APPLICATIONS OF BOUNDARY ELEMENT METHOD TO TIME DEPENDENT PROBLEMS

BY

C.S. LAU, B.Sc.

Thesis submitted to The City University
for the Degree of Doctor of Philosophy in
the Department Of Civil Engineering

February 1985

CONTENTS

LIST OF TABLE

LIST OF FIGURES

ACKNOWLEDGEMENTS

The work reported in this thesis was carried out in the Civil Engineering Department of The City University, London. Dr. K. Arumugam's supervision of the work has been greatly appreciated and the assistance of colleagues at The City University has been of considerable value. The author wishes to thank [redacted] in particular for his guidance and consultations throughout this study.

Thanks are also extended to the following: [redacted] for his special lectures on classical potential theory; [redacted] for his assistance on the numerical analysis; Dr. D. J. Lacey for his kind permission to use his experimental data.

Finally, special thanks go to [redacted] who gave me support and encouragement throughout this study and patiently typed the manuscript.

This work was made possible by the award of maintenance and support grants by the Science and Engineering Research Council.

SYNOPSIS

This study is concerned with the applications of the boundary element method to solve time dependent problems in two dimensions. The applications involve ground water flow problems, free surface flow problems, heat conduction problems and numerical modelling of periodic waves in particular.

The basic derivation of the boundary integral equation is reviewed within the framework of classical potential theory. Integral equations may be derived from (a) an indirect formulation; (b) a direct formulation; or (c) by the weighted residual technique. Numerical procedures for the solution of integral equations are discussed, involving constant, linear or quadratic variation for the potential function and its normal derivative along discretised elements on the boundary. A formulation for the solution of transient potential problems is then derived by the weighted residual technique.

The basic boundary element technique is employed to model different types of periodic wave profiles, and more importantly, the progressive waves. This approach resembles the work of Longuet-Higgins and Cokelet on numerical computation of steep surface water waves. Numerical procedures for the time stepping method are discussed in detail. With a fixed horizontal circular cylinder introduced in the flow domain, pressures and forces on the cylinder are evaluated and compared with experimental measurements.

Computer programs incorporating the above work were developed with illustrated examples throughout this study.

CHAPTER 1 - INTRODUCTION

With the advent of high speed computers, most engineering problems that may be represented by differential equations are solved by means of a numerical technique, e.g. finite difference or finite element method. The boundary element method is being increasingly used in solving various engineering problems and currently, several topics of applications are being actively researched, e.g. fluid flow problems, heat transfer problems and transient potential problems. Essentially, the boundary element method transforms the differential equation of the problem into an integral equation which becomes a surface integral for three dimensional problems and a line integral for two dimensional problems. Therefore, the dimension of the problem is reduced by one. Due to the fact that discretisation occurs only on the boundary, the number of algebraic equations to be solved is reduced. But the overall matrix is fully populated.

This study is concerned with the applications of the boundary element method for the solution of time dependent problems, with emphasis on the simulation of periodic waves. Time dependent problems in this context involve the diffusion equation and the Laplace's equation whose solution is time stepped. Application of the boundary element method to Laplace's equation is shown in Brebbia (1978), but it does not involve time stepping. Application of the boundary element method to the diffusion equation has been covered in Brebbia and Wrobel (1979).

The capabilities and limitations of existing formulations of the Laplace's equation and the diffusion equation have been studied by implementing computer programs and monitoring the numerical behaviour. Applications include ground water flow problems, free surface flow problems and transient potential problems (chapter 4). The confidence thus obtained is useful in extending the range of application to the simulation of periodic waves.

The numerical simulation of progressive wave motion has been carried out successfully by Longuet-Higgins and Cokelet (1976), based on potential theory and conformal mapping technique. Integral equations are written for the wave profile and the solution obtained is then time stepped. A similar concept is to be investigated using the boundary element method, but no conformal mapping technique is involved.

The present work starts by reviewing, in chapter 2, the literature on classical potential theory, the boundary element method and the existing technique on the simulation of periodic waves.

Chapter 3 shows how a problem governed by Laplace's equation (with prescribed boundary conditions) can be recast into an integral equation which, through a limiting process, produces a boundary integral equation relating only the boundary values. Both the indirect and the direct formulations of the boundary element method are discussed. The weighted residual technique is then employed to formulate a (direct) integral equation equivalent to the diffusion equation with prescribed boundary and initial conditions.

Numerical formulations for the solution of the boundary integral equation equivalent to Laplace's equation are discussed in chapter 4. It is shown how several features such as free surface boundary conditions, non-homogeneity, orthotropy and anisotropy can be included in the formulation. Results of their applications are presented. Numerical solutions to the time-dependent boundary integral equation equivalent to the diffusion equation are obtained through the use of time-dependent fundamental solutions. A time-stepping technique allows the time integrals in the boundary integral equation to be carried out analytically for time interpolation functions of any order. The remaining space integrals are computed numerically, apart from the singular ones. Two-dimensional problems are treated with comparison of numerical results with published analytical results.

Chapter 5 describes the theoretical basis of the application of the boundary element method to unsteady wave problems which require modification of the matrix equation to suit the appropriate boundary conditions. Time stepping technique by the Runge-Kutta method and the Adam-Bashforth-Molton method are discussed. Equations used for the evaluation of pressures and forces on an internal object are shown. The checks for accuracy of the computed wave profile are made through the use of the principles of the conservation of mass and the conservation of energy.

Numerical formulation of the boundary integral equation method to the simulation of surface waves are discussed in detail in chapter 6. Again, it involves a time stepping procedure. An area of achievement in this application is the evaluation of forces and pressures on an object placed under the wave. Computer programs incorporating these procedures are also shown. Test problems and case studies are carried out and discussed parametrically. Further comparisons of results with experimental measurements show the validity of the technique.

On the basis of comparisons of results on case studies with experimental measurements, the proposed technique on the application of the boundary element method to progressive wave problems is discussed in chapter 7.

Finally, chapter 8 draws the conclusions of this study and suggests improvements to the proposed technique.

All programs were written in FORTRAN, on the Honeywell Dual Level 66/60 computer of The City University. One exceptional program 'BEMW1' (Appendix A.12), which performs the simulation of periodic waves, was developed on the CDC7600 at the University of London Computer Centre.

CHAPTER 2 - LITERATURE SURVEY

Historically, the application of integral equations to formulate the fundamental boundary-value problems of potential theory dates back to 1903, when Fredholm demonstrated the existence of solutions to such equations, on the basis of a discretisation procedure. Due to the difficulty of finding analytical solutions, the use of integral equations has, to a great extent, been limited to theoretical investigations of existence and uniqueness to solutions of problems of mathematical physics. However, the advent of high speed digital computers made it possible to implement discretisation procedures algebraically and so enabled numerical solutions to be readily achieved.

Fredholm integral equations follow from the representation of harmonic potentials by simple-layer or double-layer potentials and set up the foundations of the so-called indirect boundary element method. Integral equations are set up involving the known boundary conditions and fictitious singular sources which are distributed on the boundary of the fictitious region at an initially unknown density. These equations may be discretised and solved numerically by using some approximate methods. The required solution variables at any internal field point may then be obtained by back-substitution of source densities into the integral equations.

Integral equations can alternatively be formulated through the application of Green's third identity (Kellogg, 1954). which represents a harmonic function as the superposition of simple-layer and double-layer potentials. Taking the field point to the boundary, an integral equation relating only boundary values and normal derivatives of the harmonic function is obtained. This technique is referred to as the direct boundary element method which provides values of the solution variables on the boundary in terms of the known boundary data.

More recently, it was demonstrated that the same integral relationships can be obtained through weighted residual considerations (Brebbia, 1978). Basically, a problem to be solved is mathematically described by its governing equations and corresponding boundary conditions. These equations are solved using some approximate methods, which transform them into algebraic relationships. This is done by using discrete elements for the spatial discretisation and discrete number of steps for the discretisation in time. In this way, it becomes easier to relate and combine the boundary element method with other numerical techniques, such as the finite element method, as well as to extend it for the analysis of problems governed by more complex partial differential equations, including non-linearities.

Jaswon (1963) and Symm (1963) presented a numerical technique to solve Fredholm boundary integral equations. The technique consists of discretising the boundary into a series of small segments (elements), assuming that the source density remains constant within each segment. The discretised equation is applied to a number of particular points (nodes) in each element, and the influence coefficients are computed approximately using Simpson's rule. Exception is made for the singular coefficients resulting from the self-influence of each element, which are computed either analytically or by the summation of the off-diagonal coefficients plus the free term. This produces a system of linear algebraic equations which can be solved computationally by a direct method, e.g. Gaussian elimination.

Applying such a technique, they obtained accurate solutions for simple two-dimensional Neumann or Dirichlet problems, e.g. the L-shaped domain with a Dirichlet boundary condition. They also proposed a more general numerical formulation for solving mixed boundary-value problems through the application of Green's third identity, which yields a boundary integral equation where boundary values and normal derivatives of a physical variable play the role of the fictitious source densities. Results using this formulation are reported by Symm (1963).

The basic idea of integral equation procedures to solve problems with homogeneous anisotropic zones of arbitrary shape and different material properties was first given by Butterfield and Tomlin (1972). The technique was later extended by Brebbia (1978) to solve non-homogeneous problems by the boundary element method. The non-homogeneous domain was divided into different homogeneous zones. The interfaces between adjoining zones were assumed to satisfy both the equilibrium and compatibility conditions. The final system of equations obtained was banded as opposed to the fully populated matrix in the original boundary element method.

The application of boundary element method to orthotropic problems was discussed in Brebbia and Chang (1979). Problems of this sort generally require the technique of zoning. A practical example was given on seepage under a dam with two sheet-pile walls and different permeabilities in the horizontal and vertical directions. Spurious results on the interface under the sheet pile were not accounted for.

The problem on seepage under a dam is a typical example of fluid flow problems where the domain is confined by the fixed boundaries. But there are also fluid flow problems with variable boundary surfaces. The location of free surface in porous media was first mentioned by Liggett (1977a) who used the boundary integral equation method to obtain equations for the location of discrete points on the free surface. An initial guess of free surface is necessary to produce the controlled domain. The final location of the free surface is obtained by an iterative process. The domain boundary is divided into five parts: (1) upstream face; (2) free surface; (3) seepage surface; (4) downstream face and (5) bottom surface. The same problem was later investigated by Brebbia and Wrobel (1979) who divided the boundary into four parts: (1) upstream face; (2) bottom surface; (3) downstream face and (4) free surface. Both approaches claimed results agreed very well with analytical solution. The effect of different seepage surface assumptions are investigated in chapter 4.

The above iterative technique resembles those employed in transient potential problems which are in general time dependent. Rizzo and Shippy (1970) applied a Laplace transform to remove the time dependence in the governing equation of transient potential problems. The transformed problem is then solved by the boundary element method. Once the equations are solved in the transformed space, the original variable involving the time dependence may be recovered by inverting the transformation numerically. Using this approach, the time dependence of the problem is temporarily removed.

Chang et al (1973) studied the time-dependent fundamental solutions associated with heat conduction in isotropic and anisotropic media. The discretisation of the integral equation was carried out using 'space and time' piecewise constant values for the variables. This approach was later extended by Wrobel and Brebbia (1979) to solve complex temperature problems. Their results were further improved by Fernandes and Pina (1983) who suggested that accurate solutions required a consistent choice of time step and spatial discretisation.

Another alternative integral approach for the solution of transient potential problems is the coupled boundary element-finite difference method proposed by Brebbia and Walker (1980). In this formulation, the problem is solved at each time interval and the time derivative is approximated in a step by step finite difference scheme.

One of the advantages of using a time dependent fundamental solution is that it precludes the need for any finite differences on the time derivative and produces an accurate and efficient solution especially when higher order space and time interpolation functions are employed.

Having reviewed the solution techniques to the location of free surface flow problems in porous media and the transient potential problems, the following is devoted to discussion on the solution of periodic wave problems. The location of wave surfaces varies with time.

The problems of wave hydrodynamics have been solved by the application of Green's theorem with simple sources and double sources distributed over the entire boundary of the fluid domain. Depending upon the properties of the fundamental solution chosen, wave problems with a submerged or floating object may be solved by the following two integral equation approaches. In the first approach, the fundamental solution satisfies the governing equation and all boundary conditions except that on the object surface. Therefore the only boundary is the object. In the second approach, the fundamental solution satisfies only the governing equation. All the boundary conditions, including the one on the object, will have to be satisfied by the integral equation. Numerical details on the first approach may be found in Mei (1978) and Lacey (1983). The following methods to be reviewed are based on the second approach.

Numerical solutions to diffraction problems with a floating or submerged body have been obtained by Bai and Yeung (1974). Their method is based on integral equation theory which involves the fundamental source function, $1/\gamma$ for three dimensional problems or $\log(1/\gamma)$ for two dimensional problems. Green's second identity is applied to a continuous potential function ϕ and the fundamental source function. The normal derivative of ϕ is either known or expressible in terms of ϕ itself. The fluid domain is then truncated by a radiation boundary taken to a finite distance. Integral equations are written in terms of ϕ and the fundamental source function. The resulting equation is then solved by the method of discretisation. Results of velocity potential, added-mass and damping coefficients may then be obtained for problems of a semi-submerged circular cylinder heaving in a deep fluid. Their results agreed well with other methods, e.g. the finite element method, except for the behaviour of the added-mass coefficient at low frequency in water of finite depth.

The application of the boundary element method to compute wave forces on submerged or floating offshore structures of arbitrary shape in two dimensions was investigated by Au and Brebbia (1982). The formulation was carried out by the weighted residual technique on the scatter potential, ϕ_s, which was expressed in terms of a linear wave theory potential without obstruction. The integral equations were satisfied subject to the bottom, free surface, obstruction and radiation boundary conditions, and were expressed in terms of ϕ_s or the derivative of ϕ_s. The wave surface was assumed to be a horizontal straight line. Therefore, their analysis is not of time stepping nature and is similar to that of Bai and Yeung (1974). Results of wave forces on submerged half-cylinders were presented and compared with other published solutions. Added-mass and damping coefficients of a heaving half-submerged cylinder were also presented.

Isaacson (1982) investigated a numerical method for calculating the interaction of steep (non-linear) ocean waves with large fixed or floating vertical structures of arbitrary shape. The interaction is treated as a transient problem with known initial conditions corresponding to still water in the vicinity of the structure and a prescribed incident waveform approaching it. The development of the flow, together with the associated fluid forces and structural motions, are obtained by a time-stepping procedure in which the flow at each time step is calculated by an integral equation method based on Green's theorem. Comparison of results with available solutions for the cases of both linear and solitary wave diffraction around a fixed surface-piercing vertical circular cylinder were discussed.

Au and Brebbia (1983a) presented the application of the boundary element method for computing wave forces on offshore structures of constant section throughout the depth of water. Examples studied include the vertical circular cylinder, the square caisson and the elliptical cylinder. The comparison of their results against analytical or experimental solutions validate the use of the boundary element method to study wave diffraction. Further application of the boundary element method to determine the wave forces on large three dimensional offshore structures can be found in Au and Brebbia (1983b).

Salmon et al (1980) applied the boundary integral equation method to transient wave problems. Their wave profile is linearized and therefore, the boundary condition on the wave surface is applied at the equilibrium free surface rather than at the actual free surface. Their radiation boundary is assumed vertical so that the radiation boundary condition takes the form as below, for non-dispersive waves:

$$\frac{\partial \phi}{\partial t} = -\sqrt{gh} \cdot \frac{\partial \phi}{\partial n} \tag{2.1}$$

The above radiation boundary condition was applied successfully in the problems of piston wave generation. The method was further extended to solve three-dimensional, linearized, transient water wave problems, (Lennon, Liu and Liggett, 1982).

The techniques described above for wave hydrodynamics are effectively time-independent problems. For the numerical simulation of progressive wave, Longuet-Higgins and Cokelet (1976, 1978) developed a numerical technique for solving periodic two-dimensional deep water breaking wave problems. This method is based on potential theory and a conformal mapping of the physical plane inside a closed contour in the mapped plane. A Fredholm integral equation of the first kind is obtained for the velocity normal to the free surface. The equation of motion is then solved for the normal velocity in this mapped plane. By employing a time-stepping technique, the progress of the wave may be followed, and after a sufficiently long time, the wave profile develops a saw-toothed appearance. However, by applying a 5-point or 7-point smoothing formula to the wave profile every 5 or 10 time steps, excellent agreement is obtained between the wave profile after one period and the initial starting profile obtained by a perturbation technique developed by Schwartz (1974). The implication is that they have proved the wave is travelling without change of shape. Numerical results have also been obtained for waves which steepen and overturn at the wave crest.

Vinje and Brevig (1980) developed a similar numerical technique to that of Longuet-Higgins and Cokelet (1976) to simulate breaking waves. The fluid is taken to be of finite depth and the computations are carried out in the physical plane. In the authors opinion, the introduction of a submerged cylinder may be included in the program, (Vinje and Brevig, 1981). The stream function ψ along the free surface and the velocity potential ϕ on the bed are determined from a Fredholm integral equation of the second kind. The integral equation is approximated using two point Lagrangian polynomials (i.e. linear interpolation). The method is remarkably stable, and no numerical instability was reported in any of the calculations. This method is also capable of modelling an overturning wave. Extreme wave forces on a submerged fixed or moving cylinder were obtained based on Vinje and Brevig's technique, (Brevig, Greenhow and Vinje, 1981). Given the same number of nodal points, this method is therefore computationally less expensive than the method of Longuet-Higgins and Cokelet (1976), except that additional nodal points are required along the bed.

Both methods assume that the flow is two-dimensional and periodic in the horizontal coordinate (the period is chosen to be 2π). The fluid is assumed to be inviscid and incompressible and the motion irrotational. McIver and Peregrine (1981) carried out a comparison on the two methods on waves that were starting to break. They concluded that both methods agreed very well and were capable of giving good results even when a large overhanging jet had formed.

In view of the above assumptions, similar to those made on potential flow problems which are solved by the boundary element method, application of the boundary element method to simulate surface wave problems becomes the major task of the present work. It will involve relating ϕ and $\frac{\partial \phi}{\partial n}$ on the domain boundary (including the free surface) through integral equations. The flow domain will be of finite depth and evaluation of $\frac{\partial \phi}{\partial n}$ on the free surface by the boundary integral equation method is carried out without domain transformation. Once the simulation has proved to be valid, a fixed obstacle is then introduced in the flow domain to allow forces and pressures to be evaluated.

Jeffrey et al (1976) have recorded some experimental measurements of surge and heave forces induced on a fixed horizontal circular cylinder in a laboratory wave tank in their wave energy project. Lacey (1983) has conducted experimental measurements of pressures at quarter points on a horizontal circular cylinder under a progressive wave. Therefore, it will be worthwhile to assess the validity of the proposed technique by comparing the theoretically calculated pressures and forces with those experimental measurements.

CHAPTER 3 - BOUNDARY INTEGRAL EQUATION METHOD

3.1 Introduction

This chapter shows the formulations of a problem governed by a partial differential equation with prescribed boundary conditions into an integral equation relating boundary data.

The basic formulation is illustrated in section 3.2 by using the partial differential equation, namely Laplace's equation. Harmonic functions in a domain satisfy Laplace's equation and may be represented as simple-layer potentials (section 3.3) or double-layer potentials (section 3.4), generated by hypothetical source density distributions on the boundary. The potentials thus generated constitute an indirect formulation, which will be discussed in section 3.5.

Section 3.6 shows that integral equations may be obtained through the application of Green's identities to harmonic functions. This becomes the direct formulation of the boundary integral equation technique. An alternative approach to obtain the same integral relationships can be derived through the weighted residual formulation in section 3.7. The weighted residual approach is further extended in sub-section 3.7.2 to include formulation of integral equations for time dependent problems governed by the diffusion equation.

Each of the alternative formulations results in a Fredholm integral equation of the first or second kind.

3.2 Elements of Potential Theory

The basic elements of classical potential theory that are related to the present study will be briefly reviewed (Jaswon and Symm, 1977). The most rigorous approach to the potential theory formulation was done by Kellogg (1954).

The potential at a field point p, with vector $\underset{\sim}{p}$, due to a unit simple source at a point q, with vector $\underset{\sim}{q}$, with reference to a set of coordinate axes, is defined as:

$$g(p,q) = |\underset{\sim}{p} - \underset{\sim}{q}|^{-1} \qquad \text{in three dimensions} \qquad (3.2.1a)$$

$$g(p,q) = \log|\underset{\sim}{p} - \underset{\sim}{q}| \qquad \text{in two dimensions} \qquad (3.2.1b)$$

where $$|\underset{\sim}{p} - \underset{\sim}{q}| = |\underset{\sim}{q} - \underset{\sim}{p}| = \left\{ \sum_{i=1}^{\alpha} \left[x_i(p) - x_i(q) \right]^2 \right\}^{1/2} \qquad (3.2.2)$$

and $\alpha = 2$ for two dimensions

$\alpha = 3$ for three dimensions

The potentials in (3.2.1) are continuous functions of p, differentiable to all orders, and satisfy Laplace's equation:

$$\nabla^2 g(p,q) = 0 \qquad (3.2.3)$$

everywhere except at the source point q (see Appendix A.2).

When the field point p coincides with the source point q, $g(p,q)$ satisfies Poisson's equation, (see Appendix A.2):

$$\nabla^2 g(p,q) = -4\pi\,\delta(\underset{\sim}{p}-\underset{\sim}{q}) \tag{3.2.4}$$

where δ is the Dirac delta function centred upon q and has the properties that:

$$\delta(\underset{\sim}{p}-\underset{\sim}{q}) = \begin{cases} 0 & \text{where } \underset{\sim}{p} \neq \underset{\sim}{q} \quad (3.2.5a) \\ \infty & \text{where } \underset{\sim}{p} = \underset{\sim}{q} \quad (3.2.5b) \end{cases}$$

$$\int_{-\infty}^{+\infty} \delta(\underset{\sim}{p}-\underset{\sim}{q})\,dp = 1 \tag{3.2.5c}$$

In a gravitational field, the potential is called a Newtonian potential which may be generated by a discrete distribution of simple sources of intensities $\sigma_1, \sigma_2, \ldots, \sigma_N$ located at points $q_1, q_2, \ldots, q_N$, respectively. The potential at p becomes:

$$u(p) = \sum_{i=1}^{N} \sigma_i \cdot g(p, q_i) \tag{3.2.6}$$

This potential is also a continuous function of p, differentiable to second order , everywhere except when p coincides with one of the source points q_i, for $i = 1, 2, \ldots, N$. Similarly, it satisfies Poisson's equation:

$$\nabla^2 u(p) = -4\pi \sum_{i=1}^{N} \delta(\underset{\sim}{p}-\underset{\sim}{q_i}) \cdot \sigma_i \tag{3.2.7}$$

The above limitation on singular behaviour has its physical importance when the solution domain of Laplace's equation contains a singular point, e.g. a source or a sink.

3.3 Simple-Layer Potential

Newtonian potentials may be generated by various types of distribution of sources, of which the surface distribution of simple sources and surface distribution of double sources play an important role in classical potential theory.

This section is devoted to discussing the properties of potential generated by surface distribution of simple sources. The potential generated by the surface distribution of double sources will be discussed in the next section. Other types of distributions can be found in Jaswon and Symm (1977), Kellogg (1954).

Let Ω_i denote a finite domain bounded by a smooth regular surface Γ and Ω_e denote an infinite region exterior to Ω_i. Let there be a continuous distribution of simple sources of density $\sigma(q)$ at $q \in \Gamma$. This distribution generates the simple-layer potential S at any point p of the form:

$$S(p) = \int_\Gamma \sigma(q)\, g(p,q)\, d\Gamma(q) \;;\quad \begin{array}{l} q \in \Gamma \\ p \in \Omega_i \text{ or } \Omega_e \end{array} \qquad (3.3.1)$$

where p and q are such that p specifies a field point and q specifies a source point. $g(p,q)$ is identical to the one in equations(3.2.1) in two or three dimensions.

The potential in (3.3.1) is continuous everywhere, differentiable to the second order and satisfies Laplace's equation. It is therefore a harmonic function, everywhere except at Γ. Provided that σ satisfies a Hölder condition (Kellogg, 1954) at $p \in \Gamma$, the potential would be continuous as the field point passes through the surface, i.e.

$$S(p) = \int_{\Gamma} \sigma(q)\, g(p,q)\, d\Gamma(q) \quad ; \quad p, q \in \Gamma \tag{3.3.2}$$

Although S remains continuous at Γ, its normal derivative is discontinuous (Smirnov, 1964). On the boundary at p, there exist two distinct normals, one on either side of Γ. It is assumed that these two normals have equal status, i.e. n_i, n_e both increase moving away from Γ. The results for the interior normal derivative of S at p is given by Jaswon and Symm (1977):

$$\frac{\partial S(p)}{\partial n_i} = S_i'(p) = \int_{\Gamma} \sigma(q)\, g_i'(p,q)\, d\Gamma(q) - \alpha\pi\sigma(p) \; ; \; p, q \in \Gamma \tag{3.3.3a}$$

and for the exterior normal derivative:

$$\frac{\partial S(p)}{\partial n_e} = S_e'(p) = \int_{\Gamma} \sigma(q)\, g_e'(p,q)\, d\Gamma(q) - \alpha\pi\sigma(p) \; ; \; p, q \in \Gamma \tag{3.3.3b}$$

where $\alpha = 1$ for two dimensional problems and $\alpha = 2$ for three dimensional problems. $g_i'(p,q)$ and $g_e'(p,q)$ imply that the interior and exterior normal derivative operations take place at p keeping q fixed, respectively:

$$g_i'(p,q) = \frac{\partial}{\partial n_i(p)}\, g(p,q) \tag{3.3.4a}$$

i.e.

$$g_e'(p,q) = \frac{\partial}{\partial n_e(p)}\, g(p,q) \tag{3.3.4b}$$

Since $g(p,q)$ remains continuous as p crosses Γ , it follows that:

$$g_i'(p,q) + g_e'(p,q) = 0 \tag{3.3.5}$$

and therefore

$$S_i'(p) + S_e'(p) = -2\alpha\pi\sigma(p) \quad ; \; p \in \Gamma \tag{3.3.6}$$

which exhibits a discontinuity of $-2\alpha\pi\sigma(p)$ between the inward and outward derivatives at $p \in \Gamma$.

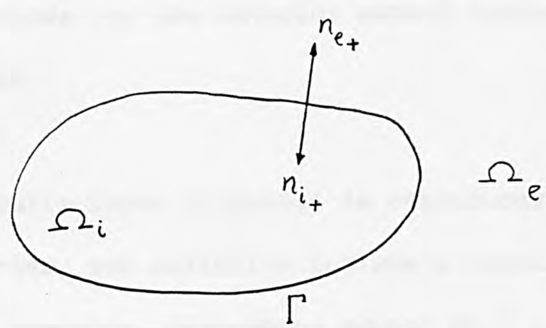

Fig. 3.3.1 Inward and outward normal directions

3.4 Double-Layer Potential

In a vector field, two simple sources, of opposite sign, separated by a small distance ε will become a dipole source or double source as ε approaches zero.

Let there be a continuous distribution of double sources over Γ (not necessarily closed) of density $\mu(q)$ at $q \in \Gamma$. The double-layer potential generated by this distribution is given by:

$$W(p) = \int_\Gamma \mu(q) \cdot g(p,q)_i' \, d\Gamma(q) \; ; \; q \in \Gamma \qquad p \in \Omega_i \text{ or } \Omega_e \tag{3.4.1}$$

where $g(p,q)_i'$ stands for the interior normal derivative of $g(p,q)$ at q keeping p fixed.

The double-layer potential is continuous and differentiable to the second order, and satisfies Laplace's equation. It is therefore a harmonic function, everywhere except at Γ.

When p approaches Γ along the normal at p on Γ, from either the interior n_i or the exterior n_e, it follows that:

$$\lim_{p_i \to p} W(p_i) = W(p) + \alpha\pi\mu(p) \tag{3.4.2a}$$

$$\lim_{p_e \to p} W(p_e) = W(p) - \alpha\pi\mu(p) \tag{3.4.2b}$$

where $\alpha = 1$ for 2-dimensional problems and $\alpha = 2$ for 3-dimensional problems.

p_i, p_e are points on the n_i, n_e normals respectively emanating from p on Γ.

Differentiating equations (3.4.2) gives:

$$\lim_{p_i \to p} \frac{\partial W(p_i)}{\partial n_i} + \lim_{p_e \to p} \frac{\partial W(p_e)}{\partial n_e} = 0 \quad ; \quad p, q \in \Gamma \tag{3.4.3}$$

which illustrates the normal derivatives are continuous at $p, q \in \Gamma$.

By putting $\mu = 1$ and letting Γ be a closed surface, Jaswon and Symm (1977) demonstrates that a jump exists in the formulations at a field point p moving from interior to exterior (interior formulae) or from exterior to interior (exterior formulae). The equations are quoted here for completeness.

Interior formulae:

$$W(p) = \int_{\Gamma} g(p,q)_i' \, d\Gamma(q) = 2\alpha\pi \quad ; \quad p \in \Omega_i \tag{3.4.4a}$$

$$W(p) = \int_{\Gamma} g(p,q)_i' \, d\Gamma(q) = \alpha\pi \quad ; \quad p \in \Gamma \tag{3.4.4b}$$

$$W(p) = \int_{\Gamma} g(p,q)_i' \, d\Gamma(q) = 0 \quad ; \quad p \in \Omega_e \tag{3.4.4c}$$

Exterior formulae:

$$W(p) = \int_{\Gamma} g(p,q)_e' \, d\Gamma(q) = -2\alpha\pi \quad ; \quad p \in \Omega_i \tag{3.4.5a}$$

$$W(p) = \int_{\Gamma} g(p,q)_e' \, d\Gamma(q) = -\alpha\pi \quad ; \quad p \in \Gamma \tag{3.4.5b}$$

$$W(p) = \int_{\Gamma} g(p,q)_e' \, d\Gamma(q) = 0 \quad ; \quad p \in \Omega_e \tag{3.4.5c}$$

3.5 Indirect Formulation

A function ϕ is said to be harmonic within a domain Ω_i, bounded by a closed surface Γ, if it satisfies the following conditions:

a) ϕ is continuous in $\Omega + \Gamma$,

b) ϕ is differentiable to at least the second order in Ω,

c) ϕ satisfies Laplace's equation in Ω,

$$\nabla^2\phi = 0 \qquad (3.5.1)$$

Since every Newtonian potential is a harmonic function, it follows that the potentials S and W in equations (3.3.1) and (3.4.1) are harmonic and satisfy Laplace's equation in Ω_i.

These two equations form the basis for the indirect formulation in classical potential theory. It is assumed that the potentials are generated by continuous source distribution on the boundary with prescribed boundary conditions which are known a priori. It is therefore an integral formulation for the unknown source intensity. These equations may be discretised and solved numerically, and potentials and their derivatives may be obtained anywhere in Ω by back-substitution of sources into equations (3.3.1) and (3.4.1).

To obtain an integral equation for the solution of Neumann problem, where the potential derivatives ϕ_i' on the boundary Γ are given, ϕ may be expressed as a simple-layer potential:

$$\phi(p) = \int_\Gamma \sigma(q)\, g(p,q)\, d\Gamma(q) \qquad p \in \Omega + \Gamma \qquad (3.5.2)$$

where σ is a source density to be determined.

$g(p,q)$ is the Newtonian potential (3.2.1) and is sometimes called the fundamental solution to Laplace's equation.

Taking the derivative of (3.5.2) in the direction of inward normal to Γ as p is taken to the boundary yields:

$$\phi_i'(p) = \int_{\Gamma} \sigma(q)\, g_i'(p,q)\, d\Gamma(q) - \alpha\pi\,\sigma(p) \qquad (3.5.3)$$

where $\alpha = 1$ for 2-dimensional problems and $\alpha = 2$ for 3-dimensional problems.

This constitutes a Fredholm integral equation of the second kind for σ in terms of ϕ_i', as the unknown appears both outside and inside the integral. According to Fredholm theory, a solution of (3.5.3) exists if the Gauss condition (equation (A.2.15)) is satisfied, and the solution is unique only up to an arbitrary additive constant. Once the system of algebraic equations is solved, values of ϕ at any interior or exterior boundary point can be calculated by using (3.5.2). Numerical examples can be found in Symm (1963) and Jaswon and Symm (1977).

For the solution of Dirichlet problem, where ϕ is prescribed on the boundary Γ, one may express ϕ as (1) a simple-layer potential with unknown density σ or (2) a double-layer potential with unknown density μ.

For the first case, ϕ takes the form of equation (3.3.2), i.e.

$$\phi(p) = \int_{\Gamma} \sigma(q)\, g(p,q)\, d\Gamma(q) \quad ; \quad p,q \in \Gamma \qquad (3.5.4)$$

which is a Fredholm integral equation of the first kind, as the unknown σ appears only inside the integral. ϕ values at any location may be uniquely obtained from equation (3.3.1), once the source density σ is solved.

For the second case, ϕ takes the form of equation (3.4.1), i.e.

$$\phi(p) = \int_{\Gamma} \mu(q)\, g(p,q)_i' \, d\Gamma(q) \quad ; \quad \begin{array}{l} q \in \Gamma \\ p \in \Omega_i \text{ or } \Omega_e \end{array} \tag{3.5.5}$$

Taking into account the jump by $-\alpha\pi\mu(p)$ at $p \in \Gamma$, in accordance with (3.4.2a), yields the boundary relation:

$$\phi(p) = \int_{\Gamma} \mu(q)\, g(p,q)_i' \, d\Gamma(q) + \alpha\pi\mu(p) \; ; \; p,q \in \Gamma \tag{3.5.6}$$

This constitutes a Fredholm integral equation of the second kind for μ in terms of ϕ. When μ is solved on the boundary, ϕ values can be computed everywhere in Ω_i or Ω_e by using equation (3.5.5).

The difference in the above two approaches lies mainly in the numerical formulation of the system of algebraic equations, obtained after discretisation. The pressence of the term outside the integral, for an equation of the second kind, ensures that the overall matrix will be diagonally dominant. An equation of the first kind with a non-singular kernel may be difficult to solve, being essentially ill-conditioned. However, in the present case, the singularity of the kernel ensures diagonal dominance in the system matrix and the problem is in general well conditioned.

Numerical solution of equation (3.5.4) can be found in Jaswon and Symm (1977) and Symm (1963).

3.6 Direct Formulation

A conceptual disadvantage of the indirect formulation is the introduction of source densities in the integral equations. The solution for ϕ or $\frac{\partial \phi}{\partial n}$ involves a two stage process: 1) solution to obtain the source densities which usually bear no physical relation to the problem; 2) back substitution of source densities to obtain ϕ or $\frac{\partial \phi}{\partial n}$.

However, the two stage process can be reduced to one stage by using Green's formula, where ϕ , $\frac{\partial \phi}{\partial n}$ over Γ play the role of source densities which generate ϕ , throughout Ω . This technique is the so-called 'Direct Formulation' of the boundary element method.

Given two different functions, ϕ and ψ, with continuous first and second derivatives in region Ω_i . From Green's second identity, (Appendix A.3, equation A.3.6) and noting that the direction of the normal is changed from outward to inward (n_i), for compatibility;

$$\int_{\Omega_i} (\phi \nabla^2 \psi - \psi \nabla^2 \phi)\, d\Omega_i = -\int_{\Gamma} (\phi \frac{\partial \psi}{\partial n_i} - \psi \frac{\partial \phi}{\partial n_i})\, d\Gamma \qquad (3.6.1)$$

If ϕ , ψ are harmonic functions in Ω_i , then

$$\nabla^2 \phi = 0 \qquad ; \qquad \nabla^2 \psi = 0$$

and the left hand side of (3.6.1) vanishes, so yielding Green's reciprocal formula:

$$\int_{\Gamma} (\phi \frac{\partial \psi}{\partial n_i} - \psi \frac{\partial \phi}{\partial n_i})\, d\Gamma = 0 \qquad (3.6.2)$$

If ϕ is a harmonic function in Ω_i and ψ is the fundamental solution:

$$\psi = g(p,q) \tag{3.6.3}$$

which satisfies Poisson's equation

$$\nabla^2 \psi = -4\pi\, \delta(\underset{\sim}{p} - \underset{\sim}{q}) \tag{3.6.4}$$

where p is the field point and q acts as a unit source point on the boundary.

From the properties of Dirac delta function, equations(3.2. 5), the left hand side of (3.6.1) becomes:

$$-4\pi \int_{\Omega_i} \phi(q)\, \delta(\underset{\sim}{p} - \underset{\sim}{q})\, d\Omega = -4\pi\, \phi(p) \; ; \quad \begin{matrix} q \in \Gamma \\ p \in \Omega_i \end{matrix} \tag{3.6.5}$$

Substituting equations (3.6.3), (3.6.5) into (3.6.1) gives:

$$\int_\Gamma \phi(q) \frac{\partial}{\partial n_i} g(p,q)\, d\Gamma - \int_\Gamma g(p,q) \frac{\partial}{\partial n_i} \phi(q)\, d\Gamma = 4\pi\, \phi(p)$$

$$; \; q \in \Gamma \; ; \; p \in \Omega_i \tag{3.6.6}$$

which is the Green's formula for potential $\phi(p)$ inside the domain and provides a fundamental link between the theory of harmonic function and potential theory.

Equation (3.6.6) exhibits ϕ in Ω_i as the superposition of a double-layer potential, generated by a source density of $\frac{-\phi}{2\pi}$ on Γ and of a simple-layer potential generated by a source density of $\frac{1}{2\pi} \cdot \frac{\partial \phi}{\partial n_i}$ on Γ .

However, according to the uniqueness theorems (Moon and Spencer,1961), either ϕ or ϕ' alone essentially suffices to determine ϕ in Ω_i .

ϕ and ϕ' must be known on Γ in (3.6.6) to enable the evaluation of $\phi(p)$ at $p \in \Omega_i$. That implies the Green's formula requires more boundary information than would be available in any well posed boundary value problem. An improvement to (3.6.6) is to move the field point p to lie on Γ , so that it can solve a boundary value problem.

In moving the point p to the boundary, the simple-layer potential remains continuous but the double-layer potential jumps by an amount $\beta\phi(p)$ depending on the type of boundary under consideration. β is an internal angle at point p, i.e. the angle in Ω_i between the tangents to Γ on either side of p and in the case of smooth boundary, $\beta = -2\pi$. Equation (3.6.6) then becomes:

$$\int_\Gamma \phi(q)\frac{\partial}{\partial n_i} g(p,q)\, d\Gamma - \int_\Gamma g(p,q)\frac{\partial}{\partial n_i}\phi(q)\, d\Gamma = 2\pi\phi(p)$$

$$; \; p, q \in \Gamma \qquad (3.6.7)$$

Equation (3.6.7) is the so-called Green's boundary formula which forms the basis of the direct boundary integral equation method. A further jump of $-2\pi\phi(p)$ occurs for smooth boundary when p lies in the exterior domain, i.e.

$$\int_\Gamma \phi(q)\frac{\partial}{\partial n_i} g(p,q)\, d\Gamma - \int_\Gamma g(p,q)\frac{\partial}{\partial n_i}\phi(q)\, d\Gamma = 0$$

$$; \; q \in \Gamma \; ; \; p \in \Omega_e \qquad (3.6.8)$$

This can be treated as a particular case of (3.6.2), since both functions ϕ and $g(p,q)$ are harmonic outside Ω_i .

Given $\phi' = \bar{\phi}'$ over Γ (interior Neumann problem), equation (3.6.7) becomes an integral equation of the second kind for ϕ in terms of ϕ' :

$$\int_\Gamma g(p,q)_i' \phi(q)\, d\Gamma - 2\pi\phi(p) = \int_\Gamma g(p,q)\, \bar{\phi}_i'(q)\, d\Gamma \quad ; p,q \in \Gamma \qquad (3.6.9)$$

This only has a solution if ϕ_i' satisfies the Gauss condition (Appendix A.2):

$$\int_\Gamma \phi'(q)\, d\Gamma = 0 \qquad (3.6.10)$$

in which case:

$$\phi = \phi_o + k$$

That means in interior Neumann problems, the solution ϕ is unique up to an arbitrary additive constant (k).

Given $\phi = \bar{\phi}$ over Γ (interior Dirichlet problem), equation (3.6.7) becomes an integral equation of the first kind for ϕ' interms of ϕ :

$$\int_\Gamma g(p,q)\, \phi_i'\, d\Gamma = -2\pi\bar{\phi}(p) + \int_\Gamma g(p,q)_i'\, \bar{\phi}(q)\, dq \quad ; p,q \in \Gamma \qquad (3.6.11)$$

Equation (3.6.11) has a unique solution, which automatically satisfies the Gauss condition.

Given $\phi = \bar{\phi}$ on a part Γ_1 of Γ and $\phi' = \bar{\phi}'_i$ on the complementary part Γ_2, where $\Gamma = \Gamma_1 + \Gamma_2$, a mixed boundary value problem is imposed. The solution is unique from the Uniqueness Theorems (Moon and Spencer 1961).

Equation (3.6.7) becomes for a smooth boundary:

$$-2\pi\phi(p)\Big|_{\Gamma} + \int_{\Gamma} g(p,q)'_i\,\phi(q)\,d\Gamma = \int_{\Gamma} g(p,q)\,\phi'_i(q)\,d\Gamma \quad ; \; p,q \in \Gamma$$

or

$$-2\pi\phi(p)\Big|_{\Gamma_2} + \int_{\Gamma_2} g(p,q)'_i\,\phi(q)\,d\Gamma - \int_{\Gamma_1} g(p,q)\,\phi'_i(q)\,d\Gamma \tag{3.6.12}$$

$$= 2\pi\bar{\phi}(p)\Big|_{\Gamma_1} - \int_{\Gamma_1} g(p,q)'_i\,\bar{\phi}(q)\,d\Gamma + \int_{\Gamma_2} g(p,q)\,\bar{\phi}'_i(q)\,d\Gamma \quad ; \; p,q \in \Gamma$$

where $\bar{\phi}$ and $\bar{\phi}'_i$ are the known values.
Hence the unknowns ϕ and ϕ'_i are on the left hand side of the equation which can then be solved by Gaussian elimination.

The mixed boundary value problems constitute most of the cases that the boundary integral equation method is applied successfully to obtain solutions.

An advantage of the direct formulation over the indirect one is that the restriction for the boundary surface to be a Liapunov (smooth) one can be relaxed, thus allowing surfaces with corners to be included.

3.7 Weighted Residual Formulation

The Green's boundary formula or the direct boundary integral equation method can alternatively be derived by the weighted residual consideration (Brebbia, 1978).

The idea of the weighted residual technique is based on the procedures for approximating numerically the solution of a set of differential equations of the form:

$$\mathcal{L}(\phi) = p \qquad \text{in} \quad \Omega \tag{3.7.1}$$

where $\mathcal{L}$ is the operator which when operating on some function ϕ produces another function, say p, with a given set of boundary conditions.

The operator can be of differential or integral type. The function ϕ is found by approximating a set of functions, such that:

$$\phi = \sum_{i=1}^{N} \alpha_i \, \phi_i \tag{3.7.2}$$

where α_i are undetermined parameters and ϕ_i are a set of 'trial' functions chosen beforehand. The ϕ_i are often chosen to be linearly independent.

It is required that these functions ϕ_i satisfy all the given boundary conditions of the problem and when substituting equations (3.7.2) into (3.7.1), the left hand side of (3.7.1) would be different from zero or produce an error function ϵ, which is called the residual,

i.e.

$$\epsilon = \nabla^2\phi - p \neq 0 \tag{3.7.3}$$

It is obvious that ϵ is equal to zero for the exact solution but not for the approximate solutions. The residual or ϵ is then forced to become zero, in the average sense, by setting weighted integrals of the residual equal to zero with the idea of orthogonalization:

$$\int \epsilon \; \omega_i \; dx = 0 \qquad\qquad i = 1,2,\ldots,N \tag{3.7.4}$$

where ω_i is a set of linearly independent weighting functions. The solutions will converge towards the exact solution as N increases.

3.7.1 Steady Potential Problems

Having given the fundamental idea of the weighted residual technique, an approximate solution is required for the problem governed by Laplace's equation:

$$\nabla^2\phi(q) = 0 \qquad ; \qquad q \in \Omega \tag{3.7.1.1}$$

with the corresponding boundary conditions:

(1) Dirichlet conditions : $\phi(q) = \bar{\phi}(q)$ on Γ_1 (3.7.1.2a)

(2) Neumann conditions : $\dfrac{\partial \phi(q)}{\partial n} = \dfrac{\partial \bar{\phi}(q)}{\partial n} = \bar{\phi}'(q)$ on Γ_2 (3.7.1.2b)

where Γ_1 and Γ_2 are part of the total boundary Γ and such that:

$$\Gamma = \Gamma_1 + \Gamma_2$$

Substituting an approximate function for ϕ into equations (3.7.1.1) and (3.7.1.2) produce errors such that:

$$\varepsilon = \nabla^2 \phi(q) \neq 0 \quad \text{in} \quad \Omega \tag{3.7.1.3a}$$

$$\varepsilon_1 = \phi(q) - \bar{\phi}(q) \neq 0 \quad \text{on} \quad \Gamma_1 \tag{3.7.1.3b}$$

$$\varepsilon_2 = \phi'(q) - \bar{\phi}'(q) \neq 0 \quad \text{on} \quad \Gamma_2 \tag{3.7.1.3c}$$

The errors must be made as small as possible over the domain and on the boundary by the above technique .

The distribution of the error functions, ε , ε_1 and ε_2 can be carried out by multiplying them by a weighting function $g^*(p,q)$ and integrating over the domain and boundary respectively, i.e.

$$\int_\Omega \varepsilon \, g^*(p,q) \, d\Omega(q) = \int_{\Gamma_2} \varepsilon_2 \, g^*(p,q) \, d\Gamma(q) - \int_{\Gamma_1} \varepsilon_1 \cdot \frac{\partial}{\partial n} g^*(p,q) \, d\Gamma(q)$$

or

$$\int_\Omega \nabla^2 \phi(q) \, g^*(p,q) \, d\Omega(q) = \int_{\Gamma_2} [\phi'(q) - \bar{\phi}'(q)] \, g^*(p,q) \, d\Gamma(q)$$
$$- \int_{\Gamma_1} [\phi(q) - \bar{\phi}(q)] \frac{\partial}{\partial n} g^*(p,q) \, d\Gamma(q) \tag{3.7.1.4}$$

where p is the field point and q is the source point, and $g^*(p,q)$ takes the value of equations(3.2.1). $\frac{\partial}{\partial n}$ represents the outward normal derivative in this technique.

Applying Green's first identity to the integral over Ω in (3.7.1.4) gives:

$$\int_{\Gamma} g^*(p,q)\,\phi'(q)\,d\Gamma(q) - \int_{\Omega} \frac{\partial \phi(q)}{\partial x_j} \cdot \frac{\partial}{\partial x_j} g^*(p,q)\,d\Omega(q)$$

$$= \int_{\Gamma_2} \left[\phi'(q) - \bar{\phi}'(q)\right] g^*(p,q)\,d\Gamma(q) - \int_{\Gamma_1} \left[\phi(q) - \bar{\phi}(q)\right] \frac{\partial}{\partial n} g^*(p,q)\,d\Gamma(q) \tag{3.7.1.5}$$

where indicial notation indicating summation has been used.

Applying Green's first identity to the integral over Ω again in (3.7.1.5) gives:

$$\int_{\Omega} \nabla^2 g^*(p,q)\,\phi(q)\,d\Omega(q) - \int_{\Gamma} \phi(q) \frac{\partial}{\partial n} g^*(p,q)\,d\Gamma(q) + \int_{\Gamma} g^*(p,q)\,\phi'(q)\,d\Gamma(q)$$

$$= \int_{\Gamma_2} \left[\phi'(q) - \bar{\phi}'(q)\right] g^*(p,q)\,d\Gamma(q) - \int_{\Gamma_1} \left[\phi(q) - \bar{\phi}(q)\right] \frac{\partial}{\partial n} g^*(p,q)\,d\Gamma(q)$$

and rearranging gives:

$$\int_{\Omega} \nabla^2 g^*(p,q)\,\phi(q)\,d\Omega(q) = -\int_{\Gamma} \phi'(q)\,g^*(p,q)\,d\Gamma(q) + \int_{\Gamma} \phi(q) \frac{\partial}{\partial n} g^*(p,q)\,d\Gamma(q) \tag{3.7.1.6}$$

where $\Gamma = \Gamma_1 + \Gamma_2$

From equation (3.6.4):

$$\nabla^2 g^*(p,q) = -4\pi\,\delta(\underset{\sim}{p} - \underset{\sim}{q}) \tag{3.7.1.7}$$

and so :

$$\int_{\Omega} \phi(q)\,\nabla^2 g^*(p,q)\,d\Omega(q) = -4\pi \int_{\Omega} \phi(q)\,\delta(\underset{\sim}{p} - \underset{\sim}{q})\,d\Omega(q)$$

$$= -4\pi\,\phi(p) \tag{3.7.1.8}$$

Substituting equations(3.7.1.8)into (3.7.1.6)gives:

$$\int_{\Gamma} \phi(q) \frac{\partial}{\partial n} g^*(p,q)\, d\Gamma(q) - \int_{\Gamma} \phi'(q)\, g^*(p,q)\, d\Gamma(q) = -4\pi\phi(p) \qquad (3.7.1.9)$$

where the field point p lies inside the domain and the source point q locates on the boundary.

When comparing the above equation with (3.6.6) a difference in sign occurs on the right hand side of the equations. This is due to the assumption made for the normal derivatives: the direct approach takes the inward normal and the weighted residual approach takes the outward normal. Both assumptions are equally valid and there is no advantage on one over the other.

When the point p is taken to the boundary and accounting for the jump in the first integral yields the more general boundary integral equation:

$$\int_{\Gamma} \phi(q) \frac{\partial}{\partial n} g^*(p,q)\, d\Gamma(q) - \int_{\Gamma} \phi'(q)\, g^*(p,q)\, d\Gamma(q) = -C(p)\,\phi(p) \qquad (3.7.1.10)$$

where $C(p)$ is a constant depending upon the type of boundary under consideration.

Two different procedures can be used to calculate the value of the coefficient C: one is through the physical consideration that a constant potential applied over a closed domain produces no flux (i.e. $\phi' = 0$), which is the one used throughout the studies and will be discussed in detail in the next chapter; the other is obtained through geometry configuration where $C(p)$ equals to the internal angle of the boundary at p (see Fig. 3.7.1.1):

$$C(p) = \pi + \theta_1 - \theta_2 \qquad (3.7.1.11)$$

where θ_1 and θ_2 are the angles between the outward normal and x axis for elements 1 and 2 respectively.

For an internal point p, $C(p)$ becomes $-2\alpha\pi$ where $\alpha = 1$ for 2-dimensional problems and $\alpha = 2$ for 3-dimensional problems.

In a well-posed boundary value problem only half of the boundary variables in (3.7.1.10) are prescribed. This equation can be employed in order to obtain the unknown boundary data. In chapter 4, a numerical scheme to solve this boundary integral equation will be presented. Then, values of the function ϕ at any internal point p can be calculated by equation (3.7.1.10). The derivatives of ϕ at p (with Cartesian coordinates $x_j(p)$, $j = 1,2,3$), if required, can be computed by differentiating equation (3.7.1.10), i.e.

$$\frac{\partial\phi(p)}{\partial x_j(p)} = \frac{1}{2\pi\alpha}\left\{\int_{\Gamma'} \phi'(q)\,\frac{\partial g^*(p,q)}{\partial x_j}\,d\Gamma(q) - \int_{\Gamma} \phi(q)\,\frac{\partial^2 g^*(p,q)}{\partial x_j\,\partial n}\,d\Gamma(q)\right\} \qquad (3.7.1.12)$$

$$j = 1,2,3$$

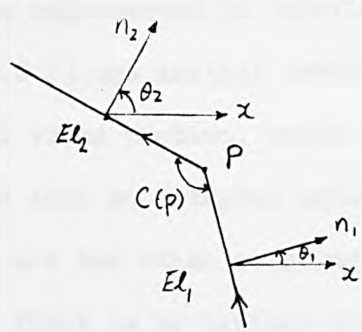

Fig. 3.7.1.1 Internal angle of the boundary at p

3.7.2 Transient Potential Problems

The foregoing deals with the boundary integral equation technique applied to problems governed by Laplace's equation. This section extends the weighted residual technique to study solutions to the diffusion equation:

$$\nabla^2\phi(q,t) - \frac{1}{K}\cdot\frac{\partial\phi(q,t)}{\partial t} = 0 \qquad ; \; q \in \Omega \qquad (3.7.2.1)$$

with boundary conditions:

$$\phi(q,t) = \bar{\phi}(q,t) \qquad \text{on } \Gamma_1 \text{ at time } t \qquad (3.7.2.2a)$$

$$\frac{\partial\phi}{\partial n}(q,t) = \frac{\partial\bar{\phi}(q,t)}{\partial n} = \bar{\phi}'(q,t) \quad \text{on } \Gamma_2 \text{ at time } t \qquad (3.7.2.2b)$$

and initial conditions:

$$\phi(q,t) = \phi_0(q,t_0) \qquad \text{given at } t_0 = 0 \quad \text{in } \Omega \qquad (3.7.2.3)$$

The coefficient K in equation (3.7.2.1) has different interpretations according to the physical problem concerned, and is assumed to be constant in space and in time.

The problem represented by equations (3.7.2.1) with boundary conditions (3.7.2.2) and initial condition (3.7.2.3) is a mixed boundary, initial value problem, which (as shown in section 3.7.1) can be transformed into an integral equation for the unknown function ϕ . There are two other existing methods to perform this transformation: the first is by Laplace transform to remove the time dependence of the problem; the second is by using the finite difference technique to replace the time derivative in equation (3.7.2.1). Details of the two existing methods are referred to Rizzo and Shippy (1970), Brebbia and Wrobel (1979).

As the problem is now time dependent, the equation will be integrated with relation to time and the weighting expression, similar to equation (3.7.1.4):

$$\int_{t=T_0}^{t=T}\int_{\Omega}\left[\nabla^2\phi(q,t)-\frac{1}{K}\cdot\frac{\partial\phi(q,t)}{\partial t}\right]g^*(p,q,t,T)\,d\Omega(q)\,dt$$
$$=\int_{t=T_0}^{t=T}\int_{\Gamma_2}\left[\phi'(q,t)-\bar{\phi}'(q,t)\right]g^*(p,q,t,T)\,d\Gamma\,dt$$
$$-\int_{t=T_0}^{t=T}\int_{\Gamma_1}\left[\phi(q,t)-\bar{\phi}(q,t)\right]\frac{\partial}{\partial n}g^*(p,q,t,T)\,d\Gamma\,dt \qquad (3.7.2.4)$$

where t_o is the initial time and T is the final time.

n is the outward normal and $g^*(p, q, t, T)$ becomes the time dependent fundamental solution of the form(Morse and Feshbach, 1953 ; Carslaw and Jaeger, 1959):

$$g^*(p,q,t,T)=\frac{1}{\left[4\pi K(T-t)\right]^{\alpha/2}}\exp\left[\frac{-r^2(p,q)}{4K(T-t)}\right]H(T-t) \qquad (3.7.2.5)$$

where α is the number of spatial dimensions of the problem, e.g.

α = 2 for two-dimensional problems.

$H(T-t)$ is the Heaviside function which becomes zero for $t>T$. This condition is known as the causality condition (Morse and Feshbach, 1953).

Applying Green's first identity twice to the integral over Ω and integrating by parts once to the time derivative $\left(\frac{\partial \phi}{\partial t}\right)$, equation (3.7.2.4) becomes:

$$\int_{t=t_0}^{t=T}\int_{\Omega}\left[\nabla^2 g^*(p,q,t,T) + \frac{1}{K}\frac{\partial}{\partial t} g^*(p,q,t,T)\right]\phi(q,t)\, d\Omega(q)\, dt$$

$$-\frac{1}{K}\left[\int_{\Omega}\phi(q,t)\, g^*(p,q,t,T)\, d\Omega(q)\right]_{t=t_0}^{t=T} = \int_{t=t_0}^{t=T}\int_{\Gamma}\phi(q,t)\frac{\partial}{\partial n} g^*(p,q,t,T)\, d\Gamma(q)\, dt$$

$$-\int_{t=t_0}^{t=T}\int_{\Gamma}\phi'(q,t)\, g^*(p,q,t,T)\, d\Gamma(q)\, dt \qquad (3.7.2.6)$$

The fundamental solution possess the following properties:

$$K\nabla^2 g^*(p,q,t,T) + \frac{\partial}{\partial n} g^*(p,q,t,T) = -\delta(\underset{\sim}{p}-\underset{\sim}{q})\,\delta(t-T) \qquad (3.7.2.7)$$

and

$$\lim_{t\to T}\int_{\Omega} g^*(p,q,t,T)\, d\Omega(q) = \delta(\underset{\sim}{p}-\underset{\sim}{q}) = \begin{cases} 0 & \text{for } \underset{\sim}{p}\neq\underset{\sim}{q} \\ \infty & \text{for } \underset{\sim}{p}=\underset{\sim}{q} \end{cases} \qquad (3.7.2.8)$$

From equation (3.7.2.7), the first term in (3.7.2.6) becomes zero in Ω for all t. From the property of Dirac delta function (3.2.5c), at $t = T$:

$$\left[\int_{\Omega}\phi(q,t)\, g^*(p,q,t,T)\, d\Omega\right]_{t=T} = \phi(p,T) \qquad (3.7.2.9)$$

Substituting equations (3.7.2.7), (3.7.2.9) into (3.7.2.6) gives the expression for the solution of diffusion equation for an internal point p:

$$\phi(p,T) + K\int_{t=t_0}^{t=T}\int_{\Gamma}\phi(q,t)\frac{\partial}{\partial n} g^*(p,q,t,T)\, d\Gamma(q)\, dt$$

$$= K\int_{t=t_0}^{t=T}\int_{\Gamma}\phi'(q,t)\, g^*(p,q,t,T)\, d\Gamma(q)\, dt + \int_{\Omega}\phi(q,t_0)\, g^*(p,q,t_0,T)\, d\Omega(q) \qquad (3.7.2.10)$$

Taking the point p in the above equation to the boundary and accounting for the jump of the left hand side integral yields the boundary integral equation;

$$C(p)\,\phi(p,T) + K\int_{t=t_0}^{t=T}\int_{\Gamma}\phi(q,t)\frac{\partial}{\partial n}g^*(p,q,t,T)\,d\Gamma(q)\,dt$$

$$= K\int_{t=t_0}^{t=T}\int_{\Gamma}\phi'(q,t)\,g^*(p,q,t,T)\,d\Gamma(q)\,dt + \int_{\Omega}\phi(q,t_0)\,g^*(p,q,t_0,T)\,d\Omega(q)$$

$$;\quad p,q\in\Gamma \qquad (3.7.2.11)$$

where $C(p)$ is a function of the internal angle on the boundary at p.

Since the time variation of functions ϕ and ϕ' is not known a priori, a time-stepping technique has to be introduced for the numerical solution of equation (3.7.2.11).

Two different time-stepping methods can be incorporated into the numerical solution technique: the first treats each time step as a new problem so the solutions inside the domain, evaluated at time step j, are used as the initial condition for time step $j+1$; the second considers the time integration process always starts at time t_0, so values of ϕ at internal points need not be computed at intermediate steps. As $T \to \infty$, a steady state solution is reached.

CHAPTER 4 - NUMERICAL FORMULATIONS AND SOLUTIONS OF PROBLEMS IN CHAPTER 3

4.1 Introduction

This chapter deals with the numerical solution of the boundary integral equations relating velocity potential ϕ and its derivative ϕ' over the boundary Γ.

The general approach involves the reduction of infinite degrees of freedom, ϕ and ϕ', to a finite set. The boundary is discretised by N nodal points with L elements of straight lines or curves. The contour integration is then performed by using a numerical quadrature scheme with the points, i , $i = 1,2,\ldots,$ N , acting successively as origins for sources or sinks. N algebraic equations are then obtained with N knowns and N unknowns in a well-posed boundary value problem. This system of equations is solved by using Gaussian elimination. Once the solutions on the boundary are known, values of ϕ and their derivatives in x and y directions at any internal point can then be calculated.

Section 4.2 examines the above approach in steady potential problems with different types of function variations along boundary elements. Although constant and linear variations were studied and discussed in the author's undergraduate project (Lau, 1980), it is repeated here for completeness.

When a problem involves domain consisting of several different homogeneous zones, or where solution becomes unstable due to singularity problems, section 4.3 illustrates how integral equations can be written for each individual zone. Each set of equations is then linked up through compatibility and equilibrium conditions on the common boundaries between zones.

The technique is further extended to solve domain problems with orthotropy and anisotropy in section 4.4; free surface flow problems in section 4.5; and transient potential problems in section 4.6.

The first boundary element program written for potential problems in this study was with linear variation along elements (Program 'BEMLVB1' in Appendix A.12). It was initially developed in the author's undergraduate project (Lau, 1980). The present version is updated with (i) evaluations of potential derivative and its direction at internal points, (ii) restructuring of computational procedure for better efficiency. A flow chart with algorithm for program 'BEMLVB1' is shown in Appendix A.11.

Computer programs incorporating the above technique are listed in Appendix A.12. Although programs were written to solve two dimensional problems only, its idea may be extended to solve three dimensional problems.

4.2 Steady Potential Problems

For steady potential problems, boundary integral equations were derived through classical potential theory and the weighted residual technique, and both approaches ended up with equations of the same form excepting the sign which depends on assumption made in taking the normal derivative inward or outward. Both approaches were programmed and gave the same results, with the signs taken into consideration. Therefore, the outward normal is chosen, unless specified, for the numerical interpretation of the boundary integral equation for steady potential problems, repeated here for clarity:

$$\int_{\Gamma} \phi(q) \frac{\partial g^*(p,q)}{\partial n} \, d\Gamma(q) - \int_{\Gamma} \phi'(q) \, g^*(p,q) \, d\Gamma(q) = -C(p)\phi(p) \qquad (4.2.1)$$

The boundary Γ is discretised into elements. Each element is defined by a set of nodal coordinates and a set of nodal values of potential ϕ and derivative ϕ', depending upon the number of nodal points on that element. Therefore the coordinates (x,y) and the functions ϕ and ϕ' at any point within an element j can be expressed in terms of some suitable interpolation functions and the nodal properties as follows:

$$x_j = \sum_{\alpha=1}^{\gamma} N_\alpha(\xi) \, x_{j\alpha} \qquad (4.2.2a)$$

$$y_j = \sum_{\alpha=1}^{\gamma} N_\alpha(\xi) \, y_{j\alpha} \qquad (4.2.2b)$$

$$\phi_j = \sum_{\alpha=1}^{\gamma} N_\alpha(\xi) \, \phi_{j\alpha} \qquad (4.2.3a)$$

$$\phi'_j = \sum_{\alpha=1}^{\gamma} N_\alpha(\xi) \, \phi'_{j\alpha} \qquad (4.2.3b)$$

where γ equals the number of nodal points on element j.

ξ is some intrinsic system of coordinates such that $\xi = -1$ at one end of an element and $\xi = 1$ at the other end (see fig. 4.2.1.1). The boundary is assumed to be discretised into L elements with N nodes. The substitution of equations (4.2.3) into (4.2.1) yields, for each nodal point i :

$$c_i \phi_i + \sum_{j=1}^{L} \int_{\Gamma_j} \frac{\partial}{\partial n} g^*\left(\sum_{\alpha=1}^{\gamma} N_\alpha \, \phi_{j\alpha}\right) d\Gamma_j = \sum_{j=1}^{L} \int_{\Gamma_j} g^*\left(\sum_{\alpha=1}^{\gamma} N_\alpha \, \phi'_{j\alpha}\right) d\Gamma$$

$$i = 1,2,\ldots,N \qquad (4.2.4)$$

Since the interpolation functions N_α are usually expressed in terms of some intrinsic system of coordinates, it is necessary to transform the integral boundary $d\Gamma$ from the global Cartesian system of coordinates, say in (x,y) plane, to the intrinsic system of coordinates, say in ξ plane. This is achieved by using a Jacobian function defined as:

$$|J(\xi)| = \frac{d\Gamma}{d\xi} = \left\{ \left(\frac{dx}{d\xi}\right)^2 + \left(\frac{dy}{d\xi}\right)^2 \right\}^{1/2} \qquad (4.2.5)$$

Hence $d\Gamma$ in equation (4.2.4) is replaced by $|J(\xi)|\,d\xi$ with the limits $\xi = -1$ to $\xi = 1$. The evaluation of $|J|$ is obtained by expressing the geometry of the element in terms of the coordinates defining the element j and the interpolation functions through equations(4.2.2).

If the expressions for N_α are known, $\frac{dx}{d\xi}$ and $\frac{dy}{d\xi}$ can be evaluated for a particular value or Gauss length ξ so $|J|$ may be calculated.

In matrix notation, equation (4.2.4) is expressed as:

$$[C_{ij}]\{\phi_i\} + [\bar{H}_{ij}]\{\phi_i\} = [G_{ij}]\{\phi'_i\} \quad , \qquad (4.2.6)$$

where

$$\bar{H}_{ij} = \int_{\Gamma_j} \frac{\partial}{\partial n} g^* \left(\sum_{\alpha=1}^{\gamma} N_\alpha \right) d\Gamma_j = \int_{-1}^{1} \frac{\partial}{\partial n} g^*(\xi) \left[\sum_{\alpha=1}^{\gamma} N_\alpha(\xi) \right] \cdot |J| \, d\xi \qquad (4.2.7a)$$

$$G_{ij} = \int_{\Gamma_j} g^* \cdot \left(\sum_{\alpha=1}^{\gamma} N_\alpha \right) d\Gamma_j = \int_{-1}^{1} g^*(\xi) \left[\sum_{\alpha=1}^{\gamma} N_\alpha(\xi) \right] |J| \, d\xi \qquad (4.2.7b)$$

Equations(4.2.7) are very general expressions. The actual values that go into $\bar{H}_{ij}$ or G_{ij} depend on the number of nodal points on element j, and will be discussed in the following sub-sections.

$[C_{ij}]$ is a diagonal matrix which may be incorporated into $[\bar{H}_{ij}]$ to form $[H_{ij}]$, i.e.

$$H_{ii} = \bar{H}_{ii} + C_{ii} \qquad (4.2.8)$$

and therefore

$$[H_{ij}]\{\phi_i\} = [G_{ij}]\{\phi_i'\} \qquad (4.2.9)$$

For the particular cases, H_{ii} and G_{ii}, due to the presence of singularity, the integrals will be evaluated analytically.

For a particular node $i = 3$, equation (4.2.9) would look like:

$$\begin{bmatrix} & & & & \cdots & \\ & & & & \cdots & \\ \bar{H}_{31} & \bar{H}_{32} & \bar{H}_{33}+\frac{1}{2} & \bar{H}_{34} & \cdots & \bar{H}_{3N} \\ & & & & \cdots & \\ & & & & \vdots & \\ & & & & \cdots & \end{bmatrix} \begin{Bmatrix} \phi_1 \\ \phi_2 \\ \phi_3 \\ \phi_4 \\ \vdots \\ \phi_N \end{Bmatrix} = \begin{bmatrix} & & & & \cdots & \\ & & & & \cdots & \\ G_{31} & G_{32} & G_{33} & G_{34} & \cdots & G_{3N} \\ & & & & \cdots & \\ & & & & \vdots & \\ & & & & \cdots & \end{bmatrix} \begin{Bmatrix} \phi_1' \\ \phi_2' \\ \phi_3' \\ \phi_4' \\ \vdots \\ \phi_N' \end{Bmatrix}$$

As discussed earlier in section 3.7, a simple approach to evaluate the diagonal matrix $[C_{ij}]$ in (4.2.6), or indeed the diagonal matrix in $[H_{ij}]$ in (4.2.9), is to apply a uniform potential to the whole boundary. The potential derivative must then be zero and equation (4.2.9) reduces to, assuming ϕ_i is a unit potential;

$$\left[H_{ij}\right]\left\{I\right\} = \left[H_{ij}\right] = 0 \tag{4.2.10}$$

Hence, the sum of all the coefficients of matrix $\left[H\right]$ in a row ought to be zero, and the coefficients on the leading diagonal can be computed as:

$$H_{ij} = -\sum_{j=1}^{L} H_{ij} \qquad ; \quad i = 1, 2, \cdots, N \tag{4.2.11}$$

Since either ϕ or ϕ' is known at each node, the set of equations can be solved for the N unknowns after re-ordering in matrix form :

$$\left[A\right]\left\{x\right\} = \left\{F\right\} \tag{4.2.12}$$

where $[A]$ is a fully populated matrix of order $N \times N$.

$\{x\}$ contains the unknowns ϕ or ϕ'.

$\{F\}$ is obtained by multiplying the known ϕ or ϕ' with the appropriate coefficients in the matrices $[H_{ij}]$ or $[G_{ij}]$ in (4.2.9).

Equation (4.2.12) is then solved by Gaussian elimination.

Once the value of ϕ and ϕ' on the whole boundary are known, the values of ϕ_i , $\frac{\partial \phi_i}{\partial x}$ in the x-direction and $\frac{\partial \phi_i}{\partial y}$ in the y -direction, at any interior point, can be calculated using equations (4.2.1) or (4.2.4), i.e.

$$\phi_i = \sum_{j=1}^{L} \int_{\Gamma_j} g^* \cdot \left(\sum_{\alpha=1}^{\gamma} N_\alpha \cdot \phi'_{j\alpha} \right) d\Gamma_j - \sum_{j=1}^{L} \int_{\Gamma_j} \frac{\partial}{\partial n} g^* \left(\sum_{\alpha=1}^{\gamma} N_\alpha \phi_{j\alpha} \right) d\Gamma_j \tag{4.2.13a}$$

$$\frac{\partial \phi_i}{\partial x} = \sum_{j=1}^{L} \int_{\Gamma_j} \frac{\partial g^*}{\partial x} \left(\sum_{\alpha=1}^{\gamma} N_\alpha \phi'_{j\alpha} \right) d\Gamma_j - \sum_{j=1}^{L} \int_{\Gamma_j} \frac{\partial^2 g^*}{\partial x \cdot \partial n} \left(\sum_{\alpha=1}^{\gamma} N_\alpha \phi_{j\alpha} \right) d\Gamma_j \tag{4.2.13b}$$

$$\frac{\partial \phi_i}{\partial y} = \sum_{j=1}^{L} \int_{\Gamma_j} \frac{\partial g^*}{\partial y} \left(\sum_{\alpha=1}^{\gamma} N_\alpha \phi'_{j\alpha} \right) d\Gamma_j - \sum_{j=1}^{L} \int_{\Gamma_j} \frac{\partial^2 g^*}{\partial y \partial n} \left(\sum_{\alpha=1}^{\gamma} N_\alpha \phi_{j\alpha} \right) d\Gamma_j \qquad (4.2.13c)$$

Since C_i becomes 1 for an internal point completely surrounded by the boundary.

The direction of potential derivative θ is obtained from:

$$\theta = \tan^{-1}\left(\frac{\partial \phi}{\partial y} \Big/ \frac{\partial \phi}{\partial x} \right) \qquad (4.2.14)$$

Different orders of approximation can be used to describe the boundary geometry, the potential and its normal derivative along an element, depending upon the behaviour of the boundary concerned. The nodes where the unknown values are required will depend upon the type of approximation used. If the boundary is approximated by straight line elements with constant variation, the nodes are taken to be in the middle of each interval (Fig. 4.2.1a) and the functions ϕ and ϕ' are assumed to be constant along that element. If the boundary is approximated by straight line elements with linear variation, the nodes are taken to be at the intersection between two elements (Fig. 4.2.1b). The functions ϕ and ϕ' are assumed to vary linearly. In both cases, the number of nodes is equal to the number of elements.

Quadratic elements (Fig. 4.2.1c) can also be used to discretise the boundary with quadratic variation for the functions ϕ and ϕ' An extra mid-element node is needed in the computation. Therefore, the number of nodes would not be equal to the number of elements.

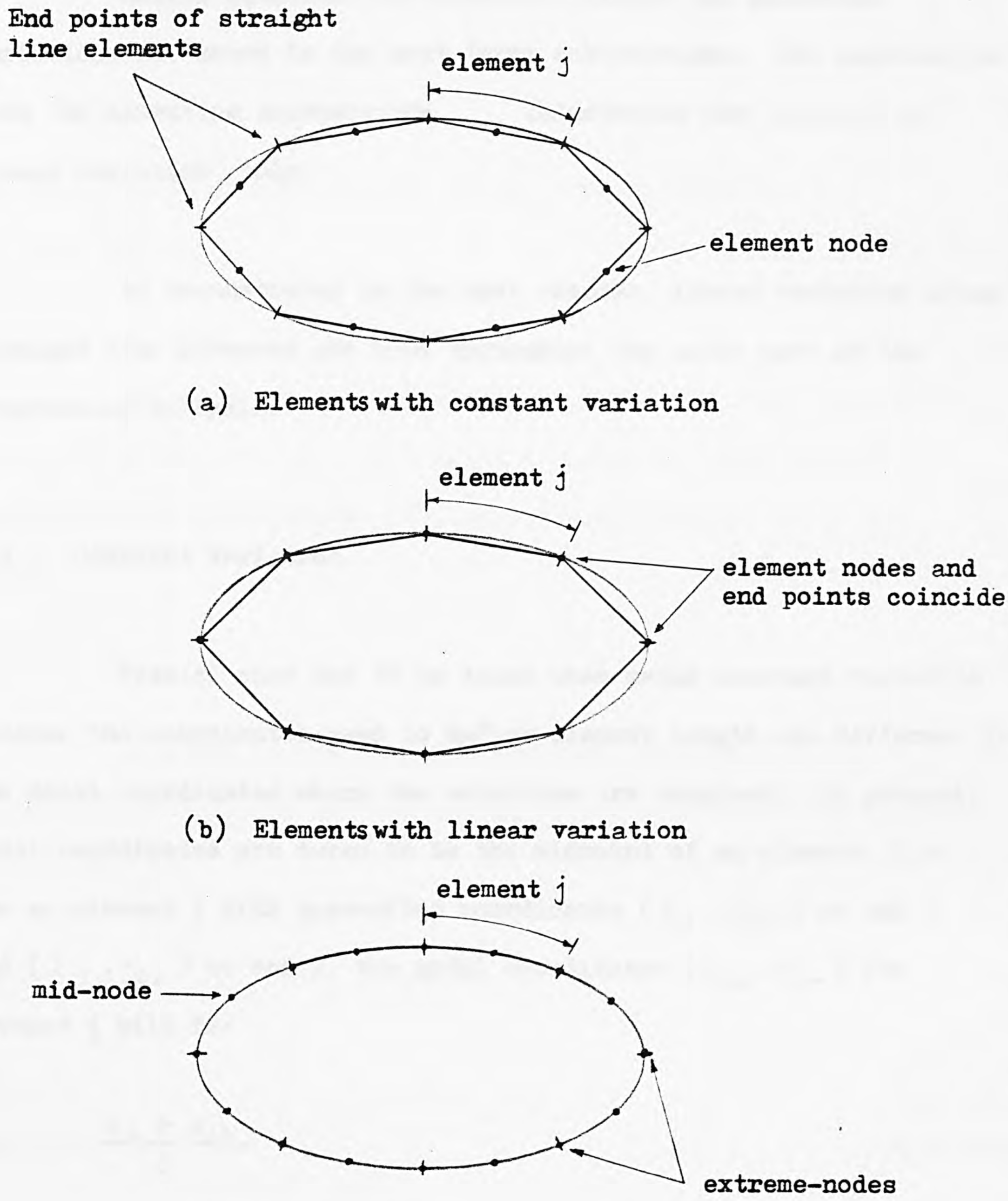

(a) Elements with constant variation

(b) Elements with linear variation

(c) Elements with quadratic variation

Fig. 4.2.1 Different types of boundary elements

Matrix equations for constant, linear and quadratic variations are shown in the next three sub-sections. But expressions used for computing purposes are illustrated for constant or linear variation only.

As demonstrated in the next chapter, linear variation along straight line elements are used throughout the major part of the programming analysis.

4.2.1 Constant Variation

Special care has to be taken when using constant variation because the coordinates used to define element length are different from the nodal coordinates where the solutions are required. In general, nodal coordinates are taken to be the midpoint of an element, i.e. for an element j with prescribed coordinates (x_{j1} , y_{j1}) at end 1 and (x_{j2} , y_{j2}) at end 2, the nodal coordinates (x_{jm} , y_{jm}) for element j will be:

$$x_{jm} = \frac{x_{j1} + x_{j2}}{2} \tag{4.2.1.1a}$$

$$y_{jm} = \frac{y_{j1} + y_{j2}}{2} \tag{4.2.1.1b}$$

The coordinates (x_j , y_j) at any point on element j can be expressed in terms of the linear interpolation functions N_α and the coordinates at end 1 and end 2, as follows:

$$x_j(\xi) = N_1(\xi)\, x_{j1} + N_2(\xi)\, x_{j2} \tag{4.2.1.2a}$$

$$y_j(\xi) = N_1(\xi)\, y_{j1} + N_2(\xi)\, y_{j2} \tag{4.2.1.2b}$$

where ξ is the intrinsic coordinate (Fig. 4.2.1.1) such that:

$$\xi = \frac{X}{l_j/2} \qquad (4.2.1.3)$$

and the interpolation functions become (Fig. 4.2.1.2):

$$N_1(\xi) = \frac{1}{2}(1-\xi) \qquad (4.2.1.4a)$$

$$N_2(\xi) = \frac{1}{2}(1+\xi) \qquad (4.2.1.4b)$$

The prescribed functions ϕ or ϕ' will be associated with the nodal point (not the end points) of element j and assumed constant along the element. So, in equation (4.2.3), γ =1 and hence :

$$N_1 = 1$$

$$\phi_j = \phi_{jm} \quad ; \quad \phi_j' = \phi_{jm}' \qquad (4.2.1.5)$$

In order to evaluate the Jacobian function, $|J|$, equation (4.2.1.2a) is written out in full and differentiated with respect to ξ :

$$x_j(\xi) = \frac{1}{2}(1-\xi)x_{j_1} + \frac{1}{2}(1+\xi)x_{j_2}$$

$$\frac{dx_j(\xi)}{d\xi} = -\frac{1}{2}x_{j_1} + \frac{1}{2}x_{j_2} = \frac{1}{2}(x_{j_2} - x_{j_1}) \qquad (4.2.1.6a)$$

Similarly, for equation (4.2.1.2b):

$$\frac{dy_j(\xi)}{d\xi} = \frac{1}{2}(y_{j_2} - y_{j_1}) \qquad (4.2.1.6b)$$

Substituting the above results into equation (4.2.5) gives:

$$|J| = \left\{\frac{1}{4}(x_{j_2}-x_{j_1})^2 + \frac{1}{4}(y_{j_2}-y_{j_1})^2\right\}^{1/2} = \frac{l_j}{2} \qquad (4.2.1.7)$$

So, the Jacobian $|J|$ for constant variation equals half the length of element j.

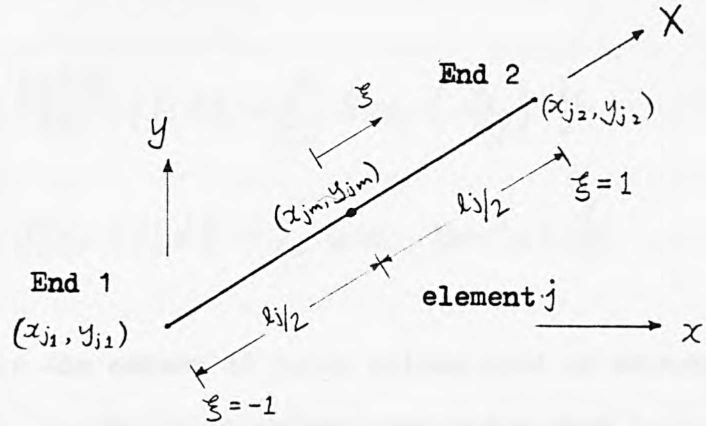

Fig. 4.2.1.1 Intrinsic coordinate system

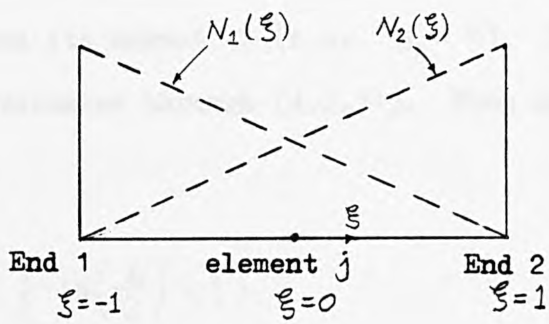

Fig. 4.2.1.2 Linear interpolation functions

The integrals in equations (4.2.7) are evaluated numerically using Gaussian quadrature scheme. With $\gamma = 1$, $N_1 = 1$ and $g^*(p,q) = \ln|\underset{\sim}{p}-\underset{\sim}{q}| = \ln(r)$, the integrals $\bar{H}_{ij}$ and G_{ij} become (see Appendix A.4):

$$\bar{H}_{ij} = \int_{-1}^{1} \frac{\partial g^*(\xi)}{\partial n} \cdot |J|\, d\xi = \sum_{k=1}^{M} GW_k \cdot \left(\frac{y_p}{r_{ik}^2}\right) \frac{\ell_j}{2} \tag{4.2.1.8a}$$

$$G_{ij} = \int_{-1}^{1} g^*(\xi) \cdot |J|\, d\xi = \sum_{k=1}^{M} GW_k \cdot \ln(r_{ik}) \cdot \frac{\ell_j}{2} \tag{4.2.1.8b}$$

where M is the number of Gauss points used on element j.

GW_k is the Gauss weight associated with Gauss point k.

y_p is the perpendicular distance from nodal point i to the tangent of element j.

ℓ_j is the length of element j.

For the diagonal terms $\bar{H}_{ij}$ and G_{ij}, the integrals become singular and have to be evaluated analytically in the Cauchy principal value sense. That implies a small segment of length 2ε around the singular point excluded from the integration and then the limit of $\varepsilon \to 0$ is taken. $\bar{H}_{ij}$ is zero due to the orthogonality of r along element i and its normal n (i.e. $y_p = 0$). Therefore, H_{ii} equals to C_{ii} and is evaluated through (4.2.11). From appendix A.5, G_{ii} is shown to be:

$$G_{ii} = \ell_i \left\{ \ln\left(\frac{\ell_i}{2}\right) - 1 \right\} \tag{4.2.1.9}$$

4.2.2 Linear Variation

The nodes are now considered to be at the ends of an element or where two straight line elements meet (Fig. 4.2.1b). Therefore, nodal coordinates are the same as element coordinates. Equations (4.2.1.2), (4.2.1.3) and (4.2.1.4) are applicable to obtain coordinates of a point on element j and hence the Jacobian function, $|J|$, remains the same as for the constant case.

Prescribed values of ϕ or ϕ' are at the nodal points, assuming varying linearly within each element. Therefore, values of ϕ and ϕ' at any point on element j may be defined by equations (4.2.3) with $\gamma = 2$, i.e.

$$\phi_j(\xi) = N_1(\xi)\,\phi_{j1} + N_2(\xi)\,\phi_{j2} \qquad (4.2.2.1a)$$

$$\phi'_j(\xi) = N_1(\xi)\,\phi'_{j1} + N_2(\xi)\,\phi'_{j2} \qquad (4.2.2.1b)$$

where N_1 and N_2 have the same expressions as (4.2.1.4). The expressions for $\overline{H}_{ij}$ and G_{ij} then become:

$$\overline{H}_{ij} = \int_{-1}^{1} N_1(\xi)\cdot\frac{\partial}{\partial n}g^*(\xi)\cdot\frac{l_j}{2}\,d\xi + \int_{-1}^{1} N_2(\xi)\frac{\partial}{\partial n}g^*(\xi)\frac{l_{j-1}}{2}\,d\xi$$

$$= \sum_{k=1}^{M} GW_k\cdot\frac{1}{2}(1-\xi)_k\cdot\left(\frac{y_p}{\gamma_{ik}^2}\right)_j\frac{l_j}{2} + \sum_{k=1}^{M} GW_k\cdot\frac{1}{2}(1+\xi)_k\left(\frac{y_p}{\gamma_{ik}^2}\right)_{j-1}\frac{l_{j-1}}{2} \qquad (4.2.2.2a)$$

$$G_{ij} = \int_{-1}^{1} N_1(\xi)\,g^*(\xi)\frac{l_j}{2}\,d\xi + \int_{-1}^{1} N_2(\xi)\,g^*(\xi)\,\frac{l_{j-1}}{2}\,d\xi$$

$$= \sum_{k=1}^{M} GW_k\frac{1}{2}(1-\xi)_k\ln(\gamma_{ik})_j\frac{l_j}{2} + \sum_{k=1}^{M} GW_k\frac{1}{2}(1+\xi)_k\ln(\gamma_{ik})_{j-1}\frac{l_{j-1}}{2} \qquad (4.2.2.2b)$$

where ξ , M, GW_k , y_p , ℓ_j have the same meaning as for constant variation .

From equations (4.2.2.2), it can be seen that the first integral accounts for the contribution of element j at node j (i.e. end 1 of element j) and the second integral accounts for the contribution from element $j-1$ at node j (i.e. end 2 of element $j-1$). This is due to the fact that for linear variation , node j lies at the intersection of elements j and $j-1$.

For the diagonal terms, $\bar{H}_{ii}$ again equals zero and hence H_{ii} is obtained through equation (4.2.11). The evaluation of G_{ii} is shown in Appendix A.5 and it has the following form:

$$G_{ii} = \frac{\ell_i}{2}\left\{ \ln(\ell_i) - 1.5 \right\} + \frac{\ell_{i-1}}{2}\left\{ \ln(\ell_{i-1}) - 0.5 \right\} \qquad (4.2.2.3)$$

where ℓ_i is the length of element i.

Again, it can be seen that coefficients in equation (4.2.2.3) involve contributions from elements $i-1$ as well as i, as compared to equation (4.2.1.9) which only involves a contribution from element i containing nodal point i.

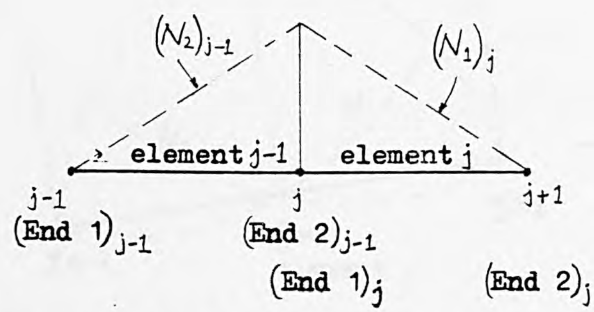

Fig. 4.2.2.1 Contributions from neighbouring elements to node j

4.2.3 Quadratic Variation

The nodes considered in this case are not only at the end intersections of elements but also an additional node located in the middle of an element or somewhere between the end nodes (see Fig. 4.2.1c). Therefore $\gamma = 3$ in equation (4.2.3). As for the linear variation, element coordinates are the same as the nodal coordinates. Both the coordinates and functions ϕ and ϕ' vary quadratically within each element. At any point on an element, its coordinates and functions may be defined in terms of its nodal values and the interpolation functions for an element j as:

$$x_j(\xi) = N_1(\xi)\,x_{j1} + N_2(\xi)\,x_{j2} + N_3(\xi)\,x_{j3} \tag{4.2.3.1a}$$

$$y_j(\xi) = N_1(\xi)\,y_{j1} + N_2(\xi)\,y_{j2} + N_3(\xi)\,y_{j3} \tag{4.2.3.1b}$$

$$\phi_j(\xi) = N_1(\xi)\,\phi_{j1} + N_2(\xi)\,\phi_{j2} + N_3(\xi)\,\phi_{j3} \tag{4.2.3.2a}$$

$$\phi'_j(\xi) = N_1(\xi)\,\phi'_{j1} + N_2(\xi)\,\phi'_{j2} + N_3(\xi)\,\phi'_{j3} \tag{4.2.3.2b}$$

where ξ is an intrinic coordinate and has the same expression as equation (4.2.1.3), i.e.

$$\xi = \frac{X}{l_j/2} \tag{4.2.3.3}$$

The interpolation functions become (see Fig. 4.2.3.1):

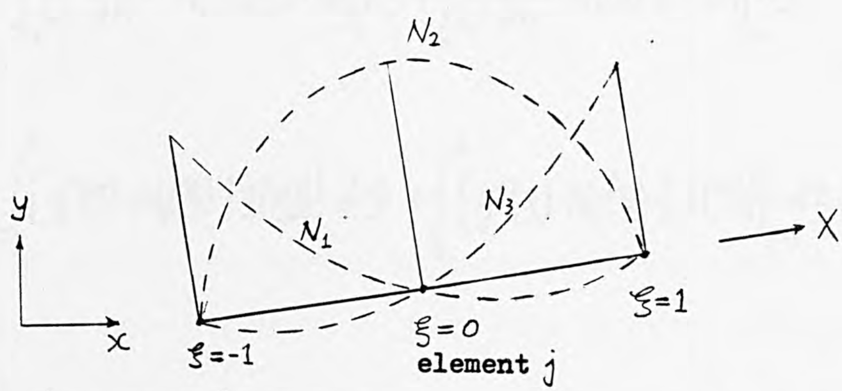

Fig. 4.2.3.1 Quadratic Variation

$$N_1 = \frac{-\xi}{2}(1-\xi) \tag{4.2.3.4a}$$

$$N_2 = (1-\xi)(1+\xi) \tag{4.2.3.4b}$$

$$N_3 = \frac{\xi}{2}(1+\xi) \tag{4.2.3.4c}$$

Substituting equations (4.2.3.4) into (4.2.3.1) and after differentiation gives:

$$\frac{dx}{d\xi} = \frac{x_{j3} - x_{j1}}{2} + \xi(x_{j1} + x_{j3} - 2x_{j2}) \tag{4.2.3.5a}$$

$$\frac{dy}{d\xi} = \frac{y_{j3} - y_{j1}}{2} + \xi(y_{j1} + y_{j3} - 2y_{j2}) \tag{4.2.3.5b}$$

With ξ equals to a Gauss length chosen, $|J|$ is obtained by:

$$|J(\xi)| = \left[\left(\frac{dx}{d\xi}\right)^2 + \left(\frac{dy}{d\xi}\right)^2\right]^{1/2} \tag{4.2.3.6}$$

The equivalent expressions for $\bar{H}_{ij}$ and G_{ij} in equations (4.2.7) for quadratic variation are given by, γ = 3 in this case:

for end-nodal points :

$$\bar{H}_{ij} = \int_{-1}^{1}\left[\frac{\partial g^*(\xi)}{\partial n}\cdot N_1(\xi)\cdot|J(\xi)|\right]_j d\xi + \int_{-1}^{1}\left[\frac{\partial g^*(\xi)}{\partial n}\cdot N_3(\xi)\cdot|J(\xi)|\right]_{j-1} d\xi \tag{4.2.3.7a}$$

$$G_{ij} = \int_{-1}^{1}\left[g^*(\xi)\cdot N_1(\xi)\,|J(\xi)|\right]_j d\xi + \int_{-1}^{1}\left[g^*(\xi)\cdot N_3(\xi)\cdot|J(\xi)|\right]_{j-1} d\xi \tag{4.2.3.7b}$$

for mid-nodal point:

$$\bar{H}_{ij} = \int_{-1}^{1} \left[\frac{\partial g^*(\xi)}{\partial n} \cdot N_2(\xi) \cdot |J(\xi)| \right]_j d\xi \qquad (4.2.3.8a)$$

$$G_{ij} = \int_{-1}^{1} \left[g^*(\xi) \cdot N_2(\xi) \cdot |J(\xi)| \right]_j d\xi \qquad (4.2.3.8b)$$

It is interesting to see that equations (4.2.3.7) have two integral terms similar to (4.2.2.2) for linear variation , and equations (4.2.38) have only one integral contribution from its own element, similar to (4.2.1.8) for constant variation . This reaffirms the fact that a node located between two elements will have contributions from both elements but a node within an element will only have a contribution from its own element.

The H_{ii} coefficients may again be obtained through equation (4.2.11) while the G_{ii} terms are of the form:

for end-nodal points:

$$G_{ii} = \frac{1}{2} \int_{-1}^{1} \left[\ln\left(r(\xi)\right) \cdot \xi\,(\xi - 1) \cdot |J(\xi)| \right]_j d\xi$$
$$+ \frac{1}{2} \int_{-1}^{1} \left[\ln\left(r(\xi)\right) \cdot \xi\,(\xi + 1) \cdot |J(\xi)| \right]_{j-1} d\xi \qquad (4.2.3.9a)$$

for mid-nodal point:

$$G_{ii} = \int_{-1}^{1} \left[\ln\left(r(\xi)\right) (1 - \xi^2) \cdot |J(\xi)| \right]_j d\xi \qquad (4.2.3.9b)$$

Since the Jacobian function involves ξ terms in it, the integral terms in G_{ii} become difficult to be evaluated analytically and may be solved by using a logarithmic Gaussian quadrature formula (Brebbia, 1978).

4.3 Combination of Zones

In many practical problems it may be necessary to divide the domain into several zones, (Brebbia,1978; Brebbia and Walker, 1980). This may be due to : (1) a non-homogeneous body constituted of several homogeneous zones with different physical properties; (2) bodies of irregular shape where re-entrant corners or singular behaviour occur . Integral equation will first be written for each zone and then linked together through compatibility and equilibrium conditions on the common boundary between the zones.

Consider for instance the case of a two-dimensional domain, divided into three different zones, Ω_1 , Ω_2 and Ω_3 (see Fig. 4.3.1) and the whole domain Ω is:

$$\Omega = \Omega_1 + \Omega_2 + \Omega_3 \tag{4.3.1}$$

The outer boundaries are denoted by Γ_1 on Ω_1 ; Γ_2 as the first part and $\underline{\Gamma}_2$ as the second part on Ω_2 ; Γ_3 on Ω_3 . The interfaces

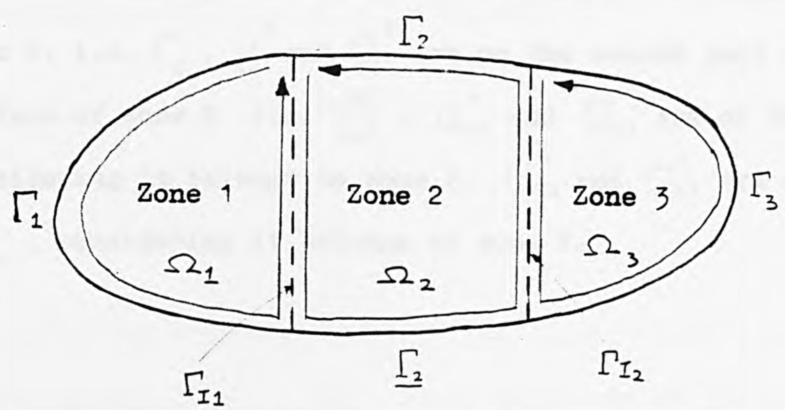

Fig. 4.3.1 Division of domain

between the three zones will be called Γ_{I1} and Γ_{I2}. Integral equations will be obtained over each zone independently. The node numbering system will be anti-clockwise in each zone (see direction of arrows in Fig. 4.3.1).

Let U represents potential ϕ and Q represents potential derivative ϕ', the integral equation in matrix form (4.2.9) becomes, for zone 1:

$$\begin{bmatrix} H^1 & H^1_{I1} \end{bmatrix} \begin{Bmatrix} U^1 \\ U^1_{I1} \end{Bmatrix} = \begin{bmatrix} G^1 & G^1_{I1} \end{bmatrix} \begin{Bmatrix} Q^1 \\ Q^1_{I1} \end{Bmatrix} \tag{4.3.2}$$

where U^1 and Q^1 are on the external surface of zone 1. U^1_{I1} and Q^1_{I1} are on the interface Γ_{I1} considering that it belongs to zone 1.

Similarly, for zone 2, the equation in matrix form becomes:

$$\begin{bmatrix} H^2 & H^2_{I1} & \underline{H}^2 & H^2_{I2} \end{bmatrix} \begin{Bmatrix} U^2 \\ U^2_{I1} \\ \underline{U}^2 \\ U^2_{I2} \end{Bmatrix} = \begin{bmatrix} G^2 & G^2_{I1} & \underline{G}^2 & G^2_{I2} \end{bmatrix} \begin{Bmatrix} Q^2 \\ Q^2_{I1} \\ \underline{Q}^2 \\ Q^2_{I2} \end{Bmatrix} \tag{4.3.3}$$

where U^2 and Q^2 are on the first part of the external surface of zone 2, i.e. Γ_2, $\underline{U}^2$ and $\underline{Q}^2$ are on the second part of the external surface of zone 2 i.e. $\underline{\Gamma}_2$. U^2_{I1} and Q^2_{I1} are on the interface Γ_{I1}, considering it belongs to zone 2. U^2_{I2} and Q^2_{I2} are on the interface Γ_{I2}, considering it belongs to zone 2.

For zone 3, the matrix form is:

$$\begin{bmatrix} H_{I2}^3 & H^3 \end{bmatrix} \begin{Bmatrix} U_{I2}^3 \\ U^3 \end{Bmatrix} = \begin{bmatrix} G_{I2}^3 & G^3 \end{bmatrix} \begin{Bmatrix} Q_{I2}^3 \\ Q^3 \end{Bmatrix} \tag{4.3.4}$$

where U^3 and Q^3 are on the external surface of zone 3. U_{I2}^3 and Q_{I2}^3 are on the interface Γ_{I2}, considering that Γ_{I2} belongs to zone 3.

The interfaces may be treated as imaginary boundaries which may not exist in the original problem. Therefore U and Q on the interfaces are unknowns. Additional equations are needed to enable the problem to be solved. Two conditions must be satisfied on the interfaces. They are:

(1) the condition of compatibility:

i.e.
$$U_{I1}^1 = U_{I1}^2 \tag{4.3.5a}$$

$$U_{I2}^2 = U_{I2}^3 \tag{4.3.5b}$$

(2) the condition of equilibrium :

$$Q_{I1}^1 = -Q_{I1}^2 \tag{4.3.6a}$$

$$Q_{I2}^2 = -Q_{I2}^3 \tag{4.3.6b}$$

Rearranging equation (4.3.2) yields:

$$\begin{bmatrix} H^1 \end{bmatrix} \begin{Bmatrix} U^1 \end{Bmatrix} = \begin{bmatrix} G^1 & G_{I1}^1 & -H_{I1}^1 \end{bmatrix} \begin{Bmatrix} Q^1 \\ Q_{I1}^1 \\ U_{I1}^1 \end{Bmatrix} \tag{4.3.7}$$

Substituting equations (4.3.5) and (4.3.6) into (4.3.3) and after rearranging the nodal equations on the common boundary due to opposite node numbering, (see Fig. 4.3.1 or Fig. 4.3.6) gives:

$$\begin{bmatrix} H^2 & \underline{H}^2 \end{bmatrix} \begin{Bmatrix} U^2 \\ \underline{U}^2 \end{Bmatrix} = \begin{bmatrix} -G^2_{I1} & -H^2_{I1} & G^2 & \underline{G}^2 & G^2_{I2} & -H^2_{I2} \end{bmatrix} \begin{Bmatrix} Q^1_{I1} \\ U^1_{I1} \\ Q^2 \\ \underline{Q}^2 \\ Q^2_{I2} \\ U^2_{I2} \end{Bmatrix} \tag{4.3.8}$$

The above substitution and re-arrangement of the equations on the common boundary are repeated in equation (4.3.4) and hence:

$$\begin{bmatrix} H^3 \end{bmatrix} \begin{Bmatrix} U^3 \end{Bmatrix} = \begin{bmatrix} -G^3_{I2} & -H^3_{I2} & G^3 \end{bmatrix} \begin{Bmatrix} Q^2_{I2} \\ U^2_{I2} \\ Q^3 \end{Bmatrix} \tag{4.3.9}$$

Combining equations (4.3.7), (4.3.8) and (4.3.9) produces:

$$\begin{bmatrix} H^1 & 0 & 0 & 0 \\ 0 & H^2 & \underline{H}^2 & 0 \\ 0 & 0 & 0 & H^3 \end{bmatrix} \begin{Bmatrix} U^1 \\ U^2 \\ \underline{U}^2 \\ U^3 \end{Bmatrix} = \left[\begin{array}{c|cc|cc|ccc} G^1 & G^1_{I1} & -H^1_{I1} & 0 & 0 & 0 & 0 & 0 \\ 0 & -G^2_{I1} & -H^2_{I1} & G^2 & \underline{G}^2 & G^2_{I2} & -H^2_{I2} & 0 \\ 0 & 0 & 0 & 0 & 0 & -G^3_{I2} & -H^3_{I2} & G^3 \end{array}\right] \begin{Bmatrix} Q^1 \\ Q^1_{I1} \\ U^1_{I1} \\ Q^2 \\ \underline{Q}^2 \\ Q^2_{I2} \\ U^2_{I2} \\ Q^3 \end{Bmatrix} \tag{4.3.10}$$

or $$\begin{bmatrix} H \end{bmatrix} \begin{Bmatrix} U \end{Bmatrix} = \begin{bmatrix} A \end{bmatrix} \begin{Bmatrix} X \end{Bmatrix} \tag{4.3.11}$$

Assuming the external boundaries are prescribed with potential U, and hence $\{X\}$ contains all the unknowns. Equation (4.3.11) can further be reduced to :

$$\begin{bmatrix} A \end{bmatrix} \begin{Bmatrix} X \end{Bmatrix} = \begin{Bmatrix} B \end{Bmatrix} \tag{4.3.12}$$

where $\{B\} = [H]\{U\}$

This system of equations is similar to (4.2.12) except that the matrix $[A]$ becomes banded, as shown in (4.3.10). This banded matrix will make the boundary integral equation method more attractive not only to reduce the behaviour of the singularity if it exists in the problem but also to reduce the computing time in the formation of matrices $[H]$ and $[G]$ and the solution routine. The band width of $[A]$ relies on the maximum size of a block matrix, or in other words, the number of nodes on the boundary and on the common boundary in a zone. If the number of boundary nodes is fixed in a problem, the smaller the number of nodes on the boundary and the common boundary in a zone, the smaller the band width in the matrix $[A]$. This is usually done by dividing the problem domain into as many zones as possible. The resultant matrix, even though it remains non-symmetric, becomes banded. Therefore, it is computationally economical to solve.

In the case where part of the boundaries are prescribed with potential derivatives Q, say in zone 1, then the Q values on the right of equation (4.3.2) would interchange with the corresponding U values on the left. The corresponding columns of matrices in $[H]$ and $[G]$ are also interchanged with the reversal of signs.

Although three zones were used for the above derivation, the technique can be applied to problems with infinite number of zones by taking equations (4.3.2) for the first zone, (4.3.4) for the last zone concerned, and repeating equation (4.3.3) for the intermediate zones.

Example 4.3.1

The following example demonstrates the credibility of the technique of combination of zones. It is a problem on seepage under a dam with a vertical cut-off wall. This problem was originally set up and solved by the finite element method, conducted by Coates (1977), a result of which is shown in Fig. 4.3.2. Although it is not an exact solution, it is still useful to compare the solution obtained by the boundary element technique against the well developed finite element result.

The boundary conditions for the problem are shown in Fig. 4.3.3:

$\phi = 100$ on upstream side of the dam

$\phi = 0$ on downstream side of the dam

$\phi' = 0$ on all other boundaries

The dimension of the domain was also taken from Coates (1977): the horizontal length of flow domain being 12 units; the vertical depth being 8 units; the depth of cut-off wall being 2 units. The thickness of the cut-off wall may vary from 1/10 to 1/1000 of a unit, but in this example, 1/1000 of a unit was chosen.

The problem was first solved by program 'BEMLVB1', which is a boundary element program for one zone domain with linear variation along elements. The domain was discretised into 34 elements by 34 nodes (see Fig. 4.3.4). The split node system is adopted at locations where the boundary conditions change from one type to another. The separation is 1/1000 of a unit in horizontal and vertical directions.

23 internal points were also allocated over the domain to determine the overall variation of ϕ values. The result of ϕ at each node is shown in Fig. 4.3.5, from which the ϕ values at nodes opposite to each other on the cut-off wall are identical. The results at internal points under the dam are poor as well, when compared with the finite element results in Fig. 4.3.2. This is because the cut-off wall resembles a re-entrant conner where its tip represents a singular point. One might say the nodes are too close to each other and hence the matrix equations become singular or at least weak.

The problem was solved again by another program 'BEMA3Z', which in addition to the functions in 'BEMLVB1', also can cope with multi-zoned domain problems and orthotropic problems. The orthotropic problems will be discussed in the next section. Therefore, the domain in this example was divided into two zones with a common boundary vertically underneath the cut-off wall. Zone 1 was discretised by 22 nodes and zone 2 by 23 nodes. 5 nodes were on the common boundary (See Fig. 4.3.6). The distance between nodes on the common boundary was not equal. In fact, element lengths were decreasing towards the tip of the cut-off wall. Theoretically, the singular point at the tip had been removed by the common boundary or at least its strength of singularity had been reduced. This idea is similar to that discussed by Liggett (1977b), who suggested higher number of points on singular element modelled better the behaviour of ϕ at singular point.

The result of ϕ at each node for the two zones is shown in Fig. 4.3.7, from which ϕ values on the cut-off wall are well behaved. Values of ϕ at internal points under the dam are comparable to those obtained by the finite element method in Fig. 4.3.2.

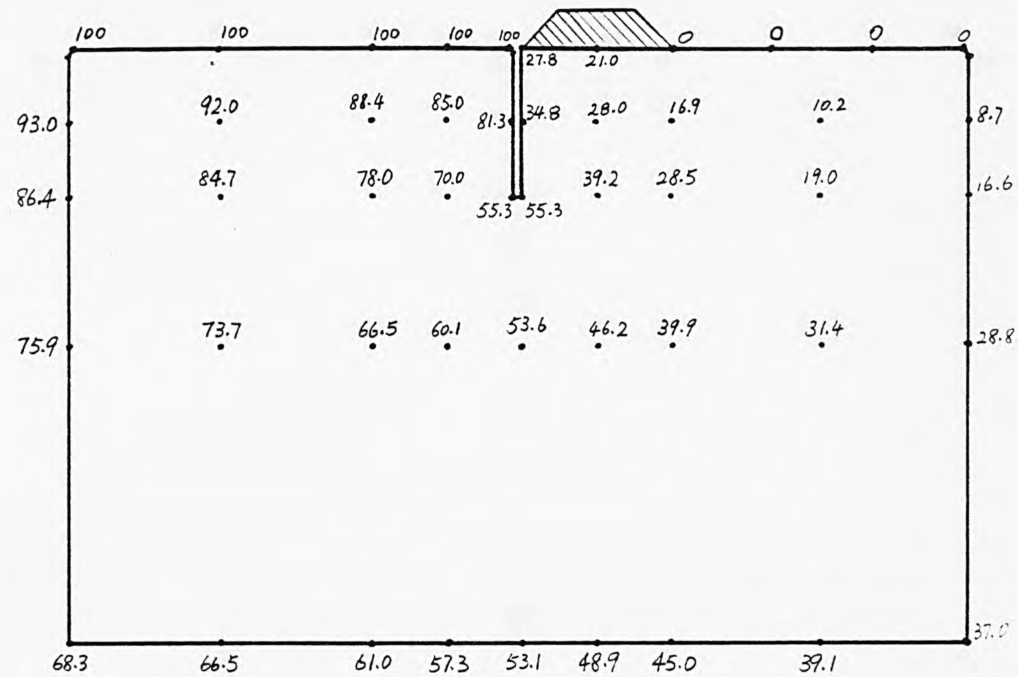

Fig. 4.3.2 A sketch of ϕ values obtained by finite element method (after Coates, 1977)

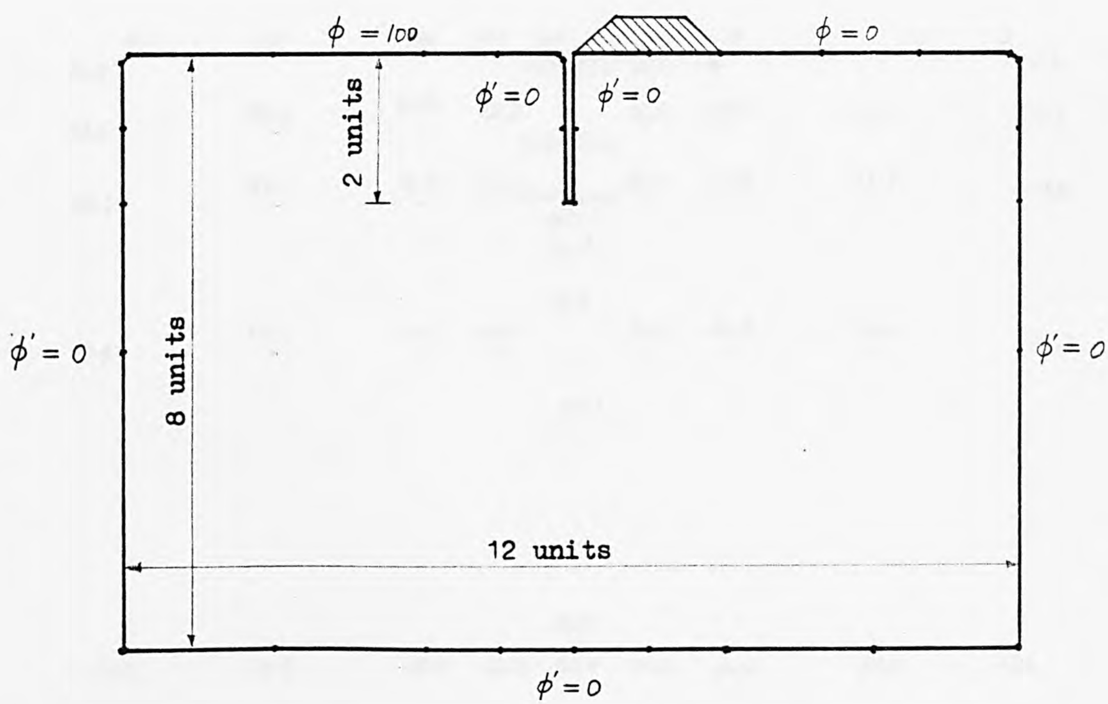

Fig. 4.3.3 Boundary conditions for example 4.3.1

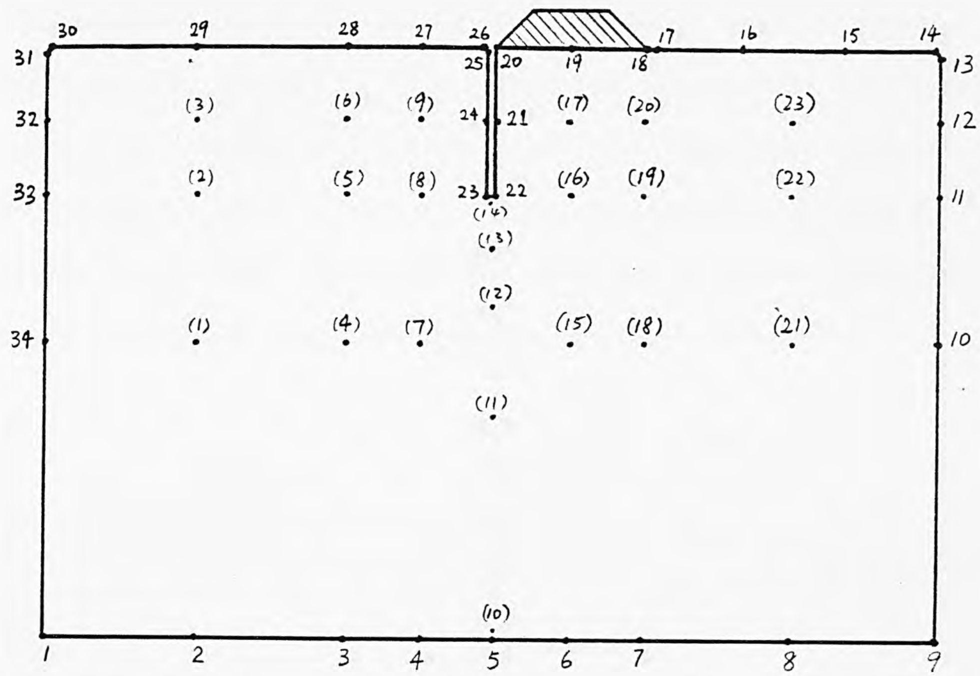

Fig. 4.3.4 A sketch of node numbers and internal point numbers

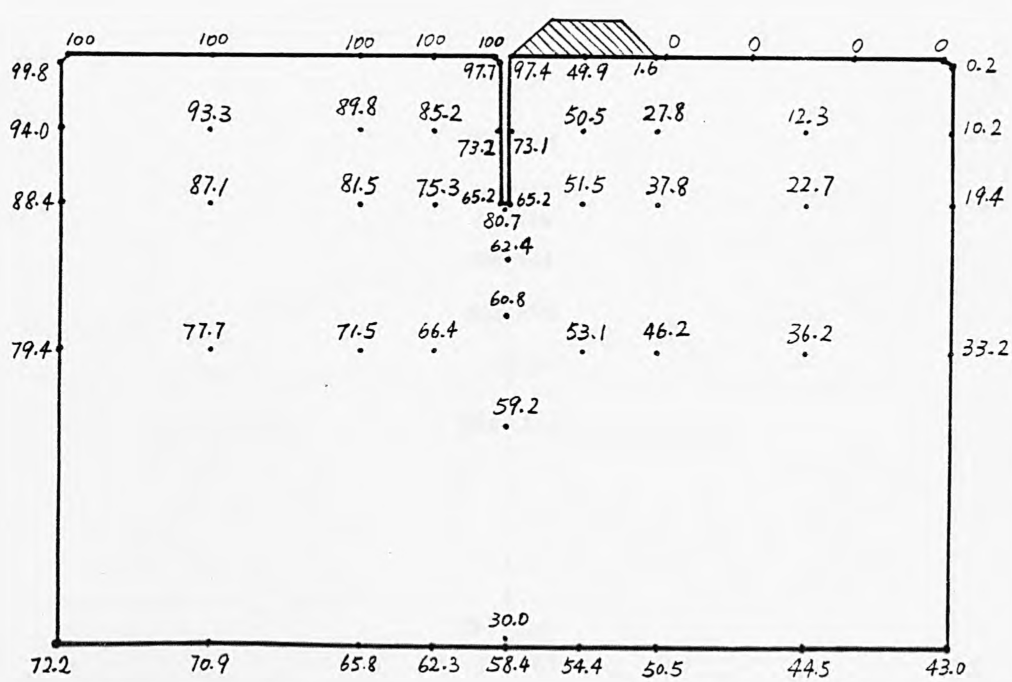

Fig. 4.3.5 A sketch of ϕ values by boundary element method treating domain as one zone

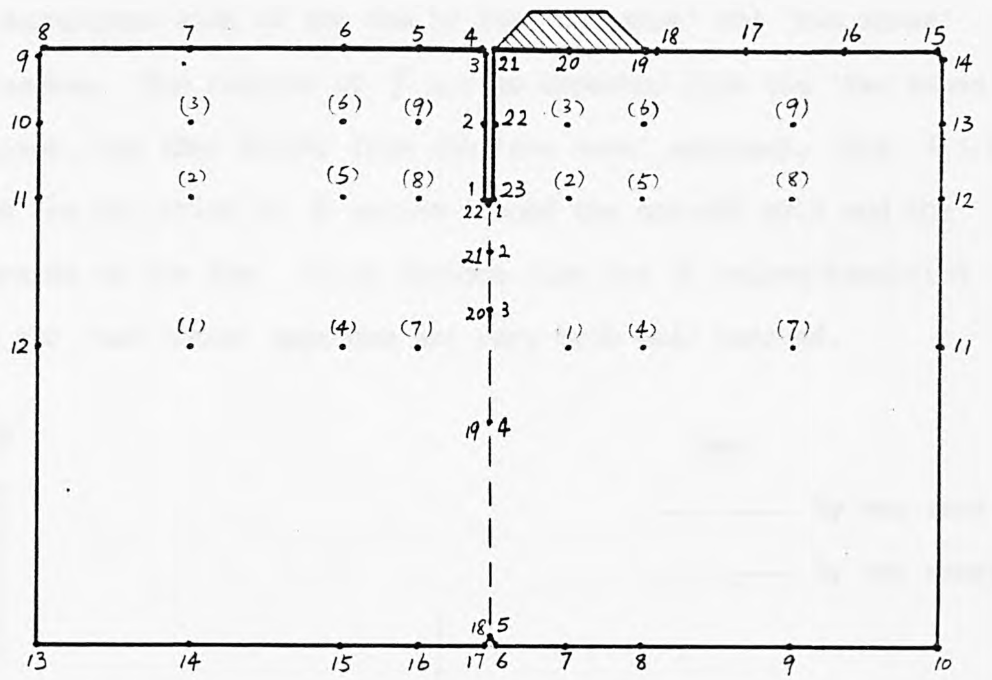

Fig. 4.3.6 A sketch of division of zones and node numbering system

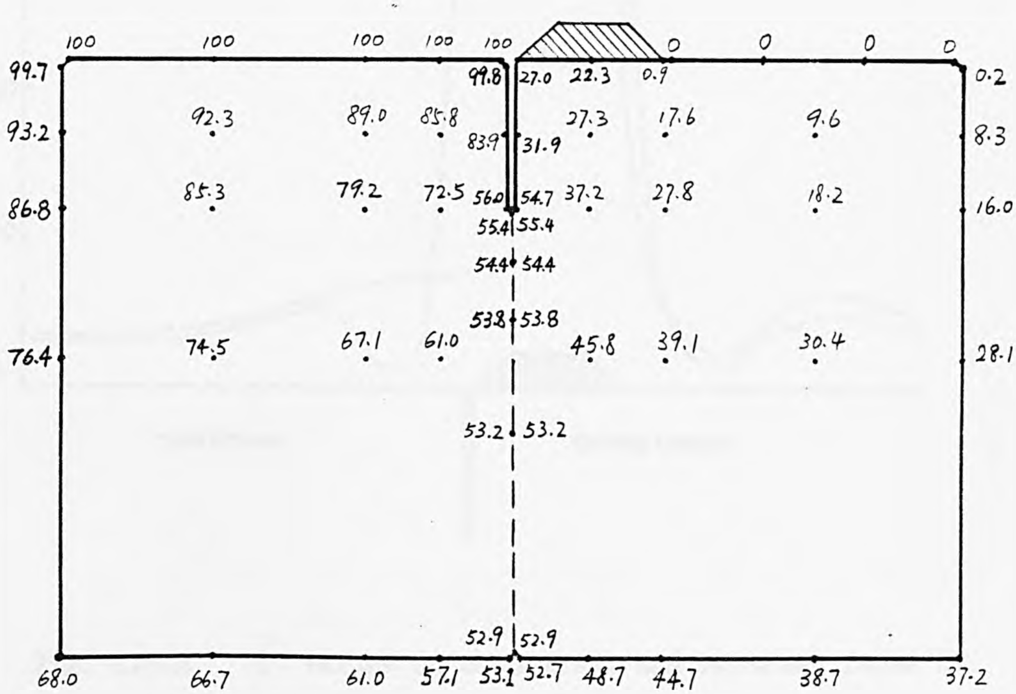

Fig. 4.3.7 A sketch of ϕ values by boundary element method with domain divided into two zones

Fig. 4.3.8 shows the variation of ϕ' on the upstream and the downstream side of the dam by the 'one zone' and 'two zones' approaches. The results of ϕ' are as expected from the 'two zones' approach, but they differ from the 'one zone' approach. Fig. 4.3.9 shows the variation of ϕ values around the cut-off wall and the underside of the dam. It is obvious that the ϕ values resulting from the 'two zones' approach are very much well behaved.

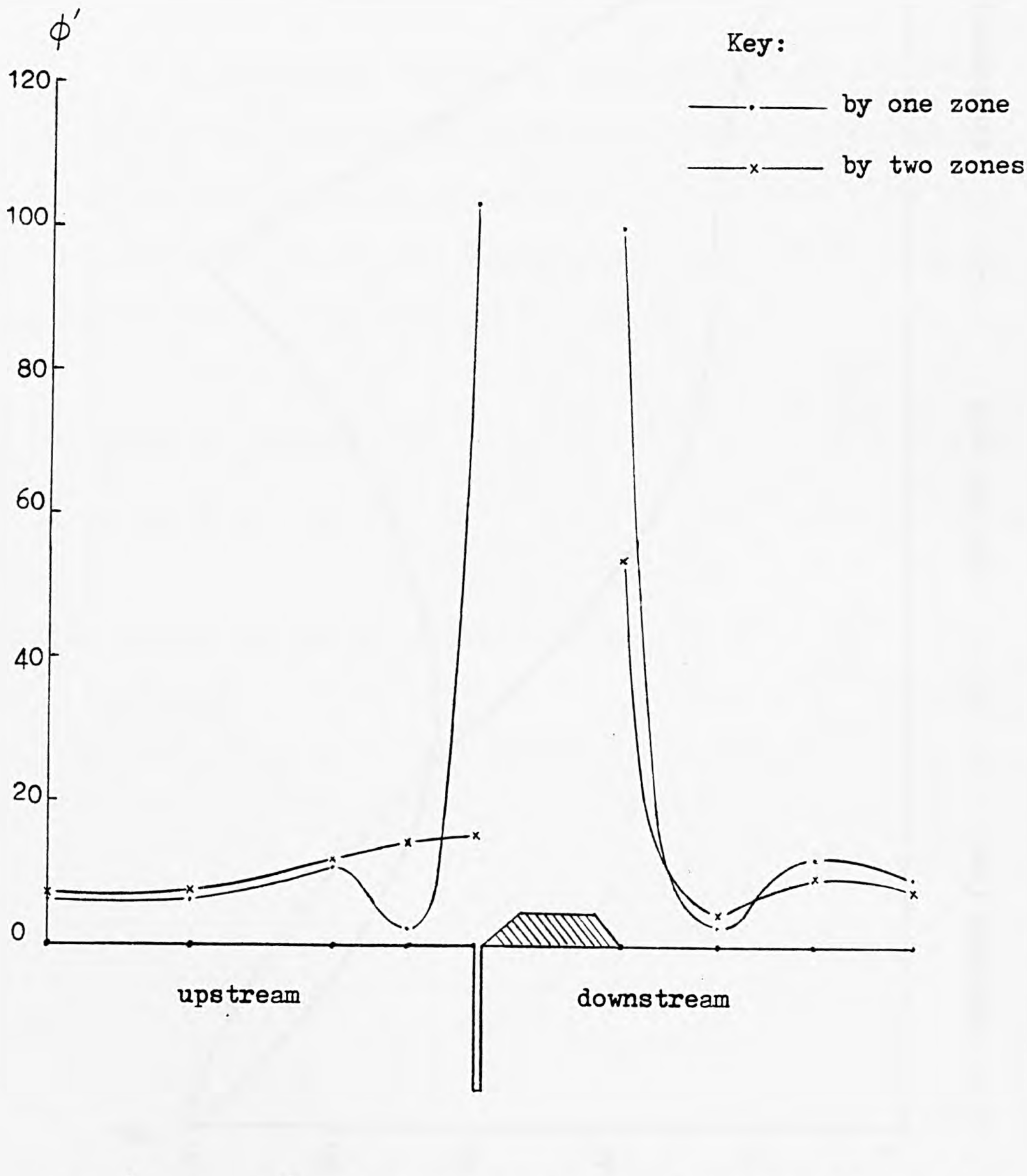

Fig. 4.3.8 ϕ' values on downstream and upstream faces of dam by zoning and without zoning

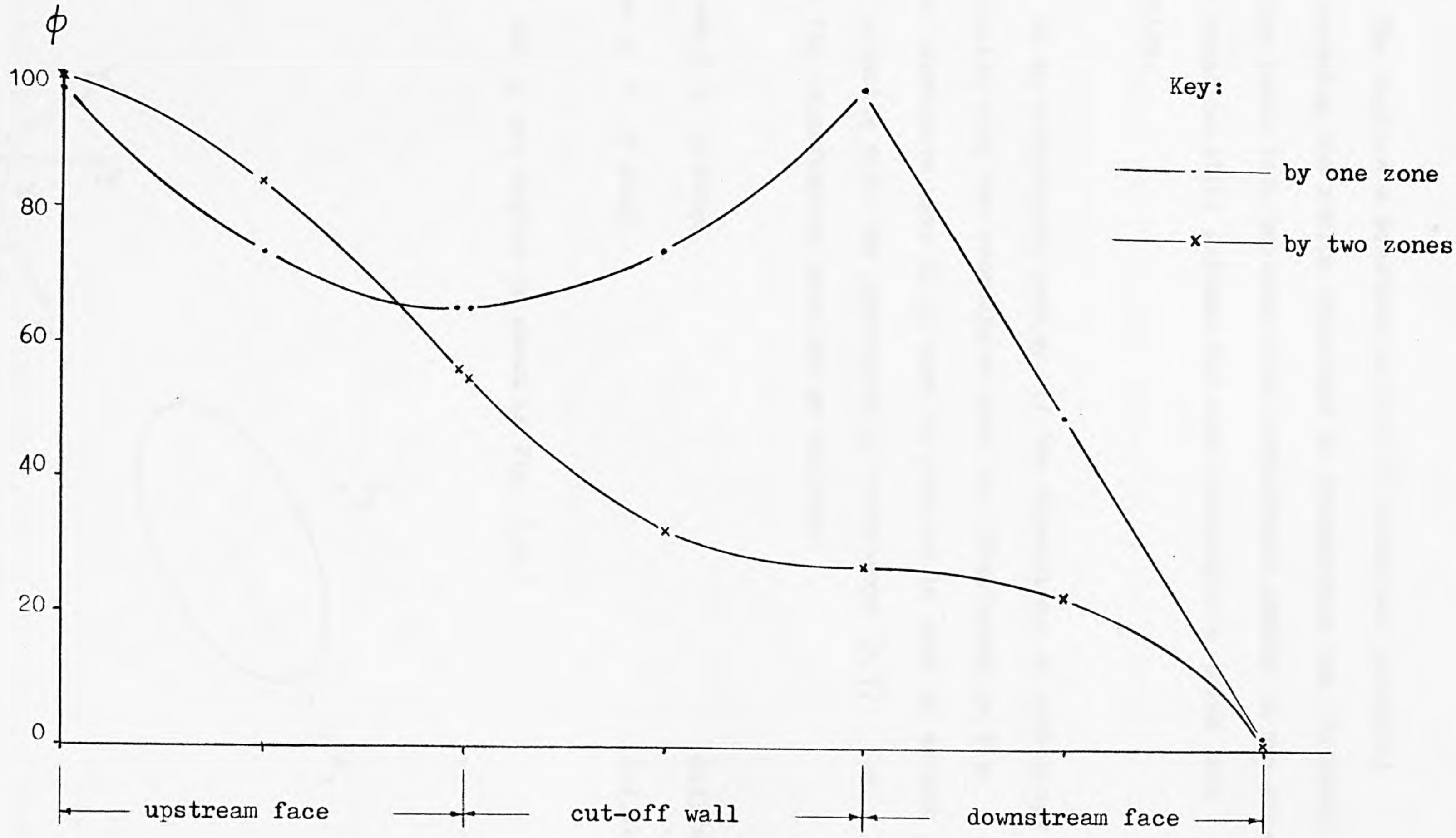

Fig. 4.3.9 A plot of ϕ values around cut-off wall and underside of dam

4.4 Orthotropic Problems

The Laplace's equation in (3.2.3) describes potential problems assuming the medium concerned is homogeneous and isotropic. This section looks into problems with orthotropic medium in two dimensions. Laplace's equation still governs but with permeability taken into consideration.

In an orthotropic medium, if the directions of orthotropy do not coincide with the coordinate axes, as illustrated in Fig. 4.4.1, the coordinate axes (x,y) must be rotated to such an extent that they coincide with the directions of orthotropy (X,Y). The equations for transferring axes are as follows:

$$X = x \cos\alpha + y \sin\alpha \tag{4.4.1a}$$

$$Y = x \cos\beta + y \sin\beta \tag{4.4.1b}$$

where α and β are angles as shown in Fig. 4.4.1

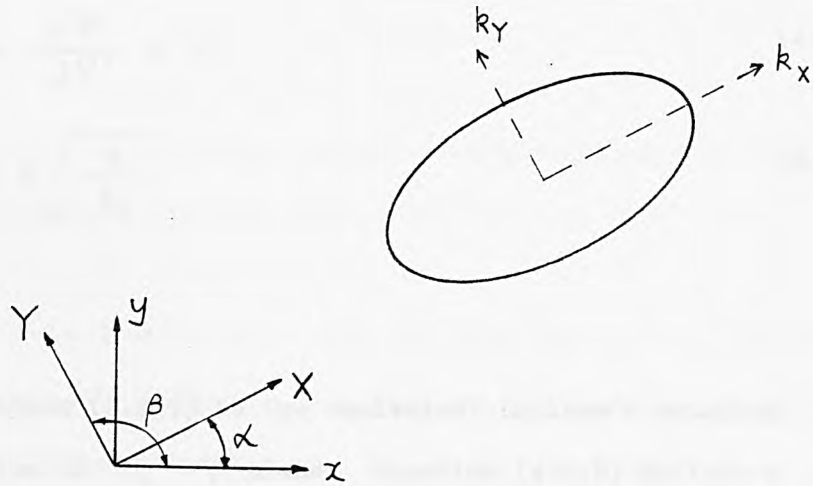

Fig. 4.4.1 Directions of orthotrophy X , Y

The generalised form of Darcy's law, for orthotropic problems, is:

$$u = -k_X \frac{\partial \phi}{\partial X} \tag{4.4.2a}$$

$$v = -k_Y \frac{\partial \phi}{\partial Y} \tag{4.4.2b}$$

where ϕ represents the total head decreasing in the directions of discharge velocities, u and v, in X and Y directions respectively. k_X and k_Y are the permeabilities in the directions of orthotropy, (see Fig. 4.4.1).

From Appendix A.6, the continuity equation in two-dimensions is shown to be:

$$\frac{\partial u}{\partial X} + \frac{\partial v}{\partial Y} = 0 \tag{4.4.3}$$

Substituting equations (4.4.2) into (4.4.3) yields:

$$k_X \frac{\partial^2 \phi}{\partial X^2} + k_Y \frac{\partial^2 \phi}{\partial Y^2} = 0 \tag{4.4.4}$$

or $$\frac{\partial^2 \phi}{\partial X_t^2} + \frac{\partial^2 \phi}{\partial Y^2} = 0 \tag{4.4.5}$$

where $$X_t = X \cdot \sqrt{\frac{k_Y}{k_X}} \tag{4.4.6}$$

Equation (4.4.5) is the equivalent Laplace's equation for isotropic medium in X_t - Y plane. Equation (4.4.6) defines a scale factor which can be applied in the X-direction to transform a given orthotropic flow domain into a fictitious isotropic flow domain (Lambe and Whitman, 1969), where solutions may be obtained through similar procedure described in section 4.2 . The equivalent coefficient of permeability applying to the transformed section, referred to as the equivalent isotropic coefficient is:

$$k_e = \sqrt{k_X \cdot k_Y} \tag{4.4.7}$$

where k_e is called the effective permeability of the transformed section. Hence the fundamental solution g^* to equation (4.4.5) is of the form, in two dimensions:

$$g^*(p,q) = \frac{1}{k_e} \ln|\underset{\sim}{p} - \underset{\sim}{q}| \tag{4.4.8}$$

where p and q are points on the $X_* - Y$ plane.

The integral equation (4.2.1) remains the same form except the term $C(p)$ becomes $C(p)/k_e$, i.e.

$$\int_\Gamma \phi(q) \frac{\partial g^*(p,q)}{\partial n} d\Gamma(q) - \int_\Gamma \phi'(q)\, g^*(p,q)\, d\Gamma(q) = -\frac{C(p)}{k_e}\phi(p) \tag{4.4.9}$$

But the change would not affect equation (4.2.9) since H_{ii} terms are evaluated through equation (4.2.11).

Once the results have been computed for the transformed section, results for the natural section can be obtained by applying the inverse of the scaling factor. The transformation in X - direction may equally be made in the Y-direction.

The above approach may be applied to anisotropic problems, details of which can be found in Wrobel (1981);Chang et al (1973). Numerical results for orthotropic problems are presented in Brebbia and Chang(1979) and for anisotropic problems in Chang et al (1973).

Example 4.4.1

The example shown in Brebbia and Chang (1979), the flow under a dam with two different orthotropic strata, was taken while the program 'BEMA3Z' was under developing stage. Fig. 4.4.2 gives the results of ϕ and equipotential lines in the flow domain, from program 'BEMA3Z'. Linear variation is assumed along elements. The results are very similar to that obtained in Brebbia and Chang (1979) with constant variation along elements. In Fig. 4.4.2 one of the ϕ values on the common boundary between equipotential lines 17 and 15 is spurious. The cause of its occurence have been searched for, but still remains unknown.

4.5 Free Surface Flow Problems

The previous section dealt with orthotropic problems where fluid flows through saturated, confined, porous media governed by Darcy's law. Integral equations are then written for the transformed domain and solved for the unknowns, which are finally converted back to the natural domain.

This section discusses the same problems but with unconfined fluid flow in which Darcy's law and Laplace's equation still apply. The additional boundary condition is on the free surface where the following conditions apply:

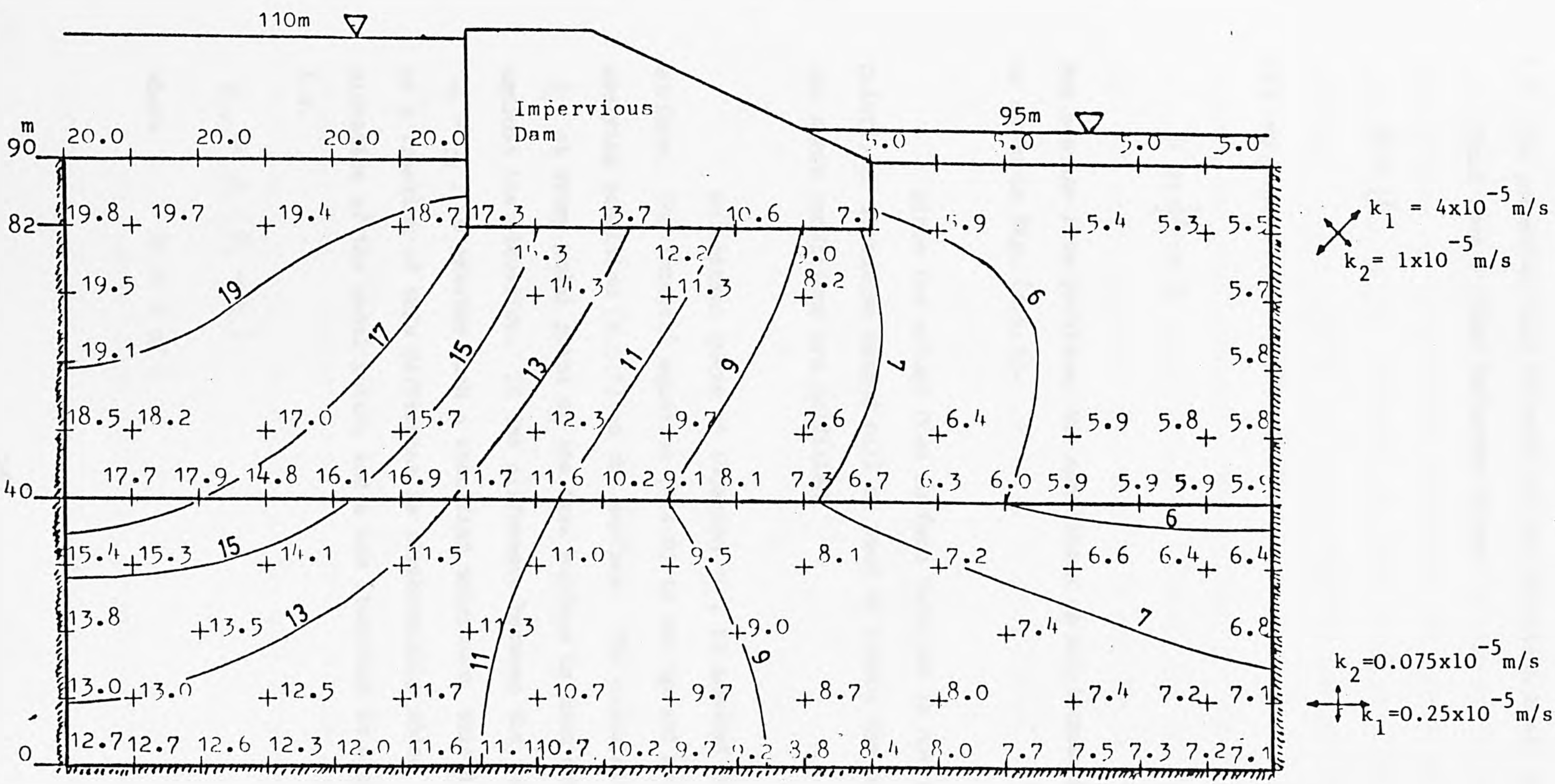

Fig. 4.4.2 Seepage flow in two **orthotropic** soils

(1) the potential head is equal to the elevation head, y, of the fluid from a fixed reference datum:

$$\phi = y \tag{4.5.1}$$

(2) no flux across the free surface;

$$\phi' = \frac{\partial \phi}{\partial n} = 0 \tag{4.5.2}$$

For seepage flow problems, the conditions on all boundaries are as shown in Fig. (4.5.1).

Since the actual free surface location is not known a priori, an iterative method will be used to locate the surface until the above conditions are fulfilled.

An initial guess of location y_i, is assumed for the free surface. The integral equation (4.4.9) is set up and solved for ϕ applying condition (4.5.2) on the surface. The calculated potential, ϕ_c, at every nodal point on the free surface is then compared against its elevation. If the difference between the two values, $\phi_c - y_i$, is greater than a specified tolerance, this difference or a fraction of this difference is algebracially added to the elevation of the nodal point, and a new iteration is carried out, i.e.

$$y_{i+1} = k\,(\phi_c - y_i) \tag{4.5.3}$$

where $0 < k \leqslant 1$

Apart from the free surface, the location of other boundaries and their conditions are fixed throughout the iterations. One may make use of these fixed properties and divide the domain into two zones: zone 1 contains the fixed boundaries and a common boundary; zone 2 contains the moving free surface and the common boundary (see Fig. 4.5.1). The initial guess of free surface has to be above the common boundary. The matrices $[H]$ and $[G]$ for zone 1 are identical for every iteration, so they will only be set up once and stored for other iterations. In addition to the computing time saved in zone 1, the overall matrix $[A]$ in equations (4.2.12) or (4.3.12) will have the advantage of being banded, (see section 4.3).

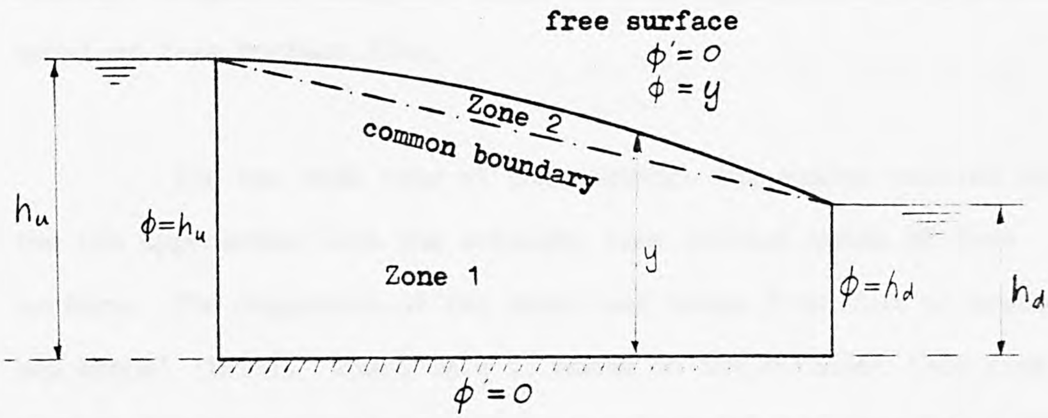

Fig. 4.5.1 Division of domain and boundary conditions in free surface flow problems

Example 4.5.1

Examples of free surface flow problems can be found in Liggett (1977a); Brebbia and Wrobel (1979). The idealisation of the free surface flow problems is the main difference in the two approaches.

Liggett (1977a) proposed a seepage surface existed in setting up the numerical model. Therefore the entire boundary was divided into five parts: impervious bottom surface; downstream face; seepage surface; free surface and upstream face. Brebbia and Wrobel (1979) assumed the boundary to be divided into four parts: impervious bottom surface; downstream face; free surface and upstream face. The boundary condition on the seepage surface is $\phi = y$.

The initial guess of free surface was a curve in Liggett's approach and a straight line in Brebbia and Wrobel's approach. Although the two types of initial guess of free surface would converge to the exact location after some number of iterations, the convergence would enhance with a sensible guess of free surface. Clearly, Liggett's numerical model is more appropriate to a physical model of free surface flow.

For the same rate of convergence, the author carried out the two approaches with the straight line initial guess of free surface. The dimension of the model was taken from that in Brebbia and Wrobel (1979). There were 17 nodes on the straight line free surface for the two models, but Liggett's model had an extra 4 nodes on the seepage surface, (see Figs. 4.5.2). The problems were run in program 'BEMFS1' with the constant $k = 1.0$ and 0.5. The program 'BEMFS1' was obtained by modifying program 'BEMLVB1'. Therefore, one zone domain was assumed with linear variation along elements.

For $k = 1.0$, when convergence had been achieved, Brebbia and Wrobel's model developed a kink at the so-called free surface and the seepage surface intersection (see Fig.4.5.3). This kink was eliminated with $k = 0.5$, (see Fig. 4.5.4). Liggett's model developed a smooth surface at the intersection for both $k = 1.0$ and $k = 0.5$ (see Figs. 4.5.3 and 4.5.4). The constant k affects

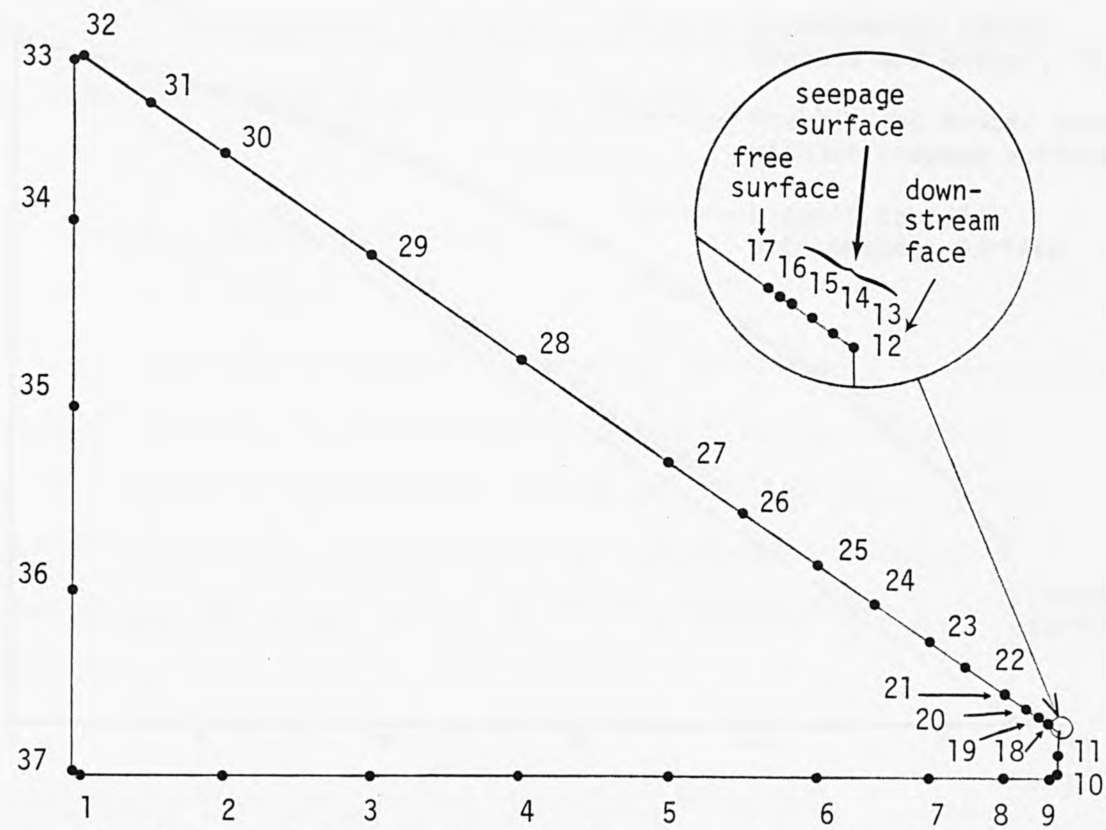

Fig. 4.5.2a A sketch of node numbers on free surface flow problem using Liggett's approach

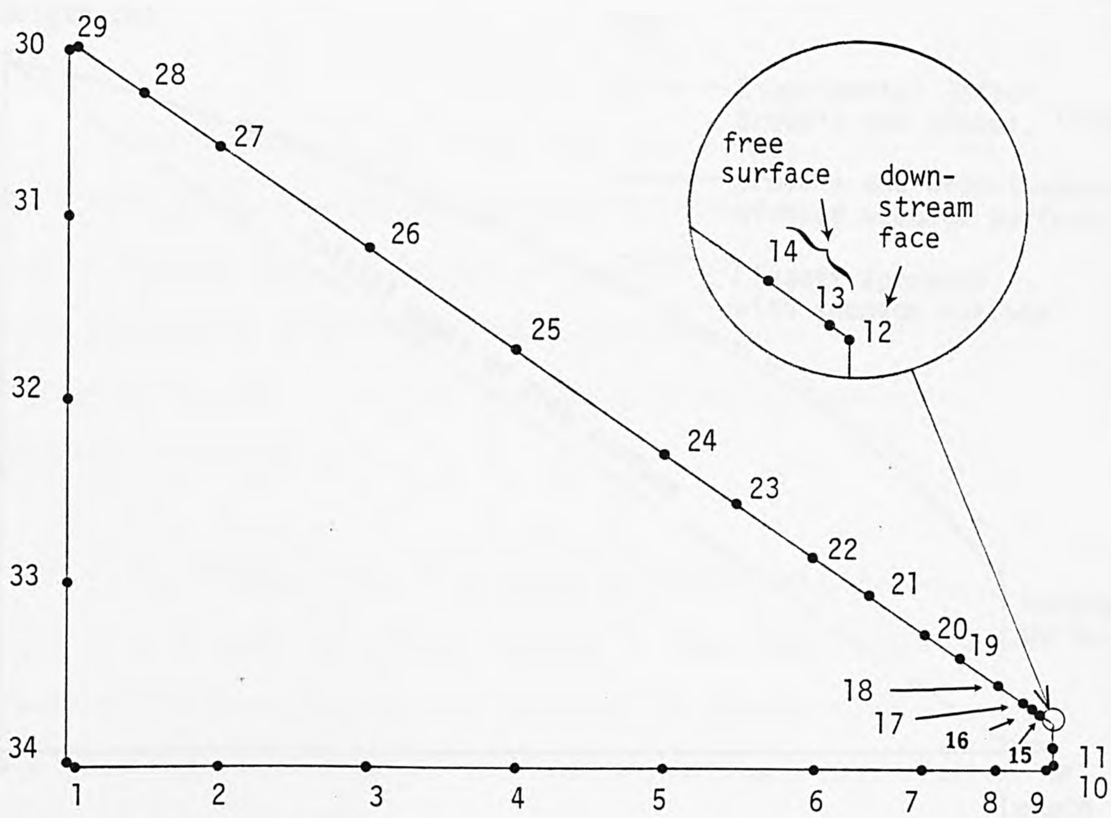

Fig. 4.5.2b A sketch of node numbers on free surface flow problem using Brebbia and Wrobel's approach

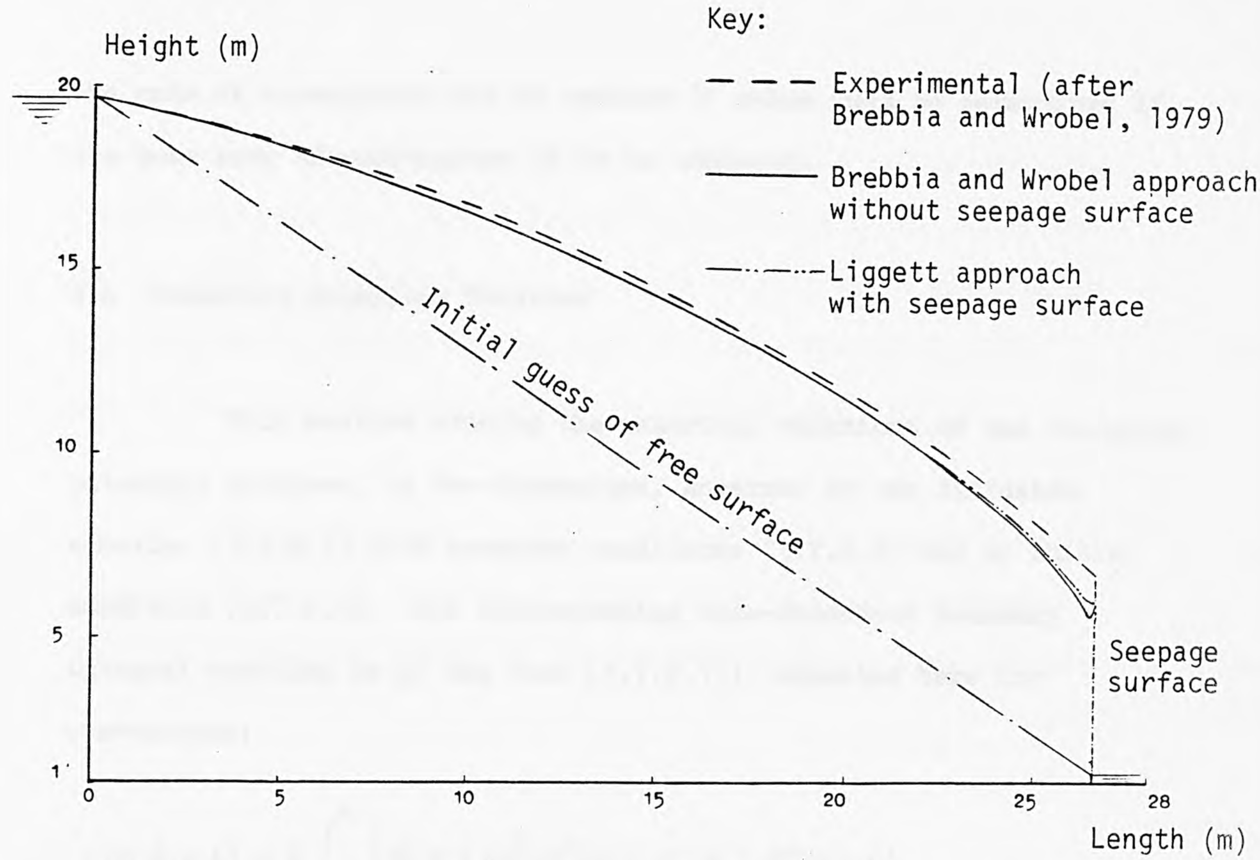

Fig. 4.5.3 Free surface profiles after 20 iterations, with $k = 1.0$

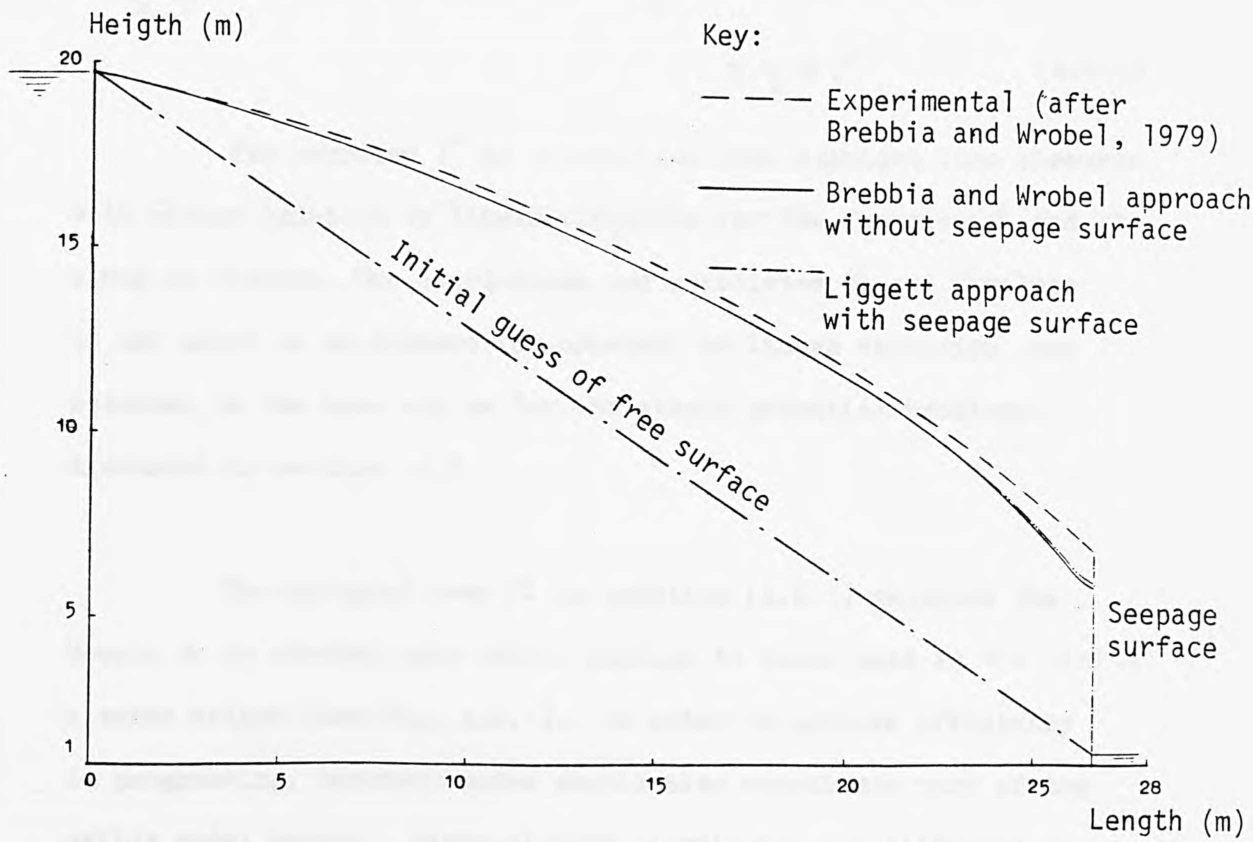

Fig. 4.5.4 Free surface profiles after 20 iterations, with $k = 0.5$

the rate of convergence and an optimum k value must be determined if the best rate of convergence is to be achieved.

4.6 Transient Potential Problems

This section studies the numerical solutions of the transient potential problems, in two-dimensions, governed by the diffusion equation (3.7.2.1) with boundary conditions (3.7.2.2) and an initial condition (3.7.2.3). The corresponding time-dependent boundary integral equation is of the form (3.7.2.11), repeated here for convenience:

$$C(p)\,\phi(p,t_2) + K\int_{t_1}^{t_2}\int_{\Gamma}\phi(q,t)\frac{\partial}{\partial n}g^*(p,q,t,t_2)\,d\Gamma(q)\,dt$$

$$= K\int_{t_1}^{t_2}\int_{\Gamma}\phi'(q,t)\,g^*(p,q,t,t_2)\,d\Gamma(q)\,dt + \int_{\Omega}\phi(q,t_1)\,g^*(p,q,t_1,t_2)\,d\Omega(q)$$

$$; \; p,q \in \Gamma \qquad (4.6.1)$$

The boundary Γ is discretised into straight line elements with either constant or linear variation for the functions ϕ and ϕ' along an element. The coordinates and associated ϕ and ϕ' values at any point on an element for constant or linear variation are obtained in the same way as for the steady potential problems discussed in section 4.2 .

The integral over Ω in equation (4.6.1) requires the domain to be divided into cells, similar to those used in the finite element method (see Fig. 4.6.1). In order to achieve efficiency in programming, boundary nodes should also constitute part of the cell's nodal points. Since element coordinates are different from nodal coordinates for constant variation on the boundary (see section 4.2.1), extra effort to compute ϕ values for cell nodal points on the boundary are undesirable and subject to instability. Linear variation was used in programming analysis and therefore the numerical interpretation of equation (4.6.1) to be given below will only be considered for the case of linear variation . The case of quadratic variation may be found in Wrobel (1981).

If the boundary Γ is discretised into N elements with N nodes, the domain Ω is divided into L_c triangular or rectangular cells, and assuming ϕ and ϕ' are constant over the time integral

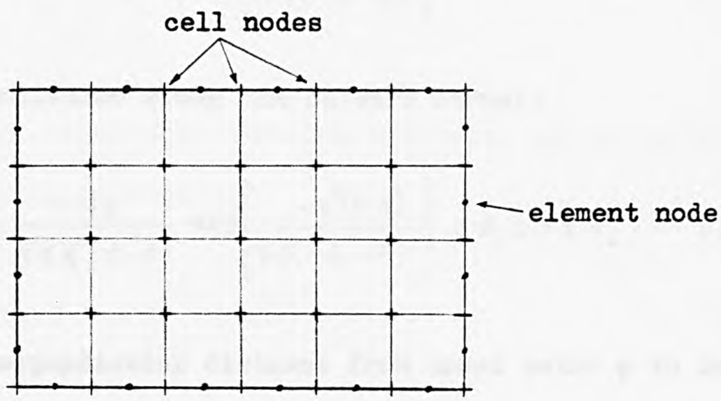

Fig. 4.6.1 Discretisations of domain and boundary with constant variation on the boundary

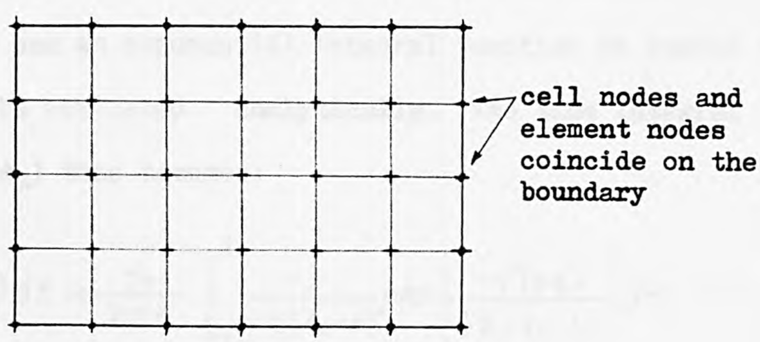

Fig. 4.6.2 Discretisations of domain and boundary with linear variation on the boundary

from t_1 to t_2, the integral equation (4.6.1) becomes:

$$C(p)\phi(p,t_2) + K\sum_{j=1}^{N}\left\{\int_{\Gamma_j}\phi(q)\int_{t_1}^{t_2}\frac{\partial}{\partial n}g^*(p,q,t,t_2)\,dt\,d\Gamma(q)\right\}$$

$$= K\sum_{j=1}^{N}\left\{\int_{\Gamma_j}\phi'(q)\int_{t_1}^{t_2}g^*(p,q,t,t_2)\,dt\,d\Gamma(q)\right\}$$

$$+ \sum_{l=1}^{L_c}\int_{\Omega_l}\phi(q,t_1)\,g^*(p,q,t_1,t_2)\,d\Omega \qquad (4.6.2)$$

The fundamental solution $g^*(p,q,t,t_2)$ is given by (3.7.2.5), in two-dimensions:

$$g^*(p,q,t,t_2) = \frac{1}{4\pi K(t_2-t)}\exp\left[\frac{-r^2(p,q)}{4K(t_2-t)}\right] \quad ; t_1 \leqslant t \leqslant t_2 \qquad (4.6.3)$$

and after differentiation along the outward normal:

$$\frac{\partial}{\partial n}g^*(p,q,t,t_2) = \frac{-y_p}{8\pi K^2(t_2-t)^2}\exp\left[\frac{-r^2(p,q)}{4K(t_2-t)}\right] \quad ; t_1 \leqslant t \leqslant t_2 \qquad (4.6.4)$$

where y_p is the perpendicular distance from nodal point p to the tangent of element q.

The complexity of the fundamental solution necessitates series expansions and an exponential integral function to enable the time integral to be evaluated analytically. The time integral in $\frac{\partial}{\partial n}g^*(p,q,t,t_2)$ thus becomes:

$$\int_{t_1}^{t_2}\frac{\partial}{\partial n}g^*(p,q,t,t_2)\,dt = \frac{y_p}{2\pi K}\int_{t_1}^{t_2}\frac{-1}{4K(t_2-t)^2}\exp\left[\frac{-r^2(p,q)}{4K(t_2-t)}\right]dt$$

$$= \frac{-y_p}{2\pi K r^2(p,q)}\exp\left[\frac{-r^2(p,q)}{4K(t_2-t_1)}\right] \qquad (4.6.5)$$

For the time integral in $g^{*}(p,q,t,t_2)$, an appropriate change of variable is needed with

$$\chi_t = \frac{r^2(p,q)}{4K(t_2-t)} \tag{4.6.6}$$

and the time integral becomes:

$$\begin{aligned}\int_{t_1}^{t_2} g^{*}(p,q,t,t_2)\,dt &= \frac{1}{\pi r^2(p,q)}\cdot\int_{t_1}^{t_2}\frac{r^2(p,q)}{4K(t_2-t)}\exp\left[\frac{-r^2}{4K(t_2-t)}\right]dt \\ &= \frac{1}{4\pi K}\left\{\int_{t_1}^{\infty}\frac{e^{-\chi_t}}{\chi_t}d\chi_t - \int_{t_2}^{\infty}\frac{e^{-\chi_t}}{\chi_t}d\chi_t\right\} \\ &= \frac{1}{4\pi K}\left[\mathrm{Ei}\,(\chi_{t_1}) - \mathrm{Ei}\,(\chi_{t_2})\right]\end{aligned} \tag{4.6.7}$$

where $\mathrm{Ei}(a)$ is the exponential-integral function, which can be evaluated by the following series:

$$\mathrm{Ei}\,(a) = -C_E - \ln(a) - \sum_{n=1}^{\infty}(-1)^{n-1}\frac{a^n}{n\cdot n!} \tag{4.6.8}$$

C_E is the Euler's constant and :

$$C_E = 0.57721566 \tag{4.6.9}$$

It is noted that when $t = t_2$;

$$\mathrm{Ei}\,(\chi_{t_2}) = 0 \tag{4.6.10}$$

The series in equation (4.6.8), although convergent for all values of a, is not suitable for computation when a is large ($|a| > 8$) as it will require a great number of terms in the calculations. To overcome this difficulty, the following asymptotic expansion series can be used (Brebbia and Wrobel, 1979):

$$\mathrm{Ei}(a) \simeq e^{-a} \sum_{n=1}^{\infty} \frac{(-1)^{n-1}(n-1)!}{a^n} \tag{4.6.11}$$

Since equation (4.6.11) is an asymptotic series, that means the series would converge and then diverge as n towards infinity. Care must be taken in evaluating the series and the following shows the technique applicable to ensure convergence.

Equation (4.6.11) can be re-written in full as:

$$\mathrm{Ei}(a) \simeq e^{-a}\left(\frac{1}{a} - \frac{1}{a^2} + \frac{2!}{a^3} - \frac{3!}{a^4} + \cdots + \frac{(-1)^{n-1}(n-1)!}{a^n} + \cdots\right)$$

$$\simeq e^{-a}\left\{\frac{1}{a} + \left(\frac{1}{a}\right)\left[\frac{-1}{a}\right] + \left(\frac{1}{a}\right)\left(\frac{-1}{a}\right)\left[\frac{-2}{a}\right] + \left(\frac{1}{a}\right)\left(\frac{-1}{a}\right)\left(\frac{-2}{a}\right)\left[\frac{-3}{a}\right] + \cdots\right\} \tag{4.6.12}$$

From the above equation, the 2nd term equals the 1st term $\times\left[\frac{-1}{a}\right]$; the 3rd term equals the 2nd term x $\left[\frac{-2}{a}\right]$ and so on.... If the square bracket terms are called the multiplier $\left[\frac{-n}{a}\right]$ for the $(n+1)^{\text{th}}$ term, when the series is convergent, the multiplier would be less than 1, and vice versa. So, the magnitude of the multiplier may be tested and if it is bigger than 1 in the n^{th} term, the sum of the series would be up to and including the $(n-1)^{\text{th}}$ term which is the smallest in magnitude in the whole series. The error induced in the series should be less than the n^{th} term.

Since linear variation is assumed over the boundary elements, ϕ and ϕ' in (4.6.2) take the form of (4.2.3) with $\gamma = 2$.

Substituting equations (4.2.3), (4.6.5), (4.6.7) and (4.6.10) into (4.6.2) yields, for boundary point i :

$$c_i \phi_i - \frac{1}{2\pi}\sum_{j=1}^{N}\int_{\Gamma_j}\frac{y_p}{\gamma^2}\exp\left[\frac{-\gamma^2}{4K(t_2-t_1)}\right]\left[\sum_{\alpha=1}^{\gamma} N_\alpha \phi_{j\alpha}\right] d\Gamma_j$$

$$= \frac{1}{4\pi}\sum_{j=1}^{N}\int_{\Gamma_j}\mathrm{Ei}\,(\chi_{t_1})\left[\sum_{\alpha=1}^{\gamma} N_\alpha \phi'_{j\alpha}\right] d\Gamma_j + \frac{1}{4\pi K(t_2-t_1)}\sum_{m=1}^{L_c}\int_{\Omega_m}\phi_{t_1}\exp\left[\frac{-\gamma^2}{4K(t_2-t_1)}\right] d\Omega_m$$

(4.6.13)

The remaining integrals in the above equation are carried out numerically over each space. The integration over the domain is performed by dividing it into triangular cells and using Hammer's quadrature scheme (Brebbia,1978). In matrix notation, equation (4.6.13) is written as:

$$\left[C_{ij}\right]\left\{\phi_i\right\} + \left[\overline{H}_{ij}\right]\left\{\phi_i\right\} = \left[G_{ij}\right]\left\{\phi'_i\right\} + \left\{P_i\right\}$$

where

$$\overline{H}_{ij} = \int_{-1}^{1} N_1(\xi)\, Z_j \cdot \frac{l_j}{2} d\xi + \int_{-1}^{1} N_2(\xi)\cdot Z_{j-1}\cdot\frac{l_{j-1}}{2} d\xi$$

$$= \sum_{k=1}^{M} GW_k \cdot \tfrac{1}{2}(1-\xi)_k (Z_j)_k \cdot \frac{l_j}{2} + \sum_{k=1}^{M} GW_k \cdot \tfrac{1}{2}(1+\xi)_k (Z_{j-1})_k \frac{l_{j-1}}{2} \quad (4.6.14a)$$

$$G_{ij} = \int_{-1}^{1} N_1(\xi)\left[\mathrm{Ei}(\chi_{t_1})_j\right]\frac{l_j}{2} d\xi + \int_{-1}^{1} N_2(\xi)\left[\mathrm{Ei}(\chi_{t_1})_{j-1}\right]\frac{l_{j-1}}{2} d\xi$$

$$= \sum_{k=1}^{M} GW_k \cdot \tfrac{1}{2}(1-\xi)_k \left[\mathrm{Ei}\,(\chi_{t_1})_j\right]_k \frac{l_j}{2} + \sum_{k=1}^{M} GW_k \tfrac{1}{2}(1+\xi)_k \left[\mathrm{Ei}\,(\chi_{t_1})_{j-1}\right]_k \frac{l_{j-1}}{2} \quad (4.6.14b)$$

$$P_i = \frac{1}{4\pi K(t_2-t_1)}\sum_{m=1}^{L}\left\{\sum_{k=1}^{M_T} WT_k \cdot \phi_k \exp\left[\frac{-\gamma_{ik}^2}{4K(t_2-t_1)}\right]\right\} A_m \quad (4.6.14c)$$

and

$$Z_j = \frac{y_p}{2\pi\gamma_{ij}^2}\exp\left[\frac{-\gamma_{ij}^2}{4K(t_2-t_1)}\right] \quad (4.6.14d)$$

ξ, M, GW_k, y_p, ℓ_j have the same meaning as for constant variation (4.2.1.8).

A_m is the area of triangular element m.

M_T is the number of Gauss points used in triangular element m.

WT_k is the Gauss weight at Gauss point k.

Y_{ik} is the distance between nodal point i and Gauss point k.

Matrix $[C_{ij}]$ can be included into $[\overline{H}_{ij}]$ to form $[H_{ij}]$, i.e.

$$[H_{ij}]\{\phi_i\} = [G_{ij}]\{\phi_i'\} + \{P_i\} \tag{4.6.15}$$

H_{ii} is obtained by applying unit potential to the domain so that:

$$H_{ii} = -\sum_{j=1}^{N} H_{ij} + P_i \tag{4.6.16}$$

For G_{ii} term, expression (4.6.8) is used for $Ei(a)$ and from Appendix A.5, equation A.5.12, G_{ii} becomes:

$$G_{ii} = \frac{\ell_i}{2}\cdot\left(3 - C_E - \ln\left|R\ell_i^2\right|\right) + \sum_{n=1}^{\infty} \frac{(-1)^{n-1} R^n \ell_i^{2n+1}}{(2n+1)(2n+2)\cdot n\cdot n!}$$
$$+ \frac{\ell_{i-1}}{2}\left(1 - C_E - \ln\left|R\ell_{i-1}^2\right|\right) + \sum_{n=1}^{\infty} \frac{(-1)^{n-1} R^n \ell_{i-1}^{2n+1}}{(2n+2)\cdot n\cdot n!} \tag{4.6.17}$$

where $R = \dfrac{1}{4K(t_2 - t_1)}$

With specified boundary conditions and initial condition, equation (4.6.15) is further reduced to:

$$[A]\{x\}=\{B\} \tag{4.6.18}$$

which can be solved by Gaussian elimination.

Once all the ϕ and ϕ' values on the boundary at $t = t_2$ are known, the ϕ value at triangular cell's nodal points inside the boundary may be computed through (4.6.13) with $C_i = 1$.

The ϕ values obtained at $t = t_2$ can be treated as an initial condition for the next time interval, say t_2 to t_3. When the initial and final times are specified, say from t_0 to t_n, one might carry out the computation by n steps with $\delta t = \frac{t_n - t_0}{n}$ or in one big step from t_0 to t_n, (Brebbia and Wrobel 1979).

Example 4.6.1

A computer program called 'BEMTDLV1' for transient potential problems was written. The program listing is shown in Appendix A.12. Linear variation is assumed along boundary elements, and triangular cells are adopted for discretisation of the domain. An example taken from Brebbia and Wrobel (1979) was used for the development of the program.

Again, it is a case of mixed boundary conditions on a rectangular plate with two insulated opposite sides and the two others subject to a uniform unit temperature (see Fig. 4.6.3).

Internal temperatures at time t = 1.0 sec and 5 sec along AB were obtained and shown in Fig. (4.6.4). The difference between the exact solutions of Carslaw and Jaeger (1959) and those by the boundary element method are similar to those obtained by Brebbia and Wrobel (1979). Although they did not mention any numerical deficiency, it was later pointed out by Fernandes and Pina (1982).

More numerical examples may be found in Fernandes and Pina (1982), who studied the influence of different numerical evaluation of the resulting integrals. A consistent choice of the time step and the spatial discretisation were discussed.

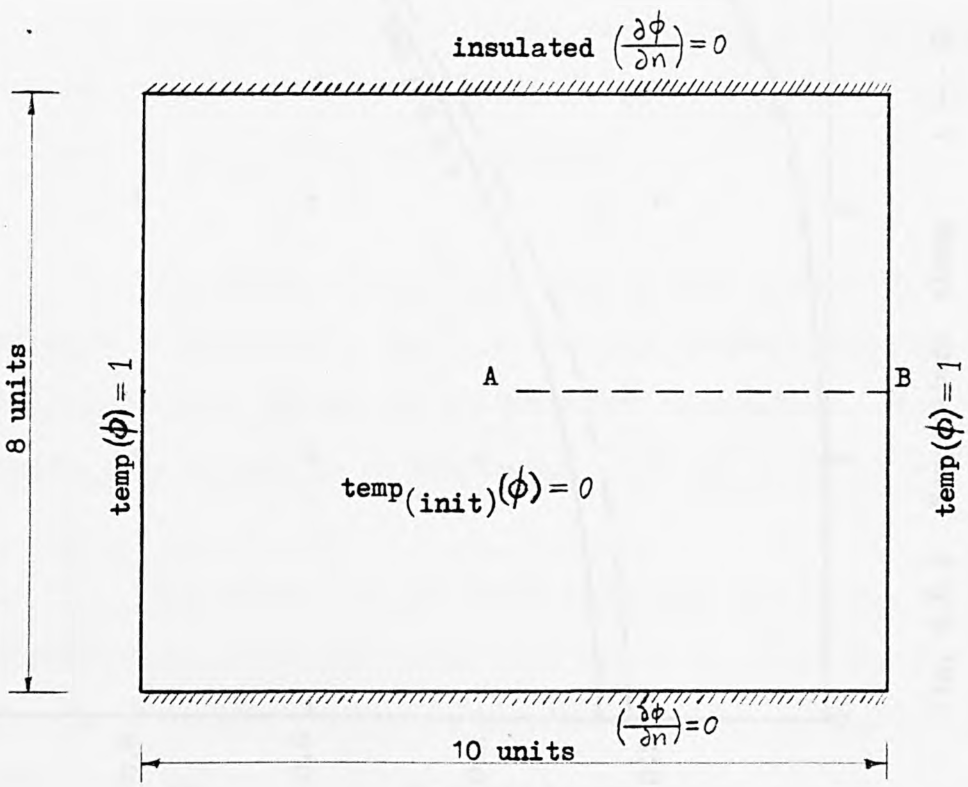

Fig. 4.6.3 Boundary conditions for transient potential problem

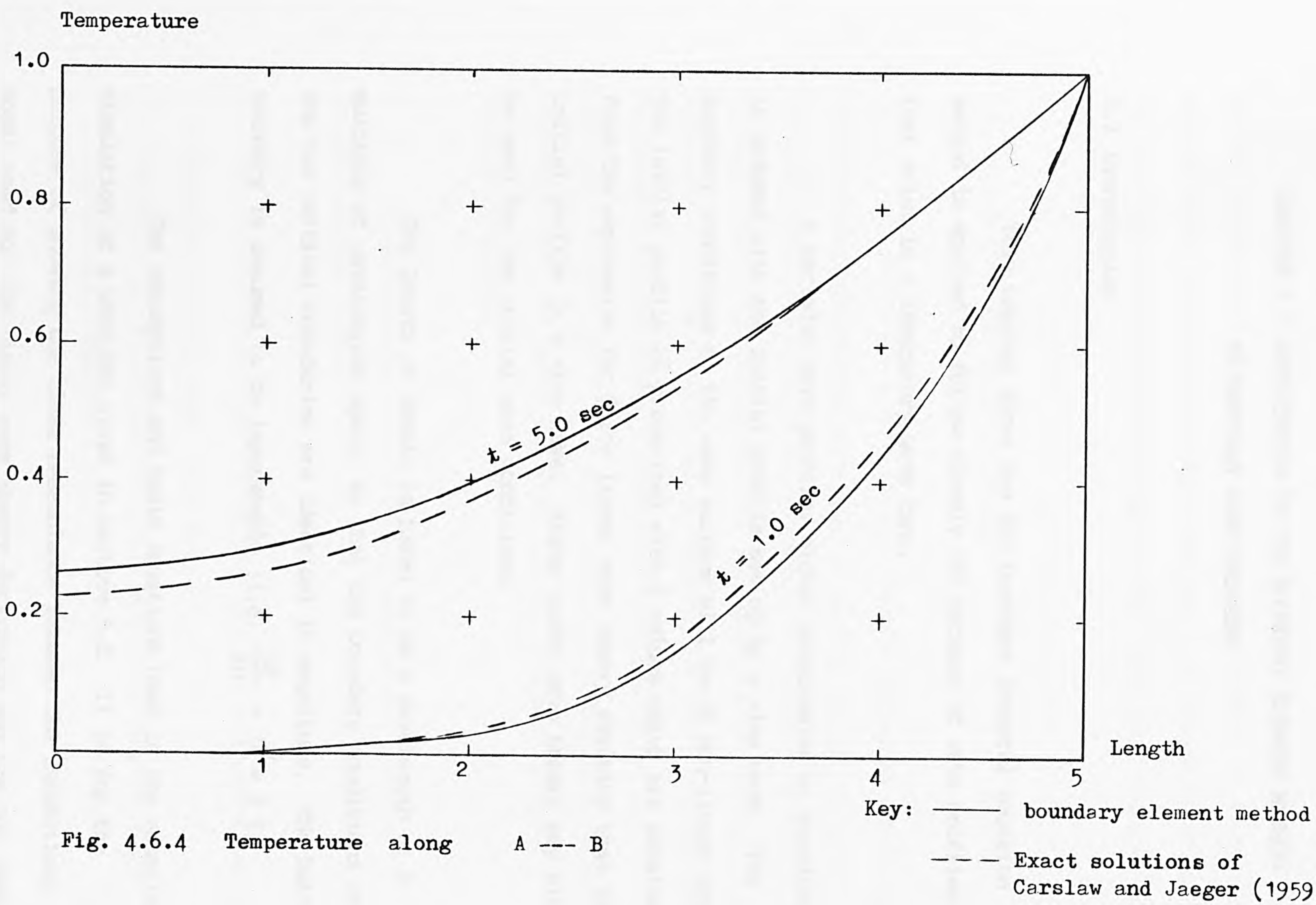

Fig. 4.6.4 Temperature along A --- B

CHAPTER 5 - APPLICATION OF THE BOUNDARY ELEMENT METHOD TO UNSTEADY WAVE PROBLEMS

5.1 Introduction

This chapter shows how the boundary integral equation method is applied to follow closely the pattern of wave profiles that exist in a laboratory wave tank.

A periodic wave profile, either progressive or standing, is assumed with the initial profile set up by a sine wave. The boundary conditions on the wave surface will be of non-linear type. The initial profile is prescribed with ϕ values which are obtained from the expression for ϕ for linear wave theory assuming that the initial profile is a sine wave. Higher order wave theory may also be used for the initial wave conditions.

The length of domain is taken to be a wavelength or a multiple of wavelengths apart, so that the boundary conditions on the two vertical boundaries are identical in magnitude. The bottom boundary is assumed to be impermeable (i.e. $\frac{\partial \phi}{\partial n} = \phi' = 0$).

The assumptions and basic equations used in the numerical simulation of a wave are given in section 5.2. It is for the purpose of showing the close resemblance between the theoretical model used for the linear wave theory derivation and the one used in the numerical simulation. Section 5.3 illustrates how the matrix equation is modified for the wave problems. Section 5.4 describes how the profile is moved to the next time step.

In the case where an object is introduced in the flow domain, pressures and forces are induced. The details of evaluating wave loadings will be discussed in section 5.5. Means of estimating the accuracy of the proposed technique have also been included in section 5.6.

5.2 Assumptions and Basic Equations

To formulate a wave theory, whether linear or non-linear, the governing differential equation of motion is set up with certain assumptions being made concerning the equation of motion. Boundary conditions are applied and the equations are solved. The formulation will be carried out in terms of the velocity potential ϕ. The assumptions and boundary conditions described below are applicable to both the theoretical model for linear wave theory derivation and the numerical model for the boundary integral equation technique.

The following assumptions are made within the flow domain (see Fig. 5.2.1).

(a) Irrotational flow - the forces on a particular element are in equilibrium condition. Thus velocity potential ϕ exists and satisfies Laplace's equation (see Appendix A.6, equation A.6.5):

$$\frac{\partial^2\phi}{\partial x^2} + \frac{\partial^2\phi}{\partial y^2} = 0 \qquad (5.2.1)$$

(b) Incompressible flow - the fluid is considered to be homogeneous, that is, of constant density. Hence when considering an element, the mass of water entering is equal to the mass of water leaving that element.

(c) The particle velocities (u, v) are small in comparison with the wave velocity, C i.e.

$$u << C \quad \text{and} \quad v << C \tag{5.2.2}$$

(d) Pressure difference due to air between wave trough and wave crest is negligible.

(e) The wave profile assumes the equation of simple harmonic motion:

$$\eta = a\cos(kx - \sigma t - \epsilon) \quad \text{for periodic wave} \tag{5.2.3a}$$

$$\eta = a\cos(kx)\sin(\sigma t - \epsilon) \quad \text{for standing wave} \tag{5.2.3b}$$

where

η is the vertical displacement of any point on the wave surface. from mean water level.

a is the wave amplitude.

k is the wave number $\left[= 2\pi/\text{wavelength} \right]$.

σ is the radian wave frequency $\left[= 2\pi/\text{Period}(T) \right]$.

t is the time.

ϵ is the phase angle.

(f) The wave amplitude, a, is small in comparison with the water depth, d.

(g) The channel bed is horizontal, and of uniform depth, d.

(h) **Infinite crest length (i.e. two dimensional wave).**

(i) **Negligible viscosity.**

(j) No underlying currents and surface tension to be negligible.

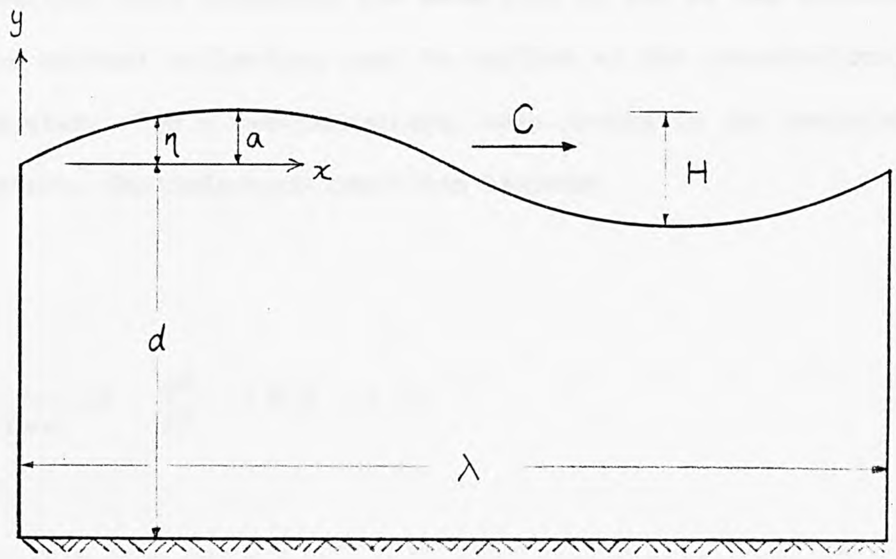

Fig. 5.2.1 Symbols used in flow domain

Before moving on to the boundary conditions of the flow domain in Fig. 5.2.1, it is useful to specify the term 'Radiation Condition' in this study. Waves being generated in water of a specified depth and infinite horizontal extent require a radiation condition to be applied at infinity. Physically, this condition requires that the generated waves must propagate away from the generation region. For three-dimensional water waves the mathematical expression for the general radiation boundary condition is: ϕ is bounded as $r \rightarrow \infty$; where r is equal to the distance from the centre of the generation area. In numerical computations, the infinite domain is truncated by the use of computational boundaries. A condition that transmits the waves into or out of the solution region without reflection must be applied at the computational boundaries. For a two-dimensional wave moving in the positive x-direction, the radiation condition becomes:

$$\lim_{r \to \infty} \sqrt{r} \left(\frac{\partial \phi}{\partial r} - i k \phi \right) = 0 \qquad (5.2.4)$$

The boundary conditions are prescribed as follows:

(i) the horizontal bed is a streamline with no flow across it. Thus the vertical component of the particle velocity is zero at depth $y = -d$, i.e.

$$v = \frac{\partial \phi}{\partial y} = 0 \qquad (5.2.5)$$

(ii) the conditions on the two vertical sides are treated as unspecified.

(iii) the conditions on the free surface profile consist of two parts:

1. linearized kinematic boundary condition:

$$\frac{\partial \eta}{\partial t}(x,t) = \frac{\partial \phi}{\partial y}(x,0,t) = v \tag{5.2.6}$$

2. linearized dynamic boundary condition, obtained from the Bernoulli's equation (A.6.6) assuming constant pressure p and $C(t) = \frac{p}{t}$:

$$\frac{\partial \phi}{\partial t} + g\eta = 0$$

or

$$\eta = \frac{-1}{g} \cdot \frac{\partial \phi}{\partial t} \quad \text{at} \quad y = \eta \tag{5.2.7}$$

Since the vertical component of particle velocity is expressed as:

$$v = \frac{\partial \eta}{\partial t} = \frac{\partial \phi}{\partial y}$$

and from equation (5.2.7):

$$\frac{\partial \eta}{\partial t} = \frac{-1}{g} \frac{\partial^2 \phi}{\partial t^2} = \frac{\partial \phi}{\partial y}$$

the following equation is derived:

$$\frac{\partial \phi}{\partial y} + \frac{1}{g} \cdot \frac{\partial^2 \phi}{\partial t^2} = 0 \quad \text{at} \quad y = \eta$$

To obtain the solution of Laplace's Equation (5.2.1), the following form for ϕ is assumed:

$$\phi = \left[A e^{ky} + B e^{-ky}\right] \sin(kx - \sigma t - \epsilon) \qquad (5.2.8)$$

Differentiating with respect to y gives:

$$\frac{\partial \phi}{\partial y} = k\left[A e^{ky} - B e^{-ky}\right] \sin(kx - \sigma t - \epsilon) \qquad (5.2.9)$$

From the boundary condition (5.2.5):

$$\frac{\partial \phi}{\partial y} = k\left[A e^{-kd} - B e^{kd}\right] \sin(kx - \sigma t - \epsilon) = 0 \qquad (5.2.10)$$

$$\therefore \quad A e^{-kd} = B e^{kd} = \tfrac{1}{2} D \quad \text{(say)}$$

Hence

$$A = \frac{1}{2} D e^{kd} \qquad (5.2.11a)$$

$$B = \frac{1}{2} D e^{-kd} \qquad (5.2.11b)$$

Substituting equations (5.2.11) into (5.2.8) yields:

$$\phi = \frac{1}{2} D \left[e^{k(d+y)} + e^{-k(d+y)}\right] \cdot \sin(kx - \sigma t - \epsilon)$$

or

$$\phi = D \cosh k(d+y) \cdot \sin(kx - \sigma t - \epsilon) \qquad (5.2.12)$$

From equations (5.2.7) and (5.2.3), differentiating ϕ with respect to t gives:

$$\frac{\partial \phi}{\partial t} = -D\sigma \cosh k(d+\eta) \cos(kx - \sigma t - \epsilon) = -ga \cdot \cos(kx - \sigma t - \epsilon)$$

Simplifying gives:

$$D = \frac{ag}{\sigma} \cdot \frac{1}{\cosh k(d+\eta)} \tag{5.2.13}$$

Substituting equations (5.2.13) into (5.2.12) yields the expression for ϕ in linear wave theory :

$$\phi = \frac{ag}{\sigma} \cdot \frac{\cosh k(y+d)}{\cosh kd} \cdot \sin(kx - \sigma t - \epsilon) \tag{5.2.14}$$

Equation (5.2.14) together with equation (5.2.3) are used as initial conditions for the numerical simulation of a wave by the boundary integral equation method. Expressions for higher order wave theory may also be used as initial conditions. The corresponding equations to (5.2.3) and (5.2.14) for second, third and fifth order wave theories are given in Appendix A.7.

The wave velocity, or phase velocity, C, is given by the equation:

$$C = \frac{\sigma}{k} = \frac{gT}{2\pi} \tanh \frac{2\pi d}{\lambda} = \left(\frac{g\lambda}{2\pi} \tanh \frac{2\pi d}{\lambda}\right)^{1/2} \tag{5.2.15}$$

Since the initial wave profile is evaluated at $t = 0$, equations (5.2.3) and (5.2.14) simplify to:

$$\eta = a \cos(kx - \epsilon) \tag{5.2.16a}$$

$$\phi = \frac{ag}{\sigma} \cdot \frac{\cosh k(y+d)}{\cosh (kd)} \cdot \sin(kx - \epsilon) \tag{5.2.16b}$$

which are the equations used in the computer program 'BEMW1'.

5.3 Modification of the Matrix Equation

As can be seen from the boundary conditions in section 5.2, the conditions on the two vertical sides must satisfy the radiation condition which may be unspecified. Thus, additional information is needed in order to solve a set of integral equations.

Since the wave to be analysed is periodic, one may make use of the periodicity and set the length of domain equal to one wavelength or a multiple of wavelengths. Then the values of potential ϕ will be identical on the two vertical boundaries (compatibility condition), whereas the values for the derivative ϕ' will have the same magnitude but of opposite sign (equilibrium condition), i.e. (Fig. 5.3.1)

$$\phi_{\Gamma_2} = \phi_{\Gamma_4} = \Phi \tag{5.3.1a}$$

$$\phi'_{\Gamma_2} = -\phi'_{\Gamma_4} = \Phi' \tag{5.3.1b}$$

The integral equation applicable to the wave problem is still of the same form as equation (4.2.1). The matrix equation will have to be modified to incorporate conditions (5.3.1). For generality, consider the domain shown in Fig. (5.3.1), and assumming the whole boundary, Γ , is divided into five parts, denoted by Γ_1, Γ_2 , Γ_3 , Γ_4 , and Γ_5 , i.e.

$$\Gamma = \Gamma_1 + \Gamma_2 + \Gamma_3 + \Gamma_4 + \Gamma_5 \tag{5.3.2}$$

the matrix equation (4.2.9) would become, in partition matrix form:

$$\left[H_{\Gamma_1} \;\vdots\; H_{\Gamma_2} \;\vdots\; H_{\Gamma_3} \;\vdots\; H_{\Gamma_4} \;\vdots\; H_{\Gamma_5} \right] \begin{Bmatrix} \phi_{\Gamma_1} \\ \hdashline \phi_{\Gamma_2} \\ \hdashline \phi_{\Gamma_3} \\ \hdashline \phi_{\Gamma_4} \\ \hdashline \phi_{\Gamma_5} \end{Bmatrix} = \left[G_{\Gamma_1} \;\vdots\; G_{\Gamma_2} \;\vdots\; G_{\Gamma_3} \;\vdots\; G_{\Gamma_4} \;\vdots\; G_{\Gamma_5} \right] \begin{Bmatrix} \phi'_{\Gamma_1} \\ \hdashline \phi'_{\Gamma_2} \\ \hdashline \phi'_{\Gamma_3} \\ \hdashline \phi'_{\Gamma_4} \\ \hdashline \phi'_{\Gamma_5} \end{Bmatrix} \qquad (5.3.3)$$

Substituting equations (5.3.1) into (5.3.3) and rearranging give :

$$\left[-G_{\Gamma_1} \;\vdots\; H_{\Gamma_3} \;\vdots\; -G_{\Gamma_5} \right] \begin{Bmatrix} \phi'_{\Gamma_1} \\ \hdashline \phi_{\Gamma_3} \\ \hdashline \phi'_{\Gamma_5} \end{Bmatrix} = \left[-H_{\Gamma_1} \;\vdots\; G_{\Gamma_2} - G_{\Gamma_4} \;\vdots\; G_{\Gamma_3} \;\vdots\; -(H_{\Gamma_2} + H_{\Gamma_4}) \;\vdots\; -H_{\Gamma_5} \right] \begin{Bmatrix} \phi_{\Gamma_1} \\ \hdashline \Phi' \\ \hdashline \phi'_{\Gamma_3} \\ \hdashline \Phi \\ \hdashline \phi_{\Gamma_5} \end{Bmatrix} \qquad (5.3.4)$$

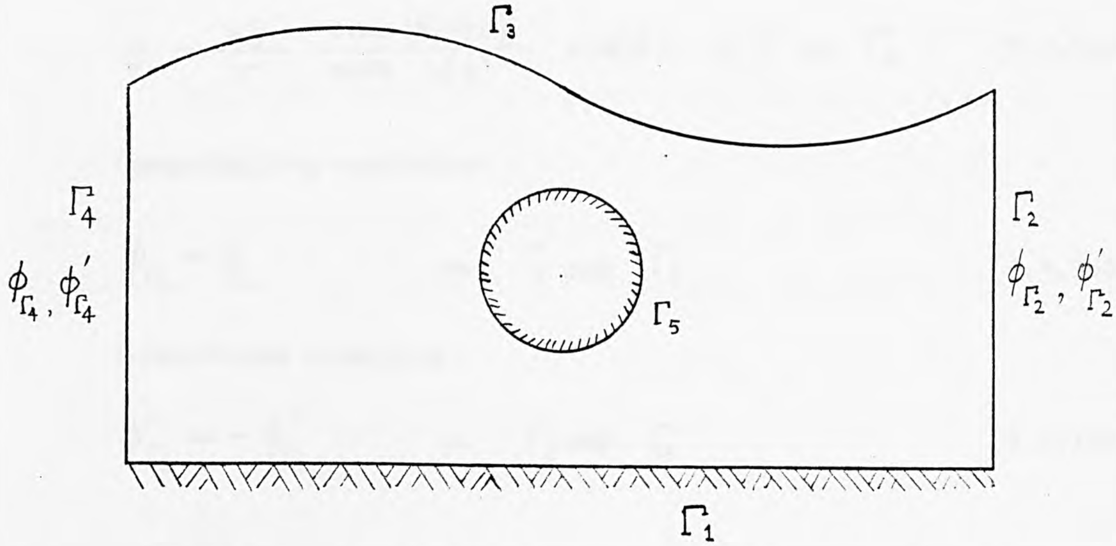

Fig. 5.3.1 Flow domain with fixed object inside

The boundary condition on an object inside the flow domain is:

$$\phi'_{\Gamma_5} = 0 \tag{5.3.5}$$

Therefore, the column matrix on the left hand side of equation (5.3.4) are known and those on the right hand side are unknown, the system of equations can be reduced to the form of equation (4.2.12), i.e.

$$[A]\{x\}=\{F\} \tag{5.3.6}$$

which can be solved by Gaussian elimination.

The associated boundary conditions for progressive and standing waves are repeated here for completeness, referred to Fig. 5.3.1.

(a) Progressive wave :

$$\phi' = 0 \quad \text{on} \quad \Gamma_1 \tag{5.3.7a}$$

$$\phi = \frac{ag}{\sigma} \cdot \frac{\cosh\left[k(y+d)\right]}{\cosh\,(kd)} \sin(kx - \epsilon) \quad \text{on} \quad \Gamma_3 \tag{5.3.7b}$$

Compatibility condition:

$$\phi_{\Gamma_2} = \phi_{\Gamma_4} \quad \text{on} \quad \Gamma_2 \text{ and } \Gamma_4 \tag{5.3.7c}$$

Equilibrium condition:

$$\phi'_{\Gamma_2} = -\phi'_{\Gamma_4} \quad \text{on} \quad \Gamma_2 \text{ and } \Gamma_4 \tag{5.3.7d}$$

$$\phi' = 0 \quad \text{on} \quad \Gamma_5 \tag{5.3.7e}$$

(b) **Standing wave :**

$$\phi' = 0 \quad \text{on} \quad \Gamma_1 \tag{5.3.8a}$$

$$\phi = \frac{-ag}{\sigma} \cdot \frac{\cosh k(y+d)}{\cosh (kd)} \cos(kx) \cdot \cos(\sigma \cdot t + \epsilon) \text{ on } \Gamma_3 \tag{5.3.8b}$$

$$\phi' = 0 \quad \text{on} \quad \Gamma_2 \text{ and } \Gamma_4 \tag{5.3.8c}$$

$$\phi' = 0 \quad \text{on} \quad \Gamma_5 \tag{5.3.8d}$$

It is noted that the equations for ϕ on Γ_3 are of first order. Higher order equations may also be used (Appendix A.7). The non-dimensionalisation of the above equations is shown in Appendix A.8.

5.4 Prediction of Wave Profile and Time Stepping Technique

The formulation described so far is considered as a boundary value problem with the wave profile taken instantaneously. No allowance has been made for the wave to move. This section will discuss the approach for allowing the wave profile evolving with time, similar to the technique applied successfully by Longuet-Higgins and Cokelet (1976).

Since the position of a particle on the wave surface is a function of time as well as space, i.e. x, y and t. The rate of change following the motion is expressed by using the Stokes derivative $\frac{D}{Dt}$, defined as in two dimensions (Kinsman, 1965):

$$\frac{D}{Dt} = \frac{\partial}{\partial t} + u\frac{\partial}{\partial x} + v\frac{\partial}{\partial y}$$

$$= \frac{\partial}{\partial t} + \nabla\phi \cdot \nabla \tag{5.4.1}$$

where u and v are particle velocities in the x and y directions. respectively. ϕ is the velocity potential.

By using the Stokes derivative, the following describes how the velocity potential and the position of individual fluid particles change as the wave moves.

By setting the constant C to zero in equation (A.6.6), the unsteady Bernoulli's equation becomes:

$$\frac{\partial\phi}{\partial t} + \frac{p}{\rho} + \frac{1}{2}(\nabla\phi)^2 + gy = 0 \qquad (5.4.2)$$

where p is the pressure acting along the free surface of the wave. Combining equations (5.4.1) and (5.4.2) gives:

$$\begin{aligned}\frac{D\phi}{Dt} &= \frac{\partial\phi}{\partial t} + \nabla\phi\cdot\nabla\phi \\ &= -\frac{p}{\rho} - \frac{1}{2}(\nabla\phi\cdot\nabla\phi) - gy + \nabla\phi\cdot\nabla\phi \\ &= \frac{1}{2}(\nabla\phi)^2 - \frac{p}{\rho} - gy \qquad (5.4.3)\end{aligned}$$

where $$(\nabla\phi)^2 = u^2 + v^2$$

Equation (5.4.3) is the dynamical boundary condition applied to the wave surface.

By the definitions of Stokes derivative and velocity potential, Longuet-Higgins and Cokelet (1976) showed that:

$$\frac{Dx}{Dt} = u = \frac{\partial\phi}{\partial x} \qquad (5.4.4a)$$

$$\frac{Dy}{Dt} = v = \frac{\partial\phi}{\partial y} \qquad (5.4.4b)$$

which are the kinematic boundary conditions applied to the wave surface.

Since ϕ' is the direct result of a boundary integral equation on the wave surface, and $\frac{\partial \phi}{\partial s}$ may be determined by the position of fluid particles and its velocity potential, both of which are given, equations (5.4.3) and (5.4.4) are rewritten as follows:

$$\frac{Dx}{Dt} = \frac{\partial \phi}{\partial s} \cos\beta - \phi' \sin\beta \tag{5.4.5a}$$

$$\frac{Dy}{Dt} = \frac{\partial \phi}{\partial s} \sin\beta + \phi' \cos\beta \tag{5.4.5b}$$

$$\frac{D\phi}{Dt} = \frac{1}{2}\left[(\phi')^2 + \left(\frac{\partial \phi}{\partial s}\right)^2\right] - \frac{p}{\rho} - gy$$

or
$$\frac{D\phi}{Dt} = \frac{1}{2}\left[\left(\frac{Dx}{Dt}\right)^2 + \left(\frac{Dy}{Dt}\right)^2\right] - \frac{p}{\rho} - gy \tag{5.4.5c}$$

where $\phi' = \frac{\partial \phi}{\partial n}$

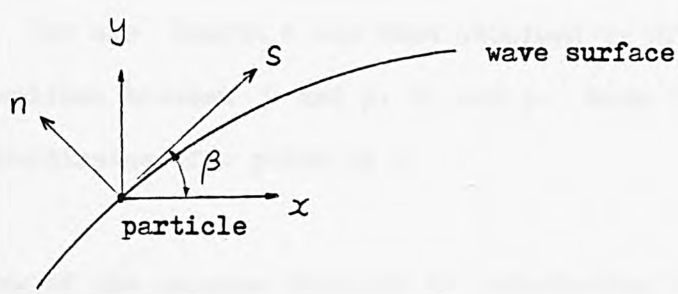

Fig. 5.4.1 Tangential and normal directions to a particle on wave surface

where β is the angle between the horizontal and the positive s axis.

Equations (5.4.5a) and (5.4.5b) shows how the position of a fluid particle changes with time, and equation (5.4.5c) shows how its velocity potential changes as the wave moves.

The evaluations of $\cos\beta$ and $\sin\beta$ necessitate the length s along the wave surface, Γ_3, to be known first. Each nodal point on Γ_3 is associated with a unique value of s, x and y. A three point Lagrangian polynomial fit was thought to be capable of handling these evaluations; but it was found later that the Lagrangian technique was very crude and inapplicable if it was to cater for an overturning wave profile.

Longuet-Higgins and Cokelet (1976) also had the same problem when the free surface was transformed into a closed contour C, on which each point had a unique value of s, and the points are not equally spaced with regard to s. To overcome this problem, they introduced a new parameter, p, uniquely defined as the point or node number. The arc length s was then obtained by fitting periodic cubic splines between r and p; θ and p. Both r and θ are polar coordinates of a point on C.

In view of the success obtained by introducing the parameter, p, the same principle is employed in this case. Periodic cubic splines are fitted between $x-2\pi p$ and p; y and p; ϕ and p to obtain $\frac{dx}{dp}+2\pi$; $\frac{dy}{dp}$ and $\frac{d\phi}{dp}$ respectively. The distance at point $p = j$, s_j, is expressed as:

$$s_j = \int \left(\frac{ds}{dp}\right)_j dp_j \tag{5.4.6}$$

where

$$\left(\frac{ds}{dp}\right)_j = \sqrt{\left(\frac{dx}{dp}\right)_j^2 + \left(\frac{dy}{dp}\right)_j^2} \tag{5.4.7}$$

The integration is carried out by Simpson's rule (see Apendix A.10), with local error of the order $(\Delta s)^4$.

One may note that $x-2\pi p$ is used for the periodic spline fit instead of x. This is because the periodic spline curve requires the ordinate and slope of the first and last nodes to be the same. For point j, $\cos\beta$ and $\sin\beta$ are calculated as:

$$\cos\beta = \left(\frac{dx}{ds}\right)_j = \frac{(dx/dp)_j}{(ds/dp)_j} \tag{5.4.8a}$$

$$\sin\beta = \left(\frac{dy}{ds}\right)_j = \frac{(dy/dp)_j}{(ds/dp)_j} \tag{5.4.8b}$$

and

$$\left(\frac{\partial\phi}{\partial s}\right)_j = \frac{(d\phi/dp)_j}{(ds/dp)_j} \tag{5.4.8c}$$

Assuming the time step, δt, being small, the changes in x, y and ϕ may be obtained from the following equations:

$$\delta x = \frac{Dx}{Dt} \cdot \delta t \tag{5.4.9a}$$

$$\delta y = \frac{Dy}{Dt} \cdot \delta t \tag{5.4.9b}$$

$$\delta\phi = \frac{D\phi}{Dt}\cdot\delta t \qquad (5.4.9c)$$

and the new position at the beginning of loop $(j + 1)$ becomes:

$$x_{(j+1)} = x_{(j)} + \delta x \qquad (5.4.10a)$$

$$y_{(j+1)} = y_{(j)} + \delta y \qquad (5.4.10b)$$

$$\phi_{(j+1)} = \phi_{(j)} + \delta\phi \qquad (5.4.10c)$$

Although equations (5.4.9) are of first order, the error induced in δx, δy and $\delta\phi$ must be kept to a minimum if the wave profile is to remain in shape for a substantial length of time or number of loops.

A fourth-order Adam -Bashforth-Moulton scheme is used for the majority of time stepping (Acton, 1970). It is a predictor-corrector method, local error being $O(\delta t)^5$.

If a first order ordinary differential equation is of the form:

$$\frac{dy(t)}{dt} = f(t, y) \qquad (5.4.11)$$

the predictor equation is:

$$y_{1p} = y_0 + \frac{\delta t}{24}\left(55f_0 - 59f_{-1} + 37f_{-2} - 9f_{-3}\right) \qquad (5.4.12)$$

and the corrector equation is:

$$y_{1c} = y_0 + \frac{\delta t}{24}\left(9f_{1p} + 19f_0 - 5f_{-1} + f_{-2}\right) \tag{5.4.13}$$

The subscripts "p" and "c" in the above equations refer to predicted and corrected values, and the subscripts -3, -2, -1, 0, 1, refer to the time steps. The y terms in equations (5.4.12) and (5.4.13) may be substituted by x and ϕ .

The method takes the time derivatives at the current time step, 0 , and three previous time steps, -1, -2, -3 to predict a value for y at the next time step, y_{1p}. By the same procedure, the predicted values of x and ϕ, i.e. x_{1p} , ϕ_{1p} , are obtained.

All predicted values are then used to solve for the integral equations by the boundary element method. Hence, f_{1p} for x , y and ϕ are obtained from equation (5.4.12). These values are fed into equation (5.4.13) to find x , y and ϕ at the new time step, i.e. x_{1c} , y_{1c} and ϕ_{1c} respectively. Having found these, f_{1p} is calculated and the cycle begins again. It can be seen that the integral equations are solved twice in each time step.

Since the Adam-Bashforth-Moulton method requires information at three previous time steps, a fourth-order Runge-Kutta technique is used to take the first three steps from the initial conditions or when the numerical accuracy is not achieved and the time step length is halved (Gerald,1970). Such a method discards all information above previous time steps and takes four mini steps forward in time from the current time step. A weighted average of these is then used to calculate the functions at the new time step. The equation used is:

$$y_1 = y_0 + \frac{1}{6}\left(k_a + 2k_b + 2k_c + 2k_d \right) \tag{5.4.14}$$

where

$$k_a = \delta t \cdot f(t_0, y_0) \tag{5.4.15a}$$

$$k_b = \delta t \cdot f\left(t_0 + \frac{1}{2}\delta t,\ y_0 + \frac{1}{2}k_a \right) \tag{5.4.15b}$$

$$k_c = \delta t \cdot f\left(t_0 + \frac{1}{2}\delta t,\ y_0 + \frac{1}{2}k_b \right) \tag{5.4.15c}$$

$$k_d = \delta t \cdot f\left(t_0 + \delta t,\ y_0 + k_c \right) \tag{5.4.15d}$$

The Runge-Kutta method requires four evaluations of the integral equations per time step and is thus twice as time-consuming as the Adam-Bashforth-Moulton method. The local error term for the fourth-order Runge-Kutta method is $O(\delta t)^5$; the global error would be about $O(\delta t)^4$.

5.5 Pressures and Forces on an Internal Object

When a stationary object is introduced into the flow domain, wave loadings are then induced on the object. The boundary condition on the object is, in general:

$$\phi' = \frac{\partial \phi}{\partial n} = 0 \tag{5.5.1}$$

assuming the object boundary is impermeable.

The velocity potential, ϕ , is then obtained when the boundary integral equations are solved. Once ϕ is known on the object boundary, non-linear pressure may then be calculated from the Bernoulli's equation (5.4.2):

$$p = -\rho \left\{ \underset{\text{hydrostatic pressure}}{gy} + \underbrace{\frac{1}{2}(\nabla\phi)^2 + \frac{\partial\phi}{\partial t}}_{\text{hydrodynamic pressure}} \right\} \tag{5.5.2}$$

where $(\nabla\phi)^2 = \left(\frac{\partial\phi}{\partial x}\right)^2 + \left(\frac{\partial\phi}{\partial y}\right)^2 = u^2 + v^2$ which can be worked out at any point inside the domain.

Since the hydrostatic pressure is fixed by the location of the object, it is only the pressures induced by the wave, i.e. the hydrodynamic pressures that are of interest in the analysis. The actual equation used in the computation then becomes:

$$p = -\rho \left\{ \frac{1}{2}(\nabla\phi)^2 + \frac{\partial\phi}{\partial t} \right\} \tag{5.5.3}$$

The method chosen to evaluate $\frac{\partial\phi}{\partial t}$ is the Lagrangian polynomials. A parabola is fitted through three values of ϕ over three consecutive times (i.e. t_{i-2} , t_{i-1} , t_i) at a particular point. Its gradient ($\frac{\partial\phi}{\partial t}$) is then calculated at time t_i . ϕ and t values of the last two time steps on the object or at any internal point are required to be stored in a matrix set up for this purpose. The gradient ($\frac{\partial\phi}{\partial t}$) may also be obtained at time t_{i-2} and t_{i-1} .

Both horizontal and vertical forces exerted on the object by the wave are obtained through integration of pressures around the object, i.e.

$$F_x(t) = \int -P(t)\cos\theta \cdot r\,d\theta \qquad (5.5.4a)$$

$$F_y(t) = \int -P(t)\sin\theta \cdot r\,d\theta \qquad (5.5.4b)$$

where r and θ are polar coordinates of a point on the object, and the integrations are carried out by Simpson's rule.

The evaluations of pressures and forces are in non-dimensional forms. Expression of pressures in millimetres may then be obtained by multiplying the appropriate dimensional constant by the non-dimensional pressure. The forces may also be normalised by the term $\rho g r \frac{H}{2}$, where H is the wave height and r is a dimension , e.g. radius, of the object.

5.6 Checks of Accuracy

Most of the numerical computations involving iteration technique would require some kind of checks on computed solutions, in case results become divergent instead of convergent. In the wave program 'BEMW1', a very basic check is employed, which is:

$$|\phi| \text{ or } |\phi'| < 50 \qquad (5.6.1)$$

The above condition may not be justified mathematically but it seems reasonable to make that assumption since the computations of ϕ and ϕ' are in non-dimensional forms. Once the above condition is not satisfied, the execution would come to a halt. Otherwise, solutions become infinite.

Apart from the above intuitive check, four other checks can be made on the numerical solutions.

The first one is a check on the Gauss condition. Letting $u = \phi$, equation (A.3.8) becomes:

$$\int_{\Gamma} \frac{\partial \phi}{\partial n} d\Gamma = \int_{\Gamma} \phi' d\Gamma = 0 \tag{5.6.2}$$

From equation (5.3.2), the boundary Γ may be divided into five parts, and from the boundary conditions of equation (5.3.7) or (5.3.8), equation (5.6.2) can be reduced to:

$$Q = \int_{\Gamma_3} \phi' d\Gamma = 0 \tag{5.6.3}$$

where Γ_3 represents the free surface of the wave. Equation (5.6.3) implies that the total outflow through the wave surface, Q, should be zero. The amount that the resulting answer differs from zero is an indication of the accuracy of ϕ' on the wave surface.

Conservations of mass and energy should theoretically be maintained throughout, but this cannot be guaranteed due to truncation and rounding off errors. It is still useful to monitor them as the calculations progress, so that information may be extracted in relation to the behaviour of an unsteady water wave using the proposed integral equation technique.

The conservation of mass implies the total flow area under the wave surface in the flow domain remains constant. In other words, the mean water level, $\bar{y}$, should remain constant if mass is conserved, since its wavelength , λ , remains constant:

$$\bar{y} = \frac{1}{\lambda}\int_0^\lambda y \, dx \tag{5.6.4}$$

The kinetic energy, Ke , and potential energy, Pe , are expressed as (Longuet-Higgins and Cokelet,1976):

$$Ke = \frac{1}{2\lambda}\int_\Gamma \phi \cdot \phi' \, d\Gamma \tag{5.6.5}$$

$$Pe = \frac{1}{\lambda}\int_0^\lambda \frac{1}{2} y^2 \, dx \tag{5.6.6}$$

From the boundary conditions of equation (5.3.7) or (5.3.8), i.e.

$\phi' = 0$ on Γ_1

$\phi'_{\Gamma_2} = -\phi'_{\Gamma_4}$ (from equation 5.3.7)

$\phi'_{\Gamma_2} = \phi'_{\Gamma_4} = 0$ (from equation 5.3.8)

$\phi' = 0$ on Γ_5

the expression for kinetic energy is reduced to:

$$Ke = \frac{1}{2\lambda}\int_{\Gamma_3} \phi \cdot \phi' \, d\Gamma \tag{5.6.7}$$

When no pressure forcing is being applied at the free surface, the total energy :

$$Te = Ke + Pe \tag{5.6.8}$$

must be constant.

As discussed in section (5.4), the above integrations are conducted through the point number parameter, p, with Simpson's rule. Hence, equations (5.6.3), (5.6.4), (5.6.6) and (5.6.7) will be written as:

$$Q = \int_{\Gamma_3} \phi' \cdot \frac{ds}{dp}\, dp \tag{5.6.9a}$$

$$\bar{y} = \frac{1}{\lambda} \int_{\Gamma_3} y \cdot \frac{dx}{dp}\, dp \tag{5.6.9b}$$

$$Ke = \frac{1}{2\lambda} \int_{\Gamma_3} \phi \cdot \phi' \frac{ds}{dp}\, dp \tag{5.6.9c}$$

$$Pe = \frac{1}{\lambda} \int_{\Gamma_3} \frac{1}{2} y^2 \frac{dx}{dp}\, dp \tag{5.6.9d}$$

CHAPTER 6 - NUMERICAL COMPUTATIONS AND RESULTS OF PROBLEMS IN CHAPTER 5

6.1 Introduction

This chapter serves two purposes: firstly, the development of wave program 'BEMW1' which has been written to perform the simulation of periodic waves is described; and secondly, the proposed method of carrying out test problems, case studies and comparison with solutions obtained by other sources is assessed. The program was written according to the theory presented, regardless of the properties and approximation of different types of wave. Nevertheless, the limitation of the proposed technique will be explored in this chapter.

Section 6.2 briefly outlines the program 'BEMW1' with a simplified flow chart and a description of its structure. It is described mainly in terms of subroutines, which will further be dealt with under four sub-sections. The input format, order of equations used and setting up of data will be discussed in sub-section 6.2.1. The fundamental theory of the boundary element technique incorporated into the wave program is coded in a subroutine called 'BEM'. Its modification to suit wave modelling will be discussed in sub-section 6.2.2. The coding of the time-stepping technique, selection of time step, spacing of nodal points on the surface and its stability will be covered in sub-section 6.2.3. Sub-section 6.2.4 presents equations for evaluation of pressures and forces on obstacle or pressures at internal points.

Section 6.3 is devoted to discussing the evolution of numerical technique for program 'BEMW1' through test problems on progressive waves without an obstacle. A typical result for the standing wave case is also shown with additional plots for the variations of energy and mean water level, and related phenomena. Section 6.4 moves on to test problems of progressive waves with the introduction of a horizontal circular object into the flow domain. Section 6.5 presents results based on experimental data extracted from Lacey, 1983. The main aim of the comparison with experimental results is the validation of the results of the proposed technique.

The program 'BEMW1' has been tested under the following conditons:

(1) Linear variation along elements.

(2) Standing and progressive waves.

(3) When an object is introduced in the progressive wave, the boundary conditions on the two vertical side boundaries, Γ_2 and Γ_4 ,are not specified. (see section 6.4)

(4) Linear, second, and third order equations for the evaluations of the wave profile and its velocity potential.

(5) Periodic cubic spline as numerical curve fitting.

At the initial stage, the program 'BEMW1' was developed using the Honeywell 66/60 level computer at the computer centre of The City University. Due to the limited capacity of the Honeywell machine, and a large number of students running programs during term time, the central processor of the machine was heavily loaded. A large job, in general, would have to wait for several hours on a batch queue before it was executed. A large job usually involves storage of 32 K bytes or more and the run time is more than 0.1 of an hour. Owing to the nature of the proposed technique involving iterations, a more powerful computer was felt necessary for the task. Therefore, a major part of program development were carried out using the CDC7600 computer at the University of London Computer Centre. The program 'BEMW1' could still be run on the Honeywell computer when it was not heavily loaded, e.g. during holidays, and the number of iterations involved in a particular job was within the run time capacity of the Honeywell computer.

6.2 Description of program 'BEMW1'

Based on the technique proposed in chapter 5, a computer program was written in Fortran language for the solution of two dimensional unsteady wave problems using linear variation along boundary elements.

The following gives an outline of program 'BEMW1' in terms of subroutines shown in the simplified flow chart in Fig. 6.2.1. The subroutines are substantial and will require further detailed explanation in the following sub-sections, especially those which presented difficulties during the course of program development. Subroutines DRAW, GRAPH and FXFYPT are for plotting graphs and wave profiles only. Therefore, they will not appear in Fig. 6.2.1 or in any discussion. There are subroutines which were used at the beginning of the program development but later on found un-suitable. They remain in the program listing in Appendix A.12. There are some other small subroutines which are elementary and will not be discussed (e.g. evaluation of length of element, shifting of end nodal points in the wave profile). The description given here will follow the steps listed out in the simplified flow-chart in Fig. 6.2.1. The names used in the flow-chart have the following representation:

LOOPS = Number of loops to be executed

NLOOP = Loop counter

NNI = Number of nodes on internal boundary

NI = Number of internal points

NCT = Loop counter for each fresh δt or surface redistribution

ϕ = Velocity potential

ϕ' = Potential derivative

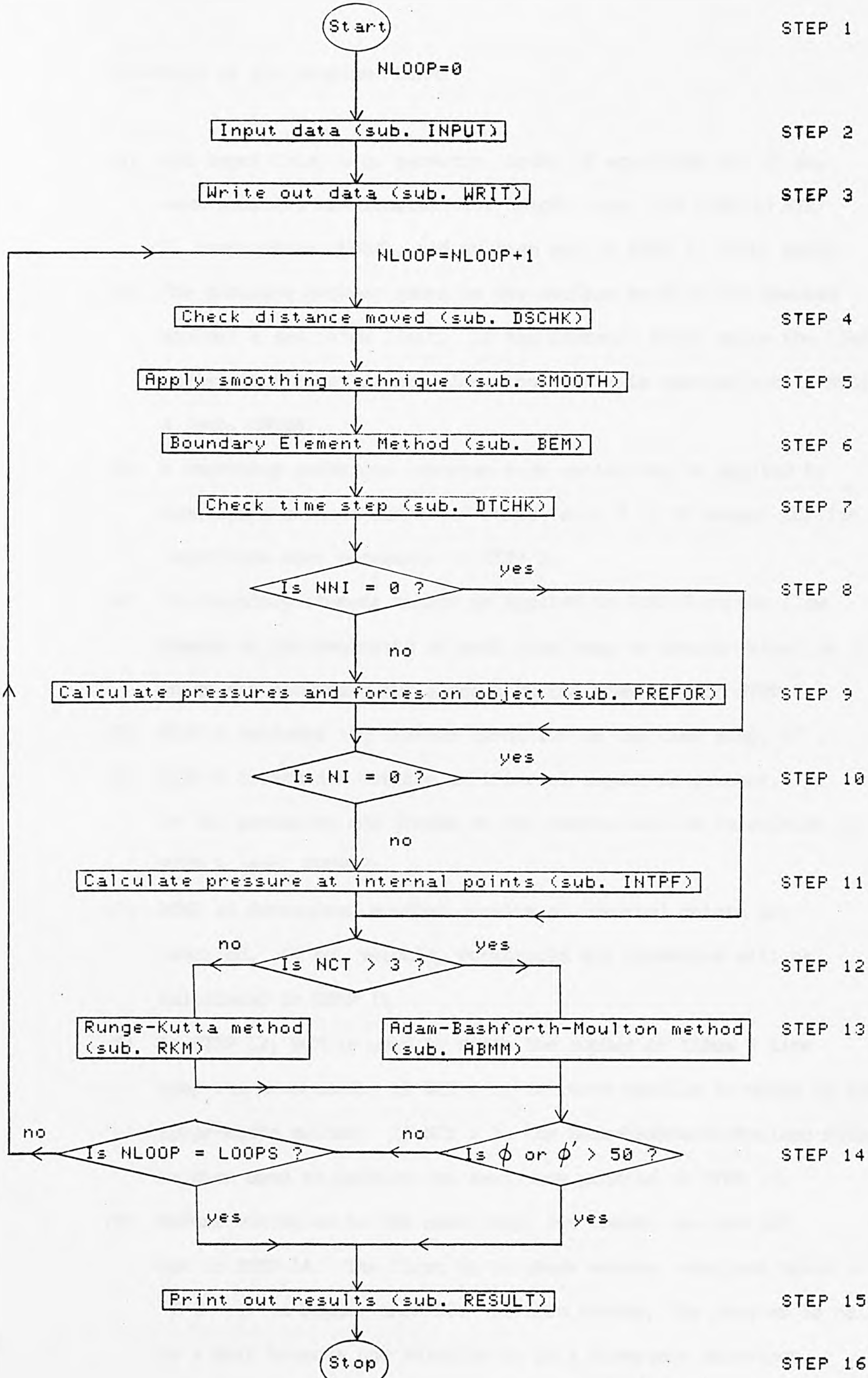

Fig. 6.2.1 Simplified flow chart for 'BEMW1'

Structure of the program 'BEMW1'

(1) All input data, e.g. geometry, order of equations for ϕ and wave profile, wavelength, wave height, etc. are read in STEP 2, (subroutine INPUT), and written out in STEP 3, (sub. WRIT).

(2) The distance between nodes on the surface profile are checked against a specified limit. If the distance drops below the limit, redistribution of points along the x-axis is carried out in STEP 4 (sub. DSCHK).

(3) A smoothing technique (section 6.3) option may be applied by specifying a fixed number of steps (e.g. 5 or 10 steps) for its repetition when necessary in STEP 5.

(4) The boundary element method is applied in STEP 6 to the flow domain at the beginning of each time step to obtain values of ϕ' which are necessary for a check on the time step in STEP 7.

(5) STEP 6 performs the Courant condition on the time step, δt .

(6) STEP 8 determines whether an internal object is present. If it is, pressures and forces on the object will be calculated in STEP 9 (sub. PREFOR).

(7) STEP 10 determines whether results at internal points are required. If so, velocity potentials and pressures will be calculated in STEP 11.

(8) In STEP 12, NCT is used to store the number of times a time step has been used. If NCT $\leqslant$ 3, the wave profile is moved by the Runge-Kutta method. If NCT > 3, the Adam-Bashforth-Moulton method is then used to predict the next wave profile in STEP 13.

(9) Before moving on to the next loop, two checks are carried out in STEP 14. The first is to check whether absolute value of ϕ or ϕ' is bigger than 50. If this occurs, the program is called to a halt because the solution is in a divergent behaviour.

The second is to check whether the counter for loops has reached the specified number of loops in the input data. If either of the two checks is satisfied, it will print out the last result in sub. RESULT before the execution is stopped automatically.

6.2.1 Input Format - Subroutine INPUT

In the wave program, 'BEMW1', the fluid domain is enclosed by an external boundary Γ_e and, an internal boundary Γ_I , if present. The external boundary is further divided into smaller parts depending on the boundary conditions and shape of domain. In a typical wave problem, the external boundary is divided into four parts, Γ_1 , Γ_2 , Γ_3 and Γ_4 , (see Fig. 6.2.1.1), such that:

$$\Gamma_e = \Gamma_1 + \Gamma_2 + \Gamma_3 + \Gamma_4 \tag{6.2.1}$$

In general, Γ_1 represents an impermeable horizontal bed; Γ_2 and Γ_4 represent the two vertical barriers; Γ_3 represents the free surface. The boundary condition associated with each part is:

$$\frac{\partial \phi}{\partial n} = 0 \qquad \text{on } \Gamma_1 \tag{6.2.2a}$$

$$\phi = \text{prescribed value on } \Gamma_3 \tag{6.2.2b}$$

$$\frac{\partial \phi}{\partial n} = 0 \text{ or unspecified on } \Gamma_2 \text{ and } \Gamma_4 \tag{6.2.2c}$$

depending on the type of problem sought

The internal boundary, Γ_I , depicts the shape of structure in the flow field, e.g. a horizontal circular cylinder, with the following boundary condition:

$$\frac{\partial \phi}{\partial n} = 0 \tag{6.2.2d}$$

If the boundary Γ_1 is discretised by M1 nodes, and similarly Γ_2 by M2; Γ_3 by M3; Γ_4 by M4, the total number of nodes on the external boundary becomes:

$$NNE = M1 + M2 + M3 + M4 \tag{6.2.3}$$

As will be explained later, it is necessary that M2 be equal to M4.

If the internal boundary Γ_I is discretised by NNI nodes, the total number of nodes on the boundaries would become:

$$NN = NNE + NNI \tag{6.2.4}$$

For constant or linear variation along an element, the total number of nodes is equal to the total number of elements, i.e.

$$NE = NN \tag{6.2.5}$$

But if quadratic variation along an element is used, the number of nodes will not be equal to the number of elements (see section 4.2).

The coordinates of nodal points (X,Y) on the external boundary are generated by specifying the starting position (XF,YF) and finishing position (XL,YL) on each boundary and the number of nodes (NX(I)) on the Ith boundary. The coordinates of nodal points on the internal boundary, in the case of a circular cylinder, are generated by specifying the centre of cylinder (XCENTD, YCENTD), its radius (RADIUD) and the number of nodes (NNI) on the cylinder.

The node numbers on the ends of the elements are generated within the program automatically, so as to keep input to a minimum.

For linear and constant variations:

NEN(I,1) specifies the node No. at the beginning of element I.

NEN(I,2) specifies the node No. at the end of element I.

For quadratic variation :

NEN(I,1) specifies the node No. at the beginning of element I.

NEN(I,2) specifies the middle node No. of element I.

NEN(I,3) specifies the node No. at the end of element I.

The type of variation along an element is designated by the parameter (NVARY) with:

NVARY = 1 for constant variation (6.2.6a)

NVARY = 2 for linear variation (6.2.6b)

NVARY = 3 for quadratic variation (6.2.6c)

As mentioned in section 6.1, although an automatic node numbering system has catered for constant, linear and quadratic variations, other parts of the program, originally developed with linear variation, have not been amended accordingly. So, throughout the analysis, the program 'BEMW1' is operational with linear variation only. It is, of course, possible to convert the entire program to include constant and quadratic variations along boundary elements.

In 'BEMW1', it was initially attempted to solve for different types of wave, specified by the parameter (NTW) with:

NTW = 1 for progressive wave cases. (6.2.7a)

NTW = 2 for standing wave cases. (6.2.7b)

NTW = 3 for wave generated from rest, similar to an instant when a wave generator is switched on, in a calm wave channel. (6.2.7c)

NTW = 4 for solitrary wave cases. (6.2.7d)

Due to the time limit in the present studies, the program is only capable of solving progressive and standing wave problems.

The expressions for the free surface profile, η , and velocity potential, ϕ , may be of linear theory or higher order equations. The program has included expressions for both η and ϕ for 1st, 2nd, 3rd or 5th order equations. The parameter specifying the order of equation is given by:

NORDER = 1 for 1st order theory (6.2.8a)

NORDER = 2 for 2nd order theory (6.2.8b)

NORDER = 3 for 3rd order theory (6.2.8c)

NORDER = 5 for 5th order theory (6.2.8d)

The equations used for 1st order theory are shown in section 5.2., i.e. equations (5.2.16a) for η and equation (5.2.16b) for ϕ , with (5.2.15) for the phase velocity. The corresponding higher order expressions are listed in Appendix A.7. With the conditions of wave profile specified (i.e. wavelength , wave height and water depth), the computations for η and ϕ are straight forward for 1st, 2nd or 3rd order theory. But in the 3rd order theory, the evaluation of wave amplitude from wave height requires Newton-Raphson's iterative process. For the 5th order theory, the constants in expressions for velocity potential and wave profile are typed in as input data obtained from tables provided in Skjelbreia and Hendrickson (1961). Newton-Raphson's method is also employed in computing the term in equation (A.7.13) in Appendix A.7.

Once the x coordinates on the wave surface have been set up, the actual y coordinates and ϕ values on the wave surface are then calculated in subroutine PW1 for progressive wave problems or SW1 for standing wave problems. Both y and ϕ values on the surface may therefore be set to zero in the input data.

When the y coordinates on the wave surface have been calculated, the nodal coordinates on the two vertical side boundaries, Γ_2 and Γ_4, may have to be readjusted in geometric proportion according to the change in y coordinate from zero position at the end points of the wave surface. This is because the initial coordinates on the sides assume the end points of wave profile at still water level or $y = 0$ (see Fig. 6.2.1.1). The shifting of the above nodes are carried out in subroutine MOVE, which can actually shift nodes in both x and y directions, as may be the case when a progressive wave moves in space.

Various curve fitting procedures have been attempted in the course of development of the program, e.g. Lagrangian polynomial, spline fitting. They are identified by specifying the parameter (NTCF) with:

NTCF = 1	for Lagrangian polynomial	(6.2.9a)
NTCF = 2	for cubic spline	(6.2.9b)
NTCF = 3	for periodic spline	(6.2.9c)

The program was initially developed by using Lagrangian polynomial curve fitting with points 'borrowed' from either end of the free surface. The number of points borrowed is indicated by the parameter (NTP). For example, NTP = 2 means two points are borrowed from either end except the end points. The borrowing operation is carried out in subroutine SHIFT. But for cubic or periodic spline curve fitting, no points need to be borrowed from either end, hence NTP = 0.

The desired number of loops to be executed in a typical run might be specified by the parameter (LOOPS). During the course of analysis, LOOPS was assigned a value of 500. In order to reduce computing time to a minimum level, the number of gauss points (NGP) used was set to 2.

For the progressive wave problems, provision is made for the pressure forcing function on the wave profile, the amplitude of which is specified by the parameter PAMPD.

As soon as coordinates are set up on the boundary and all the data are read from a data file, non-dimensionalisation, as described in Appendix A.8 is carried out, so that results thus obtained may be presented in non-dimensional form.

The type of boundary condition for node number, I, (i.e. whether ϕ or ϕ' or unspecified) is stored in matrix NFLG(I) where:

NFLG(I) = 1 represents ϕ specified at node I (6.2.10a)

NFLG(I) = 2 represents ϕ' specified at node I (6.2.10b)

NFLG(I) = 3 represents no boundary condition at node I on the out-flow vertical boundary (6.2.10c)

NFLG(I) = 4 represents no boundary condition at node I on the in-flow vertical boundary (6.2.10d)

The actual value of the boundary condition is stored in matrix VAL(I,J) where J = NFLG(I) for element I. So, with NFLG(I) equal to 3 or 4, VAL(I,J) equal to zero.

The rectangular coordinate system is defined as shown in Fig. 6.2.1.1, with origin at still water level and y-axis directed positive upwards. The wave is assumed to travel in the positive x-direction in water of constant depth. The node numbering sequence is anti-clockwise on the external boundary and clockwise on the internal boundary (see Fig. 6.4.10).

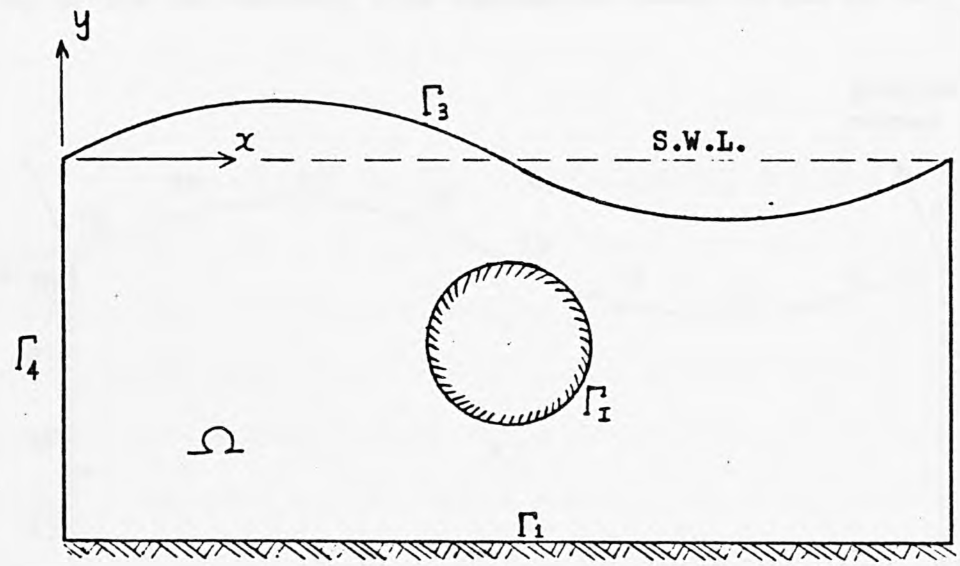

Fig. 6.2.1.1 Division of fluid boundaries

6.2.2 Boundary Element Routine - Subroutine BEM

The boundary element subroutine employed in program 'BEMW1' was basically taken from program 'BEMLVB1', and then modified to suit wave problems. The following describes the modifications implemented in sub. BEM , and also those considered during the development but found unsuitable.

Referring back to section 5.3, the compatibility and equilibrium conditions (5.3.1) were used on the two vertical side boundaries, Γ_2 and Γ_4 of Fig. 6.2.2.1, if a progressive wave problem was to be solved. Therefore, the solutions of derivative ϕ' on the two sides would have the same magnitude but opposite sign. Since a periodic spline curve was used in the numerical stepping process, it required the first and last node of wave surface to have the same ordinate and slope and be a wavelength apart. In view of the periodic spline requirement and the outcome of the equilibrium condition (5.3.1b), the author deliberately defined the top of the two vertical side boundaries, nodes 10 and 20 on Γ_2 and

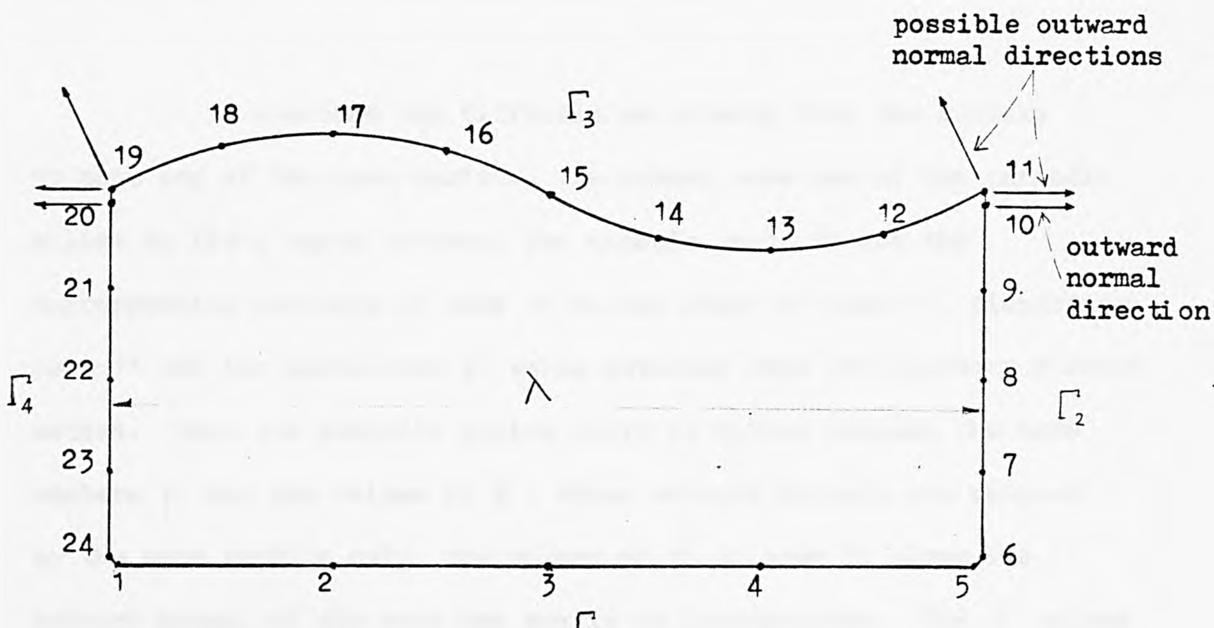

Fig. 6.2.2.1 Example of boundary discretisation with node number and outward normal direction

Γ_4 respectively, to be just under the wave surface with end nodes 11 and 19, (see Fig. 6.2.2.1). It was hoped that the above procedure would enable nodes 11 and 19 to be exempted from the equilibrium condition and resulted with ϕ' values being the same in magnitude and direction.

When the integral equations were solved from the initial wave profile and conditions, nodes 11 and 19 resulted with ϕ' values being the same in magnitude but with different signs. It seemed that the equilibrium condition still applied to nodes 11 and 19 even though they did not belong to the two vertical boundaries. It is understood that the above boundary element theory assumes ϕ' as being along the outward normal to the boundary. If the domain boundary was investigated more closely, a problem existed at a corner node where the actual outward normal was not clearly defined, (see Fig. 6.2.2.1). For example, node 11 in Fig. 6.2.2.1, belongs to two elements. Their outward normals are in different directions. Although one may take the vectorial sum as the mean of the two outward normals, this procedure invariably induces numerical instability once the wave has moved several time steps.

To overcome the difficulties arising from the corners at both end of the wave surface, the author made use of the periodic spline to fit a curve between, for example, node 18 and the corresponding position of node 18 to the right of node 11, discarding node 11 and its associated ϕ' value obtained from the boundary element method. Once the periodic spline curve is fitted between the node numbers p and the values of ϕ', whose outward normals are related to the wave profile only, the values of ϕ' at node 11 along the outward normal of the wave may easily be interpolated. The ϕ' values at node 19 will then be obtained. The above curve fitting and interpolation procedures were written in subroutine PHIDF.

If no boundary conditions are prescribed on the two vertical sides, e.g. in progressive waves, and the compatibility and equilibrium conditions are assumed, subroutine REVER will re-arrange the corresponding equations on the two sides before Gaussian elimination being applied, as discussed in section 4.3.

For standing wave problems, the two vertical sides may be considered as solid boundaries, i.e.

$$\phi' = 0 \tag{6.2.2.1}$$

and subroutine REVER is not needed to obtain a solution. Subroutine PHIDF will not be required to interpolate ϕ' values at the ends of wave surface since the end nodes on wave surface may move in the vertical direction only (see Fig. 6.3.11).

6.2.3 Time Stepping Technique - Subroutines RKM ; ABMM

Once the unknowns in a wave problem are solved in subroutine BEM at time t , the profile may then be moved to the new position. Section 5.4 discussed the two numerical schemes to be employed in the program. Euler's predictor-corrector method and the central difference scheme were attempted at an early stage of the program development, but later found to be inefficient in this study.

For the first three loops of every new time step size, a fourth-order Runge-Kutta technique (sub. RKM) is used to provide the new wave position. Each Runge-Kutta step requires four mini steps to predict end-of-mini step wave position and hence sub. BEM is executed four times. The first end-of-mini step wave profile, equation (5.4.15a) is obtained by sub. RKM1, after the boundary unknowns are solved in sub. BEM. The second end-of-mini step wave position is obtained from the first end-of-mini step wave position, and so on until equation (5.4.15d) is completed in sub. RKM3 which will give the final position of the wave surface in that time step.

If NCT is bigger than 3, the wave profile is then moved by the Adam-Bashforth-Moulton technique, in which sub. BEM is executed twice: the first execution is for the predictor equation (5.4.12) and the second execution is for the corrector equation (5.4.13), which will give the corrected wave profile position. Therefore, the computing time per time step in the Adam-Bashforth-Moulton method is half of that needed in the Runge-Kutta method. The sole purpose of using the Runge-Kutta method is to generate the information for the three time steps required in the execution of the Adam-Bashforth-Moulton technique.

6.2.4 Evaluations of Pressure and Force - Subroutines PREFOR ; INTPF

The evaluations of pressure and force at nodes on an internal object are carried out in sub. PREFOR . Sub. INTPF only evaluates pressure at internal points in the flow domain.

According to equation (5.5.3), the pressure at a node on an object or at an internal point is calculated in sub. PRESS . $\frac{\partial \phi}{\partial n}$ is obtained directly from sub. BEM . $\frac{\partial \phi}{\partial t}$ is worked out by fitting a parabola to three consecutive time steps to work out the slope at the current time step. Once the pressures at nodes on an object are obtained, the horizontal and vertical components of force, in non-dimensional or normalised form, F_N , may be evaluated through Simpson's rule in sub. SIMPV :

$$F_N = F / \rho g r \cdot \frac{H}{2} \tag{6.2.4.0}$$

where ρ is the density of the wave fluid

g is the acceleration due to gravity

r is the radius of the submerged cylinder

H is the wave height

$\nabla\phi$ in equation (5.5.3) is evaluated through:

$$(\nabla\phi)^2 = \left(\frac{\partial \phi}{\partial s}\right)^2 + \left(\frac{\partial \phi}{\partial n}\right)^2 \tag{6.2.4.1a}$$

instead of
$$(\nabla\phi)^2 = \left(\frac{\partial \phi}{\partial x}\right)^2 + \left(\frac{\partial \phi}{\partial y}\right)^2 \tag{6.2.4.1b}$$

since $\frac{\partial \phi}{\partial n}$ is known on the internal object and $\frac{\partial \phi}{\partial s}$ is calculated by fitting a periodic spline between ϕ and arc length , s , on the object.

6.3 Test Problems of Periodic Waves without an Obstacle

During the development of the wave program 'BEMW1', various problems were encountered in the behaviour of the wave predicted by the proposed technique. The problems became more complicated when an object was introduced into the flow domain. It is best to concentrate, at this stage, on the understanding of the behaviour of the periodic wave running freely on its own without any obstacle. The next section will discuss the effect of a circular object placed under a progressive wave. The data used in the test problems may be treated as arbitrary, and Table 6.3.1 shows the wave parameter used in each problem. The domain boundary is discretised by 38 nodes, of which 17 nodes are allocated on the wave surface. The length of domain is set to one wavelength. The basic dimension of the flow domain is a one unit square. When the water depth and wavelength are specified in a typical wave problem, the domain will be stretched to the dimension of water depth and wavelength specified before the wave profile η is generated.

For many numerical methods, the time step length in a time stepping technique is determined by stability considerations, of which the Courant condition is commonly used and expressed as:

$$\frac{\Delta t}{\Delta S} < \frac{1}{C} \tag{6.3.1}$$

where Δt = time step length

ΔS = element size

C = wave velocity

If M3 represents the number of nodes on a wave surface with wavelength λ , the element size projected onto the x -axis, becomes:

$$\Delta x = \frac{\lambda}{M3-1} \tag{6.3.2}$$

From equation (6.3.1), the time step length, Δt , is related to Δs (or Δx) through the wave velocity C , and must be chosen carefully so that it is small enough to give the desired accuracy and stability and large enough to be efficient in computing time.

Longuet-Higgins and Cokelet (1976) adopted a time step criterion similar to that of Chan and Street (1970). Their time step, Δt , is restricted so that at each step no fluid particle is allowed to move more than the minimum arc-length from a particle to its nearest neighbour in the transformed ζ plane.

The same principle has been applied in this study and equation (6.3.1) is modified to:

$$\Delta t_{max} < \frac{(\Delta S_{min})_j}{C} \tag{6.3.3}$$

where (ΔS_{min})$_j$ is the minimum arc-length between j and its neighbour in the $x-y$ plane.

Equation 6.3.3 had been implemented into the program "BEMW1" in sub. DTCHK, but it did not prolong the existance nor improve the stability of the wave profiles. The interpretation of C as the particle velocity in either the horizontal or tangential direction to the particle at the wave surface had also been attempted. Again their inclusion did not improve the stability of the wave profiles. Its applicability in the work of Longuet-Higgins and Cokelet (1976) was probably due to the wave being transformed into a closed loop in the ζ plane.

The inapplicability of equation (6.3.3) in this study may be explained by the following. When the wave profile has gone through a sufficient number of time steps, there is a tendency of the nodal points to concentrate near regions of shape curvature (wave crest) and space out at the wave trough, as happened in the Longuet-Higgins and Cokelet (1976) and the Vinje and Brevig (1980) procedures. Since Δt depends on the minimum distance between two adjacent nodes (equation 6.3.3), a situation would occur such that after a sufficient number of time steps, Δt would be reduced to an extent that the wave seems not to be moving at all. When this situation occurs, one suggestion is to redistribute the nodal points on the wave surface equally in the x-direction. From equation (6.3.3), a new time step is calculated based on the new distribution of nodal points.

The above postulation has also been implemented in the wave program 'BEMW1' in sub. DSCHK. The redistribution was carried out with a periodic spline curve fitting routine on every 10 or 20 time steps. The results thus obtained indicated that the redistribution of nodes on the surface did not improve the stability or overall result for the wave profile.

An alternative method to determine the time step is to relate Δt with wave steepness and wave period such that steeper wave moves in smaller time step, i.e.

$$\Delta t \propto \frac{\text{Wave period } (T)}{\text{Wave steepness } (H/\lambda)} \tag{6.3.4}$$

Equation (6.3.4) only calculates the initial time step and does not provide any check on the time step length as the wave advances.

An initial assessment of the order of magnitude for Δt has been made and Table 6.3.1 shows that different time step lengths lead to the occurence of instability at different times. By comparing the results between test problems 6.3.1; 6.3.2; 6.3.3: 6.3.4 and 6.3.5, the rate of growth of instability, per unit time, was dependent upon the time step length calculated, and there is a threshold figure beyond which smaller time step would not reduce instability nor increase the duration of wave motion. That confirms a time step length chosen must not be too small to be inefficient in computing time, and not too big to induce instability. It also reaffirms that check on time step length is not necessary once the initial time step is determined.

After a comprehensive analysis of equation (6.3.4), the following equation has been established:

$$\Delta t = \frac{T}{\sqrt{K \cdot (H/\lambda)}} \tag{6.3.5}$$

The constant, K , was determined on the basis that extreme values of wave steepness would result in a reasonable time step length, and therefore K =300,000 was found to be an optimum figure to give accuracy as well as efficiency in computing time. The above figure was used throughout the case study in section 6.5.

Test problems 6.3.2 and 6.3.8 clearly demonstrate that the smaller the wave steepness, the bigger the time step length and the duration of wave movement would also be longer.

One of the forms of instability that can be observed from Figs. 6.3.2 and 6.3.4 is that two nodal points to the right of the wave surface move towards each other after one period, and finally lead to instability and blow up at about $t = 1.4\,T$. The cause of the instability may be due to the modelling of the boundary conditions at the ends of the wave surface.

In the numerical computational work conducted by Longuet-Higgins and Cokelet (1976), their computed wave profile, after about one period, developed a saw-toothed appearance. They removed this type of instability by applying a 5-point or 7-point smoothing formula to the profile after every 5 or 10 steps.

Although the instability that occured in this study did not appear to be saw-toothed, it was still hoped that the application of smoothing formula would reduce the instability in the wave profile. The formula used in 'BEMW1' was only the 5-point formula:

$$\bar{f}_j = \frac{1}{16}\left(-f_{j-2} + 4f_{j-1} + 10f_j + 4f_{j+1} - f_{j+2}\right) \quad (6.3.6)$$

This smoothing technique has been carried out on wave profiles of test problems 6.3.9 every 10 time steps. By comparing Fig. 6.3.4 and 6.3.9 , it is concluded that the smoothing technique does reduce the instability and prolong the duration of the wave movement by about 35% in this type of test problems.

One of the basic assumptions made in section 5.2 was that the wave profile assumed the equation of simple harmonic motion, i.e.:

$$\eta = a \cdot \cos\ (kx - \sigma t) \tag{6.3.7}$$

which is a first order equation and acceptable to model finite amplitude waves but not steep waves ($H/\lambda > 0.07$). When the modelled profile has started from the initial condition, it will have the tendency to alter its shape towards a real wave, i.e. peak at the crest and flatten out at the trough. The change in shape then follows with the relative wave height being altered to a bigger value. From Figs. 6.3.2 the wave height has increased by 20% after 1 period. By the same arguement, a wave profile with wave steepness H/λ = 0.1 would try to break after 0.6 of a period, (see Fig. 6.3.10). The exact nature of this behaviour remains unknown.

From Figs. 6.3.10, one may immediately discover that the proposed technique could not cope with a breaking wave. The reason behind this incapability may be explained by the well known behaviour of re-entrant corners, as discussed in chapter 4. When a wave profile attempts to break, a re-entrant corner immediately develops such that the solution in the region of wave breaking is subjected to numerical instability which occurs well before the expected wave breaking.

Longuet-Higgins and Cokelet (1976) obtained their initial set of data for a symmetric, progressive wave of finite amplitude in deep water by using the perturbation technique developed by Schwartz (1974) . It is a very accurate method of computing the wave profile, based on Stokes's expansion. They demonstrated that their numerical wave profile after one period compared favourably with the profile of a steady wave calculated from Stokes's series.

Due to the difference in data specification between Longuet-Higgins and Cokelet's approach and the present study, higher order wave equations for η and ϕ were tried to see if that would retain constant wave steepness throughout the wave motion. 1st , 2nd and 3rd order equations were carried out and their results are shown in Figs. 6.3.2, 6.3.6, 6.3.7 respectively. From these figures, the percentage increase in wave height for the 2nd order wave was about 10% and for the 3rd order wave, the wave height remained the same. It must be pointed out that the initial wave heights for the 1st , 2nd and 3rd order equations were the same. It is therefore concluded that for a steep wave, higher order equations for the initial wave profile are desirable, but it would not reduce the instability nor allow the wave to run for a longer duration.

Finally, test problem 6.3.11 for a standing wave without an obstacle have also been carried out and the result is shown in Figs. 6.3.11. The profile ran up to $t = 2.342T$, and then stopped because the number of loops specified was achieved. A plot of the variations between kinetic energy and potential energy is shown in Fig. 6.3.11d. Total energy increases gradually as the wave moves. Variation of $\frac{\partial\phi}{\partial n}$ with time is plotted for an end node of the wave profile. It can be seen that $\frac{\partial\phi}{\partial n}$ behaves very well in a periodic manner.

TEST PROBLEM	FIGURE	WAVE HEIGHT H (m)	WAVE LENGHT λ (m)	WAVE STEEPNESS (H/λ)	WATER DEPTH	ORDER OF EQ	SMOOT-HING	TIME STEP (SEC)	LOOPS EXECUTED	WAVE LAPSED	COMPUTER RUN TIME	REMARK
6.3.1	6.3.1	0.112	1.595	0.0703	0.555	1	NO	0.037	235	1.379T	0.2366	FAILED BY ϕ OR $d\phi/dn$ > 50.0
6.3.2	6.3.2	0.112	1.595	0.0703	0.555	1	NO	0.050	181	1.414T	0.1893	FAILED BY ϕ OR $d\phi/dn$ > 50.0
6.3.3	6.3.3	0.112	1.595	0.0703	0.555	1	NO	0.060	147	1.376T	0.1514	FAILED BY ϕ OR $d\phi/dn$ > 50.0
6.3.4	6.3.4	0.112	1.595	0.0703	0.555	1	NO	0.075	118	1.377T	0.1237	FAILED BY ϕ OR $d\phi/dn$ > 50.0
6.3.5	6.3.5	0.112	1.595	0.0703	0.555	1	NO	0.150	26	0.589T	0.0309	FAILED BY ϕ OR $d\phi/dn$ > 50.0
6.3.6	6.3.6	0.112	1.595	0.0703	0.555	2	NO	0.050	174	1.359T	0.1805	FAILED BY ϕ OR $d\phi/dn$ > 50.0
6.3.7	6.3.7	0.112	1.595	0.0703	0.555	3	NO	0.050	180	1.406T	0.1847	FAILED BY ϕ OR $d\phi/dn$ > 50.0
6.3.8	6.3.8	0.072	1.595	0.0460	0.555	1	NO	0.062	223	2.226T	0.2363	FAILED BY ϕ OR $d\phi/dn$ > 50.0
6.3.9	6.3.9	0.112	1.595	0.0703	0.555	1	YES	0.075	159	1.860T	0.2267	FAILED BY ϕ OR $d\phi/dn$ > 50.0
6.3.10	6.3.10	0.112	1.595	0.1000	0.555	1	NO	0.042	116	0.758T	0.1572	FAILED BY ϕ OR $d\phi/dn$ > 50.0
6.3.11	6.3.11	0.112	1.595	0.0703	0.555	1	NO	0.075	200	2.342T	0.2038	NATURAL STOP

TABLE 6.3.1 TEST PROBLEMS OF WAVE WITHOUT OBSTACLE

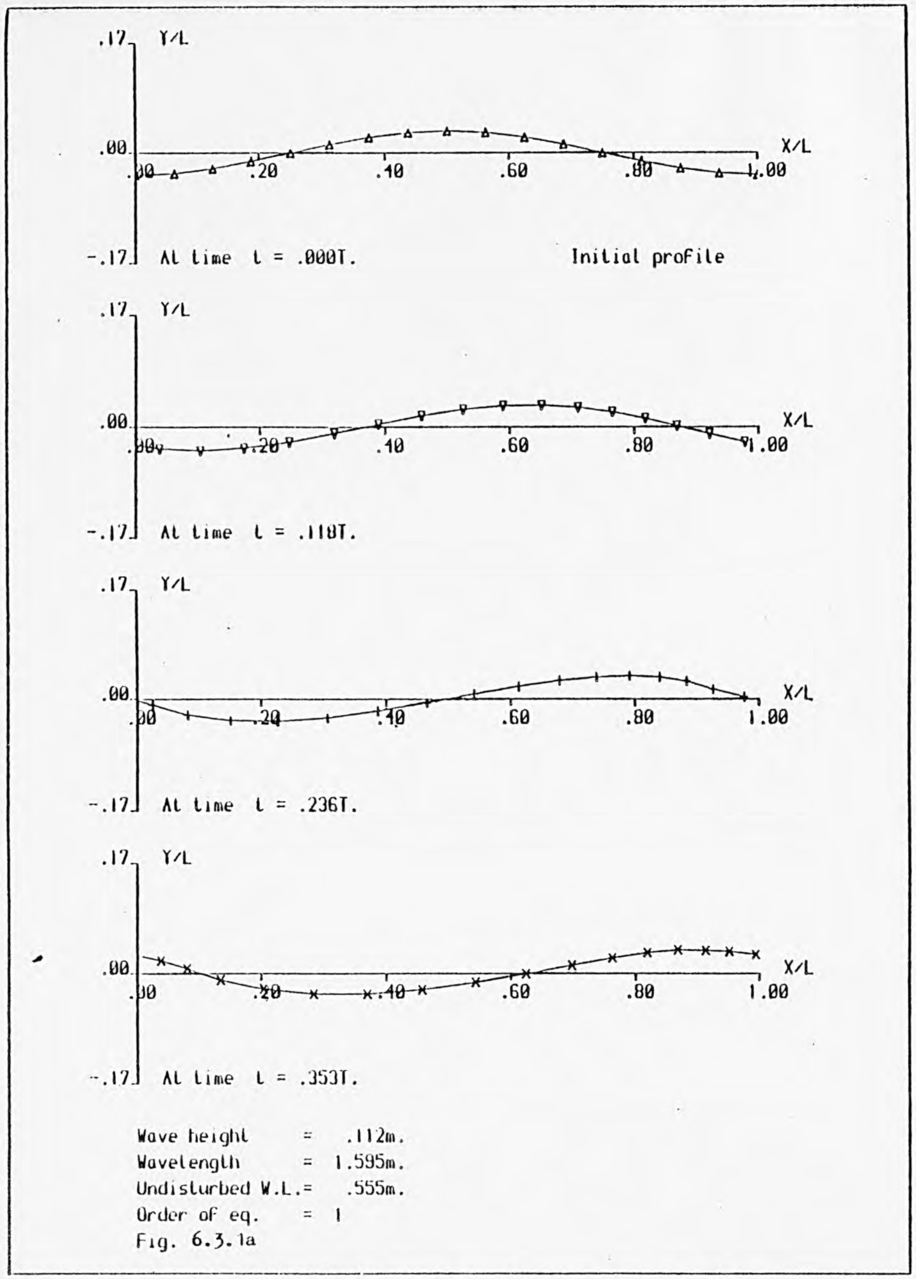

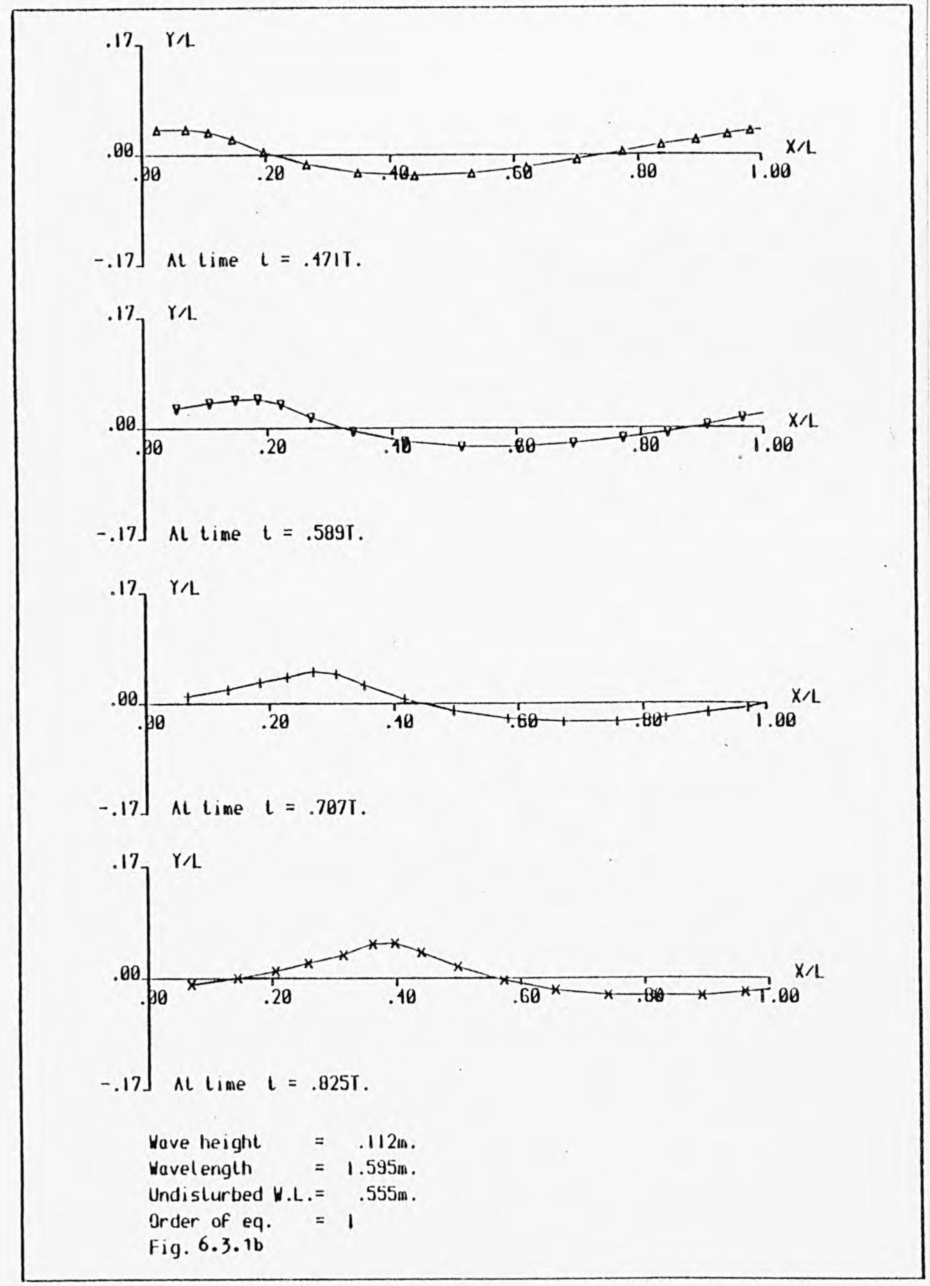

Fig. 6.3.1(a-c) A time sequence of wave profiles for test problem 6.3.1

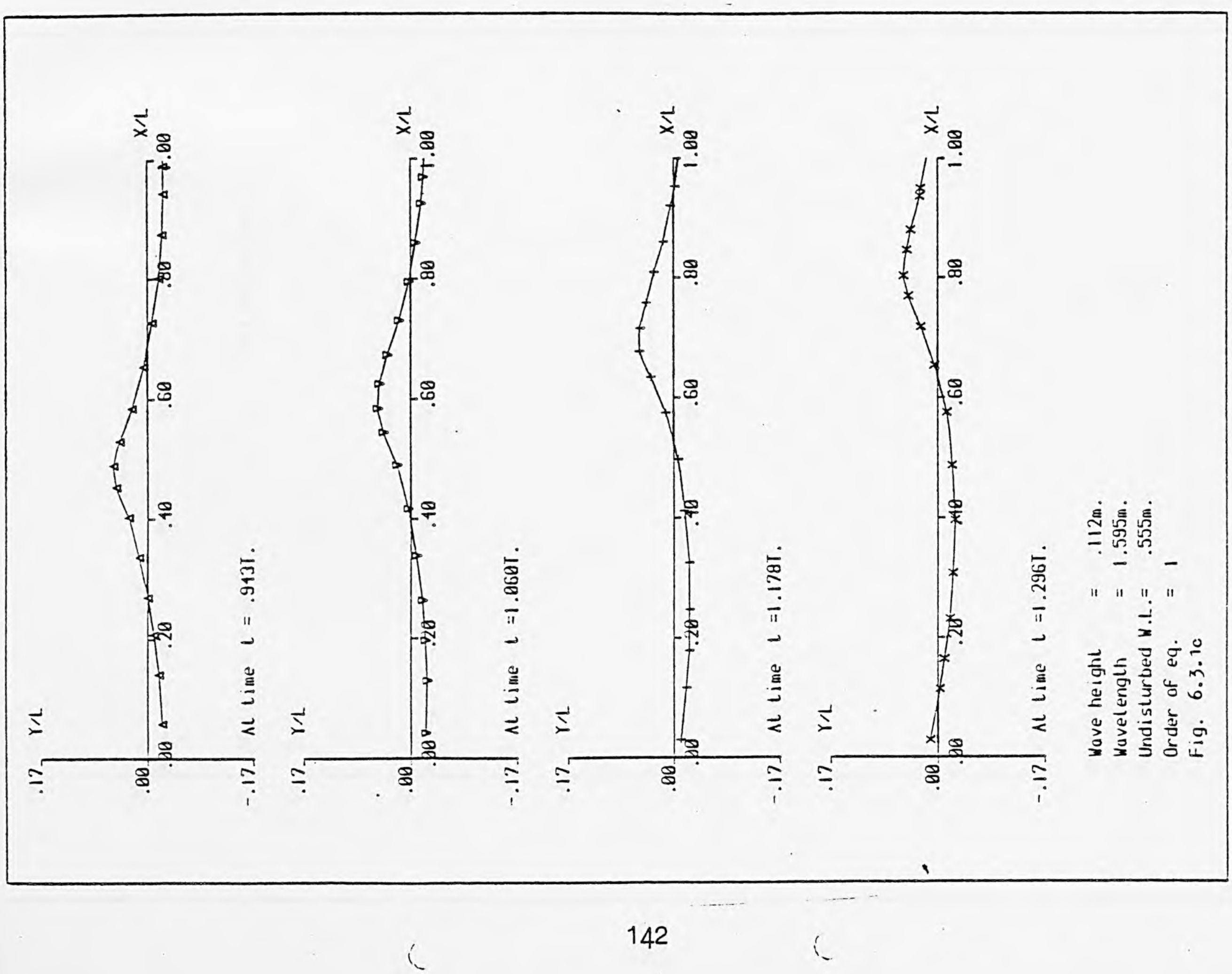
Y/L
X/L
.17
.00
-.17
.00
.20
.40
.60
.80
1.00
At time t = .913T.
At time t =1.060T.
At time t =1.178T.
At time t =1.296T.
Wave height = .112m.
Wavelength = 1.595m.
Undisturbed W.L.= .555m.
Order of eq. = 1

Fig. 6.3.1c

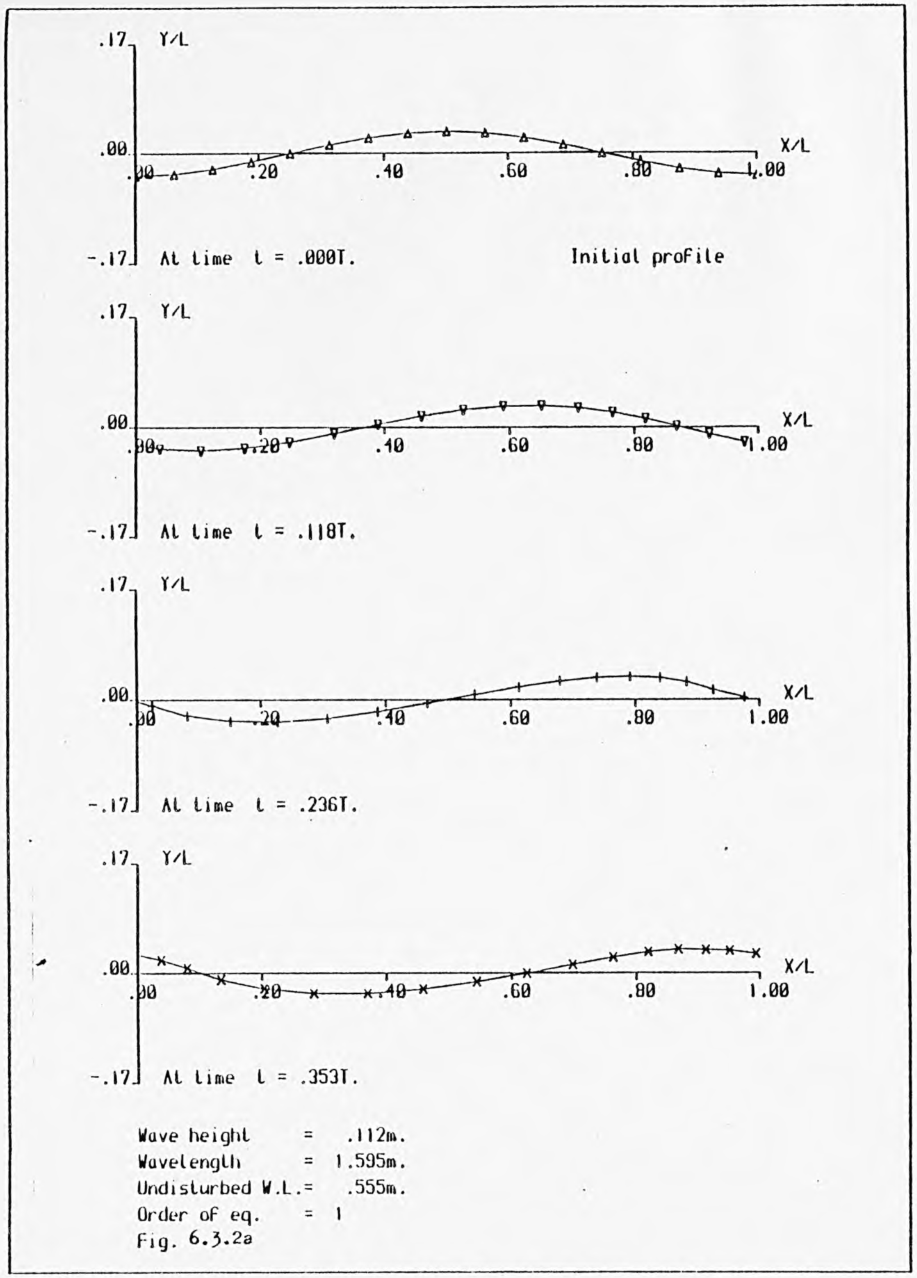

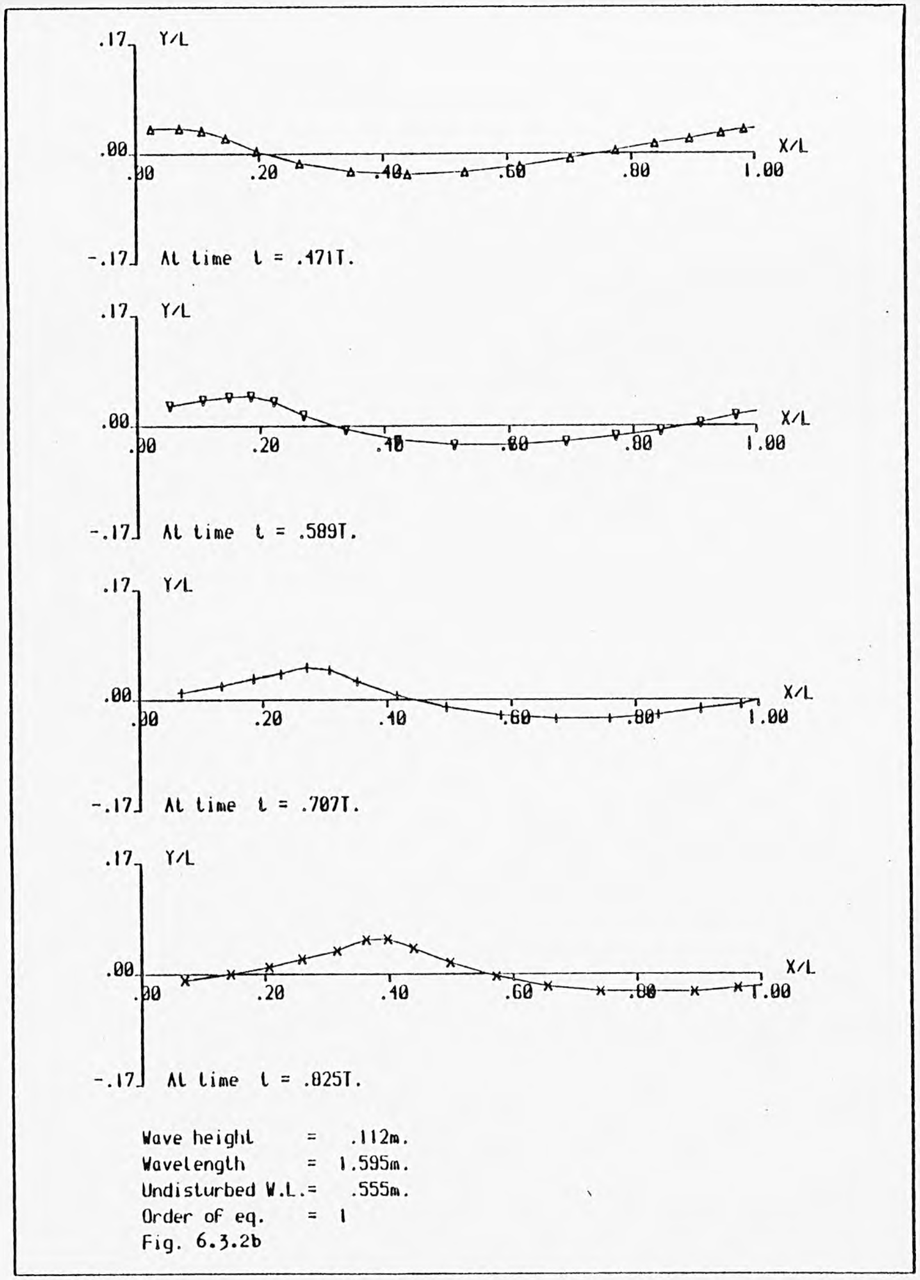

Fig. 6.3.2(a-d) A time sequence of wave profiles for test problem 6.3.2

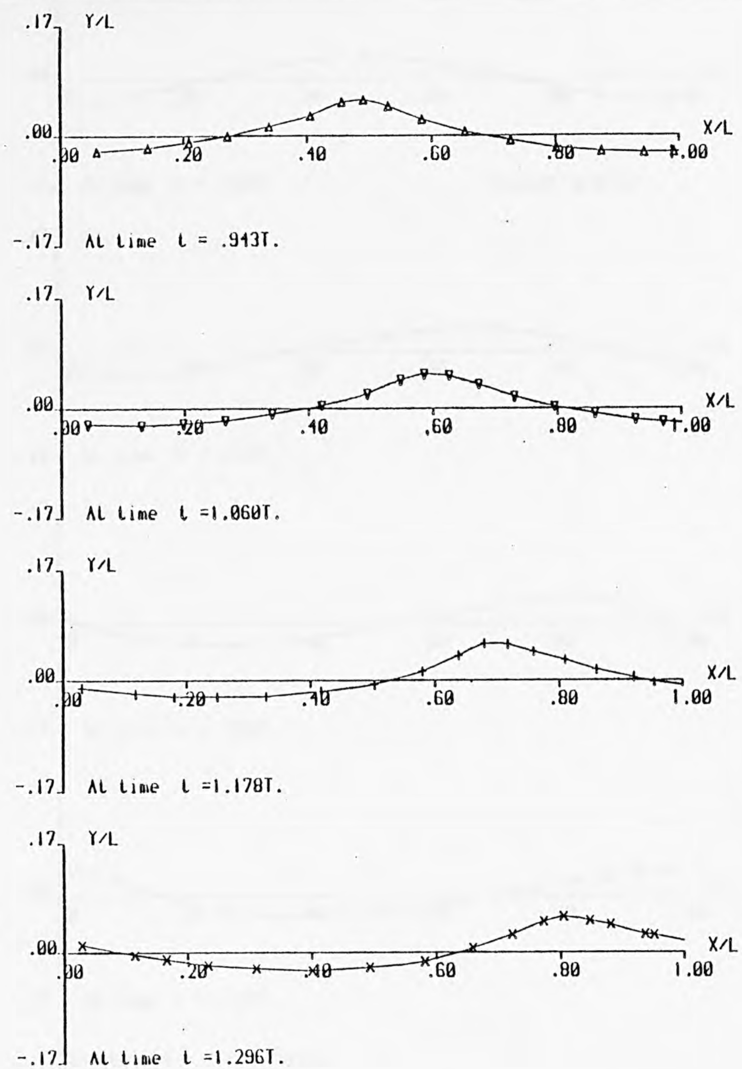

Wave height = .112m.
Wavelength = 1.595m.
Undisturbed W.L.= .555m.
Order of eq. = 1
Fig. 6.3.2c

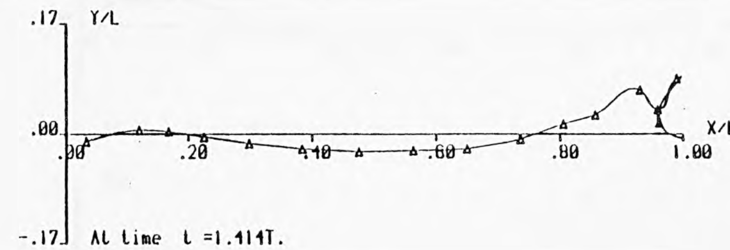

Wave height = .112m.
Wavelength = 1.595m.
Undisturbed W.L.= .555m.
Order of eq. = 1
Fig. 6.3.2d

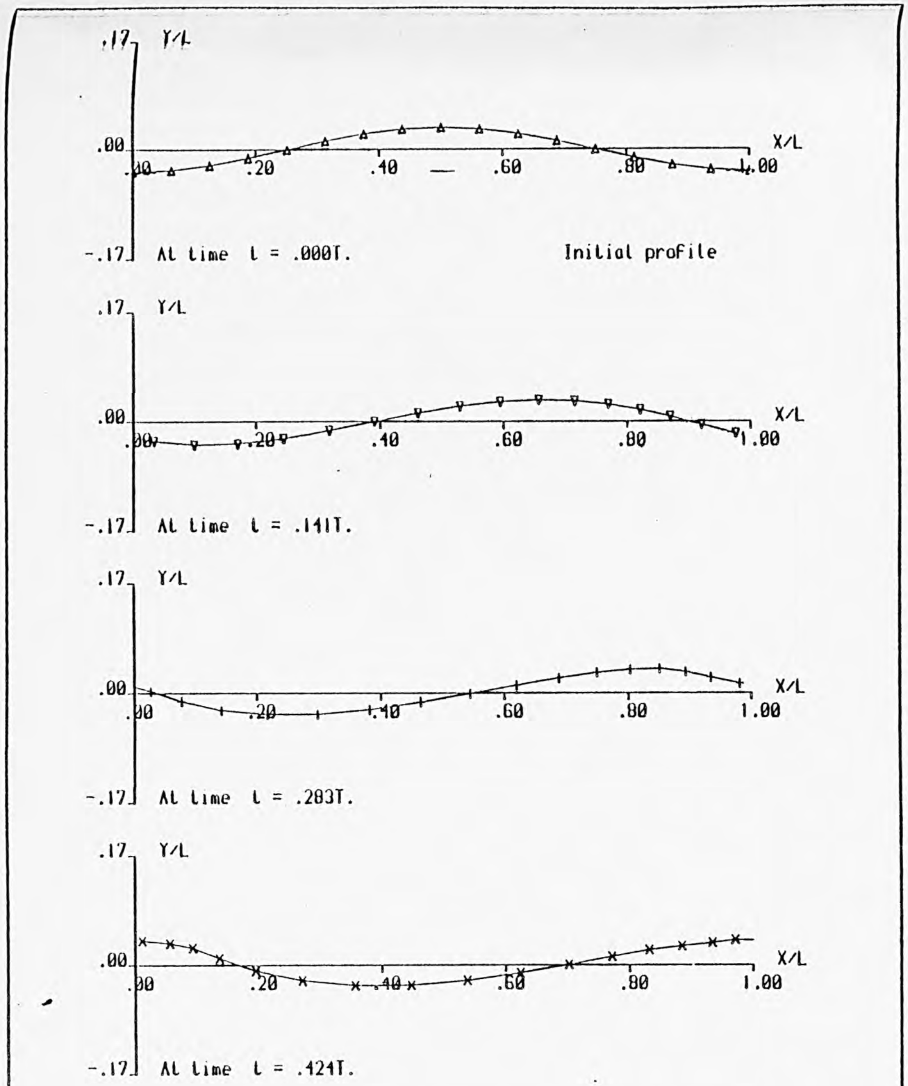

Wave height = .112m.
Wavelength = 1.595m.
Undisturbed W.L.= .555m.
Order of eq. = 1
Fig. 6.3.3a

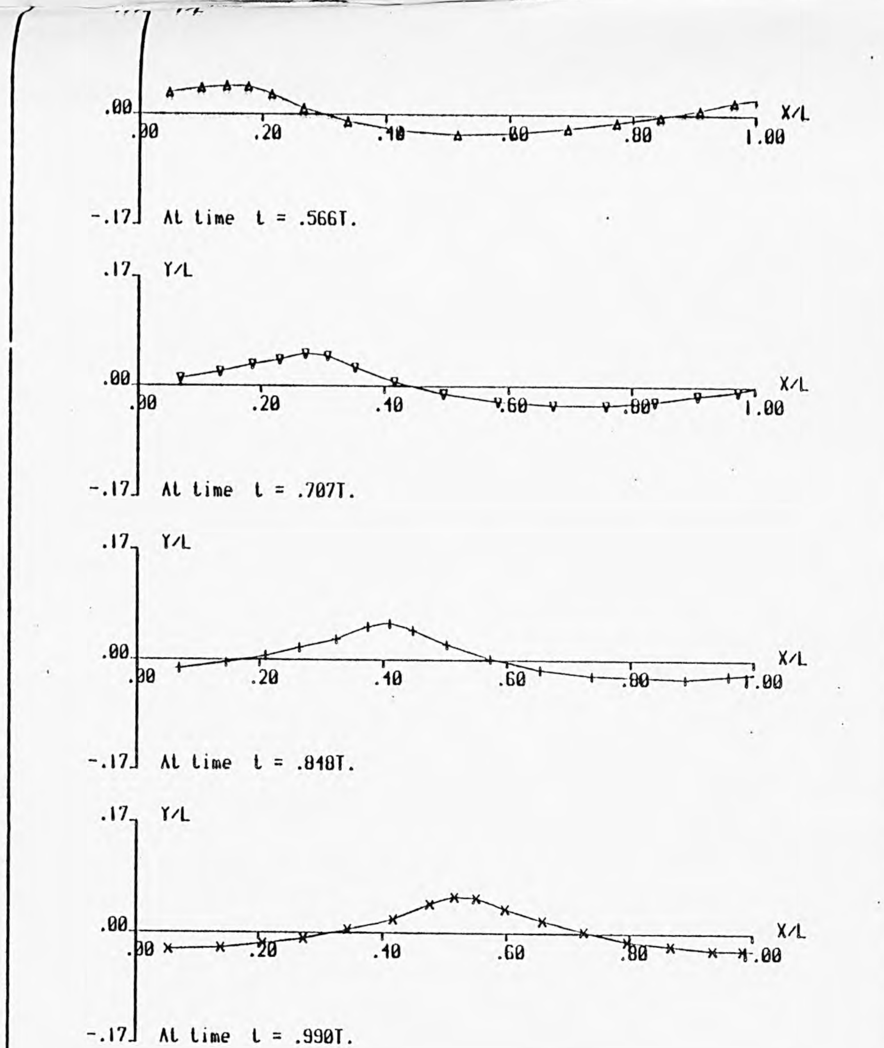

Wave height = .112m.
Wavelength = 1.595m.
Undisturbed W.L.= .555m.
Order of eq. = 1
Fig. 6.3.3b

Fig. 6.3.3(a-c) A time sequence of wave profiles for test problem 6.3.3

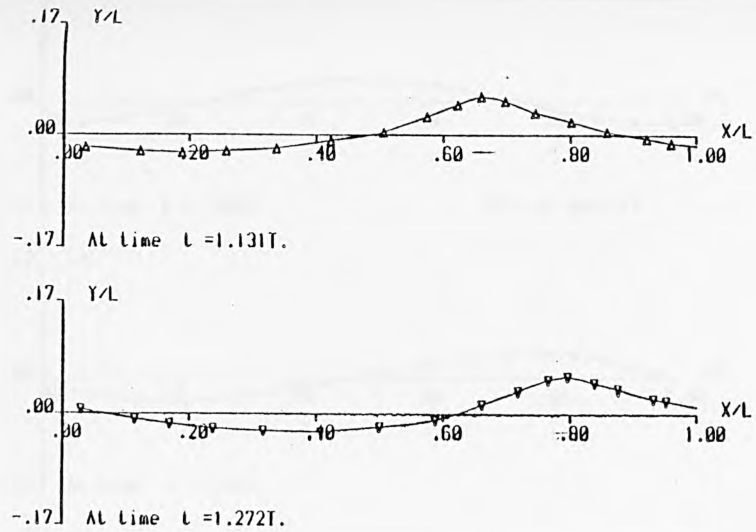

Wave height = .112m.
Wavelength = 1.595m.
Undisturbed W.L.= .555m.
Order of eq. = 1

Fig. 6.3.3c

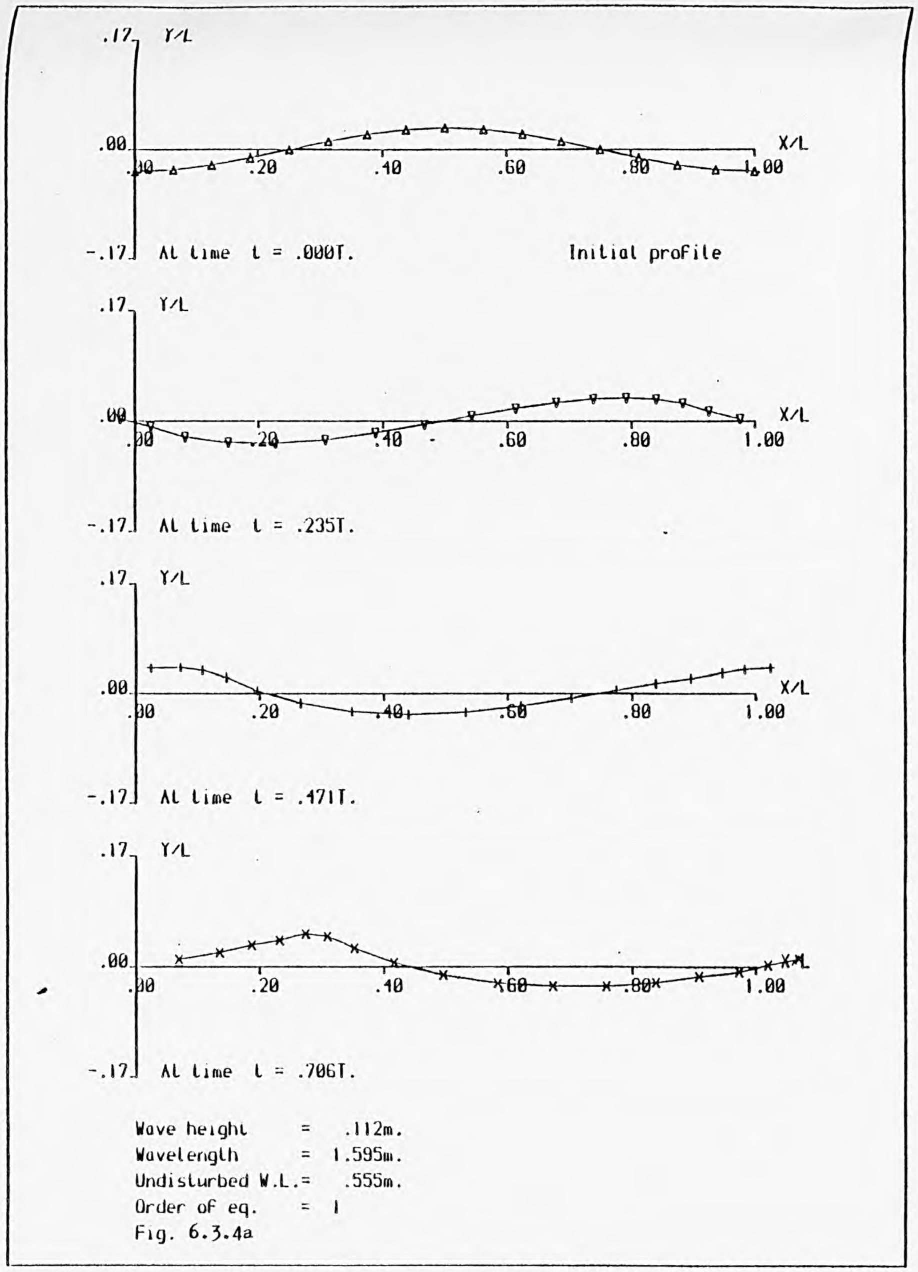

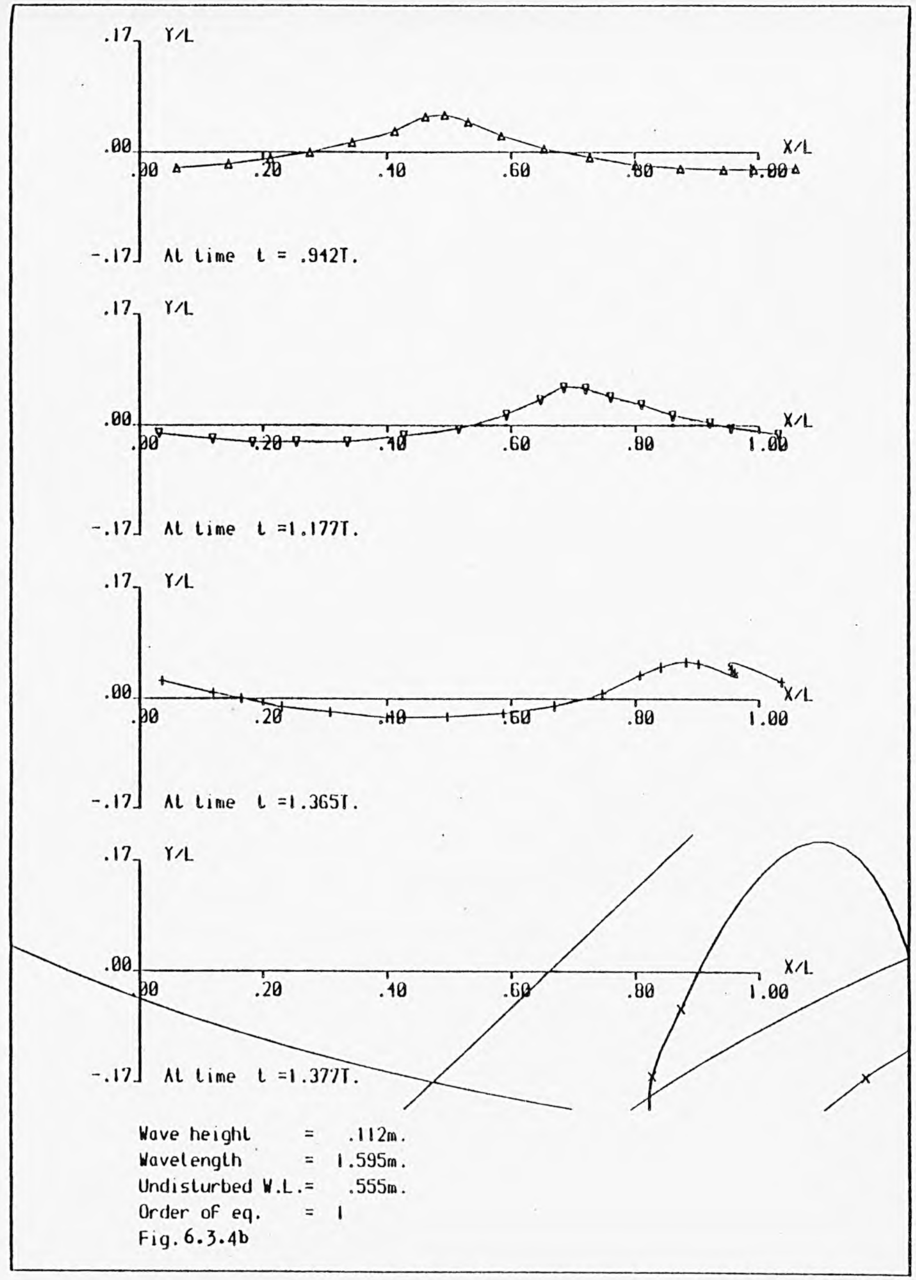

Fig. 6.3.4(a-b) A time sequence of wave profiles for test problem 6.3.4

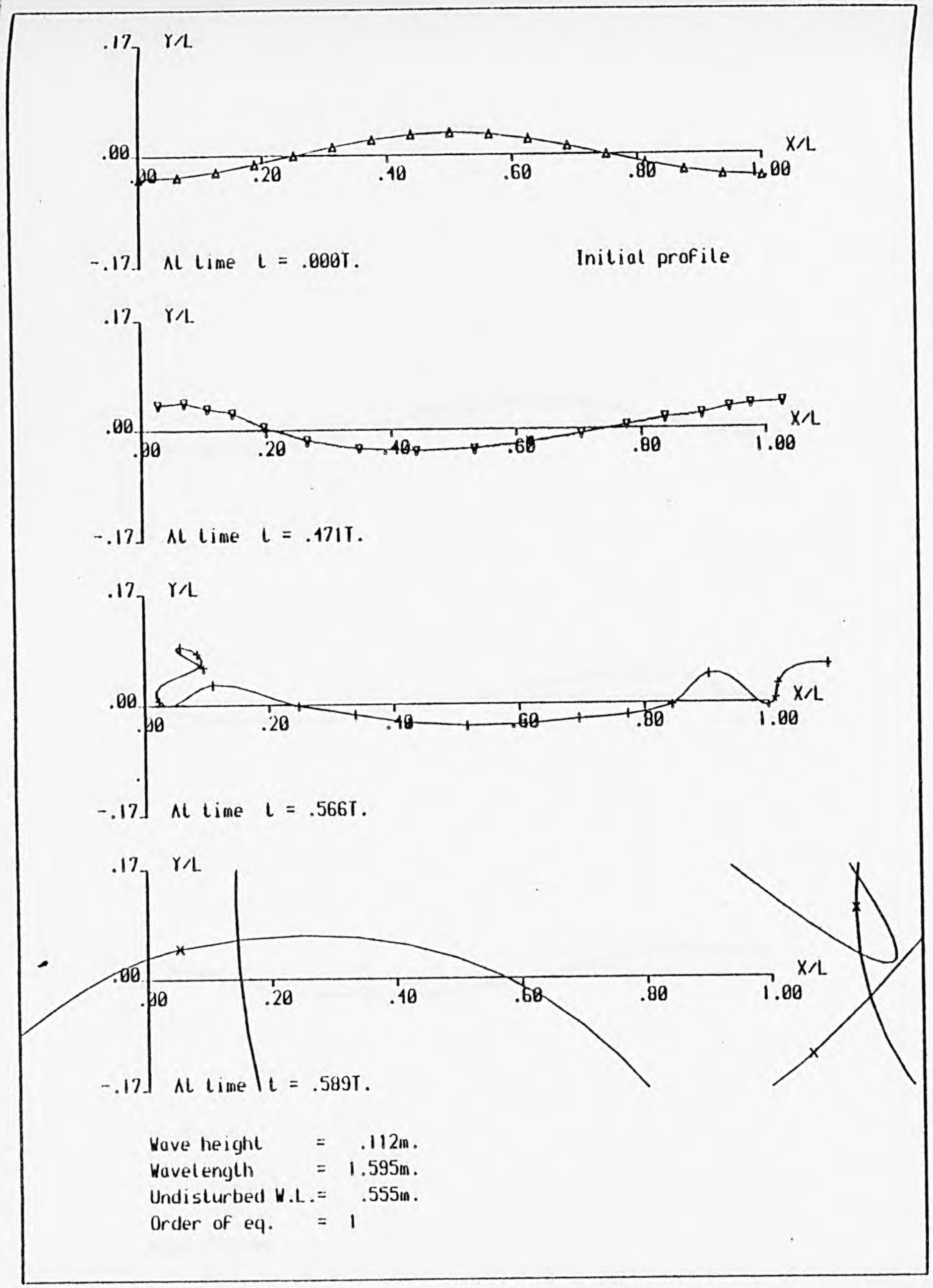

Fig. 6.3.5 A time sequence of wave profiles for test problem 6.3.5

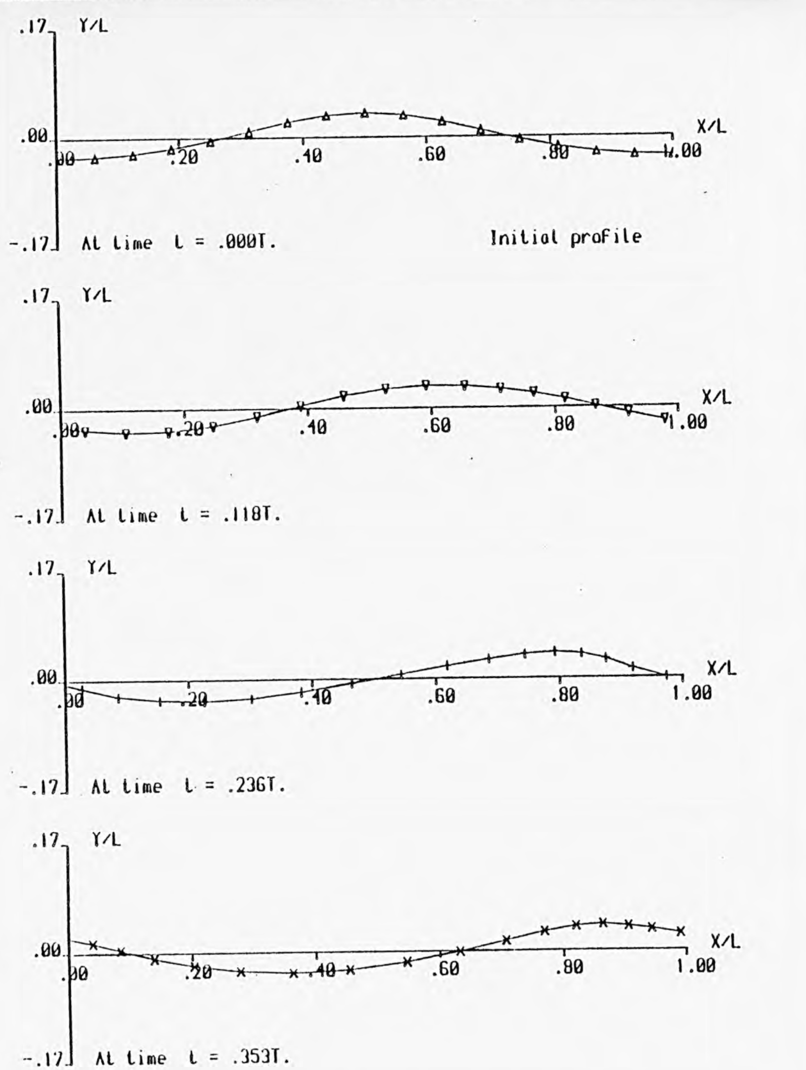

Wave height = .112m.
Wavelength = 1.595m.
Undisturbed W.L.= .555m.
Order of eq. = 2
Fig. 6.3.6a

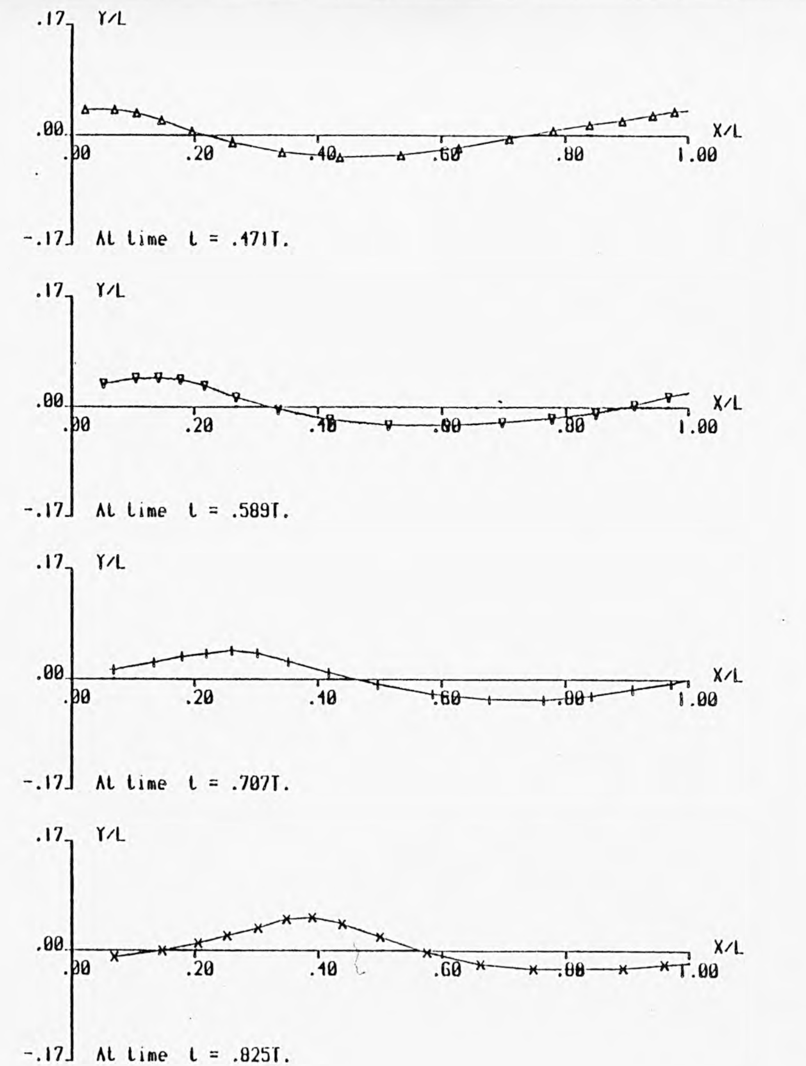

Wave height = .112m.
Wavelength = 1.595m.
Undisturbed W.L.= .555m.
Order of eq. = 2
Fig.6.3.6b

Fig. 6.3.6(a-c) A time sequence of wave profiles for test problem 6.3.6

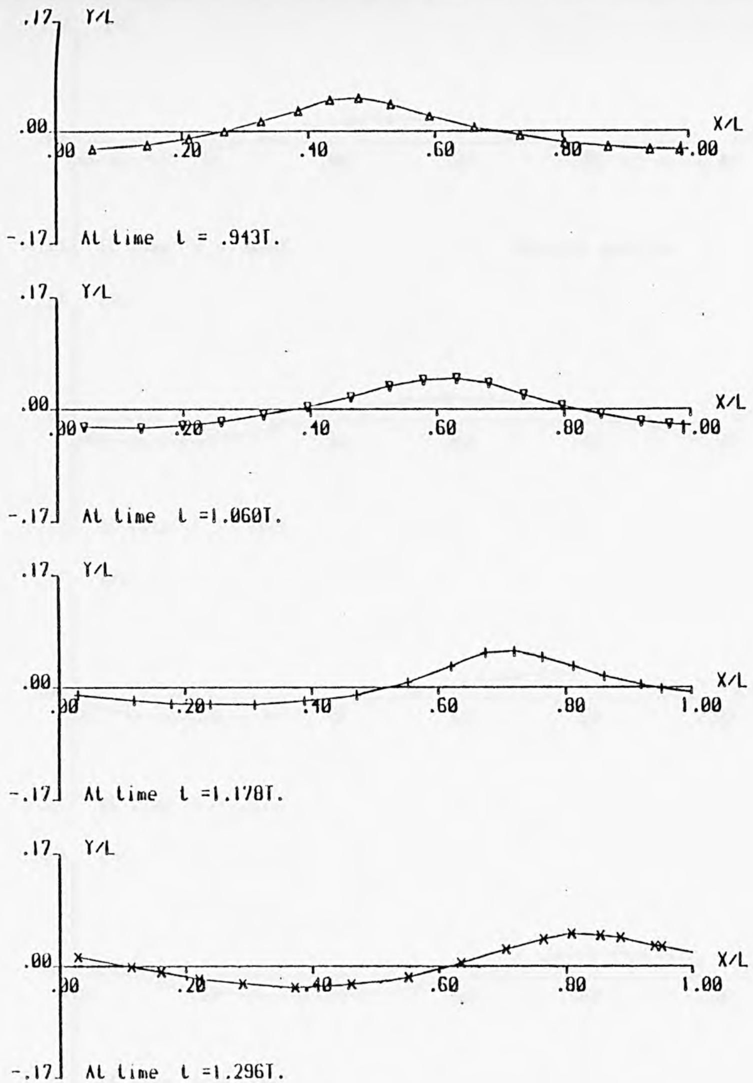

Wave height = .112m.
Wavelength = 1.595m.
Undisturbed W.L.= .555m.
Order of eq. = 2
Fig. 6.3.6c

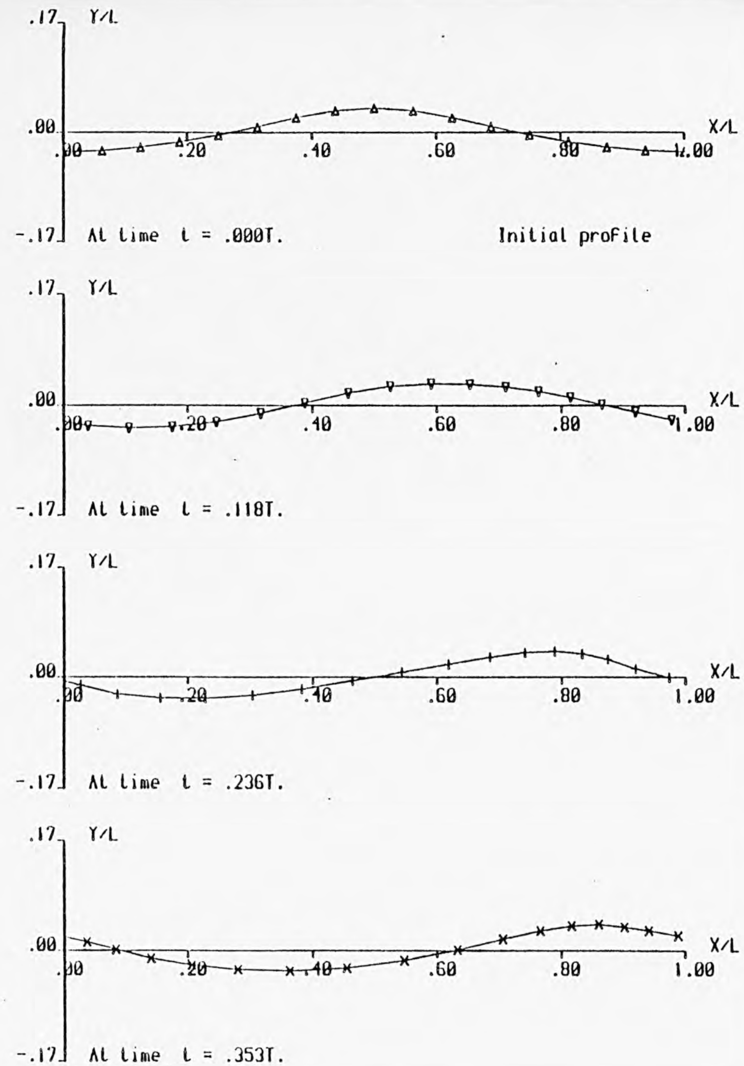

Wave height = .112m.
Wavelength = 1.595m.
Undisturbed W.L.= .555m.
Order of eq. = 3
Fig. 6.3.7a

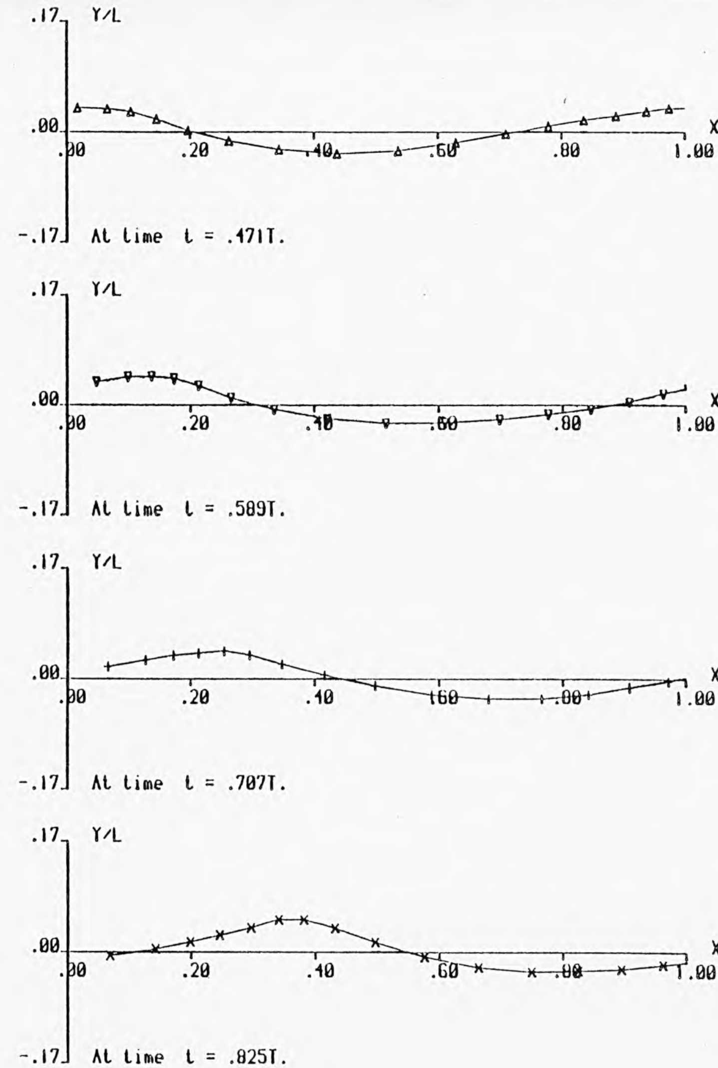

Wave height = .112m.
Wavelength = 1.595m.
Undisturbed W.L.= .555m.
Order of eq. = 3
Fig. 6.3.7b

Fig. 6.3.7(a-c) A time sequence of wave profiles for test problem 6.3.7

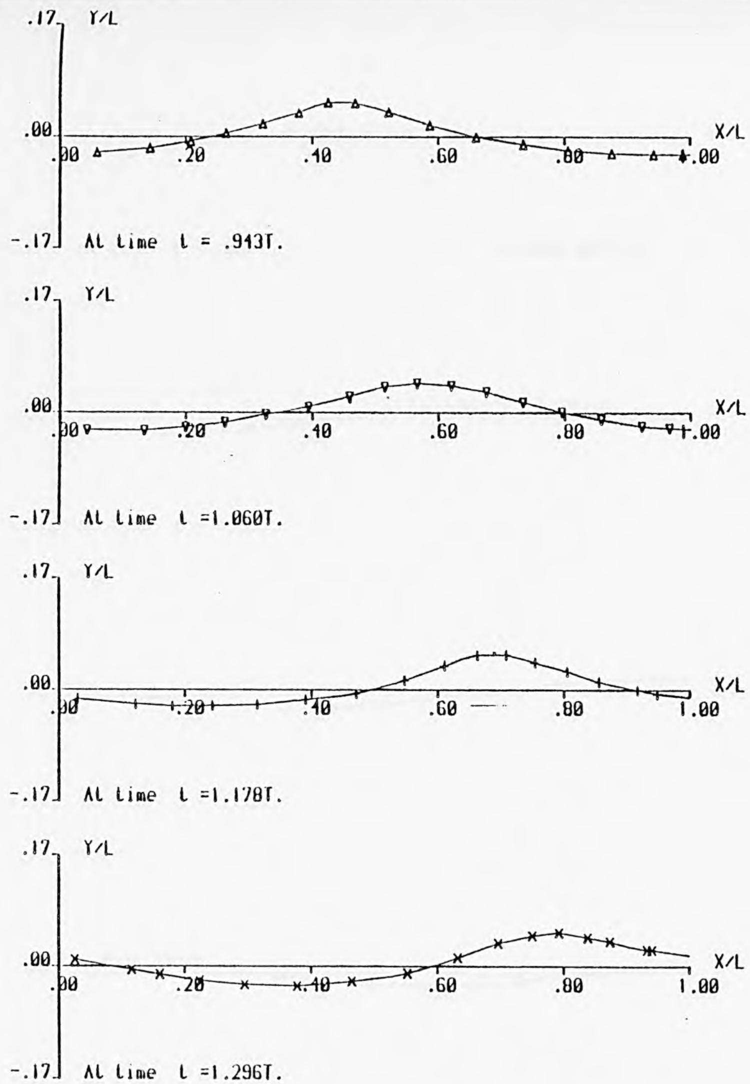

Wave height = .112m.
Wavelength = 1.595m.
Undisturbed W.L.= .555m.
Order of eq. = 3
Fig. 6.3.7c

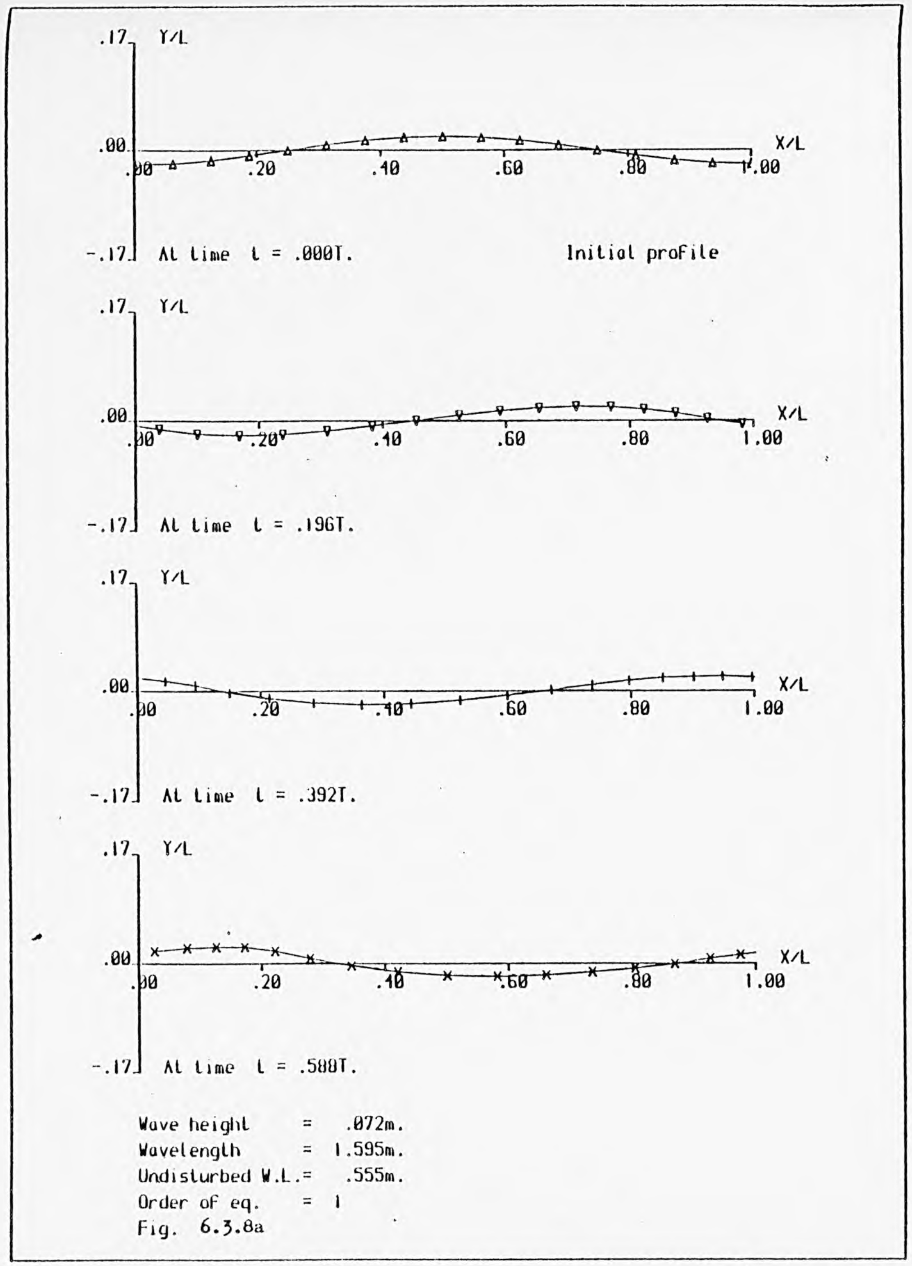

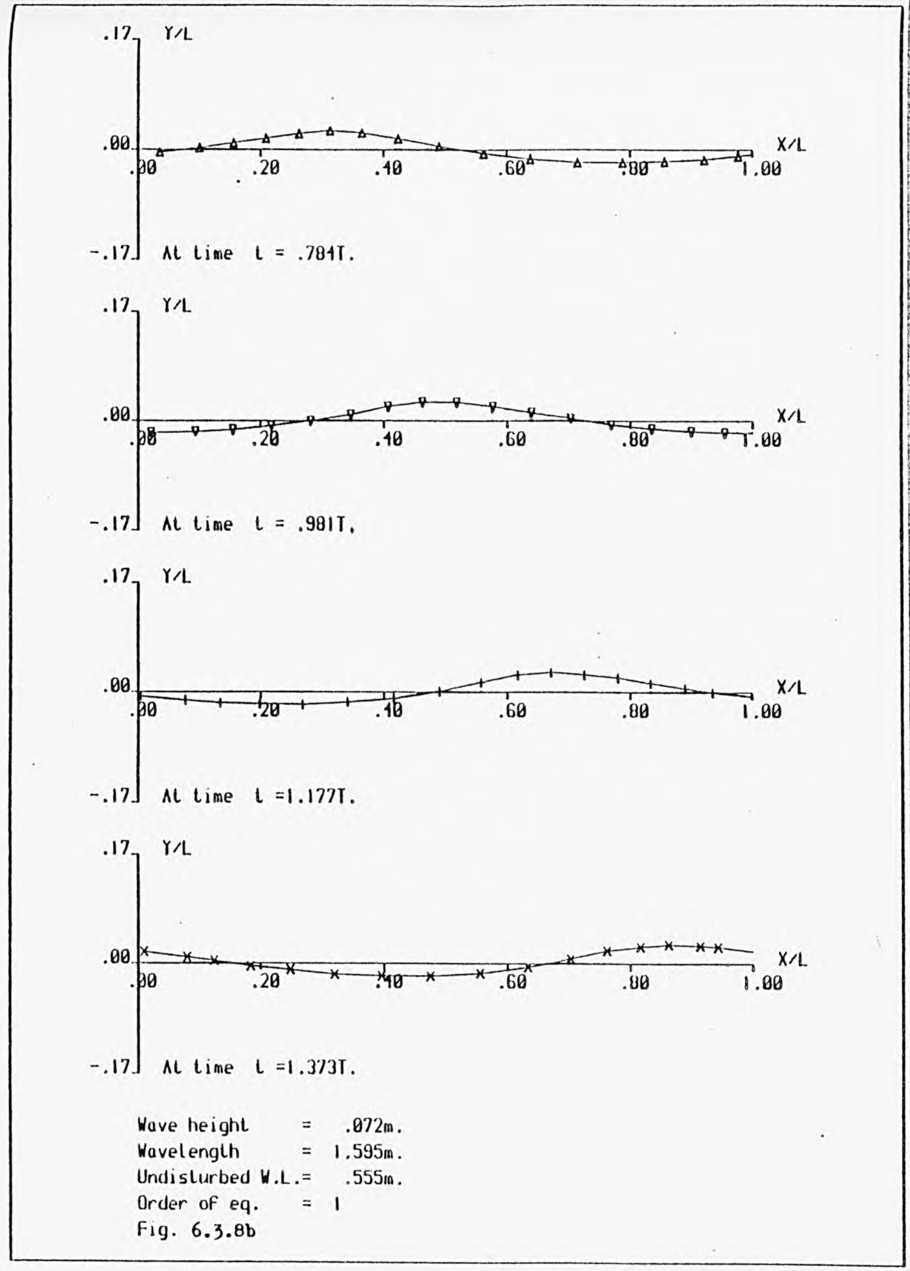

Fig. 6.3.8(a-c) A time sequence of wave profiles for test problem 6.3.8

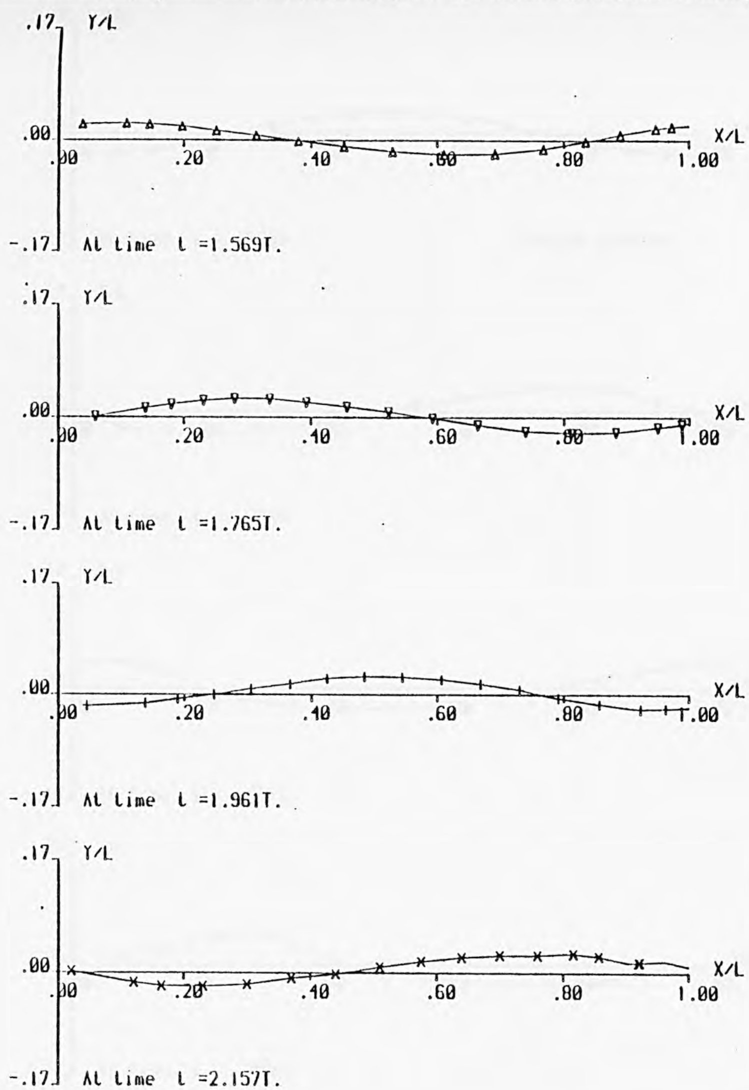

Wave height = .072m.
Wavelength = 1.595m.
Undisturbed W.L.= .555m.
Order of eq. = 1
Fig 6.3.8c

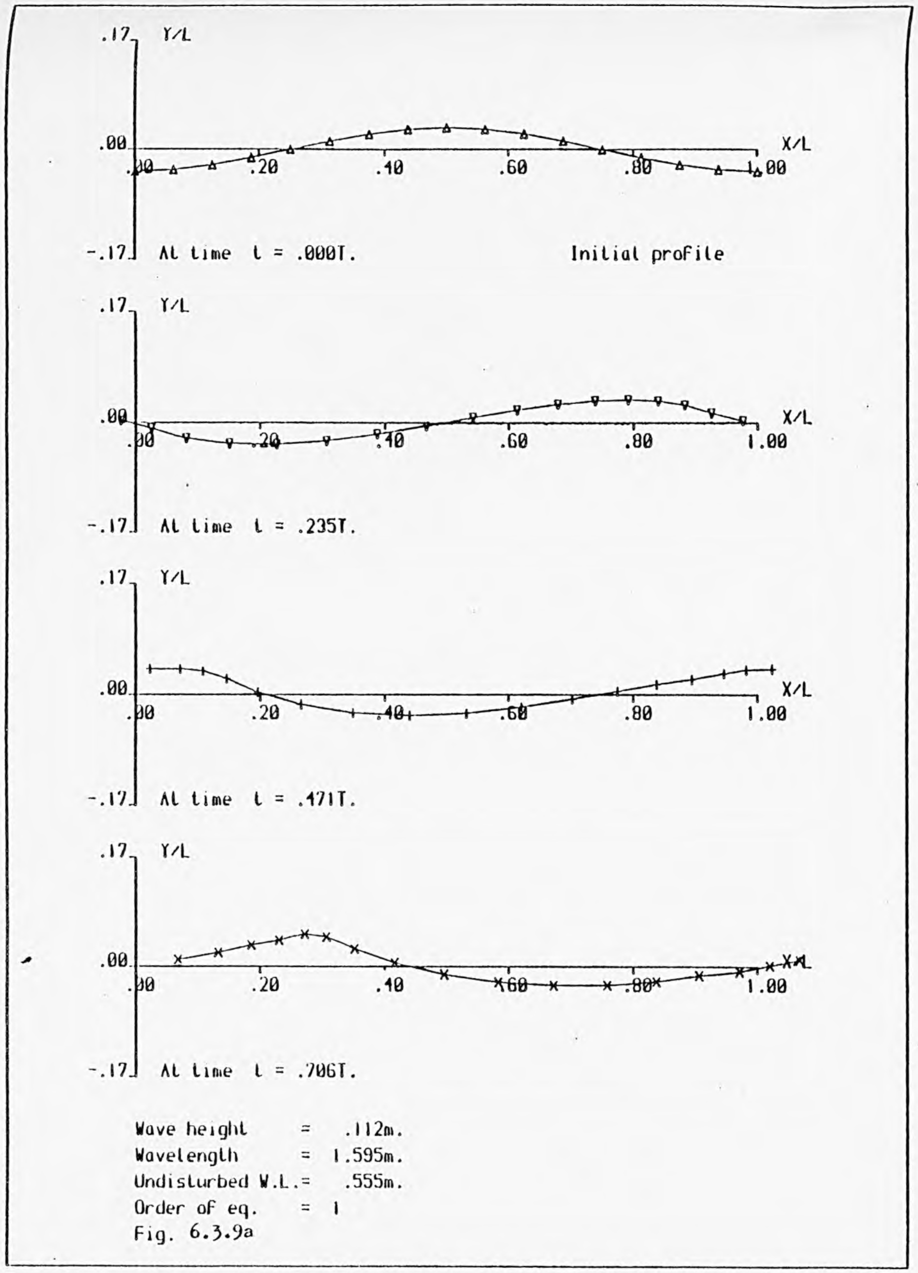

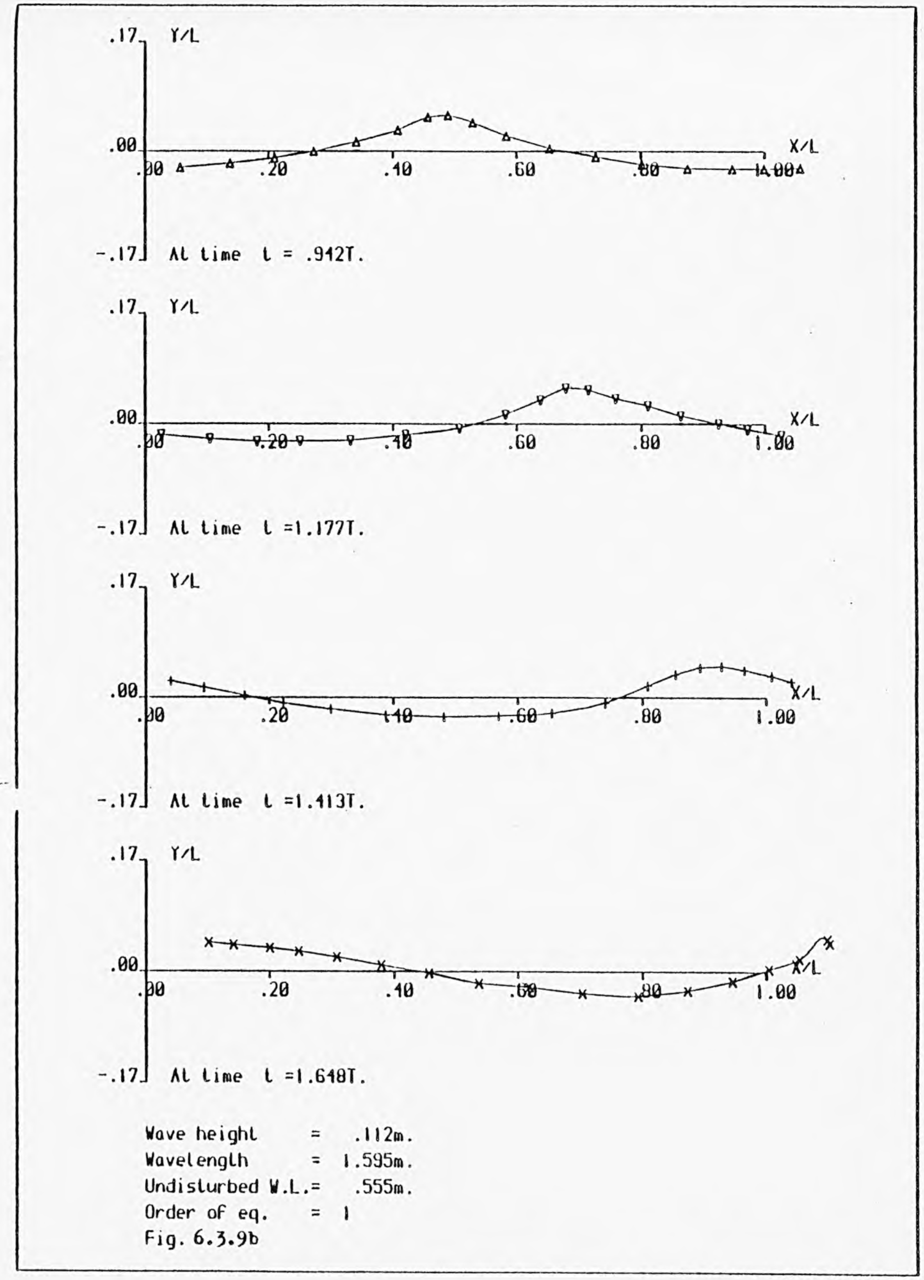

Fig. 6.3.9(a-c) A time sequence of wave profiles for test problem 6.3.9

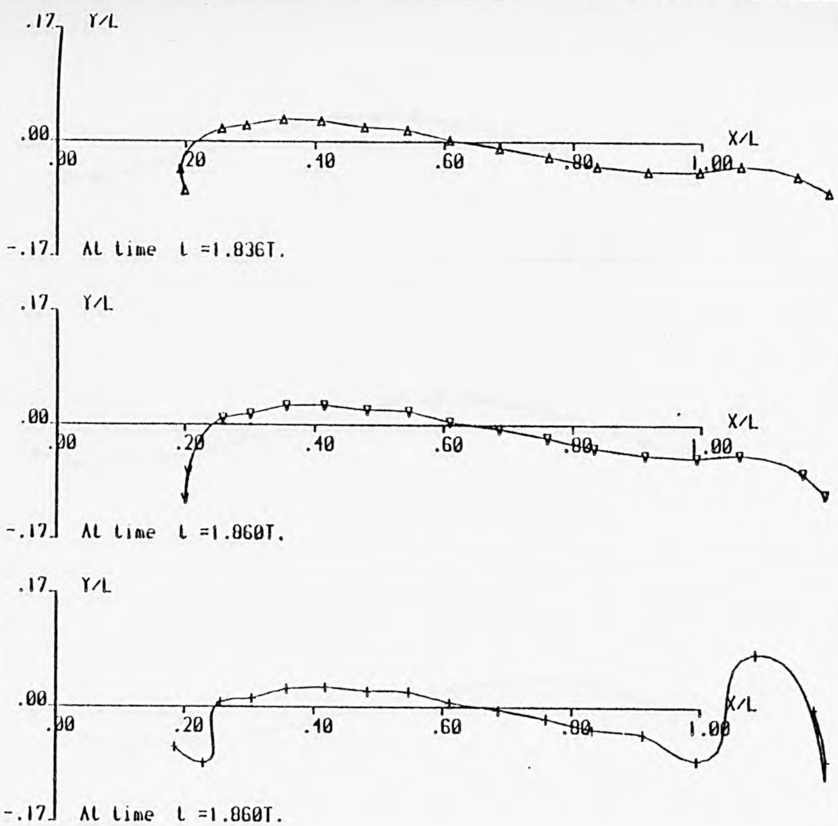

Wave height = .112m.
Wavelength = 1.595m.
Undisturbed W.L.= .555m.
Order of eq. = 1
Fig. 6.3.9c

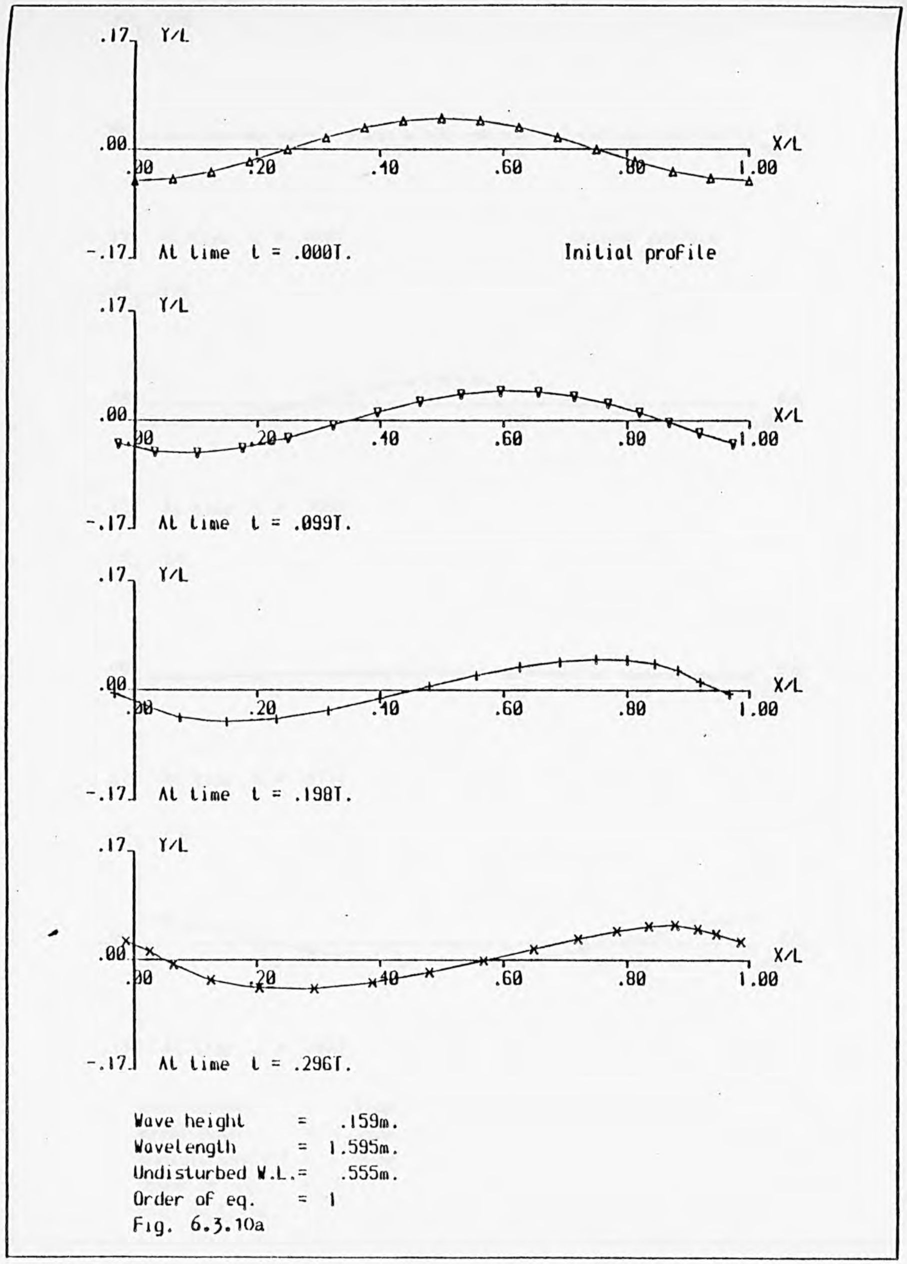

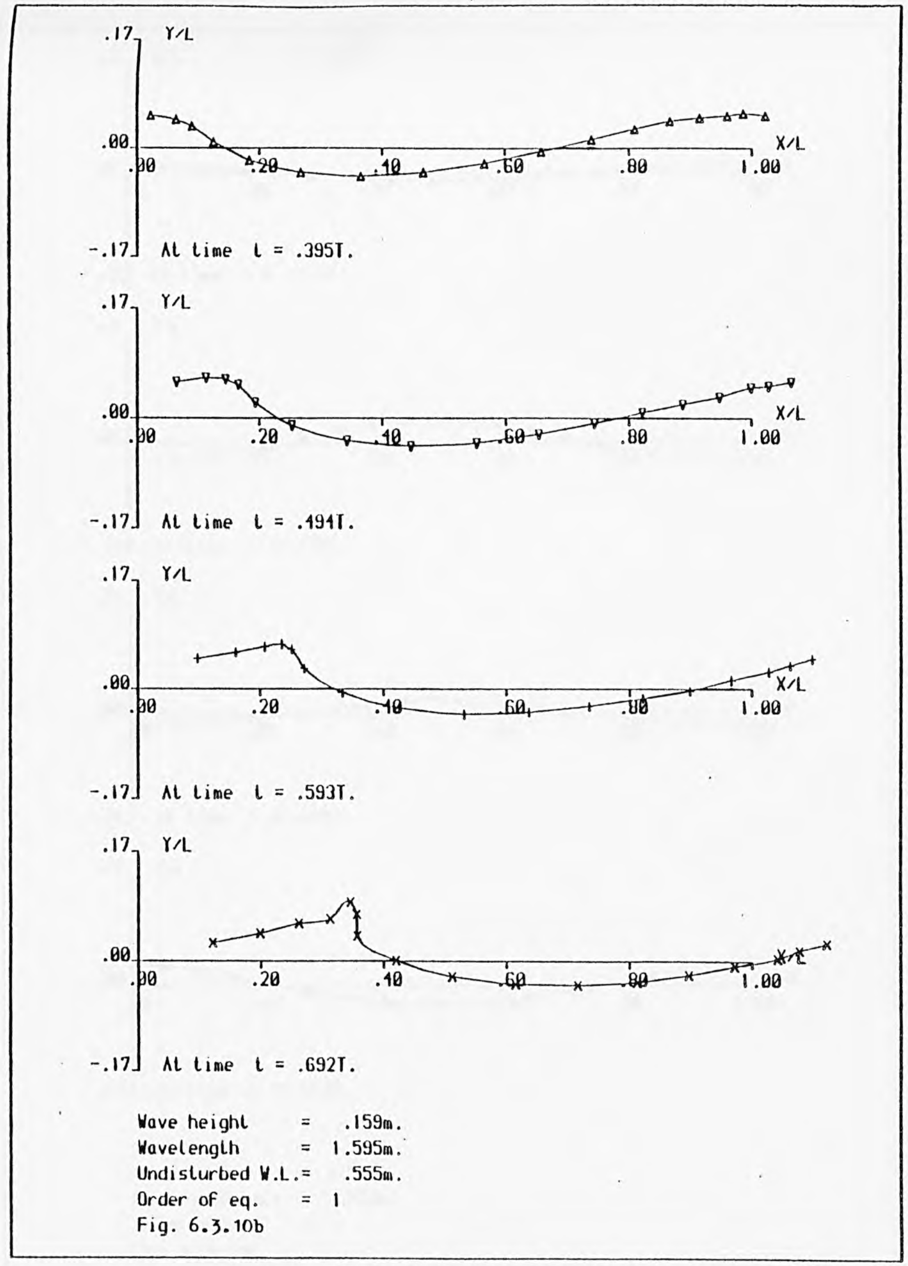

Fig. 6.3.10(a-b) A time sequence of wave profiles for test problem 6.3.10

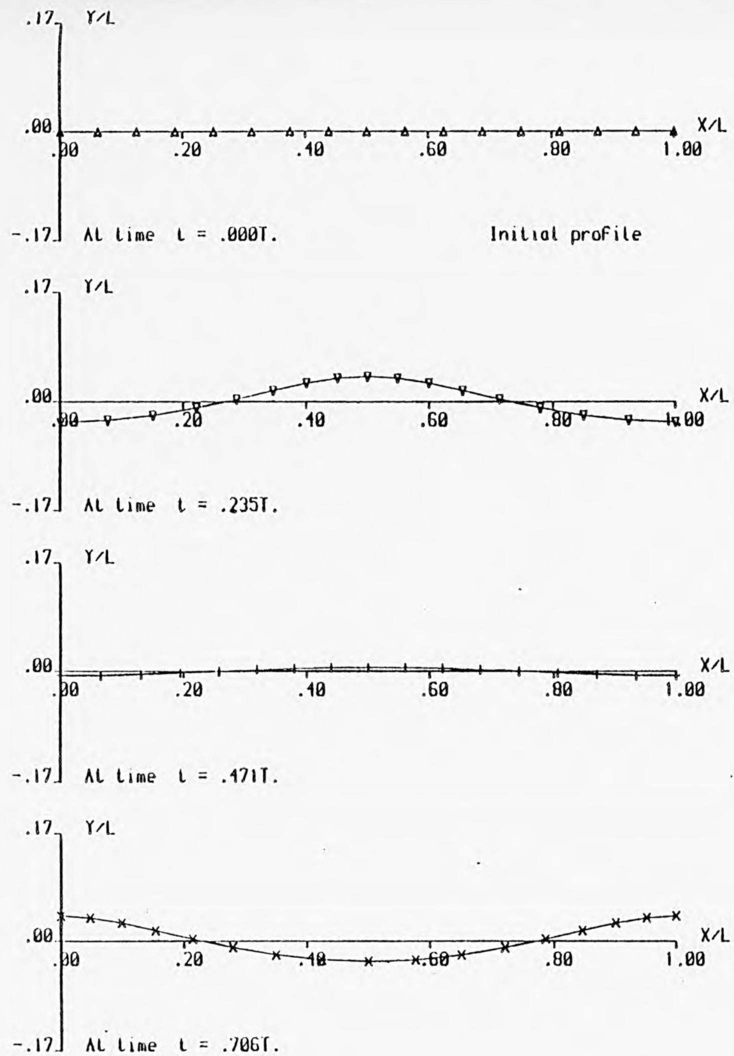

Wave height = .112m.
Wavelength = 1.595m.
Undisturbed W.L.= .555m.
Order of eq. = 1
Fig. 6.3.11a

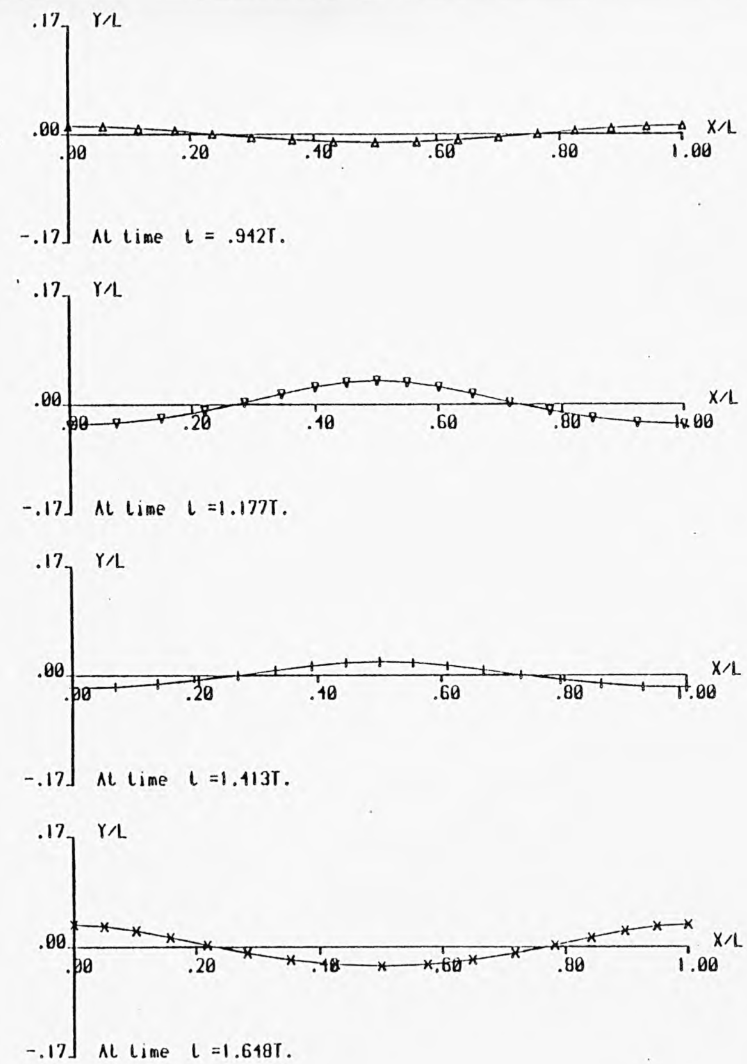

Wave height = .112m.
Wavelength = 1.595m.
Undisturbed W.L.= .555m.
Order of eq. = 1
Fig. 6.3.11b

Fig. 6.3.11(a-d) A time sequence of wave profiles for test problem 6.3.11

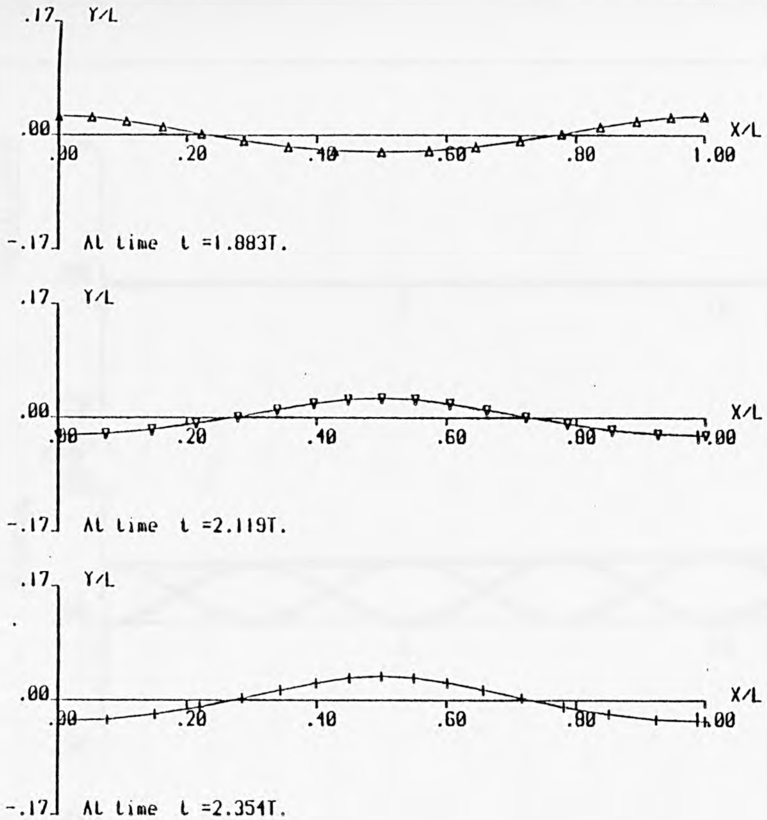

Wave height = .112m.
Wavelength = 1.595m.
Undisturbed W.L.= .555m.
Order of eq. = 1

Fig. 6.3.11c

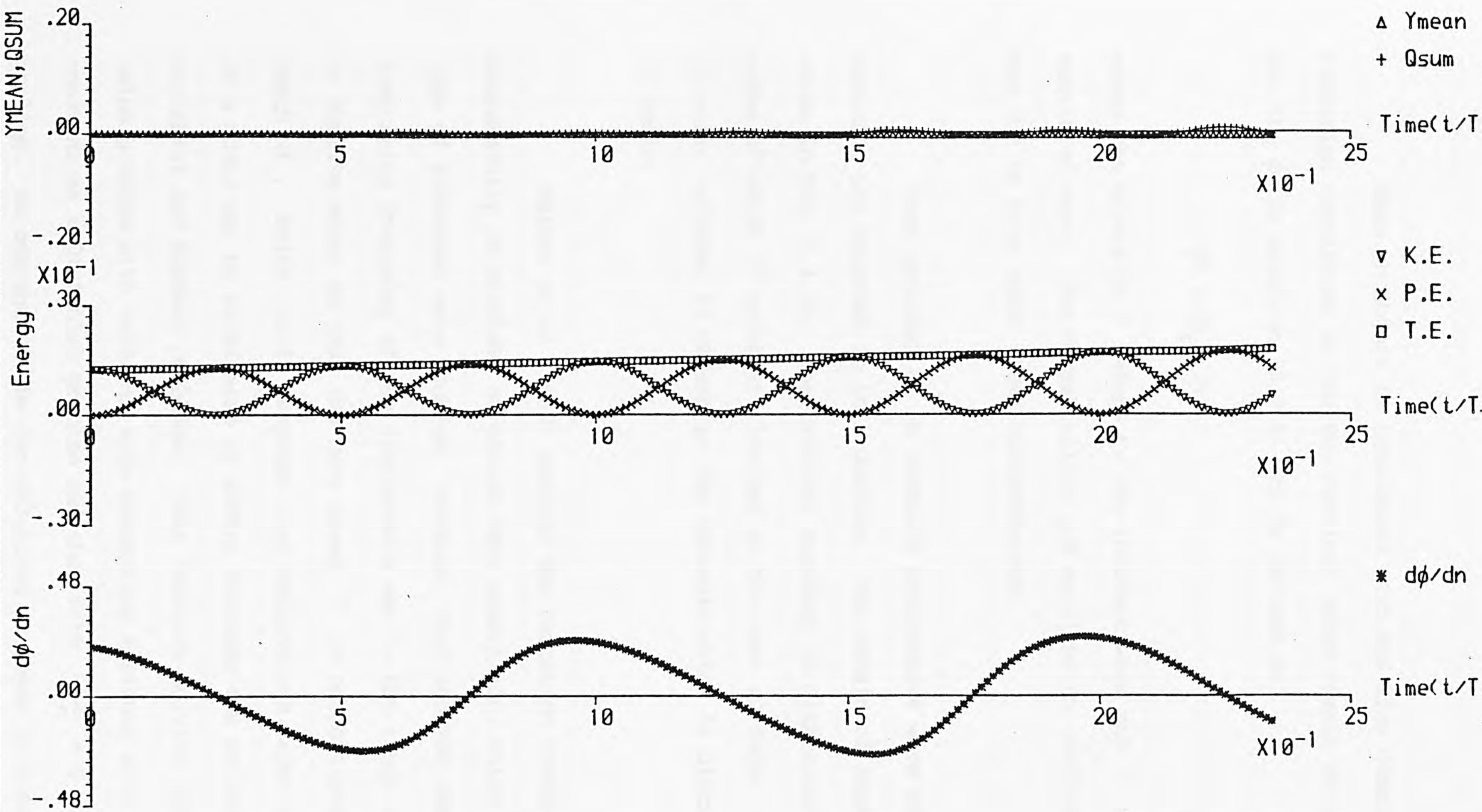

Wave height	=	.112m.	Centre X	=	.798m.
Wavelength	=	1.595m.	Centre Y	=	.000m.
Undisturbed W.L.	=	.555m.	Radius	=	.000m.
Order of eq.	=	1			

Fig. 6.3.11d

6.4 Test Problems of Progressive Waves with an Obstacle

When an object is introduced into the flow domain, the radiation conditions on the two vertical sides remain to be satisfied, but the ϕ in equation (5.2.4) may be defined as:

$$\phi = \phi_I + \phi_S \tag{6.4.1}$$

where the subscript I refers to the incident wave and S refers to the scattered wave. The compatibility and equilibrium conditions (5.3.1) may not be true under these circumstances.

Test problems of an unsteady progressive wave with an obstacle are reported in this section. The domain of analysis is shown in Fig. 6.4.10. The external boundary is discretised by 38 nodes of which 17 nodes are located on the wave surface. A horizontal circular cylinder is chosen as the obstacle which is discretised by 12 nodes.

Salmon et al (1980) applied the radiation boundary condition successfully in problems of piston wave generation, which is only one type of transient wave problem. However, they assumed that the dominating frequency of the disturbance was in the range of long waves in shallow water so that the wave speed C is proportional to water depth d. Smith (1974) proposed that reflections from the boundary of a model may be eliminated by adding together the solutions of the Dirichlet and Neumann problems. That involves solving the boundary value problem with vertical side boundaries assigned with ϕ equal to a constant as a Dirichlet problem and then with $\frac{\partial \phi}{\partial n} = 0$ as a Neumann problem. An average of the two solutions is taken to obtain a condition of no reflection.

The concept introduced by Smith was theoretically acceptable and therefore implemented in the program 'BEMW1' to solve test problem 6.4.1 (see Table 6.4.1). It was compared against unspecified boundary condition approach on the two vertical sides (section 5.3) on test problem 6.4.2. Fig. 6.4.1 shows the results with Smith's approach and Figs. 6.4.2 show the results with the unspecified boundary condition approach. It can be seen that the wave solved with Smith's approach blew up relatively earlier than that by the unspecified boundary condition approach. The wave was disturbed heavily by the Neumann boundary condition $\frac{\partial \phi}{\partial n} = 0$. Another disadvantage with Smith's approach is that for every time step, the boundary integral equation will be solved twice and hence the computing time will be double that for the unspecified boundary condition approach. Even though the unspecified boundary condition approach could not be justified theoretically, it was used to obtain induced wave forces and pressures on a fixed horizontal circular cylinder introduced in the flow domain in the next section.

The introduction of an object is assumed to be located midway between the two vertical side boundaries, Γ_2 and Γ_4 , throughout this study, see Fig. 6.4.10. Since the wave profile is obtained by evaluating equation (5.2.16) with the phase angle, ϵ , set to any arbitrary value which, together with the object, will have an impact on the duration of the wave movement. From test problems 6.4.3 , 6.4.4, 6.4.5, and 6.4.6 in Table 6.4.1, the phase angle, ϵ , at 180° gives a slightly better starting position to achieve the longest duration of wave movement than ϵ at 90°. That means the cylinder position is best placed about half a wave length behind the wave trough.

Figs. 6.4.3c; 6.4.4f; 6.4.5c and 6.4.6c show the graphs of mean water level (Ymean), total outflow through surface (Qsum), kinetic energy (K.E.), potential energy (P.E.), total energy (T.E.) and $\frac{\partial \phi}{\partial n}$ against non-dimensional time axis. They were evaluated according to equations (5.6.9). The mean water level was zero to start with and then increased gradually as the wave advanced. Since $\frac{\partial \phi}{\partial n}$ was positive in the outward direction, Qsum was also zero to start with and then the total mass increased as the wave advanced. The kinetic energy and potential energy were fairly stable over the wave's movement. Even then, a small amount of energy increase may be noticed from the total energy graph. $\frac{\partial \phi}{\partial n}$ is a plot of ϕ' values at node 16 which is at one end of the wave surface, (see Fig. 6.4.10). The result oscillated in a periodic manner.

Figs. 6.4.3d, 6.4.4g, 6.4.5e and 6.4.6d show the graphs of forces and pressures on the cylinder. The horizontal component (Fxn) and vertical component (Fyn) of force at the centre of the cylinder are expressed in normalised form [$F/\rho g r \frac{H}{2}$]. The pressures are expressed in millimetres. Point 1, 2, 3 and 4 have the positions on the cylinder as shown in Fig. 6.4.11. The accuracy of the forces and pressures on the cylinder will be discussed later.

It might be noted that the ordinate axes for the above (auxiliary) graphs differ from each other. It is caused by the method of calculating the axis scale which takes a root mean square value of all available data in each type, in that particular run. When a wave is about to blow up, the data might become enormous and hence the root mean square value would become large. If one ignores the data generated during the blow up period, the axis scale would be reduced to an extent that the auxiliary graphs would be more precisely plotted.

Test problem 6.4.7 was a repeat run for test problem 6.4.5 with a smoothing formula applied to the wave profile every 10 loops. Figs. 6.4.7 clearly indicate that the wave profile with the submerged cylinder in the flow was prolonged by about 15%. But the curves for forces and pressures (see Fig. 6.4.7e) are not as smooth as those without smoothing (see Fig. 6.4.5d). This may be caused by the numerical error present in equation (6.3.6). Therefore, smoothing is not the ultimate solution to remove numerical instability inherent in the proposed technique.

Jeffrey et al (1976) had carried out experimental measurement of forces on a horizontal circular cylinder. Some of their wave characteristics, cylinder diameters and depths of submergence are similar to the above problems tested. Therefore, it will be useful to use their experimental data to test the proposed technique. Forces computed by the boundary element method may then be compared with their measured results.

The wave characteristic chosen for the comparison are shown in Table 6.4.1 —– test problems 6.4.8. and 6.4.9. The computed forces are presented in graphical form in Figs. 6.4.8f and 6.4.9e. Dimensional forces may be obtained by multiplying the value measured on the ordinate axis scale (in non-dimensional form) by $\rho g r \frac{H}{2}$. The magnitudes of wave forces at the crest and trough behave in a diverging manner. The comparisons are given in Table 6.4.3. Figs. 6.4.12 and 6.4.13 show the pattern of force variations for both measured and theoretical results. The initial theoretical force amplitudes are more than double the measured values in Jeffrey et al (1976). The mean theoretical force amplitudes are about three times bigger than the measured values. The overestimation was caused by the cylinder being placed too closed to the wave surface; $(y_0 - r)/\lambda = 0.0064$ for test problem 6.4.8 and $(y_0 - r)/\lambda = 0.0041$ for test problem 6.4.9. From Figs. 6.4.8b and 6.4.9b, the wave profiles touch the top region of the cylinder and hence numerical instability follows.

From Figs. 6.4.8f and 6.4.9e, oscillations in force and pressure values took place in the middle of the run. Their occurences correspond to the wave trough being above the cylinder. This leads to nodes on the wave profile and on the cylinder to be too close to each other, and therefore numerical instability follows. The instability was weak in the sense that the forces and pressures recovered, once the wave trough passed over the cylinder. Termination of the two runs were due to the number of loops specified being reached.

TEST PROBLEM	WAVE HEIGHT H (m)	WAVE LENGHT λ (m)	WAVE STEEPNESS (H/λ)	WATER DEPTH	ORDER OF EQ	SMOOT-HING	PHASE ANGLE	VERTCAL SIDE B.C.	CYLINDER CENTRE X (m)	CYLINDER CENTRE Y (m)	CYLINDER RADIUS R (m)
6.4.1	0.112	1.595	0.0703	0.555	1	NO	0	$\phi=\frac{d\phi}{dn}=0$	0.798	-0.294	0.055
6.4.2	0.112	1.595	0.0703	0.555	1	NO	0	UNSPECIFIED	0.798	-0.294	0.055
6.4.3	0.112	1.595	0.0703	0.555	1	NO	0	UNSPECIFIED	0.798	-0.294	0.055
6.4.4	0.112	1.595	0.0703	0.555	1	NO	90	UNSPECIFIED	0.798	-0.294	0.055
6.4.5	0.112	1.595	0.0703	0.555	1	NO	180	UNSPECIFIED	0.798	-0.294	0.055
6.4.6	0.112	1.595	0.0703	0.555	1	NO	270	UNSPECIFIED	0.798	-0.294	0.055
6.4.7	0.112	1.595	0.0703	0.555	1	YES	180	UNSPECIFIED	0.798	-0.294	0.055
6.4.8	0.020	1.560	0.0128	0.600	1	NO	90	UNSPECIFIED	0.780	-0.060	0.050
6.4.9	0.020	2.440	0.0082	0.600	1	NO	90	UNSPECIFIED	1.220	-0.060	0.050

TABLE 6.4.1 INPUT PARAMETERS OF TEST PROBLEMS 6.4.1-6.4.9 ON WAVE WITH SUBMERGED CIRCULAR CYLINDER

TEST PROBLEM	FIGURE	TIME STEP (SEC)	LOOPS EXECUTED	WAVE LAPSED	COMPUTER RUN TIME	REMARK
6.4.1	6.4.1	0.075	26	0.295T	0.0778	FAILED BY ϕ OR $d\phi/dn$ > 50.0
6.4.2	6.4.2	0.075	124	1.449T	0.2418	FAILED BY ϕ OR $d\phi/dn$ > 50.0
6.4.3	6.4.3	0.075	68	0.789T	0.1355	FAILED BY ϕ OR $d\phi/dn$ > 50.0
6.4.4	6.4.4	0.075	128	1.497T	0.2494	FAILED BY ϕ OR $d\phi/dn$ > 50.0
6.4.5	6.4.5	0.075	122	1.426T	0.2362	FAILED BY ϕ OR $d\phi/dn$ > 50.0
6.4.6	6.4.6	0.075	86	1.002T	0.1749	FAILED BY ϕ OR $d\phi/dn$ > 50.0
6.4.7	6.4.7	0.075	140	1.638T	0.3407	FAILED BY ϕ OR $d\phi/dn$ > 50.0
6.4.8	6.4.8	0.075	200	2.357T	0.3815	NATURAL STOP
6.4.9	6.4.9	0.0375	200	1.135T	0.3822	NATURAL STOP

TABLE 6.4.2 OUTPUT PARAMETERS OF TEST PROBLEMS 6.4.1-6.4.9 ON WAVE WITH SUBMERGED CIRCULAR CYLINDER

TEST PROBLEM	HORIZONTAL FORCE, Fx (N/m)			VERTICAL FORCE, Fy (N/m)		
	JEFFREY et al, (1976)	THEORETICAL		JEFFREY et al, (1976)	THEORETICAL	
		INITIAL	MEAN		INITIAL	MEAN
6.4.8	1.80	4.17	6.61	1.13	5.47	7.22
6.4.9	1.50	3.02	3.62	0.88	4.18	6.00

Table 6.4.3 Comparisons of forces between measured and theoretical results

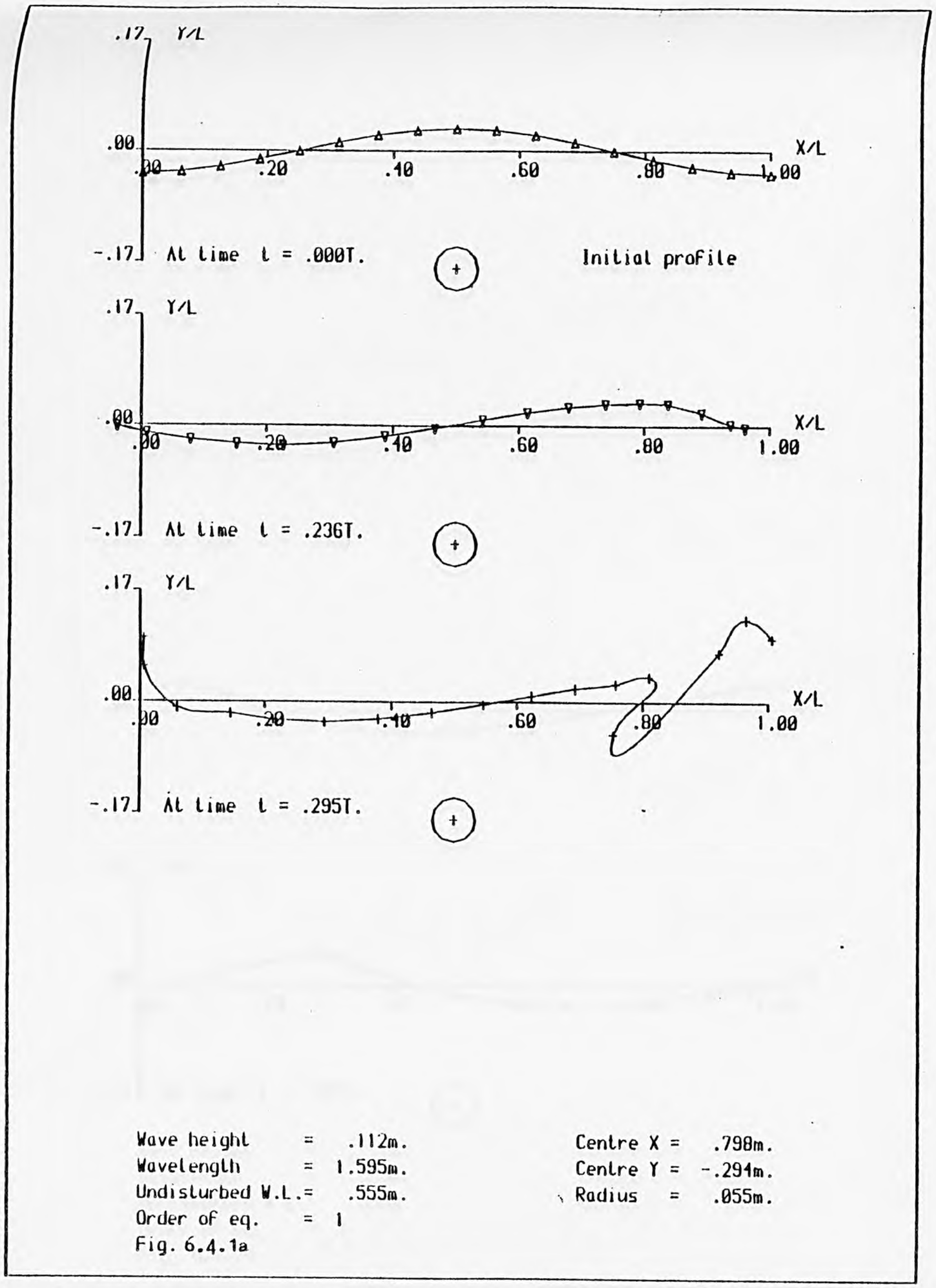

Fig. 6.4.1 A time sequence of wave profiles for test problem 6.4.1

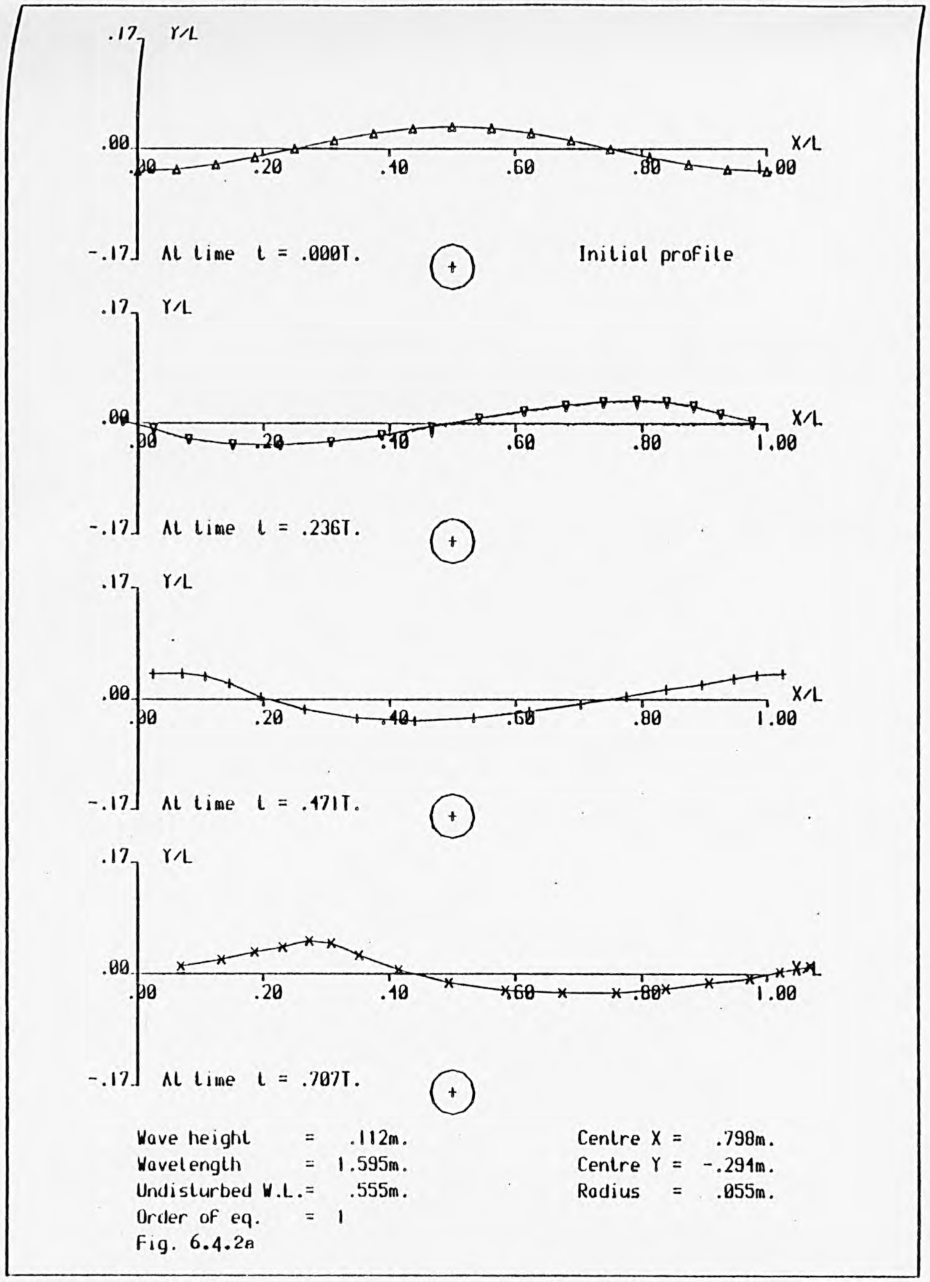

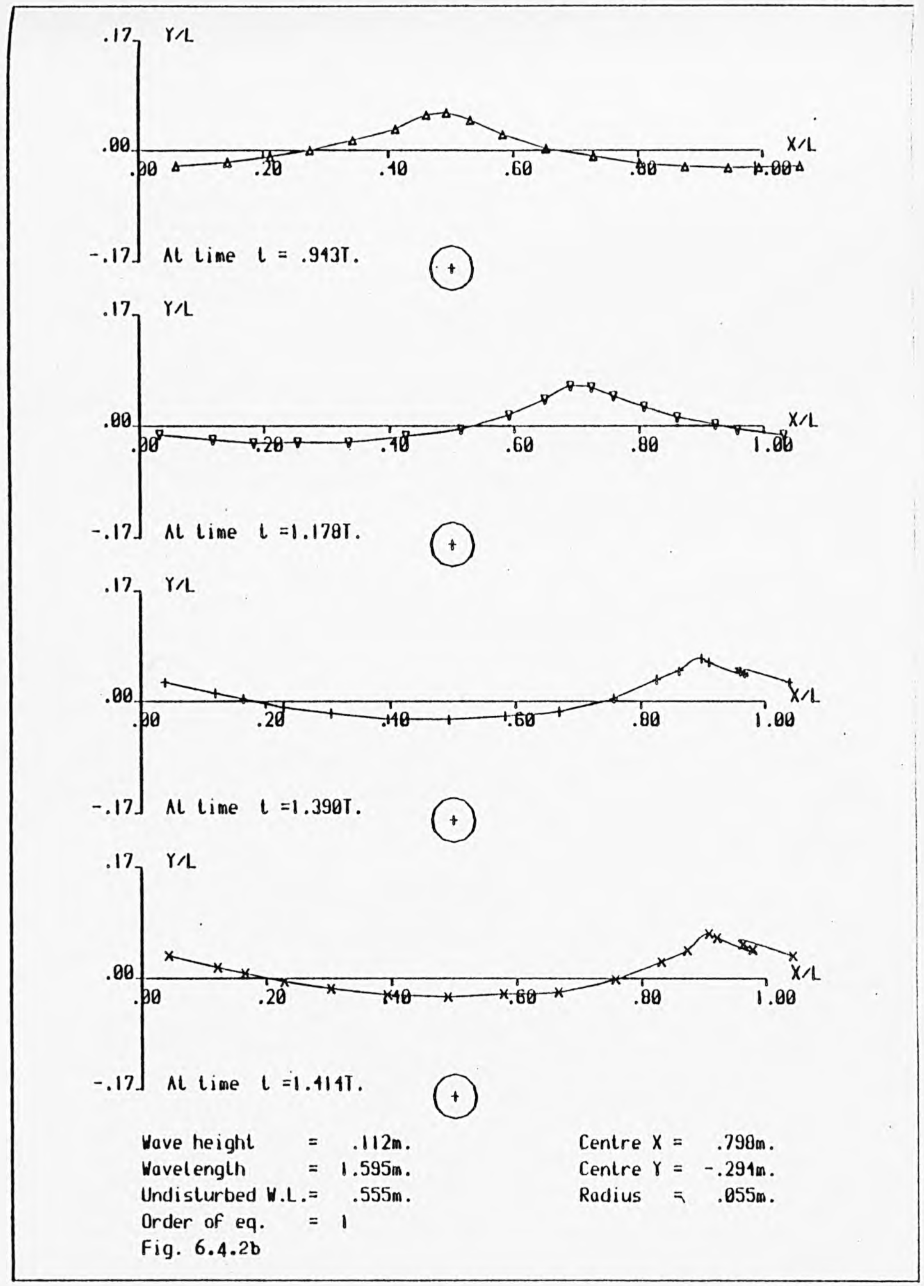

Fig. 6.4.2 (a-c) A time sequence of wave profiles for test problem 6.4.2

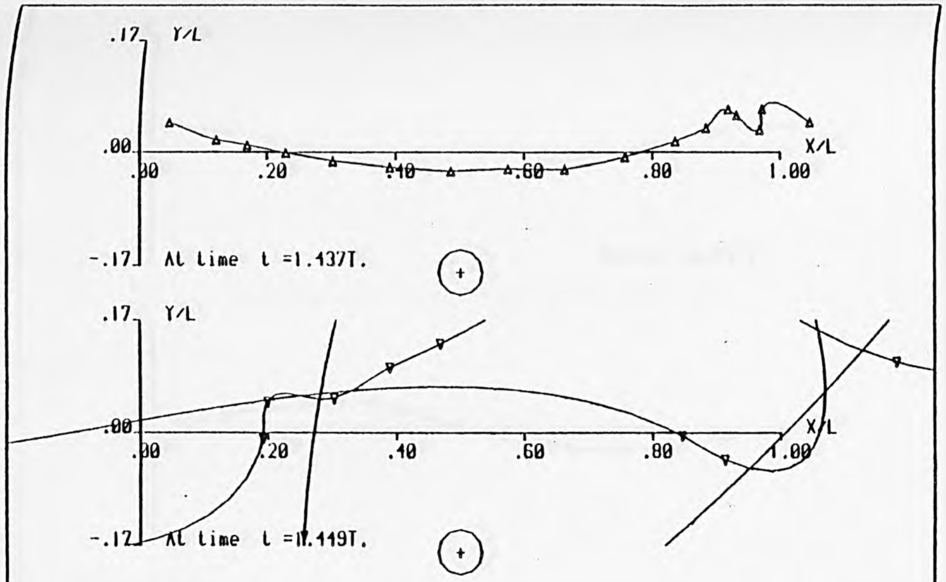

Wave height = .112m.
Wavelength = 1.595m.
Undisturbed W.L.= .555m.
Order of eq. = 1
Fig. 6.4.2c

Centre X = .798m.
Centre Y = -.294m.
Radius = .055m.

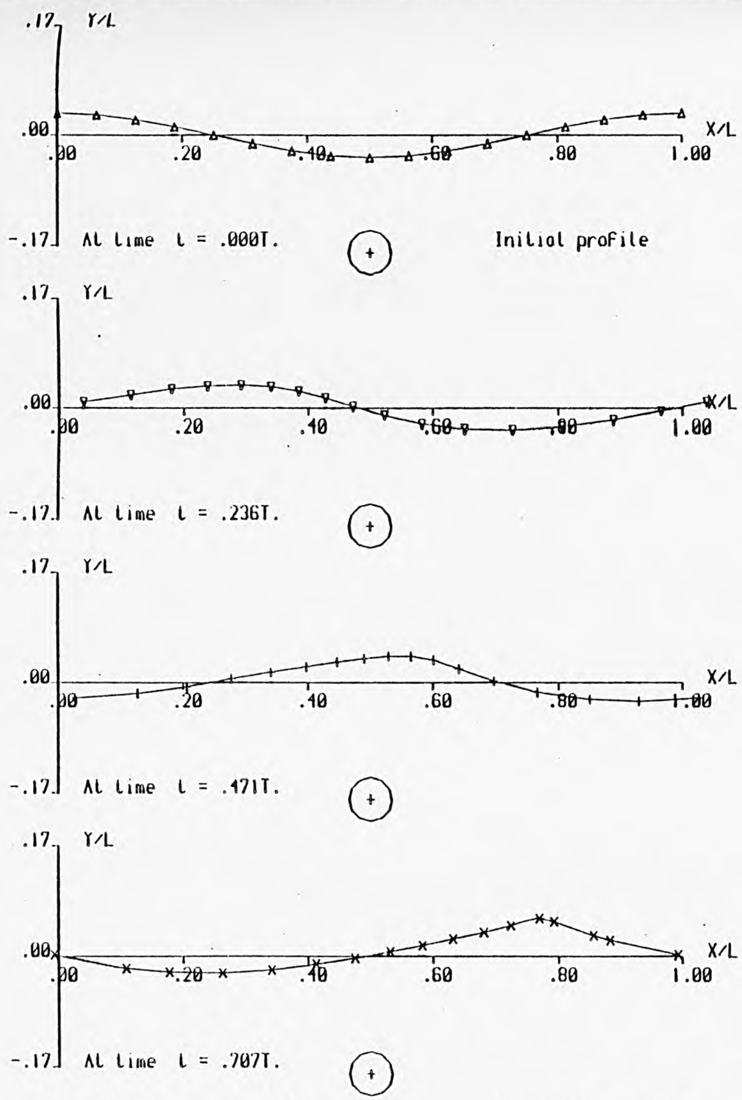

Wave height = .112m.
Wavelength = 1.595m.
Undisturbed W.L. = .555m.
Order of eq. = 1
Fig. 6.4.3a

Centre X = .798m.
Centre Y = -.294m.
Radius = .055m.

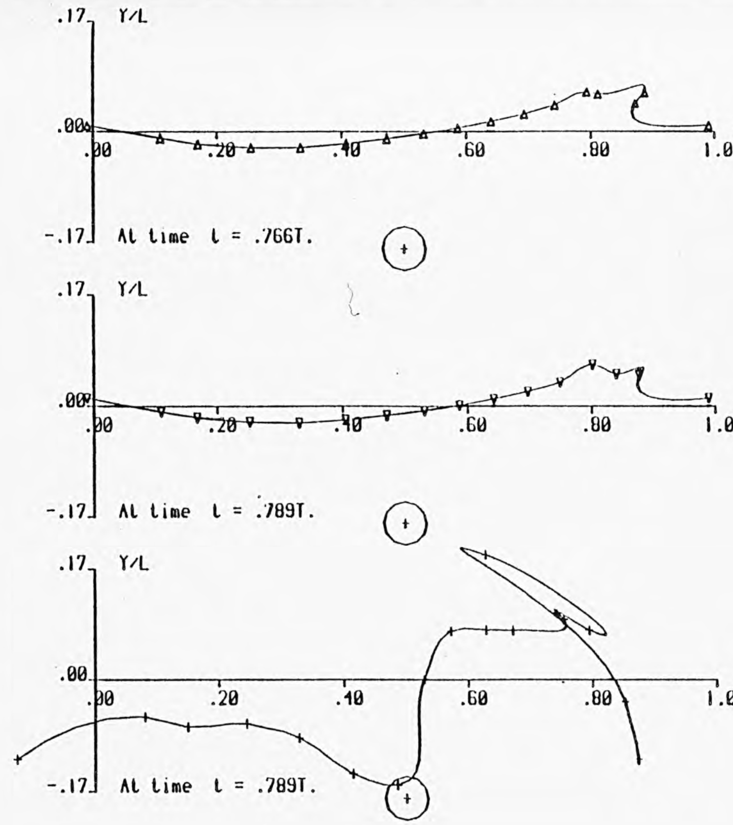

Wave height = .112m.
Wavelength = 1.595m.
Undisturbed W.L. = .555m.
Order of eq. = 1
Fig. 6.4.3b

Centre X = .798m.
Centre Y = -.294m.
Radius = .055m.

Fig. 6.4.3(a-d) A time sequence of wave profiles and auxiliary graphs for test problem 6.4.3

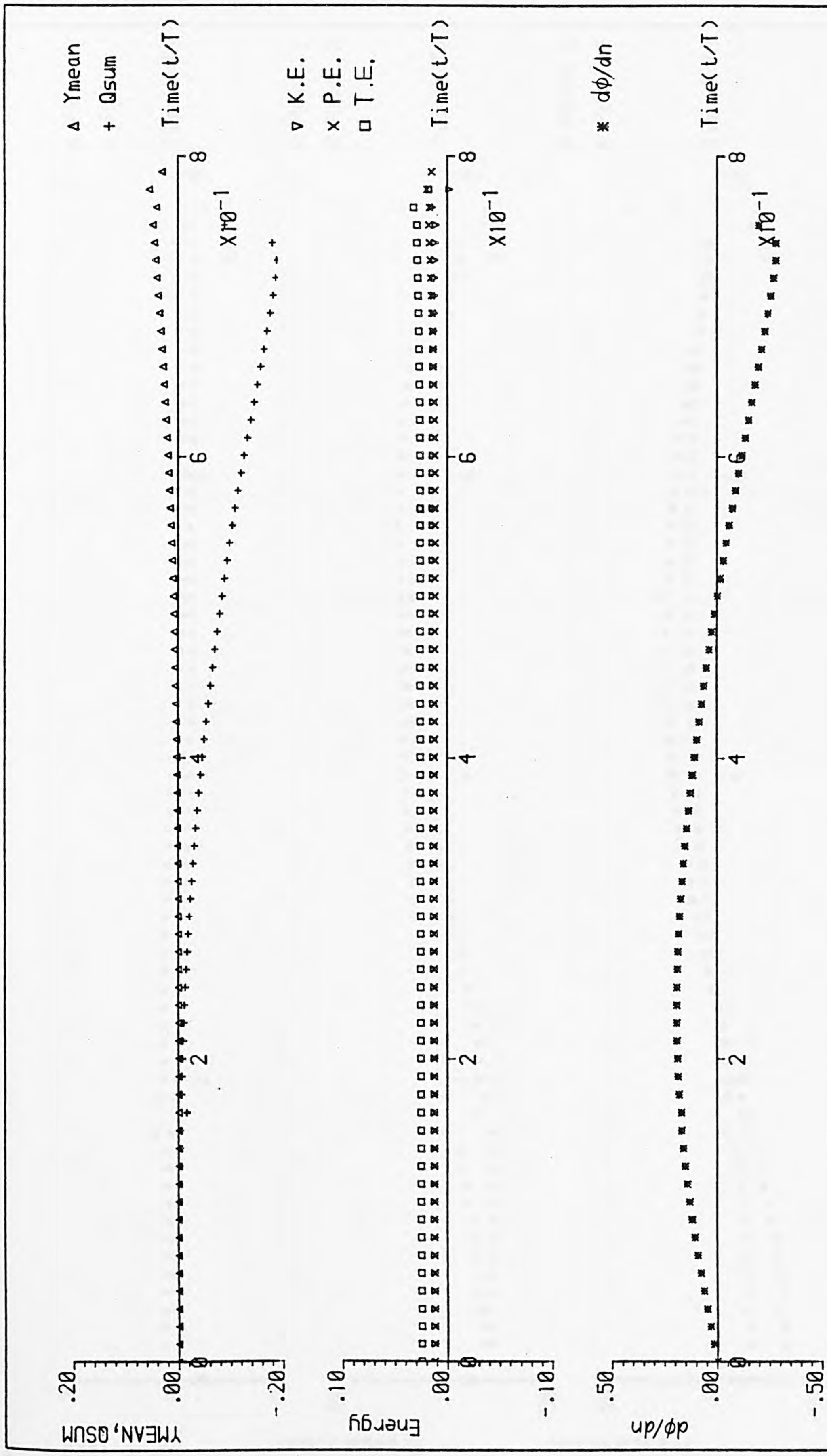

Wave height = .112m. Centre X = .798m.
Wavelength = 1.595m. Centre Y = -.294m.
Undisturbed W.L.= .555m. Radius = .055m.
Order of eq. = 1

Fig.6.4.3c

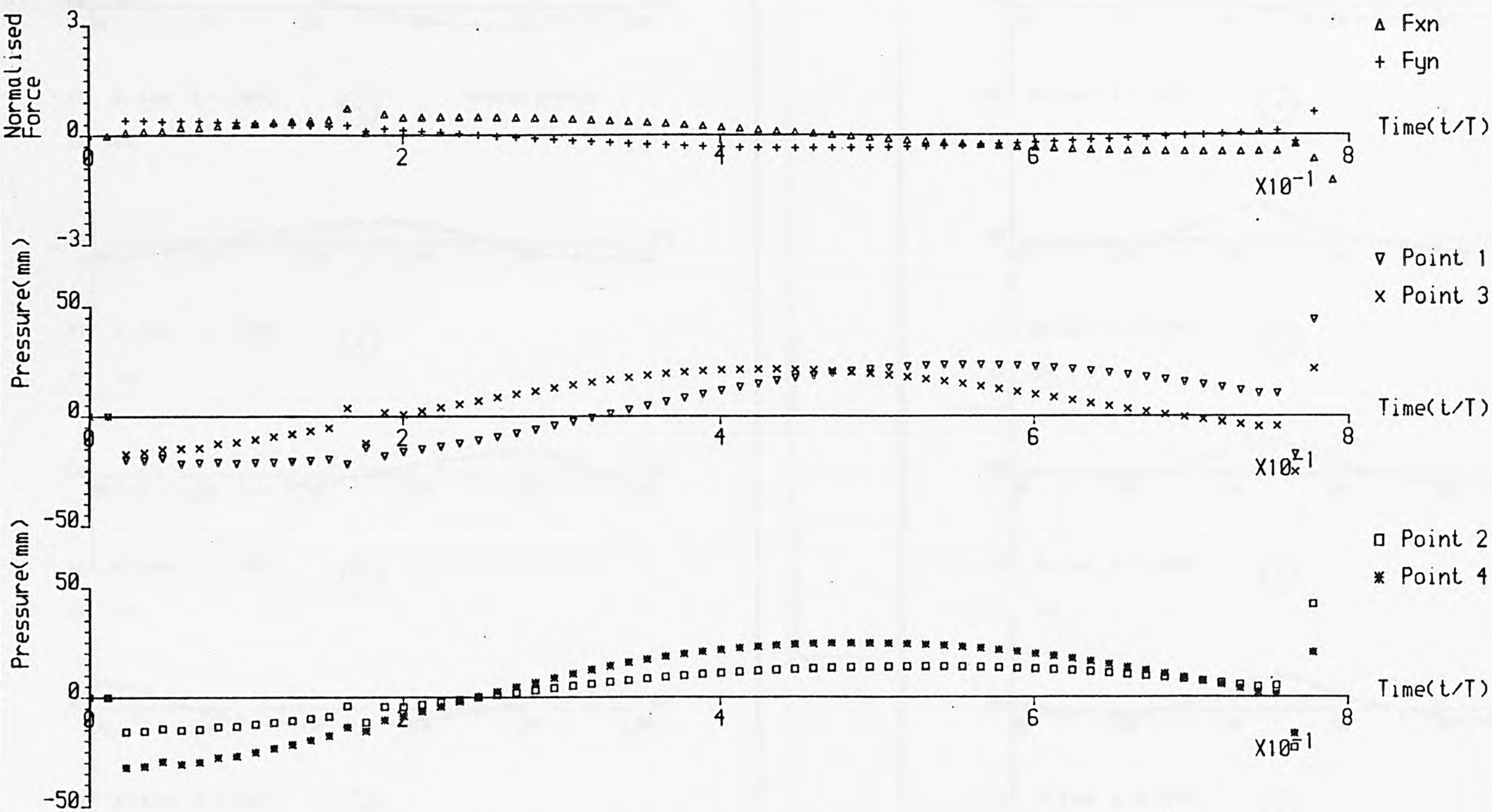

Wave height = .112m. Centre X = .798m.
Wavelength = 1.595m. Centre Y = -.294m.
Undisturbed W.L. = .555m. Radius = .055m.
Order of eq. = 1

Fig. 6.4.3d

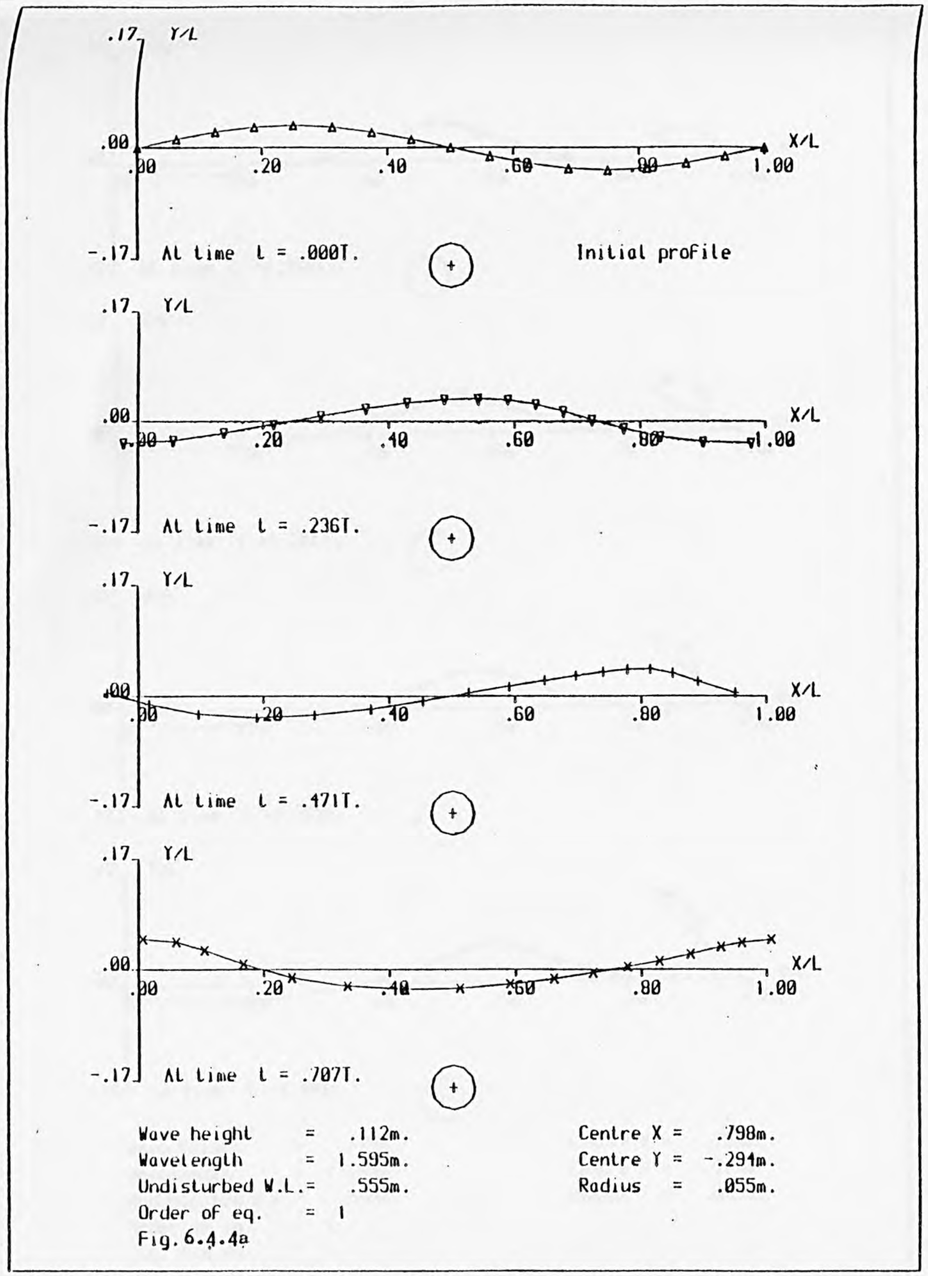

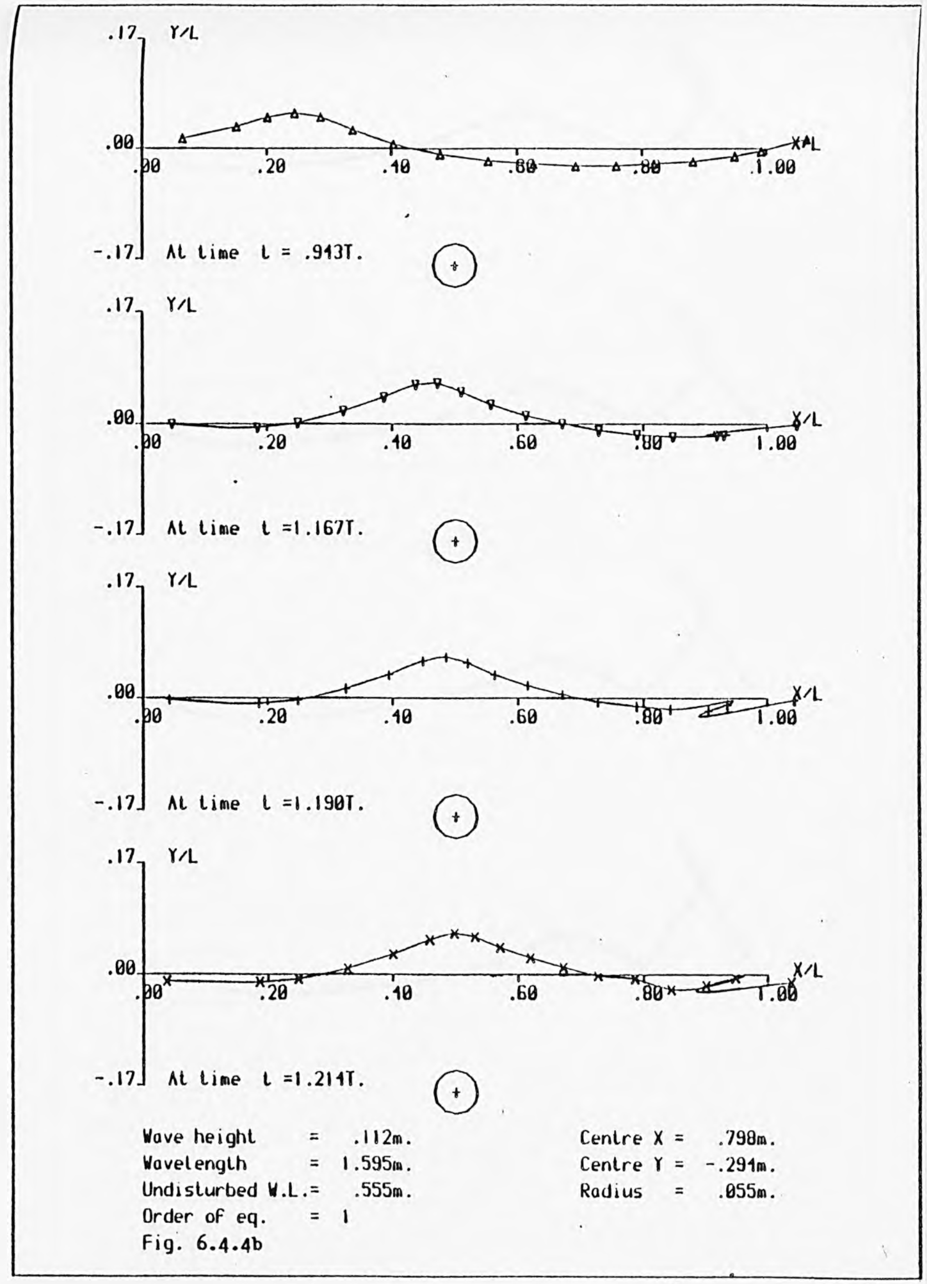

Fig 6.4.4(a-g) A time sequence of wave profiles and auxiliary graphs for test problem 6.4.4

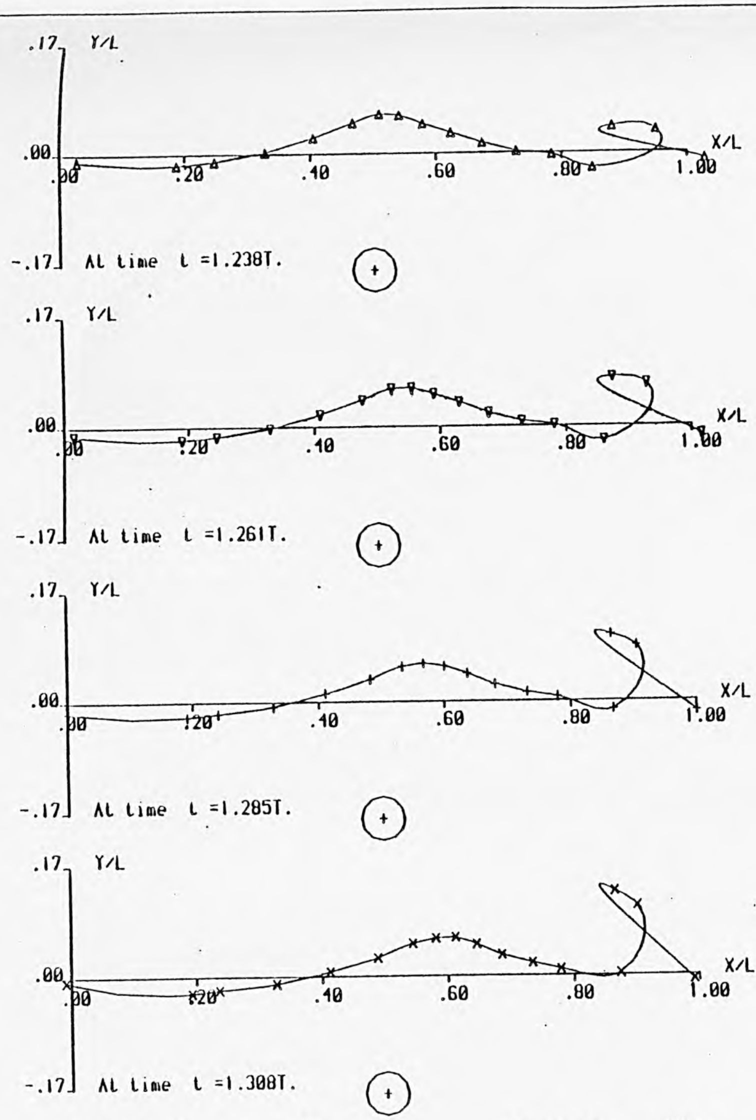

Wave height = .112m.
Wavelength = 1.595m.
Undisturbed W.L.= .555m.
Order of eq. = 1

Centre X = .798m.
Centre Y = -.294m.
Radius = .055m.

Fig. 6.4.4c

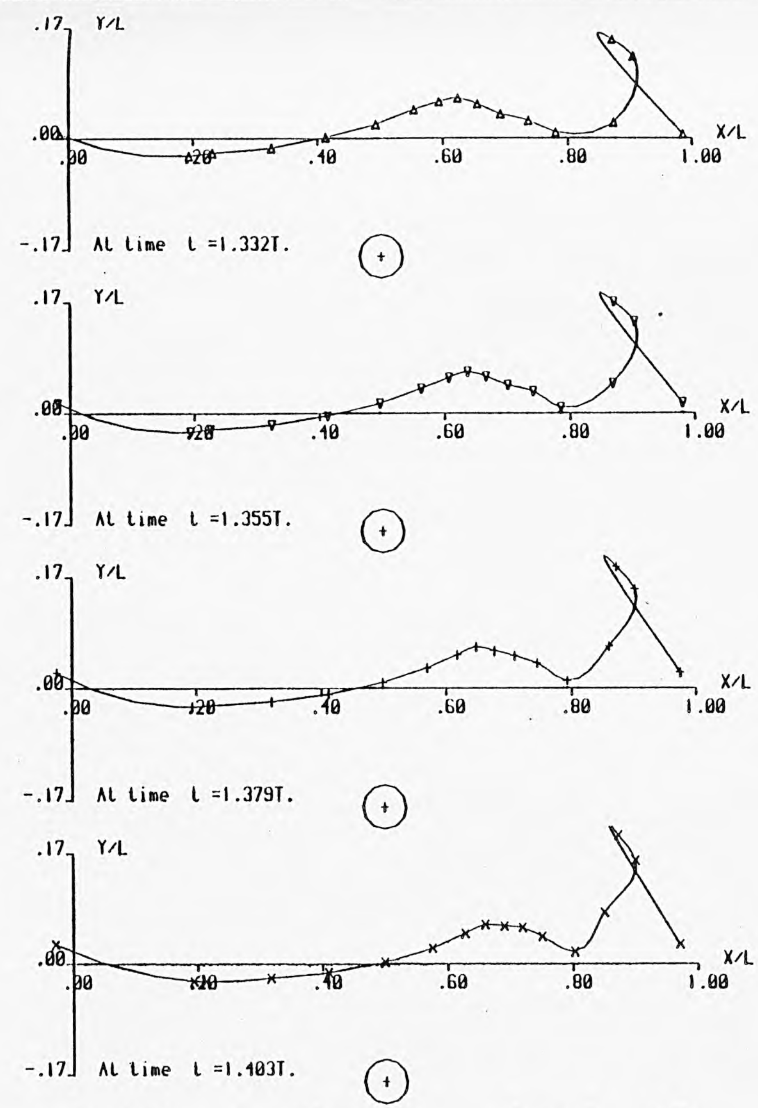

Wave height = .112m.
Wavelength = 1.595m.
Undisturbed W.L.= .555m.
Order of eq. = 1

Centre X = .798m.
Centre Y = -.294m.
Radius = .055m.

Fig. 6.4.4d

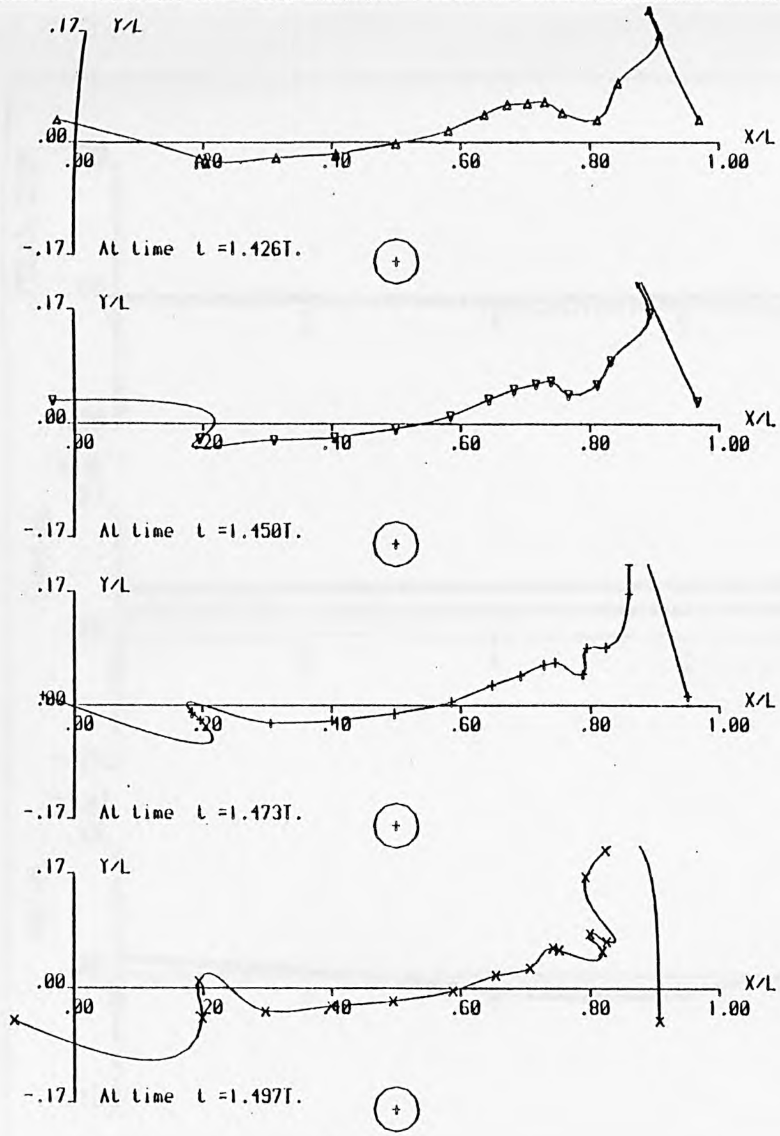

Wave height =	.112m.	Centre X =	.798m.
Wavelength =	1.595m.	Centre Y =	-.294m.
Undisturbed W.L.=	.555m.	Radius =	.055m.
Order of eq. =	1		

Fig. 6.4.4e

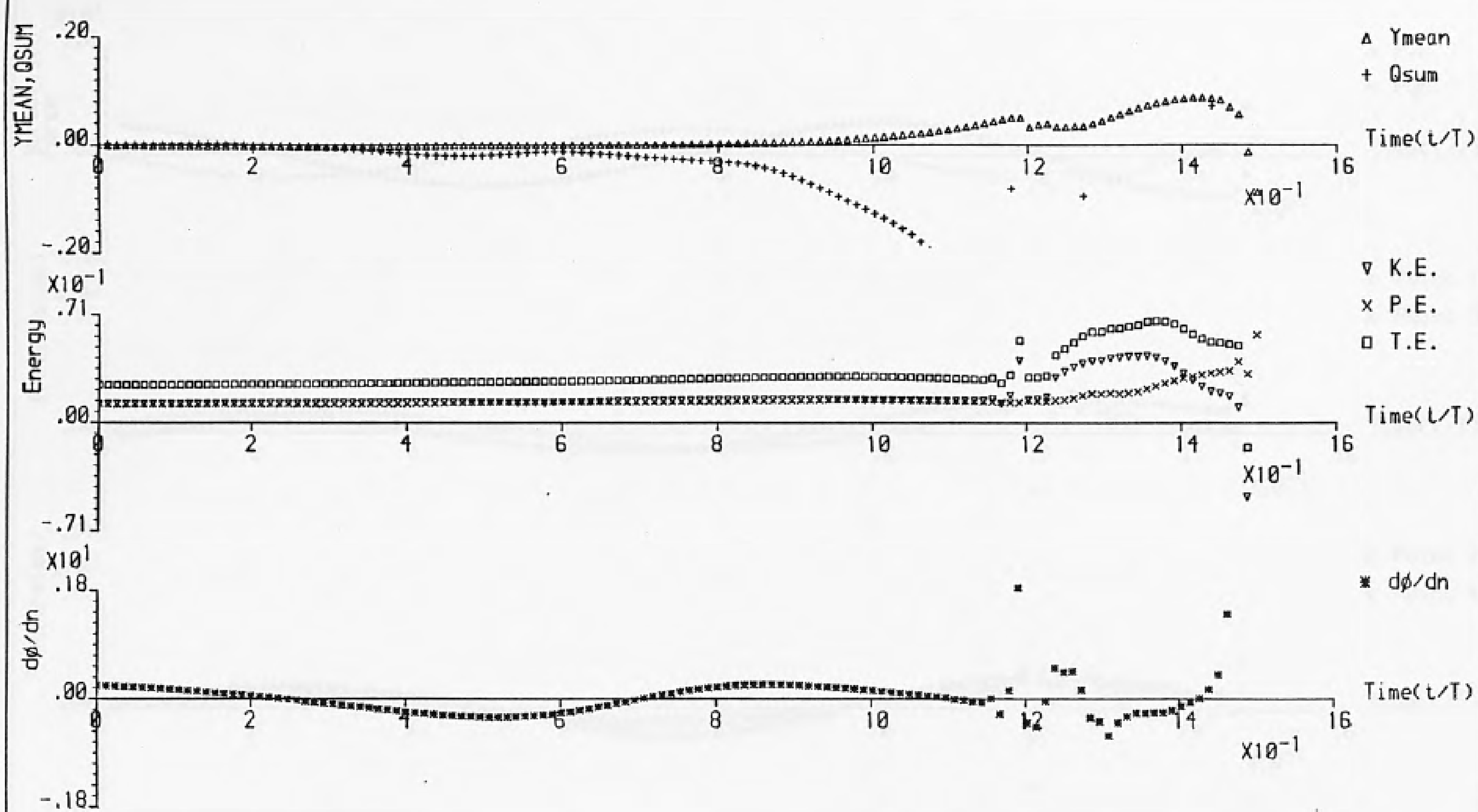

Wave height = .112m. Centre X = .798m.
Wavelength = 1.595m. Centre Y = -.294m.
Undisturbed W.L.= .555m. Radius = .055m.
Order of eq. = 1

Fig. 6.4.4f

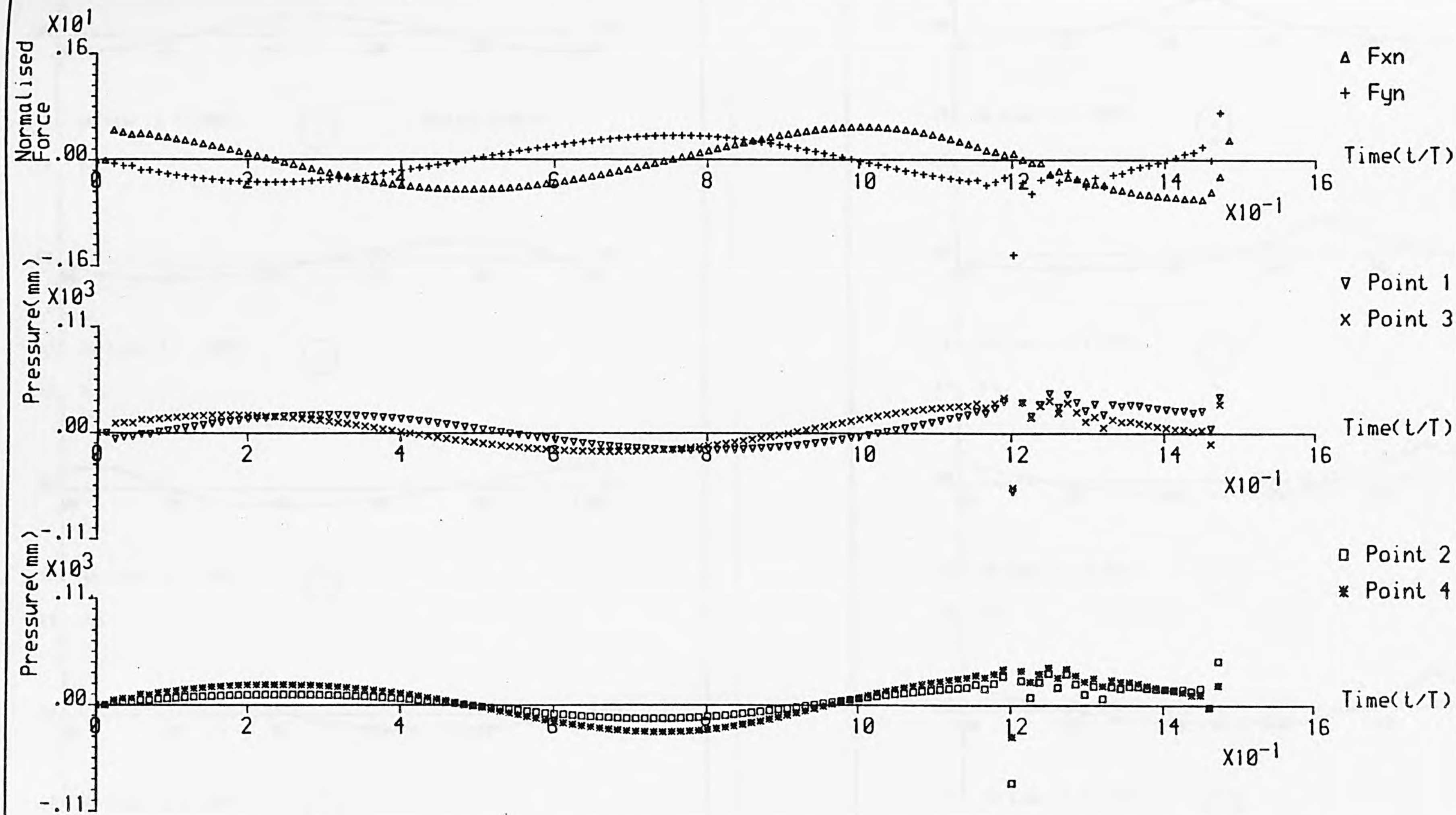

Wave height	=	.112m.	Centre X	=	.798m.
Wavelength	=	1.595m.	Centre Y	=	-.294m.
Undisturbed W.L.	=	.555m.	Radius	=	.055m.
Order of eq.	=	1			

Fig. 6.4.4g

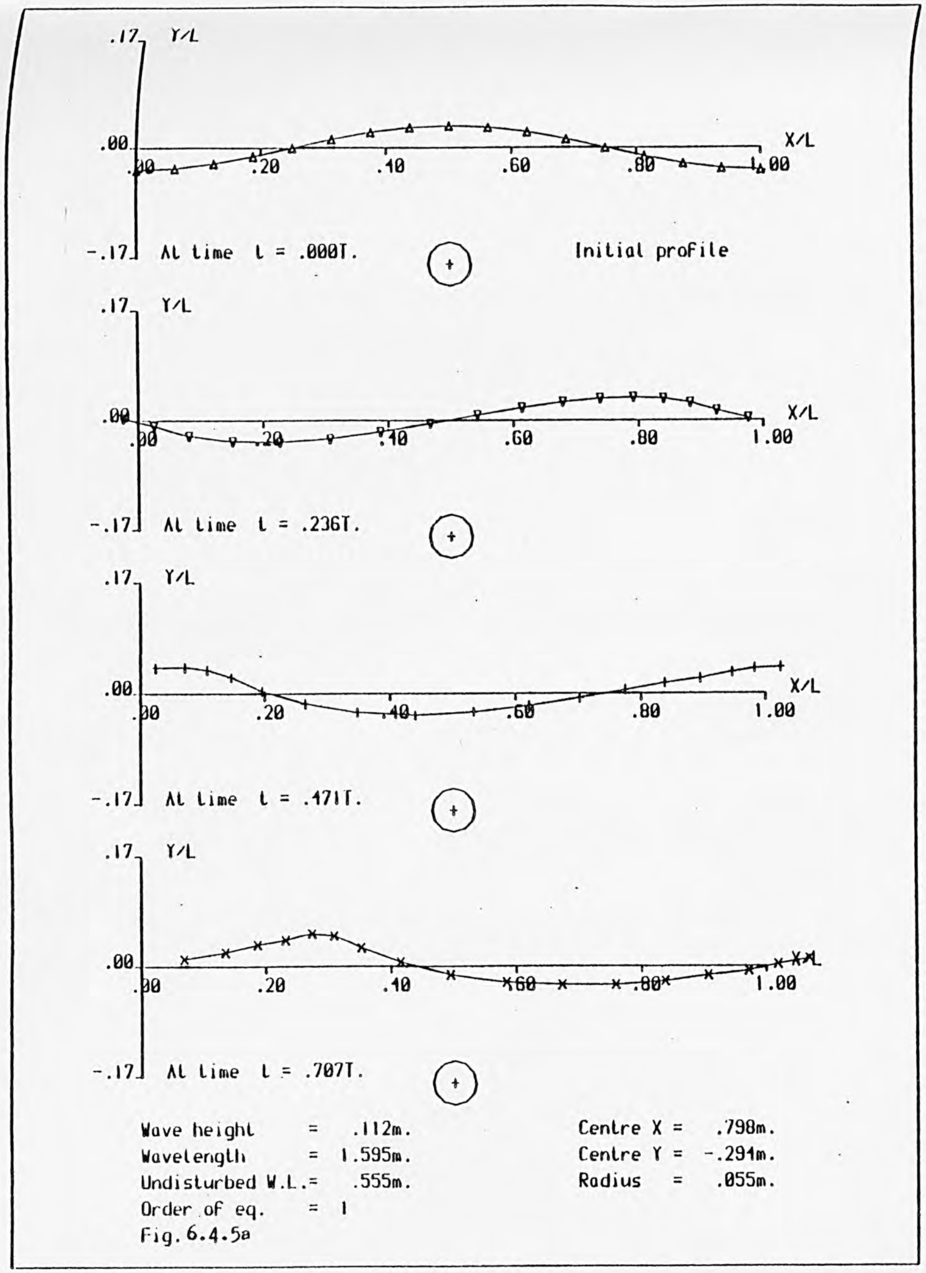

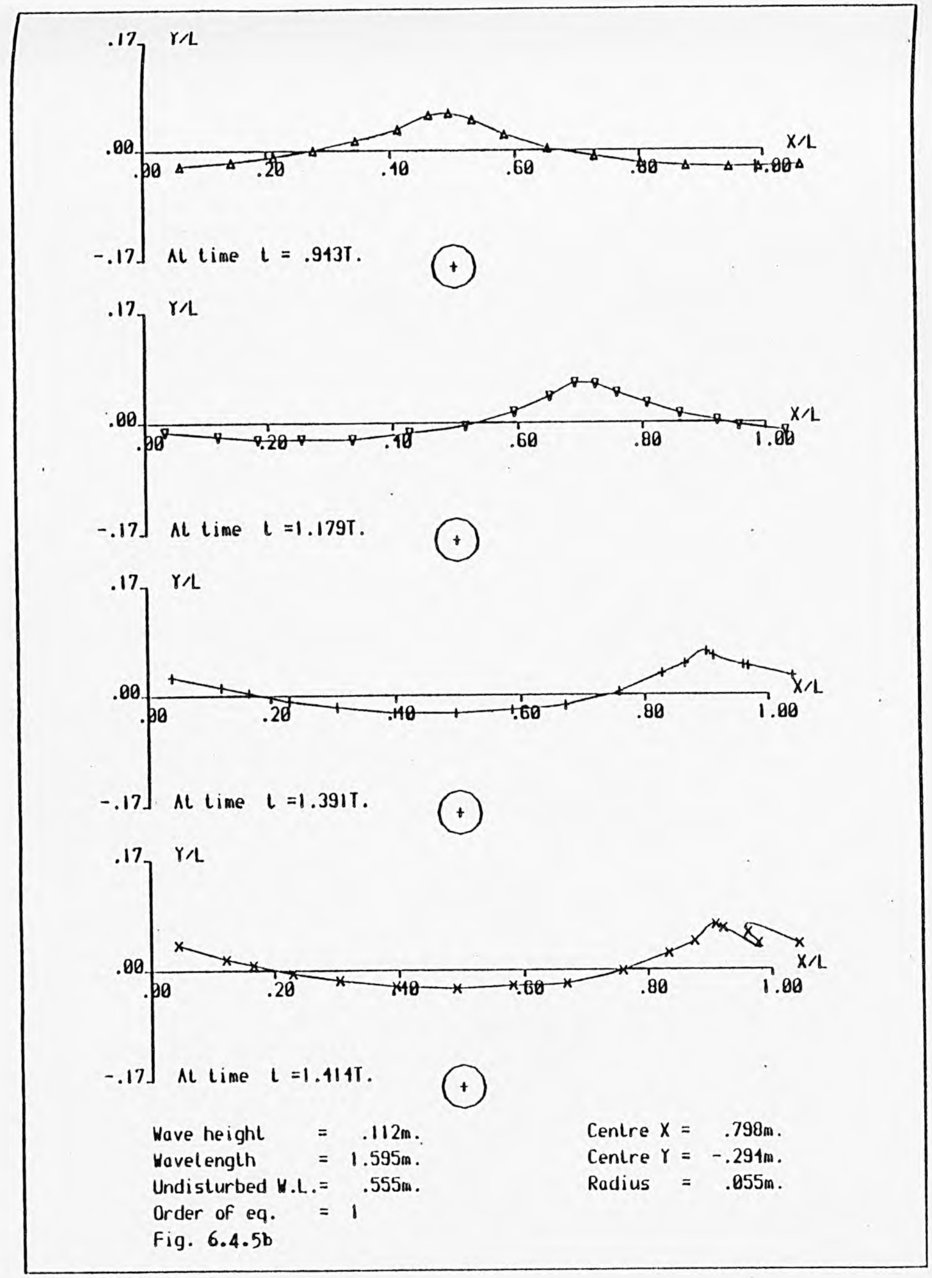

Fig. 6.4.5(a-d) A time sequence of wave profiles and auxiliary graphs for test problem 6.4.5

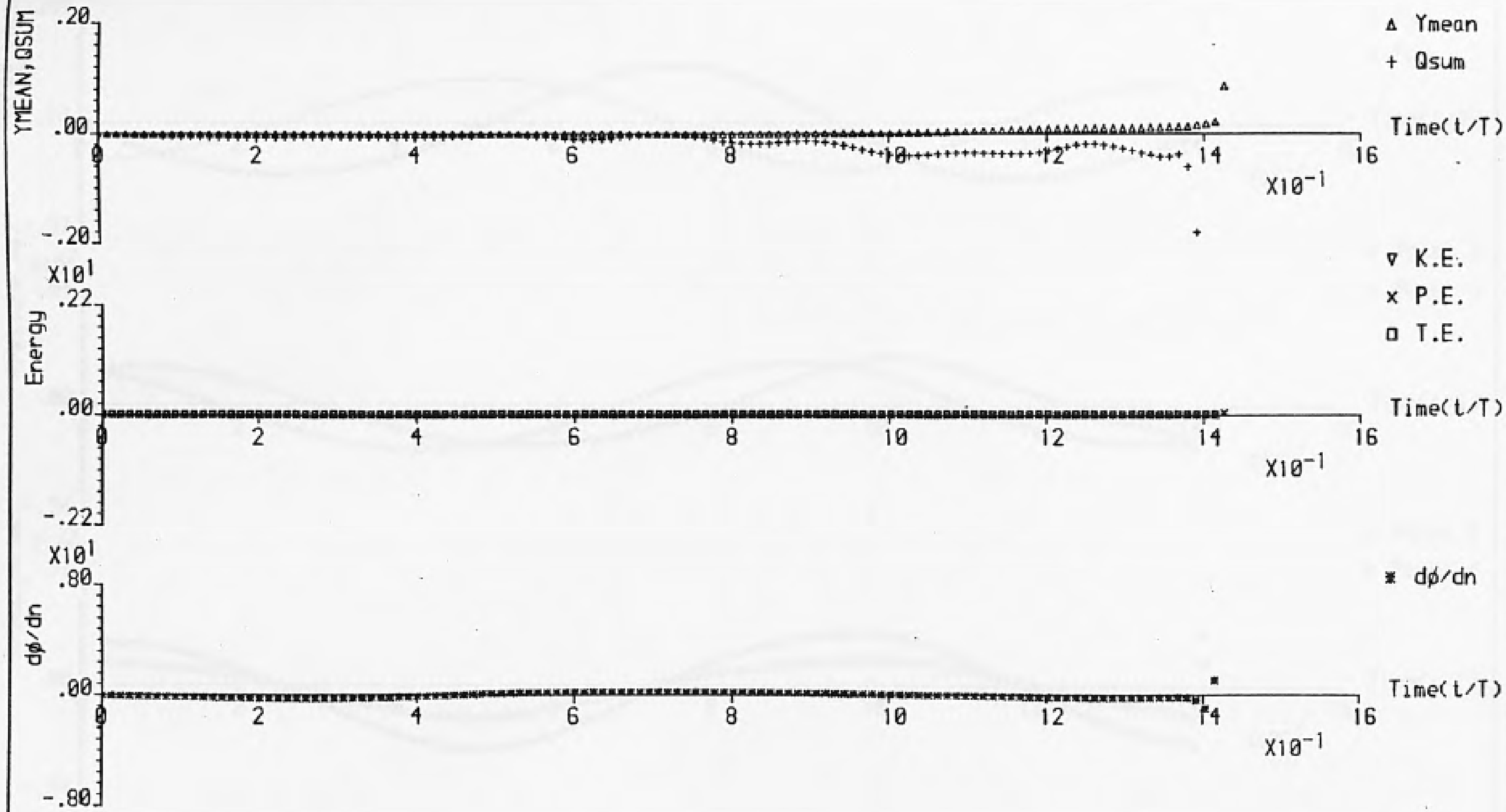

Wave height = .112m. Centre X = .798m.
Wavelength .= 1.595m. Centre Y = -.294m.
Undisturbed W.L.= .555m. Radius = .055m.
Order of eq. = 1

Fig. 6.4.5c

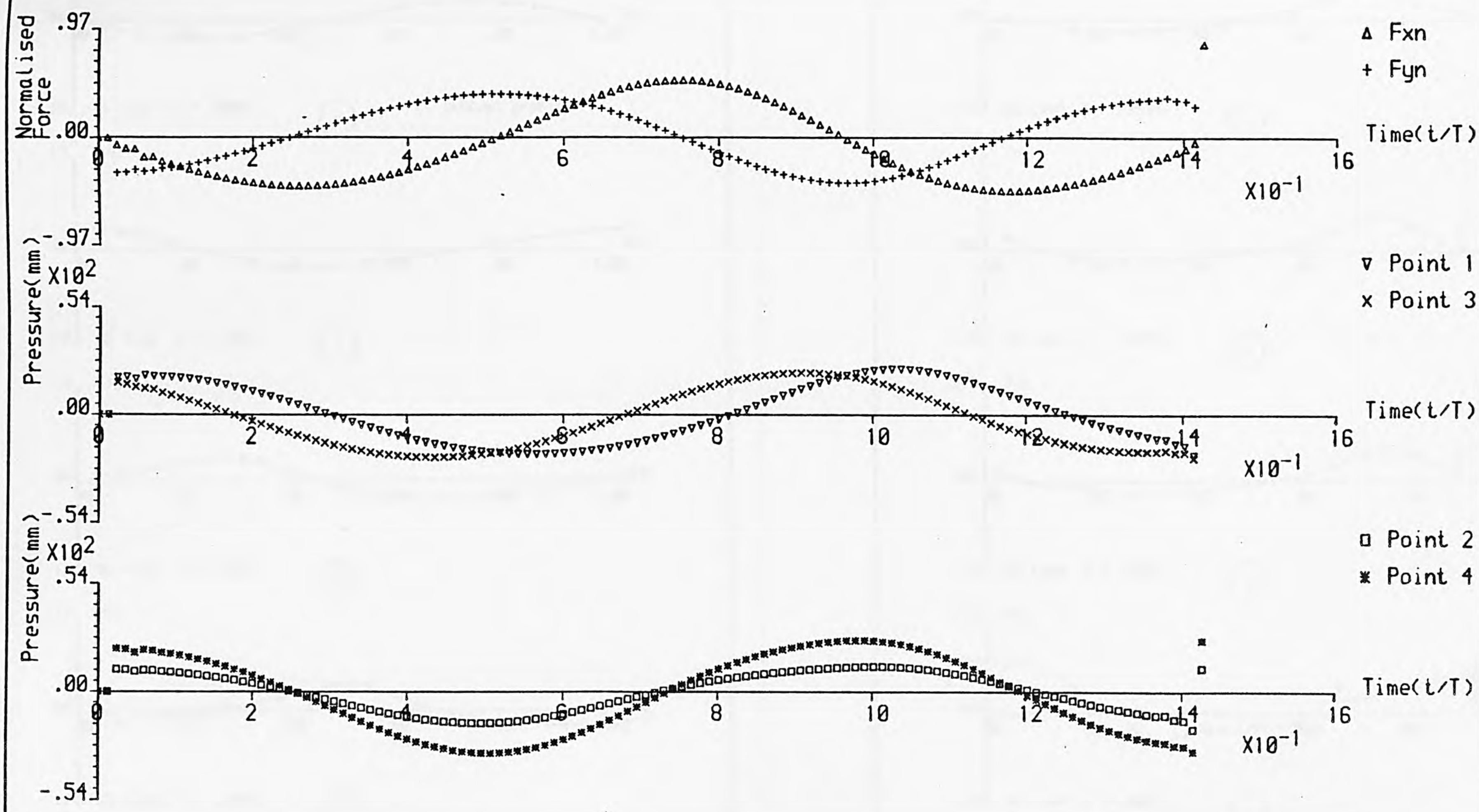

Wave height = .112m. Centre X = .798m.
Wavelength = 1.595m. Centre Y = -.294m.
Undisturbed W.L.= .555m. Radius = .055m.
Order of eq. = 1

Fig. 6.4.5d

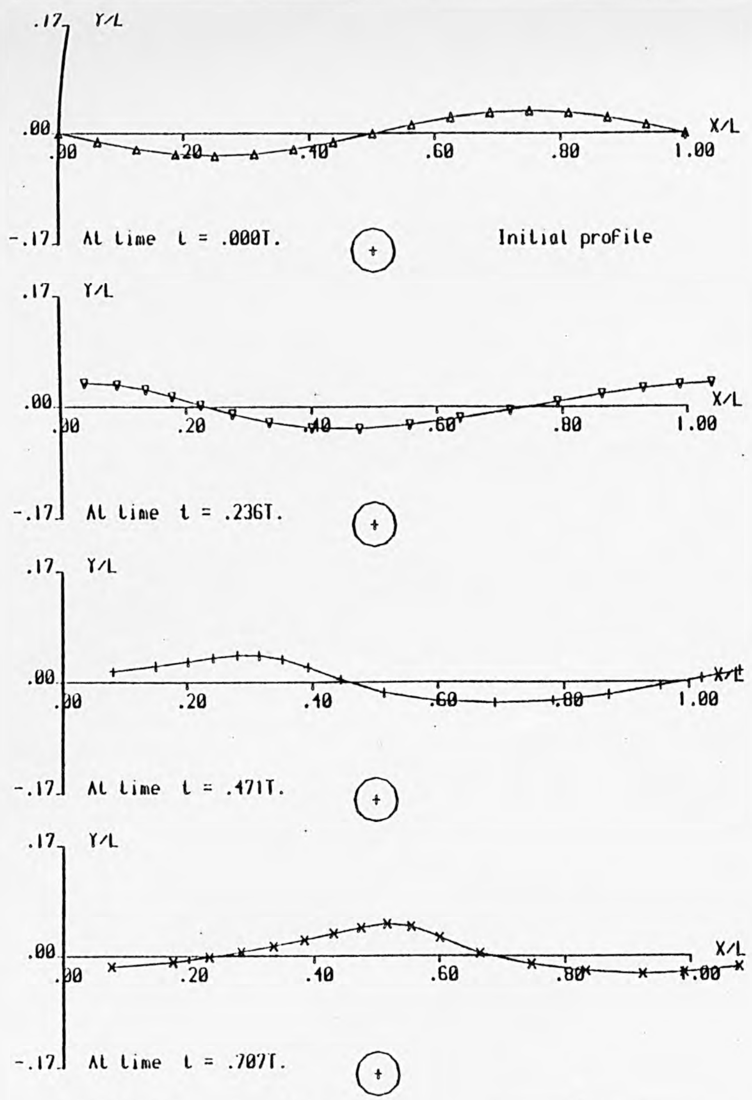

Wave height = .112m.
Wavelength = 1.595m.
Undisturbed W.L.= .555m.
Order of eq. = 1
Centre X = .798m.
Centre Y = -.294m.
Radius = .055m.

Fig. 6.4.6a

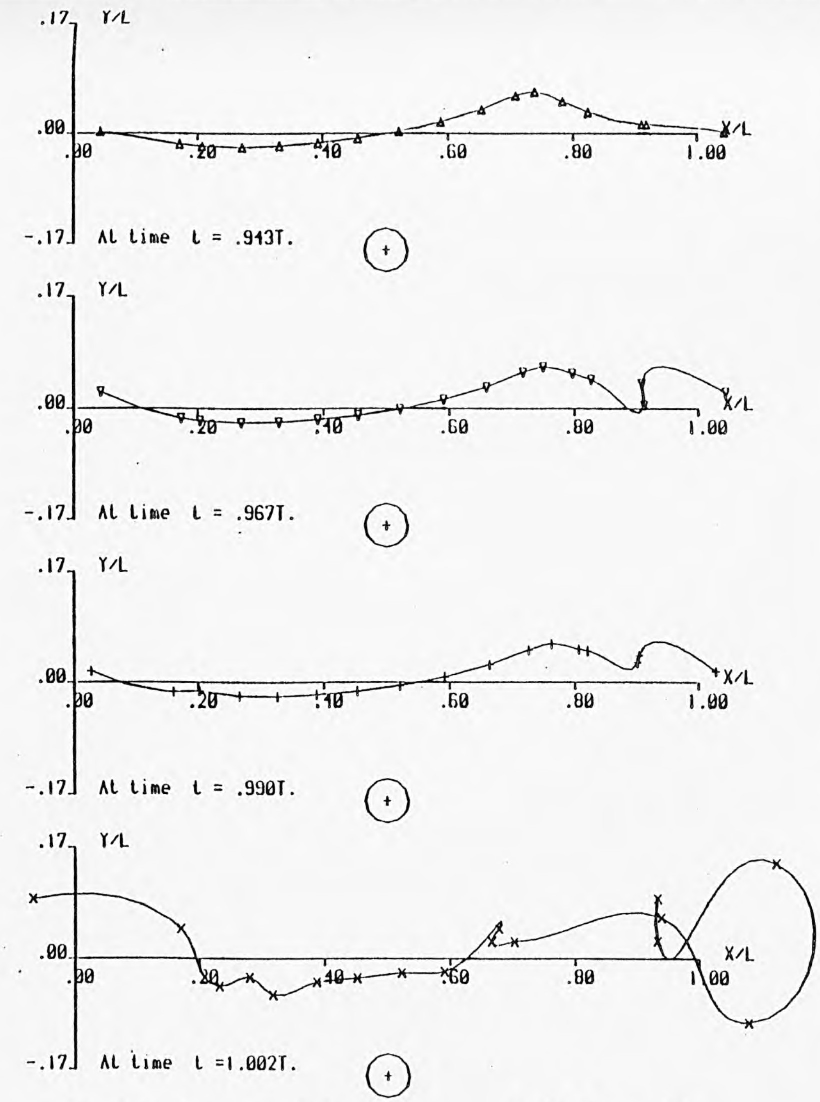

Wave height = .112m.
Wavelength = 1.595m.
Undisturbed W.L.= .555m.
Order of eq. = 1
Centre X = .798m.
Centre Y = -.294m.
Radius = .055m.

Fig. 6.4.6b

Fig. 6.4.6(a-d) A time sequence of wave profiles and auxiliary graphs for test problem 6.4.6

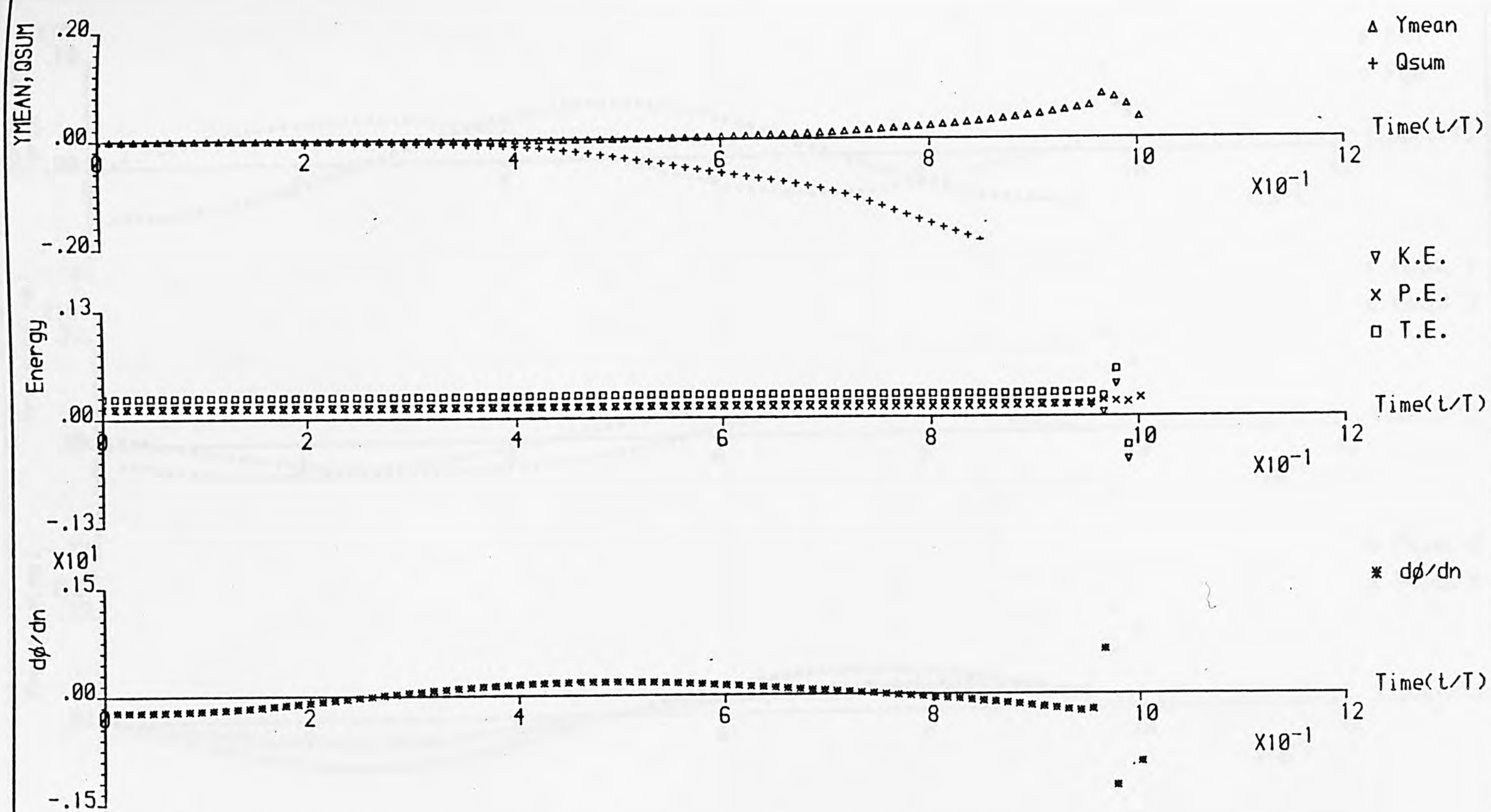

Wave height	=	.112m.	Centre X	=	.798m.
Wavelength	=	1.595m.	Centre Y	=	-.294m.
Undisturbed W.L.	=	.555m.	Radius	=	.055m.
Order of eq.	=	1			

Fig. 6.4.6c

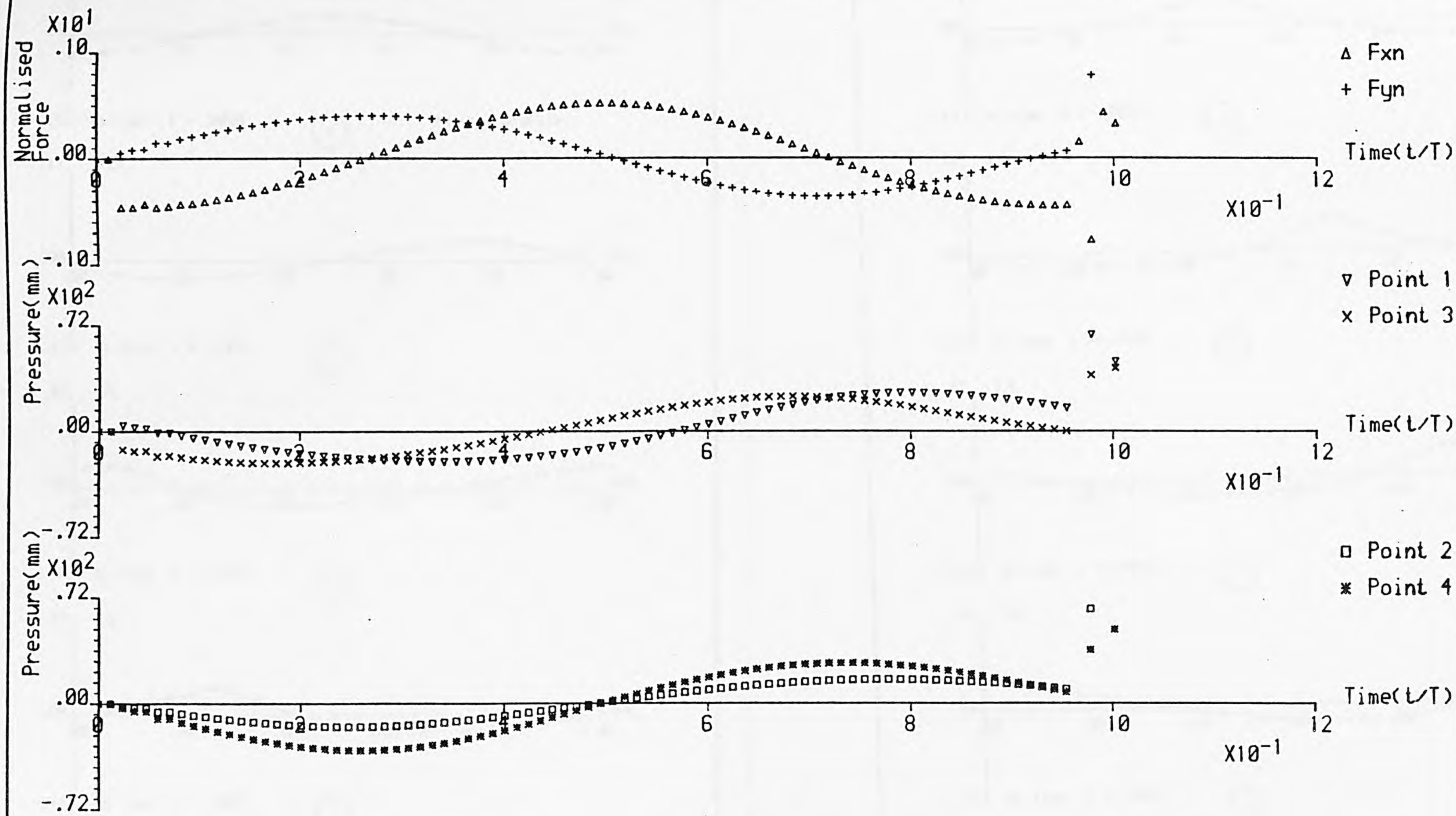

Wave height = .112m.
Wavelength = 1.595m.
Undisturbed W.L.= .555m.
Order of eq. = 1
Centre X = .798m.
Centre Y = -.294m.
Radius = .055m.

Fig. 6.4.6d

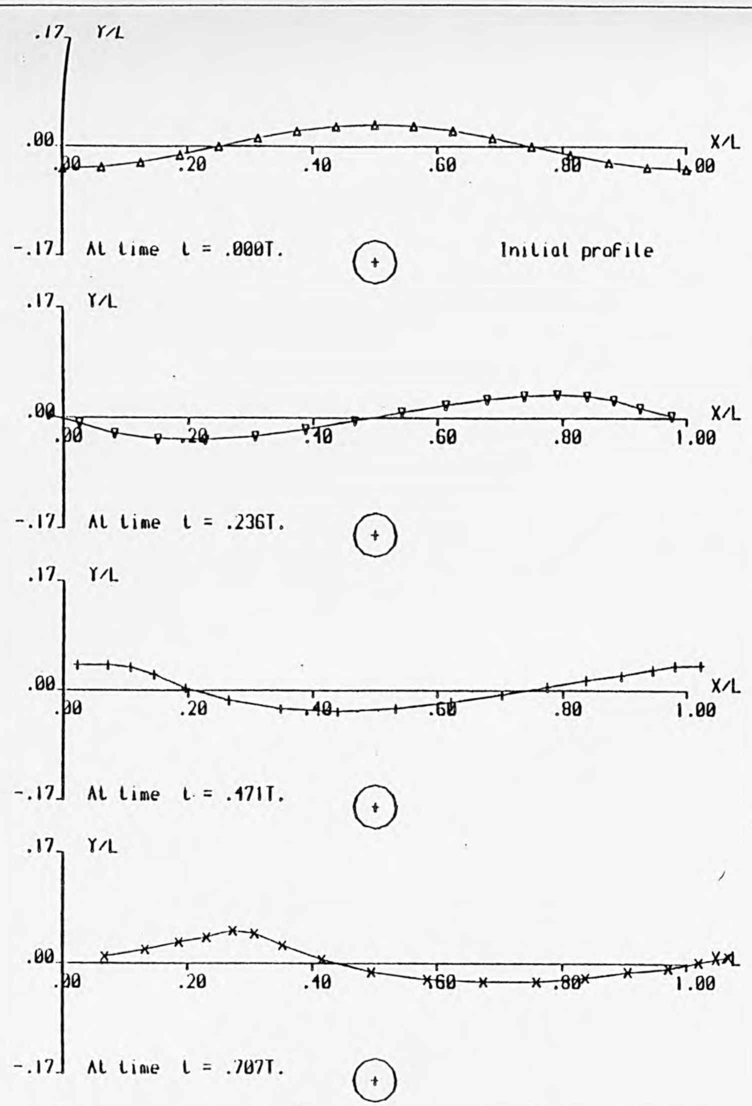

Wave height = .112m.
Wavelength = 1.595m.
Undisturbed W.L.= .555m.
Order of eq. = 1
Centre X = .798m.
Centre Y = -.294m.
Radius = .055m.

Fig. 6.4.7a

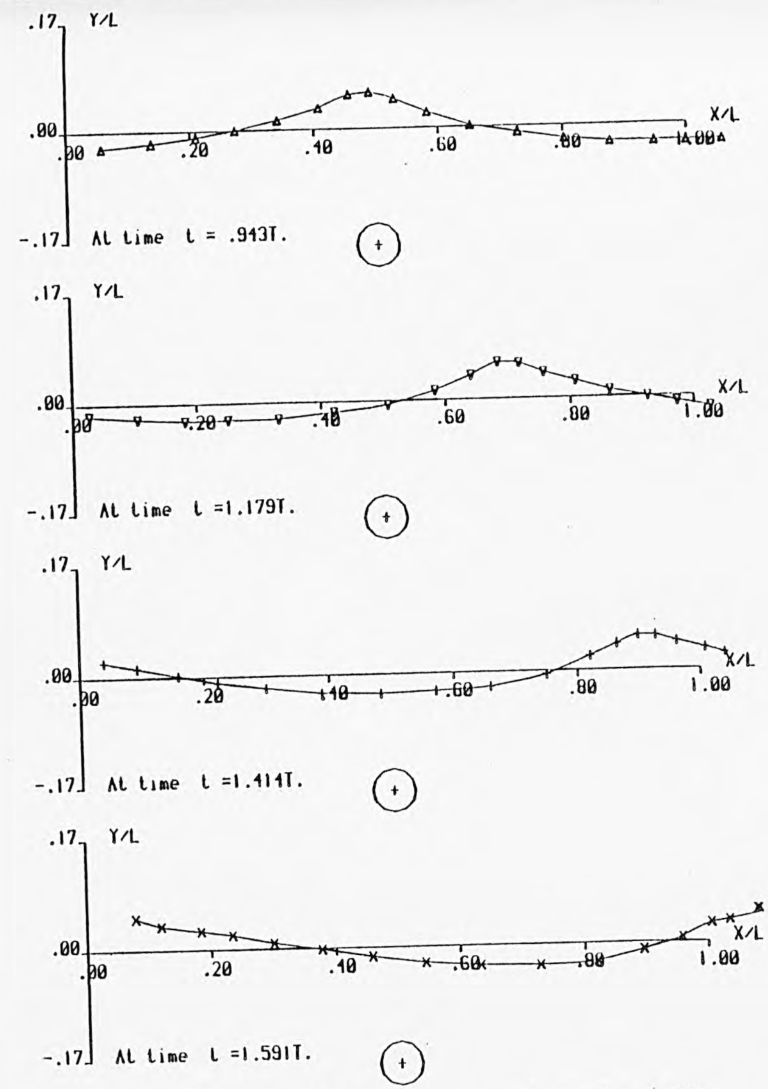

Wave height = .112m.
Wavelength = 1.595m.
Undisturbed W.L.= .555m.
Order of eq. = 1
Centre X = .798m.
Centre Y = -.294m.
Radius = .055m.

Fig. 6.4.7b

Fig. 6.4.7(a-e) A time sequence of wave profiles and auxiliary graphs for test problem 6.4.7

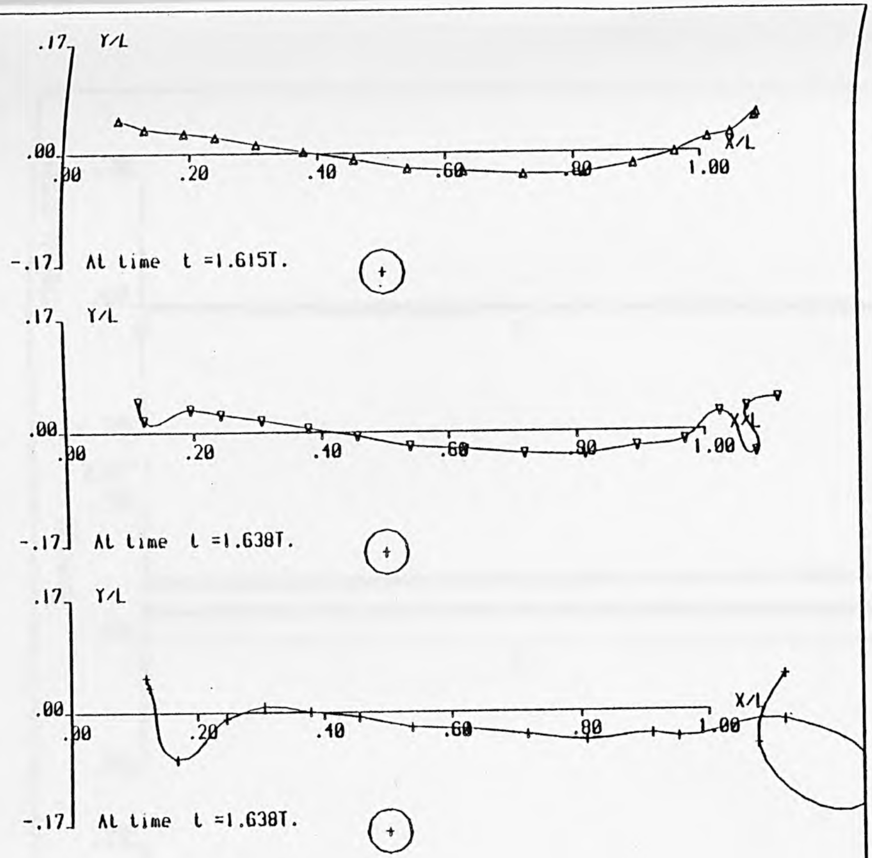

Wave height = .112m.		Centre X =	.790m.
Wavelength = 1.595m.		Centre Y =	-.294m.
Undisturbed W.L.= .555m.		Radius =	.055m.
Order of eq. = 1			

Fig.6.4.7c

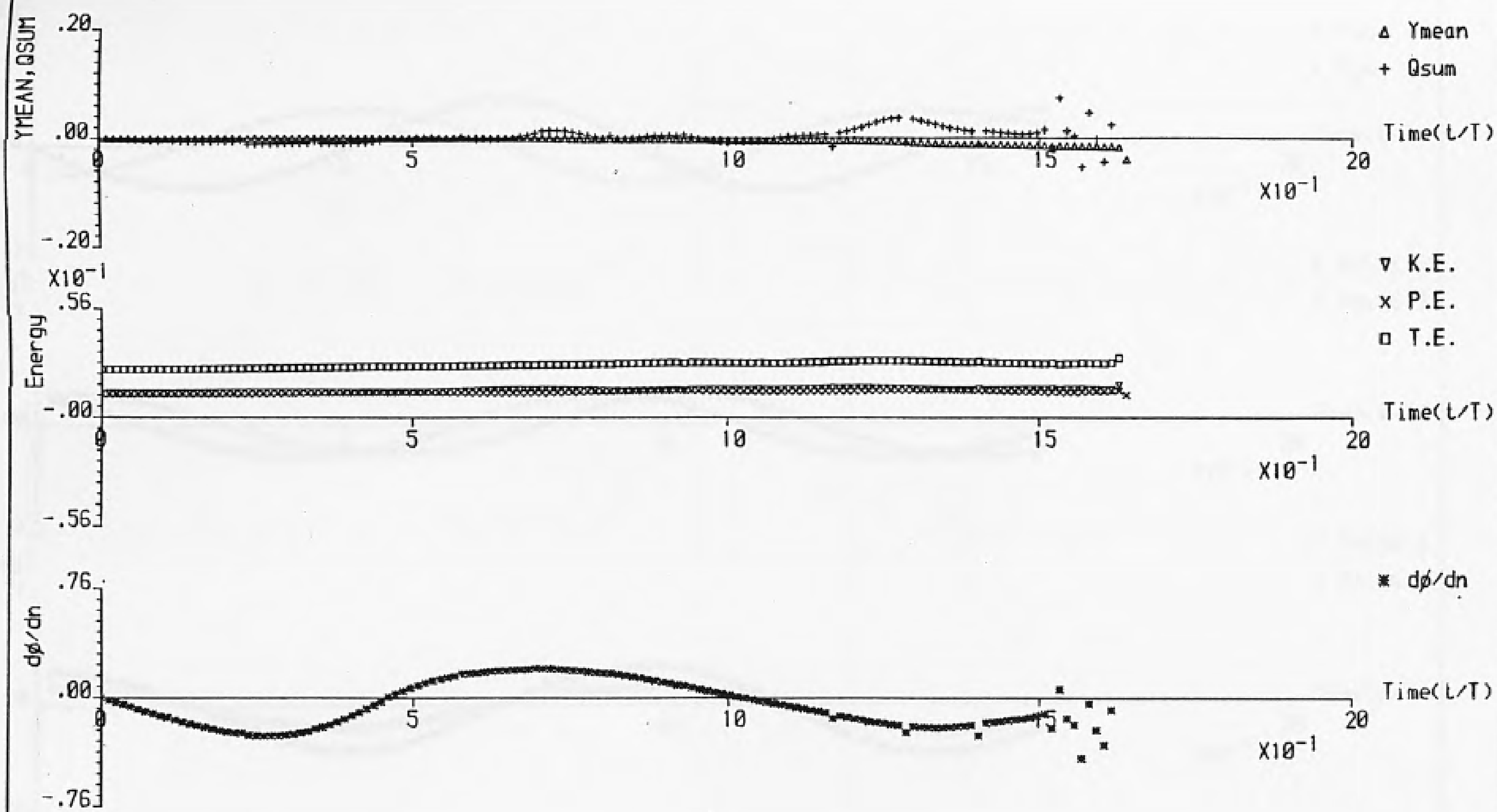

Wave height = .112m. Centre X = .798m.
Wavelength = 1.595m. Centre Y = -.294m.
Undisturbed W.L.= .555m. Radius = .055m.
Order of eq. = 1
Fig. 6.4.7d

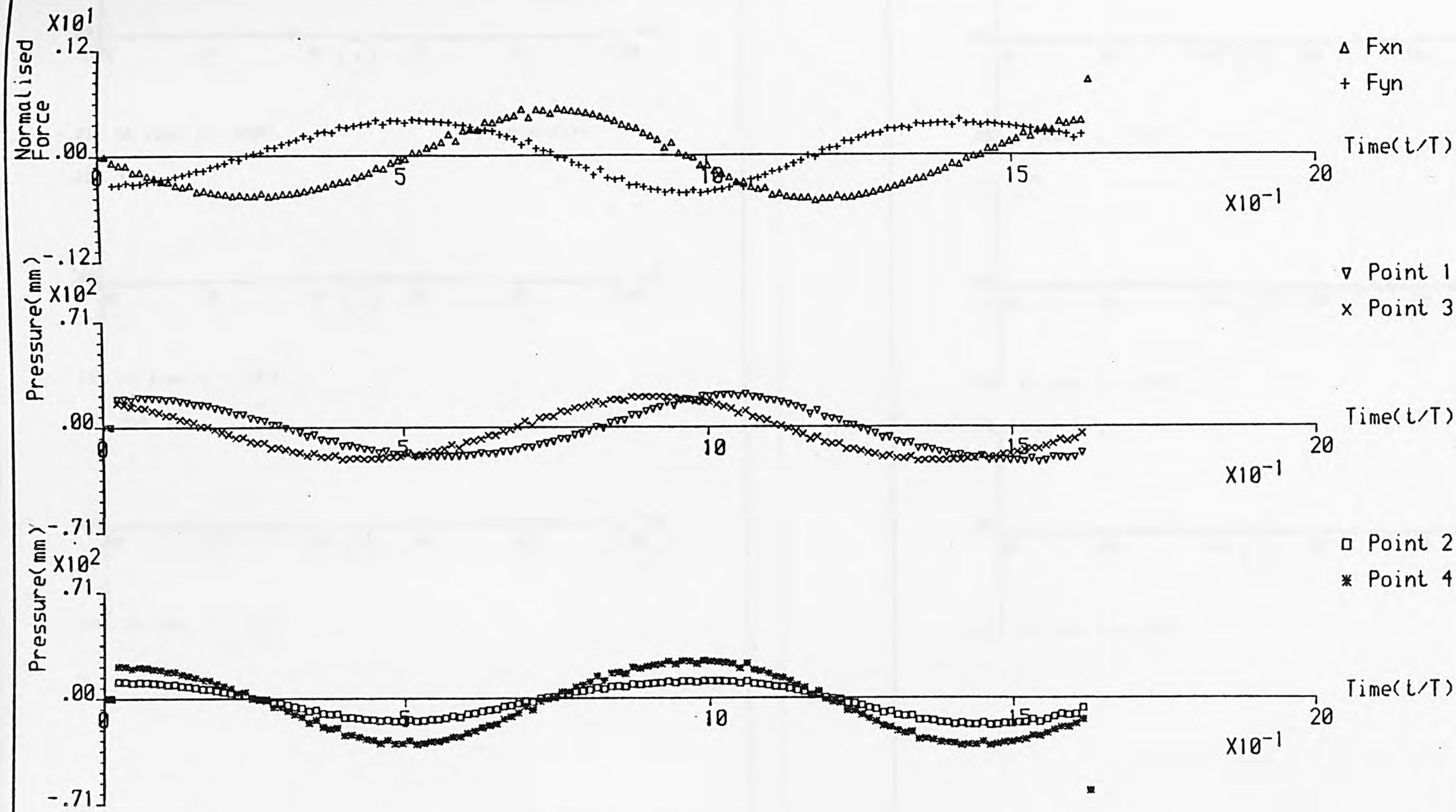

Wave height = .112m.   Centre X = .798m.
Wavelength = 1.595m.   Centre Y = -.294m.
Undisturbed W.L. = .555m.   Radius = .055m.
Order of eq. = 1

Fig. 6.4.7e

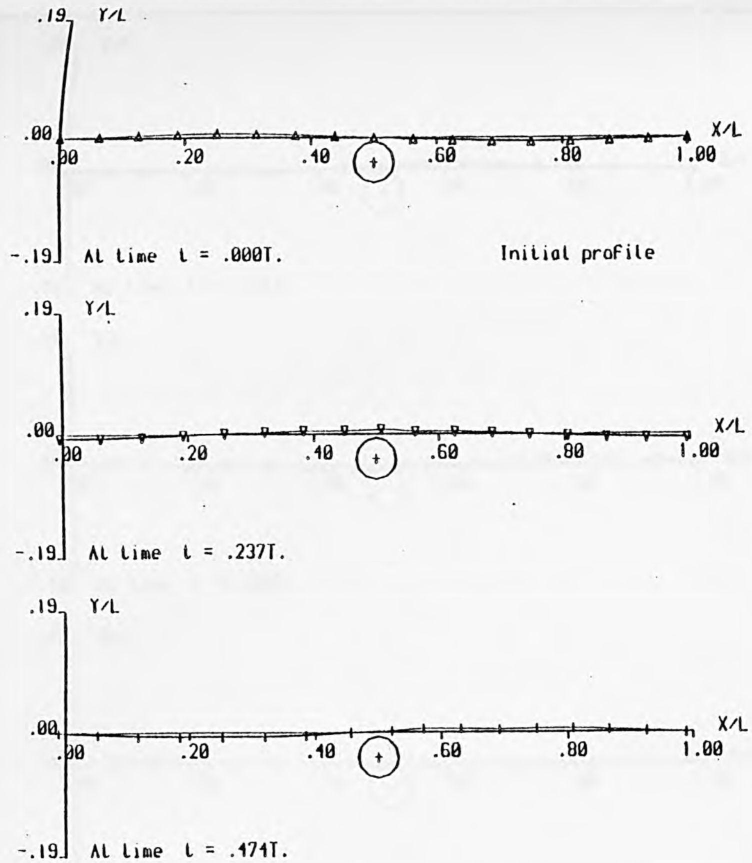

Wave height	=	.020m.	Centre X	=	.780m.
Wavelength	=	1.560m.	Centre Y	=	-.060m.
Undisturbed W.L.	=	.600m.	Radius	=	.050m.
Order of eq.	=	1			

Fig. 6.4.8a

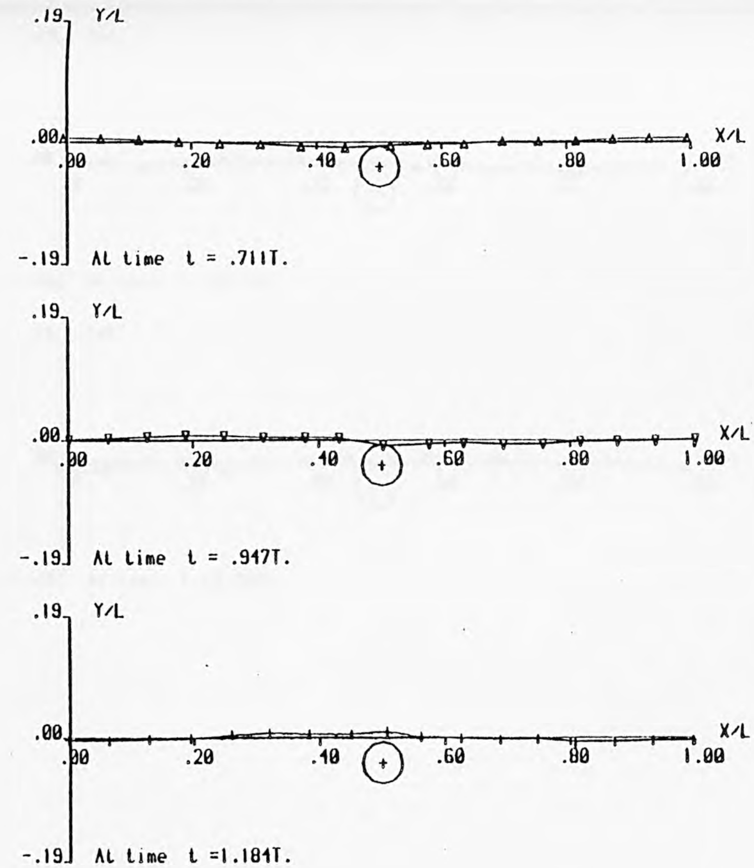

Wave height	=	.020m.	Centre X	=	.780m.
Wavelength	=	1.560m.	Centre Y	=	-.060m.
Undisturbed W.L.	=	.600m.	Radius	=	.050m.
Order of eq.	=	1			

Fig. 6.4.8b

Fig. 6.4.8(a-f) A time sequence of wave profiles and auxiliary graphs for test problem 6.4.8

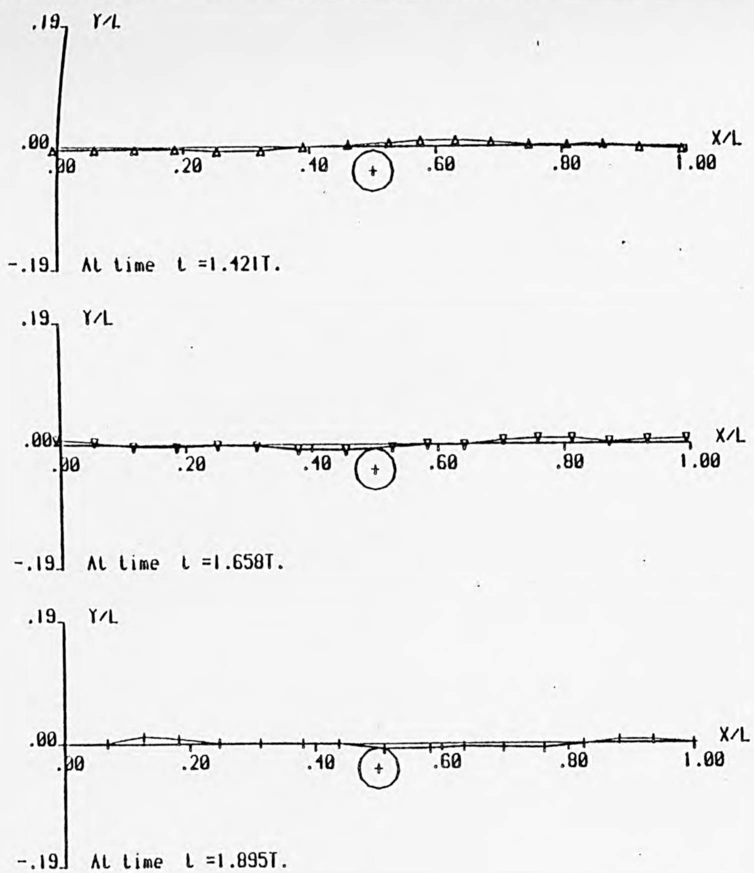

Wave height = .020m.
Wavelength = 1.560m.
Undisturbed W.L.= .600m.
Order of eq. = 1

Centre X = .780m.
Centre Y = -.060m.
Radius = .050m.

Fig. 6.4.8c

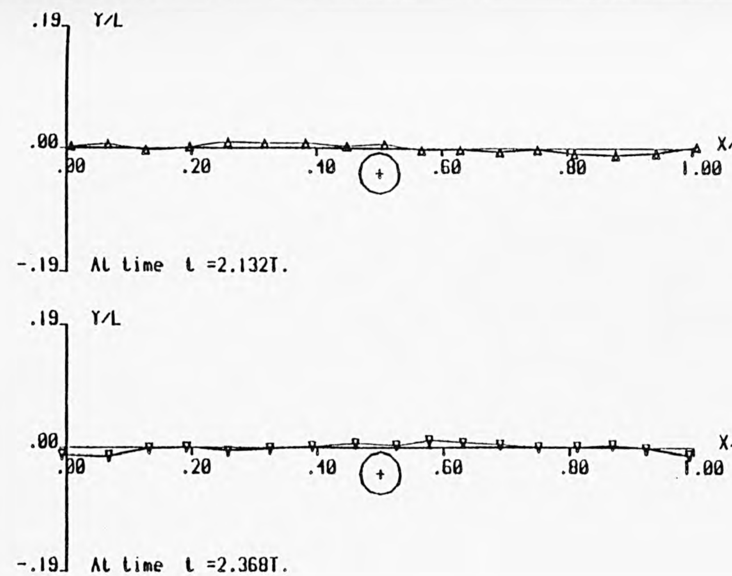

Wave height = .020m.
Wavelength = 1.560m.
Undisturbed W.L.= .600m.
Order of eq. = 1

Centre X = .780m.
Centre Y = -.060m.
Radius = .050m.

Fig. 6.4.8d

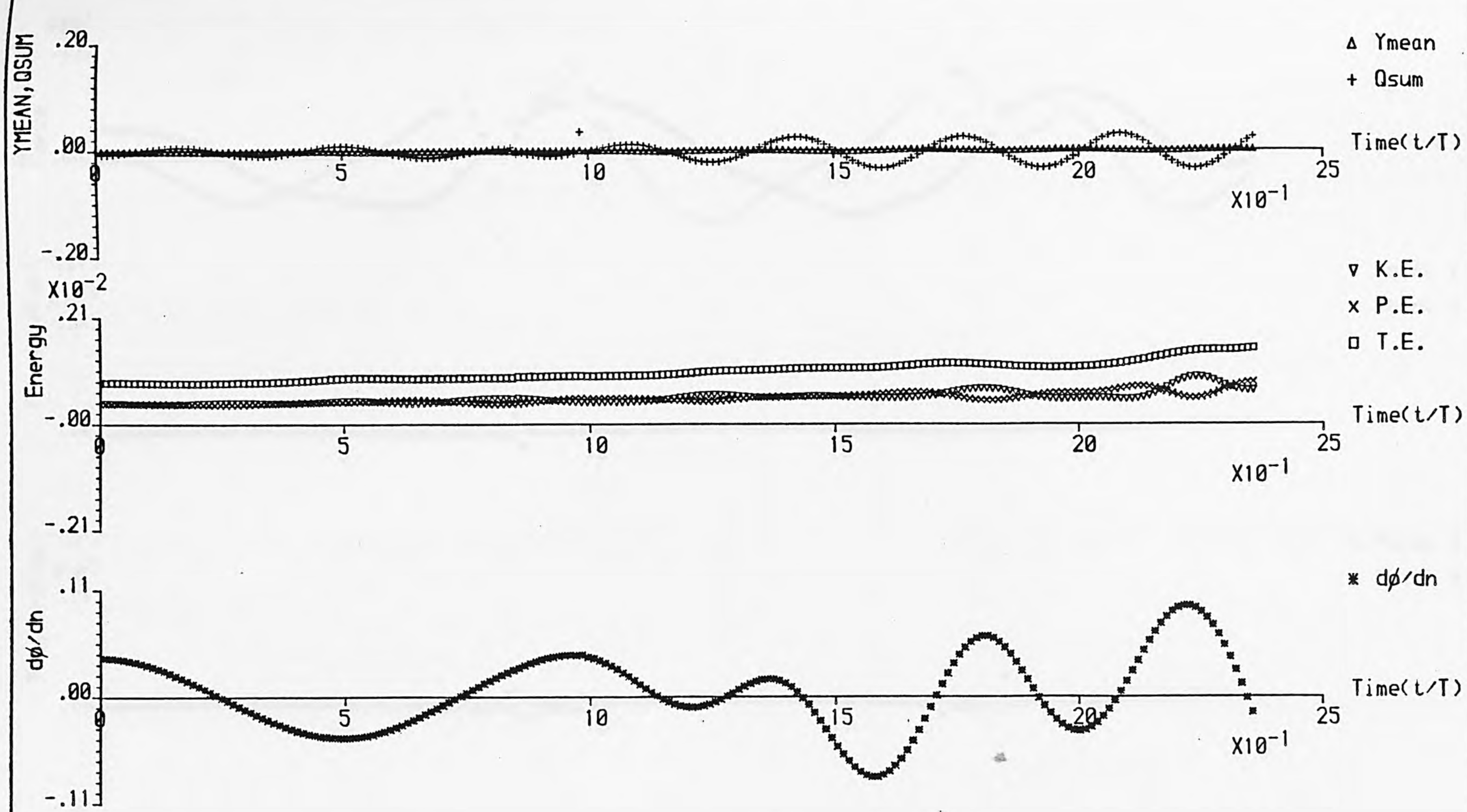

Wave height = .020m. Centre X = .780m.
Wavelength = 1.560m. Centre Y = -.060m.
Undisturbed W.L.= .600m. Radius = .050m.
Order of eq. = 1

Fig. 6.4.8e

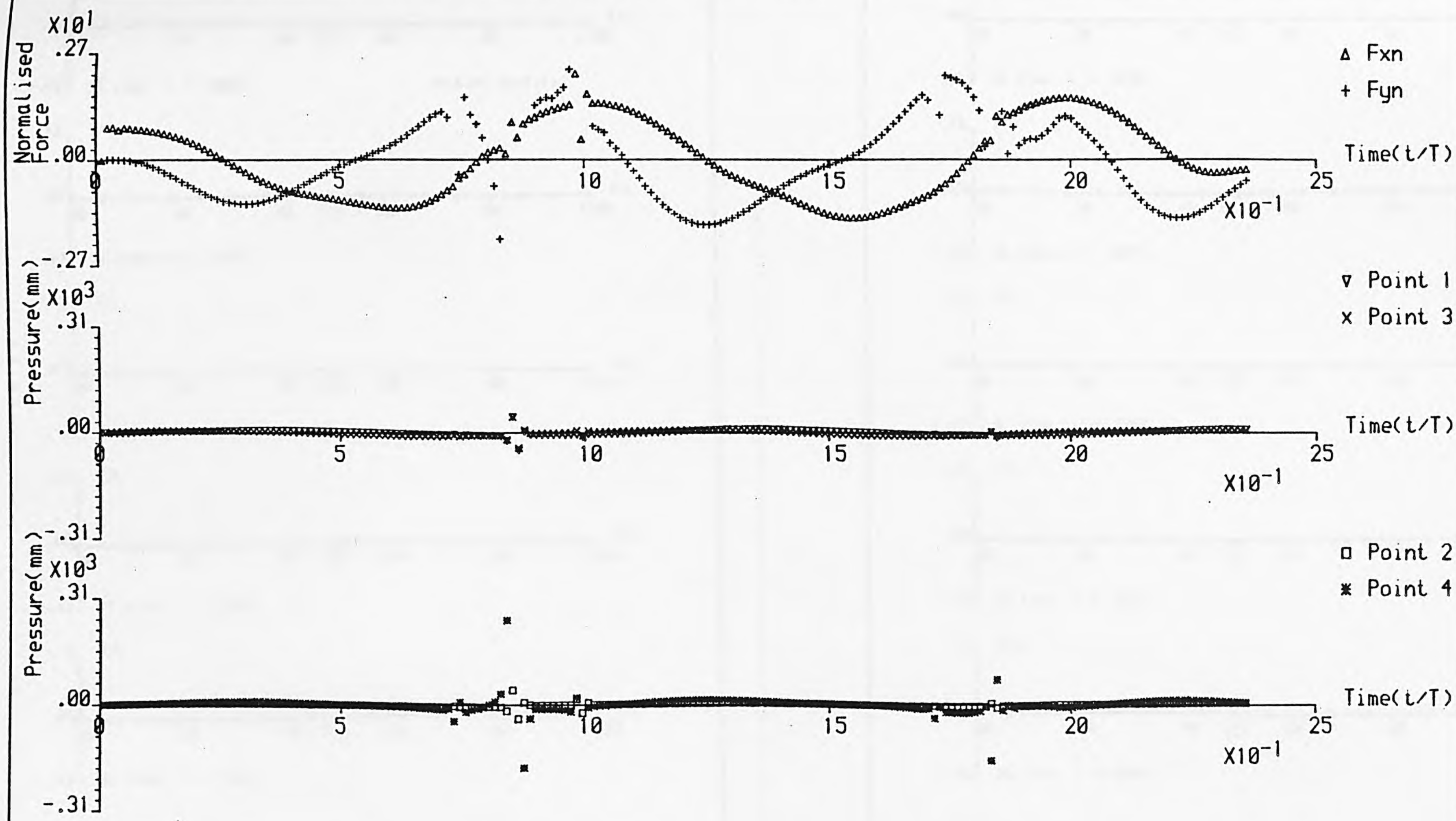

Wave height = .020m. Centre X = .780m.
Wavelength = 1.560m. Centre Y = -.060m.
Undisturbed W.L.= .600m. Radius = .050m.
Order of eq. = 1
Fig. 6.4.8f

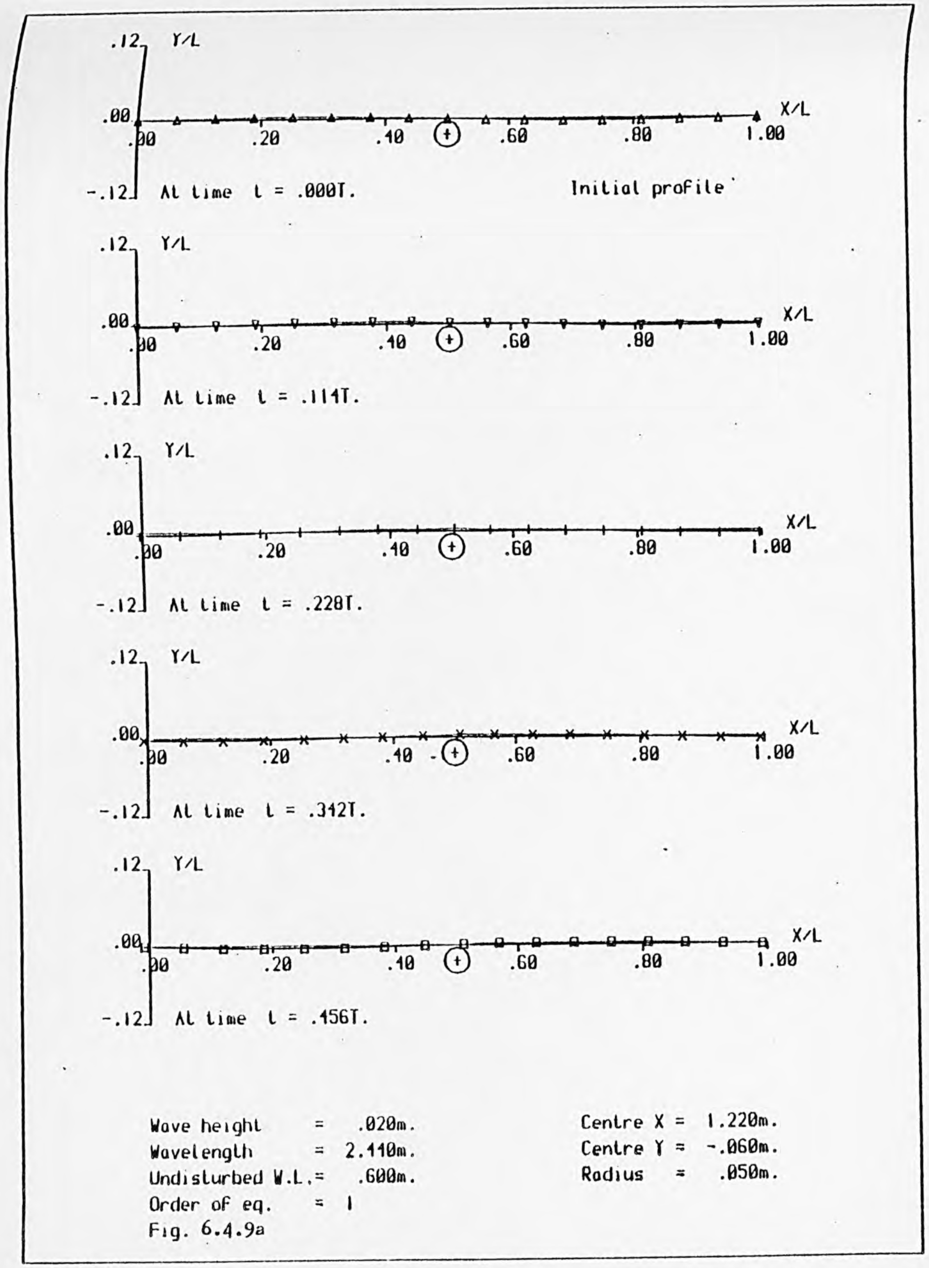

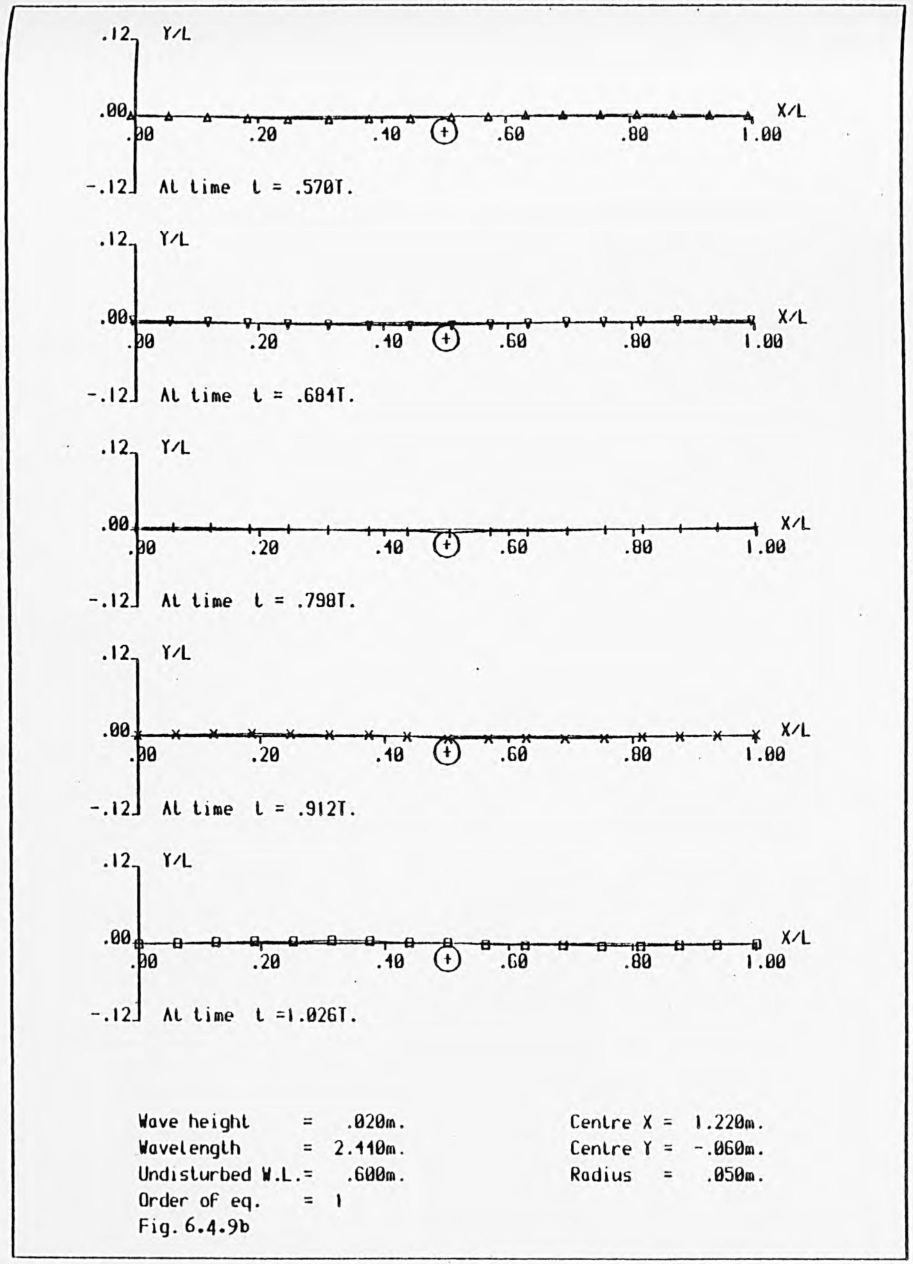

Fig. 6.4.9(a-e) A time sequence of wave profiles and auxiliary graphs for test problem 6.4.9

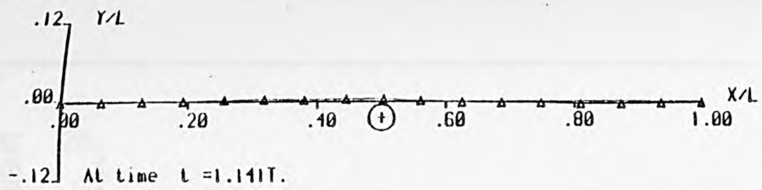

Wave height = .020m.
Wavelength = 2.440m.
Undisturbed W.L.= .600m.
Order of eq. = 1

Centre X = 1.220m.
Centre Y = -.060m.
Radius = .050m.

Fig. 6.4.9c

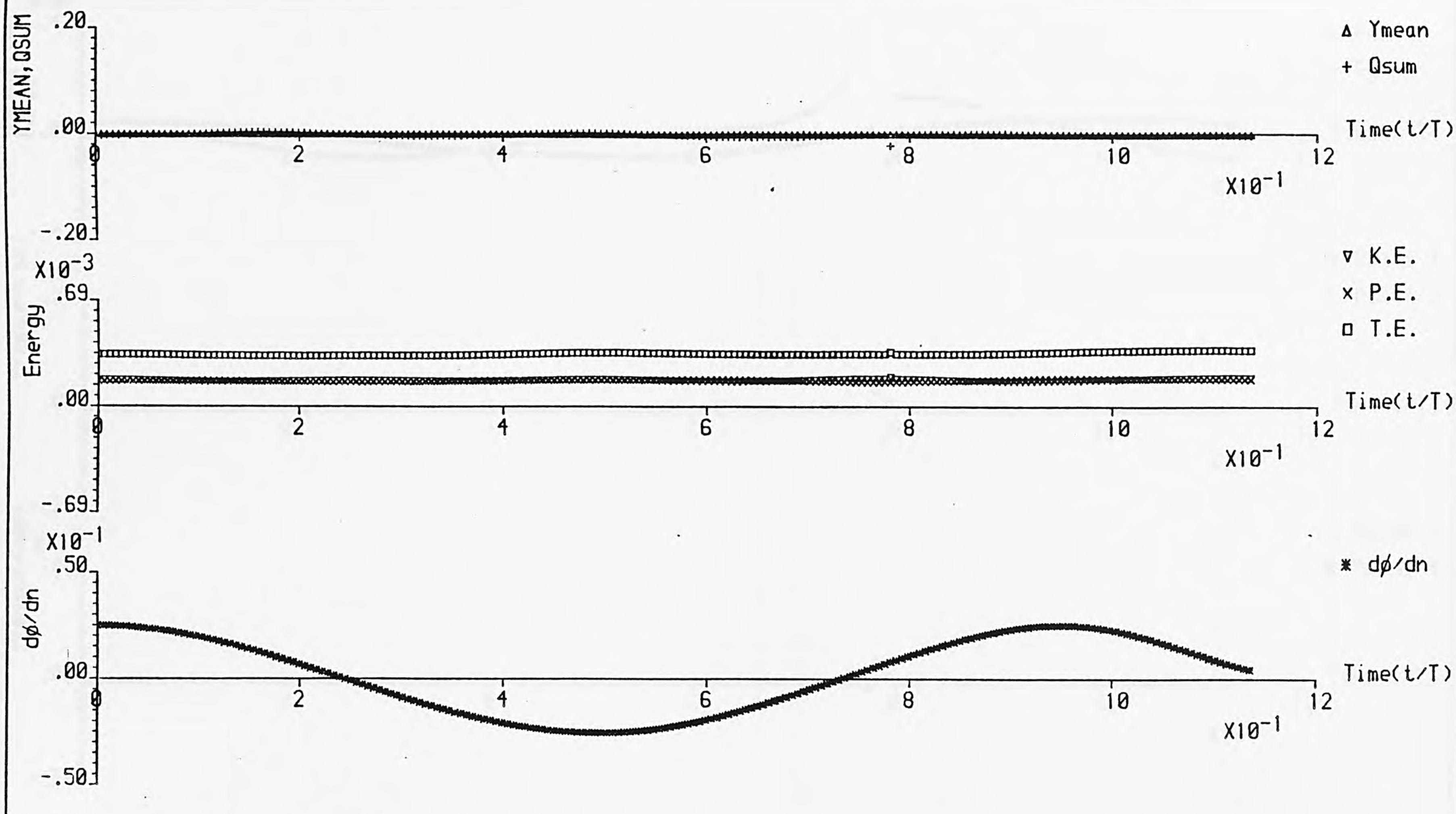

Wave height = .020m. Centre X = 1.220m.
Wavelength = 2.440m. Centre Y = -.060m.
Undisturbed W.L.= .600m. Radius = .050m.
Order of eq. = 1
Fig. 6.4.9d

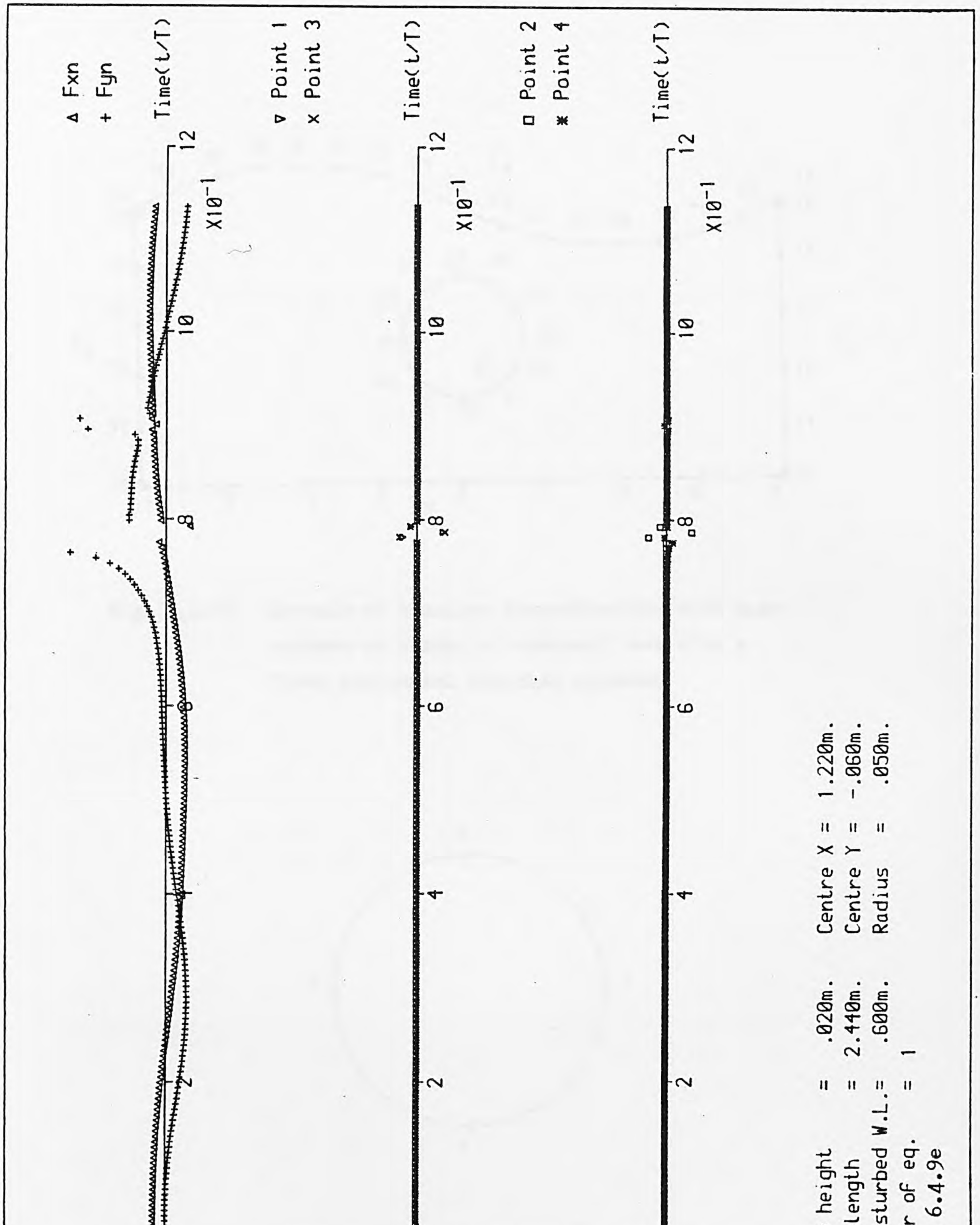

Normalised Force X10^1
.42
.00
-.42
Pressure(mm) X10^4
.28
.00
-.28
Pressure(mm) X10^4
.28
.00
-.28
0
2
4
6
8
10
12
X10^-1
Time(t/T)
Δ Fxn
+ Fyn
∇ Point 1
x Point 3
□ Point 2
✱ Point 4
Wave height = .020m.
Wavelength = 2.440m.
Undisturbed W.L.= .600m.
Order of eq. = 1
Centre X = 1.220m.
Centre Y = -.060m.
Radius = .050m.
Fig. 6.4.9e

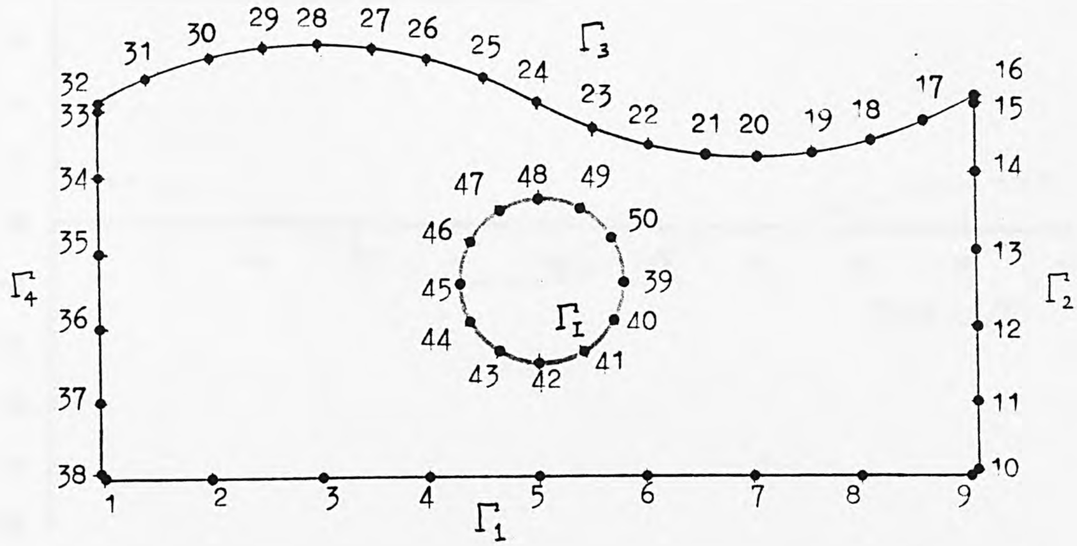

Fig. 6.4.10 Example of boundary discretisation with node numbers on domain of unsteady wave with a fixed horizontal circular cylinder

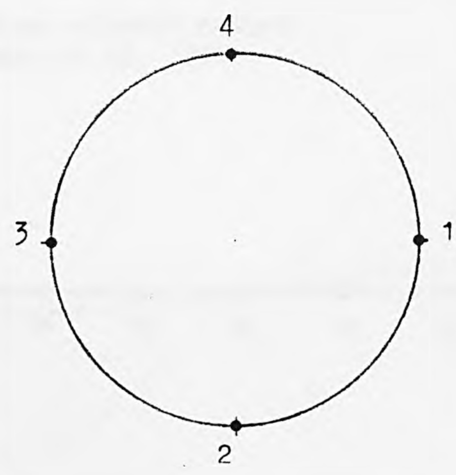

Fig. 6.4.11 Location of point numbers for pressure evaluation

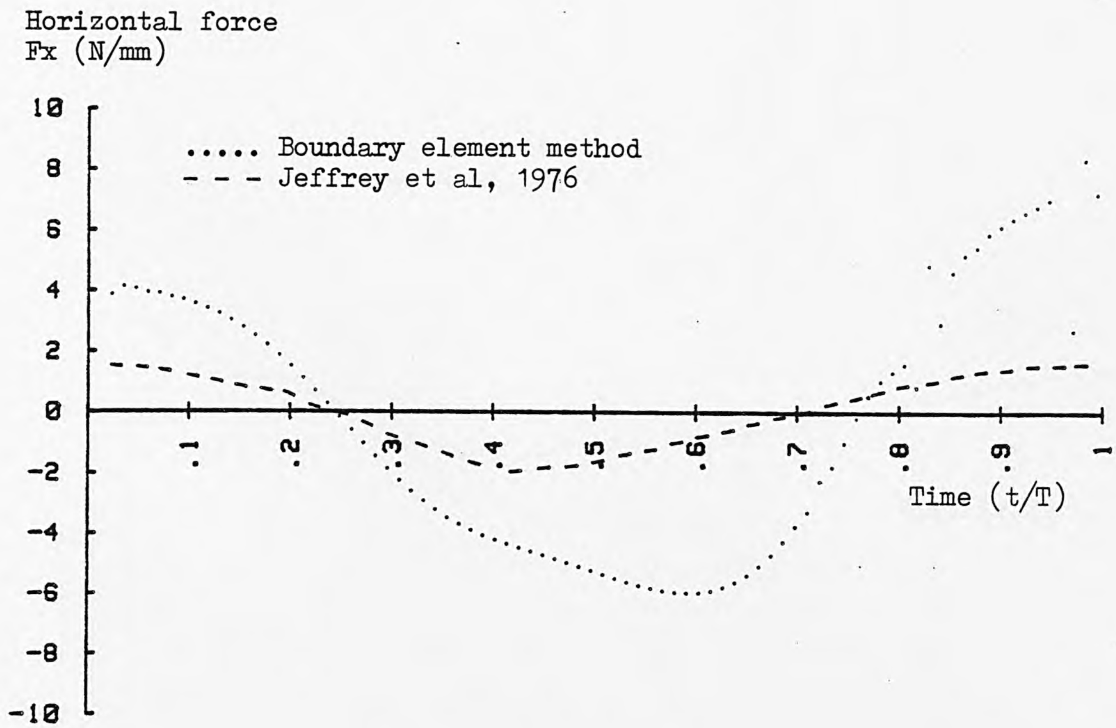

Fig. 6.4.12a Graphical representation of the comparison of horizontal forces between theoretical (BEM) and measured (Jeffrey et al, 1976) results (test problem 6.4.8)

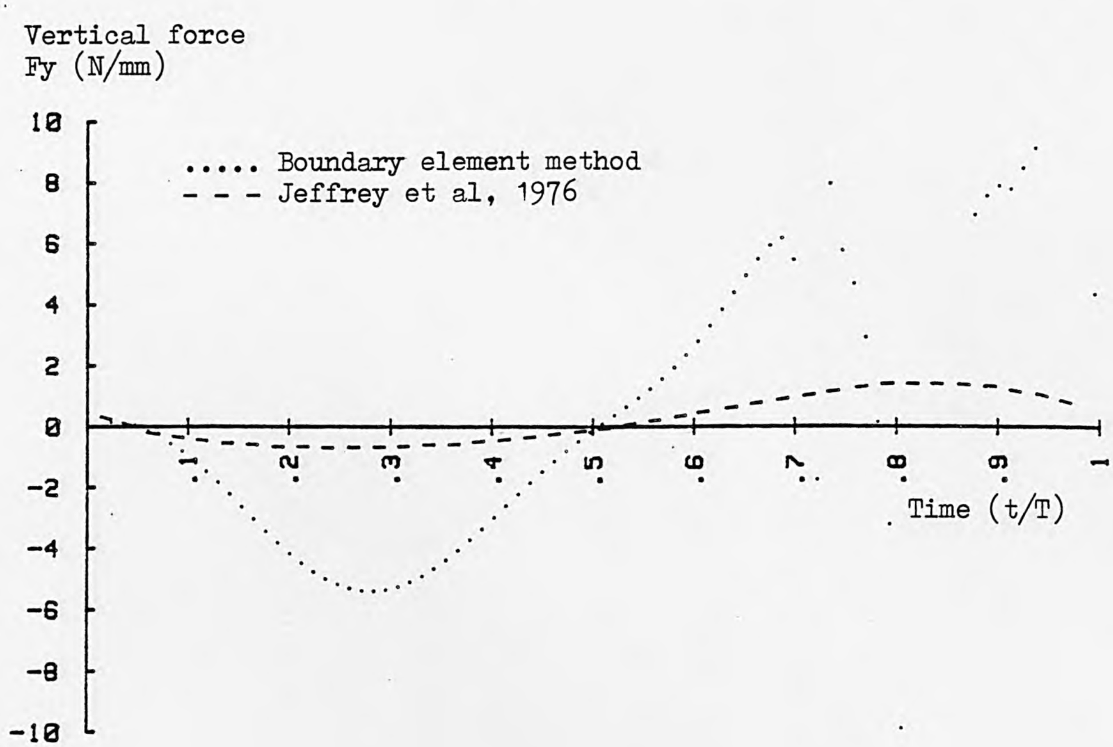

Fig. 6.4.12b Graphical representation of the comparison of vertical forces between theoretical (BEM) and measured (Jeffrey et al, 1976) results (test problem 6.4.8)

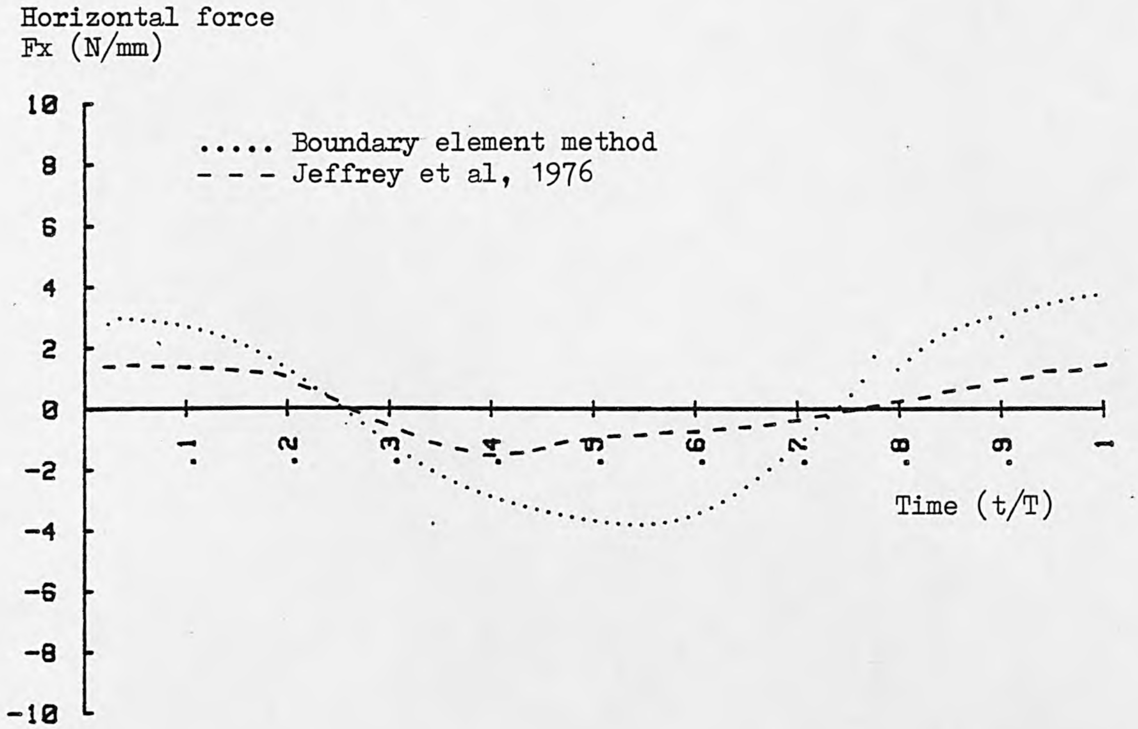

Fig. 6.4.13a Graphical representation of the comparison of horizontal forces between theoretical (BEM) and measured (Jeffrey et al, 1976) results (test problem 6.4.9)

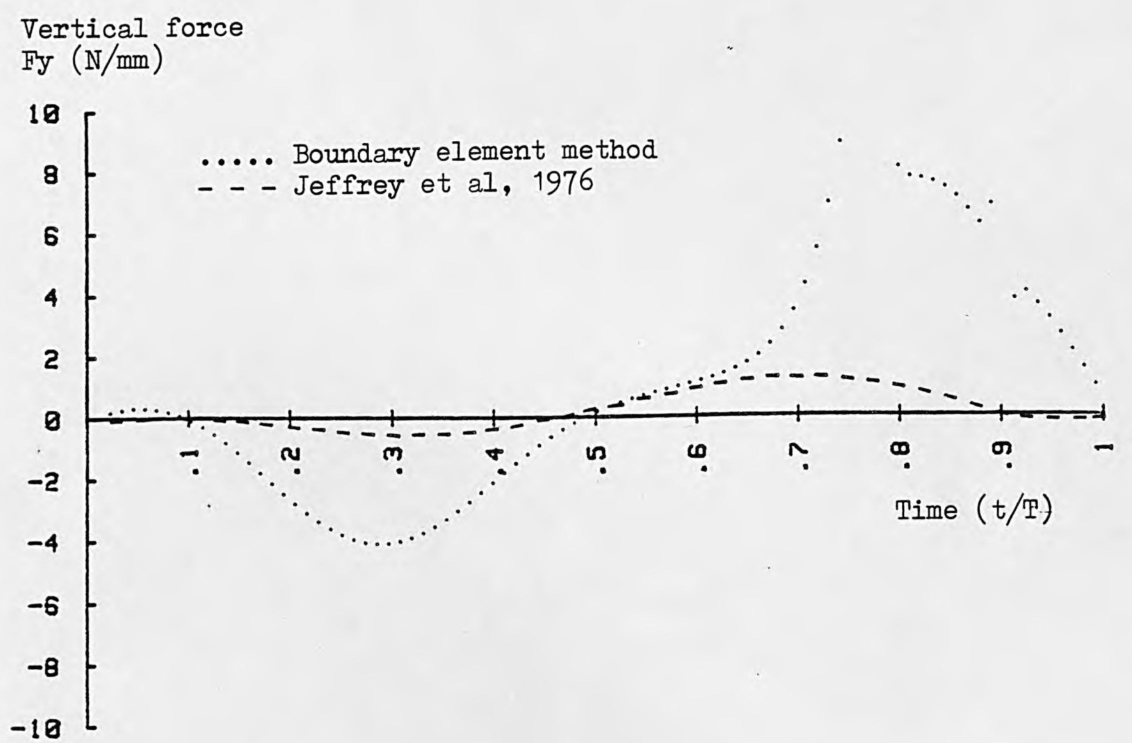

Fig. 6.4.13b Graphical representation of the comparison of vertical forces between theoretical (BEM) and measured (Jeffrey et al, 1976) results (test problem 6.4.9)

6.5 Case Studies of Experimental Results

The previous two sections discussed the limitations and reliability of the proposed technique. This section explores further, the accuracy of the method by comparing pressure results with experimental measurements which were carried out by Lacey (1983) in a wave tank at the Department of Civil Engineering, The City University.

The experimental results obtained were for a single cylinder of radius, $r = 0.055$m and a range of waves, in water of depth, $d = 0.555$m, at three frequencies $f_o = 0.977$, 1.172 and 1.367 Hz. The value of the diffraction parameter is therefore within the range $0.2 < kr < 0.5$. The cylinder is located at three depths of submergence for the sets of waves at each frequency corresponding to $(y_o - r)/\lambda = 0.05$, 0.10 and 0.15. The details of the incident wave motion are given in Table 6.5.1(a-c). It covers the intermediate water depth ($0.05 \leqslant d/\lambda \leqslant 0.5$) and deep water depth ($d/\lambda > 0.5$) ranges. $(y_o - r)/\lambda$ describes the location of the obstacle and thus gives an indication of the instantaneous shallow water region above the cylinder. Both parameters give an indication of the importance of non-linear effect.

Wave profiles and auxiliary graphs for some of the 56 cases are presented in Appendix A. 13. In a broad sense, the duration of wave movement is inversely proportional to wave height and directly proportional to the depth of submergence of the horizontal circular cylinder. Duration of wave movement of up to 6 periods is recorded in the small amplitude wave case 23.

The major source of failure occurred in the wave profile, where two nodes on the downstream side moved towards each other to produce a re-entrant boundary which finally led to the complete failure (numerical instability), as discussed in section 6.3. This type of failure occurred for all cases of depths of submergence and frequencies. Cases 1, 6, 11, 37, 44 and 51 did not show any failure, because the number of loops specified in the runs had been reached before the failure mode developed.

The depths of submergence of the cylinder may affect the shape of wave profile depending upon the water depth in the wave trough region above the cylinder. As for the cases of $(y_o - r)/\lambda =$ 0.15 and 0.10, the wave profiles in the region above the cylinder remained in-shape. But for the cases of $(y_o - r)/\lambda = 0.05$, the depth of water in the wave trough region above the cylinder became too shallow so that the existence of the cylinder had a significant impact on the shape of the wave profile. The in-coming wave seemed to stumble over the cylinder and flatten out. The disturbed profile continued to move until a re-entrant boundary developed which resulted in complete failure due to numerical instability. For the wave steepness, $H/\lambda > 0.1$, as in case 36, a plunging wave developed soon after the wave trough hit the cylinder, see Figs. A.13.36. A small amount of breaking was detected for the steeper waves, at the shallowest of the cylinder locations, during the experimental measurements.

The pressure amplitudes, together with their occurence in time for each case, have been extracted from the computer outputs. They are presented in Table 6.5.2(a-f). Points 1, 2, 3, and 4 refer to quarter positions on the cylinder in clockwise direction, see

Fig.6.5.1. Their positions are identical to the positions of pressure tapping in the experiments, whose numbering sequence are in the anti-clockwise direction, see Fig. 6.5.2. In this study, point 1 is situated on the side of the cylinder on the downstream face, and point 2 is at the bottom of the cylinder. Point 3 is on the side of the cylinder on the upstream face and point 4 is on the top of the cylinder.

From Table 6.5.2 or the pressure graphs in Figs. A.13.1 - A.13.56 , the pressure variations do not behave like a sine or cosine curve although the initial wave profile assumes simple harmonic motion. Positive pressure amplitudes do not equal the negative pressure amplitudes. Once a re-entrant boundary developed on the wave profile, the calculated pressure values fluctuated in a disordered manner until total failure occurred. In general, the pressure amplitudes behave in a periodically divergent manner with the magnitudes shifting rigidly upward (see Fig. A.13.1). The pressure graphs show clearly that pressures at point 2 and point 4 are in-phase and pressures at point 1 and point 3 and out-of-phase.

Since the durations of wave movement vary according to their wave characteristic and their pressure amplitudes diverge in all cases, mean values of pressure amplitude are calculated using a trapezoidal formula. The ratios of measured pressure, from Lacey (1983), to the theoretical mean pressure are then obtained for all cases. It is also of interest to obtain the ratios of measured pressure to the first available or initial theoretical pressure. Both ratios are presented in Table 6.5.3 (a-l). In order to allow comparisons with Lacey's theoretical results, several sets of graphs (Figs. 6.5.3 - 6.5.4) have been drawn according to the format used by Lacey whose relevant graphs are reproduced here for completeness (Figs. 6.5.7). The first set of graphs (Figs. 6.5.3a-c) are plotted with initial theoretical pressure ratio, Pm/Pti, against wave steepness H/λ for four pressure points. The second set of graphs (Figs. 6.5.4a-c) are plotted with mean theoretical pressure ratio, Pm/Ptm , against wave steepness H/λ for four pressure points. Each of the three graphs in both sets give results for a different value of the diffraction parameter and include results for each of the different cylinder locations. These graphs will indicate the significance of the finite wave height for different cylinder submergence. Scale axes for different points are identical to Lacey's presentation to give an indication that the extent of departure from the linear theory predictions varies with the positions on the cylinder.

For kr = 0.22, the initial theoretical results are very much similar to Lacey's theoretical results whereas the mean theoretical results agree very well with measured values for small wave steepness but they are under-estimated for steeper waves by about 5% at points 1 and 3, and 10% at points 2 and 4.

For kr = 0.305, the initial theoretical pressures at all points are under-estimated at large wave steepness: 5% at point 1; 50% at point 2; 10% at point 3 and 30% at point 4. The mean theoretical pressures fluctuate more than the initial theoretical pressures with over-estimation at small wave steepness and under-estimation at large wave steepness. The larger discrepancy at point 2 (bottom of the cylinder) might be attributed in part to experimental error because the amplitudes of oscillation are small.

For $kr = 0.41$ the initial theoretical pressures again resemble Lacey's theoretical pressures except at point 4 where the experimental measured values are about 30% higher than the initial theoretical values. The mean theoretical pressures reduce the difference at point 4 to about 15%. The pressures at point 1 are on average 5% higher than the measured values for the initial theoretical pressure but it becomes 5% lower for the mean theoretical pressures. At point 3 both initial and mean theoretical pressures are 10% lower than the measured values. Under-esimation also applies to point 2 which is about 10% for initial pressures and 25% for mean pressures.

The graphs have also been replotted to group them according to the format used by Lacey (reproduced here as Figs. 6.5.8). Figs. 6.5.5 shows the set of graphs for initial theoretical pressure ratio against cylinder submergence parameter. Fig.6.5.6 shows the set of graphs for mean theoretical pressure ratio against cylinder submergence parameter. The purpose of the replot is to identify the difference between experimental measurements and theoretical predictions for each of the cylinder locations.

At the deepest and intermediate submergences, the accuracy of the results of theoretical pressures decrease as wave steepness increases. But the fluctuation of initial theoretical pressure results are smaller than that of mean theoretical pressure results. At the shallowest submergemce, since the cylinder is nearer to the wave surface, the fluctuations of both initial and mean theoretical pressure results are quite poor even for the smallest values of the wave steepness parameter. For steeper waves, there is significant disagreement between the theoretical and experimental pressure amplitudes at all locations on the cylinder.

Components of horizontal and vertical forces on the circular cylinder have also been evaluated through equations 5.5.4 for all cases. They are also presented in graphical form. Since they are obtained through calculated pressure results, their behaviour resembles those for the pressure amplitudes.

Lacey (1983) has produced values of diffraction coefficient, Cx, for two sets of depth of submergence for cylinder with variable wave height and fixed wave length (see Fig. 6.5.9). Since the diffraction coefficient is a non-dimensional term, related to the corresponding wave condition and cylinder position, it may therefore be used to calculate horizontal force on the circular cylinder based on the linear diffraction theory.

Table 6.5.4 shows the magnitude of forces, expressed in Newton per metre, and their ratios of calculated value from diffraction theory to the theoretical horizontal force. Again, initial and mean forces have the same layout as for the comparison of pressure amplitudes. The ratios are reproduced in graphical form (see Figs. 6.5.10), from which variation of mean forces ratio is about ± 30% whereas the variation of initial force ratio remains at about +8% for $(y_0 - r)/\lambda = 0.10$ and +20% for $(y_0 - r)/\lambda = 0.05$. The calculated forces are based on linear diffraction theory whose results are unreliable for finite wave steepness. It may be concluded that the proposed technique behaves linearly for initial interpretations and becomes non- linear over the whole execution.

CASE No.	Yo (m)	(Yo-r)/λ	H (m)	H/λ	H/d
1	.294	.150	.028	.018	.505
2	.294	.150	.052	.033	.094
3	.294	.150	.072	.046	.130
4	.294	.150	.091	.059	.163
5	.294	.150	.112	.072	.202
6	.215	.100	.029	.018	.052
7	.215	.100	.051	.033	.093
8	.215	.100	.073	.047	.132
9	.215	.100	.922	.059	.166
10	.215	.100	.114	.072	.206
11	.135	.050	.029	.019	.052
12	.135	.050	.051	.033	.093
13	.135	.050	.073	.047	.132
14	.135	.050	.094	.060	.169
15	.135	.050	.114	.073	.205

Table 6.5.1a Incident wave characteristics at f_o = 0.98 Hz

CASE No.	Yo (m)	(Yo-r)/λ	H (m)	H/λ	H/d
16	.225	.150	.016	.014	.029
17	.225	.150	.035	.031	.063
18	.225	.150	.053	.046	.095
19	.225	.150	.071	.062	.128
20	.225	.150	.087	.077	.157
21	.225	.150	.100	.088	.181
22	.225	.150	.112	.098	.201
23	.168	.100	.017	.015	.030
24	.168	.100	.037	.032	.066
25	.168	.100	.055	.048	.098
26	.168	.100	.070	.062	.126
27	.168	.100	.087	.077	.157
28	.168	.100	.100	.088	.181
29	.168	.100	.113	.100	.204
30	.112	.050	.015	.013	.028
31	.112	.050	.037	.033	.067
32	.112	.050	.054	.048	.098
33	.112	.050	.071	.063	.128
34	.112	.050	.088	.078	.159
35	.112	.050	.101	.089	.182
36	.112	.050	.114	.100	.205

Table 6.5.1b Incident wave characteristics at f_o = 1.17 Hz

CASE No.	Yo (m)	(Yo-r)/λ	H (m)	H/λ	H/d
37	.180	.150	.018	.022	.033
38	.180	.150	.031	.037	.056
39	.180	.150	.040	.048	.072
40	.180	.150	.050	.060	.091
41	.180	.150	.060	.071	.107
42	.180	.150	.068	.082	.123
43	.180	.150	.075	.090	.136
44	.139	.100	.018	.022	.033
45	.139	.100	.030	.036	.054
46	.139	.100	.040	.048	.072
47	.139	.100	.049	.059	.089
48	.139	.100	.060	.072	.109
49	.139	.100	.069	.082	.124
50	.139	.100	.077	.092	.138
51	.097	.050	.019	.023	.035
52	.097	.050	.029	.034	.052
53	.097	.050	.041	.049	.074
54	.097	.050	.052	.063	.094
55	.097	.050	.060	.072	.108
56	.097	.050	.068	.081	.123

Table 6.5.1c Incident wave characteristics at f_0 = 1.37 Hz

CASE NUMBER	POINT 1		POINT 2		POINT 3		POINT 4	
	TIME T1 (sec)	PRESSURE P1 (mm)	TIME T2 (sec)	PRESSURE P2 (mm)	TIME T3 (sec)	PRESSURE P3 (mm)	TIME T4 (sec)	PRESSURE P4 (mm)
1	.317	+4.980	.248	+3.195	.186	+4.931	.248	+6.329
	.813	-4.836	.744	-3.374	.682	-4.965	.744	-6.825
	1.316	+5.829	1.247	+3.846	1.185	+5.725	1.247	+7.256
	1.798	-4.111	1.729	-2.580	1.660	-4.360	1.729	-6.326
	2.301	+7.046	2.246	+5.033	2.170	+6.937	2.232	+8.466
	2.777	-2.284	2.701	-1.060	2.646	-3.078	2.715	-4.806
	3.300	+9.000	3.238	+6.924	3.162	+9.076	3.224	+10.589
2	.313	+9.273	.252	+5.734	.182	+9.155	.242	+11.355
	.807	-8.926	.737	-6.530	.676	-9.314	.747	-13.130
	1.312	+11.813	1.262	+7.588	1.181	+11.305	1.251	+13.919
	1.776	-5.364	1.695	-3.132	1.635	-6.807	1.706	-10.689
	2.291	+16.067	2.251	+11.786	2.160	+15.564	2.220	+18.049
3	.309	+12.695	.249	+7.632	.180	+12.553	.241	+15.098
	.808	-11.926	.730	-9.036	.679	-12.627	.748	-18.107
	1.315	+17.230	1.272	+10.956	1.186	+15.909	1.255	+19.244
4	.306	+15.884	.245	+9.293	.184	+15.728	.237	+18.361
	.797	-14.655	.728	-11.434	.674	-15.680	.743	-22.836
	1.318	+24.100	1.295	+15.609	1.180	+20.895	1.256	+25.076
5	.303	+19.565	.248	+11.080	.179	+19.418	.234	+21.855
	.785	-17.750	.723	-14.248	.668	-19.146	.737	-28.342
6	.313	+6.598	.251	+3.945	.183	+6.528	.251	+8.511
	.822	-6.465	.747	-4.314	.686	-6.648	.754	-9.537
	1.318	+7.666	1.257	+4.661	1.189	+7.576	1.250	+9.761
	1.807	-5.811	1.732	-3.524	1.664	-6.088	1.732	-9.197
	2.310	+8.861	2.249	+5.905	2.174	+8.774	2.235	+10.904
	2.792	-3.786	2.711	-1.922	2.656	-4.780	2.731	-7.545
	3.302	+11.007	3.247	+7.913	3.166	+11.332	3.227	+13.472
7	.315	+11.768	.254	+6.737	.183	+11.593	.244	+14.512
	.824	-11.409	.742	-8.052	.681	-11.921	.753	-17.623
	1.312	+14.656	1.261	+8.576	1.190	+14.269	1.251	+17.633
	1.790	-8.413	1.709	-5.015	1.637	-9.868	1.719	-16.131
	2.288	+18.405	2.248	+12.492	2.156	+18.218	2.217	+21.366
	2.705	-.993	2.654	+.572	2.614	-5.539	2.685	-10.427
8	.307	+16.619	.247	+9.139	.187	+16.371	.239	+19.635
	.818	-15.631	.741	-11.569	.682	-16.605	.750	-25.176
	1.312	+21.792	1.270	+12.459	1.185	+20.641	1.253	+24.654

Table 6.5.2a Maximum pressure amplitude at various times

CASE NUMBER	POINT 1		POINT 2		POINT 3		POINT 4	
	TIME T1 (sec)	PRESSURE P1 (mm)	TIME T2 (sec)	PRESSURE P2 (mm)	TIME T3 (sec)	PRESSURE P3 (mm)	TIME T4 (sec)	PRESSURE P4 (mm)
9	.304	+20.793	.251	+11.037	.182	+20.519	.235	+23.660
	.813	-19.140	.737	-14.690	.676	-20.562	.752	-31.849
	1.306	+29.734	1.291	+17.196	1.177	+26.786	1.253	+31.315
10	.293	+25.633	.245	+13.046	.177	+25.345	.232	+27.876
	.804	-23.077	.729	-18.381	.675	-25.107	.750	-39.567
11	.318	+8.717	.250	+4.914	.190	+8.628	.257	+11.211
	.839	-8.672	.751	-5.685	.691	-9.068	.772	-13.622
	1.327	+10.283	1.266	+5.709	1.192	+10.168	1.252	+13.125
	1.828	-8.098	1.747	-4.961	1.672	-8.551	1.753	-13.363
	2.315	+11.103	2.268	+6.952	2.187	+10.973	2.248	+13.616
	2.830	-6.010	2.742	-3.362	2.688	-7.330	2.762	-11.770
12	.315	+15.467	.254	+8.231	.193	+15.193	.254	+18.637
	.844	-15.001	.753	-10.728	.702	-16.189	.773	-25.177
	1.322	+19.291	1.261	+10.029	1.190	+18.965	1.251	+22.926
	1.821	-12.445	1.729	-7.994	1.637	-14.204	1.749	-25.380
	2.299	+21.677	2.258	+13.361	2.176	+21.881	2.217	+25.398
	2.787	-7.957	2.685	-5.129	2.644	-13.113	2.746	-21.423
	3.285	+24.353	3.234	+14.979	3.143	+27.630	3.204	+32.840
13	.307	+22.309	.250	+10.953	.191	+21.516	.251	+24.595
	.853	-19.400	.738	-14.921	.705	-22.000	.783	-37.353
	1.315	+28.357	1.292	+14.139	1.192	+26.969	1.260	+31.166
14	.301	+27.791	.248	+13.326	.180	+27.294	.241	+29.761
	.857	-24.899	.745	-19.773	.669	-27.564	.820	-49.216
	1.301	+37.573	1.294	+17.967	1.173	+35.315	1.248	+38.671
15	.294	+33.391	.246	+15.230	.185	+32.865	.232	+33.846
	.827	-28.342	.738	-25.247	.684	-34.995	.759	-56.325
16	.340	+2.460	.263	+1.052	.170	+2.400	.247	+3.669
	.850	-2.480	.742	-1.090	.665	-2.490	.757	-4.016
	1.344	+3.110	1.267	+1.442	1.159	+2.951	1.252	+4.435
	1.839	-2.239	1.731	-.663	1.638	-2.258	1.746	-3.999
	2.349	+4.041	2.272	+2.205	2.164	+3.800	2.241	+5.414
	2.828	-1.291	2.704	+.219	2.627	-1.620	2.735	-3.346
	3.353	+5.517	3.276	+3.459	3.153	+5.300	3.245	+7.064
	3.802	+.226	3.663	+1.684	3.601	-.709	3.709	-2.419
	4.327	+7.584	4.296	+5.410	4.126	+7.396	4.219	+9.239
	4.775	+2.897	4.574	+3.797	4.574	+.954	4.667	-.391

Table 6.5.2b Maximum pressure amplitude at various times

CASE NUMBER	POINT 1		POINT 2		POINT 3		POINT 4	
	TIME T1 (sec)	PRESSURE P1 (mm)	TIME T2 (sec)	PRESSURE P2 (mm)	TIME T3 (sec)	PRESSURE P3 (mm)	TIME T4 (sec)	PRESSURE P4 (mm)
17	.344	+5.321	.250	+2.204	.156	+5.210	.250	+7.702
	.843	-5.016	.739	-2.297	.656	-5.258	.750	-8.656
	1.354	+7.357	1.281	+3.619	1.166	+6.748	1.260	+9.718
	1.812	-1.875	2.322	+7.441	1.604	-3.078	1.718	-6.397
18	.338	+7.988	.254	+3.203	.161	+7.838	.245	+11.202
	.837	-7.185	.727	-3.440	.642	-7.796	.744	-13.072
	1.353	+12.745	1.327	+6.835	1.167	+10.828	1.260	+15.181
19	.329	+10.641	.256	+4.136	.161	+10.454	.241	+14.426
	.825	-9.243	.715	-4.592	.642	-10.276	.737	-17.500
20	.323	+13.029	.250	+4.924	.158	+12.804	.231	+17.108
	.803	-10.833	.705	-5.643	.626	-12.511	.738	-21.481
21	.319	+15.010	.257	+5.552	.153	+14.754	.227	+19.184
	.791	-11.772	.699	-6.551	.619	-14.404	.736	-24.712
22	.314	+16.694	.256	+6.069	.157	+16.378	.227	+20.829
23	.347	+3.450	.256	+1.421	.151	+3.357	.256	+5.119
	.859	-3.519	.754	-1.525	.663	-3.540	.769	-5.829
	1.357	+4.329	1.266	+1.860	1.176	+4.125	1.266	+6.217
	1.854	-3.354	1.749	-1.093	1.658	-3.336	1.764	-5.961
	2.352	+5.309	2.277	+2.711	2.171	+5.022	2.262	+7.194
	2.850	-2.293	2.729	-.156	2.654	-2.738	2.759	-5.326
	3.377	+7.042	3.287	+4.063	3.166	+6.917	3.257	+9.378
	3.830	-.851	3.694	+1.350	3.618	-1.970	3.724	-4.554
	4.342	+9.109	4.312	+6.120	4.146	+9.166	4.237	+11.640
	4.779	+1.855	4.689	+3.722	4.598	-.286	4.719	-2.508
24	.334	+7.506	.253	+2.962	.162	+7.345	.253	+10.639
	.861	-7.150	.749	-3.308	.658	-7.505	.759	-12.755
	1.357	+10.050	1.286	+4.485	1.175	+9.389	1.256	+13.346
	1.833	-3.718	1.691	+.072	1.610	-5.247	1.732	-10.648
	2.339	+14.048	2.319	+8.640	2.147	+13.287	2.228	+17.235
25	.333	+11.034	.249	+4.181	.158	+10.792	.241	+14.967
	.856	-10.012	.740	-4.910	.648	-10.852	.756	-18.940
	1.347	+16.415	1.330	+7.847	1.164	+14.485	1.255	+19.802

Table 6.5.2c Maximum pressure amplitude at various times

CASE NUMBER	POINT 1 TIME T1 (sec)	POINT 1 PRESSURE P1 (mm)	POINT 2 TIME T2 (sec)	POINT 2 PRESSURE P2 (mm)	POINT 3 TIME T3 (sec)	POINT 3 PRESSURE P3 (mm)	POINT 4 TIME T4 (sec)	POINT 4 PRESSURE P4 (mm)
26	.323	+14.048	.250	+5.142	.162	+13.759	.235	+18.339
	.844	-12.295	.727	-6.326	.646	-13.694	.764	-24.351
27	.323	+17.357	.257	+6.114	.158	+17.026	.231	+21.695
	.836	-14.506	.718	-7.926	.639	-16.743	.757	-30.233
28	.313	+19.971	.257	+6.829	.159	+19.596	.227	+24.089
	.846	-16.181	.711	-9.165	.619	-19.137	.760	-34.763
29	.311	+22.522	.265	+7.494	.156	+22.101	.219	+26.225
30	.360	+4.251	.250	+1.698	.172	+4.198	.282	+6.290
	.892	-4.488	.767	-1.889	.673	-4.565	.783	-7.873
	1.377	+5.493	1.284	+2.095	1.174	+5.203	1.268	+7.916
	1.894	-4.498	1.769	-1.618	1.675	-4.439	1.784	-8.133
	2.379	+6.053	2.317	+2.895	2.191	+5.673	2.270	+8.052
	2.927	-3.894	2.771	-.970	2.692	-4.295	2.818	-8.443
	3.428	+8.021	3.303	+3.716	3.209	+8.050	3.318	+11.523
	3.866	-3.249	3.741	-.361	3.694	-3.846	3.819	-6.166
31	.343	+10.062	.252	+3.765	.172	+9.868	.263	+13.714
	.899	-9.560	.757	-4.613	.677	-10.305	.798	-18.694
	1.363	+13.332	1.303	+5.033	1.182	+12.603	1.262	+17.541
	1.878	-6.619	1.717	-1.573	1.626	-8.572	1.777	-17.871
	2.343	+15.089	2.323	+7.733	2.161	+15.124	2.242	+19.714
	2.848	-4.846	2.696	-1.093	2.676	-8.967	2.777	-16.707
32	.334	+14.610	.250	+5.191	.167	+14.299	.250	+18.694
	.893	-13.062	.743	-6.699	.651	-14.699	.801	-29.801
	1.352	+20.136	1.352	+7.792	1.168	+18.707	1.252	+24.565
33	.328	+19.019	.255	+6.427	.167	+18.624	.240	+22.911
	.917	-16.346	.735	-9.479	.677	-19.765	.750	-33.410
34	.314	+23.402	.255	+7.511	.163	+22.978	.229	+26.572
	.810	-18.137	.758	-12.317	.738	-24.349	.817	-50.979
35	.311	+26.646	.256	+8.221	.165	+26.206	.220	+28.948
	.843	-20.656	.745	-13.483	.592	-25.327	.812	-61.084

Table 6.5.2d Maximum pressure amplitude at various times

CASE NUMBER	POINT 1		POINT 2		POINT 3		POINT 4	
	TIME T1 (sec)	PRESSURE P1 (mm)	TIME T2 (sec)	PRESSURE P2 (mm)	TIME T3 (sec)	PRESSURE P3 (mm)	TIME T4 (sec)	PRESSURE P4 (mm)
36	.305	+29.791	.265	+8.843	.161	+29.344	.213	+30.990
	.830	-23.447	.755	-14.343	.599	-29.995	.732	-58.254
37	.377	+2.550	.254	+.587	.130	+2.485	.254	+4.240
	.878	-2.306	.730	-.452	.618	-2.434	.754	-4.478
	1.391	+3.531	1.311	+1.255	1.138	+3.162	1.261	+5.191
	1.867	-.988	1.669	+.881	1.589	-1.388	1.744	-3.428
38	.371	+4.310	.257	+.957	.133	+4.183	.247	+6.968
	.875	-3.737	.713	-.742	.618	-4.118	.751	-7.722
39	.366	+5.594	.258	+1.220	.133	+5.434	.241	+8.855
	.874	-4.598	.699	-.921	.607	-5.290	.749	-10.006
40	.365	+7.064	.268	+1.579	.134	+6.801	.238	+10.795
	.841	-4.412	.648	-.863	.596	-6.465	.745	-12.056
41	.355	+8.225	.267	+1.745	.130	+8.007	.239	+12.458
	.854	-5.963	.663	-1.354	.595	-7.750	.745	-14.675
42	.352	+9.626	.288	+2.185	.128	+9.191	.237	+13.991
43	.353	+10.689	.286	+2.447	.134	+10.171	.231	+15.212
44	.381	+3.446	.258	+.766	.129	+3.368	.258	+5.637
	.898	-3.223	.738	-.652	.627	-3.370	.769	-6.308
	1.402	+4.594	1.316	+1.411	1.144	+4.190	1.273	+6.891
	1.894	-1.953	1.710	+.709	1.605	-2.330	1.759	-5.348
45	.374	+5.659	.259	+1.212	.134	+5.492	.250	+8.919
	.902	-5.097	.730	-1.080	.624	-5.525	.768	-10.600
46	.368	+7.410	.259	+1.552	.134	+7.190	.243	+11.344
	.895	-6.326	.711	-1.388	.619	-7.157	.769	-13.922
47	.360	+9.157	.263	+1.878	.135	+8.880	.240	+13.605
	.893	-7.418	.698	-1.714	.608	-8.783	.766	-17.253

Table 6.5.2e Maximum pressure amplitude at various times

CASE NUMBER	POINT 1		POINT 2		POINT 3		POINT 4	
	TIME T1 (sec)	PRESSURE P1 (mm)	TIME T2 (sec)	PRESSURE P2 (mm)	TIME T3 (sec)	PRESSURE P3 (mm)	TIME T4 (sec)	PRESSURE P4 (mm)
48	.354	+11.111	.265	+2.234	.136	+10.775	.238	+15.953
	.891	-8.407	.680	-2.124	.598	-10.640	.768	-20.938
49	.350	+12.625	.268	+2.507	.134	+12.254	.229	+17.657
	.873	-8.946	.669	-2.500	.592	-12.158	.771	-23.690
50	.343	+14.113	.277	+2.784	.132	+13.692	.223	+19.218
	.728	-7.012	.668	-3.004	.590	-13.773	.734	-25.578
51	.391	+4.740	.247	+1.014	.138	+4.712	.271	+7.546
	.945	-4.543	.746	-.919	.638	-4.846	.813	-9.659
	1.421	+6.386	1.385	+1.581	1.156	+5.845	1.282	+9.619
	1.951	-3.201	1.764	+.475	1.631	-3.660	1.794	-8.299
52	.385	+7.108	.256	+1.455	.138	+6.973	.266	+10.757
	.967	-6.488	.740	-1.428	.631	-7.235	.809	-14.740
53	.372	+10.081	.256	+1.980	.140	+9.834	.256	+14.378
	.958	-8.398	.719	-2.233	.636	-10.248	.834	-23.610
54	.364	+12.858	.270	+2.443	.138	+12.521	.241	+17.419
	.969	-10.287	.736	-3.063	.619	-12.751	.773	-26.471
55	.354	+14.653	.272	+2.730	.143	+14.270	.232	+19.223
	.994	-11.589	.756	-3.442	.593	-14.459	.817	-35.536
56	.352	+16.522	.275	+3.023	.141	+16.113	.230	+20.986
	.864	-10.719	.685	-3.870	.582	-16.791	.870	-42.170

Table 6.5.2f Maximum pressure amplitude at various times

CASE NUMBER	PRESSURE (mm)			PRESSURE RATIO	
	MEASURED	THEORETICAL			
	(Pm)	INITIAL (Pti)	MEAN (Ptm)	(Pm/Pti)	(Pm/Ptm)
1	5.200	4.980	5.183	1.044	1.003
2	9.500	9.273	9.693	1.024	.980
3	13.200	12.695	13.444	1.040	.982
4	16.800	15.884	17.324	1.058	.970
5	19.100	19.565	18.657	.976	1.024
6	6.900	6.598	6.898	1.046	1.000
7	12.300	11.768	11.853	1.045	1.038
8	17.100	16.619	17.418	1.029	.982
9	21.500	20.793	22.202	1.034	.968
10	25.400	25.633	24.355	.991	1.043
11	9.200	8.717	9.104	1.055	1.011
12	15.800	15.467	16.047	1.022	.985
13	21.600	22.309	22.366	.968	.966
14	27.500	27.791	28.790	.990	.955
15	33.700	33.391	30.866	1.009	1.092

Table 6.5.3a Comparison of pressure amplitude at point 1

CASE NUMBER	PRESSURE (mm)			PRESSURE RATIO	
	MEASURED	THEORETICAL			
	(Pm)	INITIAL (Pti)	MEAN (Ptm)	(Pm/Pti)	(Pm/Ptm)
1	3.500	3.195	3.492	1.096	1.002
2	6.400	5.734	6.502	1.116	.984
3	9.100	7.632	9.165	1.192	.993
4	11.800	9.293	11.942	1.270	.988
5	13.900	11.080	12.664	1.254	1.098
6	4.200	3.945	4.376	1.065	.960
7	7.900	6.737	7.443	1.173	1.061
8	11.500	9.139	11.184	1.258	1.028
9	15.500	11.037	14.403	1.404	1.076
10	19.600	13.046	15.714	1.502	1.247
11	5.400	4.914	5.489	1.099	.984
12	10.500	8.231	9.808	1.276	1.071
13	16.200	10.953	13.734	1.479	1.180
14	20.400	13.326	17.710	1.531	1.152
15	25.100	15.230	20.239	1.648	1.240

Table 6.5.3b Comparison of pressure amplitude at point 2

CASE NUMBER	PRESSURE (mm)			PRESSURE RATIO	
	MEASURED	THEORE TICAL			
	(Pm)	INITIAL (Pti)	MEAN (Ptm)	(Pm/Pti)	(Pm/Ptm)
1	5.200	4.931	5.345	1.055	.973
2	9.500	9.155	9.947	1.038	.955
3	13.200	12.553	13.429	1.052	.983
4	17.000	15.728	16.996	1.081	1.000
5	19.800	19.418	19.282	1.020	1.027
6	6.700	6.528	7.133	1.026	.939
7	12.500	11.593	12.568	1.078	.995
8	17.300	16.371	17.556	1.057	.985
9	22.200	20.519	22.107	1.082	1.004
10	27.400	25.345	25.226	1.081	1.086
11	9.200	8.628	9.348	1.066	.984
12	16.400	15.193	17.627	1.079	.930
13	22.900	21.516	23.121	1.064	.990
14	29.300	27.294	29.434	1.073	.995
15	36.100	32.865	33.930	1.098	1.064

Table 6.5.3c Comparison of pressure amplitude at point 3

CASE NUMBER	PRESSURE (mm)			PRESSURE RATIO	
	MEASURED	THEORE TICAL			
	(Pm)	INITIAL (Pti)	MEAN (Ptm)	(Pm/Pti)	(Pm/Ptm)
1	7.100	6.329	7.023	1.122	1.011
2	12.900	11.355	13.110	1.136	.984
3	17.700	15.098	17.639	1.172	1.003
4	22.600	18.361	22.277	1.231	1.014
5	26.100	21.855	25.098	1.194	1.040
6	9.600	8.511	9.656	1.128	.994
7	17.400	14.512	17.044	1.199	1.021
8	23.800	19.635	23.660	1.212	1.006
9	29.500	23.660	29.668	1.247	.994
10	35.100	27.876	33.721	1.259	1.041
11	13.700	11.211	13.043	1.222	1.050
12	23.200	18.637	24.340	1.245	.953
13	30.200	24.595	32.617	1.228	.926
14	36.300	29.761	41.716	1.220	.870
15	39.600	33.846	45.085	1.170	.878

Table 6.5.3d Comparison of pressure amplitude at point 4

CASE NUMBER	PRESSURE (mm)			PRESSURE RATIO	
	MEASURED	THEORETICAL			
	(Pm)	INITIAL (Pti)	MEAN (Ptm)	(Pm/Pti)	(Pm/Ptm)
16	2.500	2.460	2.869	1.016	.871
17	5.400	5.321	5.324	1.015	1.014
18	8.000	7.988	8.776	1.002	.912
19	10.500	10.641	9.942	.987	1.056
20	12.900	13.029	11.931	.990	1.081
21	15.200	15.010	13.391	1.013	1.135
22	17.200	16.694	16.694	1.030	1.030
23	3.300	3.450	4.067	.957	.811
24	7.400	7.506	7.924	.986	.934
25	10.800	11.034	11.868	.979	.910
26	13.600	14.048	13.172	.968	1.033
27	16.900	17.357	15.932	.974	1.061
28	19.300	19.971	18.076	.966	1.068
29	23.900	22.522	22.522	1.061	1.061
30	4.300	4.251	5.171	1.012	.832
31	9.600	10.062	10.411	.954	.922
32	13.600	14.610	15.218	.931	.894
33	18.500	19.019	17.682	.973	1.046
34	22.000	23.402	20.770	.940	1.059
35	24.500	26.646	23.651	.919	1.036
36	28.600	29.791	26.619	.960	1.074

Table 6.5.3e Comparison of pressure amplitude at point 1

CASE NUMBER	PRESSURE (mm)			PRESSURE RATIO	
	MEASURED	THEORETICAL			
	(Pm)	INITIAL (Pti)	MEAN (Ptm)	(Pm/Pti)	(Pm/Ptm)
16	1.000	1.052	1.221	.951	.819
17	2.300	2.204	2.373	1.044	.969
18	3.400	3.203	4.229	1.062	.804
19	4.700	4.136	4.364	1.136	1.077
20	6.300	4.924	5.284	1.279	1.192
21	7.600	5.552	6.051	1.369	1.256
22	8.800	6.069	6.069	1.450	1.450
23	1.300	1.421	1.670	.915	.779
24	2.900	2.962	3.380	.979	.858
25	4.600	4.181	5.462	1.100	.842
26	6.400	5.142	5.734	1.245	1.116
27	9.300	6.114	7.020	1.521	1.325
28	10.900	6.829	7.997	1.596	1.363
29	11.900	7.494	7.494	1.588	1.588
30	1.600	1.698	2.030	.942	.788
31	4.000	3.765	4.276	1.062	.935
32	6.600	5.191	6.595	1.271	1.001
33	10.200	6.427	7.953	1.587	1.283
34	13.300	7.511	9.914	1.771	1.342
35	14.300	8.221	10.852	1.739	1.318
36	17.000	8.843	11.593	1.922	1.466

Table 6.5.3f Comparison of pressure amplitude at point 2

CASE NUMBER	PRESSURE (mm)			PRESSURE RATIO	
	MEASURED	THEORE TICAL			
		INITIAL	MEAN		
	(Pm)	(Pti)	(Ptm)	(Pm/Pti)	(Pm/Ptm)
16	2.500	2.400	3.028	1.042	.826
17	5.500	5.210	5.383	1.056	1.022
18	8.300	7.838	8.564	1.059	.969
19	11.100	10.454	10.365	1.062	1.071
20	14.000	12.804	12.658	1.093	1.106
21	16.100	14.754	14.579	1.091	1.104
22	18.700	16.378	16.378	1.142	1.142
23	3.400	3.357	4.293	1.013	.792
24	7.600	7.345	8.114	1.035	.937
25	11.400	10.792	11.745	1.056	.971
26	15.100	13.759	13.726	1.097	1.100
27	18.600	17.026	16.885	1.092	1.102
28	21.900	19.596	19.366	1.118	1.131
29	25.200	22.101	22.101	1.140	1.140
30	4.500	4.198	5.178	1.072	.869
31	10.500	9.868	11.204	1.064	.937
32	15.300	14.299	15.601	1.070	.981
33	20.500	18.624	19.194	1.101	1.068
34	24.800	22.978	23.663	1.079	1.048
35	29.300	26.206	25.766	1.118	1.137
36	33.200	29.344	29.669	1.131	1.119

Table 6.5.3g Comparison of pressure amplitude at point 3

CASE NUMBER	PRESSURE (mm)			PRESSURE RATIO	
	MEASURED	THEORE TICAL			
		INITIAL	MEAN		
	(Pm)	(Pti)	(Ptm)	(Pm/Pti)	(Pm/Ptm)
16	3.900	3.669	4.662	1.063	.836
17	8.600	7.702	8.474	1.117	1.015
18	13.000	11.202	13.132	1.161	.990
19	17.400	14.426	15.963	1.206	1.090
20	21.600	17.108	19.295	1.263	1.119
21	25.400	19.184	21.948	1.324	1.157
22	29.200	20.829	20.829	1.402	1.402
23	5.500	5.119	6.657	1.075	.826
24	12.200	10.639	12.671	1.147	.963
25	18.100	14.967	18.162	1.209	.997
26	23.800	18.339	21.345	1.298	1.115
27	27.900	21.695	25.964	1.286	1.075
28	32.300	24.089	29.426	1.341	1.098
29	38.500	26.225	26.225	1.468	1.468
30	7.400	6.290	8.310	1.177	.891
31	17.200	13.714	17.806	1.254	.966
32	23.500	18.694	25.715	1.257	.914
33	28.500	22.911	28.161	1.244	1.012
34	30.500	26.572	38.776	1.148	.787
35	31.400	28.948	45.016	1.085	.698
36	33.400	30.990	44.622	1.078	.749

Table 6.5.3h Comparison of pressure amplitude at point 4

CASE NUMBER	PRESSURE (mm)			PRESSURE RATIO	
	MEASURED	THEORETICAL			
	(Pm)	INITIAL (Pti)	MEAN (Ptm)	(Pm/Pti)	(Pm/Ptm)
37	2.500	2.550	2.535	.981	.986
38	4.300	4.310	4.023	.998	1.069
39	5.700	5.594	5.096	1.019	1.119
40	7.000	7.064	5.738	.991	1.220
41	8.100	8.225	7.094	.985	1.142
42	9.500	9.626	9.626	.987	.987
43	10.900	10.689	10.689	1.020	1.020
44	3.500	3.446	3.505	1.016	.998
45	5.600	5.659	5.378	.990	1.041
46	7.200	7.410	6.868	.972	1.048
47	8.900	9.157	8.288	.972	1.074
48	10.500	11.111	9.759	.945	1.076
49	11.900	12.625	10.785	.943	1.103
50	13.400	14.113	10.563	.949	1.269
51	5.200	4.740	4.966	1.097	1.047
52	7.300	7.108	6.798	1.027	1.074
53	9.400	10.081	9.239	.932	1.017
54	11.700	12.858	11.572	.910	1.011
55	13.300	14.653	13.121	.908	1.014
56	18.000	16.522	13.620	1.089	1.322

Table 6.5.3i Comparison of pressure amplitude at point 1

CASE NUMBER	PRESSURE (mm)			PRESSURE RATIO	
	MEASURED	THEORETICAL			
	(Pm)	INITIAL (Pti)	MEAN (Ptm)	(Pm/Pti)	(Pm/Ptm)
37	.600	.587	.520	1.021	1.154
38	1.000	.957	.850	1.045	1.177
39	1.300	1.220	1.070	1.066	1.215
40	1.600	1.579	1.221	1.014	1.311
41	2.000	1.745	1.549	1.146	1.291
42	2.400	2.185	2.185	1.098	1.098
43	3.000	2.447	2.447	1.226	1.226
44	.700	.766	.697	.913	1.004
45	1.100	1.212	1.146	.908	.960
46	1.600	1.552	1.470	1.031	1.088
47	2.000	1.878	1.796	1.065	1.114
48	2.500	2.234	2.179	1.119	1.147
49	3.300	2.507	2.504	1.316	1.318
50	4.300	2.784	2.894	1.545	1.486
51	.900	1.014	.923	.888	.975
52	1.400	1.455	1.441	.962	.971
53	2.500	1.980	2.107	1.263	1.187
54	3.800	2.443	2.753	1.555	1.380
55	5.300	2.730	3.086	1.941	1.717
56	4.200	3.023	3.446	1.389	1.219

Table 6.5.3j Comparison of pressure amplitude at point 2

CASE NUMBER	PRESSURE (mm)			PRESSURE RATIO	
	MEASURED	THEORETICAL			
	(Pm)	INITIAL (Pti)	MEAN (Ptm)	(Pm/Pti)	(Pm/Ptm)
37	2.700	2.485	2.511	1.086	1.075
38	4.500	4.183	4.150	1.076	1.084
39	5.900	5.434	5.362	1.086	1.100
40	7.500	6.801	6.633	1.103	1.131
41	8.700	8.007	7.879	1.087	1.104
42	9.900	9.191	9.191	1.077	1.077
43	11.600	10.171	10.171	1.141	1.141
44	3.600	3.368	3.470	1.069	1.038
45	5.900	5.492	5.508	1.074	1.071
46	7.700	7.190	7.173	1.071	1.073
47	9.800	8.880	8.831	1.104	1.110
48	11.800	10.775	10.707	1.095	1.102
49	13.100	12.254	12.206	1.069	1.073
50	14.800	13.692	13.733	1.081	1.078
51	5.400	4.712	4.959	1.146	1.089
52	7.900	6.973	7.104	1.133	1.112
53	11.200	9.834	10.041	1.139	1.115
54	13.900	12.521	12.636	1.110	1.100
55	16.500	14.270	14.365	1.156	1.149
56	12.700	16.113	16.452	.788	.772

Table 6.5.3k Comparison of pressure amplitude at point 3

CASE NUMBER	PRESSURE (mm)			PRESSURE RATIO	
	MEASURED	THEORETICAL			
	(Pm)	INITIAL (Pti)	MEAN (Ptm)	(Pm/Pti)	(Pm/Ptm)
37	4.500	4.240	4.501	1.061	1.000
38	7.900	6.968	7.345	1.134	1.076
39	10.400	8.855	9.430	1.175	1.103
40	13.300	10.795	11.425	1.232	1.164
41	15.600	12.458	13.567	1.252	1.150
42	18.100	13.991	13.991	1.294	1.294
43	20.600	15.212	15.212	1.354	1.354
44	6.500	5.637	6.230	1.153	1.043
45	10.500	8.919	9.759	1.177	1.076
46	13.900	11.344	12.633	1.225	1.100
47	17.700	13.605	15.429	1.301	1.147
48	21.200	15.953	18.446	1.329	1.149
49	23.300	17.657	20.673	1.320	1.127
50	25.200	19.218	22.398	1.311	1.125
51	11.200	7.546	9.067	1.484	1.235
52	15.500	10.757	12.748	1.441	1.216
53	19.300	14.378	18.994	1.342	1.016
54	21.900	17.419	21.945	1.257	.998
55	25.600	19.223	27.379	1.332	.935
56	23.300	20.986	31.578	1.110	.738

Table 6.5.3l Comparison of pressure amplitude at point 4

CASE NUMBER	HORIZONTAL FORCE (N/m)			FORCE RATIO	
	CALCULATED FROM LACEY,1983 (Fxm)	THEORE TICAL			
		INITIAL (Fxti)	MEAN (Fxtm)	(Fxm/Fxti)	(Fxm/Fxtm)
23	3.379	3.155	4.576	1.071	.738
24	7.490	7.037	8.116	1.064	.923
25	11.113	10.456	11.603	1.063	.958
26	14.247	13.241	13.567	1.076	1.050
27	17.707	16.697	16.978	1.061	1.043
28	20.434	19.295	18.680	1.059	1.094
29	23.080	21.588	20.686	1.069	1.116
30	4.587	3.861	5.181	1.188	.885
31	11.021	9.324	11.591	1.182	.951
32	16.145	13.659	16.004	1.182	1.009
33	21.209	17.961	17.236	1.181	1.230
34	26.332	22.307	20.879	1.180	1.261
35	30.145	25.554	23.582	1.180	1.278
36	33.839	28.720	25.945	1.178	1.304

Table 6.5.4 Comparison of horizontal force amplitude

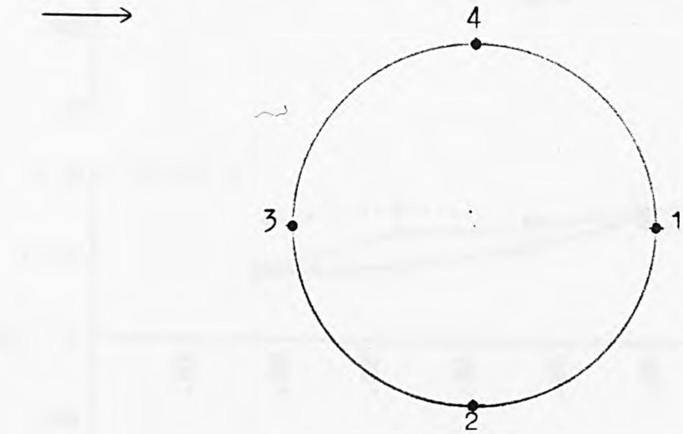

Fig. 6.5.1 Point number used in this study

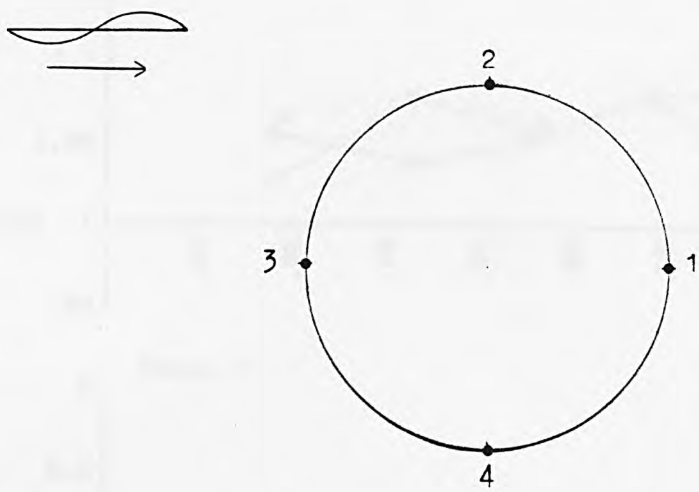

Fig. 6.5.2 Location number in Lacey, 1983

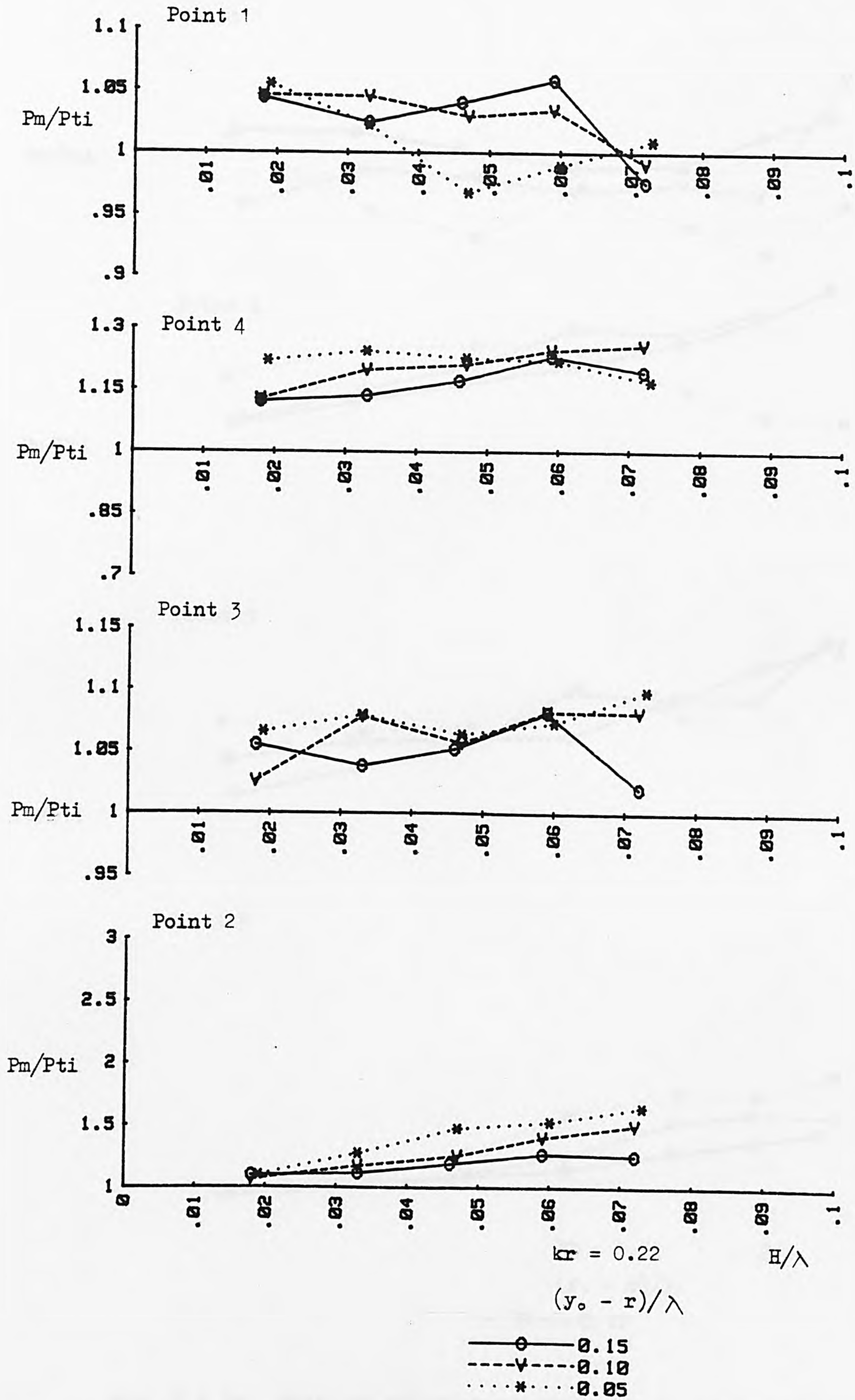

Fig. 6.5.3a Ratio of measured and theoretical (initial) pressure amplitudes

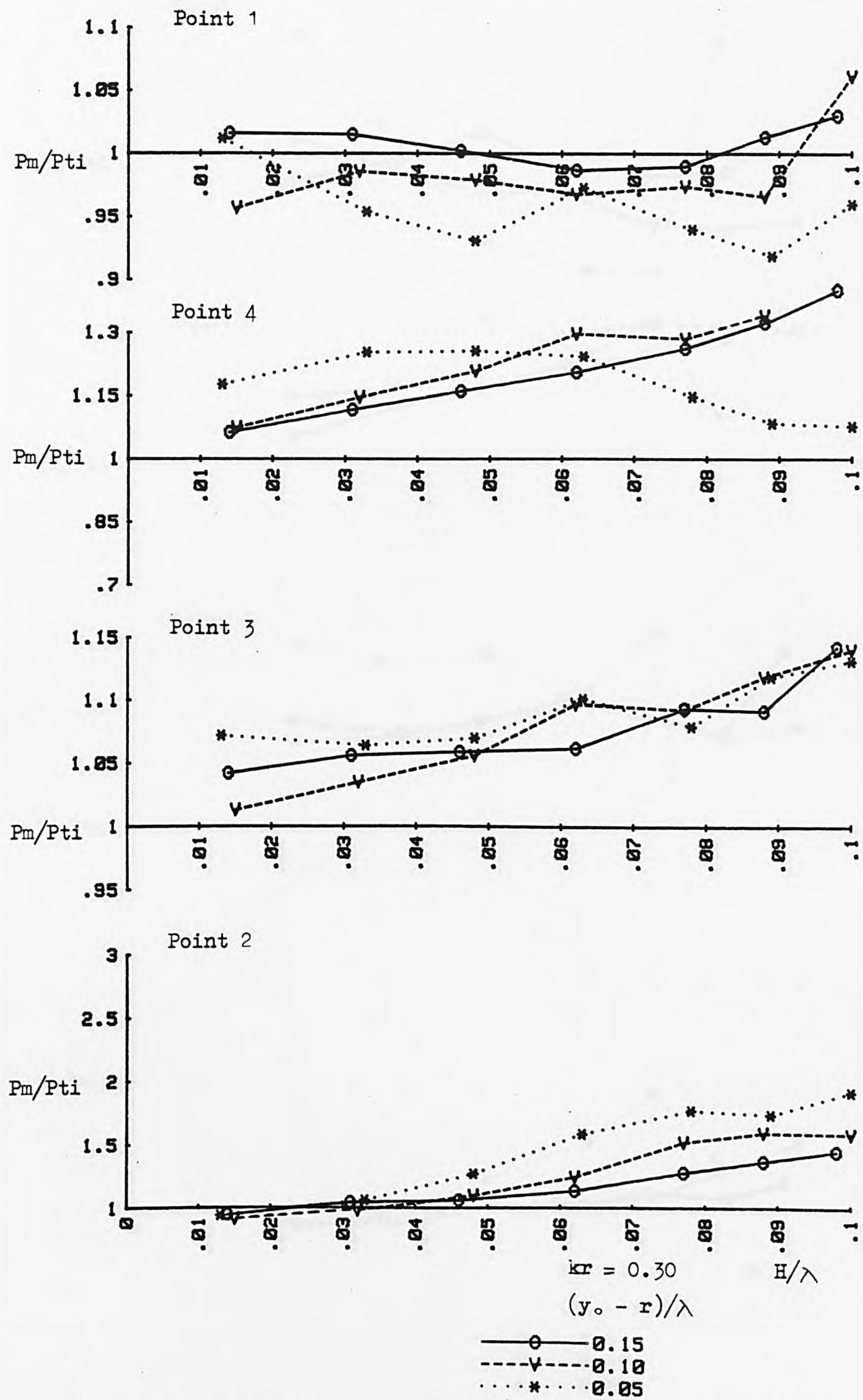

Fig. 6.5.3b Ratio of measured and theoretical (initial) pressure amplitudes

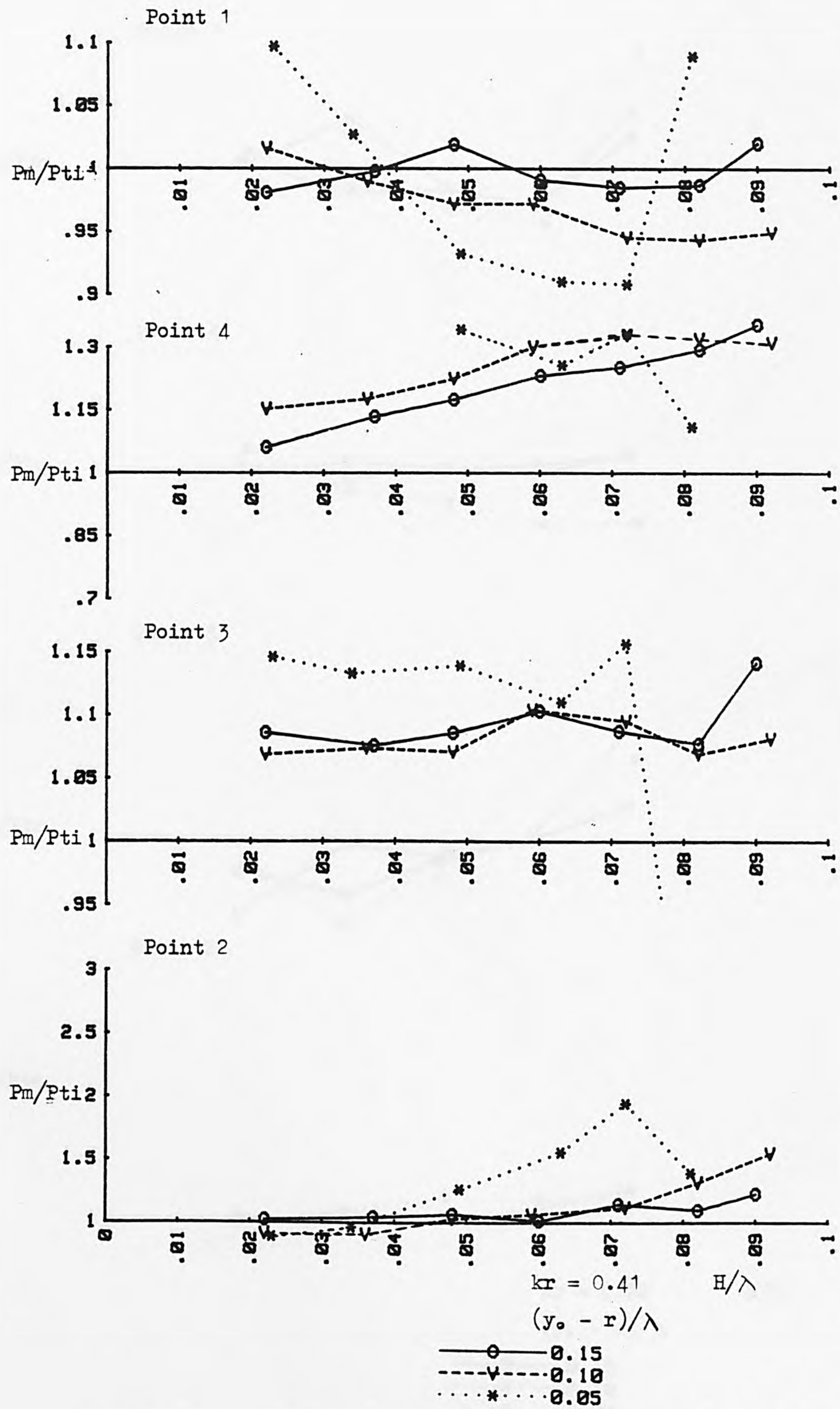

Fig. 6.5.3c Ratio of measured and theoretical (initial) pressure amplitudes

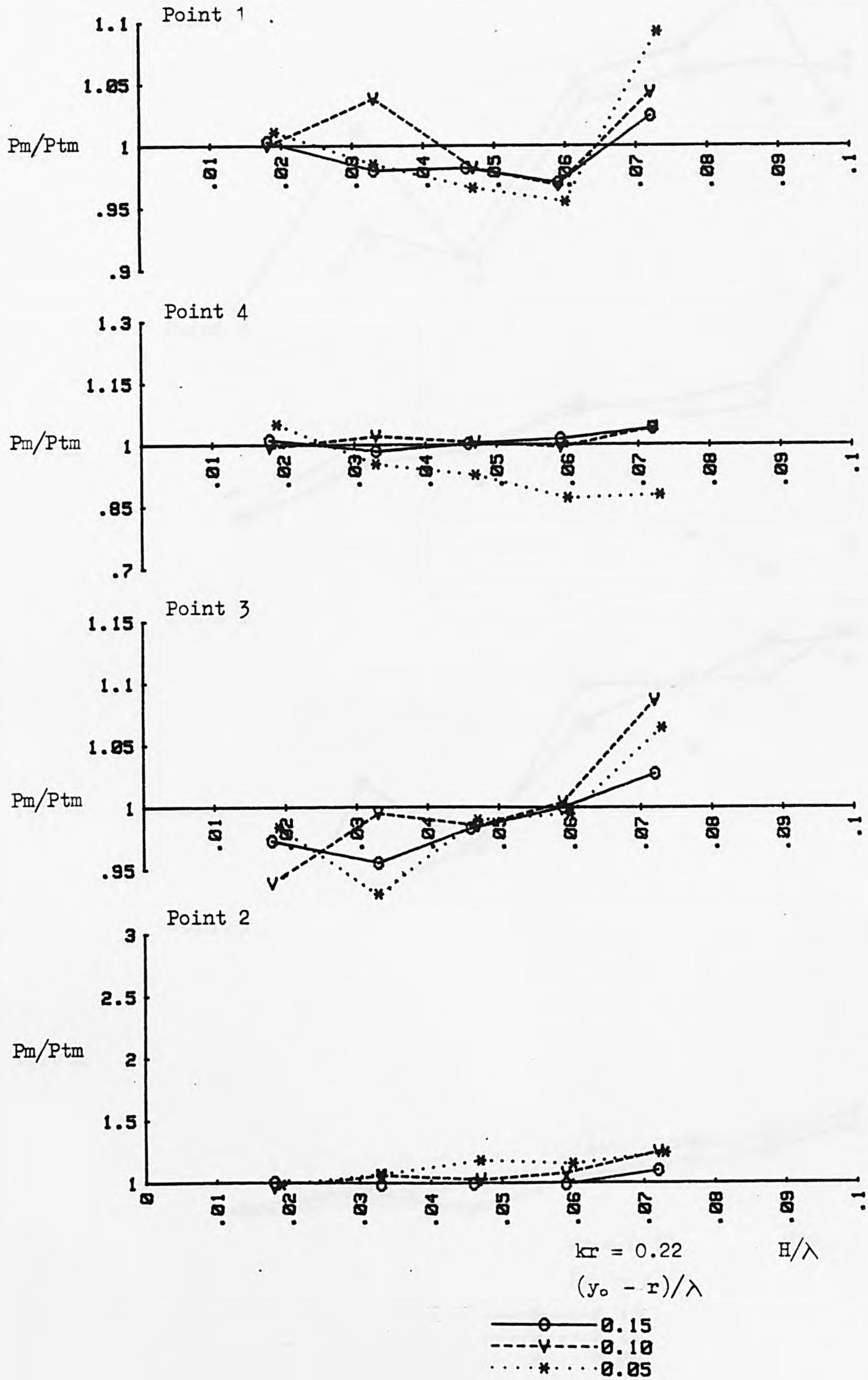

Fig. 6.5.4a Ratio of measured and theoretical (mean) pressure amplitudes

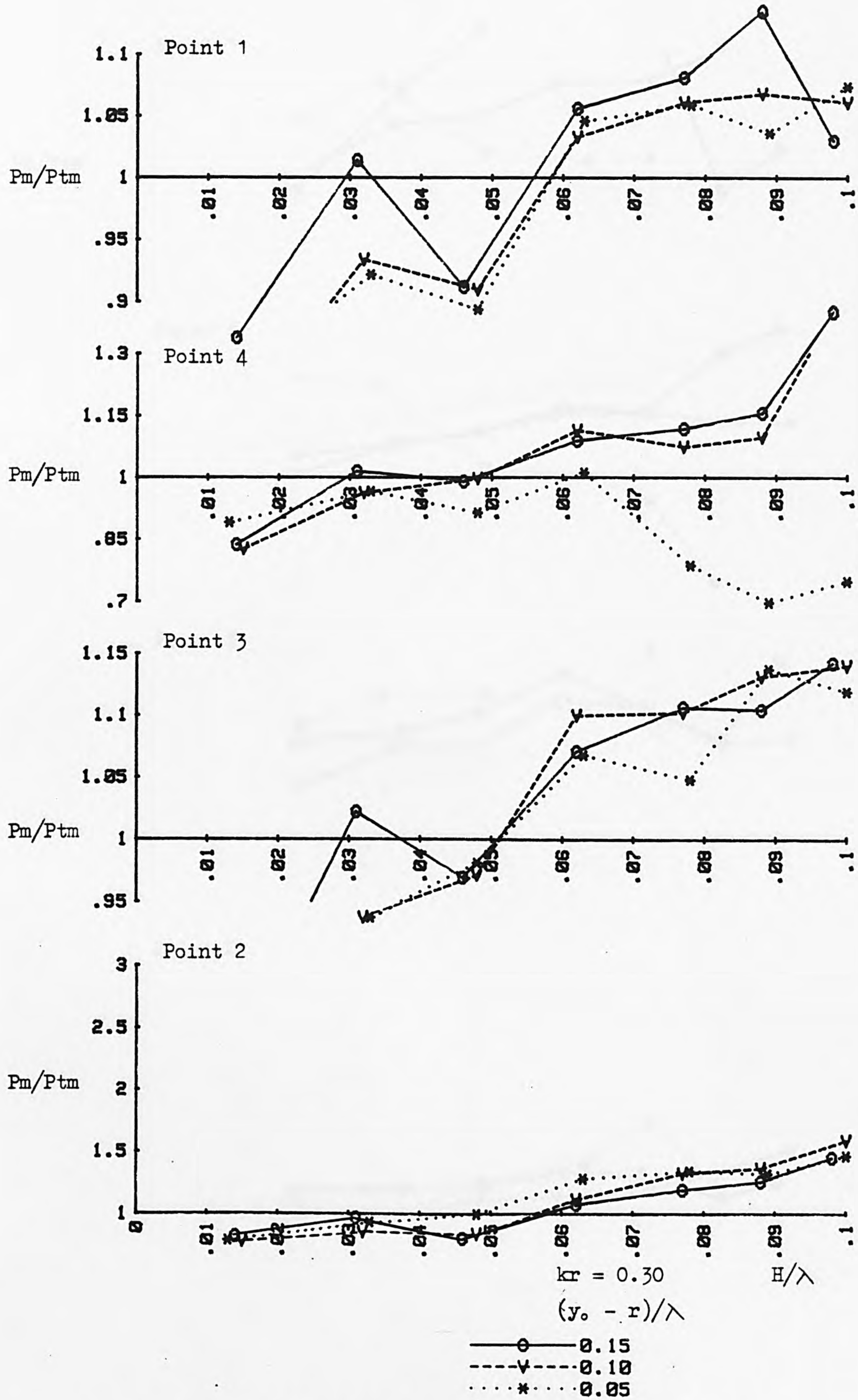

Fig. 6.5.4b Ratio of measured and theoretical (mean) pressure amplitudes

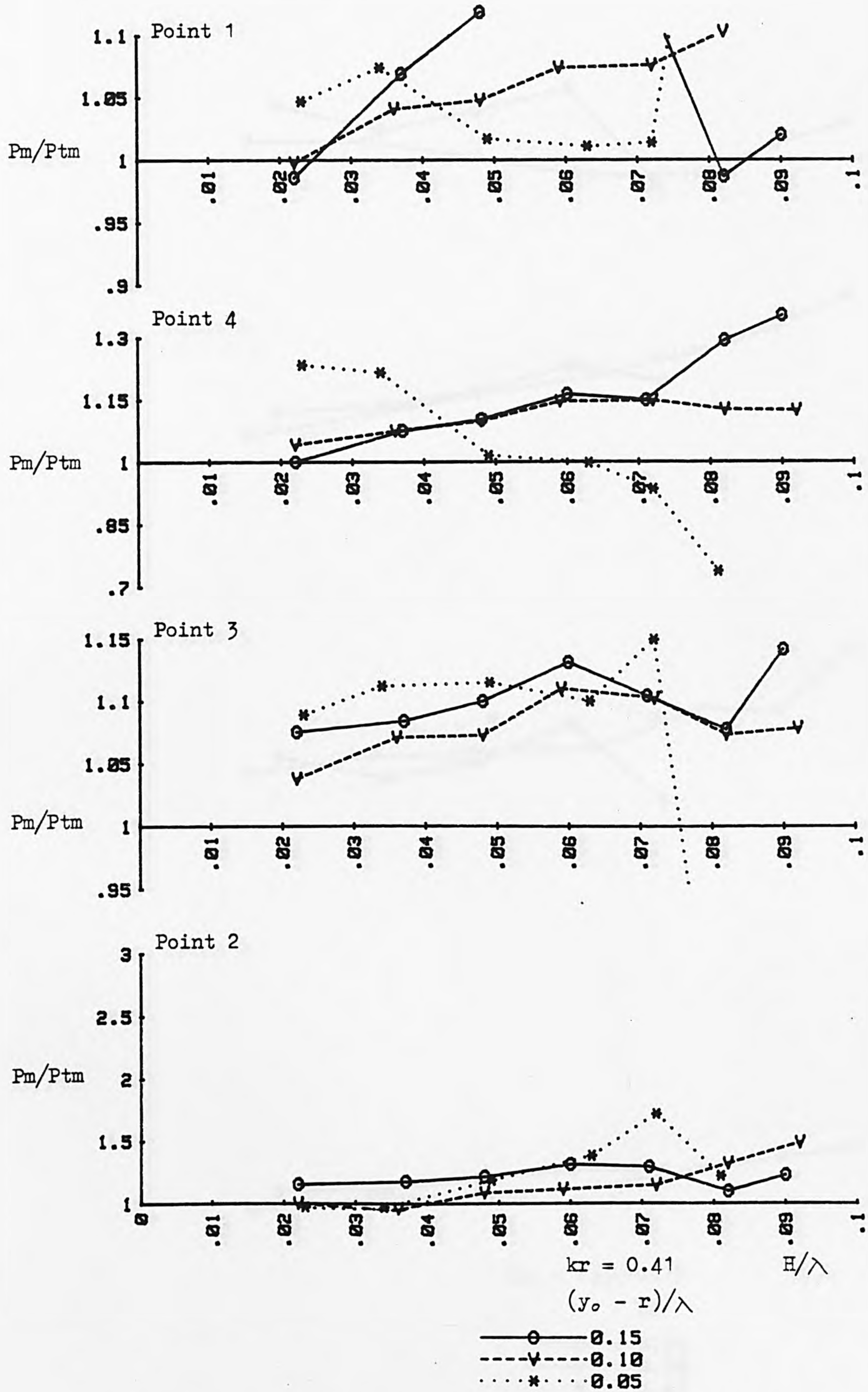

Fig. 6.5.4c Ratio of measured and theoretical (mean) pressure amplitudes

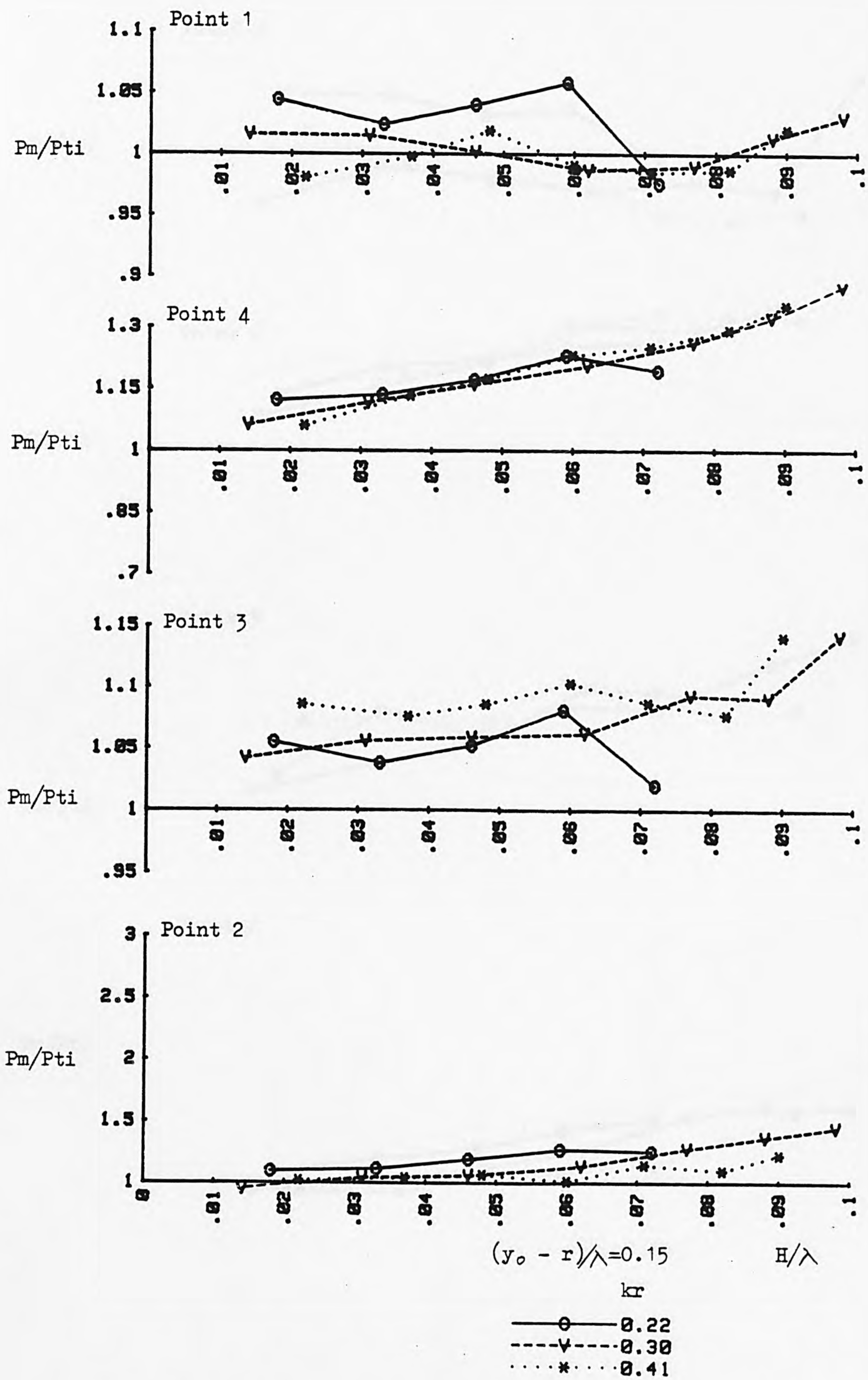

Fig. 6.5.5a Ratio of measured and theoretical (initial) pressure amplitudes

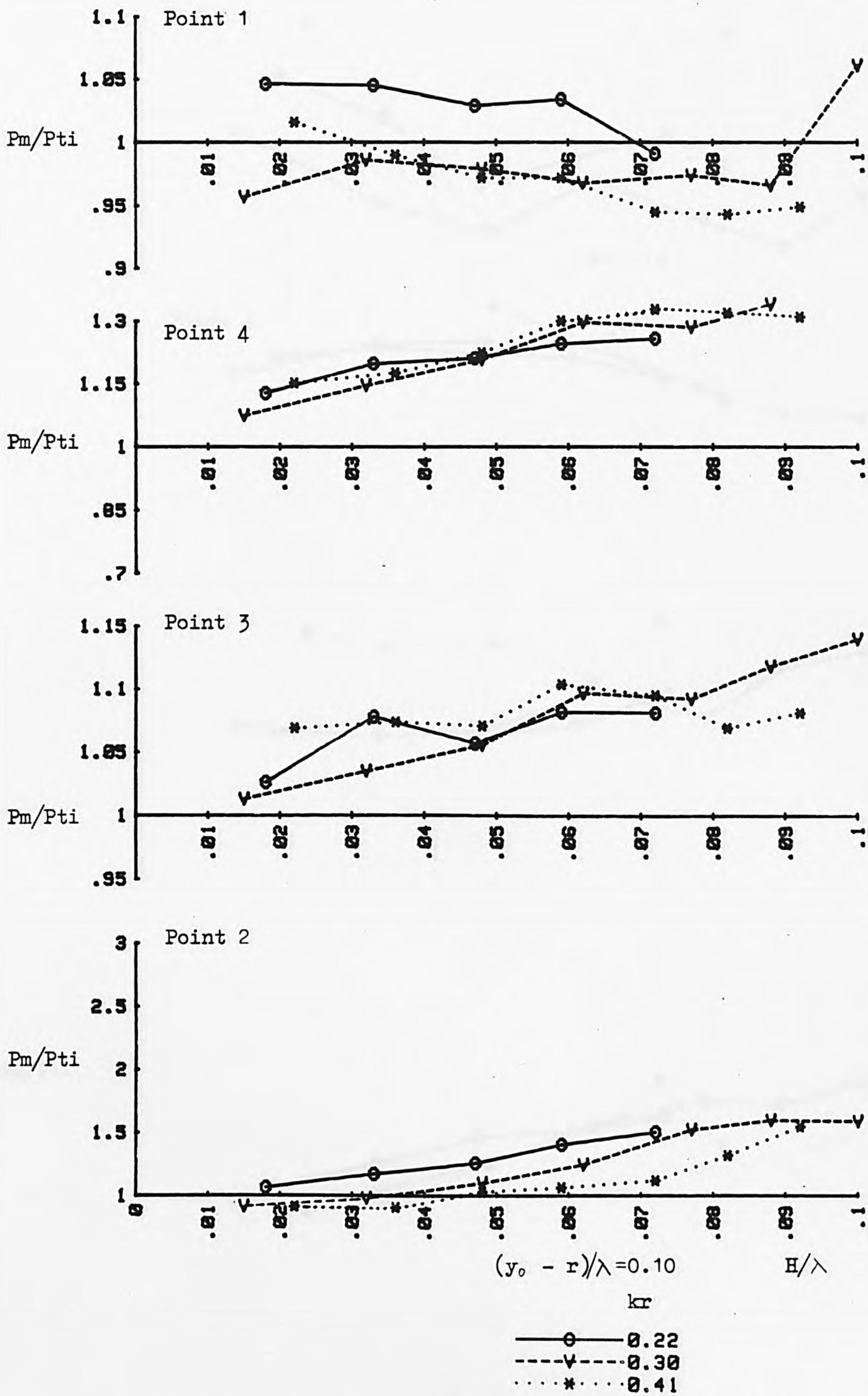

Fig. 6.5.5b Ratio of measured and theoretical (initial) pressure amplitudes

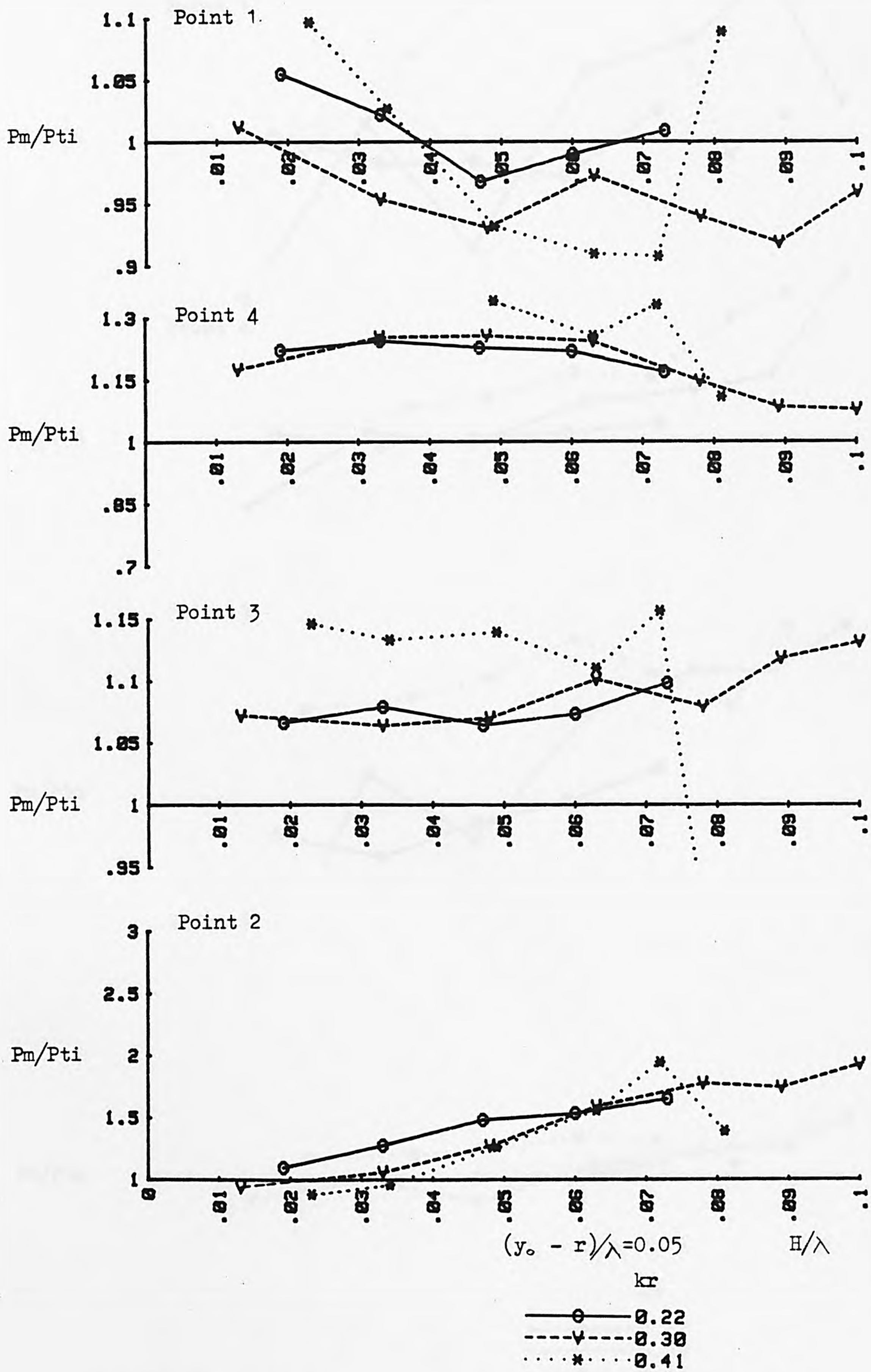

Fig. 6.5.5c Ratio of measured and theoretical (initial) pressure amplitudes

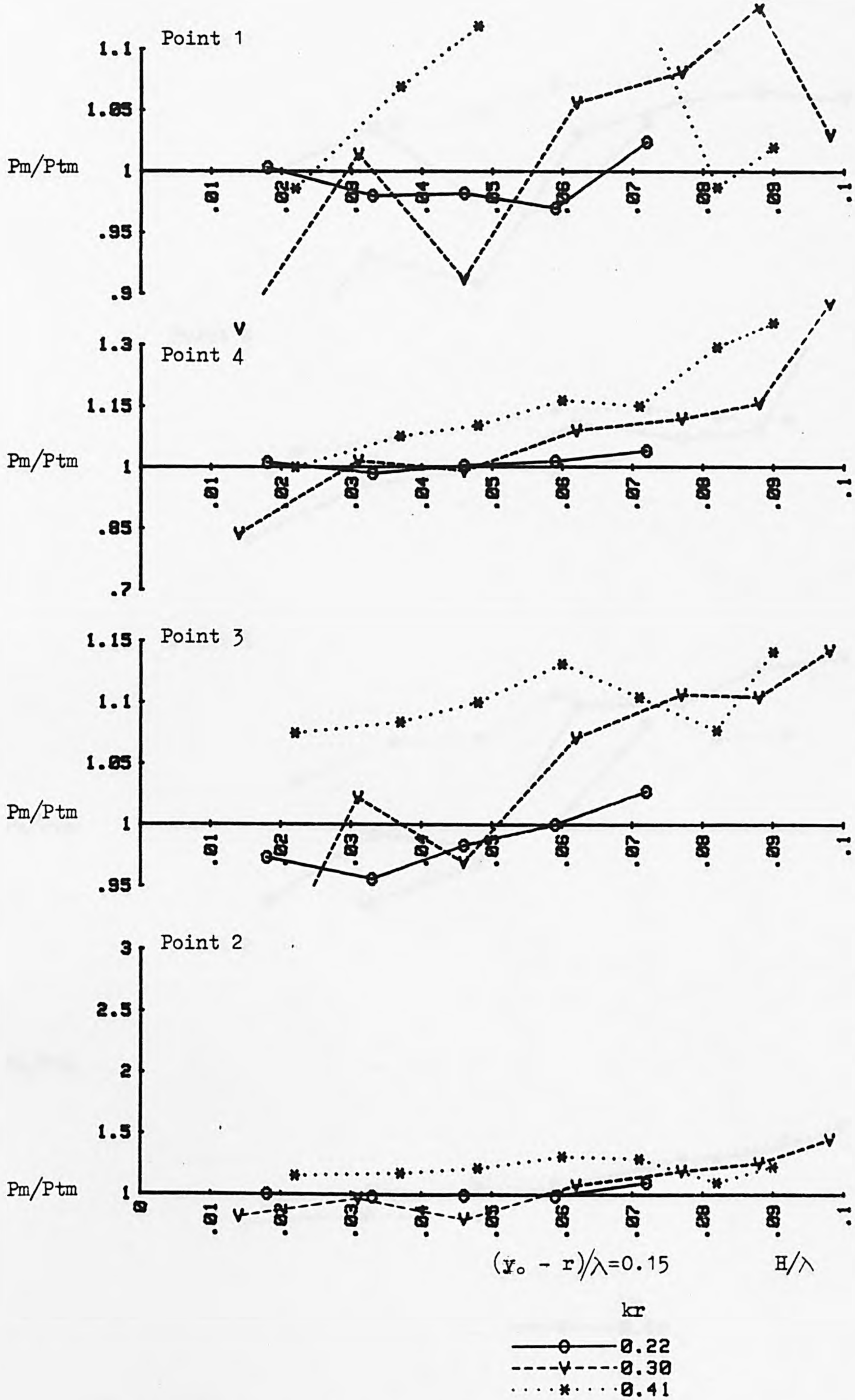

Fig. 6.5.6a Ratio of measured and theoretical (mean) pressure amplitudes

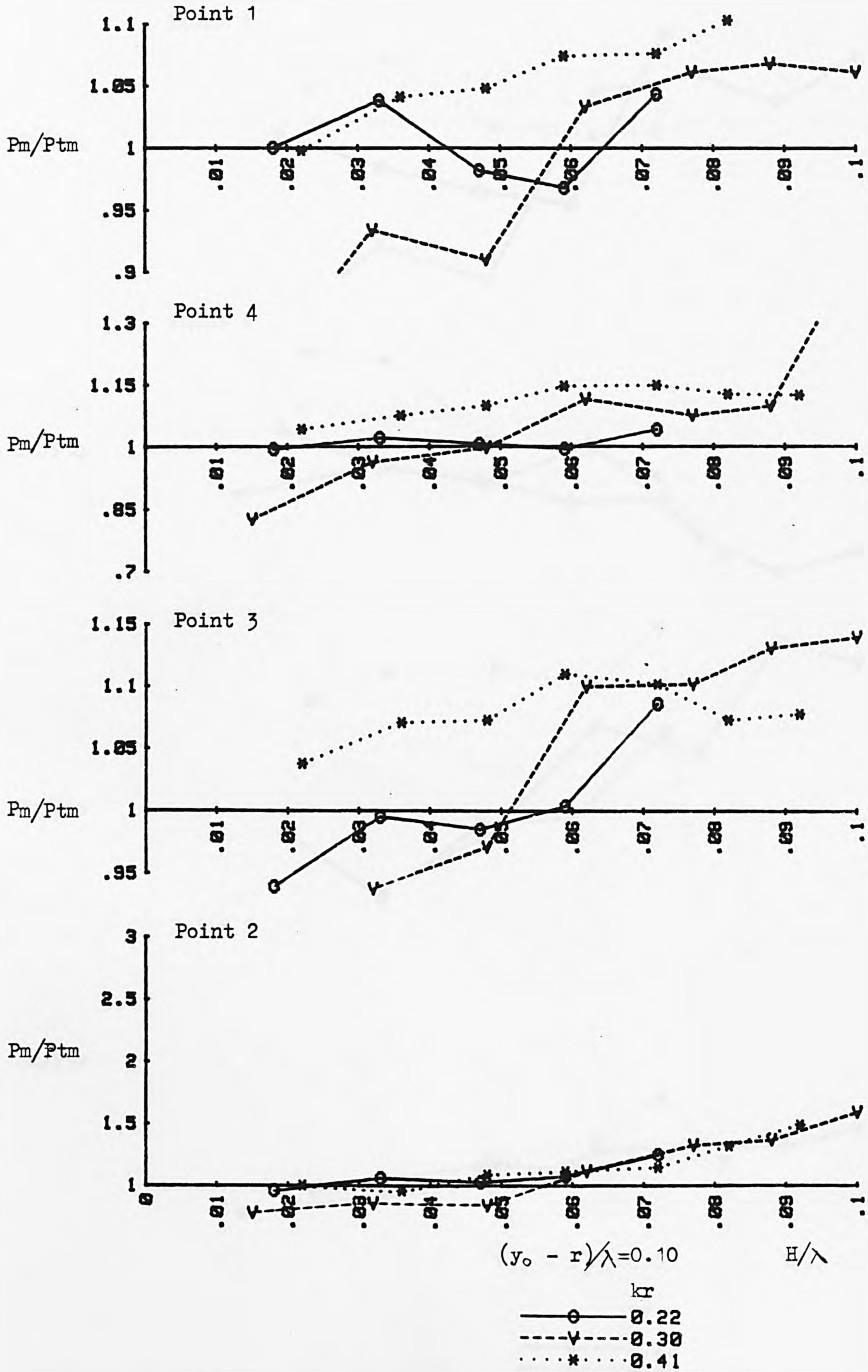

Fig. 6.5.6b Ratio of measured and theoretical (mean) pressure amplitudes

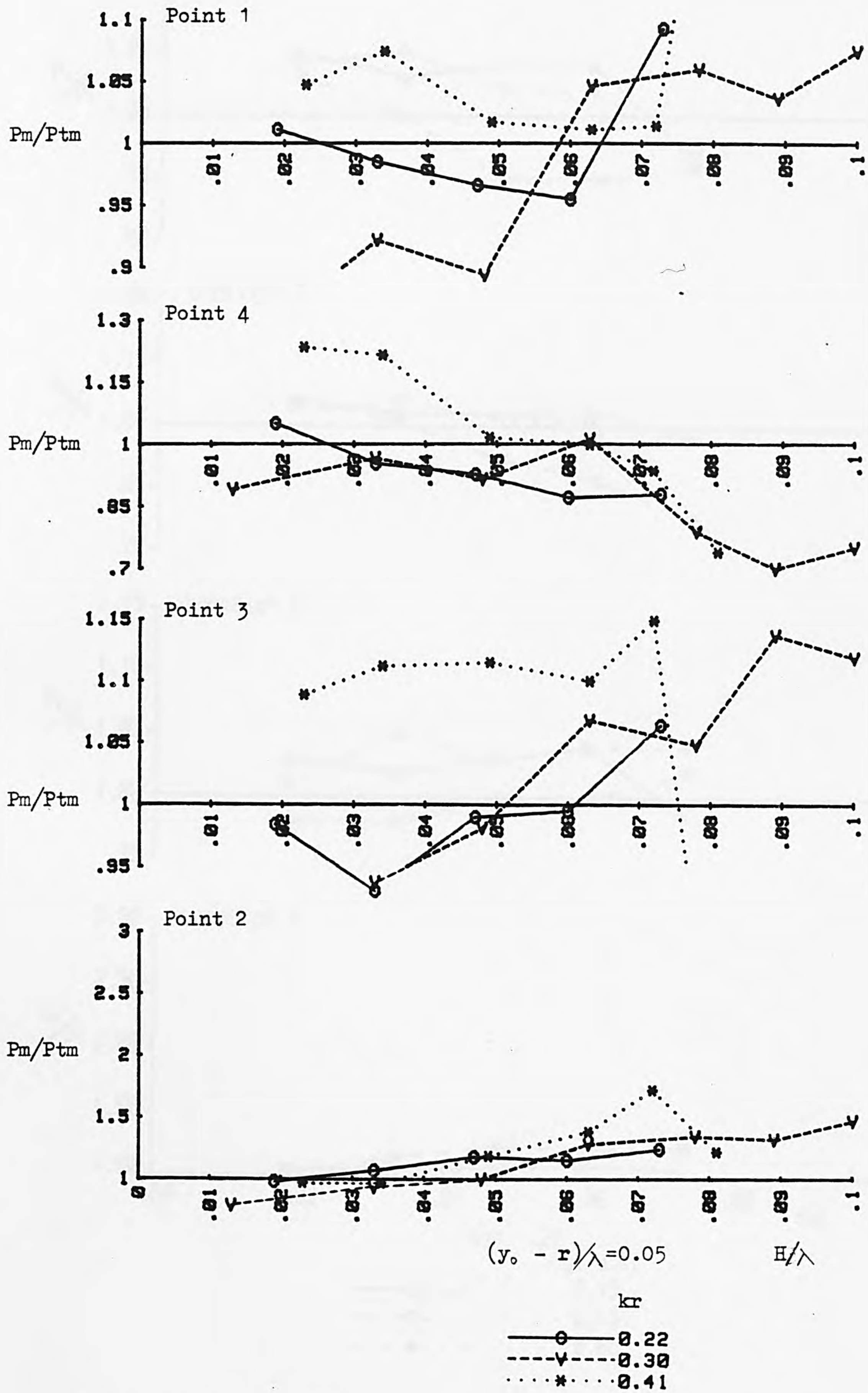

Fig. 6.5.6c   Ratio of measured and theoretical (mean) pressure amplitudes

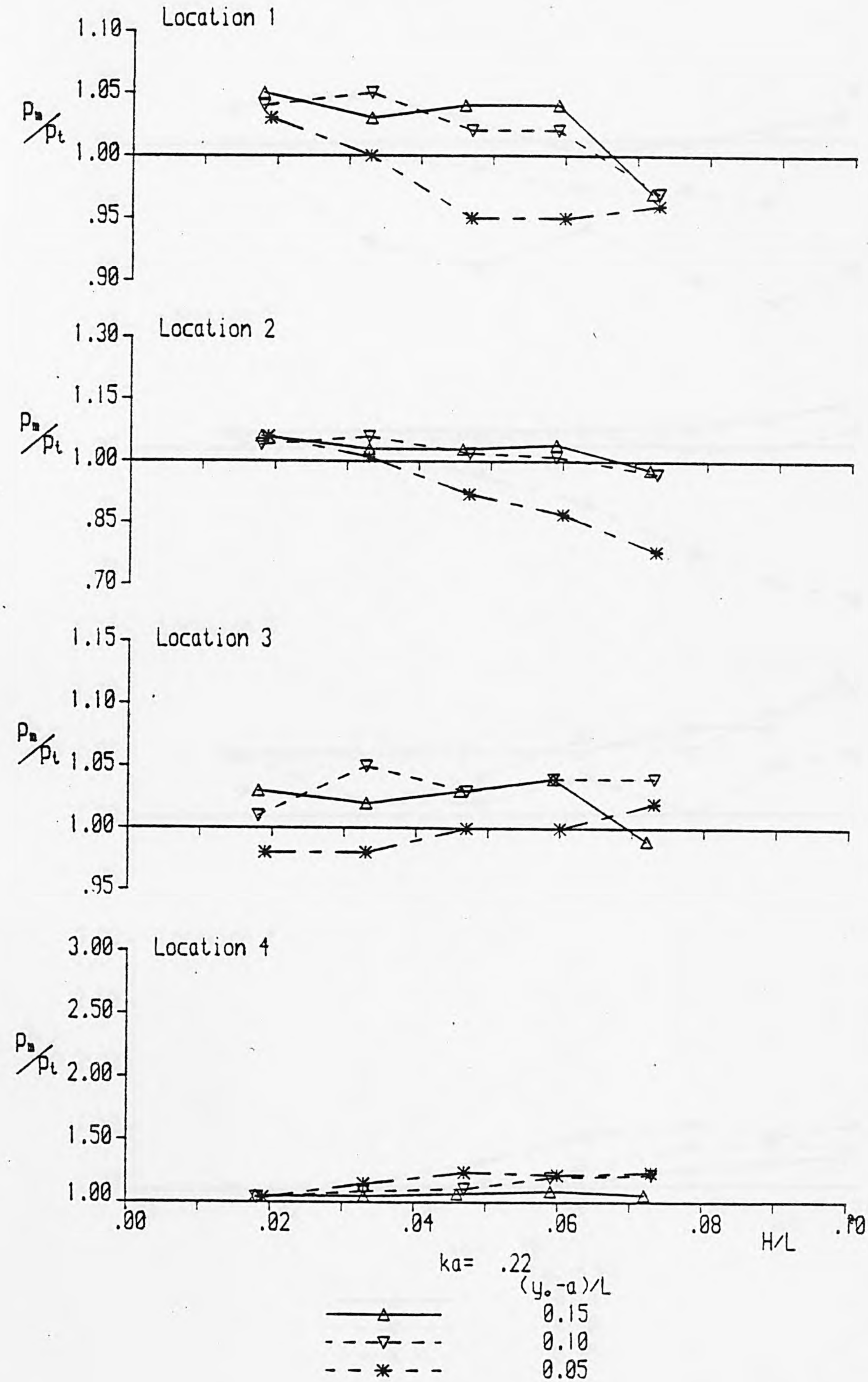

Figure 6.5.7a Ratio of measured and theoretical pressure amplitudes (after LACEY, 1983)

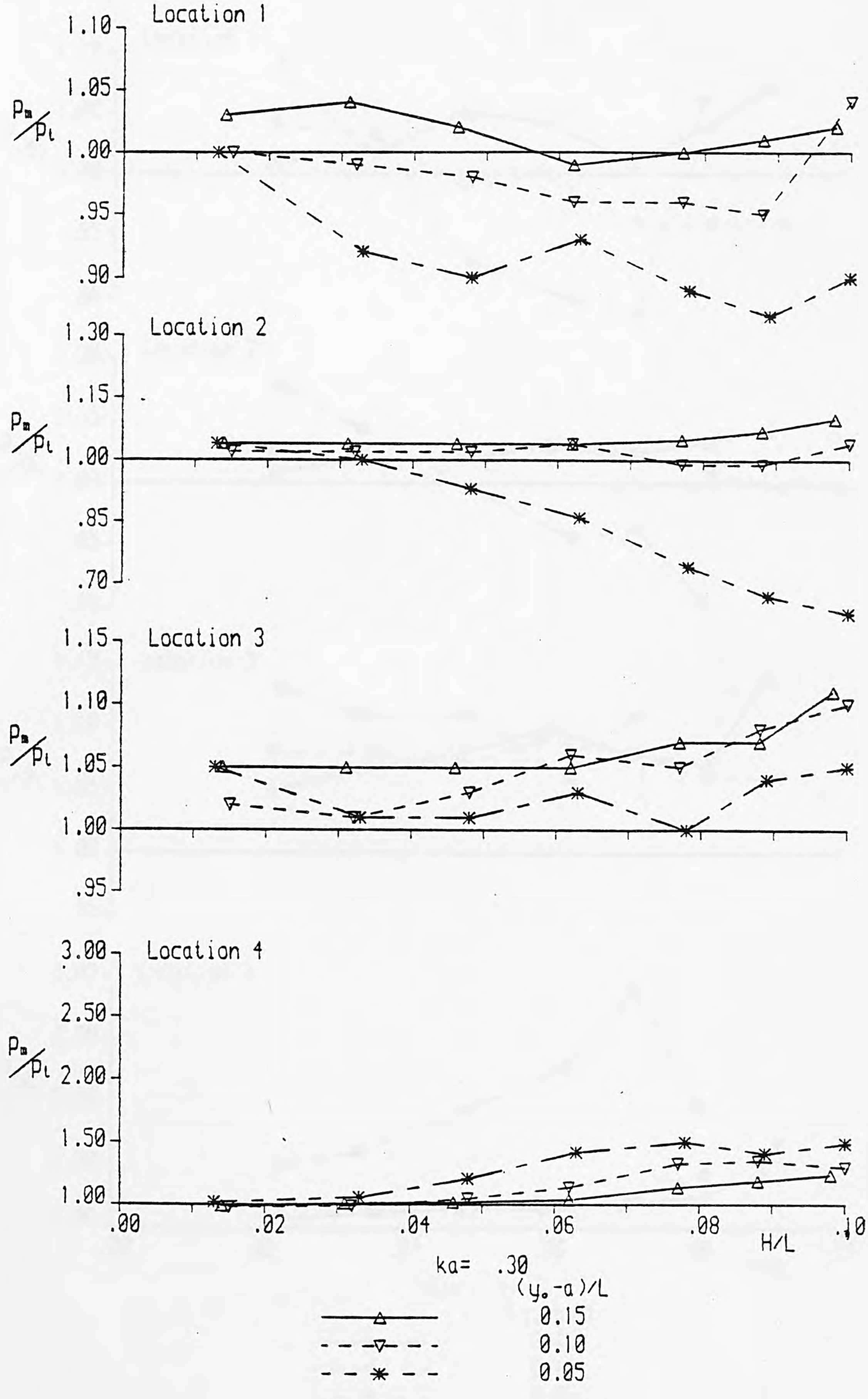

Figure 6.5.7b Ratio of measured and theoretical pressure amplitudes (after LACEY, 1983)

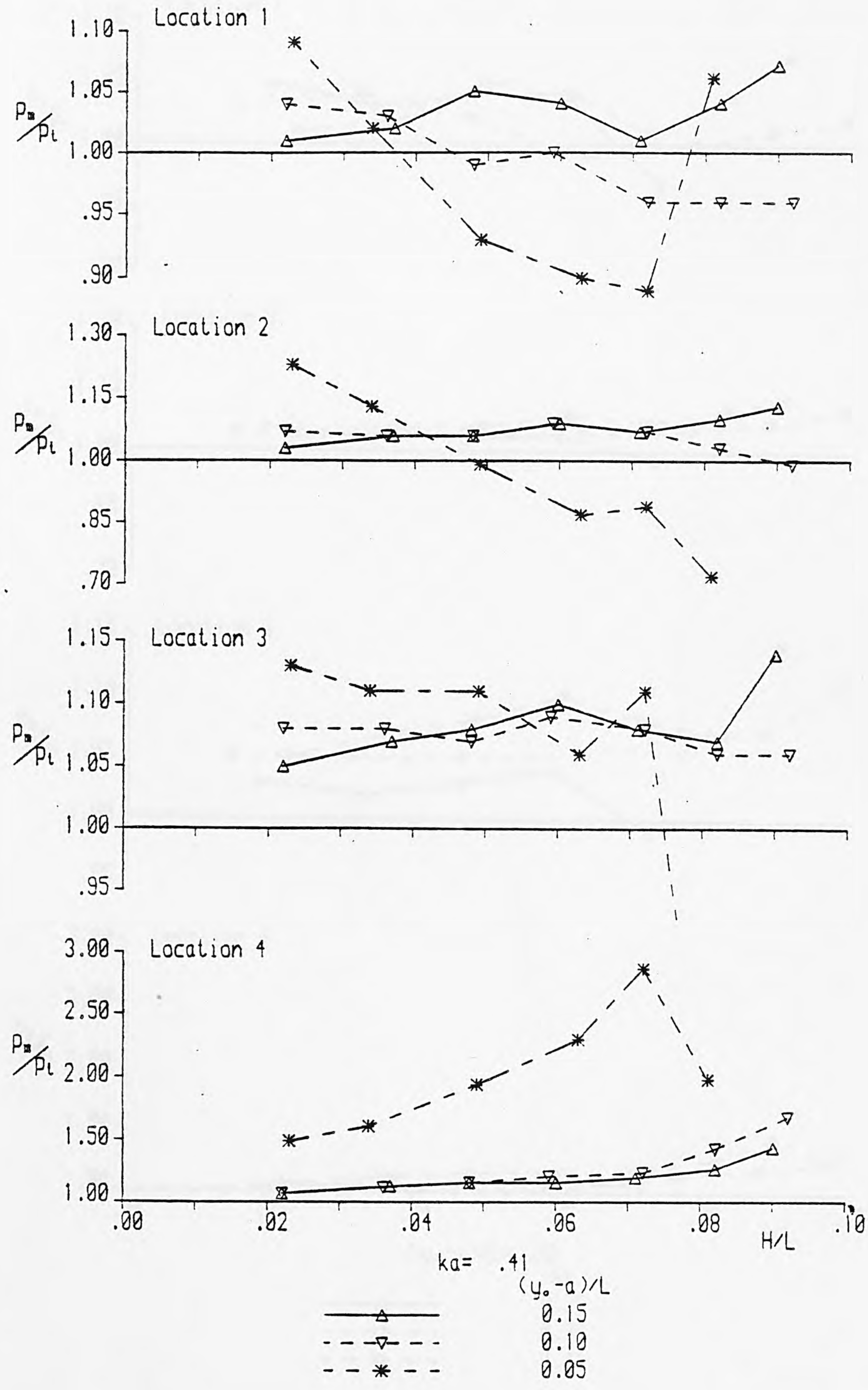

Figure 6.5.7c Ratio of measured and theoretical pressure amplitudes (after LACEY, 1983)

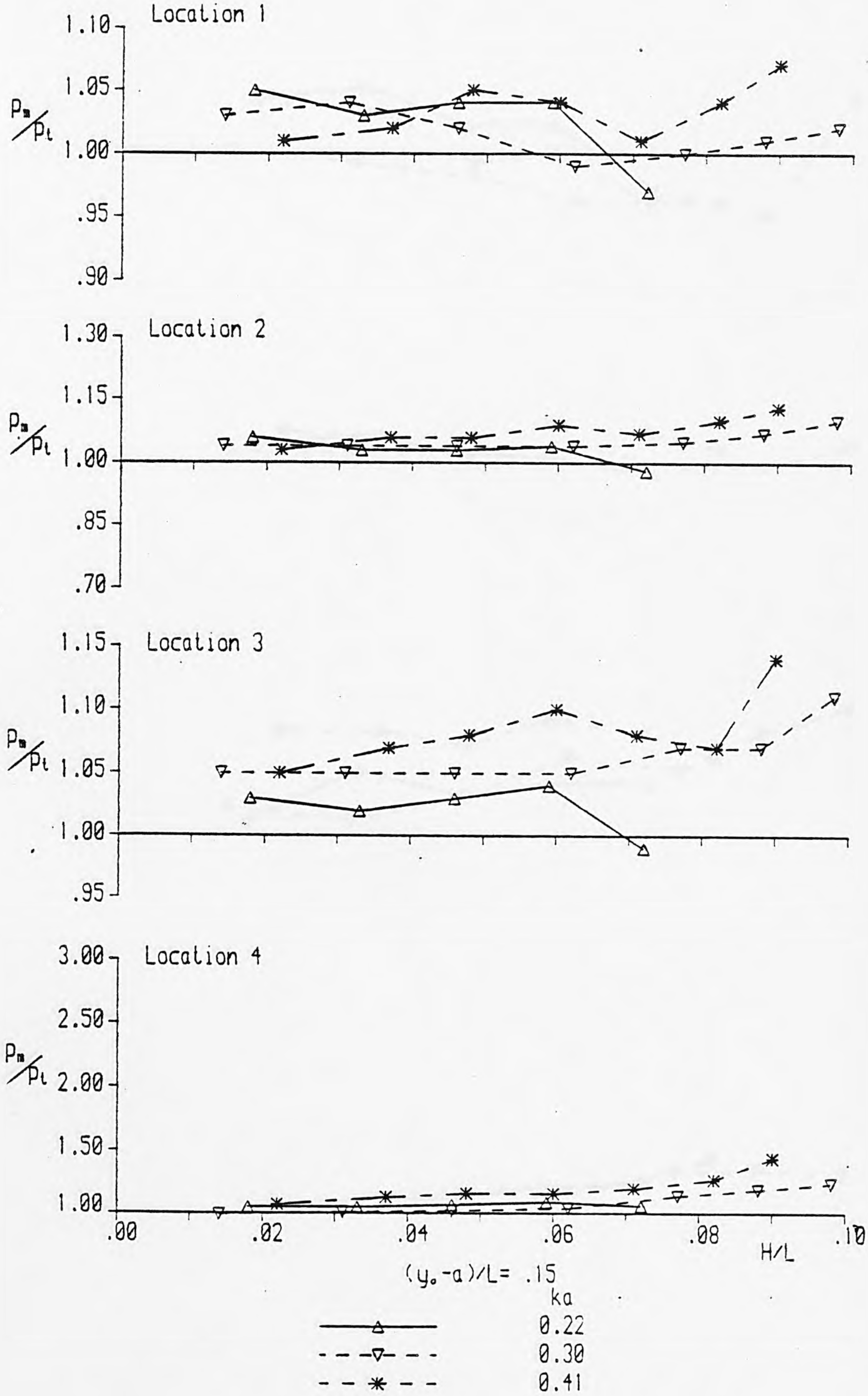

Figure 6.5.8a Ratio of measured and theoretical pressure amplitudes (after LACEY, 1983)

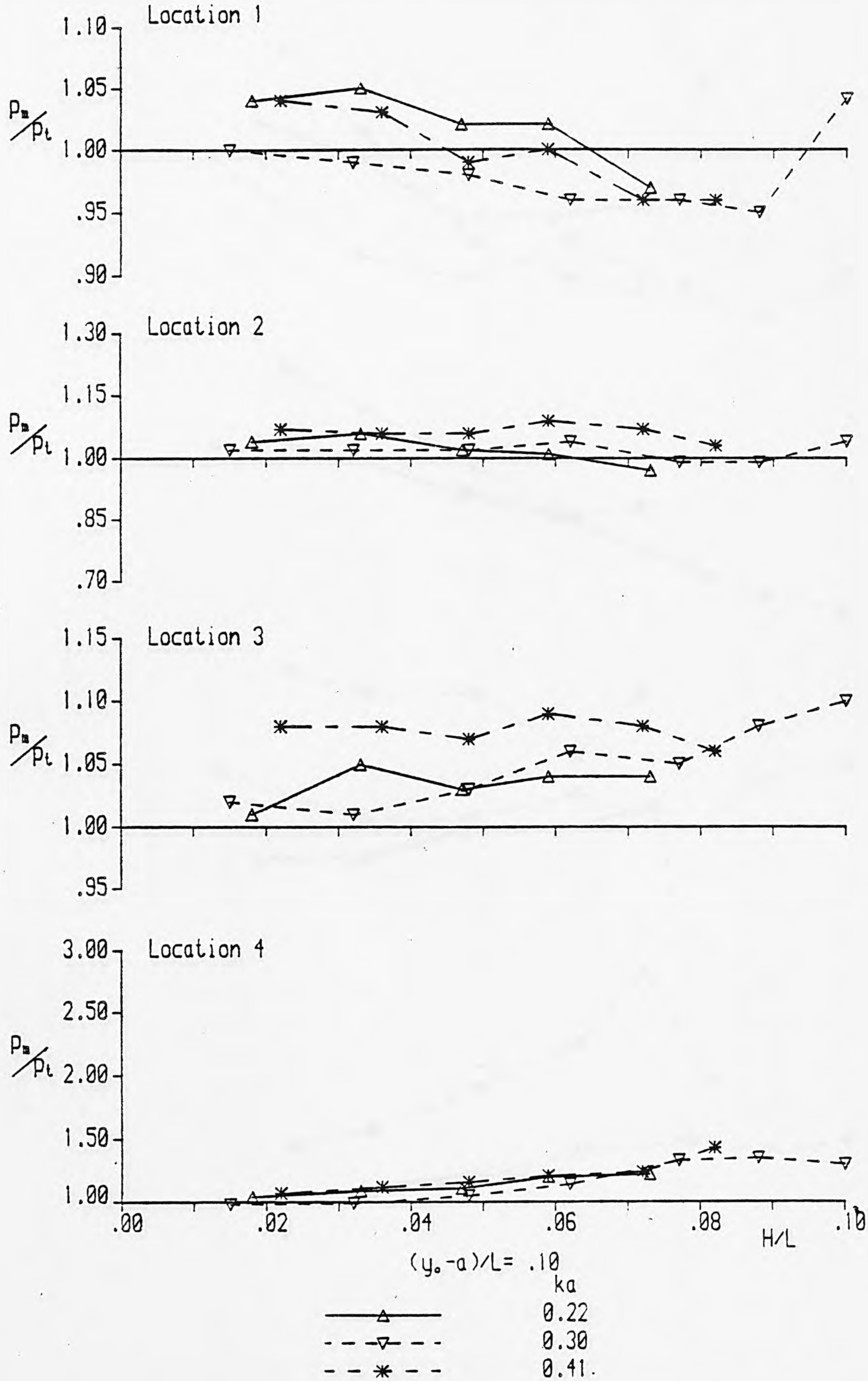

Figure 6.5. 8b Ratio of measured and theoretical pressure amplitudes (after LACEY, 1983)

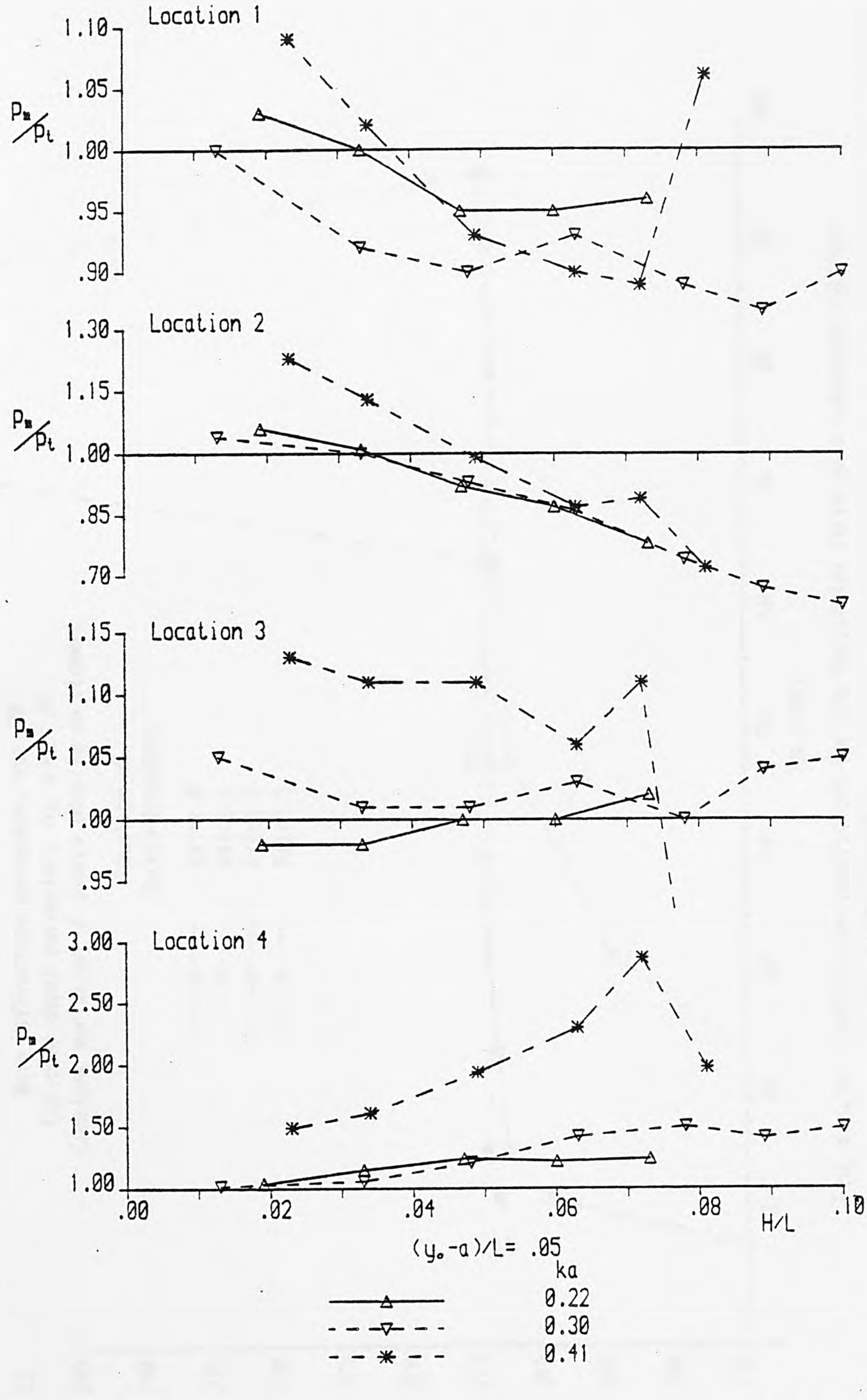

Figure 6.5.8c Ratio of measured and theoretical pressure amplitudes (after LACEY, 1983)

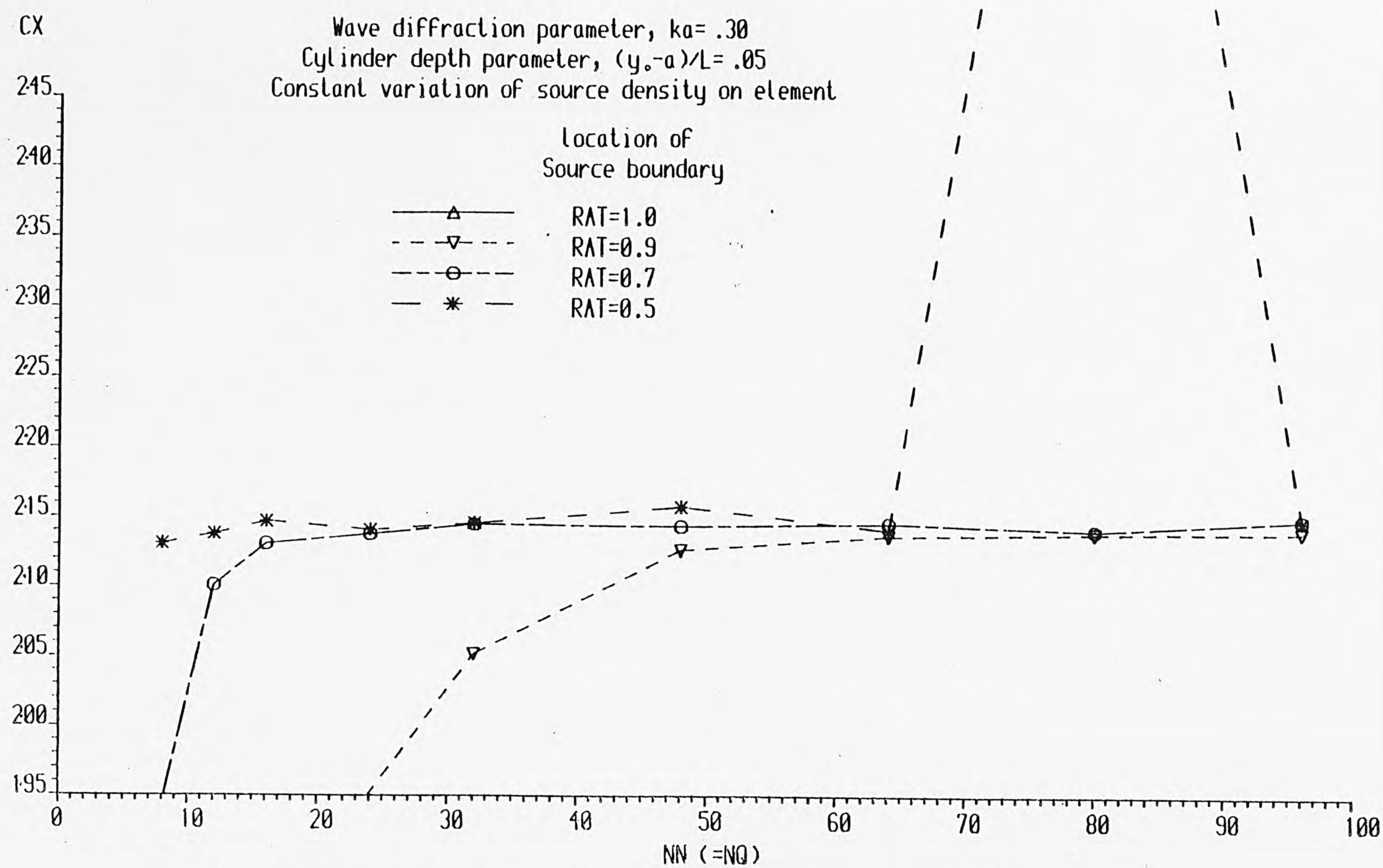

Fig. 6.5.9a Diffraction coefficient for the horizontal force on a submerged cylinder (after LACEY, 1983)

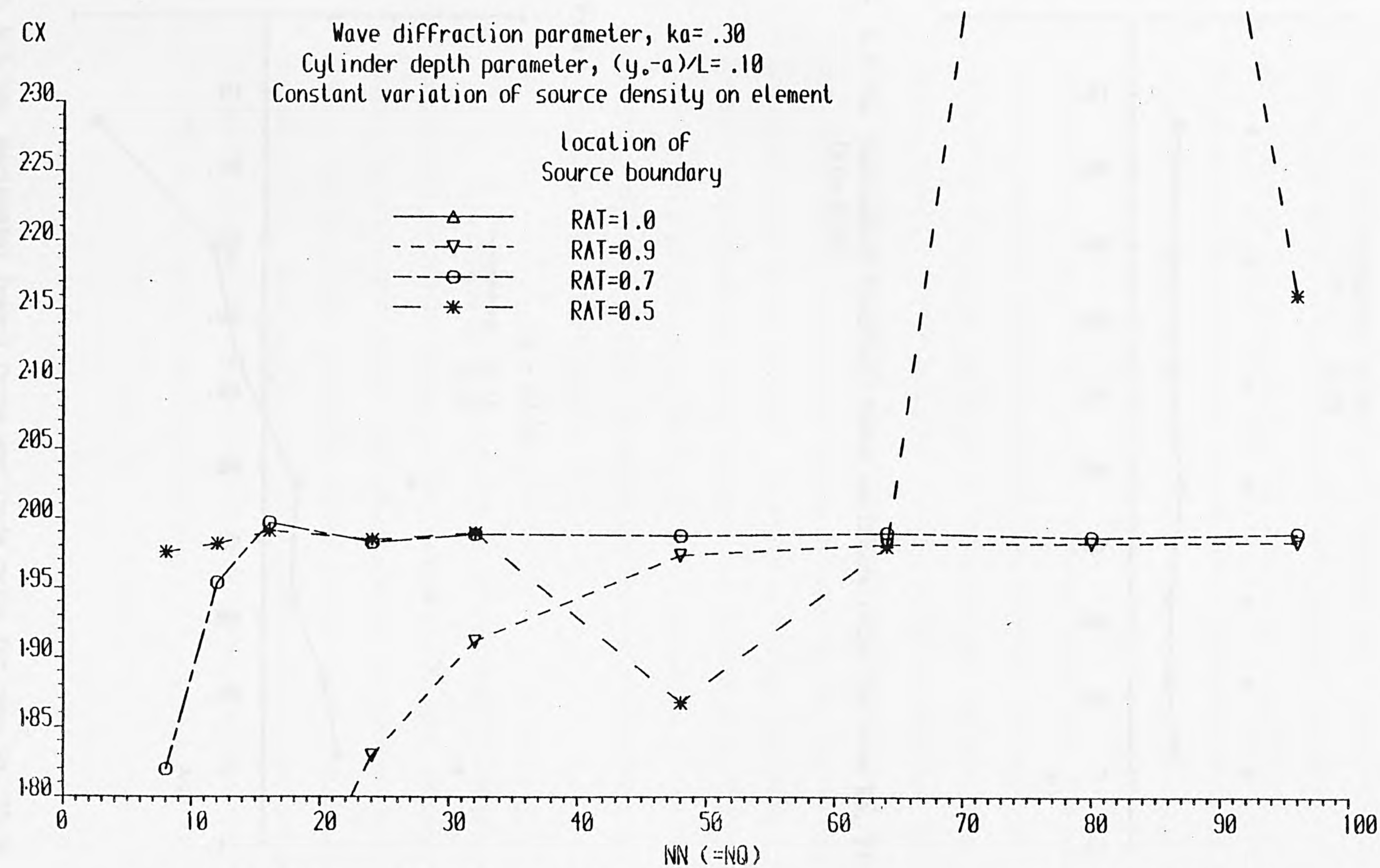

Fig. 6.5.9b Diffraction coefficient for the horizontal force on a submerged cylinder (after LACEY, 1983)

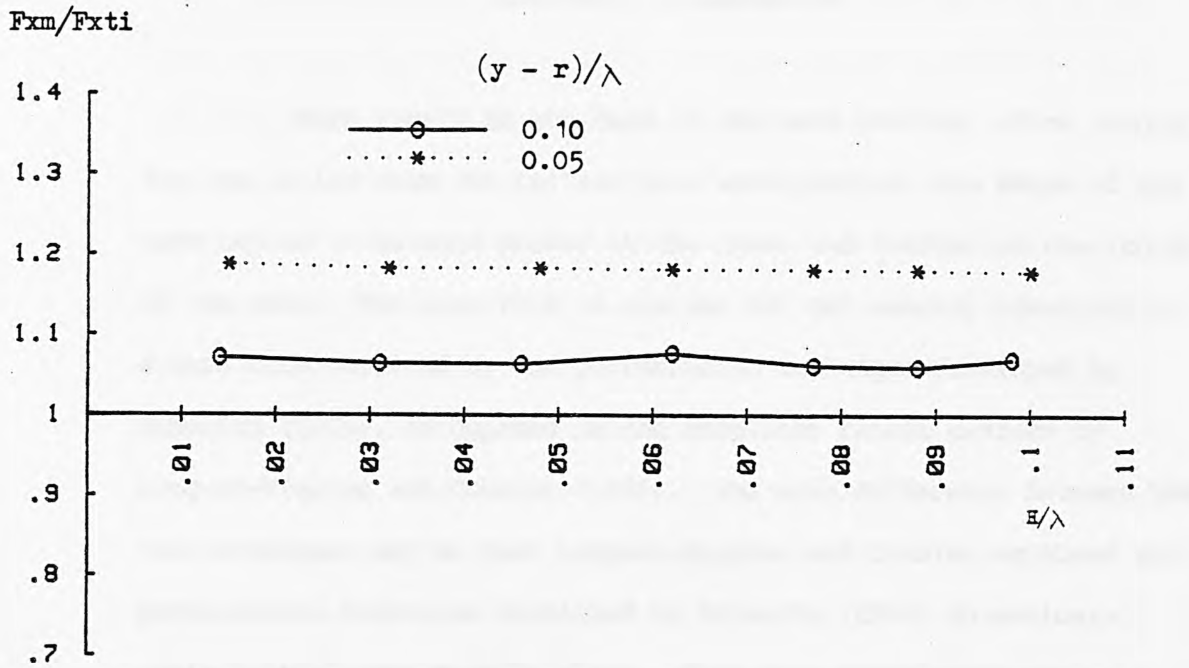

Fig. 6.5.10a Horizontal (initial) force amplitude ratio for case No. 23-36 ($k\gamma = 0.30$)

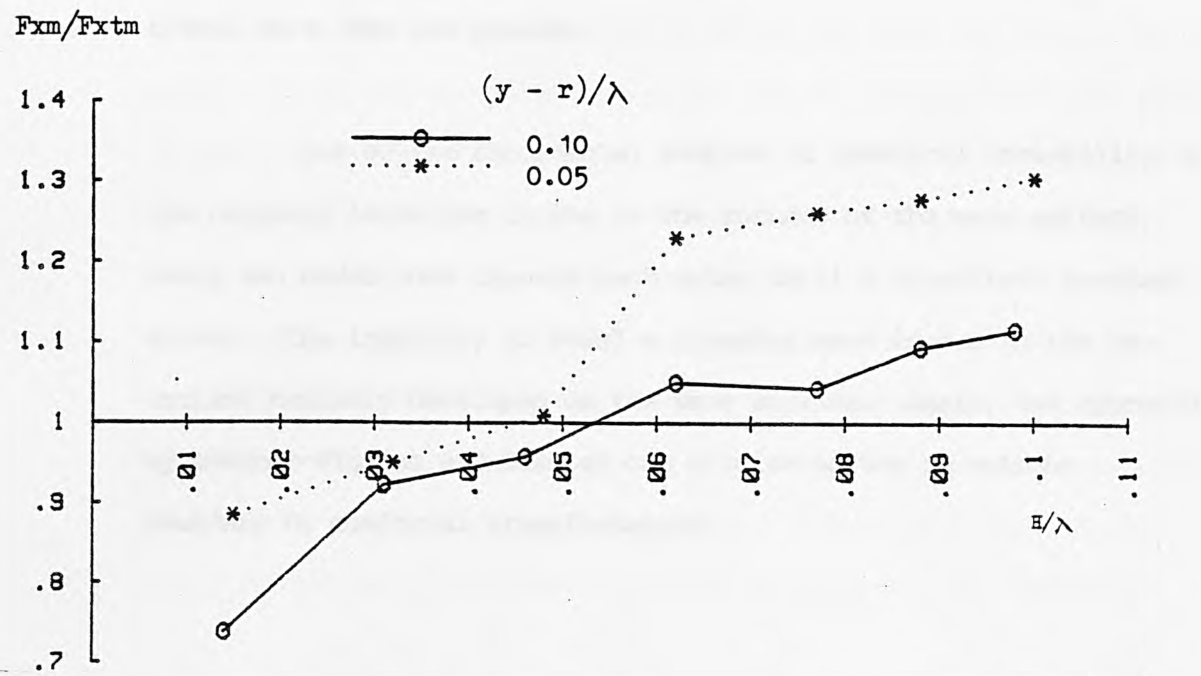

Fig. 6.5.10b Horizontal (mean) force amplitude ratio for case No. 23-36 ($k\gamma = 0.30$)

With regard to the form of the wave profile, after running for one period from the initial sine wave profile, the shape of the wave begins to be more peaked at the crest and flatter in the trough of the wave. The wave form is similar but not exactly identical to a wave form obtained by the perturbation technique developed by Schwartz (1974), as opposed to the excellent result claimed by Longuet-Higgins and Cokelet (1976). The main difference between the two techniques may be that Longuet-Higgins and Cokelet employed the perturbation technique developed by Schwartz (1974) to evaluate their initial wave profile alone. They have proved that the wave travels without change of form. Therefore, there is a possibility that the proposed technique is not as accurate as the one developed by Longuet-Higgins and Cokelet. At least, their vertical side boundary conditions and corner problems are eliminated by the conformal transformation. But the proposed method has proved that for small amplitude waves, the technique would allow the wave to travel more than six periods.

One of the fundamental sources of numerical instability in the proposed technique is due to the corners of the wave surface, where two nodes move towards each other until a re-entrant boundary exists. The inability to model a plunging wave is due to the re-entrant boundary developed on the wave surface. Again, the approach by Longuet-Higgins and Cokelet has eliminated the re-entrant boundary by conformal transformation.

The pressures obtained by the proposed technique on the fixed horizontal circular cylinder are not in good agreement with the experimental measurements for steeper waves. But the experimental results may be subject to the disturbance of the free surface and viscous effect on the cylinder. Good agreement is shown for small amplitude waves and when the cylinder is well away from the free surface. Due to the inability to model plunging waves, when the cylinder is in shallow submergence, the pressure results would not agree well with the experimental measurements. The poor comparison of forces between the proposed technique and those obtained by Jeffrey et al (1976) is caused by the cylinder being placed too closed to the surface. Good agreement is shown on forces between the proposed technique and those obtained by Lacey (1983). Results for forces and pressures might be improved if the fixed horizontal circular cylinder is placed half a wavelength behind the wave trough.

Longuet-Higgins and Cokelet (1976) have shown energy variation in time for waves with pressure amplitude applied at the wave surface. Vinge and Brevig (1980) showed the variation in time of the total energy of the deep-water waves and of their components, i.e. kinetic and potential energy. Their total energy is almost constant in time, except at the very end of the calculation where the total energy drops. Even though they have shown their energy variations, it is difficult to compare their results with the energy variations from the case studies. From their graphs, the wave moved about 0.75 of a period and then stopped. From Figs. A.13.1 - A.13.56, the energy variations in time are all fairly constant, except that the total energy increases gradually at the end of the wave movement. The durations of the wave movement in these cases range from over 6 periods for small amplitude waves to 0.55 of a period for finite amplitude waves.

Another area of concern which might contribute some numerical inaccuracy is that shown by Ogilvie (1963) who demonstrated that when a wave passed over an object, a phase lag would exist between the incident and transmitted waves. The phase lag leads to a difference in wavelengths on the wave before and after passing the object. Calculations have been carried out and show that for the wave characteristic in case 34, the phase lag is 10° which is equivalent to a difference in wavelengths of 63mm. For the wave characteristic in case 56, the phase lag is 16.6° which is equivalent to a phase difference of 77.3mm. These differences may contribute some error which the proposed method has not accounted for.

When a wave problem is to be solved using the proposed technique, there are three factors which play a significant role in determining the accuracy of the solution. The first factor is the wave characteristic. Although the method uses non-linear boundary conditions on the wave surface, numerical instability increases with increasing wave steepness. The second factor is the number of nodes used on the boundaries, especially on the wave surface. Even though this comparison has not been shown in the previous chapter, the execution time is proportional to the square of the total number of nodes used at the boundaries. The third factor relates to the introduction of an object into the flow domain. The smaller the depth of submergence of the object, the sooner the numerical instability occurs on the wave profile.

The disadvantage of the proposed technique, or even the techniques proposed by Longuet-Higgins and Cokelet (1976) and Vinje and Brevig (1980), is that the domain will repeat itself infinitely. That means if the wave profile has an object in the flow domain, the object will repeat itself an infinite number of times with the same wave profile above it. Hence the method can not be applied to a realistic problem, for example, a horizontal cylinder under wave profiles in a wave tank. An immediate answer would be to have a domain with 5 to 10 wavelengths along the length of domain, so that the influence of vertical side boundaries on the cylinder is reduced, or ultimately to replace the in-flow vertical side boundary conditions with the numerical modelling of wave generator and the out-flow vertical boundary conditions with the numerical modelling of wave absorber.

CHAPTER 8 - CONCLUSION AND RECOMMENDATIONS FOR FURTHER RESEARCH WORK

The aim of the present study has been achieved by showing the applications of the boundary element method to ground water flow problems, free surface flow problems, orthotropic problems, heat conduction problems and more extensively to the simulation of progressive and standing wave problems.

The basic formulation of the boundary element method has been presented in chapter 3. It mainly consists of dividing only the boundary of the domain into a series of elements as opposed to the division of the whole domain in the finite element method (with the exception of the application to transient potential problems). Therefore a smaller system of algebraic equations is obtained and a considerable reduction in the data required to solve a problem can be achieved. The accuracy of solutions by the boundary element method is comparable to those obtained by the finite element method.

Existing techniques for the application of the boundary element method to time dependent problems have been studied. The results of the four examples given in chapter 4 validate the programs written in this study. Accuracy of the solution technique for rigid domain problems with re-entrant corners may be improved through the division of the domain into zones, as illustrated in example 4.3.1 - seepage under a dam with vertical cut-off wall. Comparison of the boundary idealisations in the free surface flow solution procedure of Liggett (1977a) and Brebbia and Wrobel (1979), indicates that results may be improved by the inclusion of the seepage surface and a constant, k, to control the rate of convergence. Two values were assigned to the constant, $k = 1.0$ and $k = 0.5$. It was found that $k = 0.5$ gave a smoother free surface at the downstream face. The examples for orthotropic and heat conduction problems show the degree of numerical accuracy achieved in their original work.

The major achievement of the present work is the numerical simulation of periodic waves (i.e. progressive or standing) and the evaluation of pressures and forces on an internal object introduced into the flow domain.

The technique of applying the boundary element method to simulate periodic waves has been developed in chapter 5, together with the evaluation of pressures and forces on an internal object. Basically, the method involves solving integral equations along the fluid boundary, at each time step, to determine the spatial dependence of the motion at the wave surface. The wave profile is represented by the positions of wave particles. At each instant of time, boundary integral equations are set up and solved for the unknowns on the boundary. The positions of the wave particles are then advanced by a time stepping technique. Pressures and forces on an internal object may be evaluated at each time step.

A comparison of the wave profile after running for one or two periods with exact solution is not an easy task. The following points may be identified to support the validity of the application of the boundary element method to simulate periodic waves with small wave steepness. Firstly, the technique would allow the wave to travel more than six periods for small amplitude waves and, secondly, the pressures obtained on the fixed horizontal cylinder are in good agreement with the experimental measurements for small amplitude waves when the cylinder is well away from the free surface. (Numerical instability occurs when the cylinder is placed too close to the wave surface.)

The majority of wave profile failures in the case studies originate at the corner of the wave surface where two nodes moved towards each other until a re-entrant boundary developd. The larger the wave steepness in the wave problem, the sooner the failure occurs. Therefore, investigation into the corner problem of the wave surface is recommended for improvement of the proposed technique.

One of the disadvantages of the technique is that the cylinder cannot be treated as partly submerged in the wave surface, which is within the capability of the technique by Vinje and Brevig (1980). Even if the cylinder is fully submerged, the crown of the cylinder must be well below the level where the trough of the wave lies.

The development of a re-entrant boundary is clearly a numerical obstacle for the wave to become plunging. Chapter 4 has clearly demonstrated that the re-entrant corner in example 4.3.1 can be eliminated by the technique of zoning. But it has not been adopted in the unsteady wave problems. The reason is that example 4.3.1 involves a rigid domain where the re-entrant corner is explicit. In the case of unsteady wave problems the re-entrant corner does not exist when a problem was set up. One has no knowledge of where on the wave surface it will occur. Obviously, the re-entrant corner problem in a non-rigid domain is an area for further research.

Another area for the improvement of the proposed technique is the numerical modelling of proper radiation boundary conditions on the two vertical side boundaries. A more realistic approach would be the numerical modelling of the wave generator and absorber on the two vertical side boundaries to simulate a numerical wave tank.

If a vector field $\underset{\sim}{F}(x_F, y_F, z_F)$ and the divergence of $\underset{\sim}{F}$:

$$\mathrm{div}\,\underset{\sim}{F} = \frac{\partial x_F}{\partial x} + \frac{\partial y_F}{\partial y} + \frac{\partial z_F}{\partial z} \tag{A.1.1}$$

are continuous over the regular region Ω and its boundary Γ, the Divergence theorem may then be stated as (Kellogg, 1954):

$$\int_\Omega \mathrm{div}\,\underset{\sim}{F}\, d\Omega = \int_\Gamma \underset{\sim}{F_n}\, d\Gamma \tag{A.1.2}$$

where $\underset{\sim}{F_n}$ is the component of the vector field in the direction of the outward normal to the boundary Γ.

Equation (A.1.2) may be rewritten in full as:

$$\int_\Omega \left(\frac{\partial x_F}{\partial x} + \frac{\partial y_F}{\partial y} + \frac{\partial z_F}{\partial z}\right) d\Omega = \int_\Gamma (x_F \ell_1 + y_F \ell_2 + z_F \ell_3)\, d\Gamma \tag{A.1.3}$$

where ℓ_1, ℓ_2 and ℓ_3 are the direction cosines of the outward normal to Γ. The conditions for this theorem to be true are that the integrals of $\frac{\partial x_F}{\partial x}$, $\frac{\partial y_F}{\partial y}$ and $\frac{\partial z_F}{\partial z}$ through Ω exist and the region to be regular in the sense defined by Kellogg (1954), who stated that a regular region of space is a bounded closed region whose boundary is a closed regular surface.

APPENDIX A.2 FUNDAMENTAL SOLUTION AND GAUSS FLUX THEOREM

It is best to start from basic principle to prove that a function , f, involving $\frac{1}{r}$ in three-dimensional problems, or ln (r) in two-dimensional problems, may be a solution to Laplace's equation:

$$\nabla^2 f(r) = 0 \tag{A.2.1}$$

Let (x_1, x_2 , x_3), denoted by x_i , be the coordinates of a point p in space, and r, its distance from the origin o,(see Fig.A.2.1):

$$r^2 = x_1^2 + x_2^2 + x_3^2 = x_i x_i \tag{A.2.2}$$

Indicial notation indicating summation has been used in the above equation and will be used when appropriate. Differentiating equation (A.2.2) yields:

$$2r \frac{\partial r}{\partial x_i} = 2x_i$$

$$\frac{\partial r}{\partial x_i} = \frac{x_i}{r} \tag{A.2.3}$$

Therefore,

$$\frac{\partial}{\partial x_i}\left(\frac{1}{r}\right) = \frac{\partial}{\partial r}\left(\frac{1}{r}\right) \cdot \frac{\partial r}{\partial x_i} = \frac{-x_i}{r^3} \tag{A.2.4}$$

Differentiating equation (A.2.4) again gives:

$$\frac{\partial^2}{\partial x_i \partial x_i}\left(\frac{1}{r}\right) = \frac{\partial}{\partial x_i}\left(\frac{-x_i}{r^3}\right)$$

$$= \frac{-1}{r^3}\left(\frac{\partial x_i}{\partial x_i}\right) - x_i \frac{\partial}{\partial x_i}\left(\frac{1}{r^3}\right)$$

$$= \frac{-1}{r^3}(1+1+1) - x_i \frac{-3}{r^4} \cdot \frac{x_i}{r}$$

i.e. $$\frac{\partial^2}{\partial x_i \partial x_i}\left(\frac{1}{r}\right) = \nabla^2\left(\frac{1}{r}\right) = 0 \qquad \text{(A.2.5)}$$

Hence, $\frac{1}{r}$ is a solution of Laplace's equation in three dimensions except at the origin.

$\ln(r)$ may also be proved with the above approach to be a solution of Laplace's equation in two dimensions.

Now, consider the flux of the gradient of $\left(\frac{1}{r}\right)$ through a sphere Γ_s. r is the distance between point p, inside the sphere, and the origin, q, which is treated as a source point lying outside Γ_s, (see Fig. A.2.1). By applying

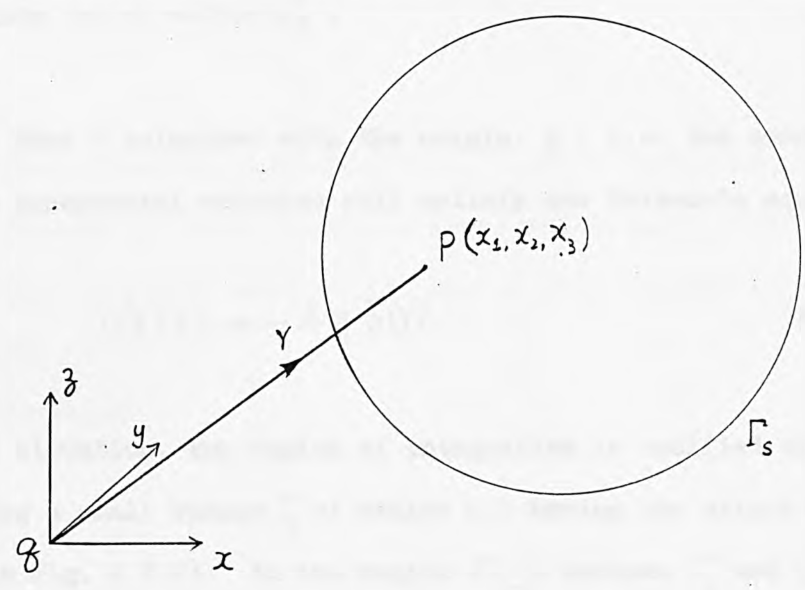

Fig. A.2.1 A point p inside a sphere in Cartesian coordinate system the Divergence theorem (see Appendix A.1) to the flux of the gradient of $(\frac{1}{\gamma})$, equation (A.1.3) becomes:

$$\int_{\Omega} \frac{\partial}{\partial x_i}\left[\frac{\partial}{\partial x_i}\left(\frac{1}{\gamma}\right)\right] d\Omega = \int_{\Gamma_s} l_i \cdot \frac{\partial}{\partial x_i}\left(\frac{1}{\gamma}\right) d\Gamma_s \tag{A.2.6}$$

where l_i is the direction cosine of the outward normal and :

$$l_i \cdot \frac{\partial}{\partial x_i}\left(\frac{1}{\gamma}\right) = \frac{\partial x_i}{\partial n} \cdot \frac{\partial}{\partial x_i}\left(\frac{1}{\gamma}\right) = \frac{\partial}{\partial n}\left(\frac{1}{\gamma}\right) \tag{A.2.7}$$

From equation (A.2.5):

$$\int_{\Omega} \frac{\partial^2}{\partial x_i^2}\left(\frac{1}{\gamma}\right) d\Omega = 0 \tag{A.2.8}$$

therefore,

$$\int_{\Omega} \frac{\partial^2}{\partial x_i^2}\left(\frac{1}{\gamma}\right) d\Omega = \int_{\Gamma_s} \frac{\partial}{\partial n}\left(\frac{1}{\gamma}\right) d\Gamma_s = 0 \tag{A.2.9}$$

Equation (A.2.9) is true provided that γ is different from zero at all points on or within Γ_s .

When p coincides with the origin, q , i.e. the source point, the fundamental solution will satisfy the Poisson's equation:

$$\nabla^2 f(\gamma) = -4\pi\,\delta(\gamma) \tag{A.2.10}$$

Under this situation, the region of integration is modified by constructing a small sphere Γ_ε of radius ε , having the origin as centre (see Fig. A.2.2). In the region $\Omega_{s-\varepsilon}$, between Γ_s and Γ_ε , the function $\frac{1}{\gamma}$ satisfies the Divergence theorem, since $\Omega_{s-\varepsilon}$ does not contain any source point and thus equation (A.1.3) becomes:

$$\int_{\Omega_{S-\varepsilon}} \frac{\partial}{\partial x_i}\left[\frac{\partial}{\partial x_i}\left(\frac{1}{r}\right)\right] d\Omega_{S-\varepsilon} = \int_{\Gamma_S} l_i \cdot \frac{\partial}{\partial x_i}\left(\frac{1}{r}\right) d\Gamma_S + \int_{\Gamma_\varepsilon} l_i \frac{\partial}{\partial x_i}\left(\frac{1}{r}\right) d\Gamma_\varepsilon \qquad \text{(A.2.11)}$$

where l_i denotes the direction cosines of the outward normals from region $\Omega_{S-\varepsilon}$ which will be outward from q over Γ_S and inward over Γ_ε .

From equations (A.2.7) and (A.2.8), equation (A.2.11) is reduced to:

$$\int_{\Gamma_S} \frac{\partial}{\partial n}\left(\frac{1}{r}\right) d\Gamma_S - \int_{\Gamma_\varepsilon} \frac{\partial}{\partial n}\left(\frac{1}{r}\right) d\Gamma_\varepsilon = 0 \qquad \text{(A.2.12)}$$

Since r and n are in the same direction. the last integral of equation (A.2.12) can be evaluated as:

$$\int_{\Gamma_\varepsilon} \frac{\partial}{\partial r}\left(\frac{1}{r}\right) d\Gamma_\varepsilon = \frac{-1}{r^2} \cdot 4\pi r^2 \qquad \text{(A.2.13)}$$

$$= -4\pi$$

Equation (A.2.12) then becomes:

$$\int_{\Gamma_S} \frac{\partial}{\partial n}\left(\frac{1}{r}\right) d\Gamma_S = -4\pi \qquad \text{(A.2.14)}$$

These results, equations (A.2.9) and (A.2.14), constitute the Gauss flux theorem or Gauss condition which states that : If Γ is a closed regular surface and q is the source point located at the origin, then,

in three-dimensions:

$$\int_{\Gamma} \frac{\partial}{\partial n}\left(\frac{1}{r}\right) d\Gamma = \begin{cases} 0 & \text{for } q \text{ outside } \Gamma \qquad \text{(A.2.15a)} \\ -4\pi & \text{for } q \text{ inside } \Gamma \qquad \text{(A.2.15b)} \end{cases}$$

and similarly in two-dimensions:

$$\int_{\Gamma} \frac{\partial}{\partial n} \ln\left(\frac{1}{r}\right) d\Gamma = \begin{cases} 0 & \text{for } q \text{ outside } \Gamma \quad \text{(A.2.16a)} \\ -2\pi & \text{for } q \text{ inside } \Gamma \quad \text{(A.2.16b)} \end{cases}$$

where $\frac{\partial}{\partial n}$ is the differentiation along the outward normal.

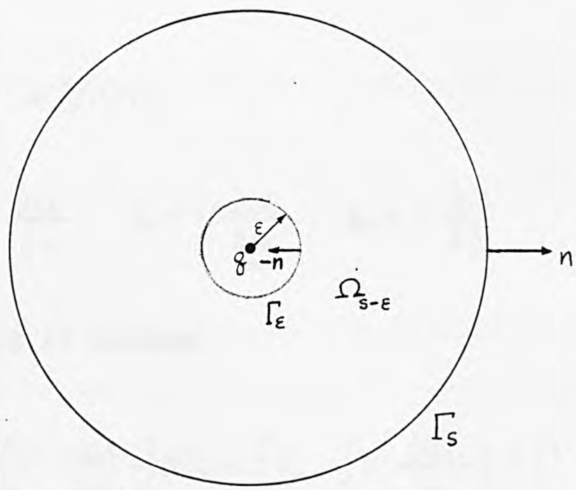

Fig. A.2.2 A singular point, q, excluded from the region by a small sphere Γ_ε

APPENDIX A.3 GREEN'S THEOREMS

Let U and V be two different functions defined in a closed regular region, Ω, in space. Both functions are continuously differentiable in Ω and have continuous partial derivatives of the second order in Ω. Then, the Divergence theorem in Appendix A.1 holds for Ω with the vector field:

$$\underset{\sim}{F} = V \cdot \nabla U$$

or
$$x_F = V\frac{\partial U}{\partial x}\ , \quad y_F = V\frac{\partial U}{\partial y}\ , \quad z_F = V\frac{\partial U}{\partial z} \tag{A.3.1}$$

Equation (A.2.2) becomes:

$$\int_\Omega \frac{\partial}{\partial x_i}\left(V \cdot \frac{\partial U}{\partial x_i}\right) d\Omega = \int_\Gamma l_i \cdot \left(V \cdot \frac{\partial U}{\partial x_i}\right) d\Gamma \tag{A.3.2}$$

where indicial notation indicating summation has been used, l_i represents the direction cosines of the outward normal n to Γ and:

$$l_i \cdot \frac{\partial U}{\partial x_i} = \frac{\partial x_i}{\partial n} \cdot \frac{\partial U}{\partial x_i} = \frac{\partial U}{\partial n} \tag{A.3.3}$$

which is the differentiation of U along the outward normal n.

Equation (A.3.2) becomes:

$$\int_\Omega V \nabla^2 U \, d\Omega + \int_\Omega \frac{\partial V}{\partial x_i} \cdot \frac{\partial U}{\partial x_i} d\Omega = \int_\Gamma V \cdot \frac{\partial U}{\partial n} d\Gamma \tag{A.3.4}$$

which is generally known as Green's first identity.

Similarly, by interchanging the roles of U and V in equation (A.3.1), the following equation may be obtained:

$$\int_{\Omega} U\nabla^2 V\, d\Omega + \int_{\Omega} \frac{\partial U}{\partial x_i}\cdot\frac{\partial V}{\partial x_i}\, d\Omega = \int_{\Gamma} U\cdot\frac{\partial V}{\partial n}\, d\Gamma \tag{A.3.5}$$

Noting that :

$$\frac{\partial U}{\partial x_i}\cdot\frac{\partial V}{\partial x_i} = \frac{\partial V}{\partial x_i}\cdot\frac{\partial U}{\partial x_i}$$

and subtracting equation (A.3.4) from (A.3.5) gives:

$$\int_{\Omega} (U\nabla^2 V - V\nabla^2 U)\, d\Omega = \int_{\Gamma} \left(U\frac{\partial V}{\partial n} - V\frac{\partial U}{\partial n}\right) d\Gamma \tag{A.3.6}$$

which is known as Green's second identity for the two functions U and V in a closed regular region Ω with boundary Γ and the normal n is directed outward from Γ.

If U and V are harmonic and continuously differentiable in the closed regular region Ω, then the Green's second identity becomes:

$$\int_{\Gamma} \left(U\frac{\partial V}{\partial n} - V\frac{\partial U}{\partial n}\right) d\Gamma = 0 \tag{A.3.7}$$

If U is harmonic and continuously differentiable in Ω, and V is assigned a constant value to it, say, $V = 1$, then the Green's first identity (A.3.4) reduces to the Gauss condition (A.2.15a):

$$\int_{\Gamma} \frac{\partial U}{\partial n}\, d\Gamma = 0 \tag{A.3.8}$$

APPENDIX A.4 EVALUATION OF $\dfrac{\partial g^*}{\partial n}$

The fundamental solution $g^*(p,q)$ in two dimensions is given by:

$$g^*(p,q) = \ln|\underset{\sim}{p} - \underset{\sim}{q}| = \ln(r) \tag{A.4.1}$$

It is assumed that $\dfrac{\partial g^*}{\partial n}$ can be resolved into radial and tangential directions, r and t, (see Fig. A.4.1). Therefore,

$$\frac{\partial g^*}{\partial n} = \frac{\partial g^*}{\partial r}\cos\alpha + \frac{\partial g^*}{\partial t}\cos\beta \tag{A.4.2}$$

Since g^* is a function of r along the radial direction only;

$$\frac{\partial g^*}{\partial t} = 0 \tag{A.4.3}$$

and therefore,

$$\frac{\partial g^*}{\partial n} = \frac{\partial g^*}{\partial r}\cos\alpha = \frac{y_p}{r^2} \tag{A.4.4}$$

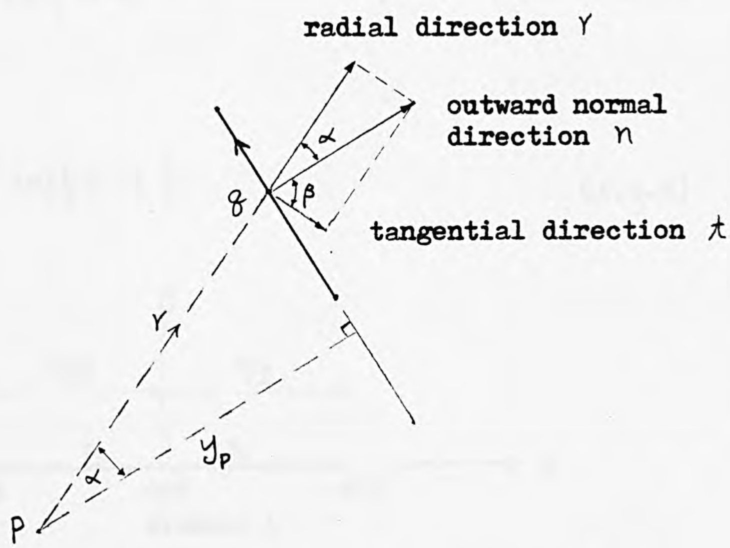

Fig. A.4.1 Radial and tangential directions to an element at q

APPENDIX A.5 EXACT INTEGRATIONS OF G_{ii}

The exact integrations of G_{ii} terms for constant or linear variation for both steady and transient potential problems are carried out in the Cauchy principal value sence.

(a) Steady potential problems

i. Constant variation (see Fig. A.5.1):

$$G_{ii} = \int_{\Gamma_i} g^* \, d\Gamma$$

$$= \int_{E(0)}^{E(1)} \ln(\gamma_1)\, d\gamma_1 + \int_{E(0)}^{E(2)} \ln(\gamma_2)\, d\gamma_2$$

$$= \Big[\gamma_1 \cdot \ln(\gamma_1) - \gamma_1\Big]_{\varepsilon}^{\frac{l_i}{2}} + \Big[\gamma_2 \cdot \ln(\gamma_2) - \gamma_2\Big]_{\varepsilon}^{\frac{l_i}{2}}$$

$$= 2 \cdot \left\{ \left[\frac{l_i}{2} \ln\left(\frac{l_i}{2}\right) - \frac{l_i}{2} \right] - \Big[\varepsilon \cdot \ln(\varepsilon) - \varepsilon \Big] \right\} \qquad \text{(A.5.1)}$$

with $\varepsilon \rightarrow 0$, from L'Hopital rule;

$$\lim_{\varepsilon \to 0} \Big[\varepsilon \cdot \ln(\varepsilon)\Big] = 0 \qquad \text{(A.5.2)}$$

Therefore,

$$G_{ii} = l_i \left\{ \ln\left(\frac{l_i}{2}\right) - 1 \right\} \qquad \text{(A.5.3)}$$

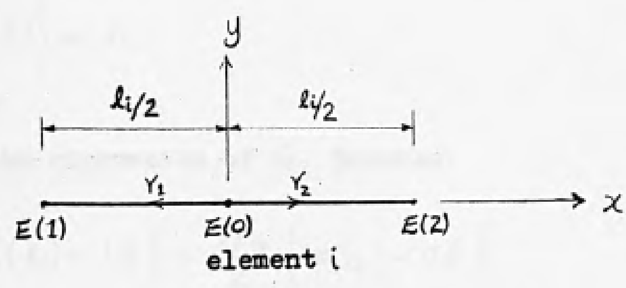

Fig. A.5.1 Exact integration for constant variation

ii. Linear variation

Since node i lies between elements i and $i-1$, the following interpolation functions are needed for the evaluation:

$$N_1 = 1 - \frac{r}{\ell_i} \qquad \text{for element } i \qquad (A.5.4a)$$

$$N_2 = \frac{r}{\ell_{i-1}} \qquad \text{for element } i-1 \qquad (A.5.4b)$$

and

$$G_{ii} = \int_{\Gamma_i} N_1\, g^*\, d\Gamma + \int_{\Gamma_{i-1}} N_2\, g^*\, d\Gamma$$

$$= \int_{\varepsilon}^{\ell_i} \left(1-\frac{r}{\ell_i}\right)\cdot \ln(r)\, dr + \int_{\varepsilon}^{\ell_{i-1}} \frac{r}{\ell_i}\cdot \ln(r)\, dr$$

$$= \left[\ln(r)\cdot\left(r-\frac{r^2}{2\ell_i}\right)\right]_{\varepsilon}^{\ell_i} - \int_{\varepsilon}^{\ell}\left(r-\frac{r^2}{2\ell_i}\right)\cdot\frac{1}{r}\, dr$$

$$+\left[\ln(r)\frac{r^2}{2\ell_{i-1}}\right]_{\varepsilon}^{\ell_{i-1}} - \int_{\varepsilon}^{\ell_{i-1}} \frac{r^2}{2\ell_{i-1}}\cdot\frac{1}{r}\, dr$$

$$= \frac{\ell_i}{2}\cdot \ln(\ell_i) - \varepsilon\cdot\ln(\varepsilon) + \frac{\varepsilon^2}{2\ell_i}\ln(\varepsilon) - \left[r - \frac{r^2}{4\ell_i}\right]_{\varepsilon}^{\ell_i}$$

$$+\frac{\ell_{i-1}}{2}\ln(\ell_{i-1}) - \frac{\varepsilon^2}{2\ell_{i-1}}\ln(\varepsilon) - \left[\frac{r^2}{4\ell_{i-1}}\right]_{\varepsilon}^{\ell_{i-1}} \qquad (A.5.5)$$

From L'Hopital rule, with the limit $\varepsilon \longrightarrow 0$:

$$\lim_{\varepsilon\to 0}\left\{\varepsilon^2 \ln(\varepsilon)\right\} = 0 \qquad (A.5.6)$$

Therefore, the expression of G_{ii} becomes:

$$G_{ii} = \frac{\ell_i}{2}\left\{\ln(\ell_i) - 1.5\right\} + \frac{\ell_{i-1}}{2}\left\{\ln(\ell_{i-1}) - 0.5\right\} \qquad (A.5.7)$$

(b) Transient potential problems

i. Linear variation

The same principle for linear variation of steady potential problems can be ultilised here, i.e.

$$G_{ii} = \int_{\Gamma_i} N_1 \, \mathrm{Ei}\,[a]\, d\Gamma + \int_{\Gamma_{i-1}} N_2 \, \mathrm{Ei}\,[a]\, d\Gamma \tag{A.5.8}$$

where N_1 and N_2 have the expressions of equations (A.5.4):

$$\mathrm{Ei}\,[a] = -C_E - \ln|a| - \sum_{n=1}^{\infty} (-1)^{n-1} \frac{a^n}{n \cdot n!} \tag{A.5.9a}$$

$$a = R r^2 \tag{A.5.9b}$$

$$R = \frac{1}{4K(t_2 - t_1)} \tag{A.5.9c}$$

Substituting equations (A.5.9) into the first integral in equation (A.5.8) yields:

$$\int_{\Gamma_i} N_1 \mathrm{Ei}[a]\, d\Gamma = \int_{\varepsilon \to 0}^{l_i} \left(1 - \frac{r}{l_i}\right) \left\{ -C_E - \ln|Rr^2| + Rr^2 - \frac{(Rr^2)^2}{2 \cdot 2!} + \frac{(Rr^2)^3}{3 \cdot 3!} - \frac{(Rr^2)^4}{4 \cdot 4!} + \cdots \right\} dr$$

which is simplified to:

$$\int_{\Gamma_i} N_1 \mathrm{Ei}\,[a]\, d\Gamma = \frac{l_i}{2}\left(3 - C_E - \ln|R l_i^2|\right) + \sum_{n=1}^{\infty} \frac{(-1)^{n-1} R^n l_i^{2n+1}}{(2n+1)\cdot(2n+2)\cdot n \cdot n!} \tag{A.5.10}$$

Similarly, for the second integral of equation (A.5.8):

$$\int_{\Gamma_{i-1}} \left(\frac{r}{l_{i-1}}\right) \mathrm{Ei}[a]\, d\Gamma = \frac{l_{i-1}}{2}\left(1 - C_E - \ln|R l_{i-1}^2|\right) + \sum_{n=1}^{\infty} \frac{(-1)^{n-1} R^n l_{i-1}^{2n+1}}{(2n+2)\cdot n \cdot n!} \tag{A.5.11}$$

Therefore, equation (A.5.8) becomes:

$$G_{ii} = \frac{l_i}{2}\left(3 - C_E - \ln|R l_i^2|\right) + \sum_{n=1}^{\infty} \frac{(-1)^{n-1} R^n l_i^{2n+1}}{(2n+1)\cdot(2n+2)\cdot n \cdot n!}$$

$$+ \frac{l_{i-1}}{2}\left(1 - C_E - \ln|R l_{i-1}^2|\right) + \sum_{n=1}^{\infty} \frac{(-1)^{n-1} R^n l_{i-1}^{2n+1}}{(2n+2)\cdot n \cdot n!} \tag{A.5.12}$$

BASIC HYDRODYNAMICS FOR TWO DIMENSIONAL FLOW

(1) Incompressible flow

Consider an element of fluid of unit dimensions, as shown in Fig. A.6.1, the horizontal and vertical inflow velocities are u and v respectively.

For incompressible flow, the density of fluid is constant:
Mass of fluid inflow = Mass of fluid outflow

$$u + v = u + \frac{\partial u}{\partial x} + v + \frac{\partial v}{\partial y}$$

Hence:

$$\frac{\partial u}{\partial x} + \frac{\partial v}{\partial y} = 0 \qquad \text{(A.6.1)}$$

Equation (A.6.1) is the well known continuity equation.

(2) Stream function "ψ"

A stream function, ψ , is defined such that:

$$\frac{\partial \psi}{\partial y} = u \qquad \text{(A.6.2a)}$$

$$\frac{\partial \psi}{\partial x} = -v \qquad \text{(A.6.2b)}$$

Substituting equations (A.6.2) into (A.6.1) yields:

$$\frac{\partial^2 \psi}{\partial x \cdot \partial y} - \frac{\partial^2 \psi}{\partial x \cdot \partial y} = 0 \qquad \text{(A.6.3)}$$

Hence the stream function ψ satisfies the continuity equation.

(3) Velocity potential " ϕ "

A velocity potential is defined such that:

$$\frac{\partial \phi}{\partial x} = u \tag{A.6.4a}$$

$$\frac{\partial \phi}{\partial y} = v \tag{A.6.4b}$$

Substituting equations (A.6.4) into (A.6.1) gives:

$$\frac{\partial^2 \phi}{\partial x^2} + \frac{\partial^2 \phi}{\partial y^2} = 0$$

or $$\nabla^2 \phi = 0 \tag{A.6.5}$$

Equation (A.6.5) is the well known Laplace's equation.

(4) Bernoulli's equation

Since the flow of an inviscid fluid is generally irrotational, but may be unsteady, the Bernoulli's equation for unsteady irrotational flows is shown to be (Newman, 1980):

$$\frac{\partial \phi}{\partial t} + \frac{p}{\rho} + \frac{1}{2}(u^2 + v^2) + g y = C(t)$$

or $$\frac{\partial \phi}{\partial t} + \frac{p}{\rho} + \frac{1}{2}(\nabla \phi)^2 + g y = C(t) \tag{A.6.6}$$

where p is the pressure.

ρ is the fluid density.

g is the acceleration due to gravity.

$C(t)$ is a constant independent of space coordinates but may depend on time.

$\nabla\phi$ is the particle velocity.

u and v are the particle velocities in x and y directions respectively, (see Fig. A.6.1).

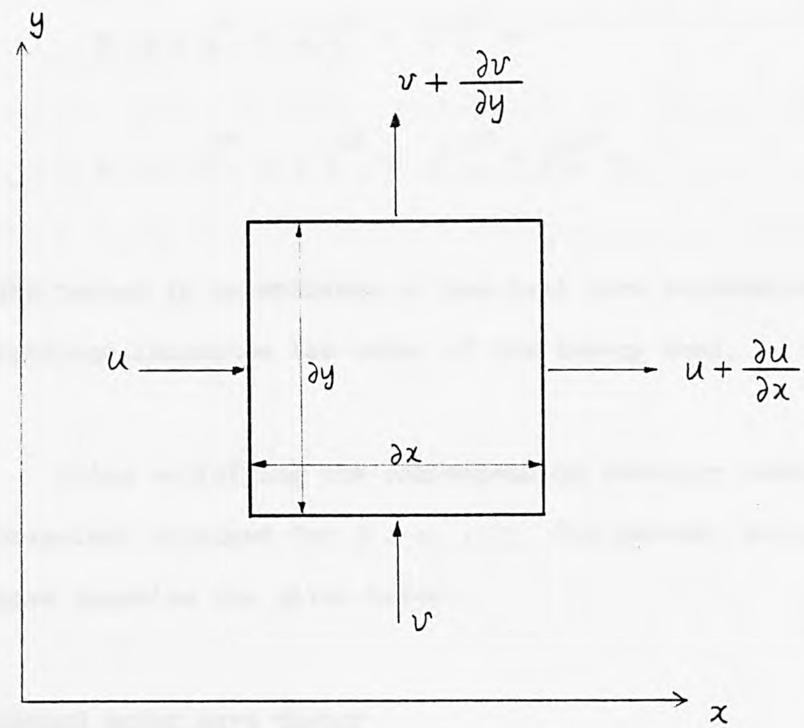

Fig. A.6.1 An element of fluid

Wehausen and Laitone (1960) assumed that the velocity potential ϕ , wave profile η , and wave velocity C could be expanded in a perturbation series in some parameter:

$$\varepsilon = a\,k \tag{A.7.1}$$

and

$$\phi = \varepsilon\,\phi^{(1)} + \varepsilon^2\phi^{(2)} + \varepsilon^3\phi^{(3)} + \cdots \tag{A.7.2a}$$

$$\eta = \varepsilon\,\eta^{(1)} + \varepsilon^2\eta^{(2)} + \varepsilon^3\eta^{(3)} + \cdots \tag{A.7.2b}$$

$$C = C^{(0)} + \varepsilon\,C^{(1)} + \varepsilon^2 C^{(2)} + \varepsilon^3 C^{(3)} + \cdots \tag{A.7.2c}$$

where the number in parentheses of the last term considered in the approximations,indicates the order of the theory used.

After satisfying the corresponding boundary conditions, the expressions obtained for ϕ , η , C for second, third and fifth order wave theories are given below.

(i) <u>Second order wave theory</u>

The following equations are identical with the ones presented in Wiegel (1964).

Velocity potential, ϕ:

$$\phi = a \cdot C \cdot \frac{\cosh k(d+y)}{\sinh\ (kd)} \cdot \sin(kx - \sigma t)$$

$$+ \frac{3}{4} \cdot \frac{\pi a^2 C}{\lambda} \cdot \frac{\cosh 2k(d+y)}{\sinh^4(kd)} \cdot \sin 2(kx - \sigma t) \tag{A.7.3}$$

Wave profile , η :

$$\eta = a\cos(kx-\sigma t)+\frac{1}{4}a^2k\frac{(2+\cosh 2kd)\cosh(kd)}{\sinh^3(kd)}\cos 2(kx-\sigma t) \qquad \text{(A.7.4)}$$

The equation for the wave velocity C is the same as for the linear wave theory, i.e.

$$C = \frac{gT}{2\pi}\cdot\tanh\left(\frac{2\pi d}{\lambda}\right)$$

or

$$C^2 = \frac{g\lambda}{2\pi}\cdot\tanh\left(\frac{2\pi d}{\lambda}\right) \qquad \text{(A.7.5)}$$

(ii) Third order wave theory

The velocity potential, wave profile and velocity computations were carried out by Stokes to the third order for pure gravity waves in fluid of finite depth. The following expressions, however, are taken from a report by Skjelbreia (1958).

Velocity potential , ϕ :

$$\phi = \frac{C}{k}\left\{F_1\cdot\cosh k(d+y)\cdot\sin(kx-\sigma t) + \frac{1}{2}F_2\cosh 2k(d+y)\cdot\sin 2(kx-\sigma t) + \frac{1}{3}F_3\cosh 3k(d+y)\cdot\sin 3(kx-\sigma t)\right\} \qquad \text{(A.7.6)}$$

where

$$F_1 = ak\frac{1}{\sinh(kd)}$$

$$F_2 = \frac{3}{4}a^2k^2\frac{1}{\sinh^4(kd)}$$

$$F_3 = \frac{3}{64}a^3k^3\frac{(11-2\cosh 2kd)}{\sinh^7(kd)}$$

Wave profile, η :

$$\eta = a\cos(kx-\sigma t)+\frac{\pi a^2}{\lambda} f_2\left(\frac{d}{\lambda}\right)\cdot \cos 2(kx-\sigma t)$$

$$+\frac{\pi^2 a^3}{\lambda^2} f_3\left(\frac{d}{\lambda}\right)\cdot\cos 3(kx-\sigma t) \tag{A.7.7}$$

where

$$f_2\left(\frac{d}{\lambda}\right)=\frac{\cosh(kd)\cdot\left[\cosh(2kd)+2\right]}{2\sinh^3(kd)}$$

$$f_3\left(\frac{d}{\lambda}\right)=\frac{3}{16}\cdot\frac{\left[1+8\cosh^6(kd)\right]}{\sinh^6(kd)}$$

Wave velocity, C :

$$C^2=\frac{g}{k}\cdot\tanh(kd)\cdot\left[1+a^2k^2\frac{8+\cosh(4kd)}{8\sinh^4(kd)}\right] \tag{A.7.8}$$

The value of wave amplitude 'a' may be determined from equation given below:

$$H=2a-\frac{2\pi^2a^3}{\lambda^2}\cdot f_3\left(\frac{d}{\lambda}\right) \tag{A.7.9}$$

where H is the wave height.

$f_3(\frac{d}{\lambda})$ has the same expression as for (A.7.7).

$k=2\pi/\lambda$.

For a specified value of H, a is obtained by using Newton-Raphson's method.

(iii) <u>Fifth order wave theory</u>

The Stokes's theory for velocity potential, wave profile and velocity was extended to the fifth order of approximation by De (1955). The expressions used in this study, were, however, taken from Skjelbreia and Hendrickson (1961).

Velocity potential, ϕ :

$$\phi = \frac{\bar{C}}{k}\Big\{(\beta A_{11} + \beta^3 A_{13} + \beta^5 A_{15}) \cosh k(d+y) \sin k(x - \bar{C}t)$$

$$+ (\beta^2 A_{22} + \beta^4 A_{24}) \cosh 2k(d+y) \sin 2k(x - \bar{C}t)$$

$$+ (\beta^3 A_{33} + \beta^5 A_{35}) \cosh 3k(d+y) \sin 3k(x - \bar{C}t)$$

$$+ \beta^4 A_{44} \cosh 4k(d+y) \sin 4k(x - \bar{C}t)$$

$$+ \beta^5 A_{55} \cosh 5k(d+y) \sin 5k(x - \bar{C}t)\Big\} \qquad \text{(A.7.10)}$$

Wave profile, η :

$$\eta = \frac{1}{k}\Big\{\beta \cos k(x - \bar{C}t) + (\beta^2 B_{22} + \beta^4 B_{24}) \cos 2k(x - \bar{C}t)$$

$$+ (\beta^3 B_{33} + \beta^5 B_{35}) \cos 3k(x - \bar{C}t)$$

$$+ \beta^4 B_{44} \cos 4k(x - \bar{C}t) + \beta^5 B_{55} \cos 5k(x - \bar{C}t)\Big\} \qquad \text{(A.7.11)}$$

Wave velocity, $\bar{C}$:

$$\bar{C}^2 = \frac{C_0^2}{k}(1 + \beta^2 C_1 + \beta^4 C_2) \qquad \text{(A.7.12)}$$

β in the above expressions is determined by the following equation, assuming the wave height H, water depth d, and wave length λ given:

$$\frac{\pi H}{d} = \frac{1}{(d/\lambda)}\Big\{\beta + \beta^3 B_{33} + \beta^5 (B_{35} + B_{55})\Big\} \qquad \text{(A.7.13)}$$

The expressions for constants A_{ij}, B_{ij} and C_i are functions of (d/λ) and listed below. Their numerical values for different values of (d/λ) are given in tables I, II and III of Skjelbreia and Hendrickson (1961). For brevity in listing the coefficients, two notations are made:

(a) $S = \sinh(2\pi d/\lambda)$ (A.7.14a)

(b) $C = \cosh(2\pi d/\lambda)$ (A.7.14b)

$$C_o^2 = g\left[\tanh(kd)\right] \tag{A.7.15a}$$

$$A_{11} = 1/S \tag{A.7.15b}$$

$$A_{13} = \frac{-C^2\ (5C^2 + 1)}{8S^5} \tag{A.7.15c}$$

$$A_{15} = \frac{-(1184C^{10} - 1440C^8 - 1992C^6 + 2641C^4 - 249C^2 + 18)}{1536S^{11}} \tag{A.7.15d}$$

$$A_{22} = \frac{3}{8S^4} \tag{A.7.15e}$$

$$A_{24} = \frac{(192C^8 - 424C^6 - 312C^4 + 480C^2 - 17)}{768S^{10}} \tag{A.7.15f}$$

$$A_{33} = \frac{13 - 4C^2}{64S^7} \tag{A.7.15g}$$

$$A_{35} = \frac{(512C^{12} + 4224C^{10} - 6800C^8 - 12808C^6 + 16704C^4 - 315C^2 + 107)}{4096S^{13}\ (6C^2 - 1)} \tag{A.7.15h}$$

$$A_{44} = \frac{(80C^6 - 816C^4 + 1338C^2 - 197)}{1536S^{10}\ (6C^2 - 1)} \tag{A.7.15i}$$

$$A_{55} = \frac{-(2880C^{10} - 72480C^8 + 324000C^6 - 432000C^4 + 163470C^2 - 16245)}{61440S^{11}\ (6C^2 - 1)\ (8C^4 - 11C^2 + 3)} \tag{A.7.15j}$$

$$B_{22} = \frac{C(2C^2 + 1)}{4S^3} \tag{A.7.15k}$$

$$B_{24} = \frac{C(272C^8 - 504C^6 - 192C^4 + 322C^2 + 21)}{384S^9} \tag{A.7.15l}$$

$$B_{33} = \frac{3(8C^6 + 1)}{64S^6} \tag{A.7.15m}$$

$$B_{35} = \frac{(88128C^{14} - 208224C^{12} + 70848C^{10} + 54000C^{8} - 21816C^{6} + 6264C^{4} - 54C^{2} - 81)}{12288S^{12}(6C^{2} - 1)} \qquad \text{(A.7.15n)}$$

$$B_{44} = \frac{C(768C^{10} - 448C^{8} - 48C^{6} + 48C^{4} + 106C^{2} - 21)}{384S^{9}(6C^{2} - 1)} \qquad \text{(A.7.15o)}$$

$$B_{55} = \frac{192000C^{16} - 262720C^{14} + 83680C^{12} + 20160C^{10} - 7280C^{8}}{12288S^{10}(6C^{2} - 1)(8C^{4} - 11C^{2} + 3)}$$

$$+ \frac{(7161C^{6} - 1800C^{4} - 1050C^{2} + 225)}{12288S^{10}(6C^{2} - 1)(8C^{4} - 11C^{2} + 3)} \qquad \text{(A.7.15p)}$$

$$C_{1} = \frac{(8C^{4} - 8C^{2} + 9)}{8S^{4}} \qquad \text{(A.7.15q)}$$

$$C_{2} = \frac{(3840C^{12} - 4096C^{10} + 2592C^{8} - 1008C^{6} + 5944C^{4} - 1830C^{2} + 147)}{512S^{10}(6C^{2} - 1)} \qquad \text{(A.7.15r)}$$

$$C_{3} = \frac{-1}{4SC} \qquad \text{(A.7.15s)}$$

$$C_{4} = \frac{(12C^{8} + 36C^{6} - 162C^{4} + 141C^{2} - 27)}{192CS^{9}} \qquad \text{(A.7.15t)}$$

If the wave period is given instead of the wave length to describe the wave profile, i.e. H , d, T are known, the wave length λ will be obtained through the following expression:

$$\frac{d}{\lambda_0} = \left(\frac{d}{\lambda}\right) \tanh(kd) \left\{ 1 + \beta^{2} C_1 + \beta^{4} C_2 \right\} \qquad \text{(A.7.16)}$$

where

$$\lambda_0 = \frac{gT^2}{2\pi}$$

g = acceleration due to gravity.

APPENDIX A.8 NON-DIMENSIONALISATION

The equations used in the computer program 'BEMW1' are in non-dimensional form.

In order to non-dimensionalise all the equations, the following reference parameters are chosen:

Reference length = $\lambda/2\pi$ (A.8.1a)

Reference velocity = $(g\lambda/2\pi)^{1/2}$ (A.8.1b)

Reference time = $(\lambda/2\pi g)^{1/2}$ (A.8.1c)

where λ is the actual dimension of wavelength.

g is the acceleration due to gravity.

Before carrying out the analysis, the following table is constructed to differentiate symbols with dimensions and those without dimensions.

Parameter	Dimensional symbol	Non-dimensional symbol
horizontal length	x	x_N
vertical length	y	y_N
wavelength	λ	λ_N
wave number	k	k_N
amplitude	a	a_N
water depth	d	d_N
velocity potential	ϕ	ϕ_N
wave velocity	C	C_N
time	t	t_N
period	T	T_N
wave frequency	σ	σ_N
acceleration due to gravity	g	g_N
density	ρ	ρ_N
pressure	p	p_N
force	F	F_N
normal direction	n	n_N
wave profile	η	η_N
phase angle	ϵ	ϵ_N
cylinder radius	r	r_N
wave height	H	H_N

Table A.8.1 Dimensional and non-dimensional symbols

From equations (A.8.1), the following identities are obtained:

$$x = x_N \frac{\lambda}{2\pi} \tag{A.8.2a}$$

$$y = y_N \frac{\lambda}{2\pi} \tag{A.8.2b}$$

$$\lambda = \lambda_N \frac{\lambda}{2\pi} \tag{A.8.2c}$$

$$a = a_N \frac{\lambda}{2\pi} \tag{A.8.2d}$$

$$d = d_N \frac{\lambda}{2\pi} \tag{A.8.2e}$$

$$k = k_N / \frac{\lambda}{2\pi} \tag{A.8.2f}$$

$$t = t_N \left(\frac{\lambda}{2\pi g}\right)^{1/2} \tag{A.8.2g}$$

$$\phi = \phi_N \left(\frac{g\lambda}{2\pi}\right)^{1/2} \left(\frac{\lambda}{2\pi}\right) = \phi_N \sqrt{\frac{g\lambda^3}{2\pi}} \tag{A.8.2h}$$

$$\sigma = \sigma_N / \left(\frac{\lambda}{2\pi g}\right)^{1/2} \tag{A.8.2i}$$

$$C = C_N \left(\frac{g\lambda}{2\pi}\right)^{1/2} \tag{A.8.2j}$$

$$p = p_N \rho g \cdot \frac{\lambda}{2\pi} \tag{A.8.2k}$$

$$F = F_N \rho g \left(\frac{\lambda}{2\pi}\right)^3 \tag{A.8.2l}$$

$$H = H_N \frac{\lambda}{2\pi} \tag{A.8.2n}$$

$$Y = Y_N \frac{\lambda}{2\pi} \tag{A.8.2m}$$

$$\eta = \eta_N \frac{\lambda}{2\pi} \tag{A.8.2o}$$

Substituting equations (A.8.2) into the relevant equations for wave profile, velocity potential, etc., the non-dimensionalised counterparts would be obtained. The following shows the non-dimensionalised, first order equations used in program 'BEMW1' for progressive wave problems:

(a) Wave profile :

$$\eta_N = a_N \cos\left(k_N x_N - \sigma_N t_N - \epsilon_N\right) \tag{A.8.3a}$$

(b) Velocity potential :

$$\phi_N = \frac{a_N g_N}{\sigma_N} \cdot \frac{\cosh\left[k_N\left(y_N + d_N\right)\right]}{\cosh\left(k_N d_N\right)} \sin\left(k_N x_N - \sigma_N t_N - \epsilon_N\right) \tag{A.8.3b}$$

where $g_N = 1$ for acceleration due to gravity in non-dimensional form.

(c) Dispersion relationship :

$$\sigma_N^2 = g_N \cdot k_N \tanh\left(k_N d_N\right) \tag{A.8.3c}$$

(d) Wave velocity :

$$C_N^2 = \frac{g_N \cdot \lambda_N}{2\pi} \tanh\left(\frac{2\pi d_N}{\lambda_N}\right) \tag{A.8.3d}$$

(e) Pressure :

$$p_N = -\rho_N \left\{ g_N y_N + \frac{1}{2}\left(\frac{\partial \phi_N}{\partial n_N}\right)^2 + \frac{\partial \phi_N}{\partial t_N} \right\} \tag{A.8.3e}$$

where $\rho_N = 1$ for fluid density in non-dimensional form.

(f) Normalised forces :

$$F_{x_N} = \int \frac{p_N \cos\theta \cdot r_N \, d\theta}{a_N \cdot \frac{H_N}{2}} \tag{A.8.3f}$$

$$F_{y_N} = \int \frac{p_N \sin\theta \cdot r_N \, d\theta}{a_N \cdot \frac{H_N}{2}} \tag{A.8.3g}$$

where r_N and θ are the polar coordinates of a point on an object.

APPENDIX A.9 SPLINE FITTING OF A CURVE

A spline is a flexible strip which can be held by weights so that it passes through each of the given points, but goes smoothly from each interval to the next according to the laws of beam flexure. A set of cubics fit through a set of data points (x_i , y_i), where $i = 1,2,\ldots, N$, using a new cubic in each interval. It corresponds to the idea of the draftsman's spline using a French curve, having the same slope and curvature for the pair of cubics that join at each point. The equations are then developed subject to these conditions. The following derivation is brief and for computational purpose. More details can be found in Ahlberg, Wilson and Walsh (1967).

Thus on interval (x_i , x_{i+1}) , from the linearity of the second derivative, the following equation is obtained:

$$\frac{\omega_i - \omega}{x_i - x} = \frac{\omega - \omega_{i+1}}{x - x_{i+1}} \tag{A.9.1}$$

where ω represents the second derivative of $y_i = f(x_i)$.

After rearranging:

$$\omega = \frac{x_{i+1} - x}{h_i}\omega_i + \frac{x - x_i}{h_i}\omega_{i+1}$$

or

$$S_i''(x) = \frac{x_{i+1} - x}{h_i}\omega_i + \frac{x - x_i}{h_i}\omega_{i+1} \tag{A.9.2}$$

where $h_i = x_{i+1} - x_i$

Integrating once:

$$S_i'(x) = \frac{-(x_{i+1}-x)^2}{2h_i}\omega_i + \frac{(x-x_i)^2}{2h_i}\omega_{i+1} + a_i \tag{A.9.3}$$

Integrating again:

$$S_i(x) = \frac{(x_{i+1}-x)^3}{6h_i}\omega_i + \frac{(x-x_i)^3}{6h_i}\omega_{i+1} + a_i(x-x_i) + b_i \tag{A.9.4}$$

The functions $S_i''(x), S_i'(x)$ and $S_i(x)$ are continuous on $[x_1, x_N]$.

When $x = x_i$, equation (A.9.4) gives:

$$b_i = y_i - \frac{h_i^2}{6}\omega_i \tag{A.9.5}$$

Substituting equations (A.9.5) into (A.9.4) and with $x = x_{i+1}$:

$$a_i = \frac{y_{i+1}}{h_i} + \frac{h_i}{6}\omega_i - \frac{h_i}{6}\omega_{i+1} - \frac{y_i}{h_i} \tag{A.9.6}$$

Hence equation (A.9.4) can be written in full as:

$$S_i(x) = \frac{(x_{i+1}-x)^3}{6h_i}\omega_i + \frac{(x-x_i)^3}{6h_i}\omega_{i+1} + \left(y_i - \frac{h_i^2}{6}\omega_i\right)\left(\frac{x_{i+1}-x}{h_i}\right)$$
$$+ \left(y_{i+1} - \frac{h_i^2}{6}\omega_{i+1}\right)\left(\frac{x-x_i}{h_i}\right) \tag{A.9.7}$$

and equation (A.9.3) becomes:

$$S_i'(x) = \frac{-(x_{i+1}-x)^2}{2h_i}\omega_i + \frac{(x-x_i)^2}{2h_i}\omega_{i+1} + \frac{(y_{i+1}-y_i)}{h_i}$$
$$- \frac{(\omega_{i+1}-\omega_i)}{6}h_i \tag{A.9.8}$$

By continuity of slope and with $x = x_i$, i.e.

$$S_i'(x_i) = S_{i-1}'(x_i)$$

the following equation is obtained:

$$\omega_{i-1}\frac{h_{i-1}}{6} + \omega_i\left(\frac{h_{i-1}+h_i}{3}\right) + \omega_{i+1}\frac{h_i}{6}$$

$$= \frac{y_{i+1}-y_i}{h_i} - \frac{y_i - y_{i-1}}{h_{i-1}} \qquad \text{for } i = 2, 3, \ldots, N-1 \qquad \text{(A.9.9)}$$

Equation (A.9.9) is used to solve for ω_i, $i = 1,\ldots,N$ and then ω_i are back substituted into equation(A.9.7) to work out ordinate or (A.9.8) to work out slope for a specified x value.

It is noted that the following equations (for ordinate and slope) are used in the subroutines instead of equations (A.9.7) and (A.9.8), for computational efficiency:

$$S_i(x) = y_{i+1}\left(\frac{x-x_i}{h_i}\right) + y_i\left(\frac{x_{i+1}-x}{h_i}\right)$$

$$- \frac{(x_{i+1}-x)(x-x_i)}{6h_i}\left[(x-x_i+h_i)\,\omega_{i+1} + (x_{i+1}-x+h_i)\,\omega_i\right] \qquad \text{(A.9.10)}$$

$$S_i'(x) = \frac{y_{i+1}}{h_i} - \frac{y_i}{h_i} - \left[D_2\ (D_2-2D_1) + (D_2-D_1)h_i\right]\frac{\omega_i}{6h_i}$$

$$- \left[D_1(2D_2-D_1) + (D_2-D_1)\ h_i\right]\frac{\omega_{i+1}}{6h_i} \qquad \text{(A.9.11)}$$

where $D_1 = x - x_i$

$D_2 = x_{i+1} - x$

There are two types of spline applicable in this situation: (1) periodic spline and (2) cubic spline. The basic difference between the two splines is that continuity of slope at every point including the ends are ensured in the periodic spline, whereas the curve fitted by a cubic spline would have continuity at every point except the end points.

In the development of the program 'BEMW1', a periodic spline was used to ensure continuity of slope at the end points of a wave because an infinite number of waves are assumed. Once the program had been developed, the cubic spline was used to solve problems where wave periodicity does not exist.

APPENDIX A.10 SIMPSON'S RULE

To evaluate $\int_a^b f(x)\,dx$, the interval from a to b is subdivided into N sub-intervals, such that the step size:

$$h = \frac{b-a}{N} \qquad \text{(A.10.1)}$$

The integration may then be carried out by Simpson's 1/3 rule (Gerald, 1970):

$$\int_a^b f(x)\,dx = \frac{h}{3}\left[f_1 + 4f_2 + 2f_3 + 4f_4 + \cdots + 2f_{N-1} + 4f_N + f_{N+1}\right] \qquad \text{(A.10.2)}$$

$$a < x < b$$

with a global error of $O(h^4)$.

A condition for equation (A.10.2) to be appliable is that N must be even.

In program 'BEMW1', the calculation of total outflow through wave surface requires the evaluation of s, distanee between adjacent nodal points on the surface. Since $\frac{ds}{dp}$ is obtained from using spline subroutine, the following equation derived from simpson's rule makes use of the first order derivative to yield s :

$$s_{N_2,N_3} = \int_{N_2}^{N_3} f'(p)\,dp = \frac{1}{24}\left\{13\left(f'_{N2} + f'_{N3}\right) - \left(f'_{N1} + f'_{N4}\right)\right\} \qquad \text{(A.10.3)}$$

where

$f'_{Nj} = \frac{ds}{dp}$ at node N_j .

$s_{N_2,N_3} =$ distance between node N_2, and node N_3 .

The error term for equation (A.10.3) is 11/720.

Appendix A.11 Description of program 'BEMLVB1'

Program 'BEMLVB1' is the basis of development for all other programs and was initially written in the author's undergraduate project. The version 'BEMLVB1' presented in this thesis is a modified undergraduate project's version to include evaluations of potential derivative and its direction at internal points. The efficiency in computational technique has also been improved since the research was initiated.

Apart from program 'BEMW1', all other programs have a common or similar flow diagram since they were obtained with minor modifications to program 'BEMLVB1'. It is therefore sufficient to present, as an example, a simplified flow chart with algorithm for program 'BEMLVB1' to illustrate the logical steps undertaken. The flow chart and algorithm for program 'BEMW1' has been shown and discussed in chapter 6, due to the complexity of formulations involved in programming. Listing of computer programs is shown in Appendix A.12.

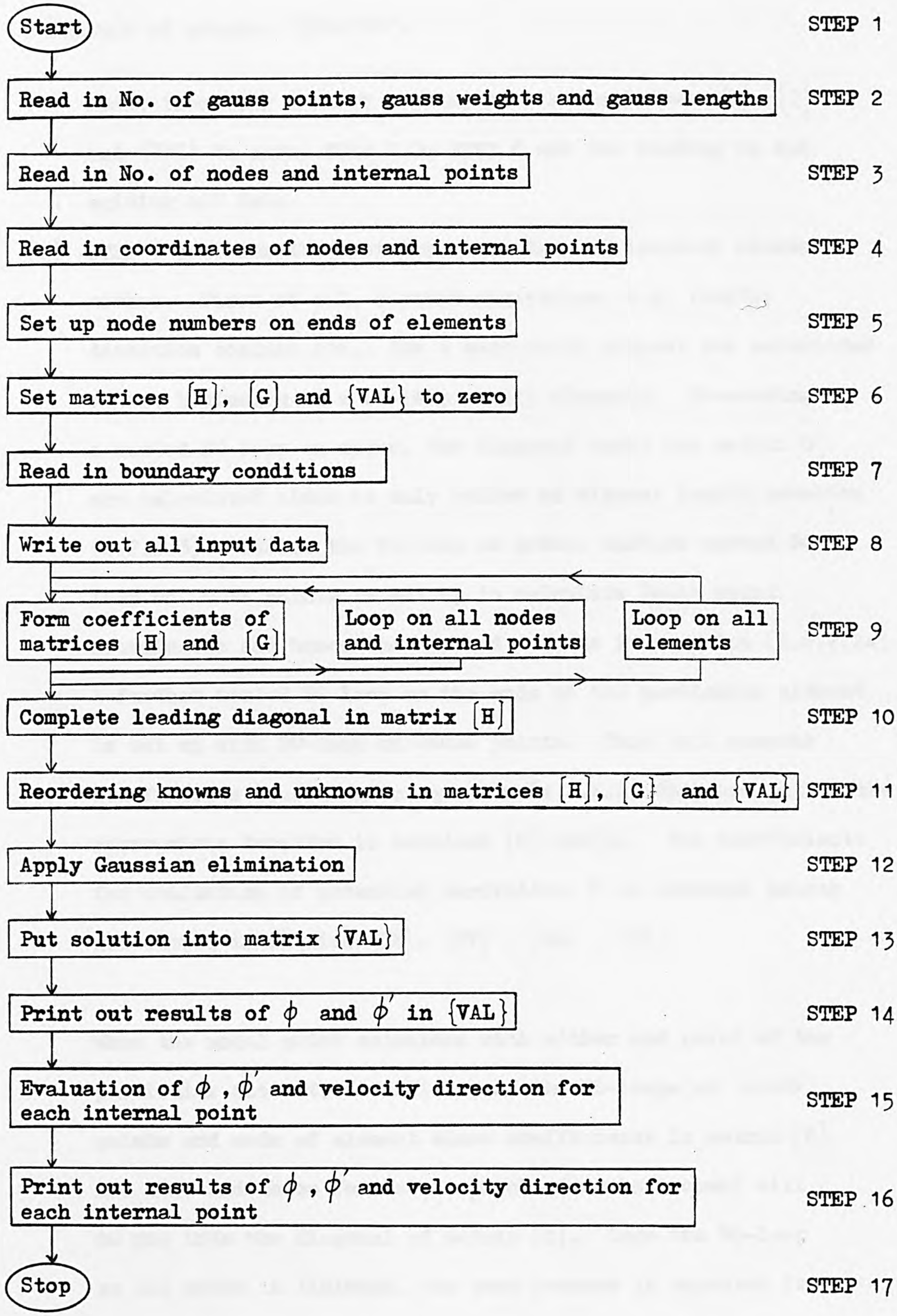

Fig. A.11.1 Flow Chart for 'BEMLVB1'

Structure of program 'BEMLVB1'.

(1) Apart from STEP 6 which is simply to set matrices [H], [G] and {VAL} to zero, STEP 1 to STEP 8 are for reading in and writing out data.

(2) STEP 9 performs the most important task of boundary element method. First of all, element geometries, e.g. length, direction cosines, etc., for a particular element are calculated at the beginning of a DO-loop on all elements. Preceeding a nested DO-loop on nodes, the diagonal terms for matrix [G] are calculated since it only relies on element length, equation (4.2.2.3). Inside the DO-loop on nodes, another nested DO-loop on Gauss points is set up to calculate Gauss point coordinates and hence the y_p and Y terms in equation (4.2.2.2a). A further nested DO-loop on the ends of the particular element is set up with DO-loop on Gauss points. This will compute coefficients according to equations (4.2.2.2). They are put in the appropriate location in matrices [H] and [G]. The coefficients for evaluation of potential derivative ϕ' at internal points are stored in matrices {PX}, {PY}, {QX}, {QY}.

When the nodal point coincides with either end point of the particular element, it will bypass the DO-loops on Gauss points and ends of element since coefficients in matrix [H] are zero and those for matrix [G] obtained beforehand will be put into the diagonal of matrix [G]. Once the DO-loop on all nodes is finished, the same process is repeated for the next element, and so on until all the coefficients are calculated and added to the appropriate locations in matrices [H] and [G].

(3) Having set up matrices $[H]$ and $[G]$, the diagonal terms in matrix $[H]$ are still unknown. As discussed in section 4.2.2 for linear variation, STEP 10 completes the diagonal terms through equation (4.2.11).

(4) STEP 11 is to perform the reordering from equations(4.2.9) to (4.2.12).

(5) Having obtained $[A]\{x\} = \{F\}$, a standard solution routine for Gaussian elimination is carried out in STEP 12.

(6) STEP 13 re-arranges solutions and put into correct columns in matrix $\{VAL\}$.

(7) Solutions, including known values, for ϕ and ϕ' are printed out in STEP 14.

(8) Expressions for ϕ, $\frac{\partial \phi}{\partial x}$ and $\frac{\partial \phi}{\partial y}$ at internal points (i.e equations 4.2.13 and 4.2.14) are evaluated in STEP 15.

(9) Results of STEP 15 are printed in STEP 16.

APPENDIX A.12 LISTING OF BOUNDARY ELEMENT PROGRAMS

Based on the numerical formulations outlined in chapters 4 and 6, computer programs were written for the solution of two dimensional potential problems using constant or linear variation along elements. The programs to be listed in this thesis are:

(1) BEMLVB1 --- Boundary element program for potential problems with linear variation along elements.

(2) BEMCVB1 --- Boundary element program for potential problems with constant variation along elements.

(3) BEMA3Z --- Boundary element program for anisotropic problems whose domain may be divided up to 3 zones, linear variation along elements.

(4) BEMFS1 --- Boundary element program for free surface flow potential problems with linear variation along elements.

(5) BEMTDLV1 -- Boundary element program for time dependent problems with triangular discretisation on domain and linear variation along elements.

(6) BEMW1 --- Boundary element program for unsteady wave problems, with linear variation along elements.

The following variable names and arrays have been used in the programs. Wherever possible variable names are chosen to coincide with the symbols employed in the text of the thesis but the use of mnemonics is frequently necessary.

AK	A constant for K
AMP	Wave amplitude
AN(J)	Shape functions for constant, linear or quadratic variation on element
ANGLE	Acute angle in direction of orthotrophy with respect to x-axis in degree
APHI	ϕ matrix for graph plotting
ARCL(I)	Arc length at node I on cylinder from a reference point
AREA	Area of triangular element
AX(I)	x coordinate at node I on free surface for moving purpose
AY(I)	y coordinate at node I on free surface for moving purpose
BK	Wave number $(=2\pi/\lambda)$
CON( )	Matrix for the evaluation of exponential integral series
CON1( )	Matrix for the evaluation of exponential integral series
CON2( )	Matrix for the evaluation of exponential integral series
CX(I)	x coordinate at node I on cylinder; x coordinate at element node of element I for constant variation
CY(I)	y coordinate at node I on cylinder; y coordinate at element node of element I for constant variation
D( )	Array for domain integral in time dependent problem
DCC1(I)	Direction cosine with x axis for node I on cylinder
DCC2(I)	Direction cosine with y axis for node I on cylinder
DCI( )	Array for domain integral in time dependent problems
DELTI	Time step, δt, based on Courant condition
DELTIX	Minimum time step
DELTMX	Maximum time step
DPDNC(L,I)	$\partial\phi/\partial n$ at point I on cylinder
DPDP(I)	Rate of change of ϕ at node I with respect to node number p

DPDS(I)	Rate of change of ϕ with respect to s at node I
DPDT(L,I)	Rate of change of ϕ with respect to time at node I
DPHIC	Change in ϕ at a node on wave surface in A.B.M. corrector formula
DPHIDS	Rate of change of ϕ with respect to s
DPHIP	Change in ϕ at a node on wave surface in A.B.M. predictor formula
DS	Distance between adjacent nodes on surface profile
DS( )	Dummy array
DSDP(I)	Rate of change of length at node I along wave surface with respect to node number
DSMAX	Maximum distance between adjacent nodes on wave surface
DSMIN	Minimum distance between adjacent nodes on wave surface
DT	Time step δt
DXC	Change in x at a node on wave surface in A.B.M. corrector formula
DXDP(I)	Rate of change of x at node I with respect to node number p
DXDS(I)	Rate of change of x with respect to s at node I
DXDT(L,I)	Rate of change of x with respect to time at node I
DXP	Change in x at a node on wave surface in A.B.M. predictor formula
DYC	Change in y at a node on wave surface in A.B.M. corrector formula
DYDP(I)	Rate of change of y at node I with respect to node number p
DYDS(I)	Rate of change of y with respect to s at node I
DYDT(L,I)	Rate of change of y with respect to time at node I
DYP	Change in y at a node on wave surface in A.B.M. predictor formula

EIA	Exponential-integral function
EKIN(L)	Array for plotting kinetic energy of wave profile
EL	Linear length of element
EPOT(L)	Array for plotting potential energy of wave profile
ETOT(L)	Array for plotting total energy of wave profile (EPOT + EKIN)
EULER	Euler's constant
F(NN)	Dummy array for Gaussian elimination
FACT(N)	Factorial N
FXNL(L)	Array for plotting nonlinear force on cylinder in x direction
FYNL(L)	Array for plotting nonlinear force on cylinder in y direction
G(L,NN,NN)	Overall matrix for zone L in zoned domain problems
G(NN,NN)	Overall matrix $[G]$
GL(K)	Gauss length at Gauss point K
GLT(K)	Gauss length at Gauss point K for triangular element
GPC1	Gauss point coordinate in x direction
GPC1T	Gauss point coordinate in x direction on triangular element
GPC2	Gauss point coordinate in y direction
GPC2T	Gauss point coordinate in y direction on triangular element
GRA	Acceleration due to gravity (=1 in non-dimensional form)
GSUM(,)	Overall matrix before Gaussian elimination in zoned domain problems
GW(K)	Gauss weight at Gauss point K
GWT(K)	Gauss weight at Gauss point K for triangular element
H(L,NN,NN)	Overall matrix for zone L in zoned domain problems
H(NN,NN)	Overall matrix $[H]$

HK	A constant for determining time step δt
HSUM(,)	Overall matrix before Gaussian elimination in zoned domain problems
HX(I)	Matrix for spline fit and Simpson's rule
IRPC	Indicator for numerical stepping technique
ISMOTH	Number of loops for the smoothing technique to be carried out
ISTOP	A flag to stop execution if numerical instability occurs
LOOPS	Number of loops to be executed
M1	Number of nodes on bottom boundary
M2	Number of nodes on right vertical side boundary
M3	Number of nodes on free surface or top boundary
M4	Number of nodes on left vertical side boundary
NCT	Loop counter for each fresh δt or surface redistribution
NDTBE	Number of sides on external boundary
NDUM	Dummy arguement
NE	Total number of elements
NEN(I,J)	Node number on ends of element I
NENT(I,J)	Node numbers on triangular element I
NFIG	Figure number for graph plotting
NFLG(I)	Type of boundary condition at each node I
NGP	Number of Gauss points used
NGPT	Number of Gauss points for triangular element
NI	Number of internal points
NITER	Number of iteration
NN	Total number of nodes
NNE	Number of nodes on external boundary
NNI	Number of nodes on internal boundary
NORDER	Order of equation for wave profile and ϕ

NTCF	Choice of numerical interpolation
NTE	No. of triangular element in a domain
NTERM	Number of terms for infinite series
NTP	Number of points to be borrowed for Lagrangian polynomial
NTW	Wave type
NVARY	Parameter to specify type of variation on element boundary
NX( )	Number of nodes on each external boundary
P(I)	Node number on free surface
PAMPD	Pressure amplitude
PERD	Wave period T
PEPSLN	Phase shift in progressive wave
PHI(I)	ϕ value at node I on free surface for moving purpose
PHIB(I)	ϕ values before moving wave surface at node I
PHIC1(L,N)	ϕ matrix for the evaluation of $\frac{\partial \phi}{\partial n}$
PI	π
P1NL(L)	Array for plotting nonlinear pressure at point 1 on cylinder
P2NL(L)	Array for plotting nonlinear pressure at point 2 on cylinder
P3NL(L)	Array for plotting nonlinear pressure at point 3 on cylinder
P4NL(L)	Array for plotting nonlinear pressure at point 4 on cylinder
PRES1(I)	Computed nonlinear pressure at node I on cylinder
PRES2(I)	Computed linear pressure at node I on cylinder
PX(I,J)	Matrix coefficients for the evaluation of $\frac{\partial \phi}{\partial x}$
PY(I,J)	Matrix coefficients for the evaluation of $\frac{\partial \phi}{\partial y}$
QM8(L)	Array for plotting potential derivative at a node on wave surface
QSUR(L)	Array for plotting total outflow through surface
QX(I,J)	Matrix coefficients for the evaluation of $\frac{\partial \phi}{\partial x}$
QY(I,J)	Matrix coefficients for the evaluation of $\frac{\partial \phi}{\partial y}$
R	Length between gauss point and nodal point
RADIUD	Radius of horizontal cylinder

RO	Density of water (= 1 in non-dimensional form)
RPHI(I)	Calculated ϕ value at internal point I
S(I)	Length of nodal point I along wave surface
SCM1	x coordinate at mid-point of element
SCM2	y coordinate at mid-point of element
SEPSLN	Phase shift in standing wave
SFACT	Specified constant for the redistribution of nodes on surface
SGDIA	Coefficient of diagonal matrix in $[G]$
SGOFF	Coefficient of off diagonal matrix in $[G]$
ST( )	Dummy matrix
SYKDXK	Effective permeability
T	Parameter for cumulation of time
TAXIS(L)	Time matrix for graphical output
TGL	True Gauss length
THEN(I)	Direction of velocity at internal point I
THET(I)	Direction of potential derivative at an internal point I
TIME	Starting time of wave profile
TMULT	Multiplication factor for time
TPERD	Non-dimensional cumulative time (T/PERD)
TT(L)	Time matrix for the evaluation of $\frac{\partial \phi}{\partial t}$
UI(I)	Initial ϕ values at node I
UTR1	ϕ value at Gauss point of triangular element
VAL(I,1)	Array for potential ϕ at node I
VAL(I,2)	Array for potential derivative $\frac{\partial \phi}{\partial n}$ at node I
VAL(I,3)	Array for unspecified boundary value at node I
VAL(I,4)	Array for unspecified boundary value at node I
VAL(L,I,1)	Array for potential ϕ at node I in zone L
VAL(L,I,2)	Array for potential derivative $\frac{\partial \phi}{\partial n}$ at node I in zone L

VAL(L,I,3)	Array for unspecified boundary value at node I in zone L
VAL(L,I,4)	Array for unspecified boundary value at node I in zone L
VALS( )	Dummy array for Gaussian elimination
WAVEC	Phase velocity or wave velocity
WAVEHD	Wave height
WX(I)	Matrix for spline fit and Simpson's rule
X(I)	x coordinate at node I
X1(L,I)	x coordinate at node I in zone L before transformation in anisotropic problems
X2(L,I)	x coordinate at node I in zone L after transformation in anisotropic problems
XB(I)	x coordinate before moving wave surface at node I
XCENTD	x coordinate at centre of horizontal cylinder
XF	x coordinate at starting point on each part of external boundary
XK	Permeability , k_x, in direction of orthotrophy
XL	x coordinate at end point on each part of external boundary
XLAMDD	Wavelength λ
XMAXD	Number of wavelength in flow domain in x direction
XYK	Coefficient of permeability (= 1 if not applicable)
Y(I)	y coordinate at node I
Y1(L,I)	y coordinate at node I in zone L before transformation in anisotropic problems
Y2(L,I)	y coordinate at node I in zone L after transformation in anisotropic problems
YB(I)	y coordinate before moving wave surface at node I
YBAR(L)	Array for plotting mean water level
YCENTD	y coordinate at centre of horizontal cylinder
YDEPD	Water depth
YF	y coordinate at starting point on each part of external boundary
YK	Permeability , k_y, in direction of orthotrophy
YL	y coordinate at end point on part of external boundary
YP	Perpendicular distance from node to tangent of element

Computer programs (pp. 294-340)
have been removed
for copyright reasons

(1) BEMLVB1

(2) BEMCVB1

(3) BEMA3Z

(4) BEMFS1

(5) BEMTDLV1

(6) BEMW1

APPENDIX A.13 GRAPHICAL OUTPUT OF CASE STUDIES IN SECTION 6.5

This appendix shows the time sequence of wave profiles and auxiliary graphs for the case studies in section 6.5. To present all the wave profiles in the Appendix would be bulky and unnecessary. Therefore, the wave profiles for frequency, f_0 = 1.172 Hz are chosen to give a good representation of the behaviour of wave profiles by the boundary element method. The auxiliary graphs for forces and pressures are shown for a majority of case numbers.

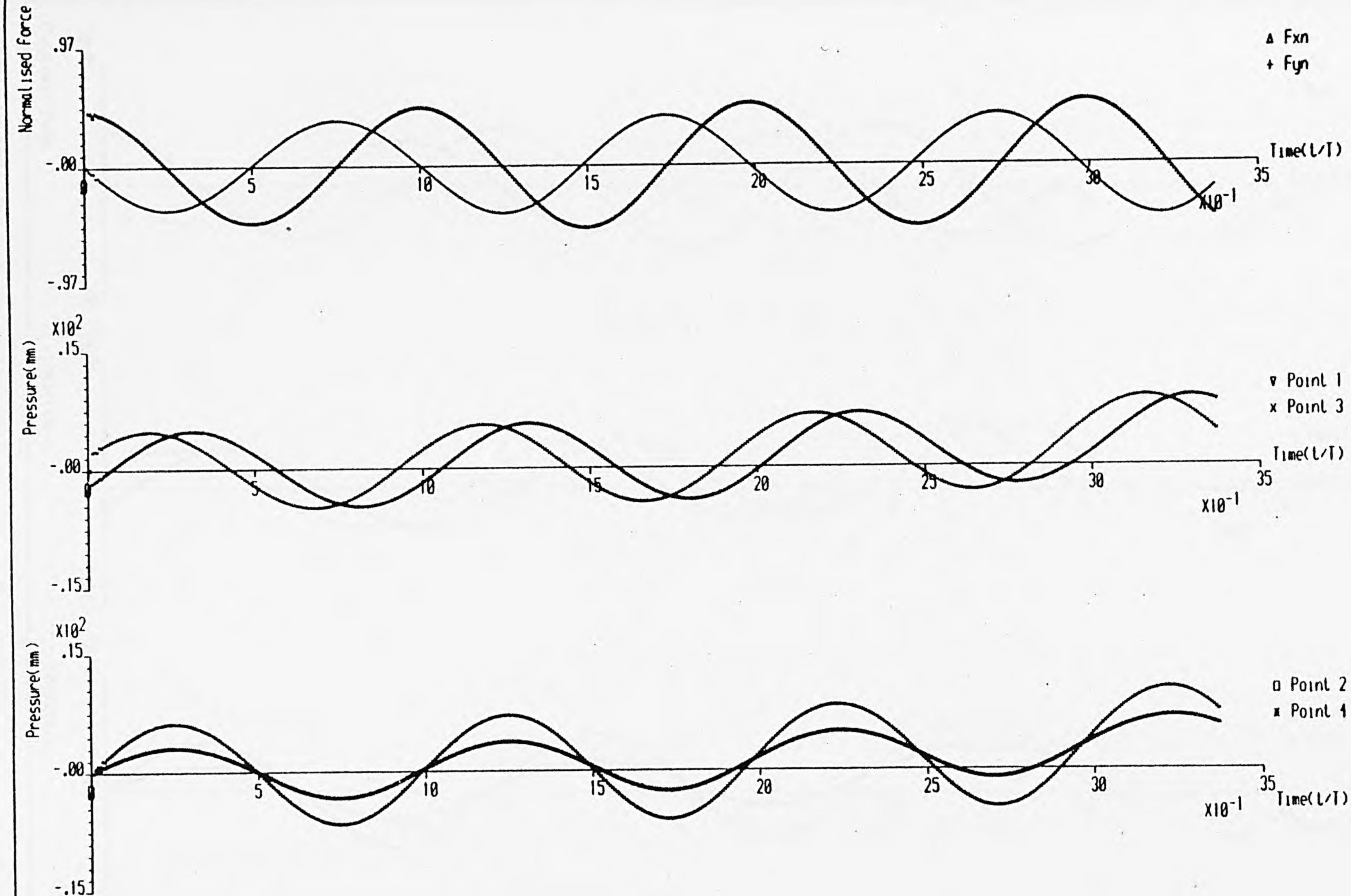

Wave height = .028m.
Wavelength = 1.595m.
Undisturbed W.L.= .555m.
Order of eq. = 1

Centre X = .797m.
Centre Y = -.294m.
Radius = .055m.

Fig. A.13. 1 Auxiliary graphs for case No. 1

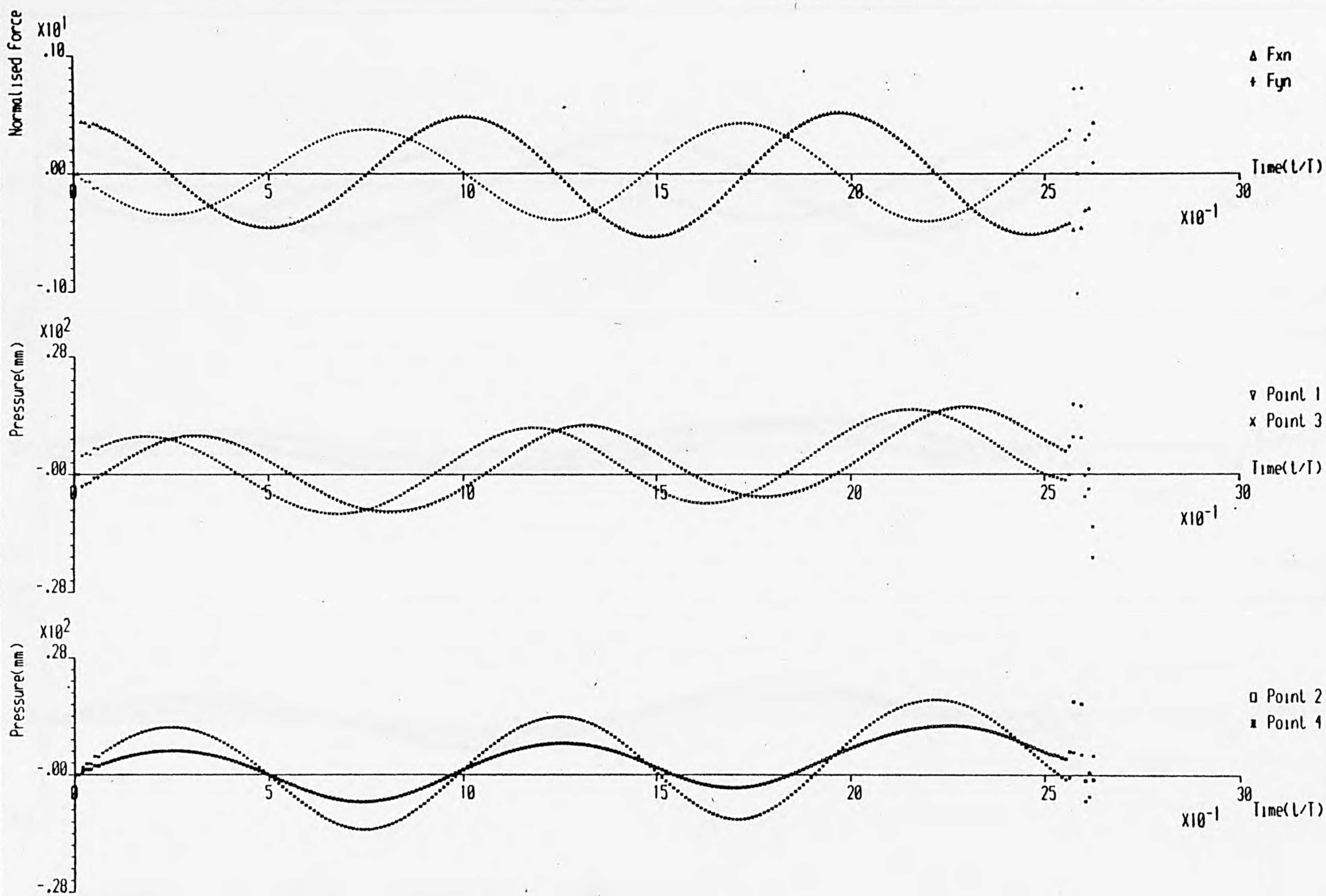

Wave height = .052m.
Wavelength = 1.595m.
Undisturbed W.L.= .555m.
Order of eq. = 1

Centre X = .797m.
Centre Y = -.294m.
Radius = .055m.

Fig. A.13. 2 Auxiliary graphs for case No. 2

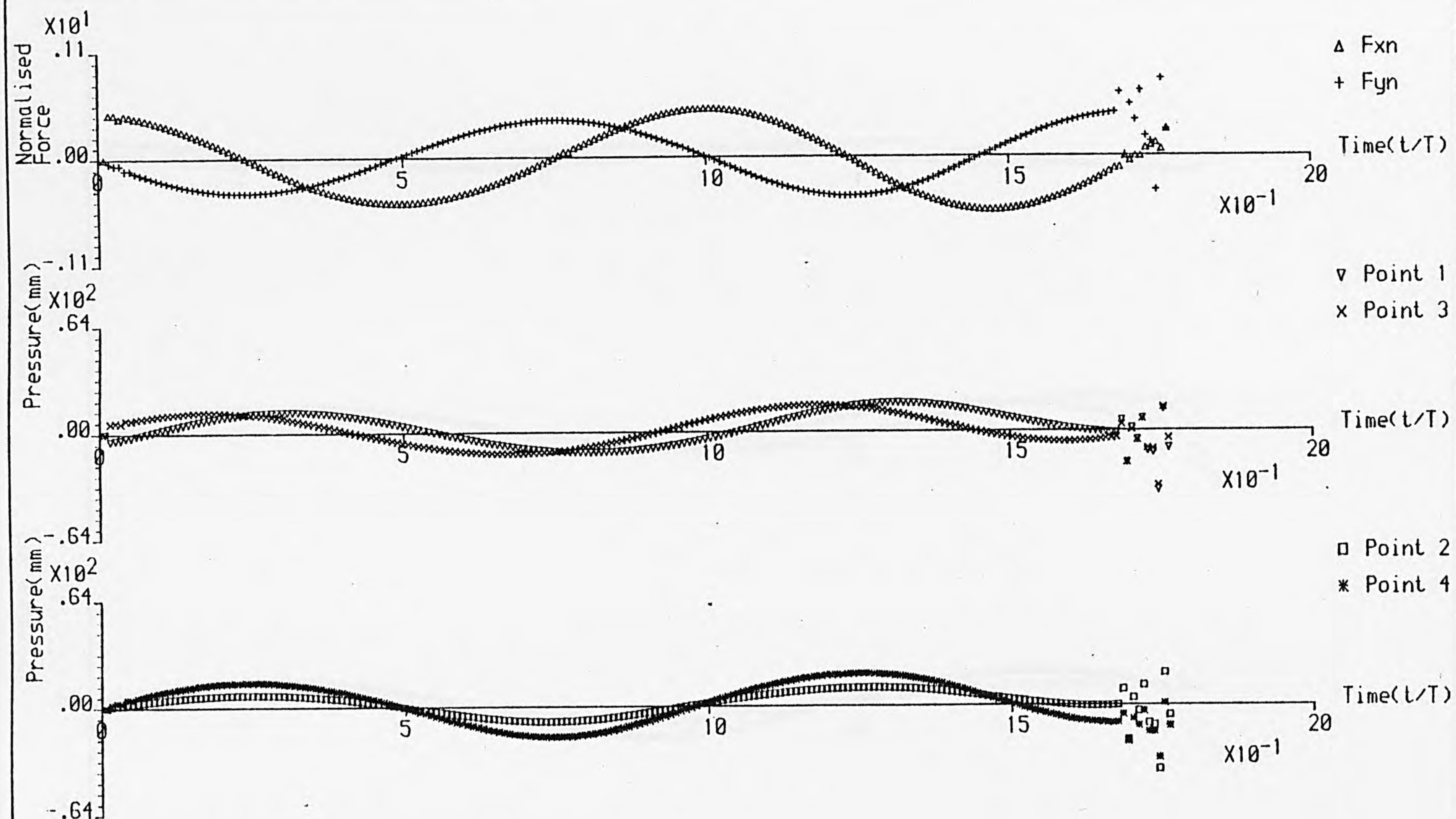

Wave height	= .072m.	Centre X	=	.798m.
Wavelength	= 1.595m.	Centre Y	=	-.294m.
Undisturbed W.L.	= .555m.	Radius	=	.055m.
Order of eq.	= 1			

Fig. A.13. 3 Auxiliary graphs for case No. 3

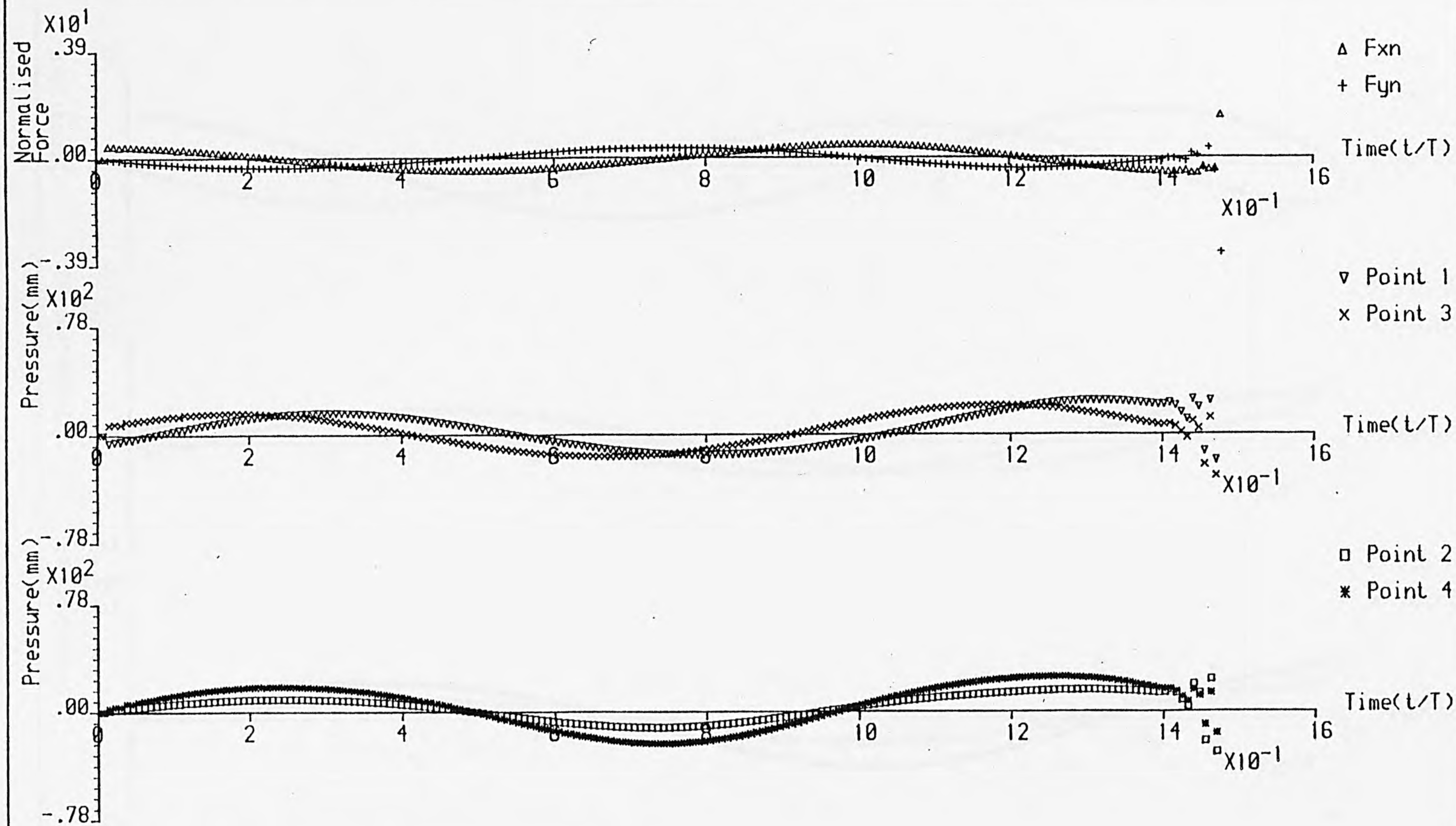

Wave height = .091m. Centre X = .798m.
Wavelength = 1.595m. Centre Y = -.294m.
Undisturbed W.L.= .555m. Radius = .055m.
Order of eq. = 1

Fig. A.13. 4 Auxiliary graphs for case No. 4

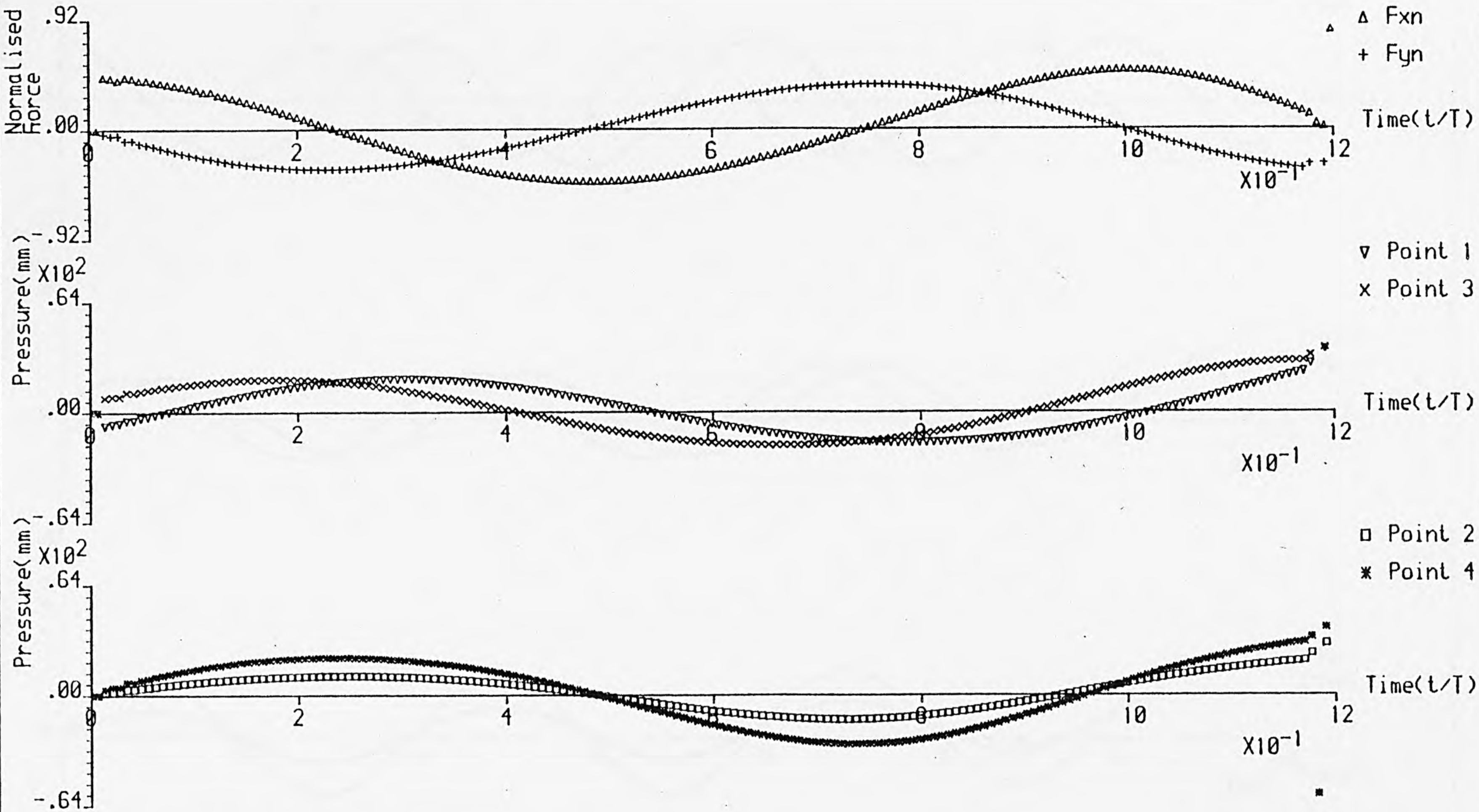

Wave height	= .112m.	Centre X	=	.798m.
Wavelength	= 1.595m.	Centre Y	=	-.294m.
Undisturbed W.L.	= .555m.	Radius	=	.055m.
Order of eq.	= 1			

Fig. A.13. 5 Auxiliary graphs for case No. 5

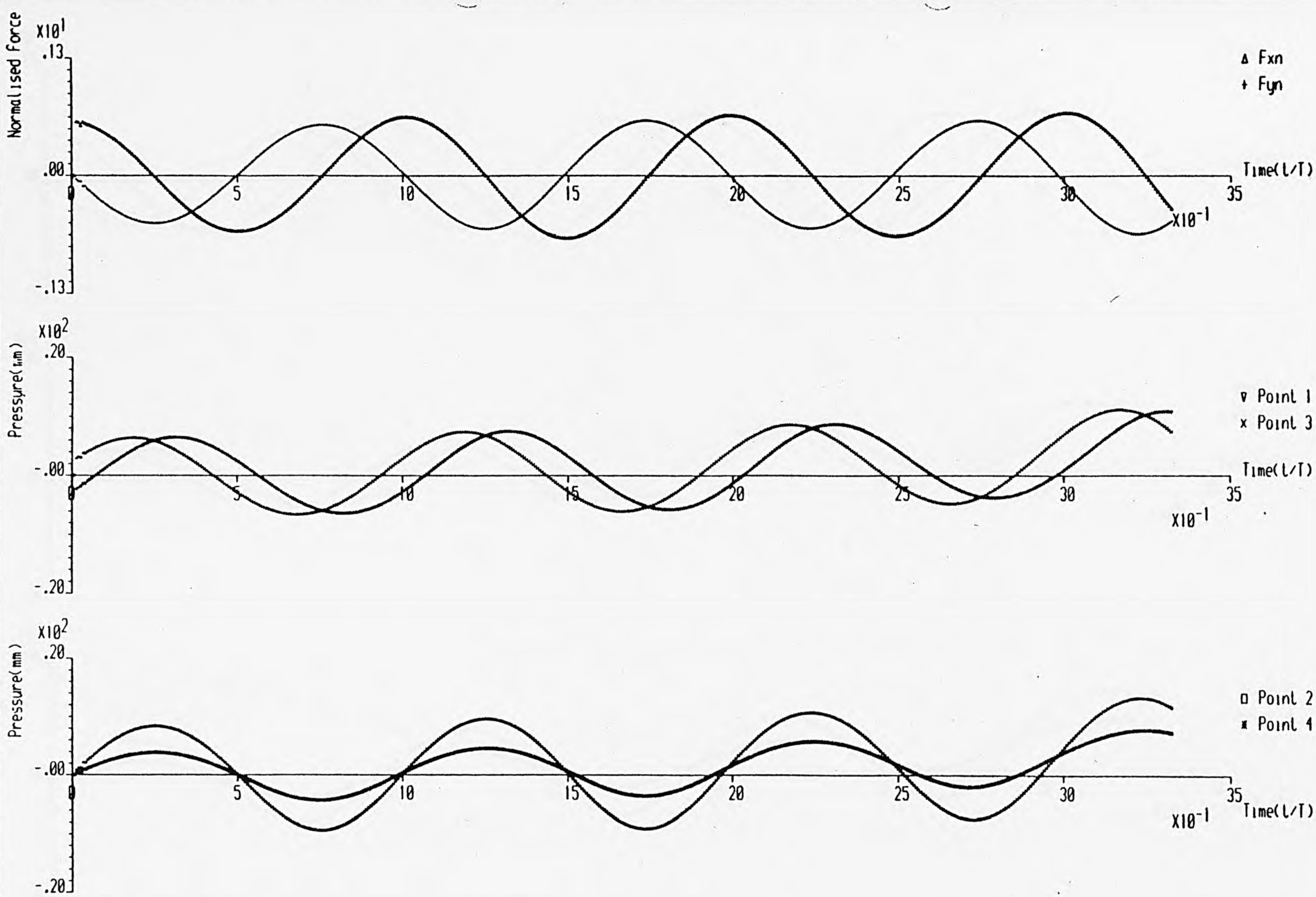

Wave height = .029m.
Wavelength = 1.595m.
Undisturbed W.L.= .555m.
Order of eq. = 1

Centre X = .797m.
Centre Y = -.214m.
Radius = .055m.

Fig. A.13. 6 Auxiliary graphs for case No. 6

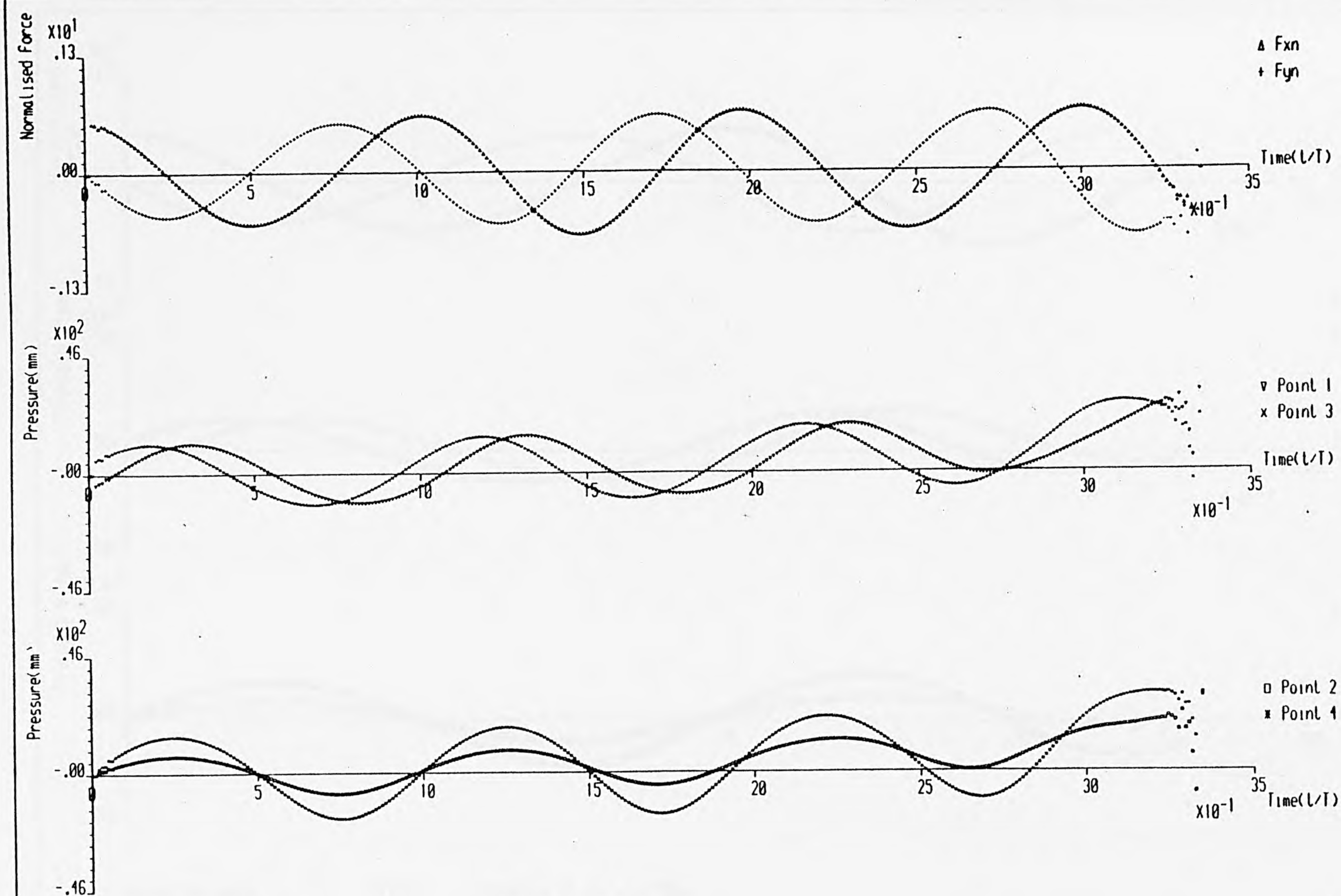

Wave height = .051m.
Wavelength = 1.595m.
Undisturbed W.L.= .555m.
Order of eq. = 1

Centre X = .797m.
Centre Y = -.214m.
Radius = .055m.

Fig. A.13. 7 Auxiliary graphs for case No. 7

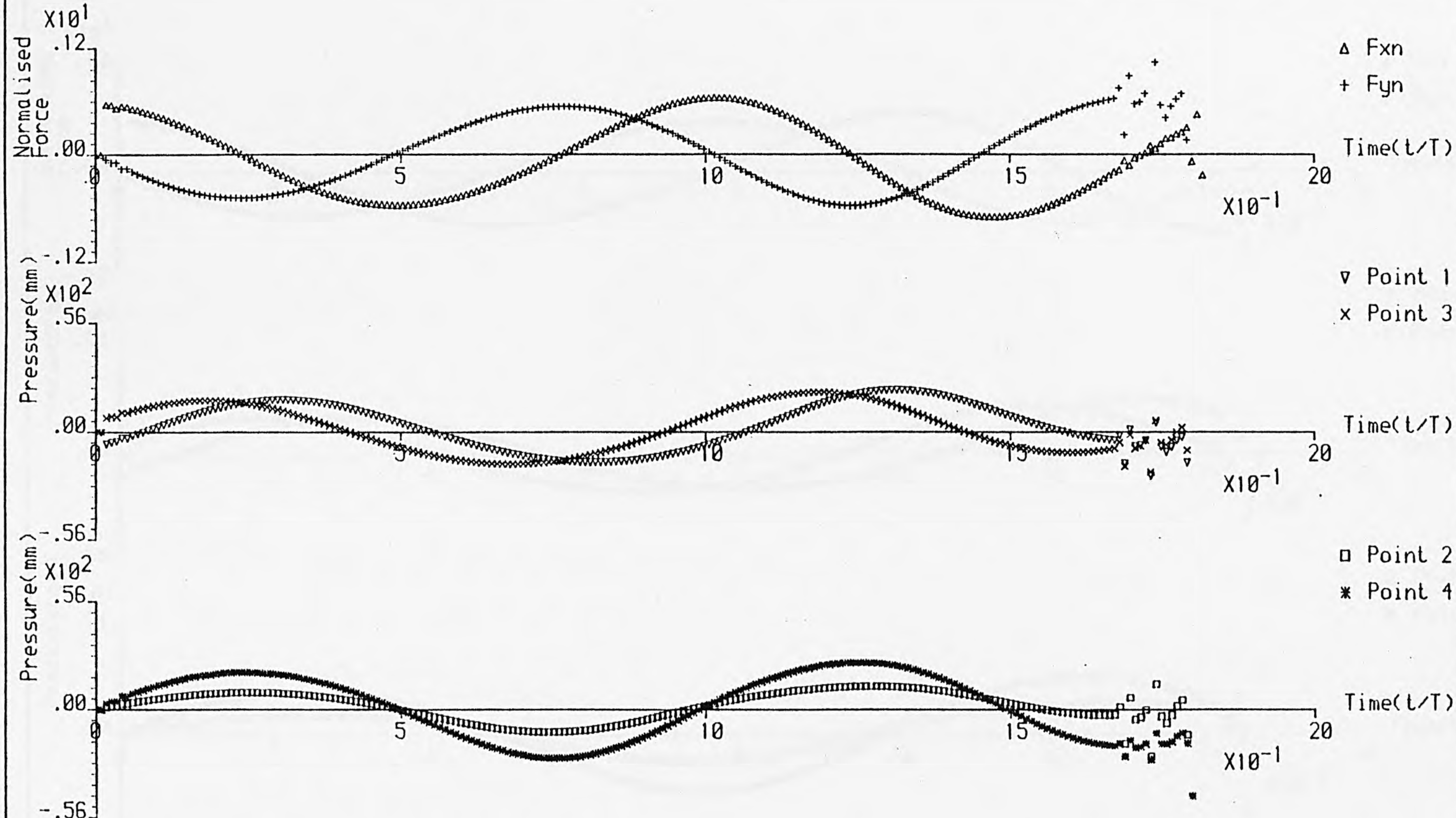

Wave height	=	.073m.	Centre X	=	.798m.
Wavelength	=	1.595m.	Centre Y	=	-.215m.
Undisturbed W.L.	=	.555m.	Radius	=	.055m.
Order of eq.	=	1			

Fig. A.13. 8 Auxiliary graphs for case No. 8

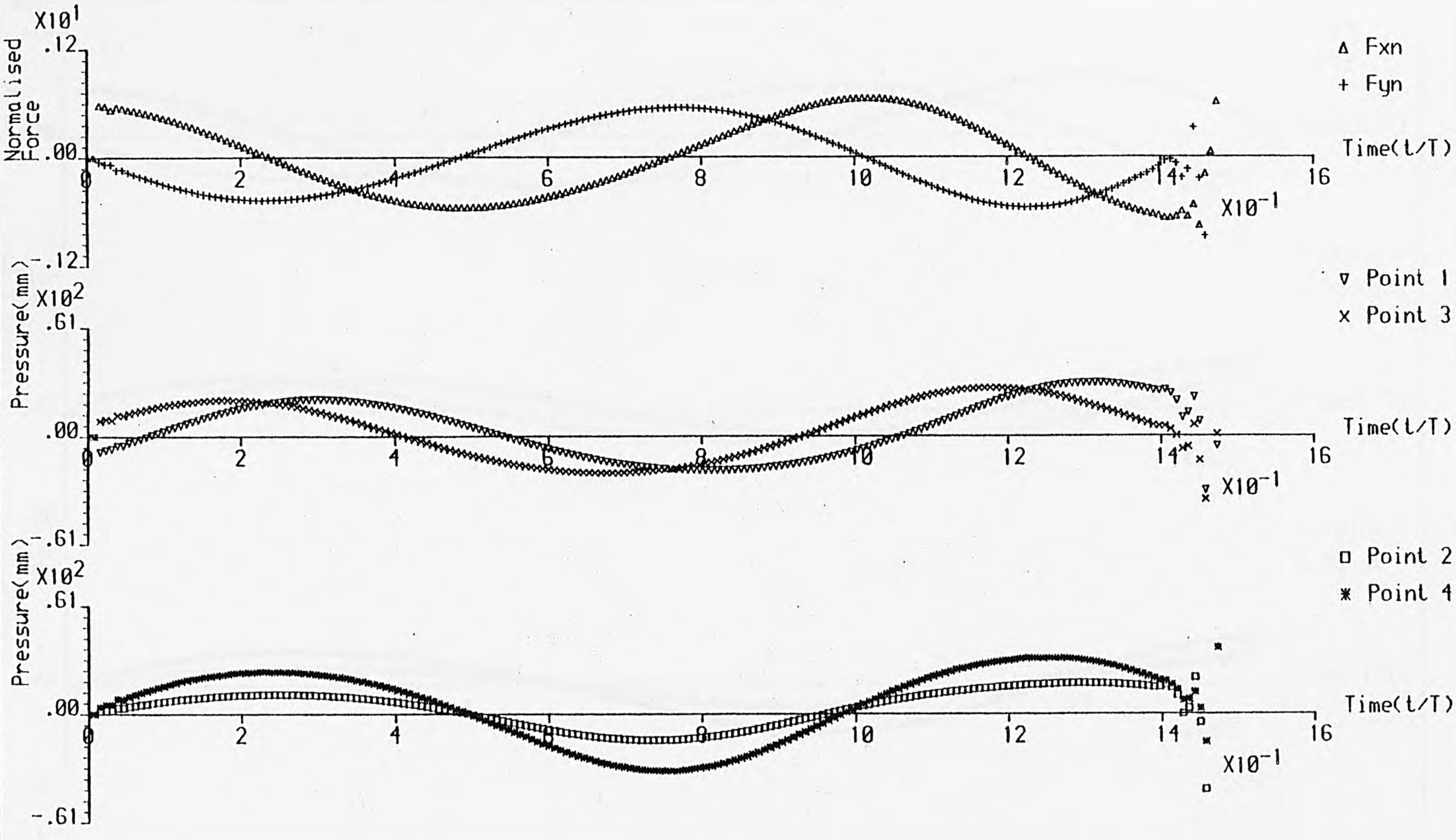

Wave height = .092m. Centre X = .798m.
Wavelength = 1.595m. Centre Y = -.215m.
Undisturbed W.L.= .555m. Radius = .055m.
Order of eq. = 1

Fig. A.13.9 Auxiliary graphs for case No. 9

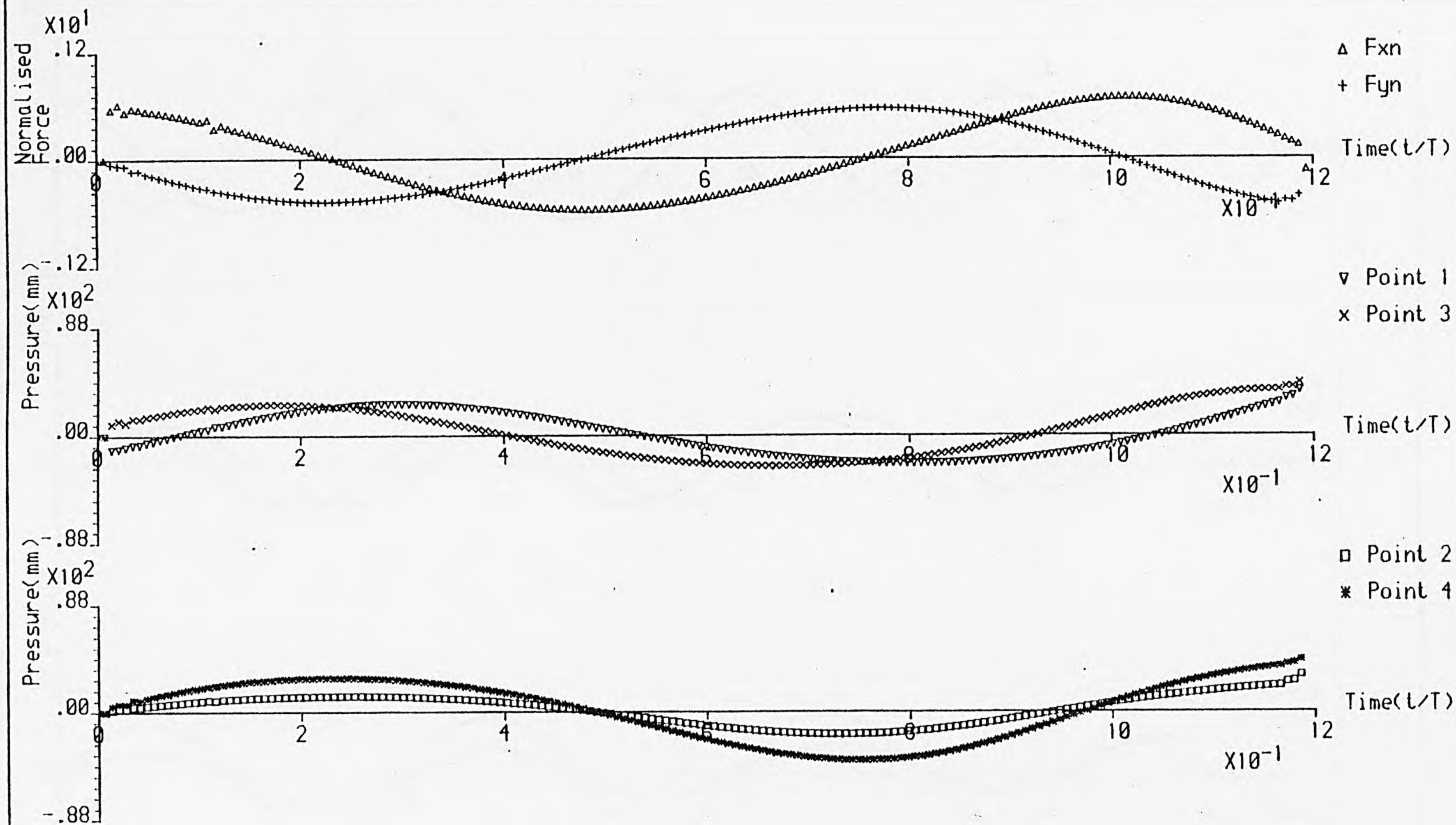

Wave height = .114m. Centre X = .798m.
Wavelength = 1.595m. Centre Y = -.215m.
Undisturbed W.L.= .555m. Radius = .055m.
Order of eq. = 1

Fig. A.13. 10 Auxiliary graphs for case No. 10

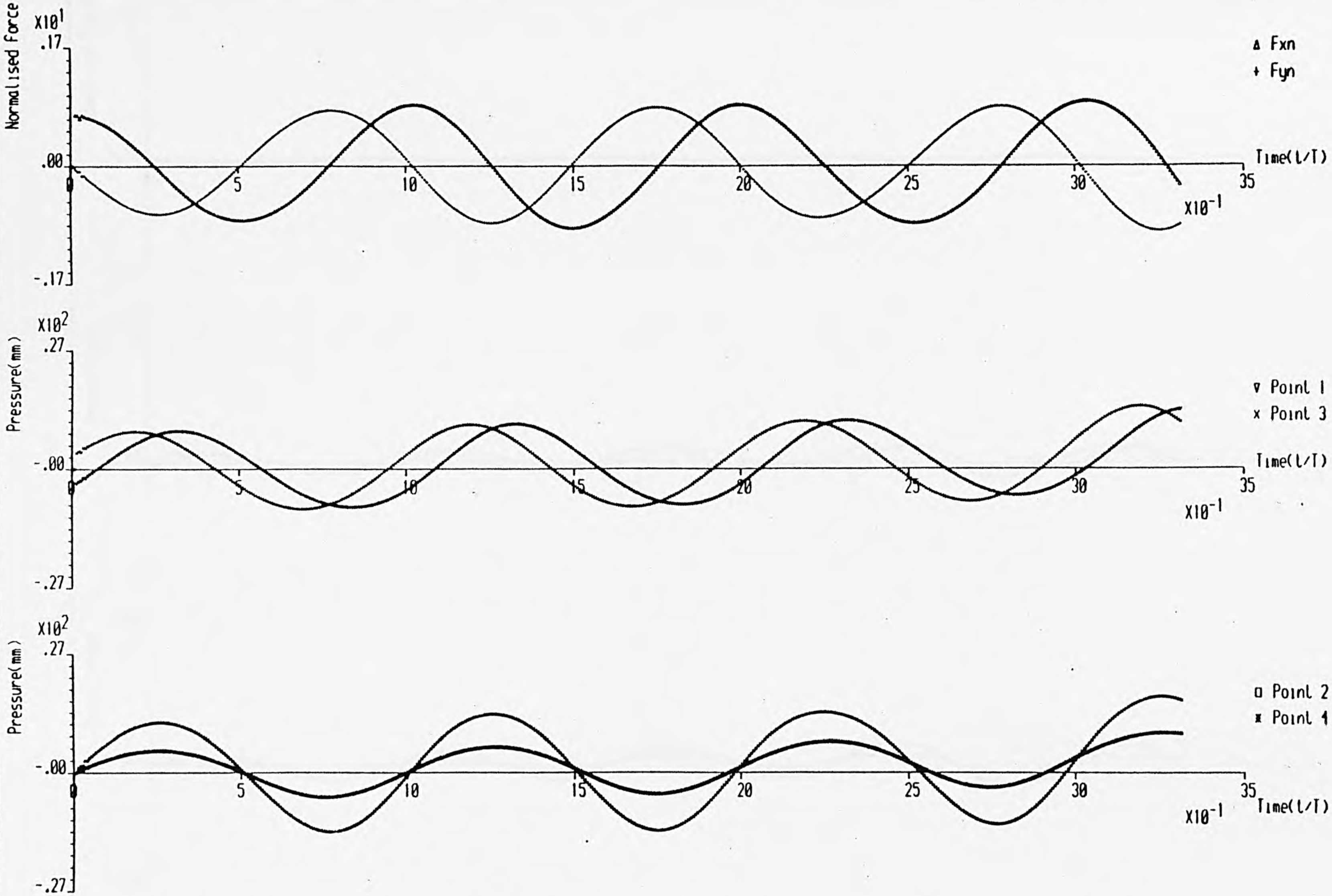

Wave height = .029m.
Wavelength = 1.595m.
Undisturbed W.L.= .555m.
Order of eq. = 1

Centre X = .797m.
Centre Y = -.135m.
Radius = .055m.

Fig. A.13. 11 Auxiliary graphs for case No. 11

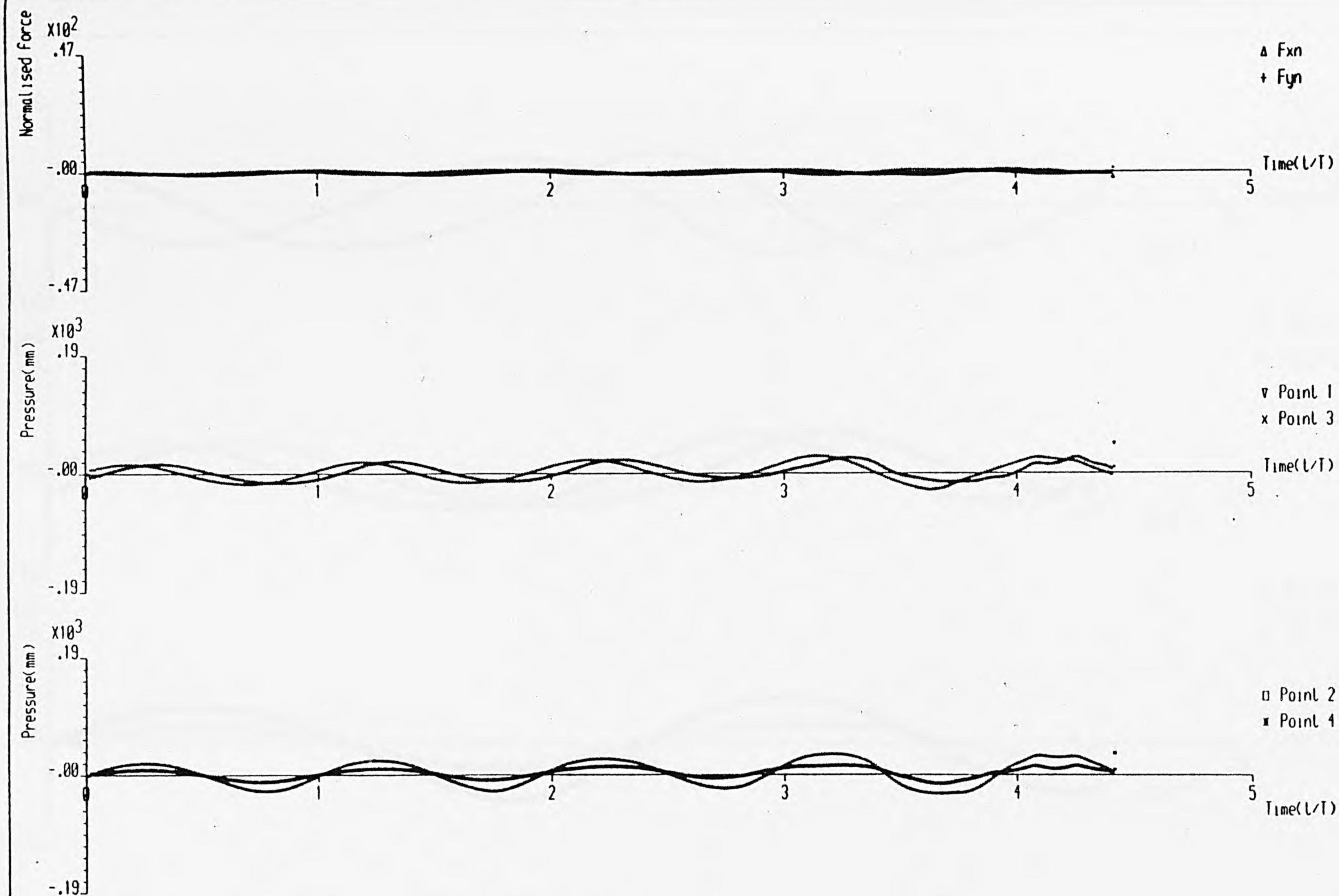

Wave height = .051m.
Wavelength = 1.595m.
Undisturbed W.L.= .555m.
Order of eq. = 1

Centre X = .797m.
Centre Y = -.135m.
Radius = .055m.

Fig. A.13. 12 Auxiliary graphs for case No. 12

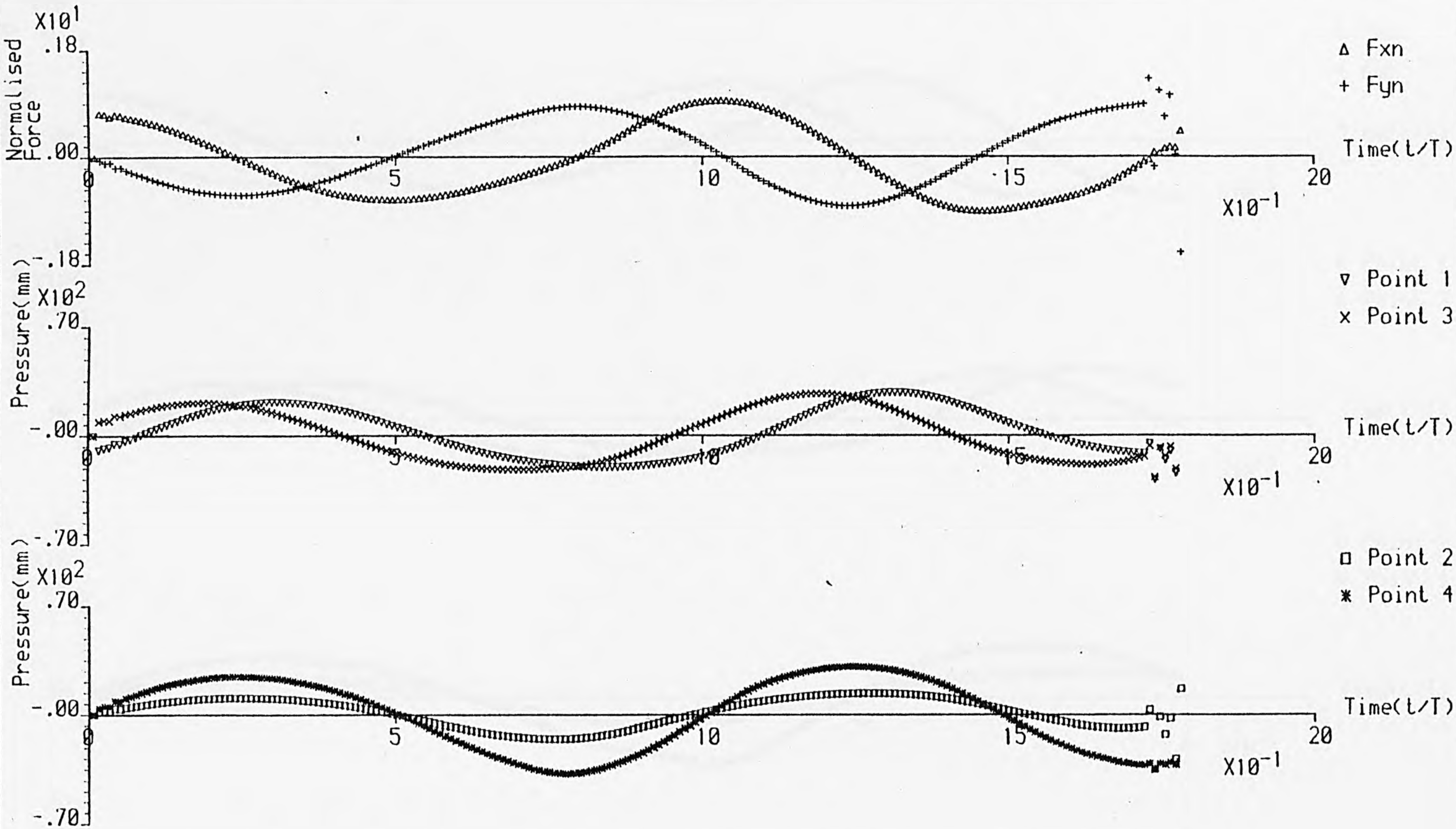

Wave height =	.073m.	Centre X =	.798m.
Wavelength =	1.595m.	Centre Y =	-.135m.
Undisturbed W.L.=	.555m.	Radius =	.055m.
Order of eq. =	1		

Fig. A.13. 13 Auxiliary graphs for case No. 13

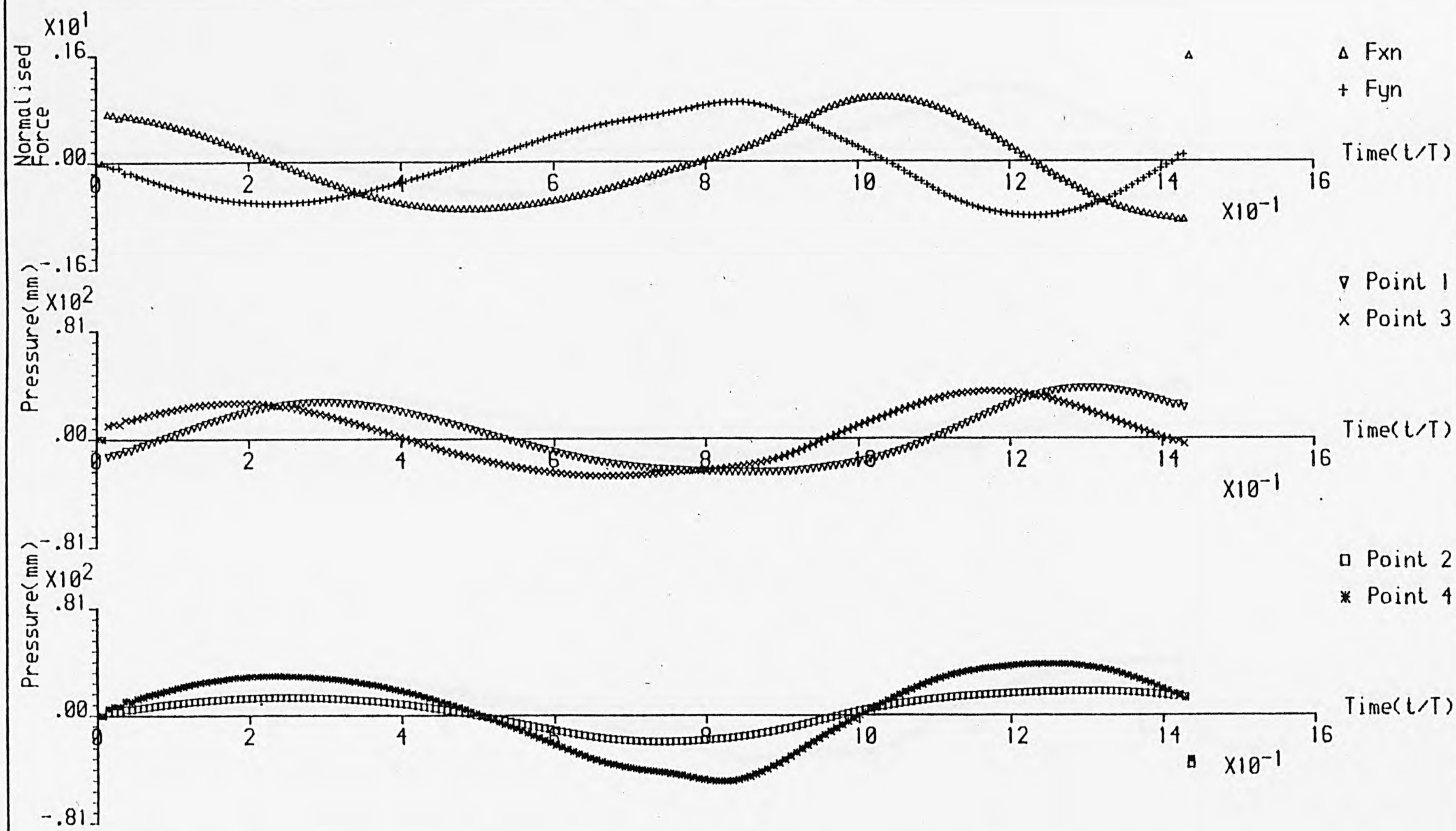

Wave height = .094m. Centre X = .798m.
Wavelength = 1.595m. Centre Y = -.135m.
Undisturbed W.L.= .555m. Radius = .055m.
Order of eq. = 1

Fig. A.13. 14 Auxiliary graphs for case No. 14

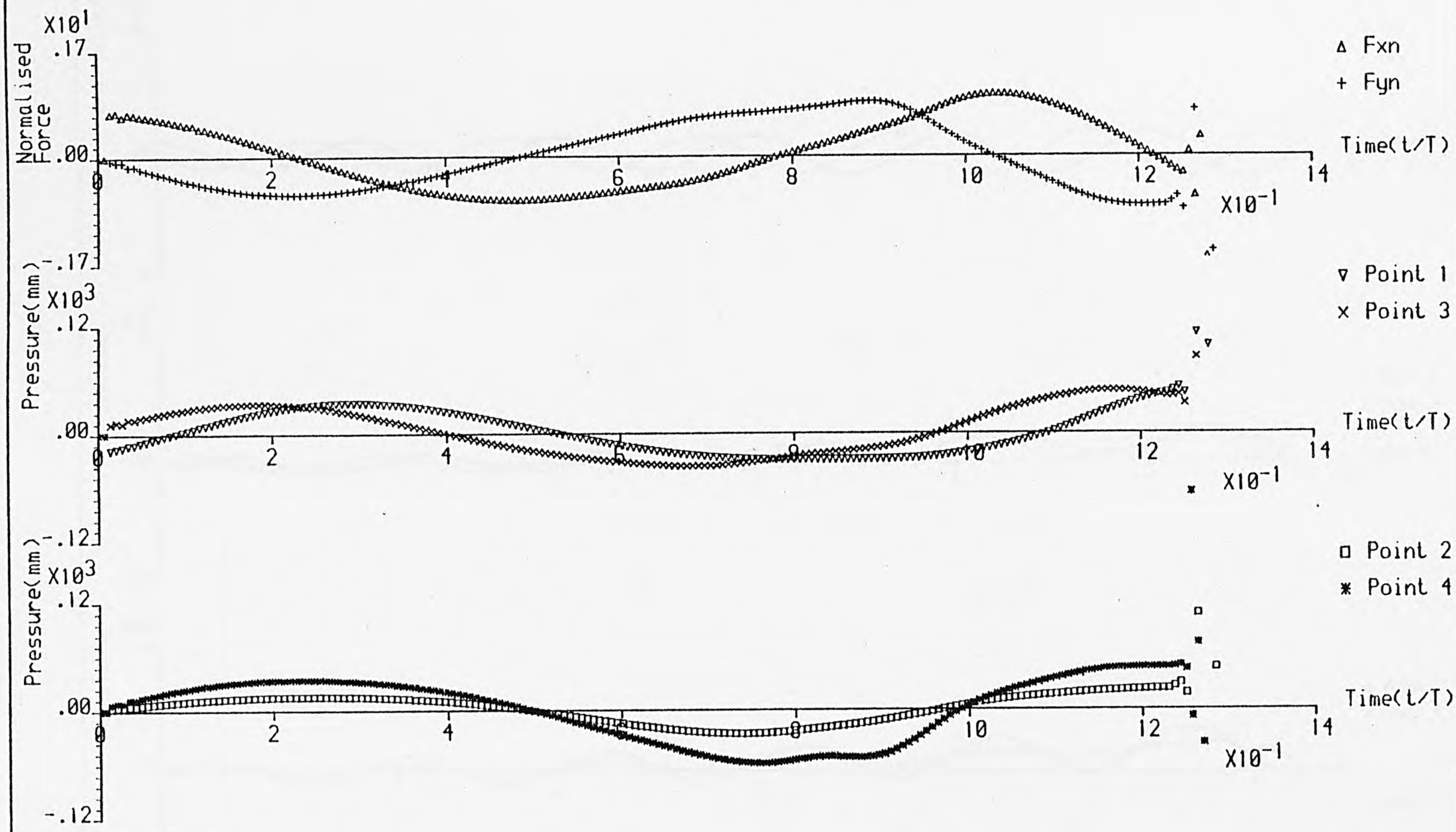

Wave height	=	.114m.	Centre X	=	.798m.
Wavelength	=	1.595m.	Centre Y	=	-.135m.
Undisturbed W.L.	=	.555m.	Radius	=	.055m.
Order of eq.	=	1			

Fig. A.13. 15 Auxiliary graphs for case No. 15

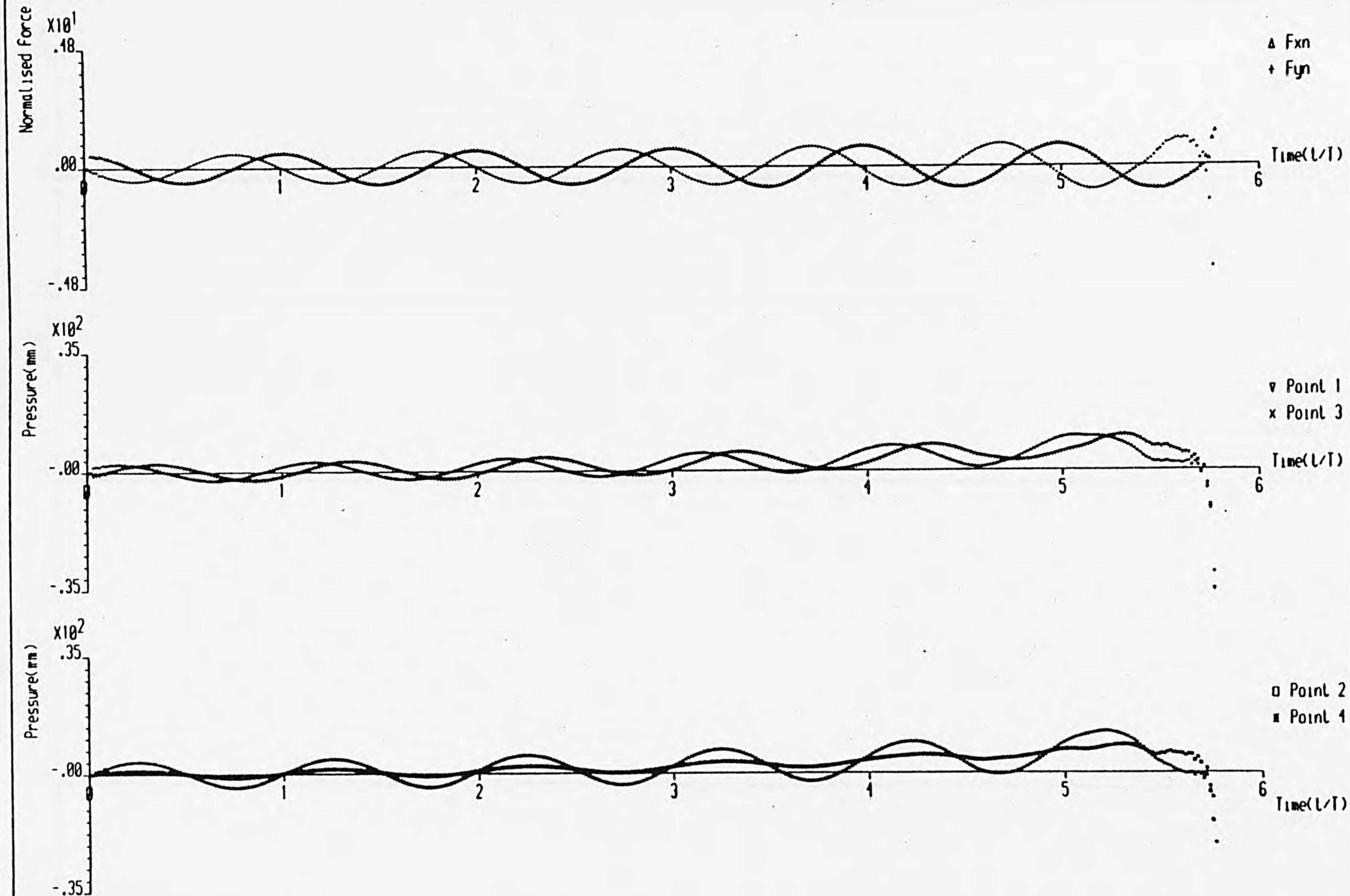

Wave height = .016m.
Wavelength = 1.132m.
Undisturbed W.L.= .555m.
Order of eq. = 1

Centre X = .566m.
Centre Y = -.225m.
Radius = .055m.

Fig. A.13. 16 Auxiliary graphs for case No. 16

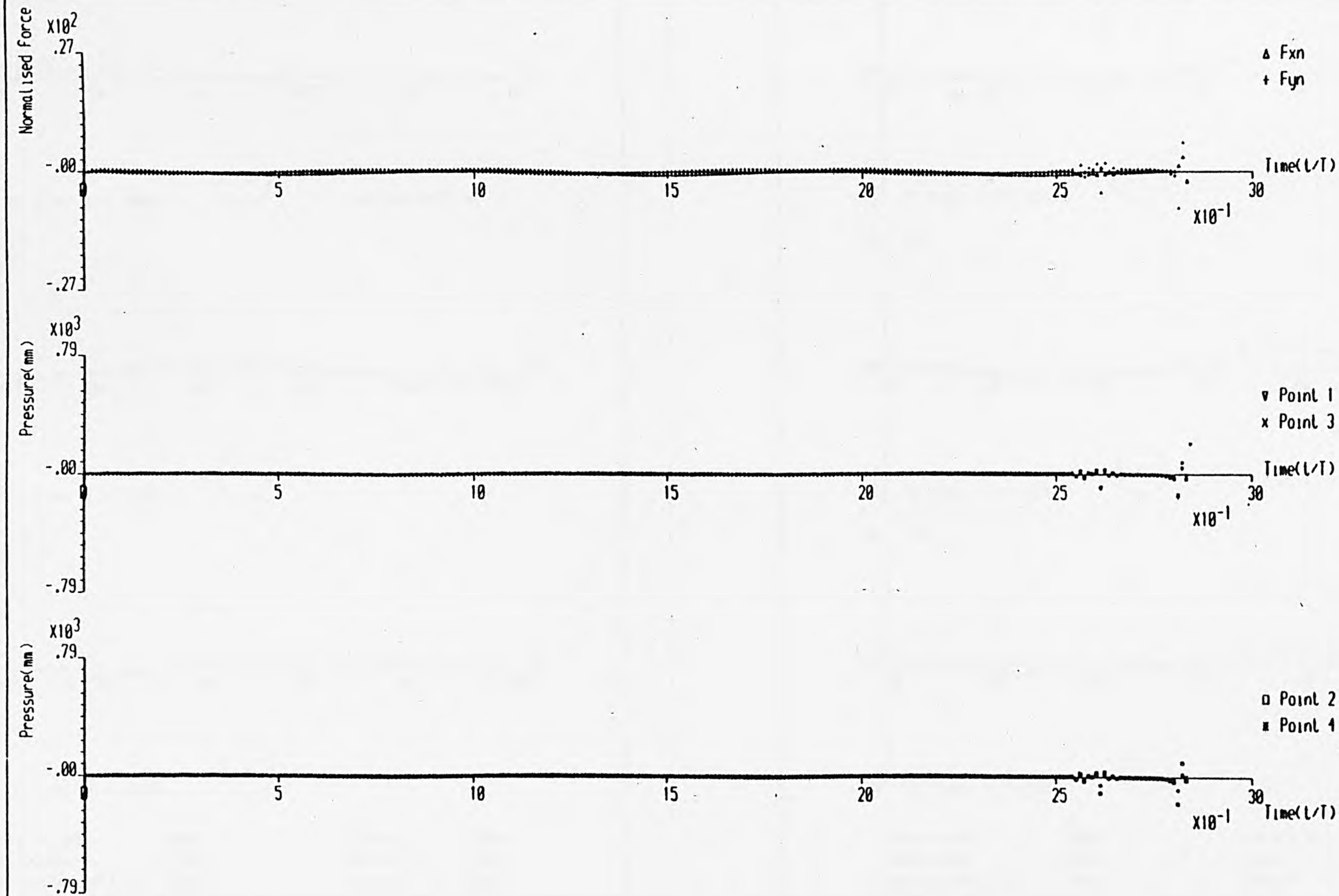

Wave height = .035m.
Wavelength = 1.132m.
Undisturbed W.L.= .555m.
Order of eq. = 1

Centre X = .566m.
Centre Y = -.225m.
Radius = .055m.

Fig. A.13. 17 Auxiliary graphs for case No. 17

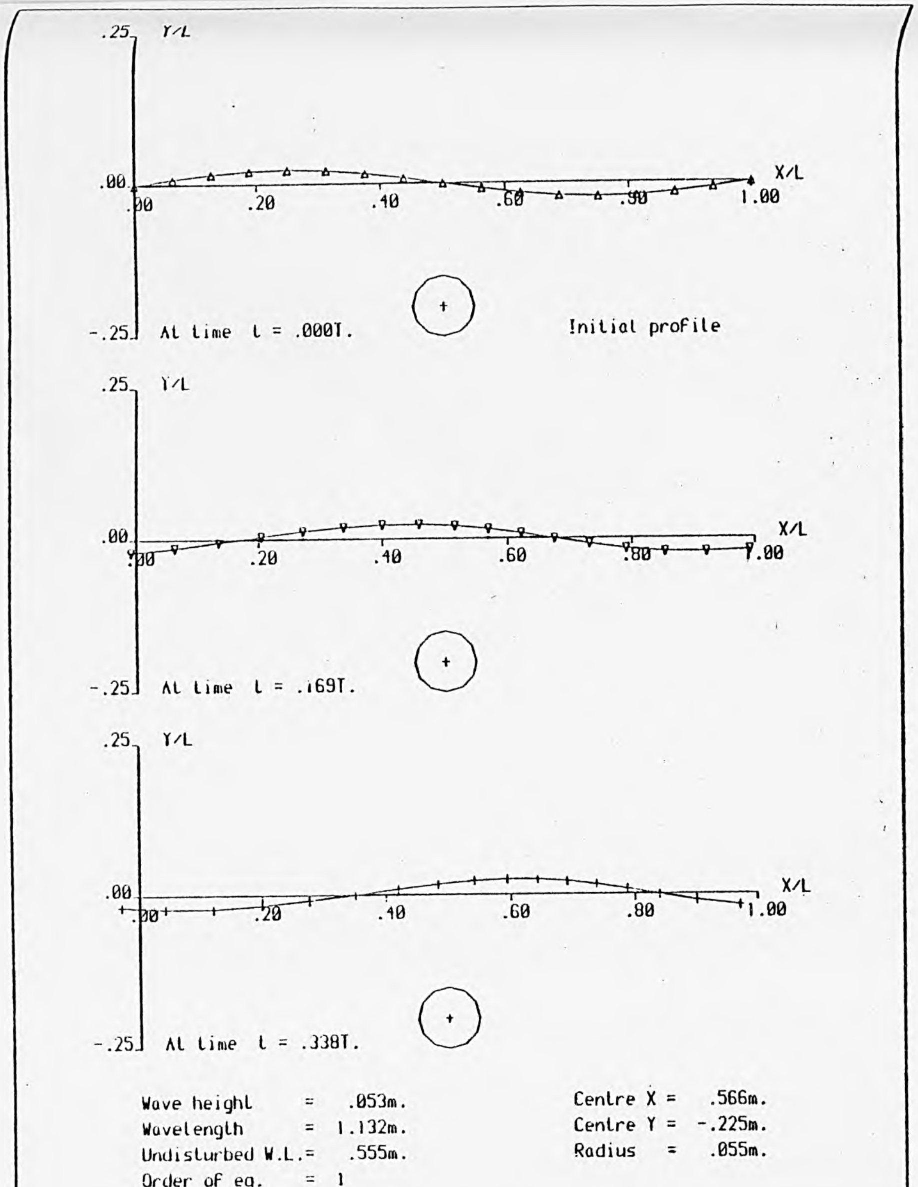

Fig. A.13.18a

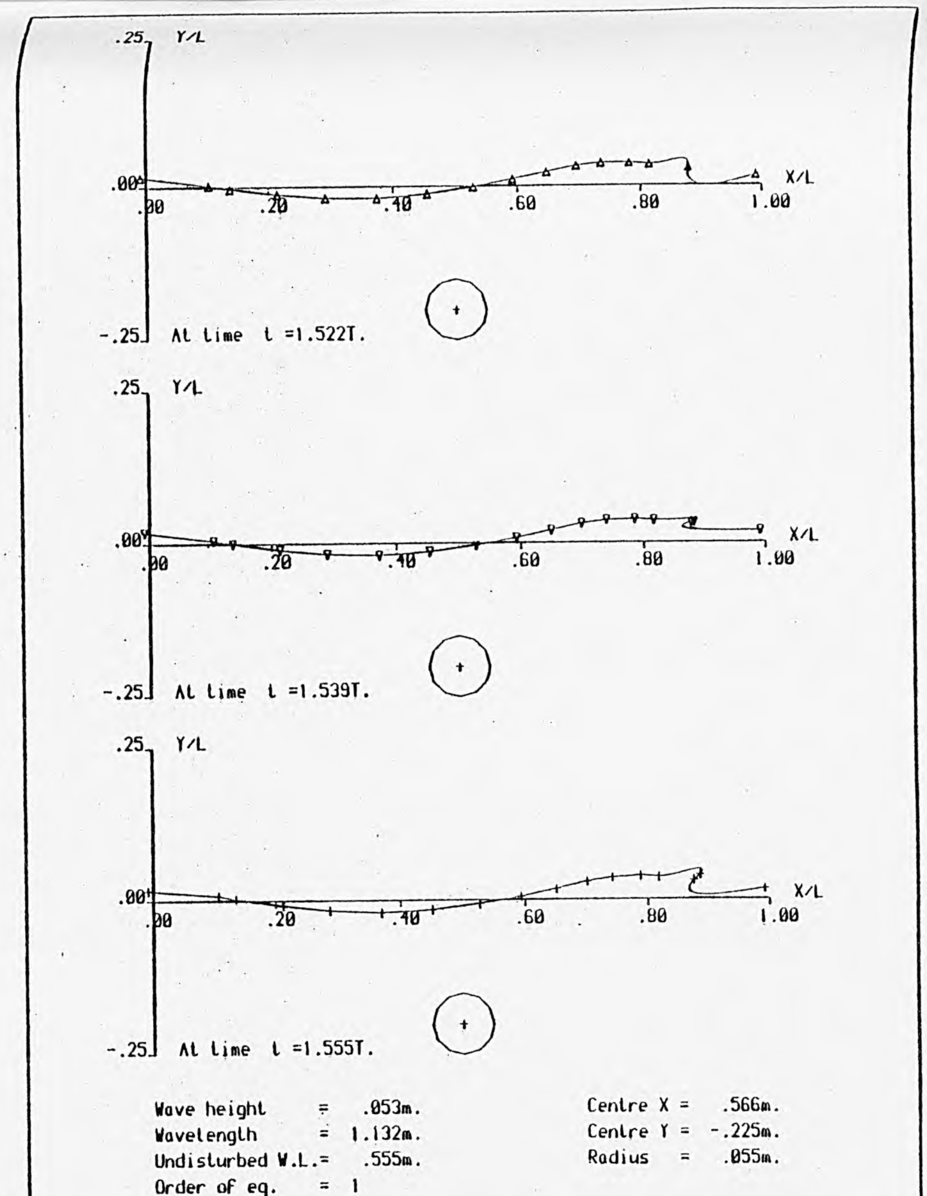

Fig. A.13.18b

Fig. A.13.18(a - f) A time sequence of wave profiles and auxiliary graphs for case No. 18

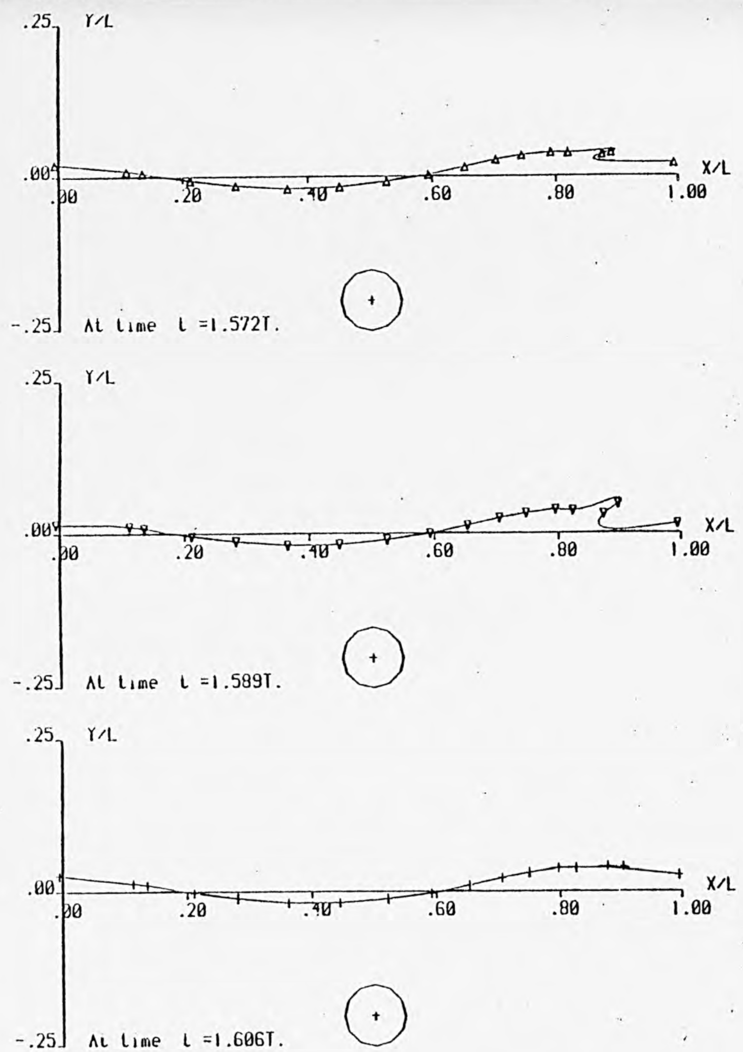

Wave height = .053m.
Wavelength = 1.132m.
Undisturbed W.L.= .555m.
Order of eq. = 1

Centre X = .566m.
Centre Y = -.225m.
Radius = .055m.

Fig. A.13.18c

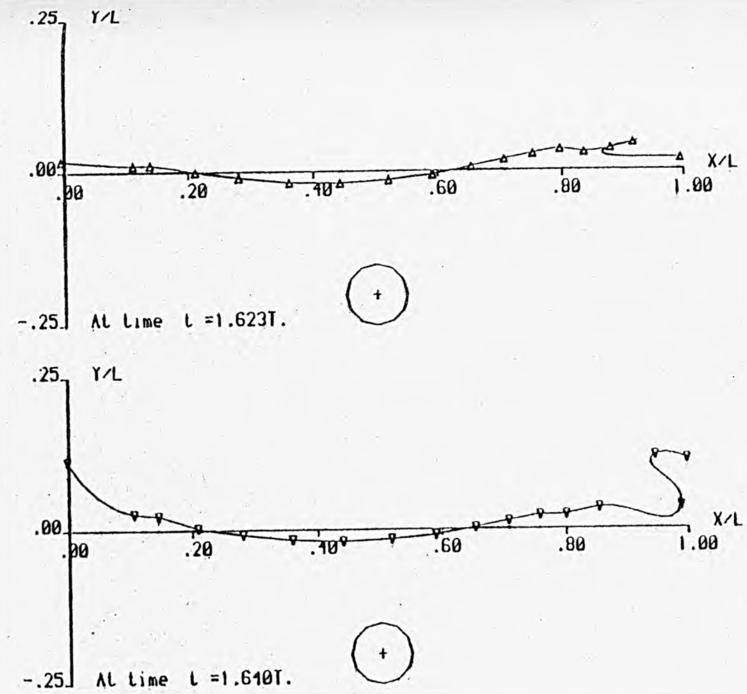

Wave height = .053m.
Wavelength = 1.132m.
Undisturbed W.L.= .555m.
Order of eq. = 1

Centre X = .566m.
Centre Y = -.225m.
Radius = .055m.

Fig. A.13.18d

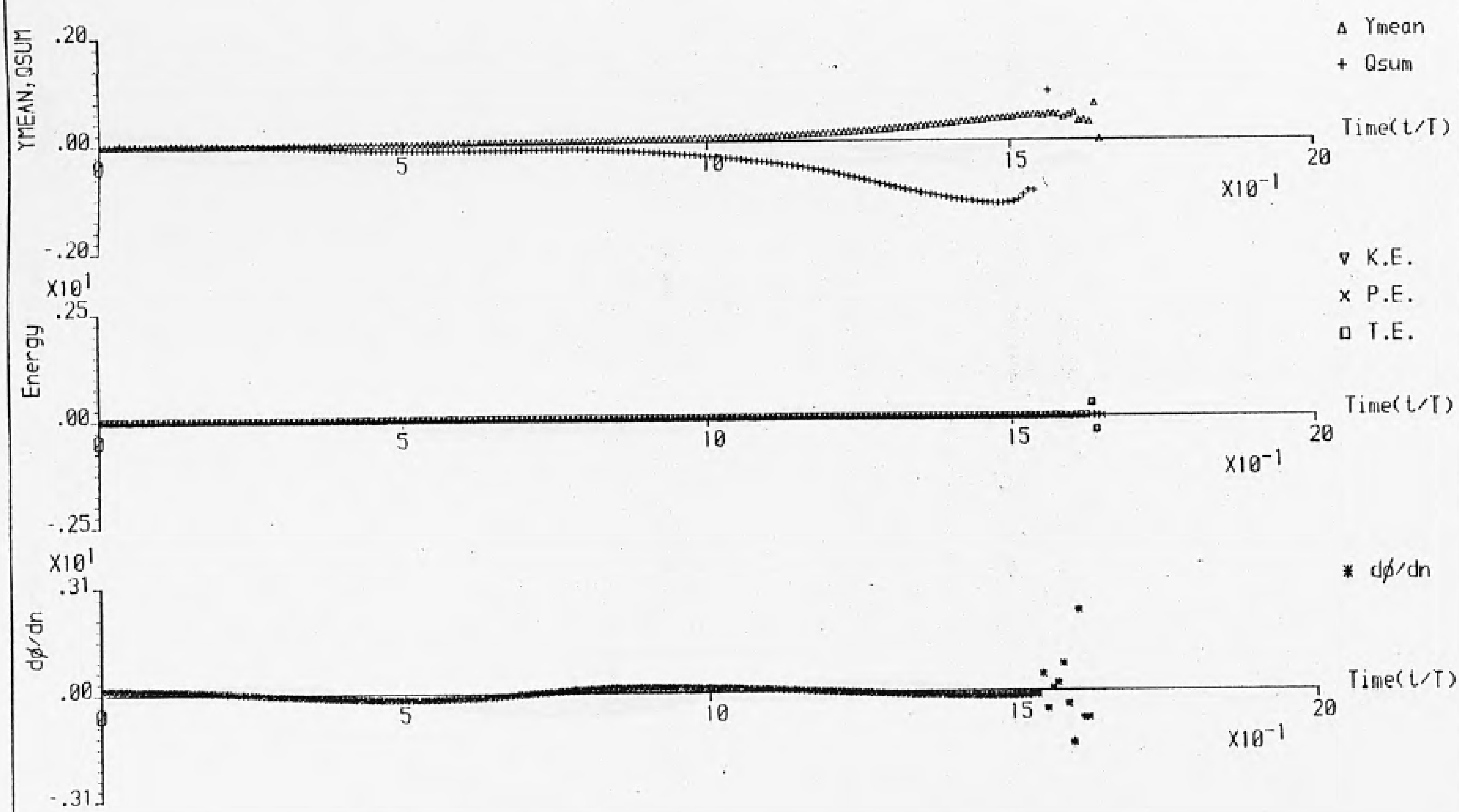

Wave height = .053m. Centre X = .566m.
Wavelength = 1.132m. Centre Y = -.225m.
Undisturbed W.L.= .555m. Radius = .055m.
Order of eq. = 1

Fig. A.13.18e

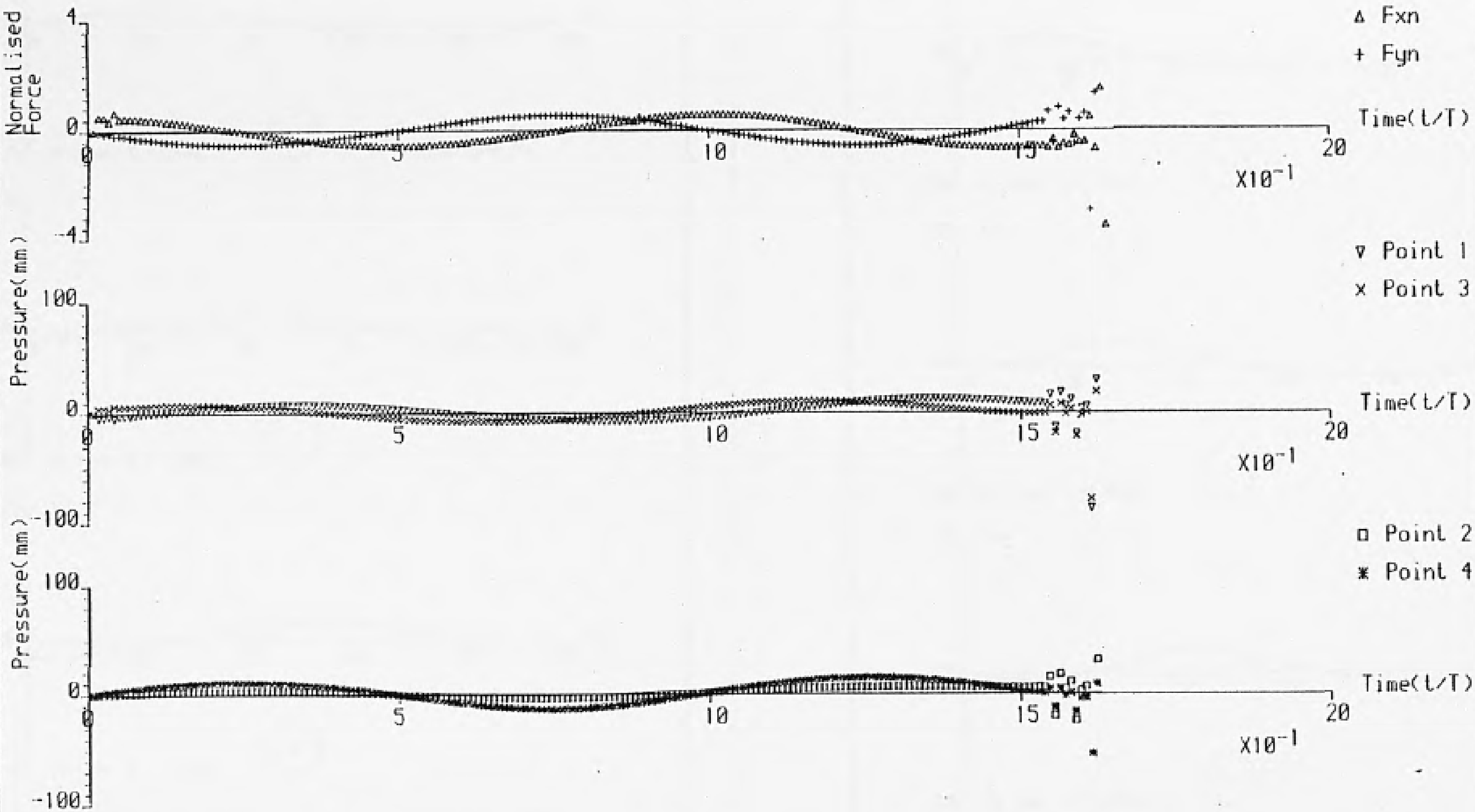

Wave height	=	.053m.	Centre X	=	.566m.
Wavelength	=	1.132m.	Centre Y	=	-.225m.
Undisturbed W.L.	=	.555m.	Radius	=	.055m.
Order of eq.	=	1			

Fig. A.13.18f

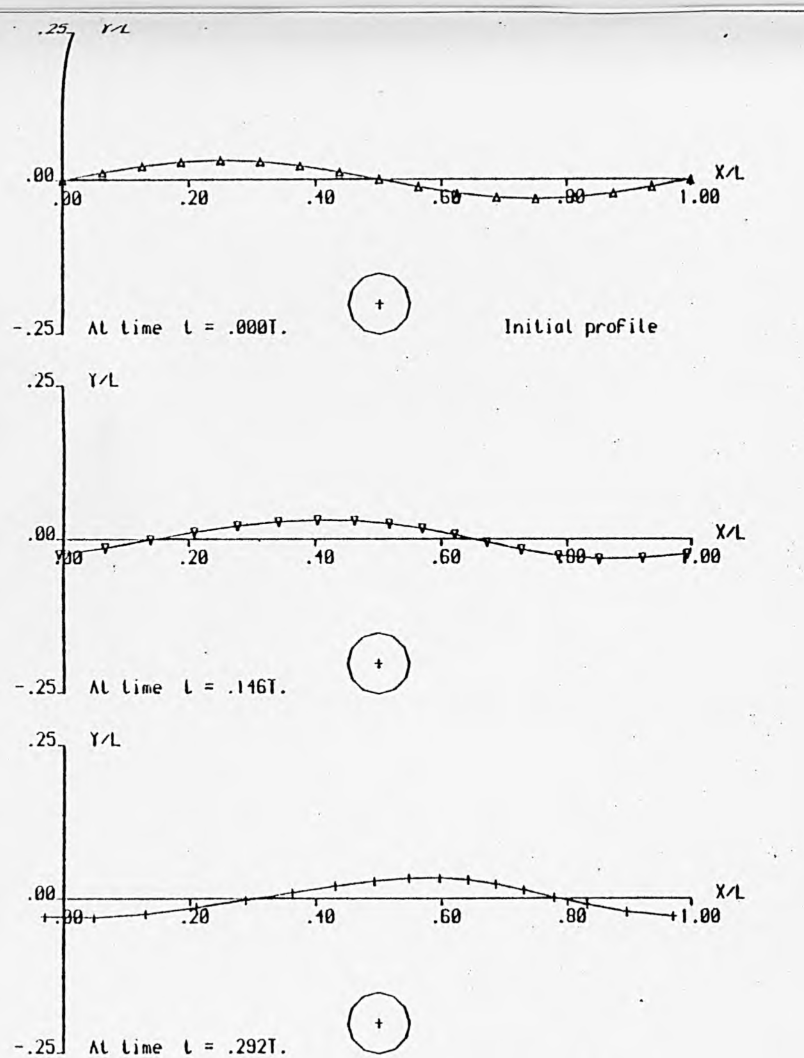

Wave height = .071m.
Wavelength = 1.132m.
Undisturbed W.L.= .555m.
Order of eq. = 1

Centre X = .566m.
Centre Y = -.225m.
Radius = .055m.

Fig. A.13.19a

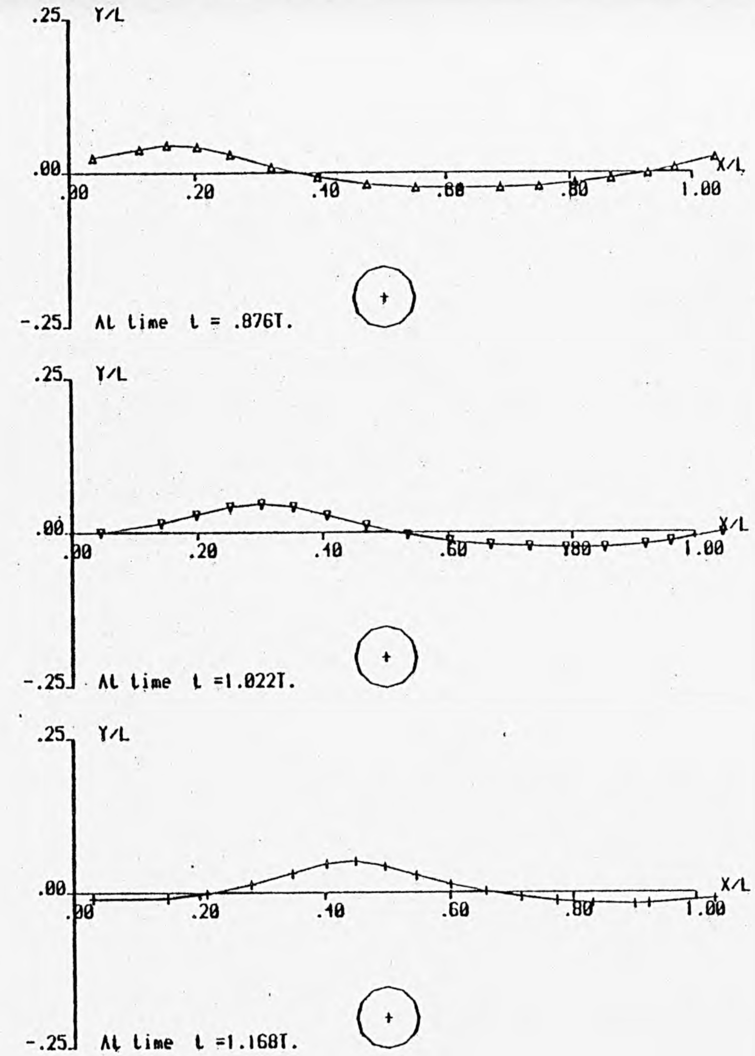

Wave height = .071m.
Wavelength = 1.132m.
Undisturbed W.L.= .555m.
Order of eq. = 1

Centre X = .566m.
Centre Y = -.225m.
Radius = .055m.

Fig. A.13.19b

Fig. A.13.19(a - f) A time sequence of wave profiles and auxiliary graphs for case No. 19

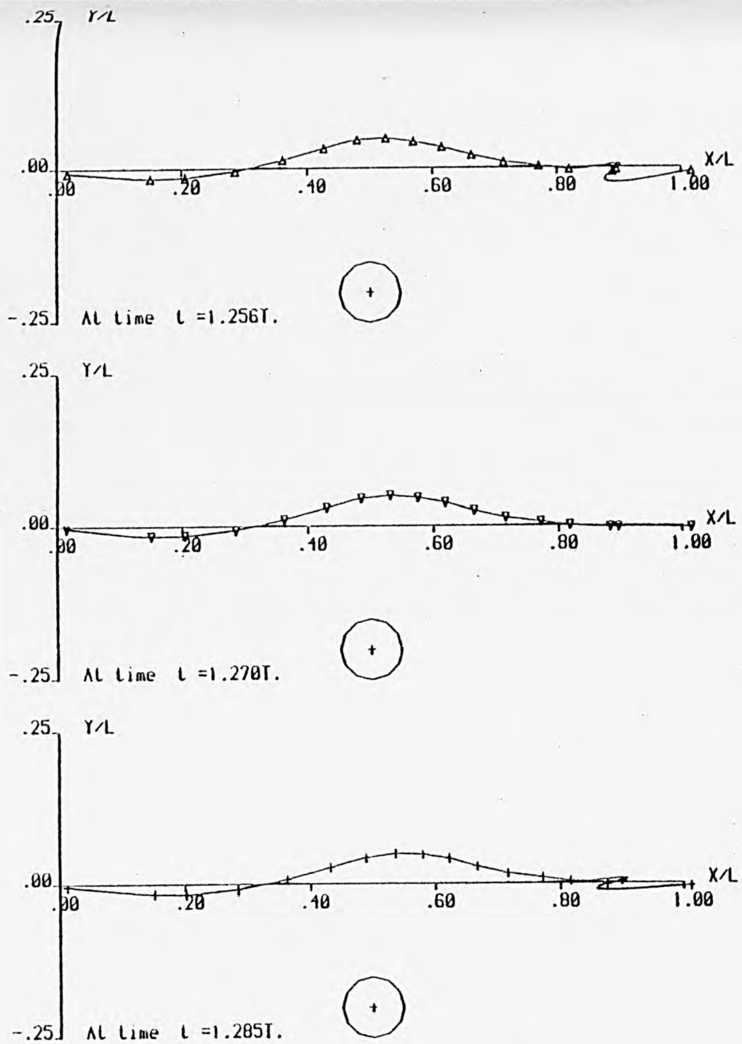

Wave height = .071m.
Wavelength = 1.132m.
Undisturbed W.L.= .555m.
Order of eq. = 1
Fig. A.13.19c

Centre X = .566m.
Centre Y = -.225m.
Radius = .055m.

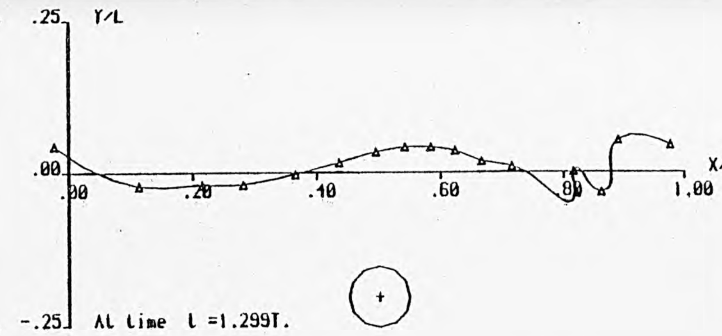

Wave height = .071m.
Wavelength = 1.132m.
Undisturbed W.L.= .555m.
Order of eq. = 1
Fig. A.13.19d

Centre X = .566m.
Centre Y = -.225m.
Radius = .055m.

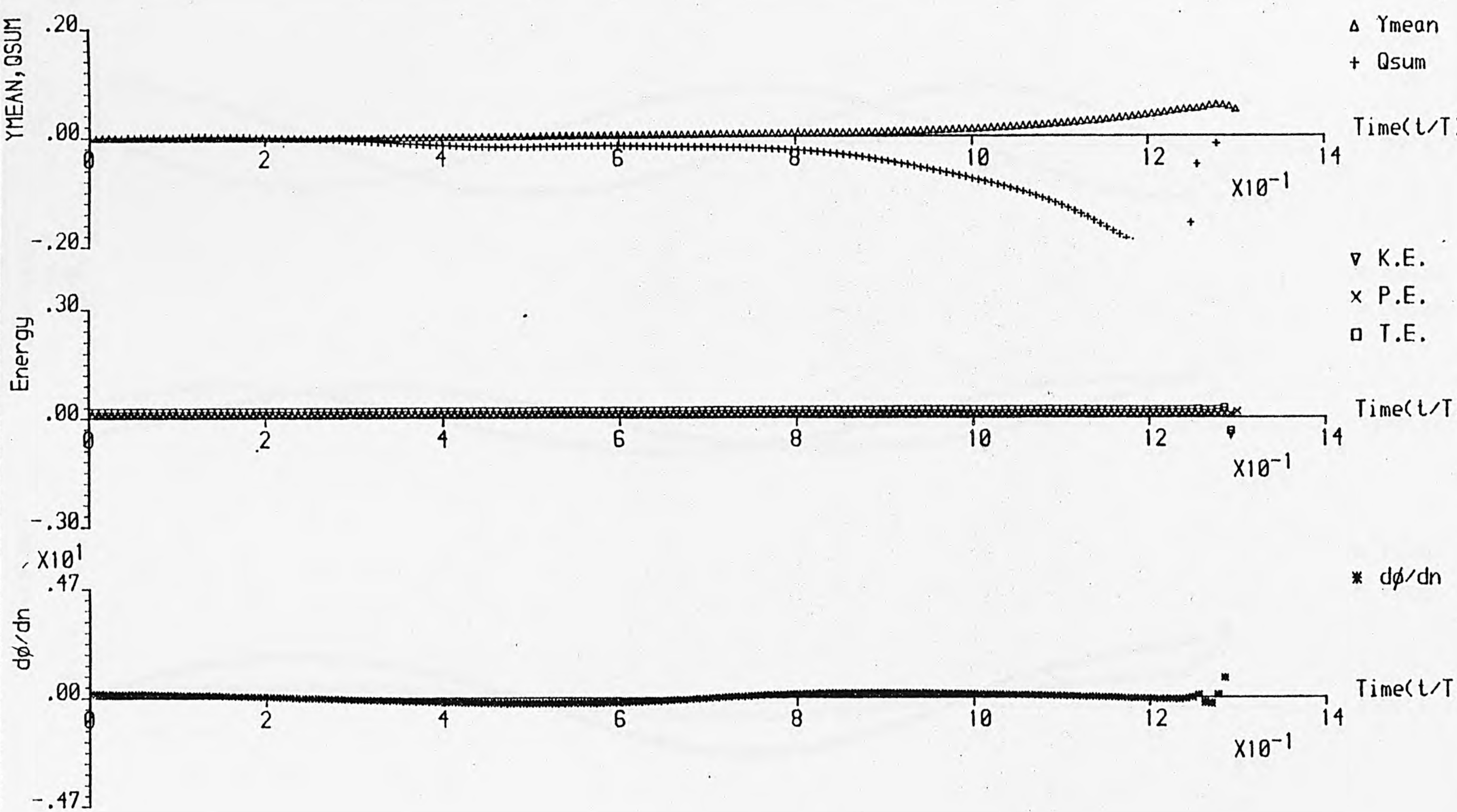

Wave height	=	.071m.	Centre X	=	.566m.
Wavelength	=	1.132m.	Centre Y	=	-.225m.
Undisturbed W.L.	=	.555m.	Radius	=	.055m.
Order of eq.	=	1			

Fig. A.13.19e

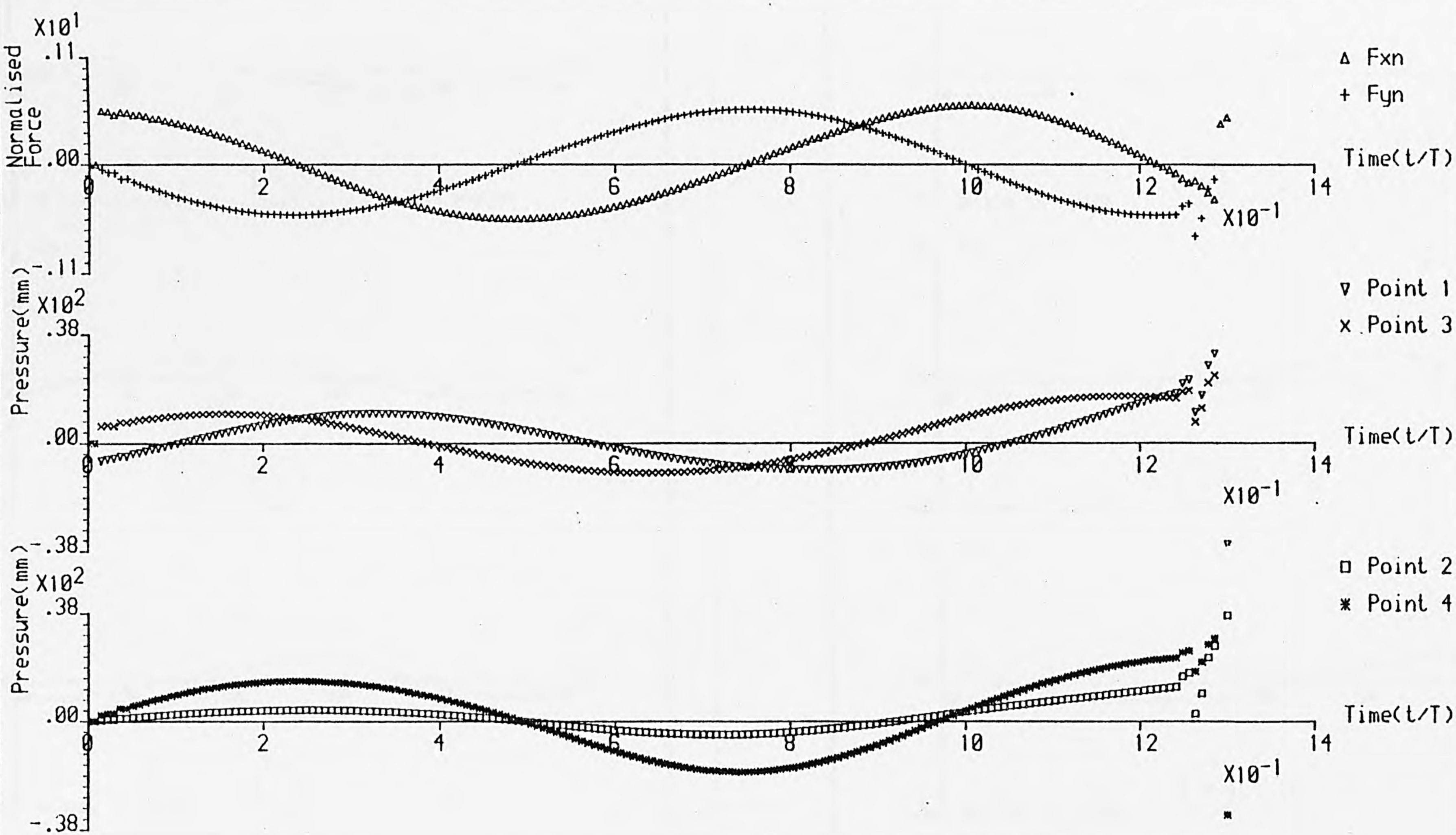

Wave height = .071m. Centre X = .566m.
Wavelength = 1.132m. Centre Y = -.225m.
Undisturbed W.L.= .555m. Radius = .055m.
Order of eq. = 1

Fig. A.13.19f

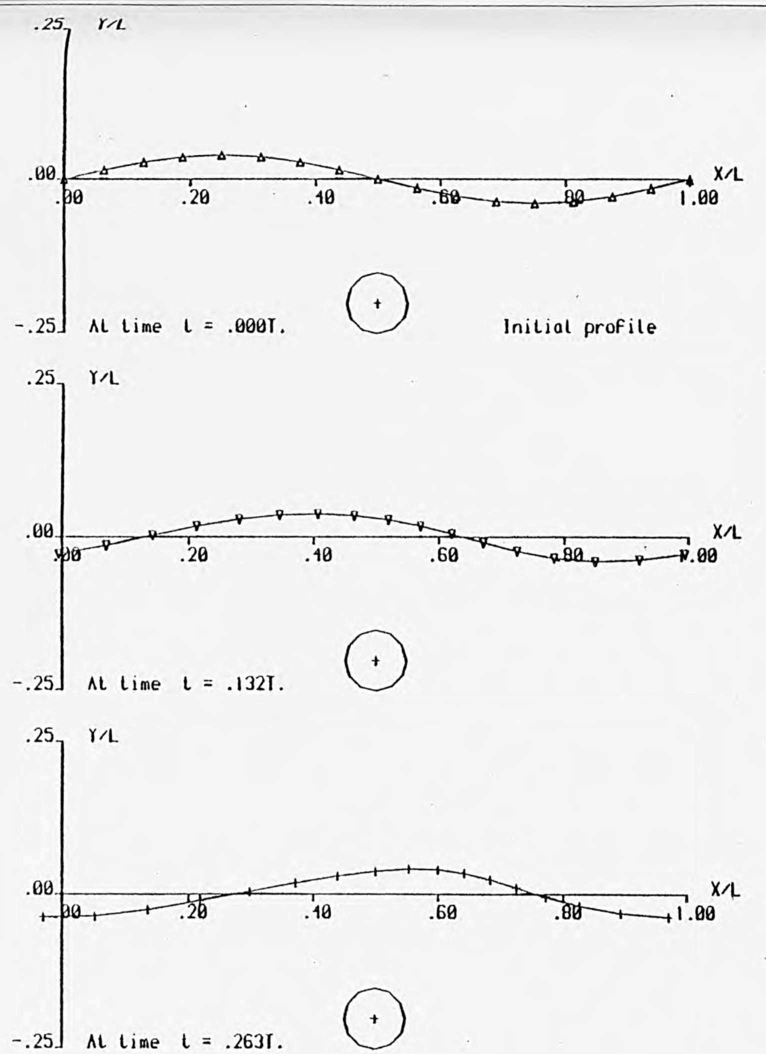

Wave height = .087m.
Wavelength = 1.132m.
Undisturbed W.L.= .555m.
Order of eq. = 1
Fig. A.13.20a

Centre X = .566m.
Centre Y = -.225m.
Radius = .055m.

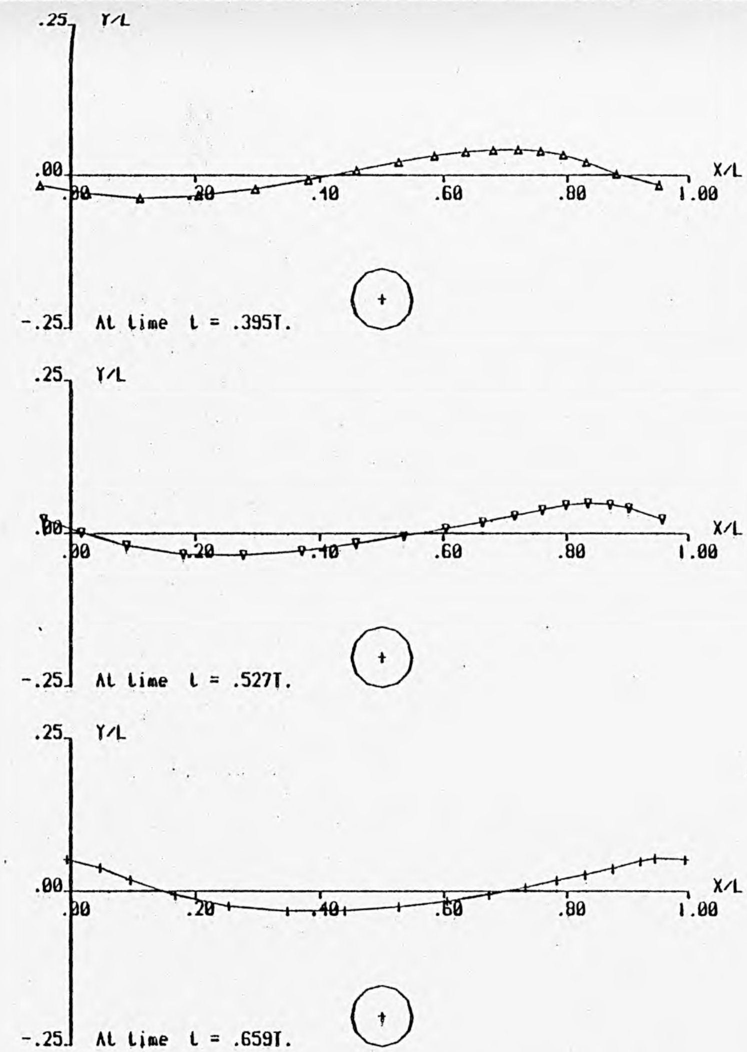

Wave height = .087m.
Wavelength = 1.132m.
Undisturbed W.L.= .555m.
Order of eq. = 1
Fig. A.13.20b

Centre X = .566m.
Centre Y = -.225m.
Radius = .055m.

Fig. A.13.20(a - f) A time sequence of wave profiles and auxiliary graphs for case No. 20

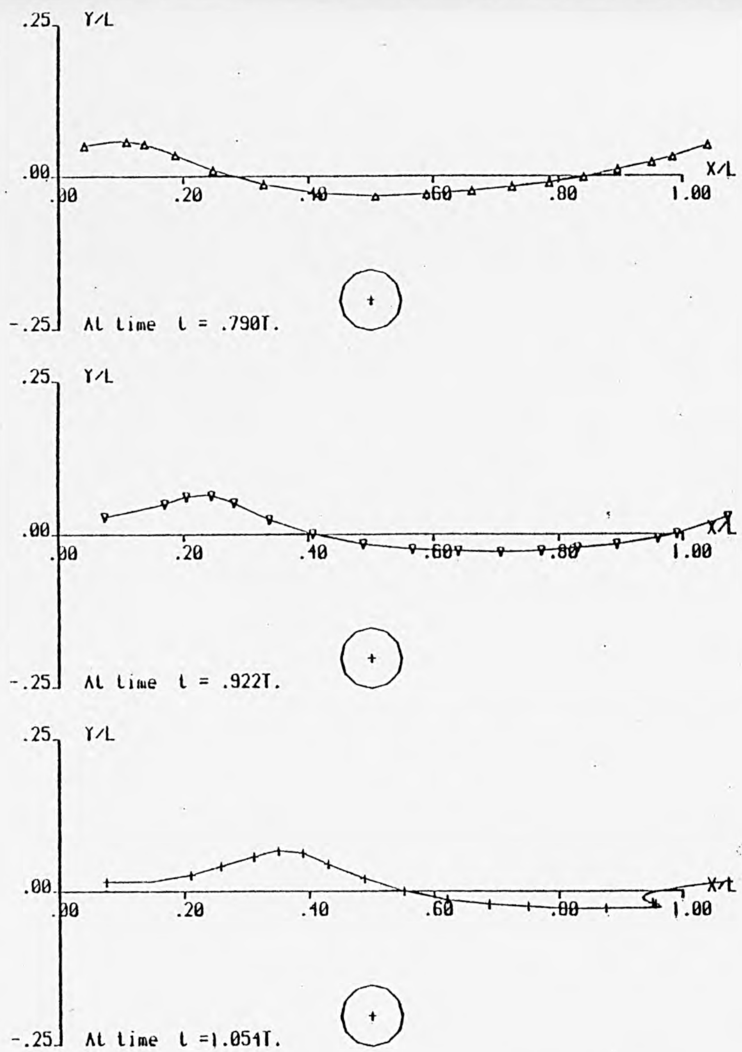

Wave height = .087m.
Wavelength = 1.132m.
Undisturbed W.L.= .555m.
Order of eq. = 1

Centre X = .566m.
Centre Y = -.225m.
Radius = .055m.

Fig.A.13.20c

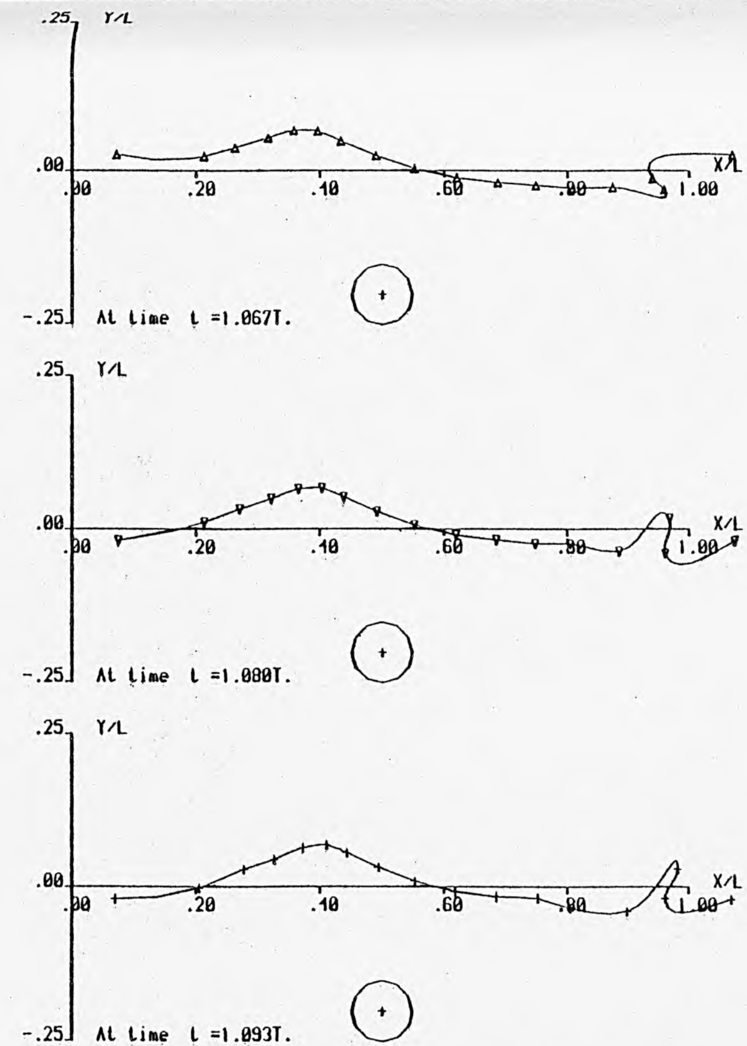

Wave height = .087m.
Wavelength = 1.132m.
Undisturbed W.L.= .555m.
Order of eq. = 1

Centre X = .566m.
Centre Y = -.225m.
Radius = .055m.

Fig. A.13.20d

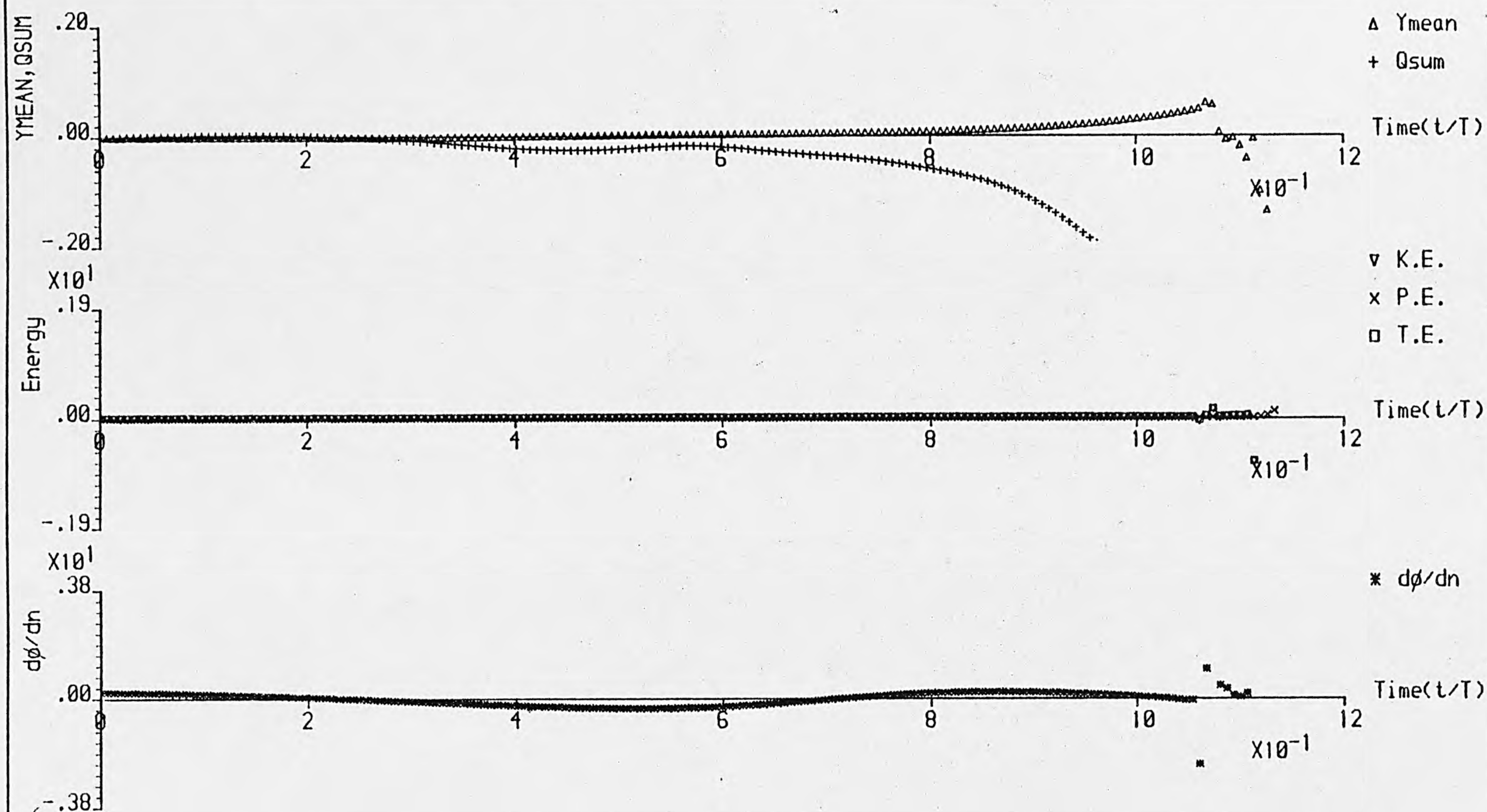

Wave height = .087m. Centre X = .566m.
Wavelength = 1.132m. Centre Y = -.225m.
Undisturbed W.L.= .555m. Radius = .055m.
Order of eq. = 1

Fig. A.13.20e

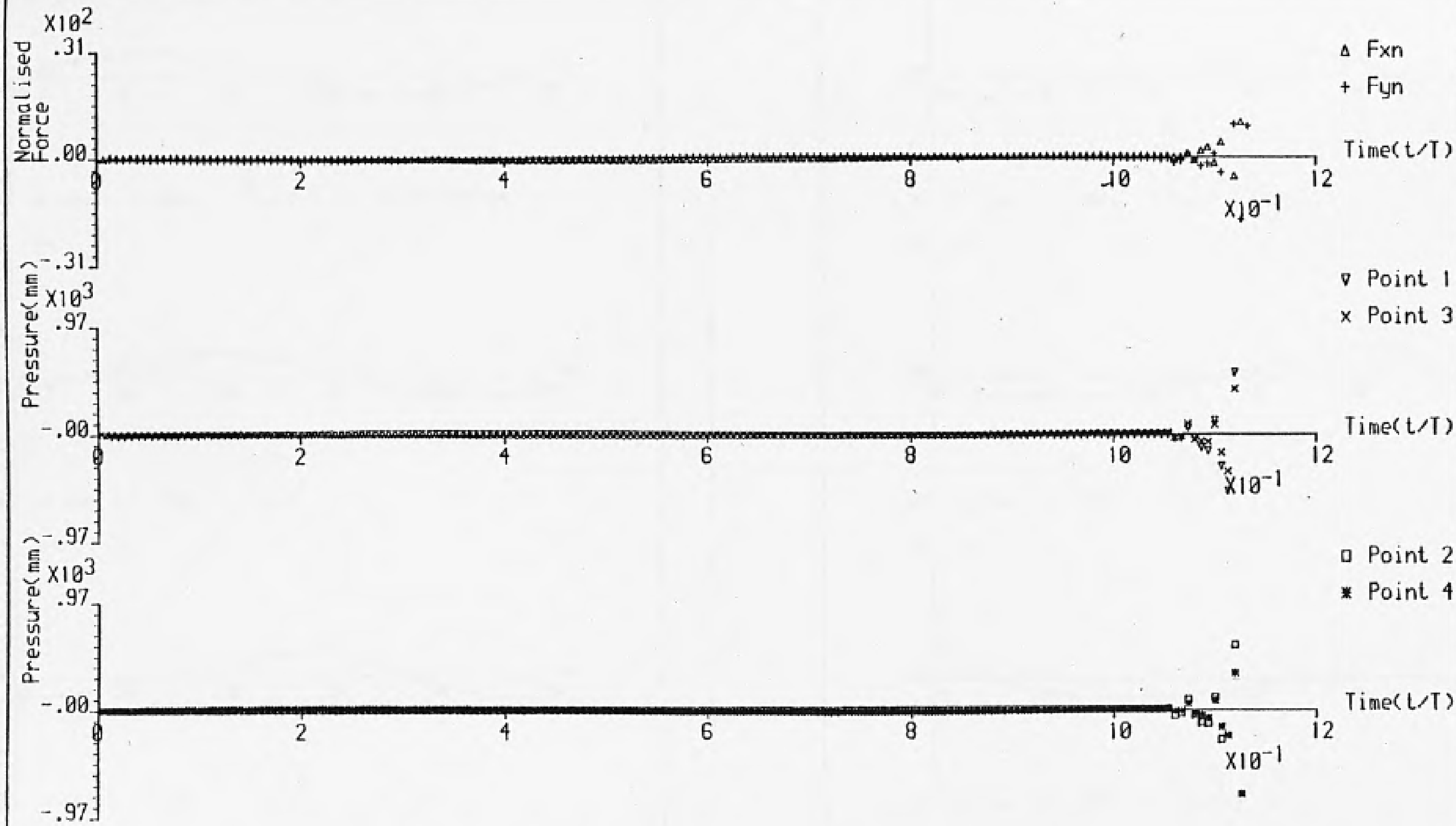

Wave height = .087m.   Centre X = .566m.
Wavelength = 1.132m.   Centre Y = -.225m.
Undisturbed W.L.= .555m.   Radius = .055m.
Order of eq. = 1

Fig. A.13.20f

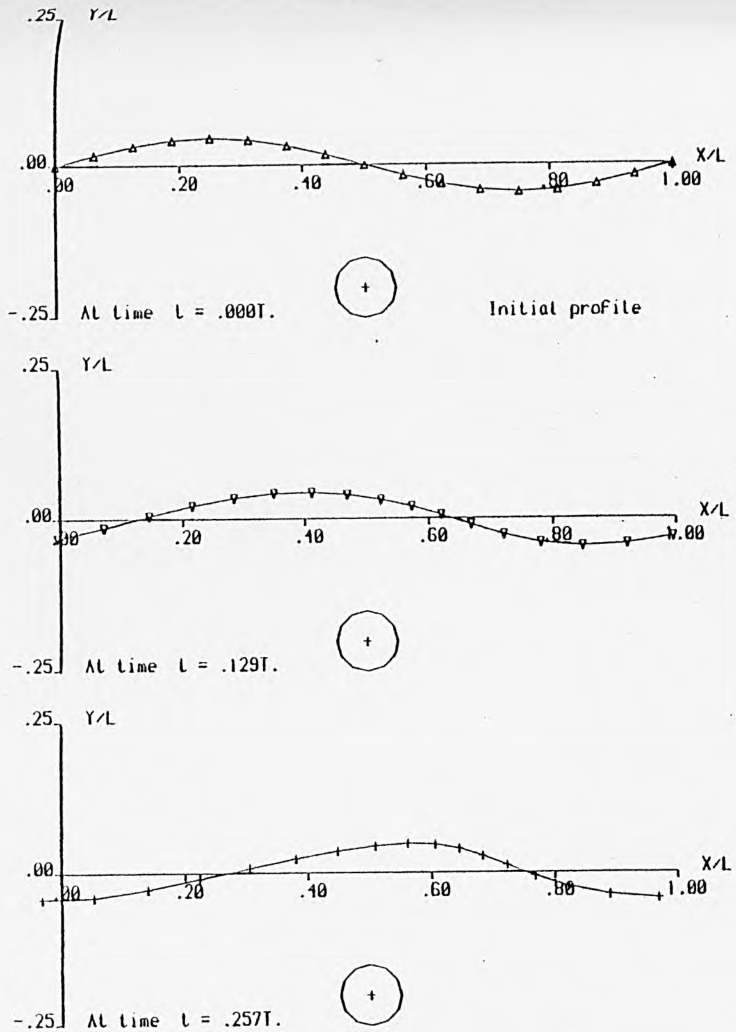

Wave height = .100m.
Wavelength = 1.132m.
Undisturbed W.L.= .555m.
Order of eq. = 1

Centre X = .566m.
Centre Y = -.225m.
Radius = .055m.

Fig. A.13.21a

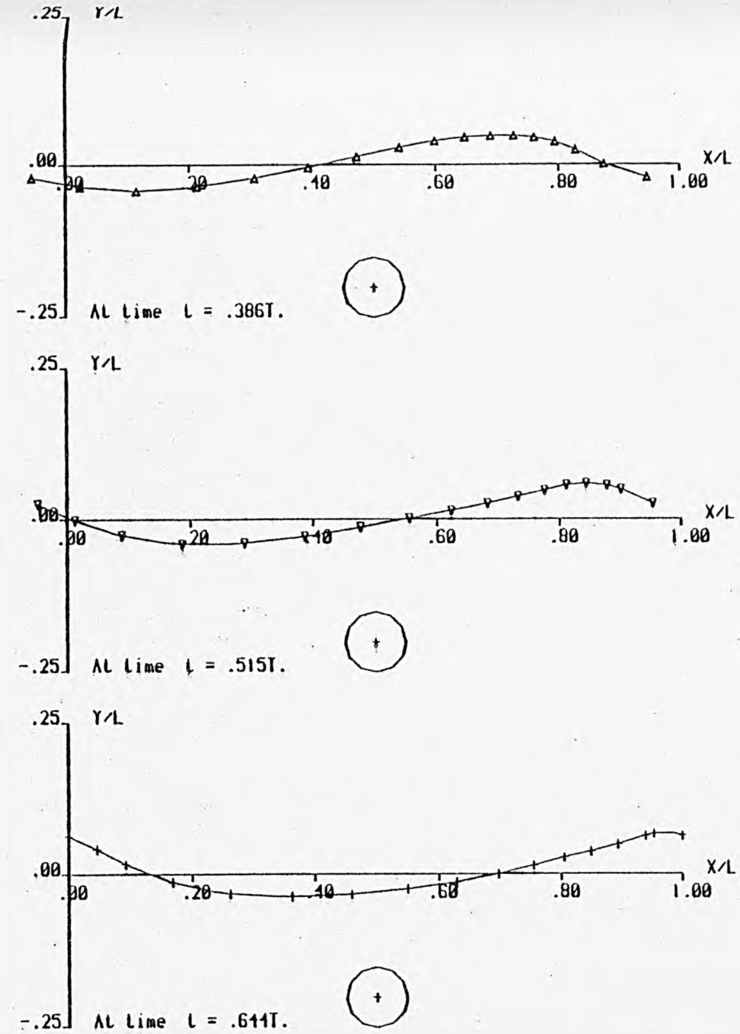

Wave height = .100m.
Wavelength = 1.132m.
Undisturbed W.L.= .555m.
Order of eq. = 1

Centre X = .566m.
Centre Y = -.225m.
Radius = .055m.

Fig. A.13.21b

Fig. A.13.21(a - e) A time sequence of wave profiles and auxiliary graphs for case No. 21

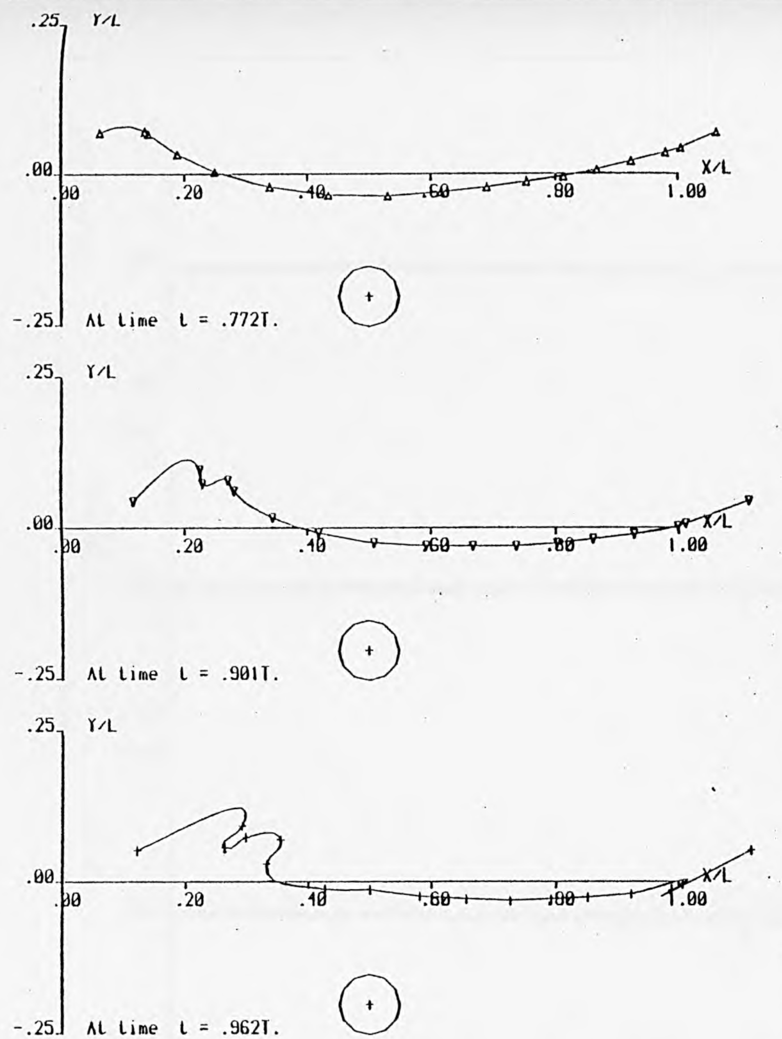

Wave height	=	.100m.	Centre X	=	.566m.
Wavelength	=	1.132m.	Centre Y	=	-.225m.
Undisturbed W.L.	=	.555m.	Radius	=	.055m.
Order of eq.	=	1			

Fig. A.13.21c

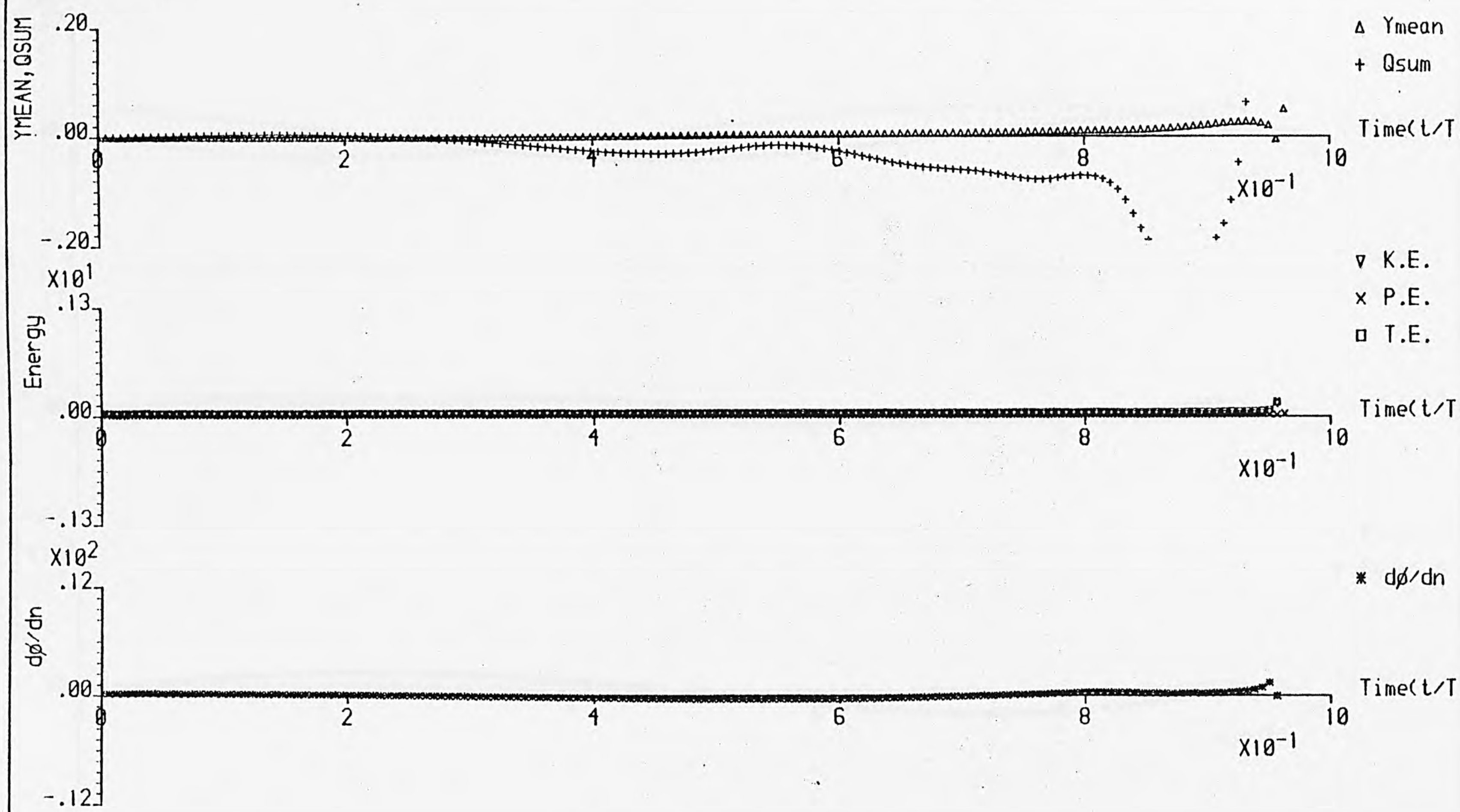

Wave height = .100m. Centre X = .566m.
Wavelength = 1.132m. Centre Y = -.225m.
Undisturbed W.L.= .555m. Radius = .055m.
Order of eq. = 1
Fig. A.13.21d

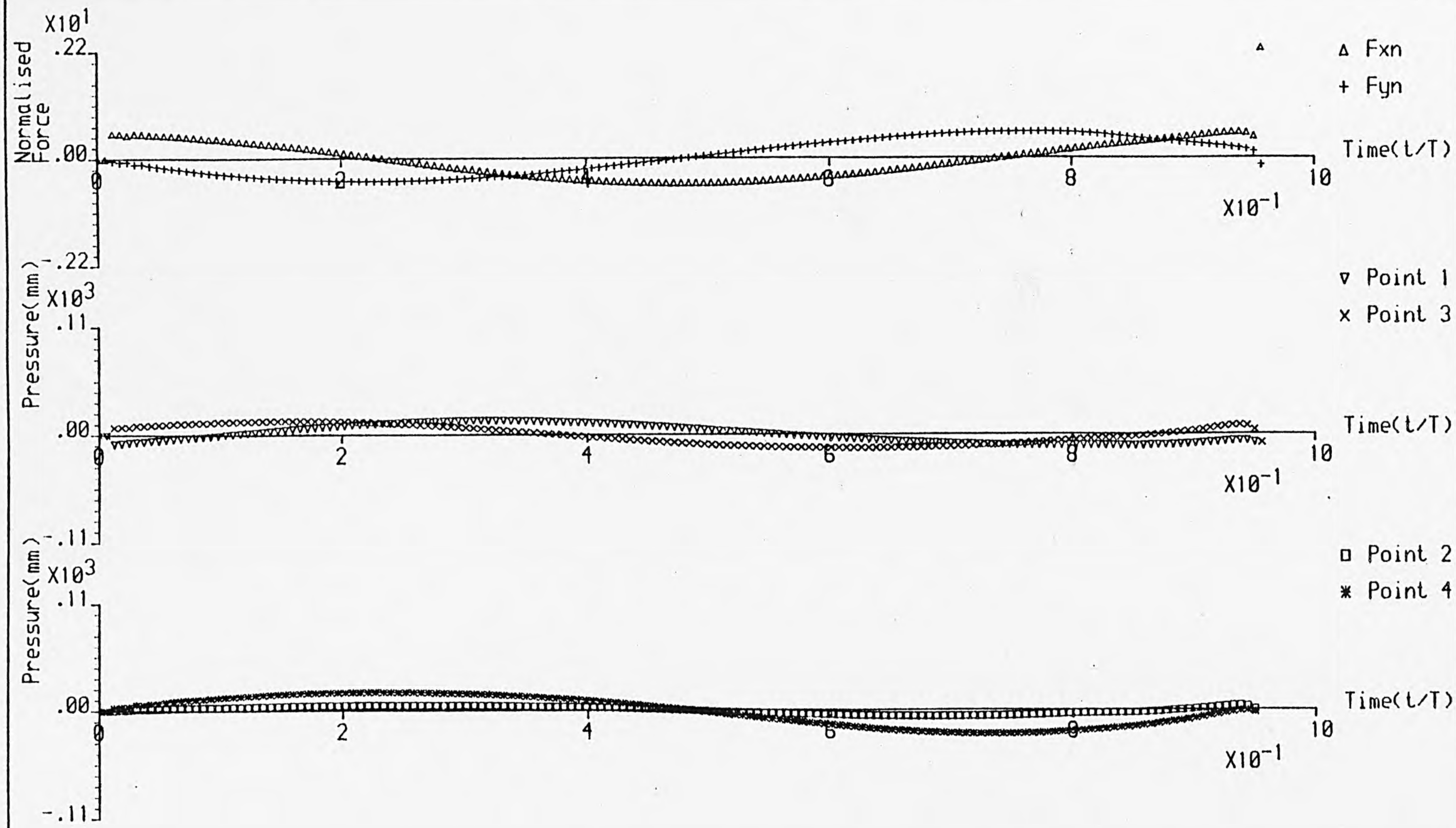

Wave height = .100m. Centre X = .566m.
Wavelength = 1.132m. Centre Y = -.225m.
Undisturbed W.L.= .555m. Radius = .055m.
Order of eq. = 1

Fig. A.13.21e

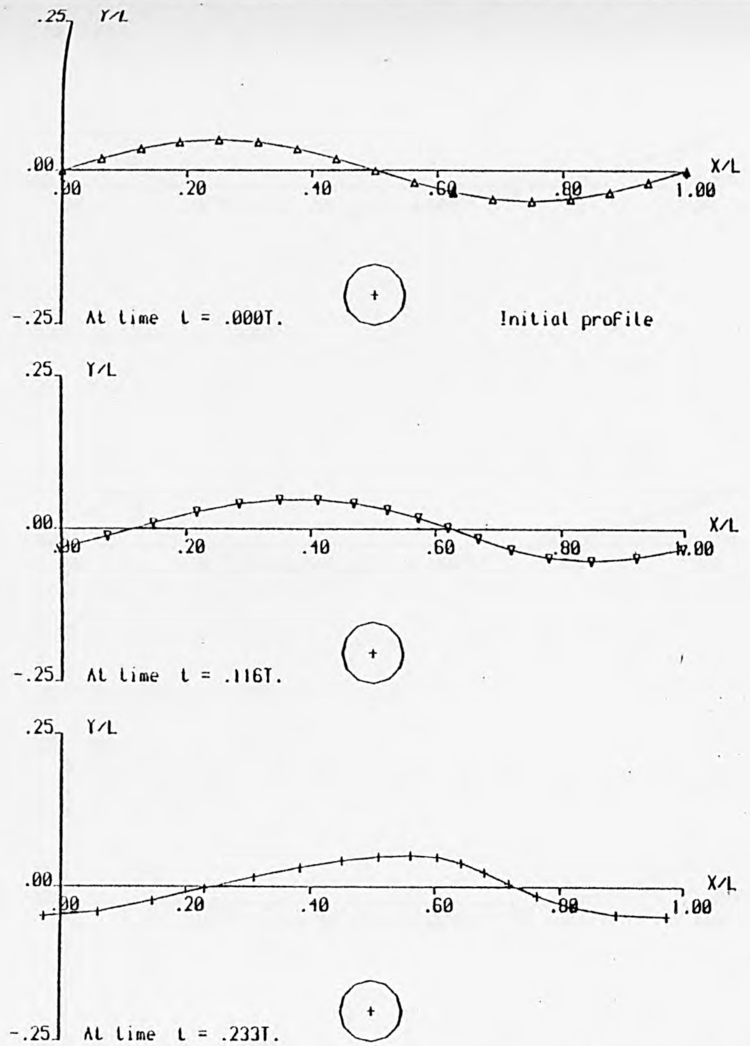

Wave height = .112m.
Wavelength = 1.132m.
Undisturbed W.L.= .555m.
Order of eq. = 1
Fig. A.13.22a

Centre X = .566m.
Centre Y = -.225m.
Radius = .055m.

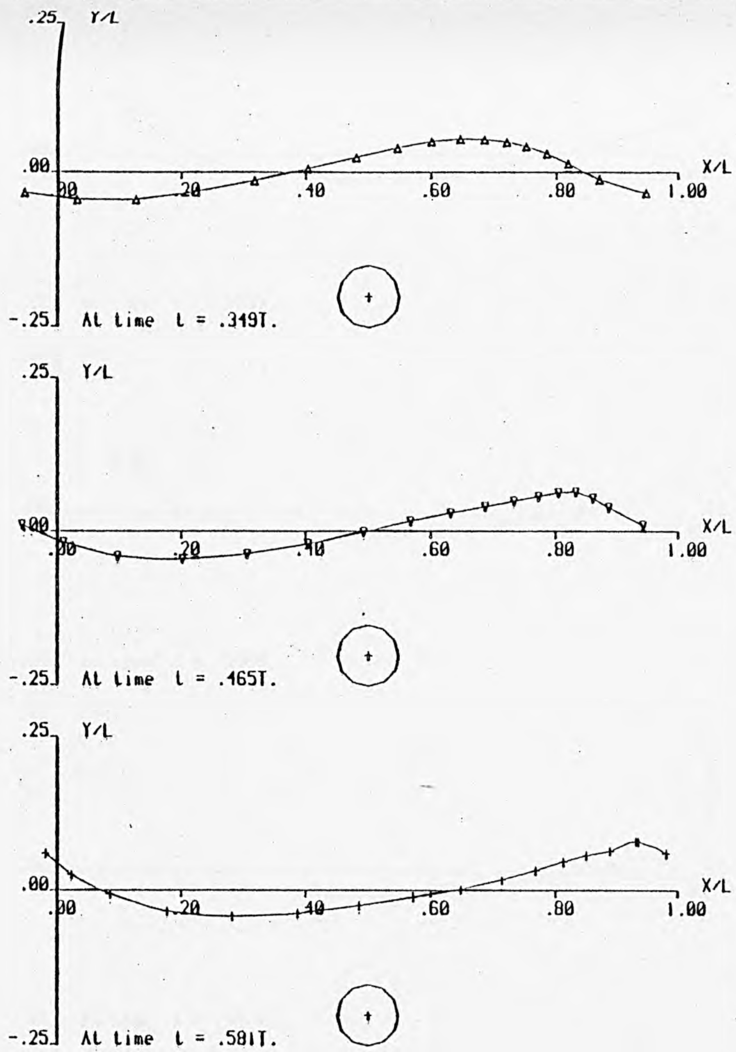

Wave height = .112m.
Wavelength = 1.132m.
Undisturbed W.L.= .555m.
Order of eq. = 1
Fig. A.13.22b

Centre X = .566m.
Centre Y = -.225m.
Radius = .055m.

Fig. A.13.22(a - f) A time sequence of wave profiles and auxiliary graphs for case No. 22

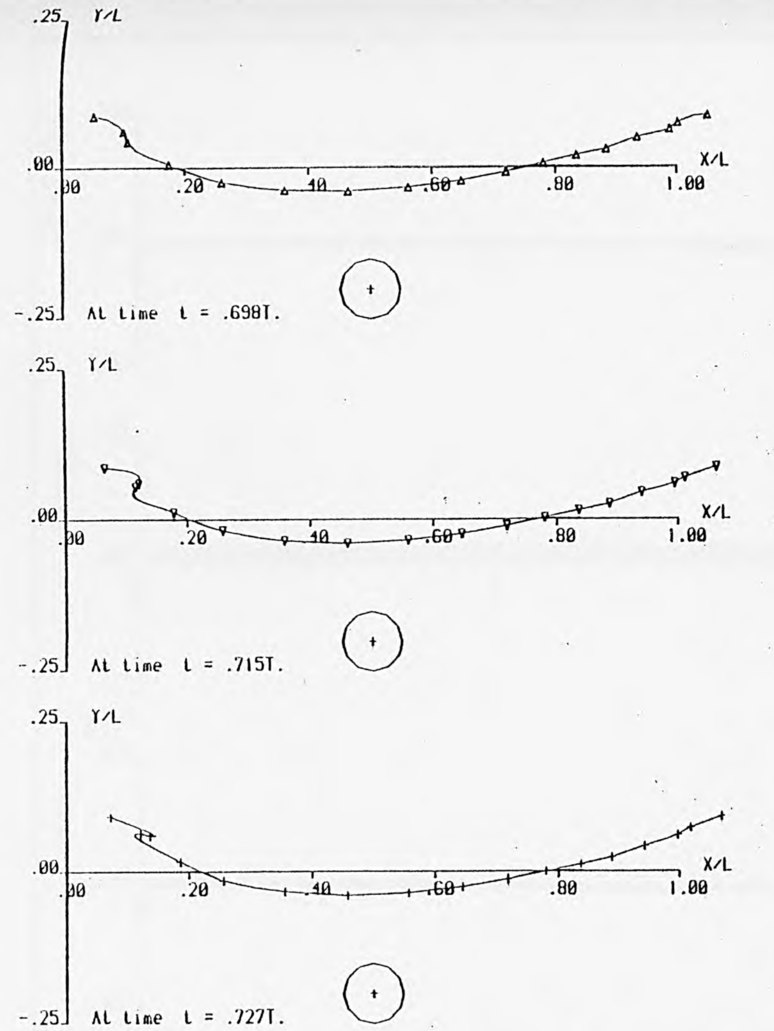

Wave height = .112m.
Wavelength = 1.132m.
Undisturbed W.L.= .555m.
Order of eq. = 1
Centre X = .566m.
Centre Y = -.225m.
Radius = .055m.

Fig. A.13.22c

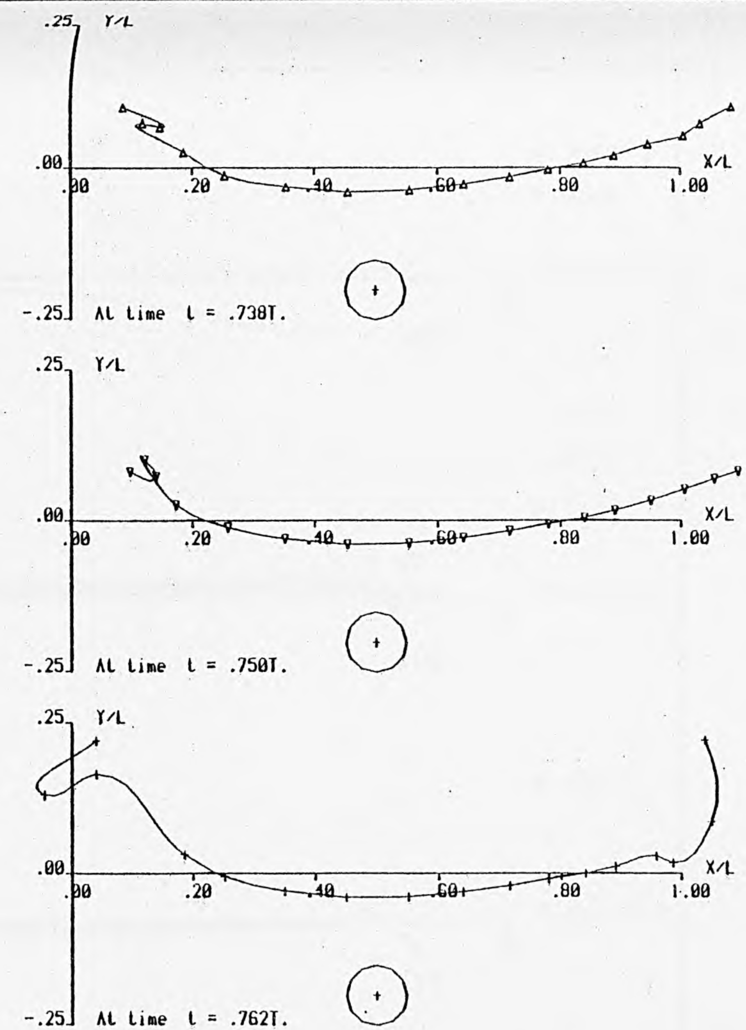

Wave height = .112m.
Wavelength = 1.132m.
Undisturbed W.L.= .555m.
Order of eq. = 1
Centre X = .566m.
Centre Y = -.225m.
Radius = .055m.

Fig. A.13.22d

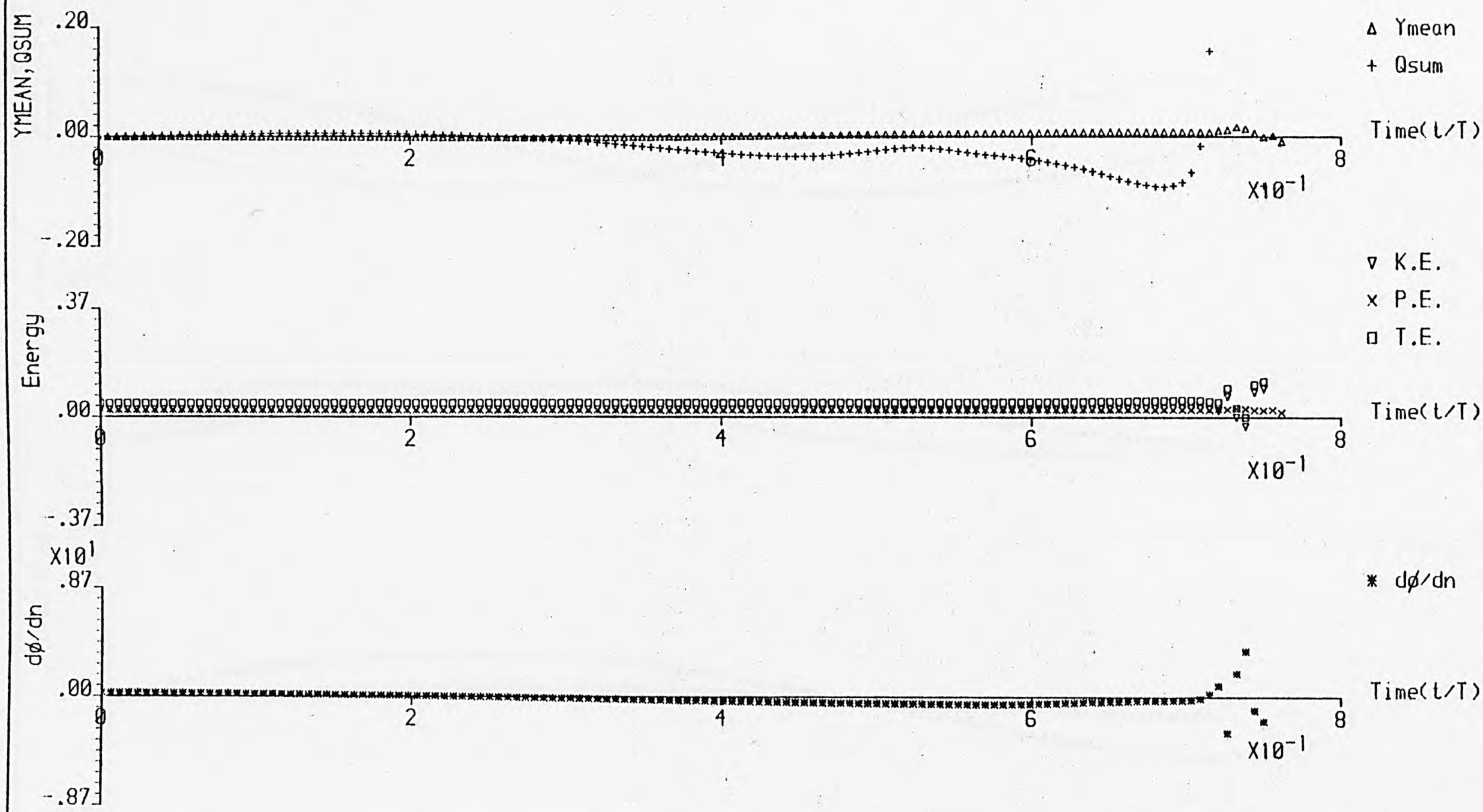

Wave height = .112m. Centre X = .566m.
Wavelength = 1.132m. Centre Y = -.225m.
Undisturbed W.L.= .555m. Radius = .055m.
Order of eq. = 1

Fig. A.13.22e

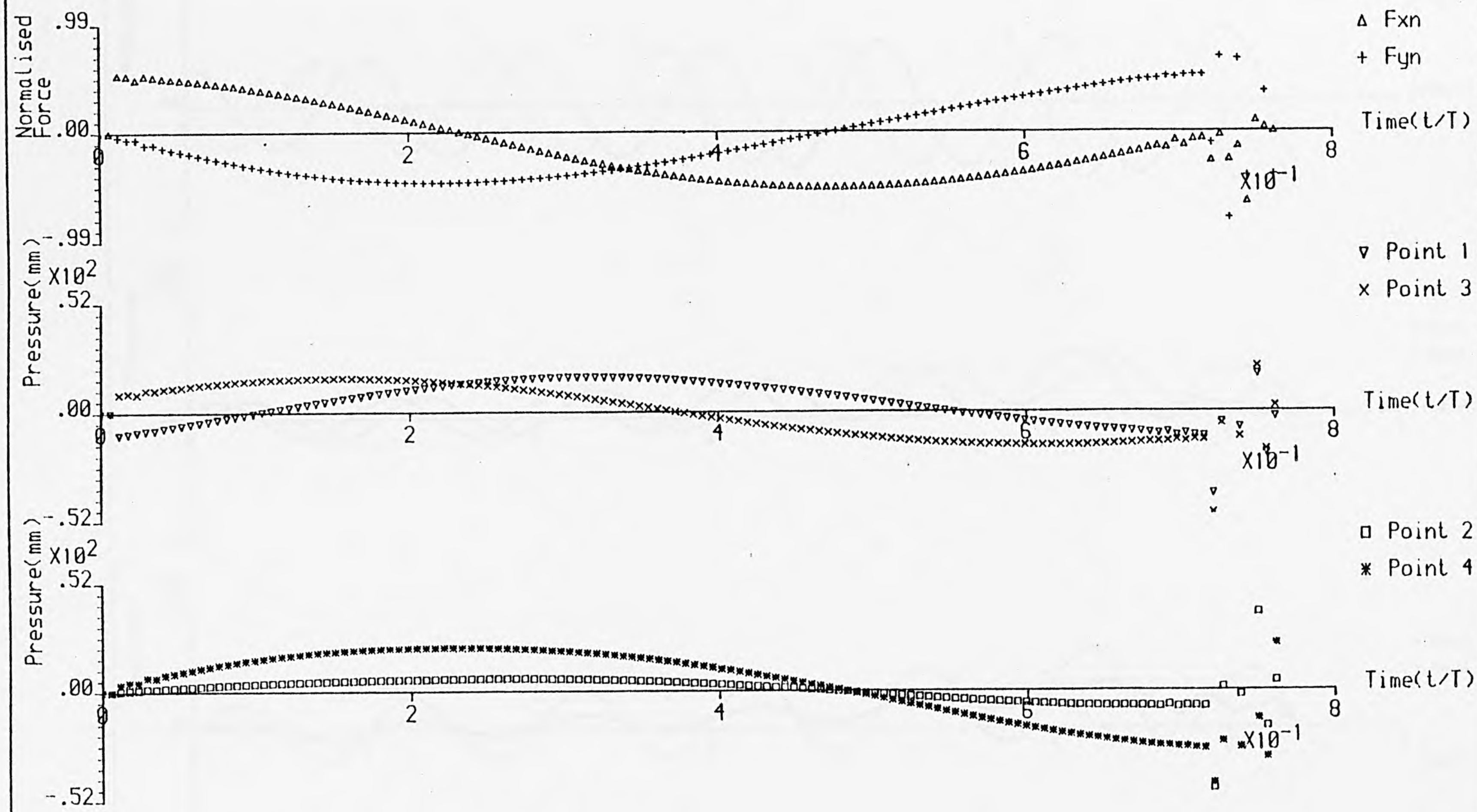

Wave height	=	.112m.	Centre X	=	.566m.
Wavelength	=	1.132m.	Centre Y	=	-.225m.
Undisturbed W.L.	=	.555m.	Radius	=	.055m.
Order of eq.	=	1			

Fig. A.13.22f

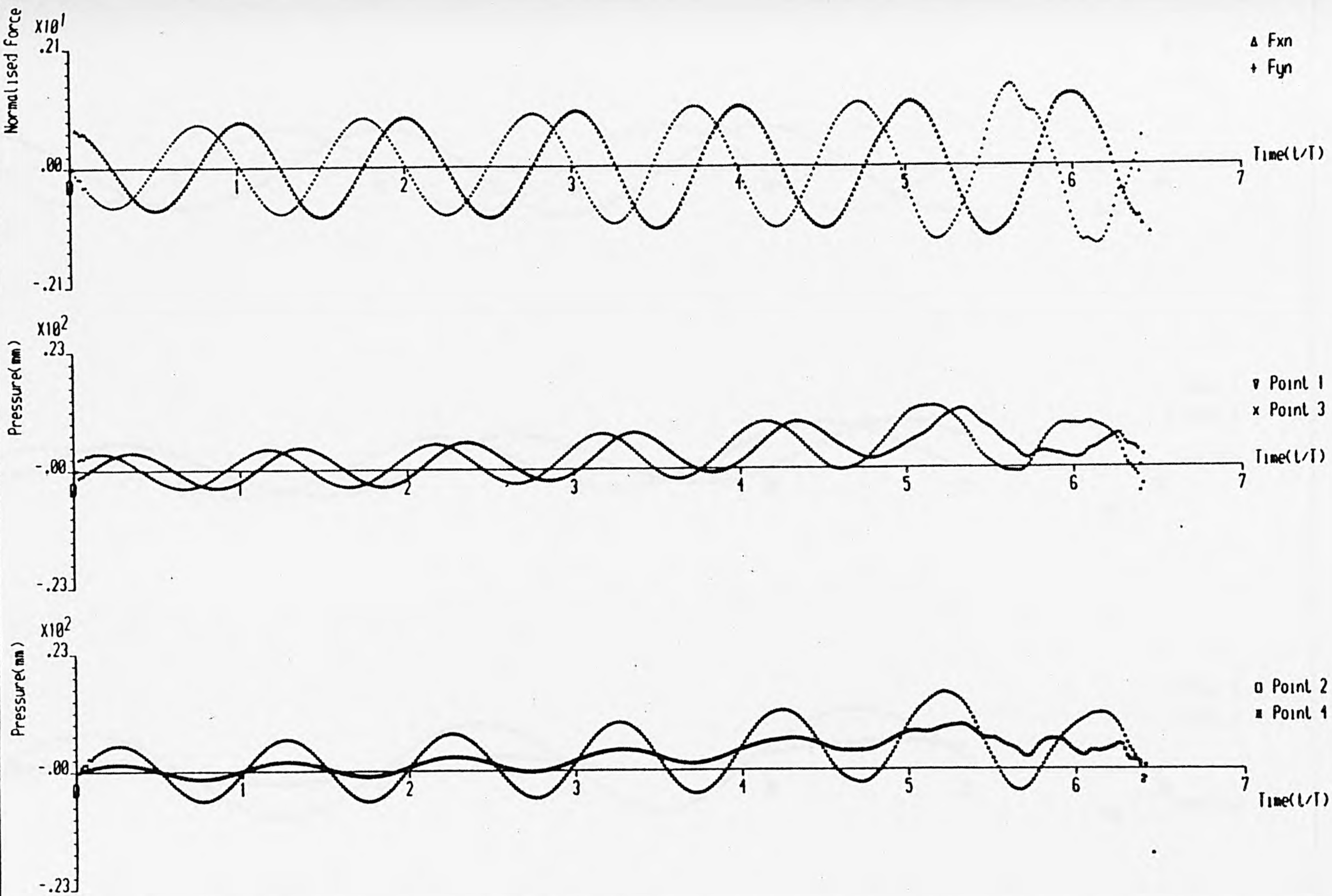

Wave height = .017m.		Centre X =	.566m.
Wavelength = 1.132m.		Centre Y =	-.168m.
Undisturbed W.L.= .555m.		Radius =	.055m.
Order of eq. = 1			

Fig. A.13. 23 Auxiliary graphs for case No. 23

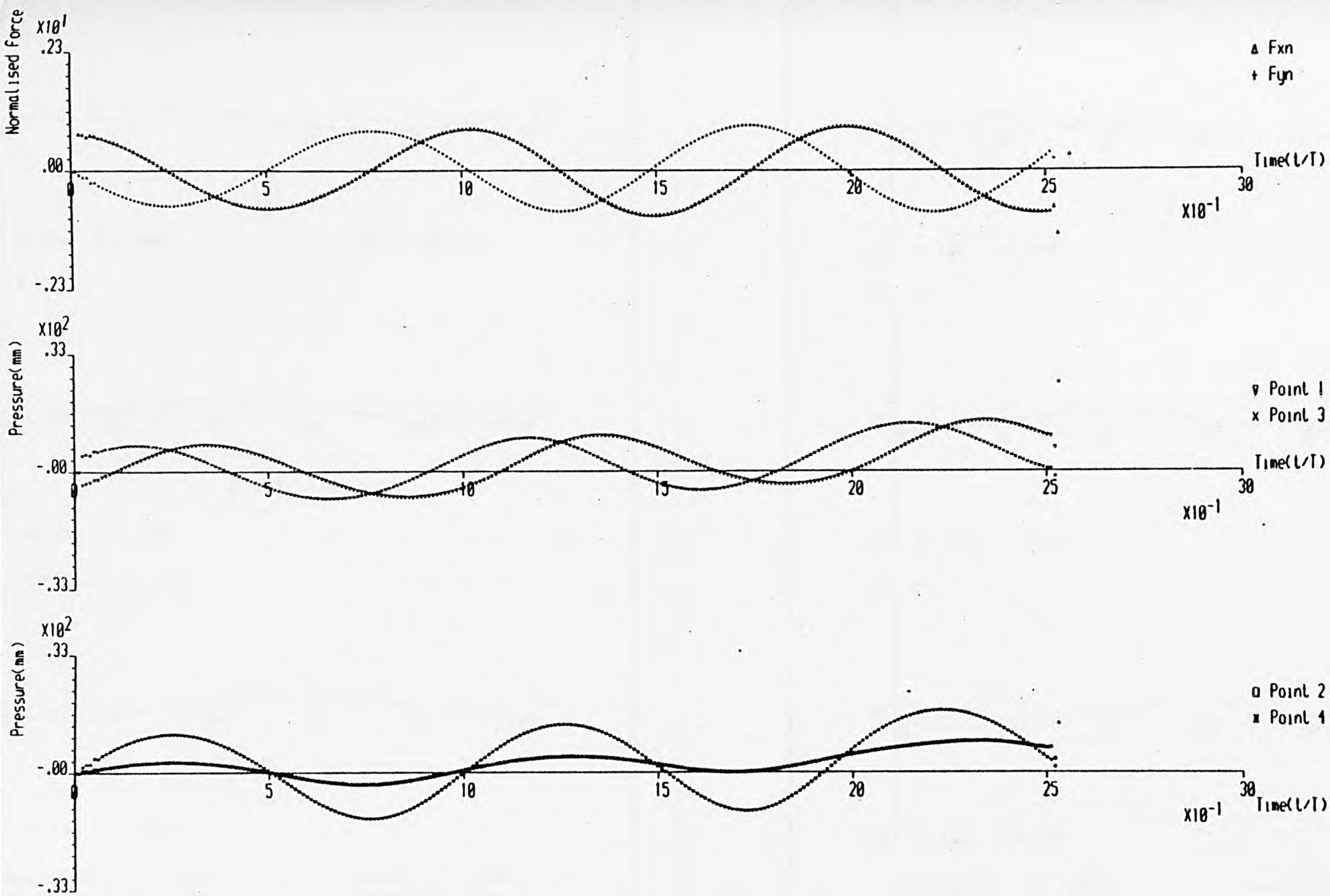

Wave height	=	.037m.
Wavelength	=	1.132m.
Undisturbed W.L.	=	.555m.
Order of eq.	=	1

Centre X	=	.566m.
Centre Y	=	-.168m.
Radius	=	.055m.

Fig. A.13. 24 Auxiliary graphs for case No. 24

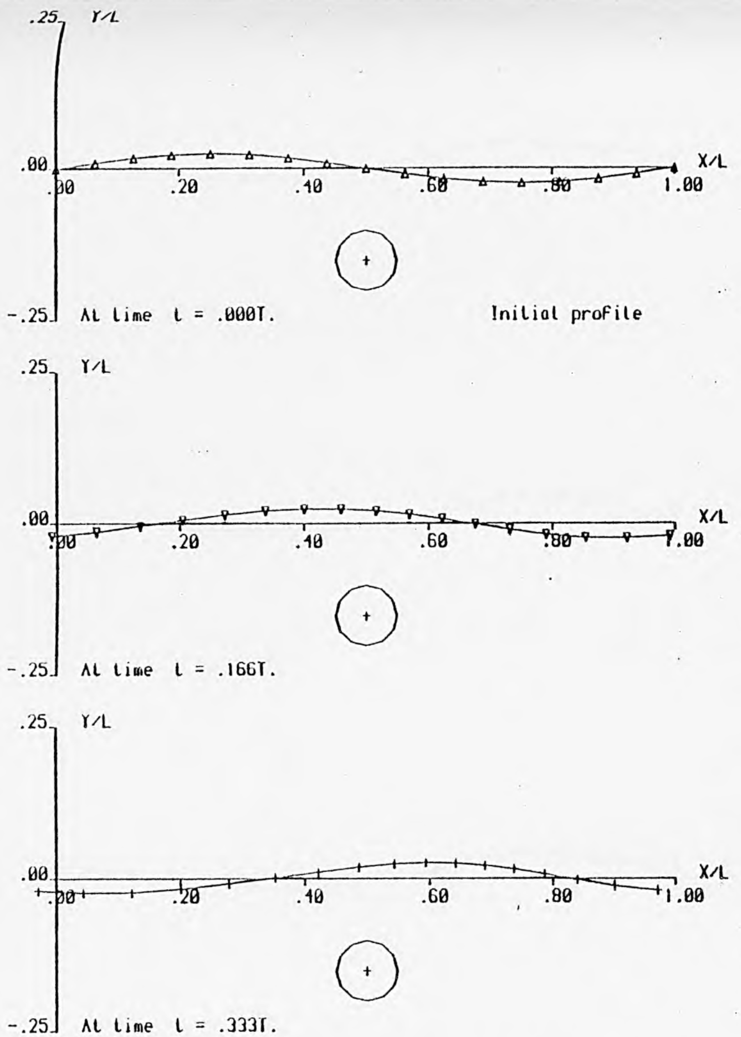

Wave height = .055m.
Wavelength = 1.132m.
Undisturbed W.L.= .555m.
Order of eq. = 1
Fig. A.13.25a

Centre X = .566m.
Centre Y = -.168m.
Radius = .055m.

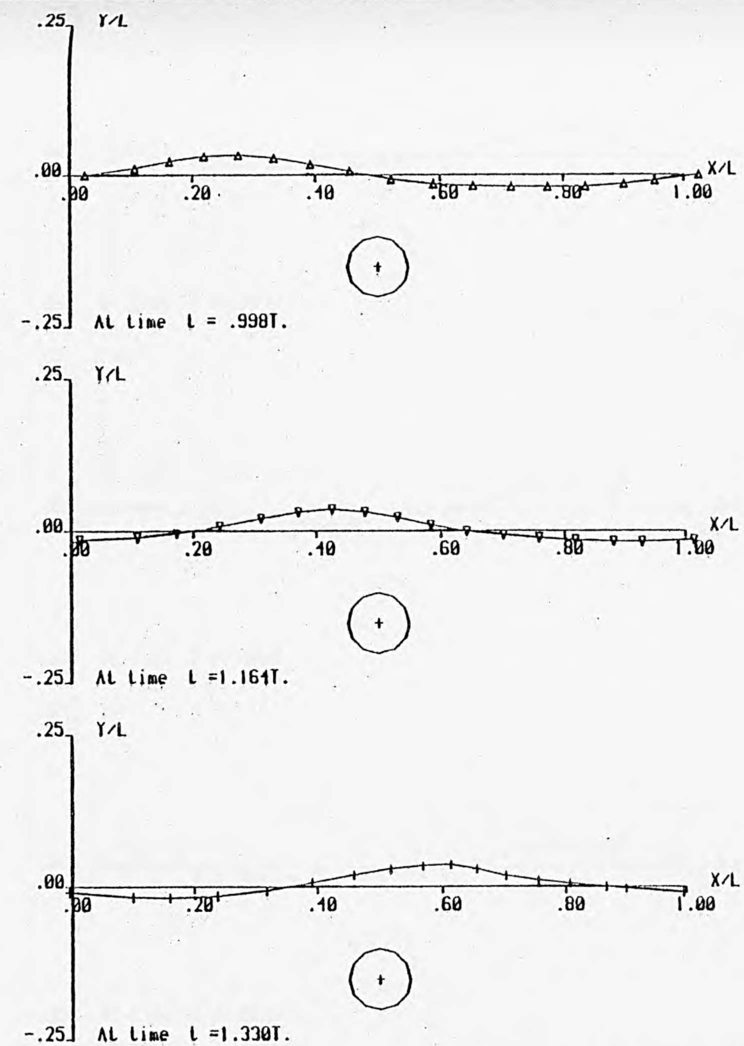

Wave height = .055m.
Wavelength = 1.132m.
Undisturbed W.L.= .555m.
Order of eq. = 1
Fig.A.13.25b

Centre X = .566m.
Centre Y = -.168m.
Radius = .055m.

Fig. A.13.25(a - h) A time sequence of wave profiles and auxiliary graphs for case No. 25

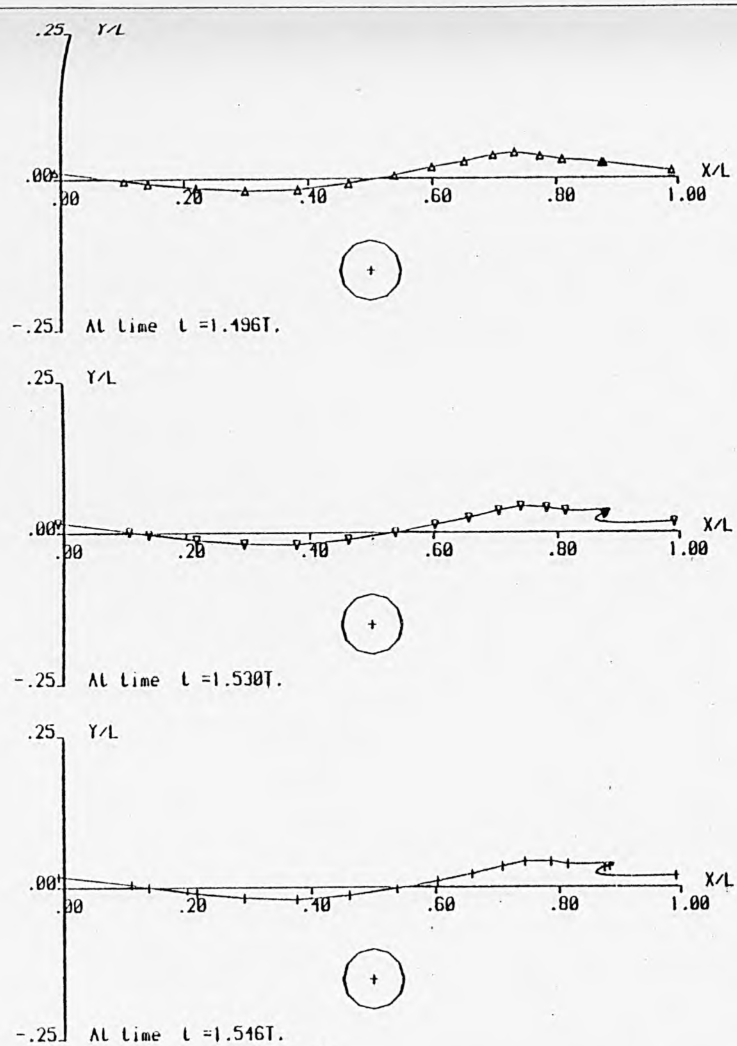

Wave height	=	.055m.	Centre X	=	.566m.
Wavelength	=	1.132m.	Centre Y	=	-.168m.
Undisturbed W.L.	=	.555m.	Radius	=	.055m.
Order of eq.	=	1			

Fig. A.13.25c

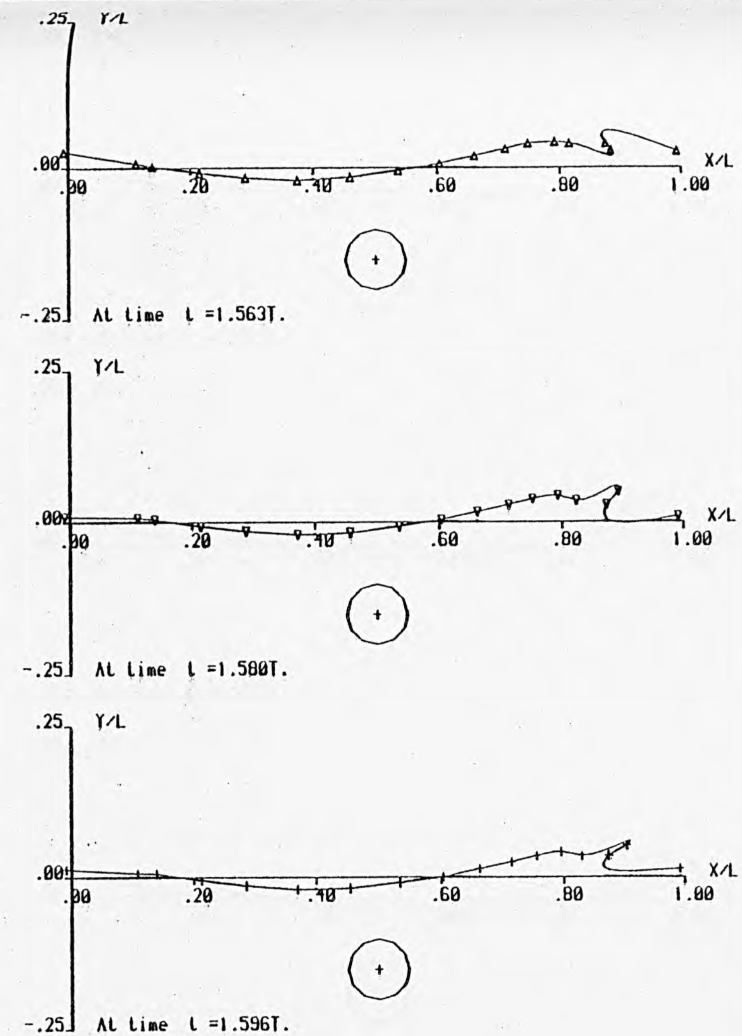

Wave height	=	.055m.	Centre X	=	.566m.
Wavelength	=	1.132m.	Centre Y	=	-.168m.
Undisturbed W.L.	=	.555m.	Radius	=	.055m.
Order of eq.	=	1			

Fig. A.13.25d

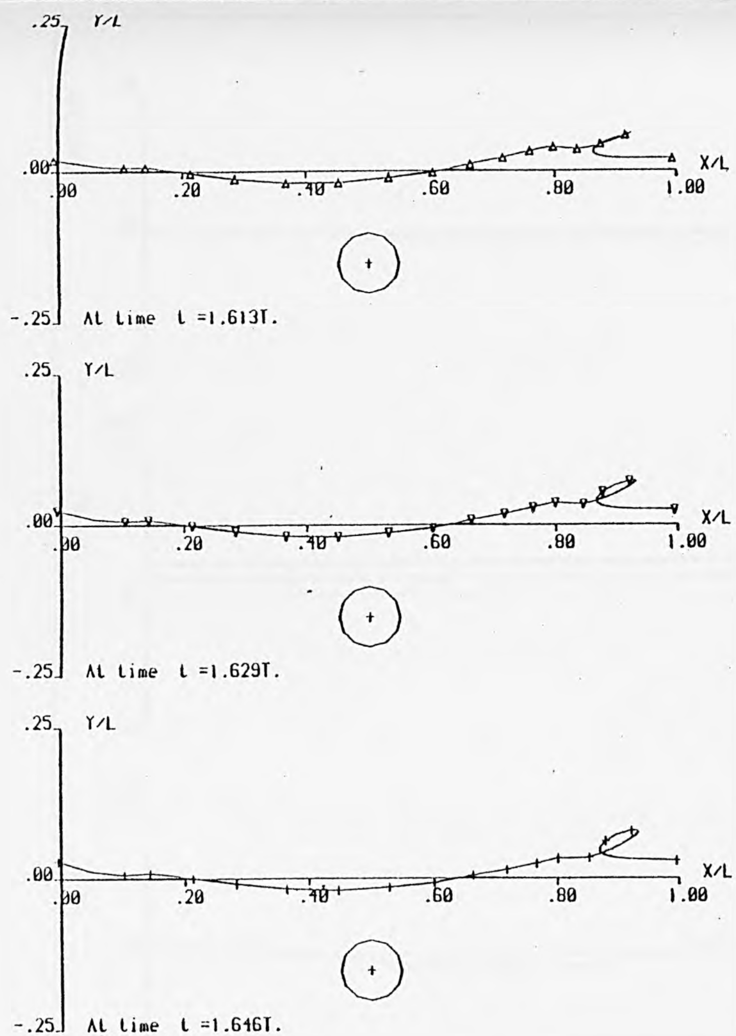

Wave height = .055m.
Wavelength = 1.132m.
Undisturbed W.L.= .555m.
Order of eq. = 1
Centre X = .566m.
Centre Y = -.168m.
Radius = .055m.
Fig. A.13.25e

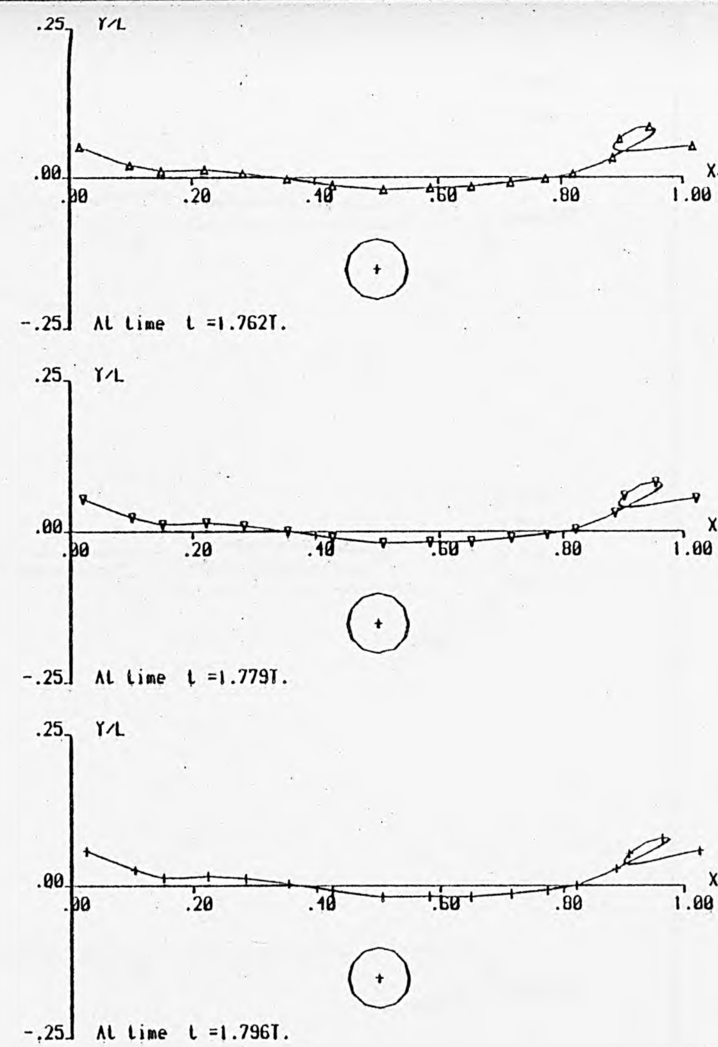

Wave height = .055m.
Wavelength = 1.132m.
Undisturbed W.L.= .555m.
Order of eq. = 1
Centre X = .566m.
Centre Y = -.168m.
Radius = .055m.
Fig. A.13.25f

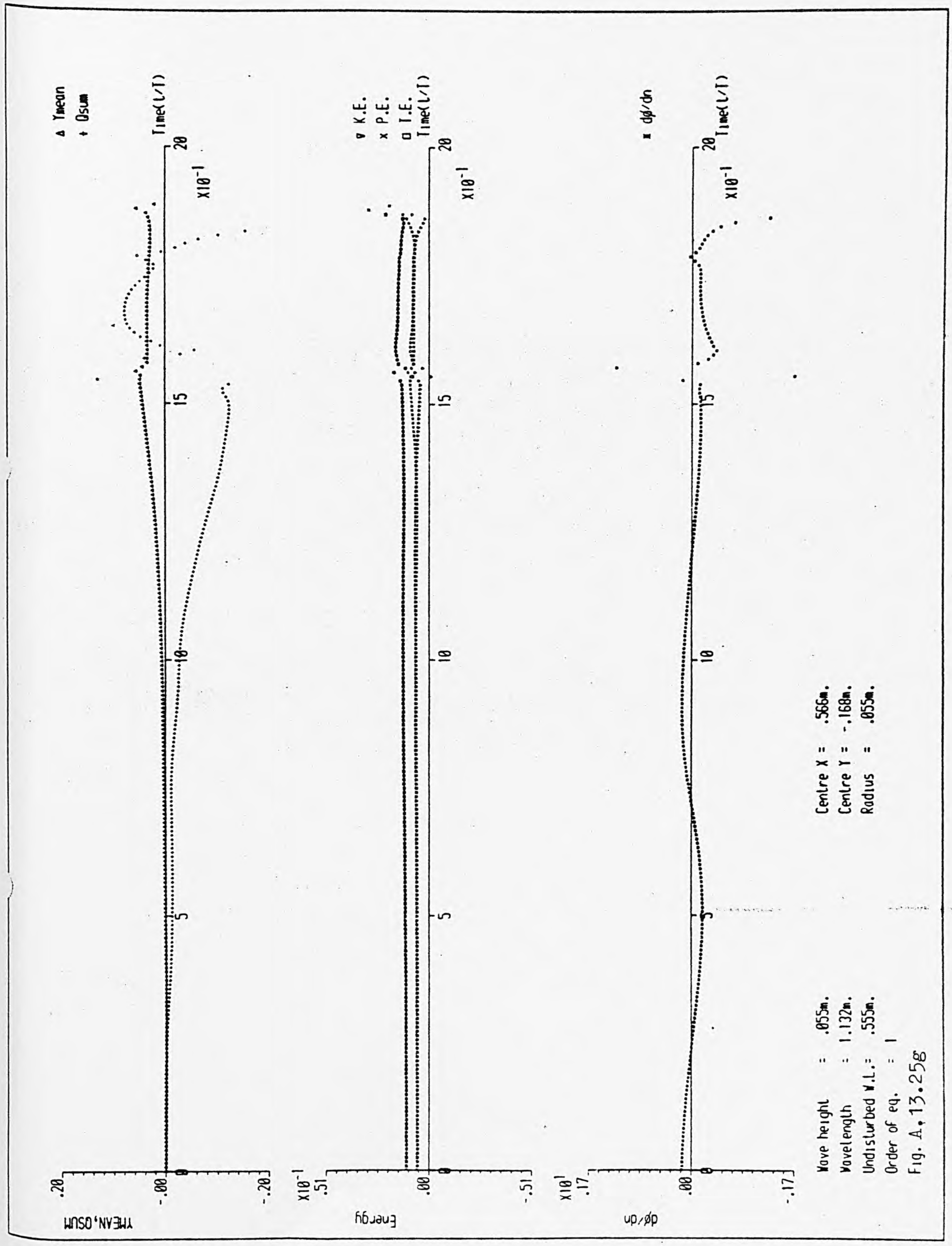
YMEAN,QSUM
.20
-.00
-.20
Δ Ymean
+ Qsum
Time(L/T)
X10^-1
5
10
15
20
Energy
X10^-1 .51
.00
-.51
∇ K.E.
x P.E.
□ T.E.
dφ/dn
X10^1 .17
-.17
Wave height : .055m.
Wavelength : 1.132m.
Undisturbed W.L.: .555m.
Order of eq. : 1
Centre X = .566m.
Centre Y = -.168m.
Radius = .055m.

Fig. A.13.25g

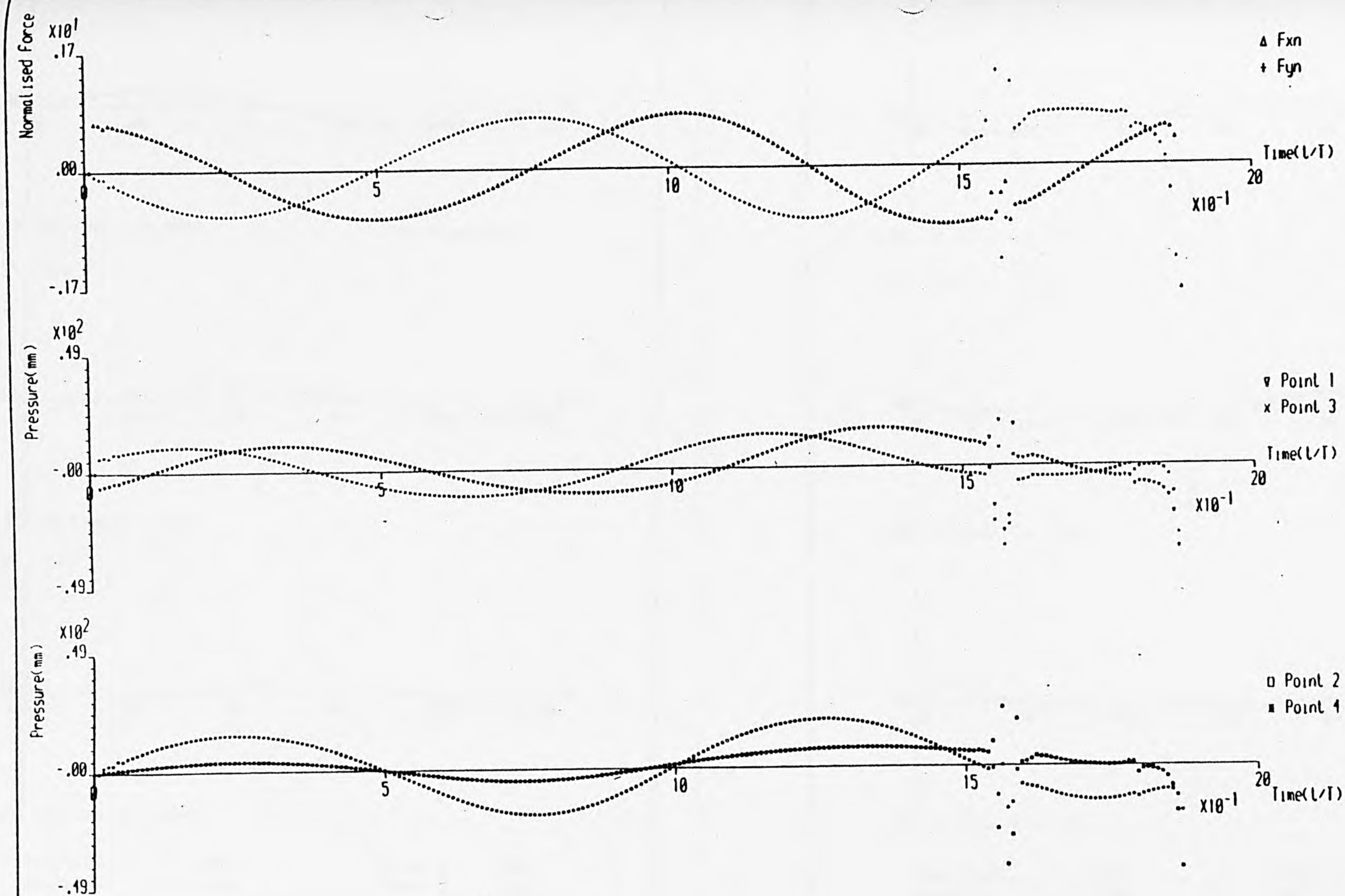

Wave height = .055m.
Wavelength = 1.132m.
Undisturbed W.L.= .555m.
Order of eq. = 1

Centre X = .566m.
Centre Y = -.168m.
Radius = .055m.

Fig. A.13.25h

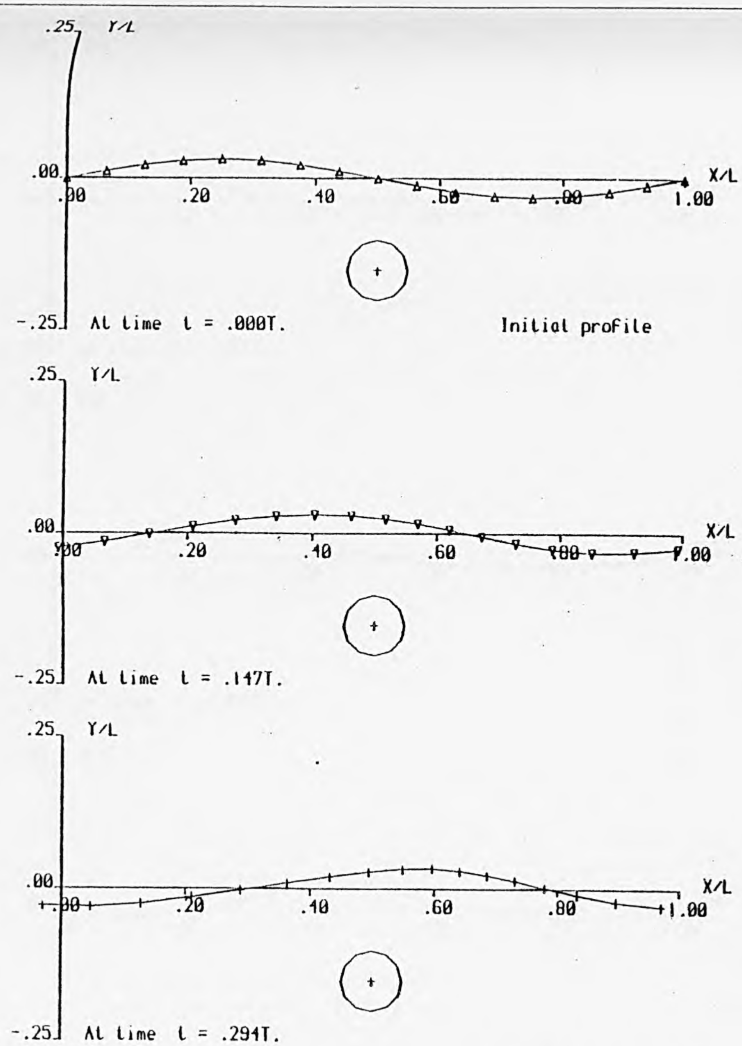

Wave height = .070m.
Wavelength = 1.132m.
Undisturbed W.L.= .555m.
Order of eq. = 1

Centre X = .566m.
Centre Y = -.168m.
Radius = .055m.

Fig. A.13.26a

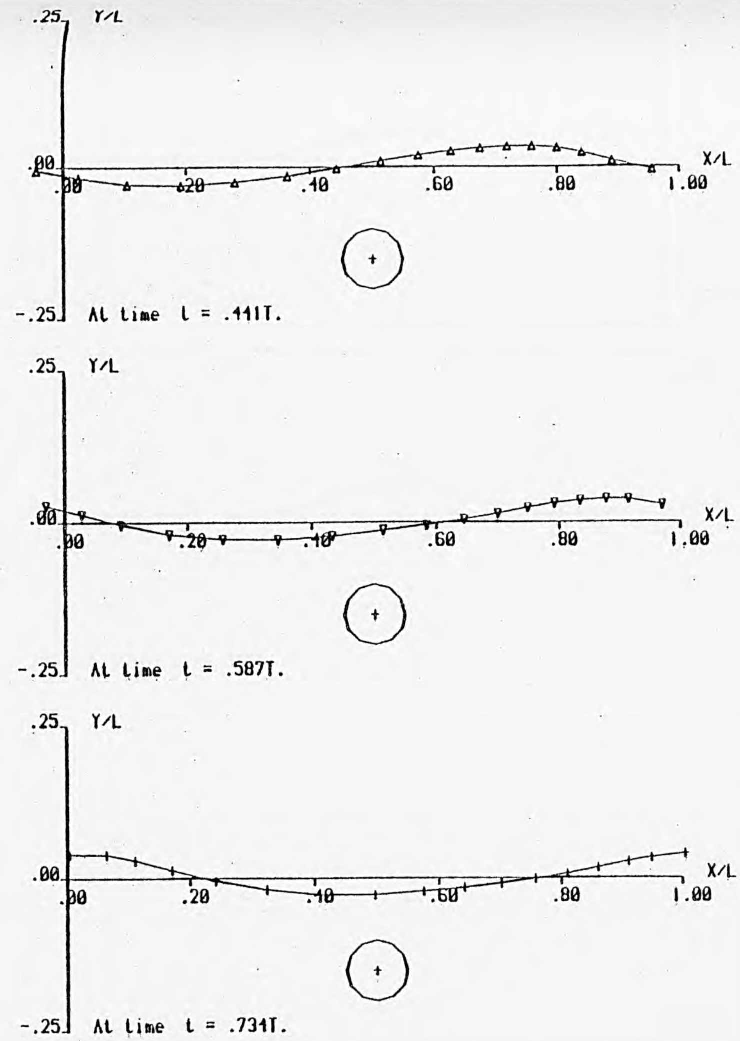

Wave height = .070m.
Wavelength = 1.132m.
Undisturbed W.L.= .555m.
Order of eq. = 1

Centre X = .566m.
Centre Y = -.168m.
Radius = .055m.

Fig. A.13.26b

Fig. A.13.26(a - f) A time sequence of wave profiles and auxiliary graphs for case No. 26

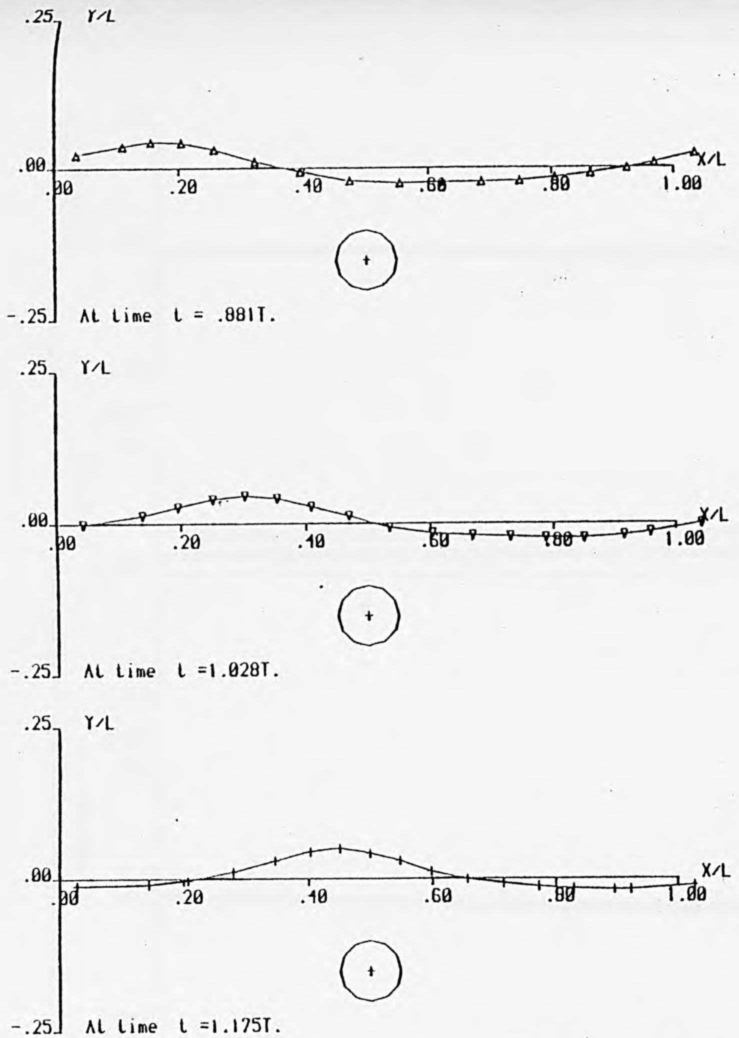

Wave height = .070m.
Wavelength = 1.132m.
Undisturbed W.L.= .555m.
Order of eq. = 1

Centre X = .566m.
Centre Y = -.168m.
Radius = .055m.

Fig. A.13.26c

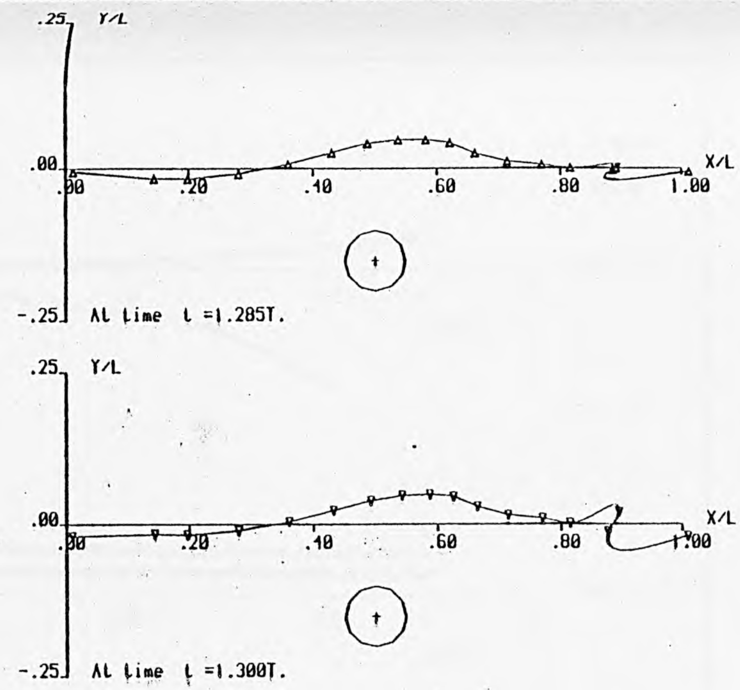

Wave height = .070m.
Wavelength = 1.132m.
Undisturbed W.L.= .555m.
Order of eq. = 1

Centre X = .566m.
Centre Y = -.168m.
Radius = .055m.

Fig. A.13.26d

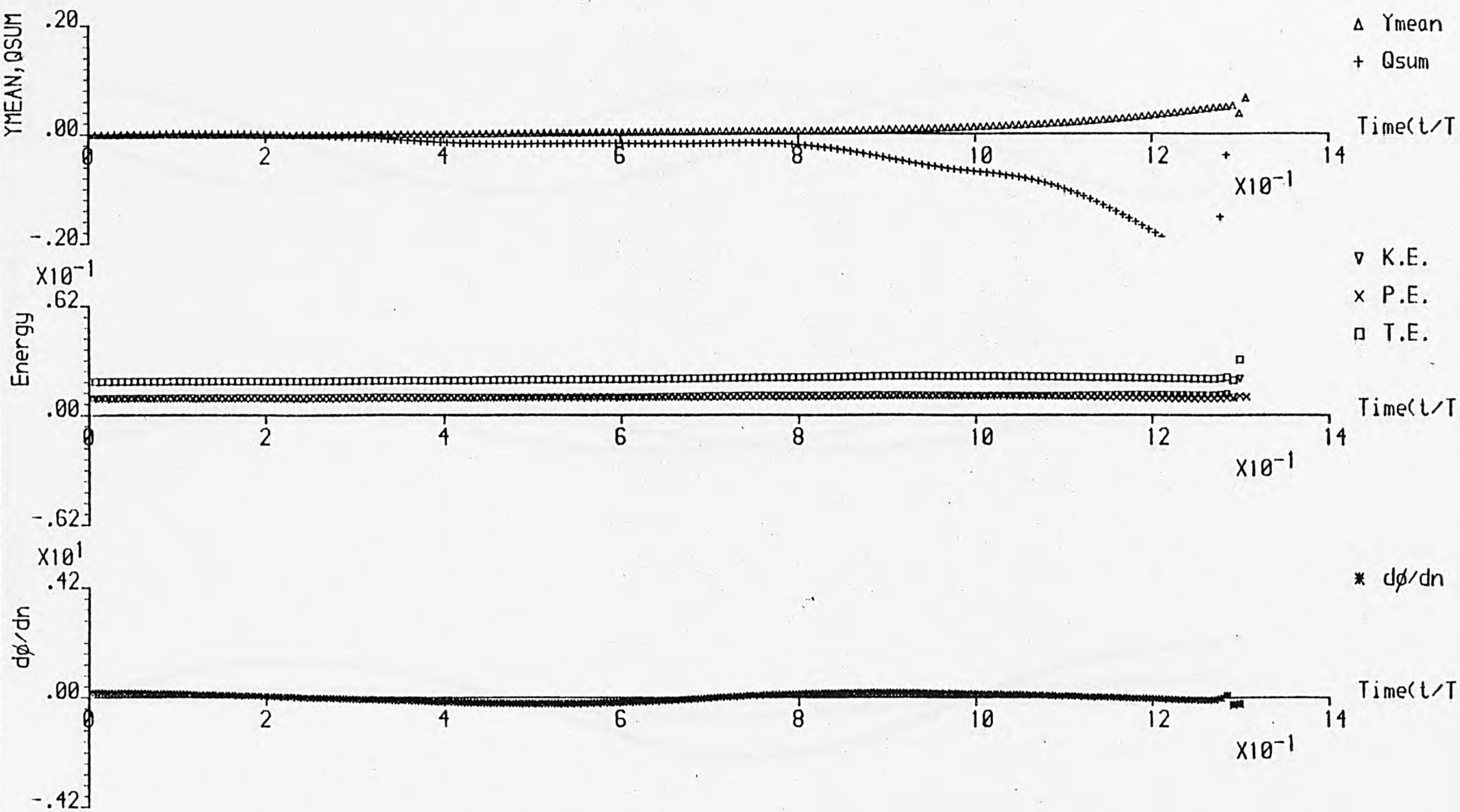

Wave height = .070m. Centre X = .566m.
Wavelength = 1.132m. Centre Y = -.168m.
Undisturbed W.L.= .555m. Radius = .055m.
Order of eq. = 1

Fig. A.13.26e

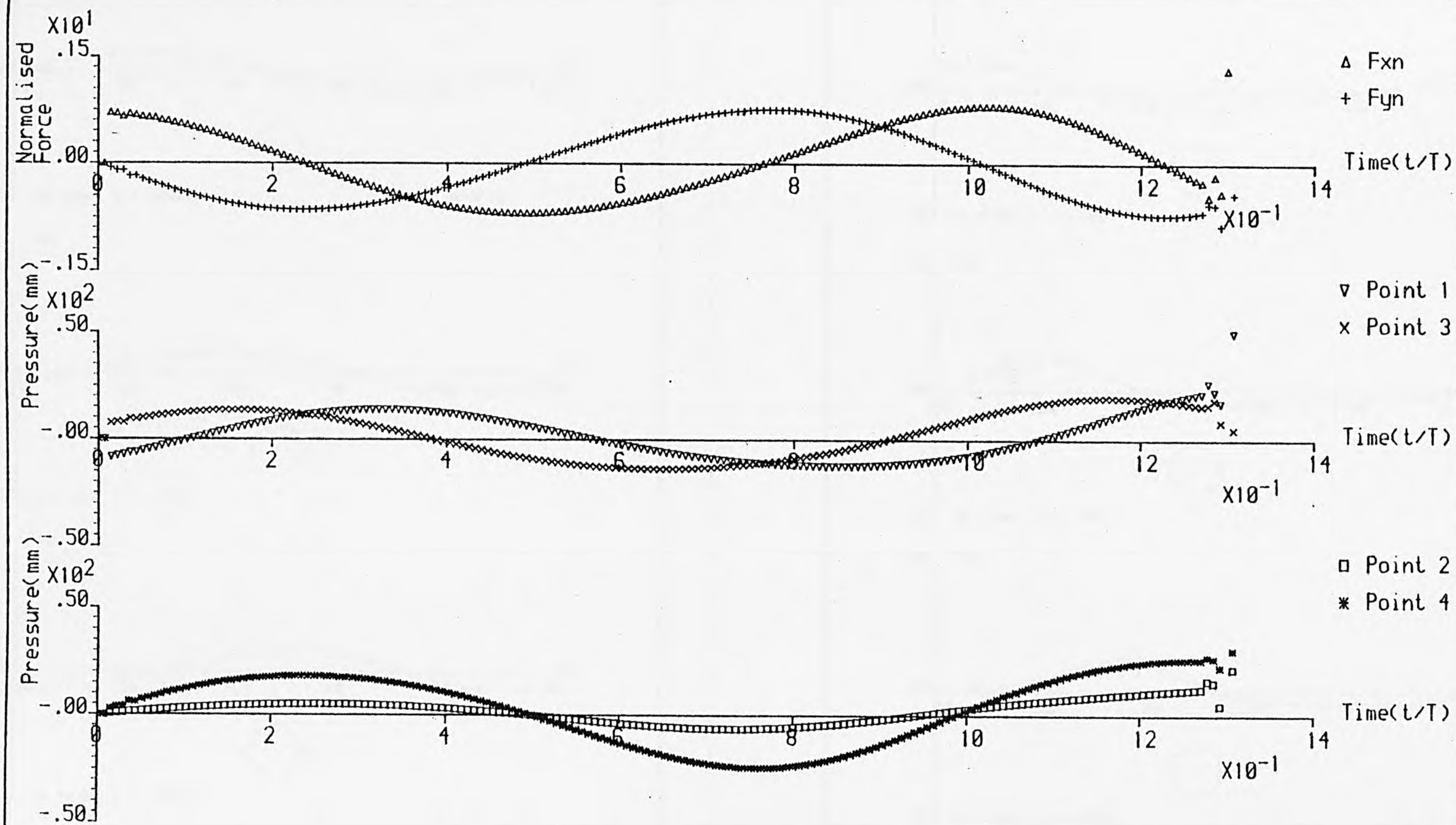

Wave height = .070m. Centre X = .566m.
Wavelength = 1.132m. Centre Y = -.168m.
Undisturbed W.L.= .555m. Radius = .055m.
Order of eq. = 1

Fig. A.13.26f

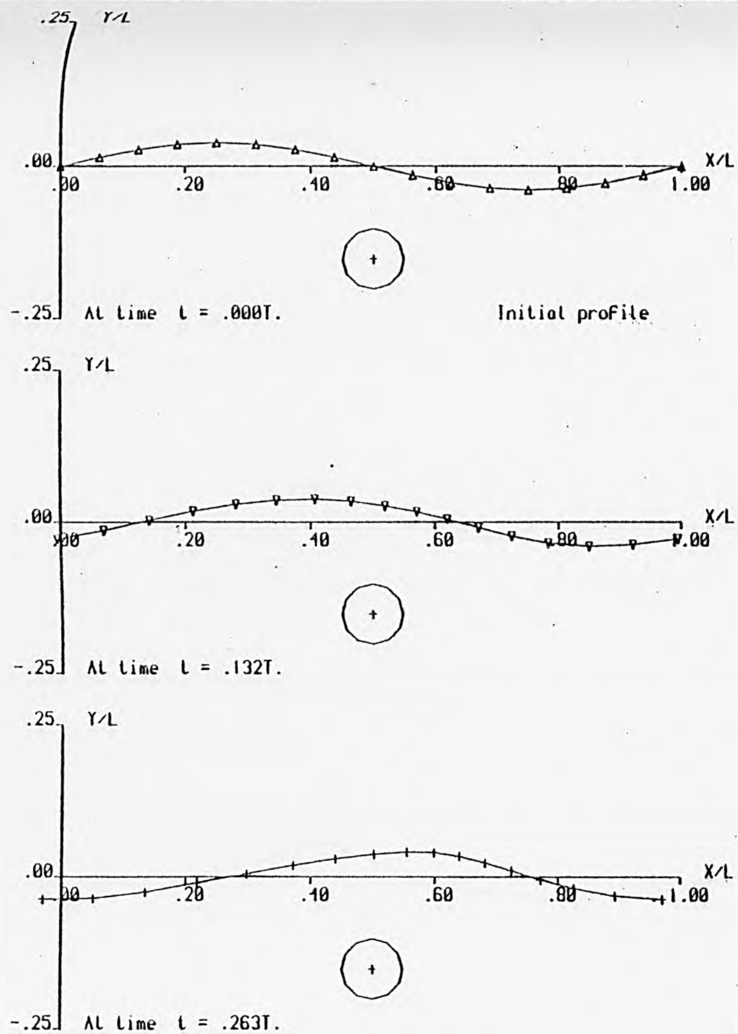

Wave height = .087m.
Wavelength = 1.132m.
Undisturbed W.L.= .555m.
Order of eq. = 1
Fig. A.13.27a

Centre X = .566m.
Centre Y = -.168m.
Radius = .055m.

Fig. A.13.27(a – f) A time sequence of wave profiles and auxiliary graphs for case No. 27

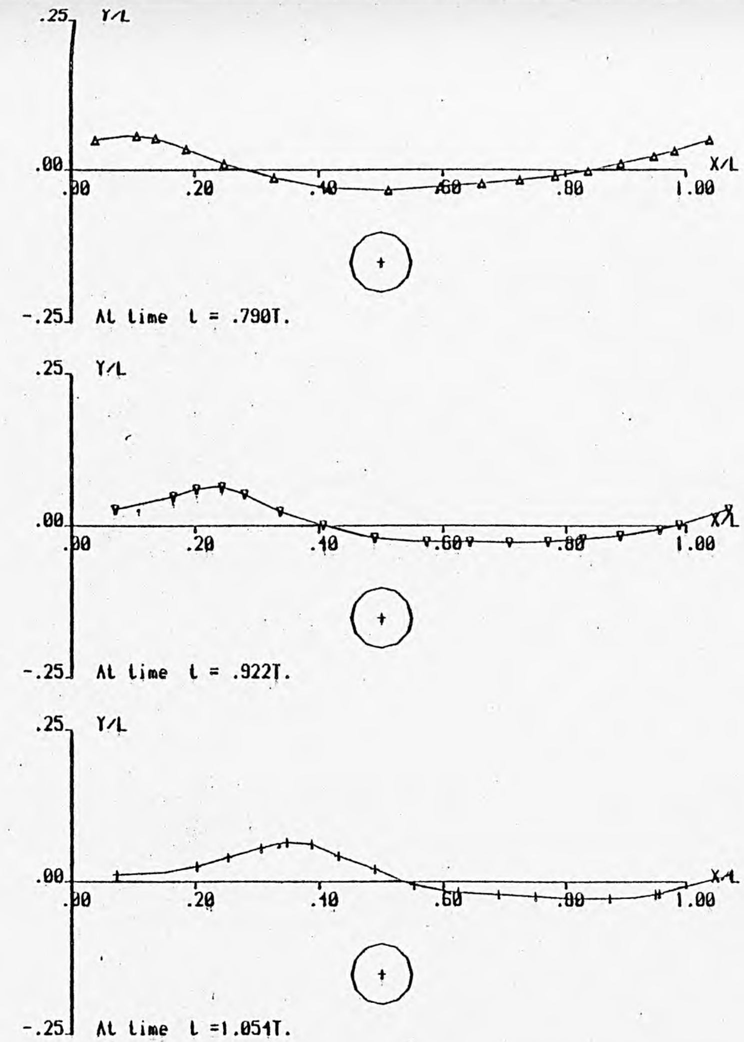

Wave height = .087m.
Wavelength = 1.132m.
Undisturbed W.L.= .555m.
Order of eq. = 1
Fig. A.13.27b

Centre X = .566m.
Centre Y = -.168m.
Radius = .055m.

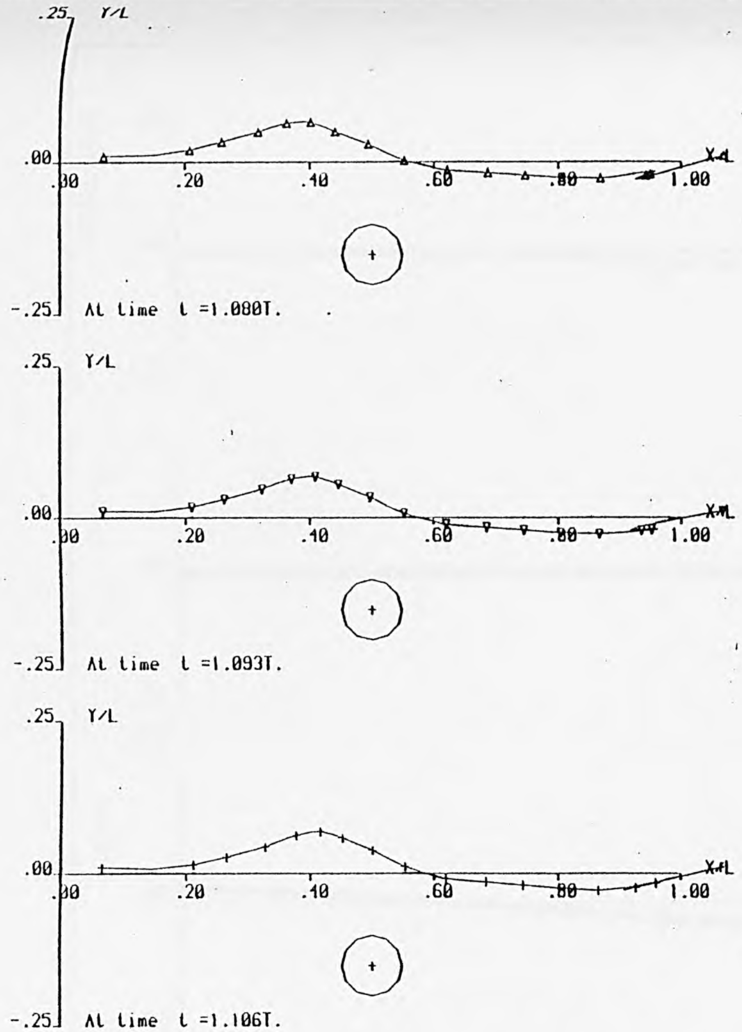

Wave height	= .087m.	Centre X =	.566m.
Wavelength	= 1.132m.	Centre Y =	-.168m.
Undisturbed W.L.=	.555m.	Radius =	.055m.
Order of eq.	= 1		

Fig. A.13.27c

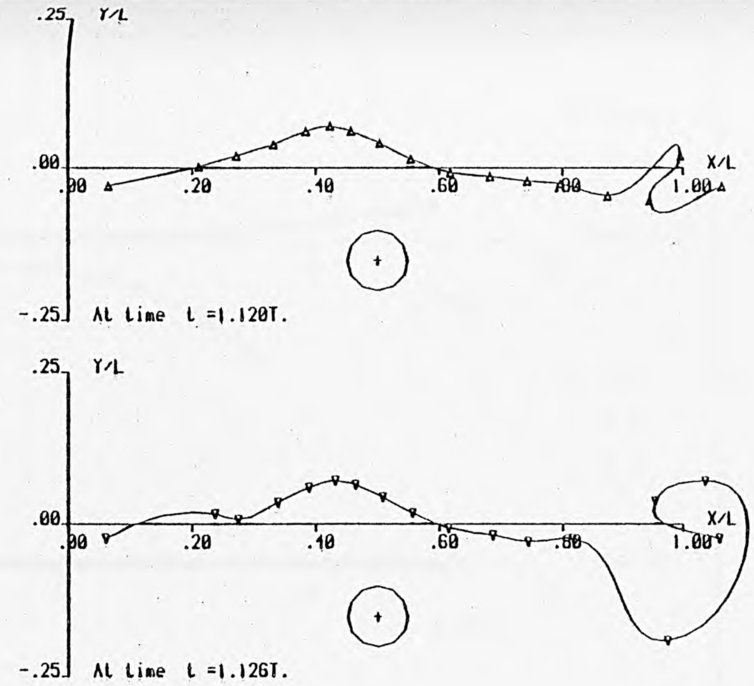

Wave height	= .087m.	Centre X =	.566m.
Wavelength	= 1.132m.	Centre Y =	-.168m.
Undisturbed W.L.=	.555m.	Radius =	.055m.
Order of eq.	= 1		

Fig. A.13.27d

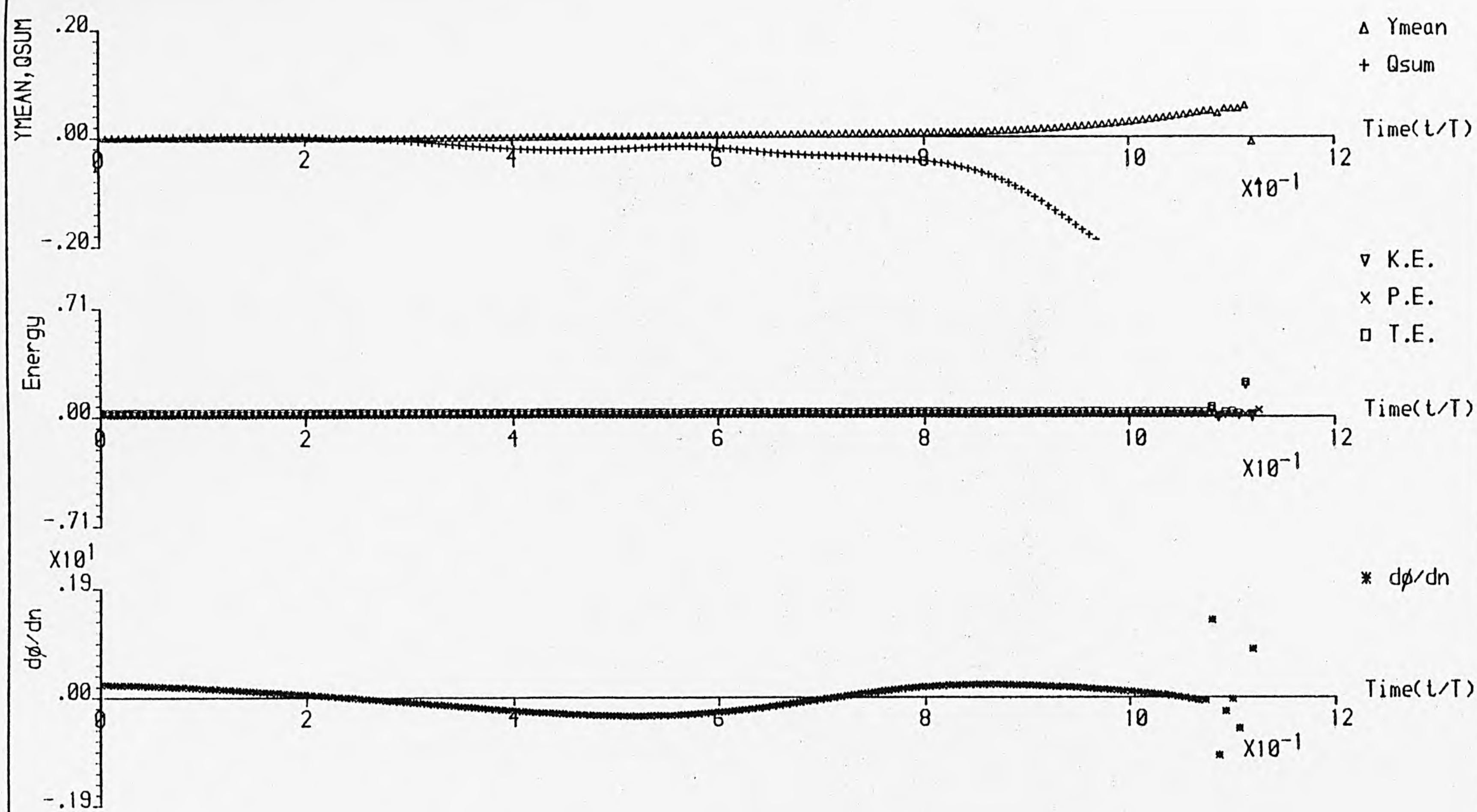

Wave height = .087m. Centre X = .566m.
Wavelength = 1.132m. Centre Y = -.168m.
Undisturbed W.L.= .555m. Radius = .055m.
Order of eq. = 1

Fig. A.13.27e

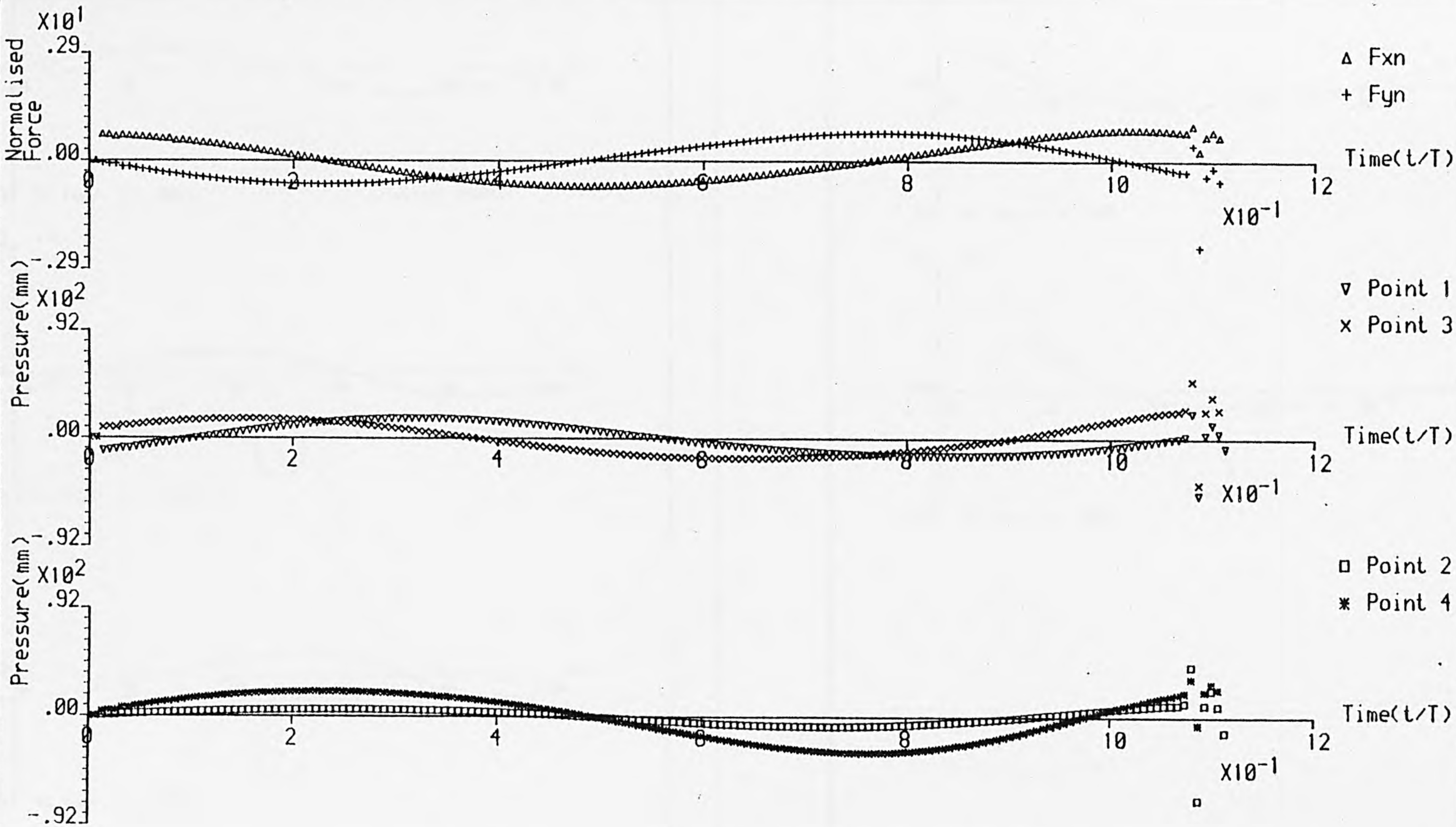

Wave height	=	.087m.	Centre X	=	.566m.
Wavelength	=	1.132m.	Centre Y	=	-.168m.
Undisturbed W.L.	=	.555m.	Radius	=	.055m.
Order of eq.	=	1			

Fig. A.13.27f

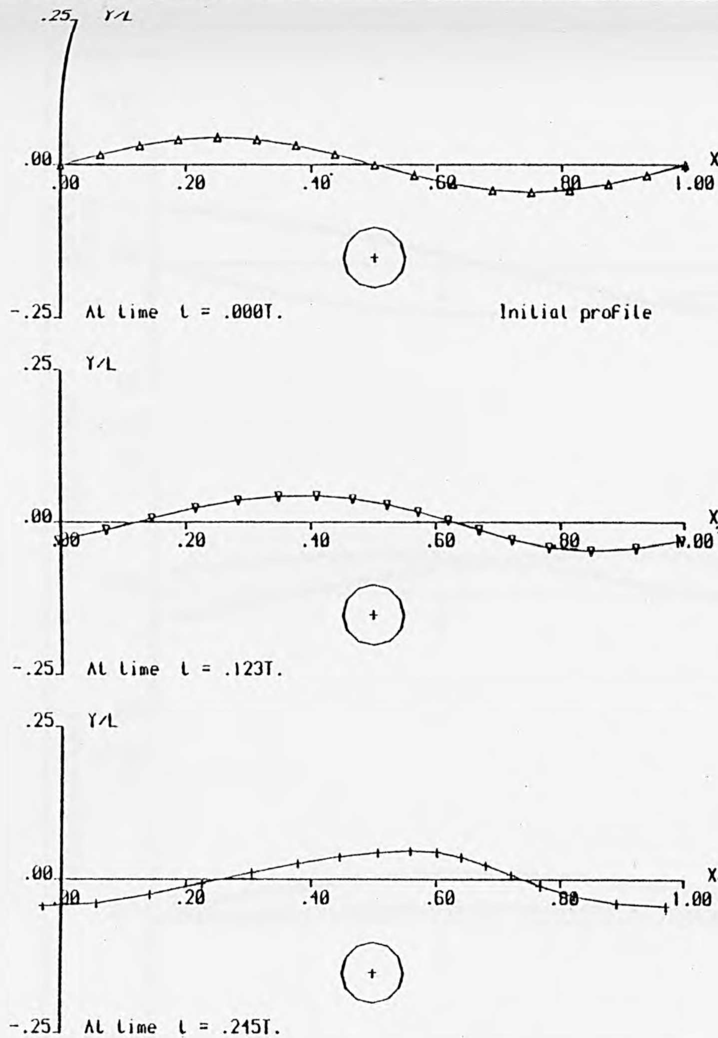

Wave height = .100m.
Wavelength = 1.132m.
Undisturbed W.L.= .555m.
Order of eq. = 1
Fig. A.13.28a

Centre X = .566m.
Centre Y = -.168m.
Radius = .055m.

Fig. A.13.28(a - d) A time sequence of wave profiles and auxiliary graphs for case No. 28

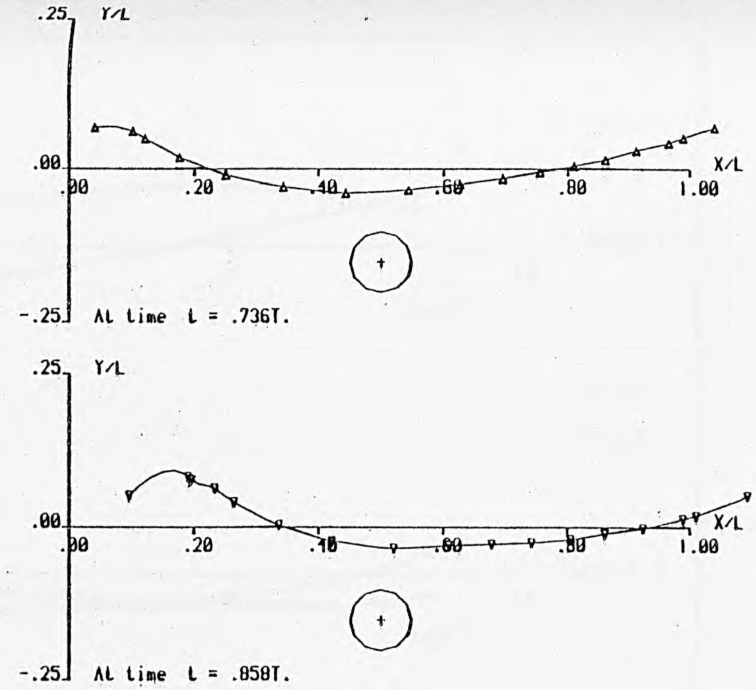

Wave height = .100m.
Wavelength = 1.132m.
Undisturbed W.L.= .555m.
Order of eq. = 1
Fig. A.13.28b

Centre X = .566m.
Centre Y = -.168m.
Radius = .055m.

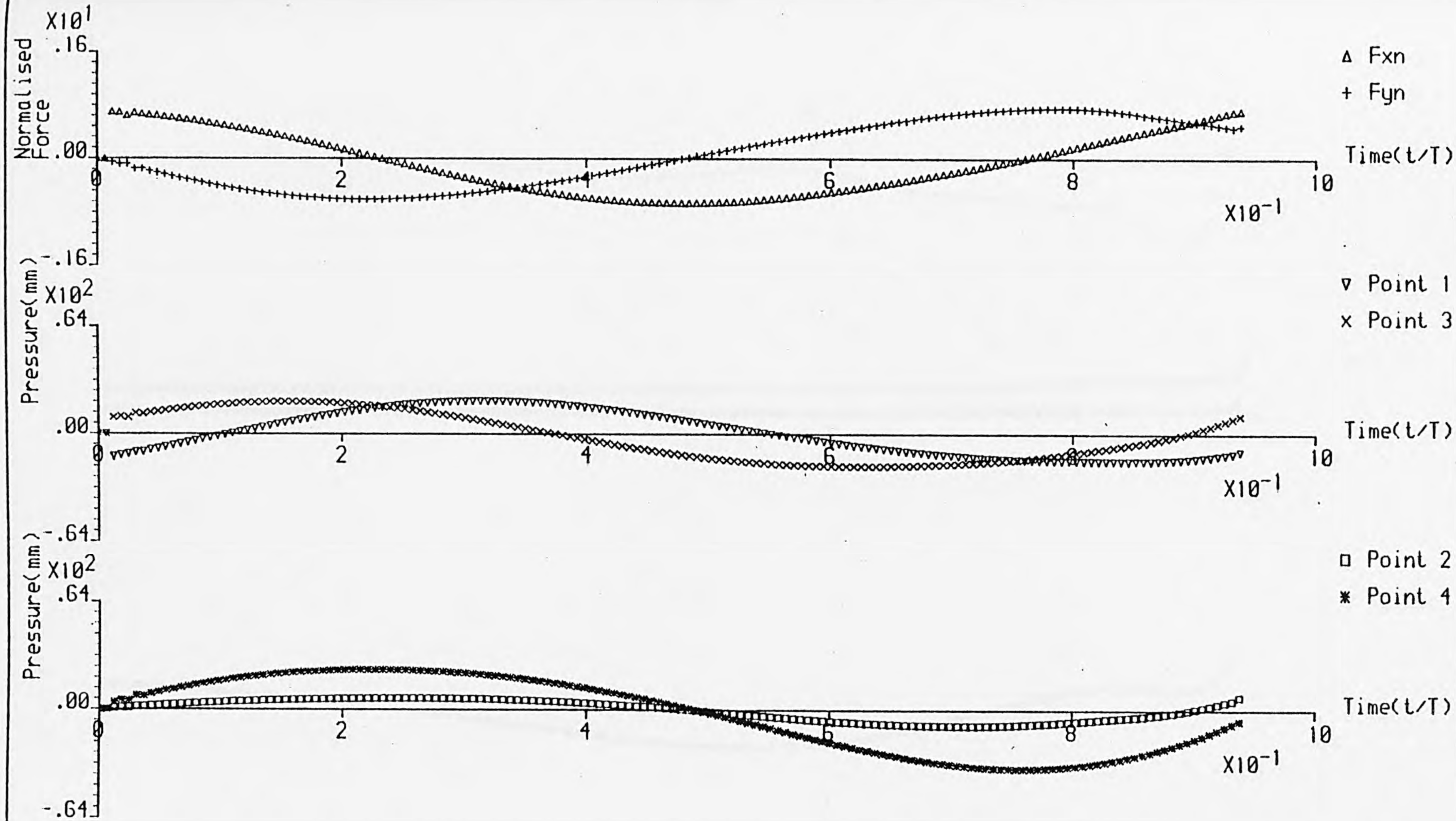

Wave height =	.100m.	Centre X =	.566m.
Wavelength =	1.132m.	Centre Y =	-.168m.
Undisturbed W.L.=	.555m.	Radius =	.055m.
Order of eq. =	1		

Fig. A.13.28c

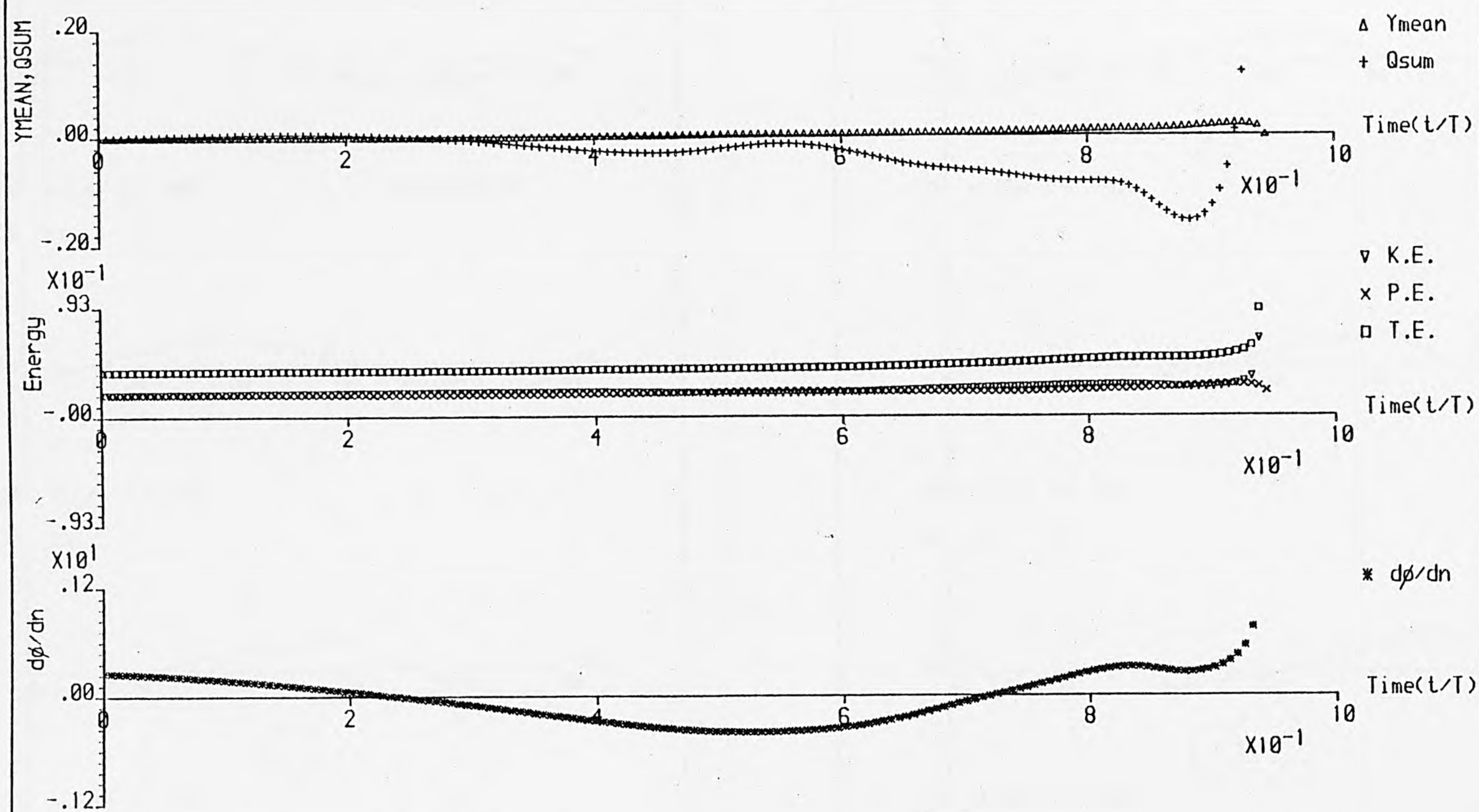

Wave height = .100m. Centre X = .566m.
Wavelength = 1.132m. Centre Y = -.168m.
Undisturbed W.L.= .555m. Radius = .055m.
Order of eq. = 1

Fig. A.13.28d

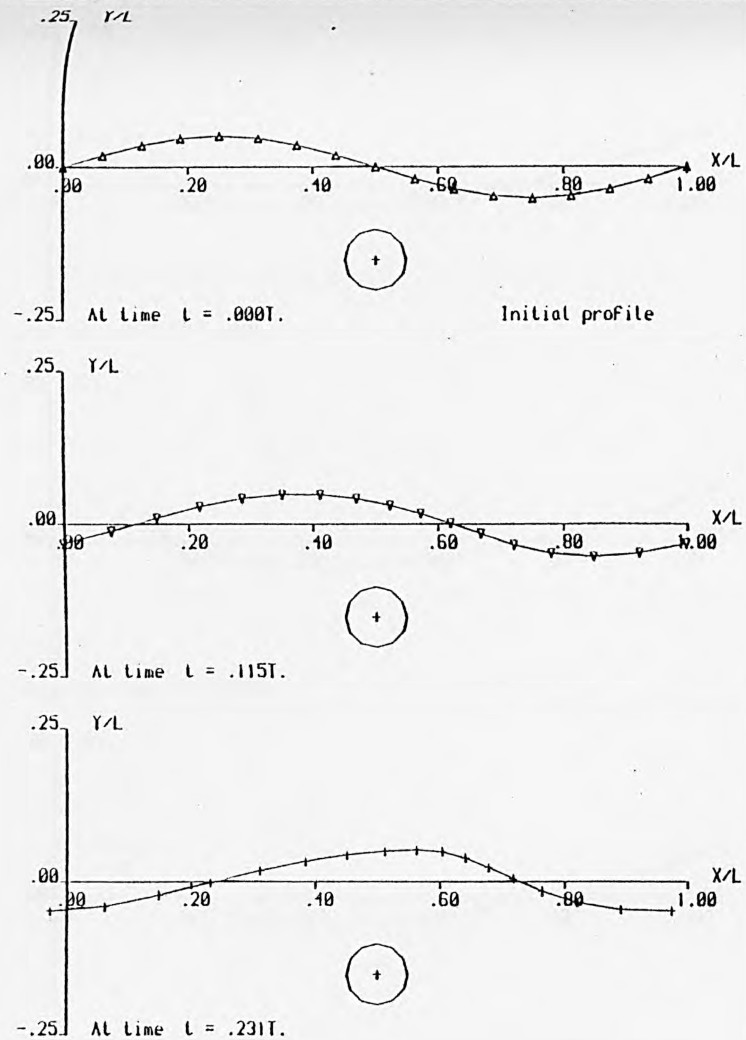

Wave height = .113m.
Wavelength = 1.132m.
Undisturbed W.L.= .555m.
Order of eq. = 1

Centre X = .566m.
Centre Y = -.168m.
Radius = .055m.

Fig. A.13.29a

Fig. A.13.29(a - f) A time sequence of wave profiles and auxiliary graphs for case No. 29

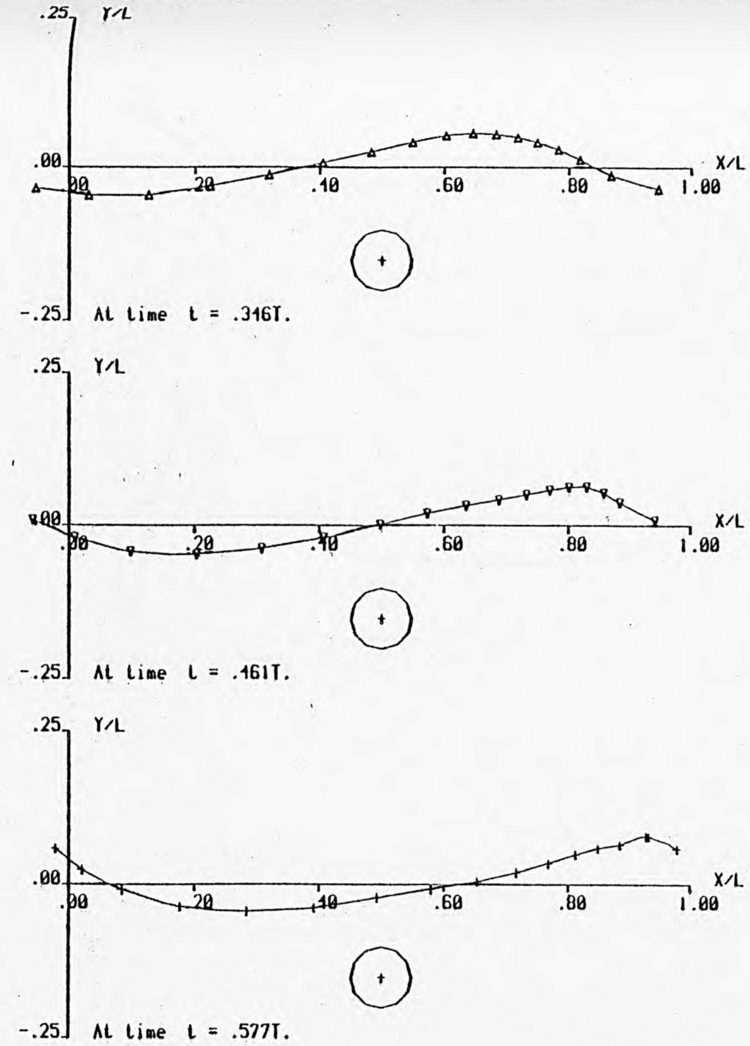

Wave height = .113m.
Wavelength = 1.132m.
Undisturbed W.L.= .555m.
Order of eq. = 1

Centre X = .566m.
Centre Y = -.168m.
Radius = .055m.

Fig. A.13.29b

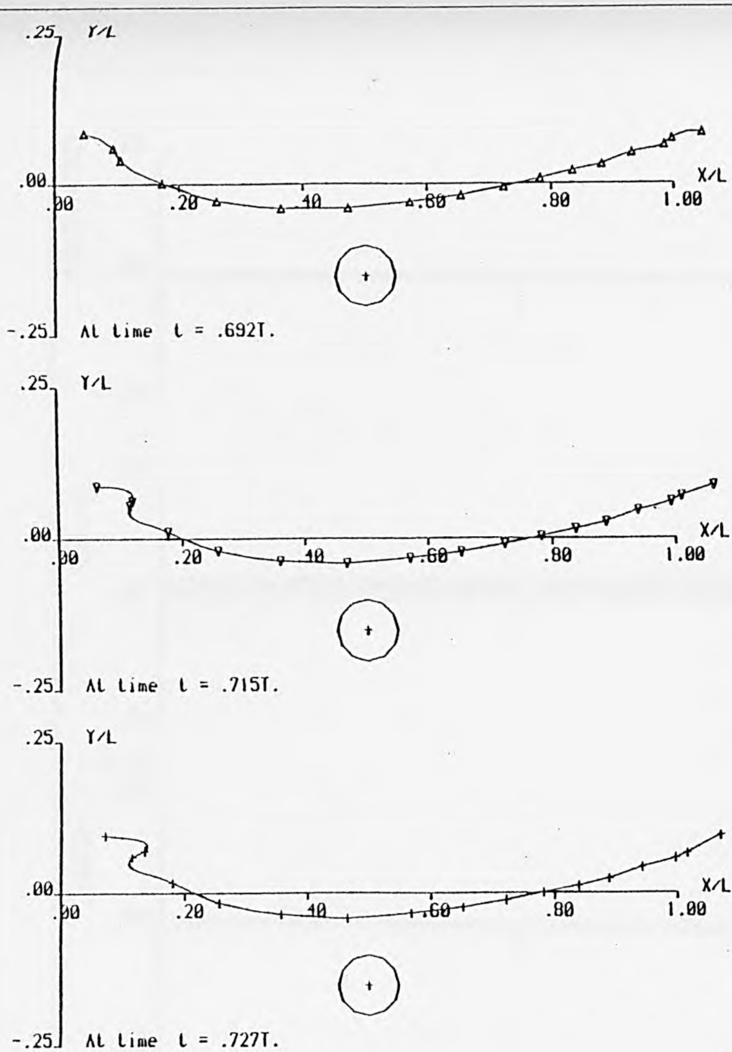

Wave height = .113m.
Wavelength = 1.132m.
Undisturbed W.L.= .555m.
Order of eq. = 1

Centre X = .566m.
Centre Y = -.168m.
Radius = .055m.

Fig. A.13.29c

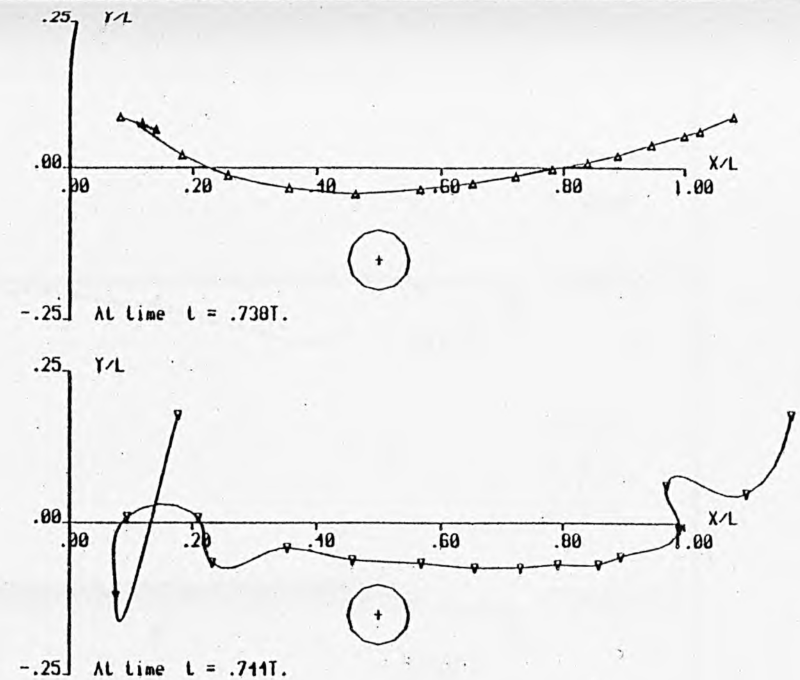

Wave height = .113m.
Wavelength = 1.132m.
Undisturbed W.L.= .555m.
Order of eq. = 1

Centre X = .566m.
Centre Y = -.168m.
Radius = .055m.

Fig. A.13.29d

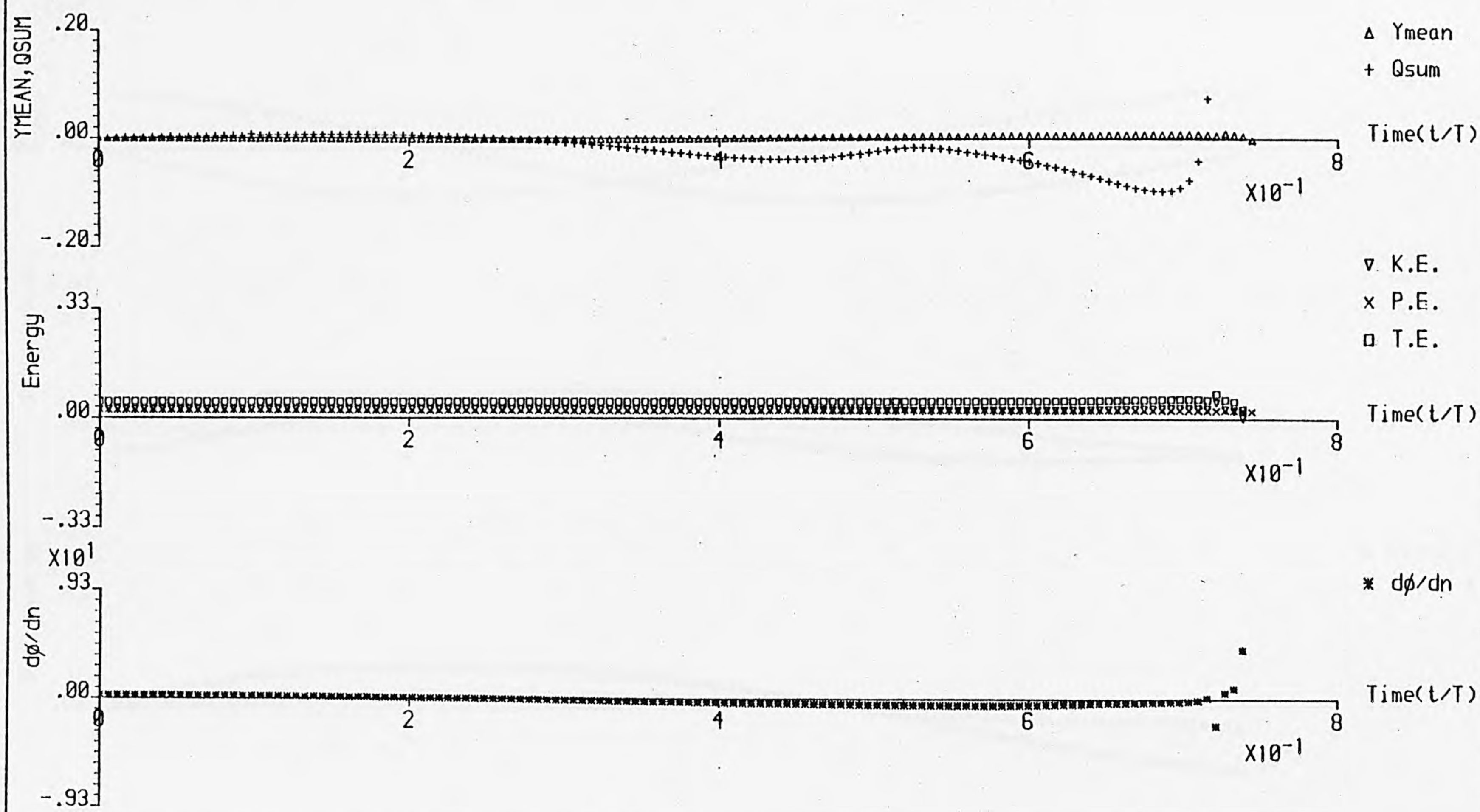

Wave height = .113m. Centre X = .566m.
Wavelength = 1.132m. Centre Y = -.168m.
Undisturbed W.L.= .555m. Radius = .055m.
Order of eq. = 1

Fig. A.13.29e

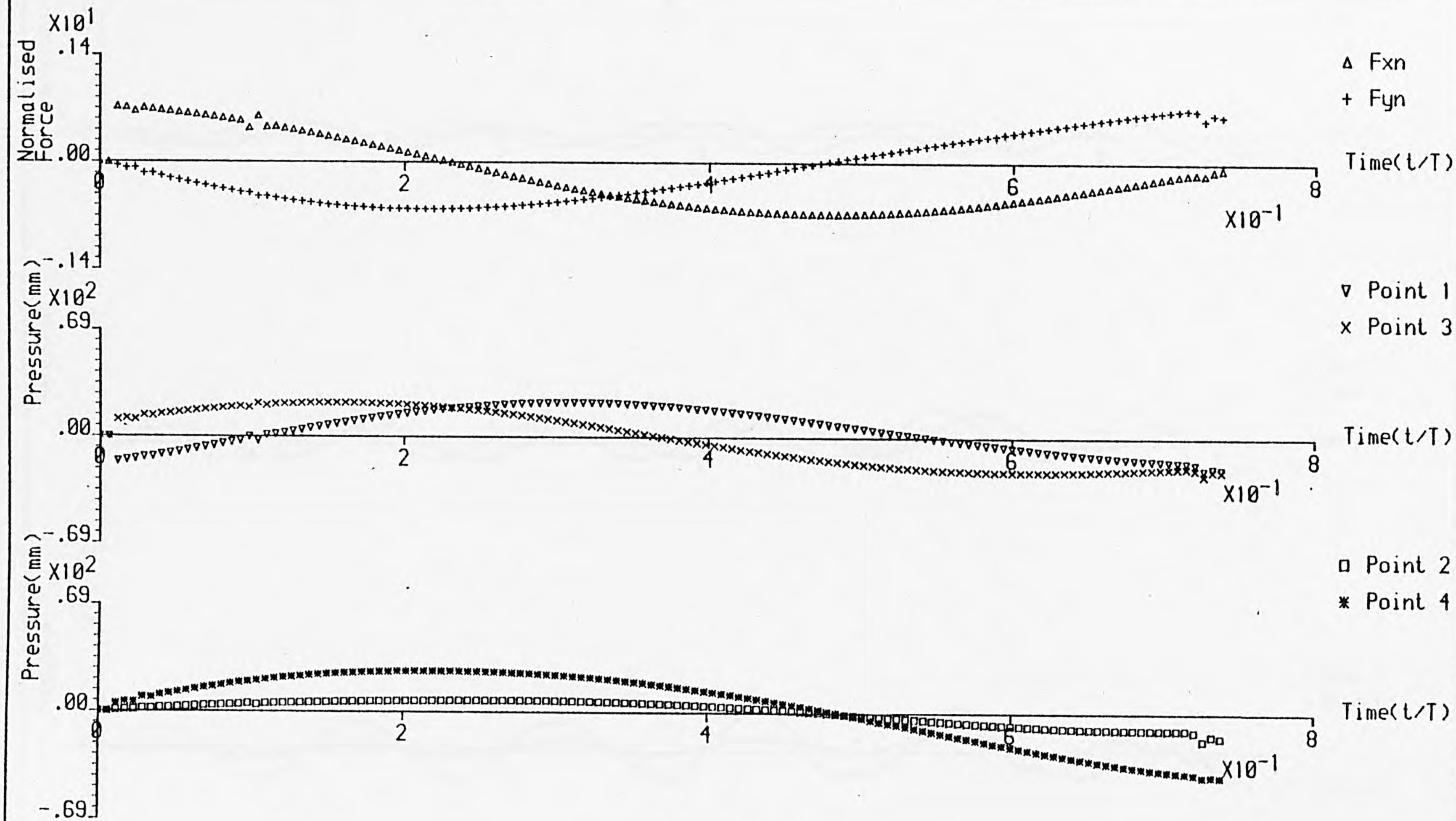

Wave height = .113m. Centre X = .566m.
Wavelength = 1.132m. Centre Y = -.168m.
Undisturbed W.L.= .555m. Radius = .055m.
Order of eq. = 1

Fig. A.13.29f

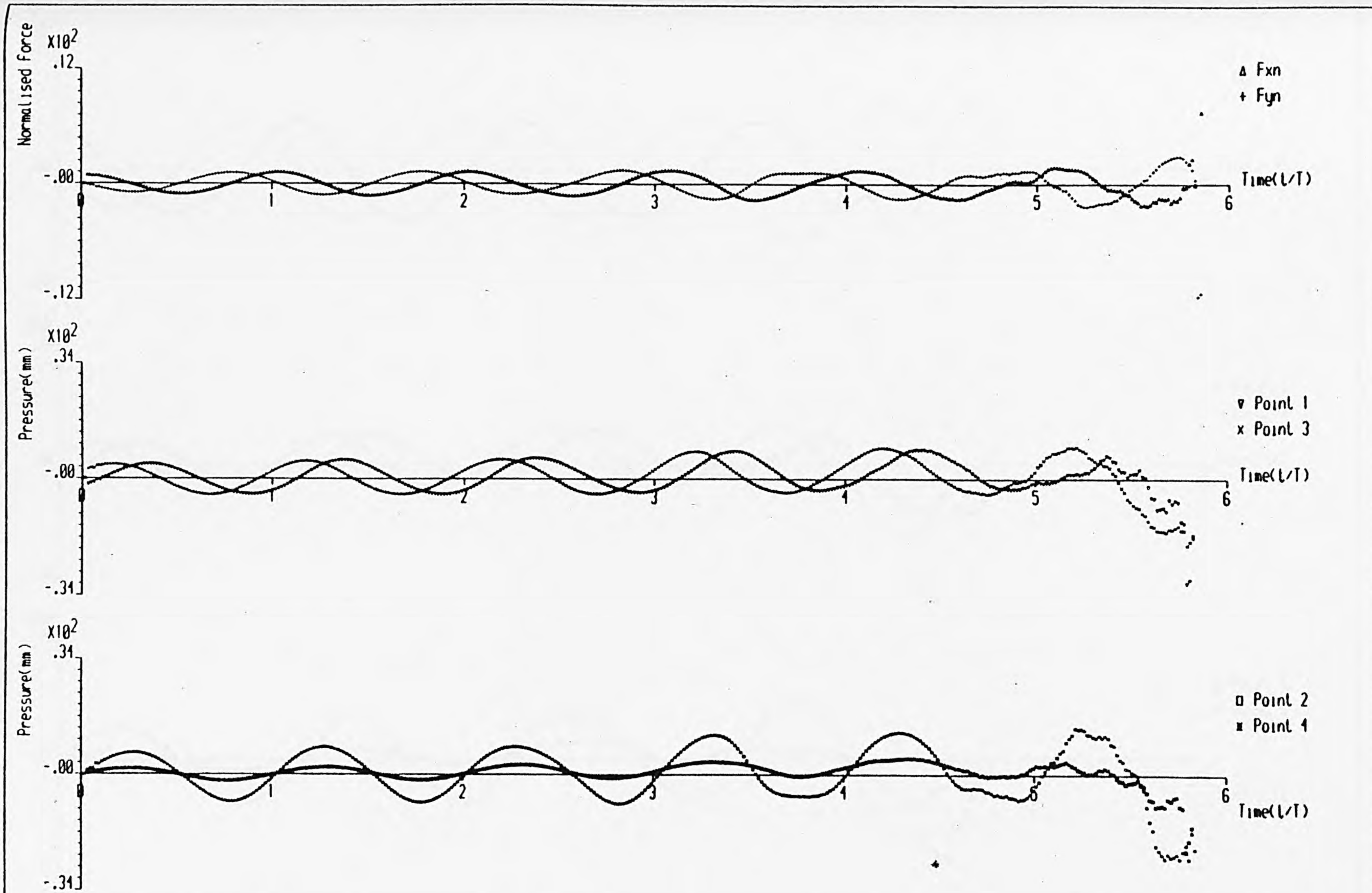

Wave height = .015m.
Wavelength = 1.132m.
Undisturbed W.L.= .555m.
Order of eq. = 1

Centre X = .566m.
Centre Y = -.112m.
Radius = .055m.

Fig. A.13. 30 Auxiliary graphs for case No. 30

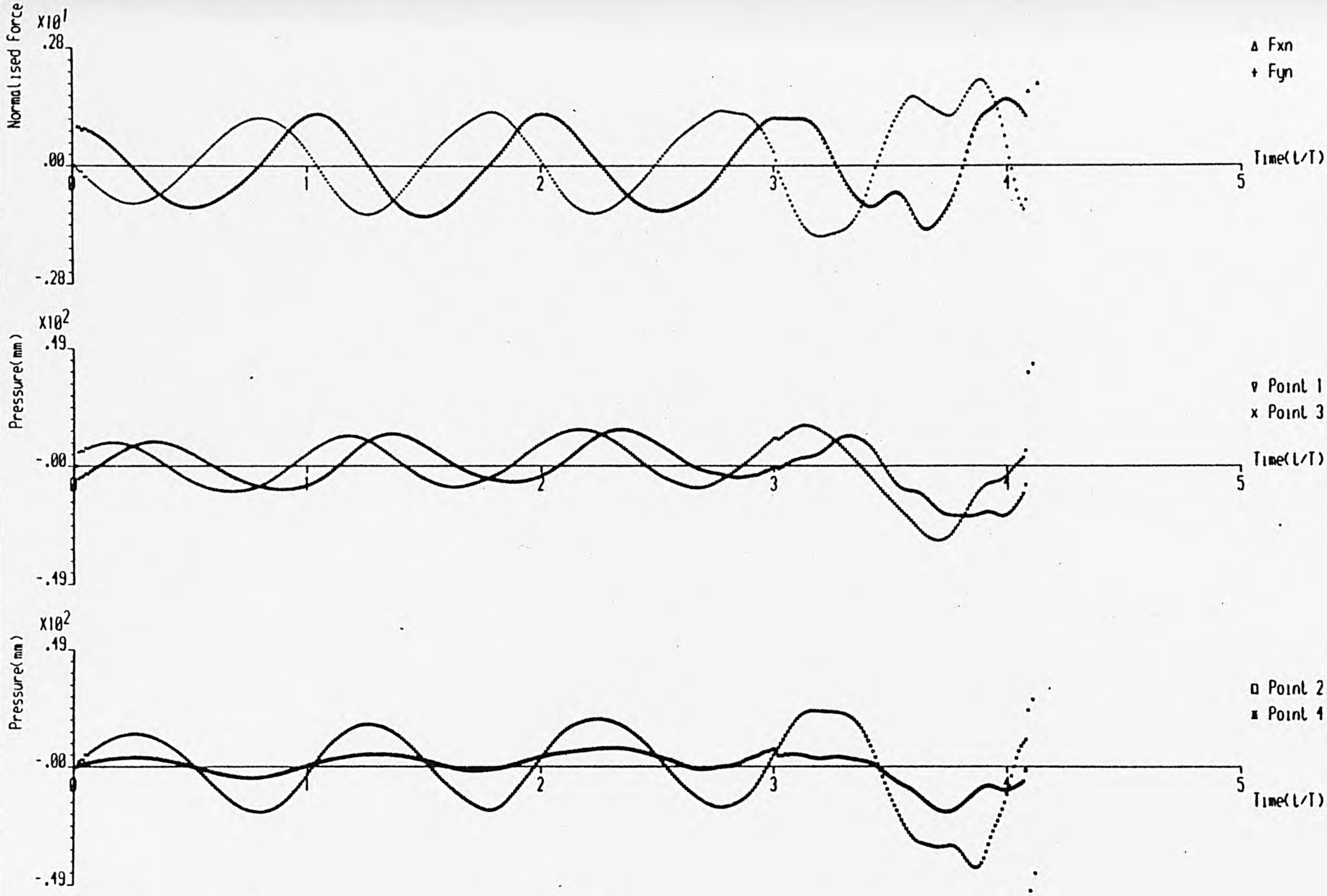

Wave height = .037m.
Wavelength = 1.132m.
Undisturbed W.L.= .555m.
Order of eq. = 1

Centre X = .566m.
Centre Y = -.112m.
Radius = .055m.

Fig. A.13. 31 Auxiliary graphs for case No. 31

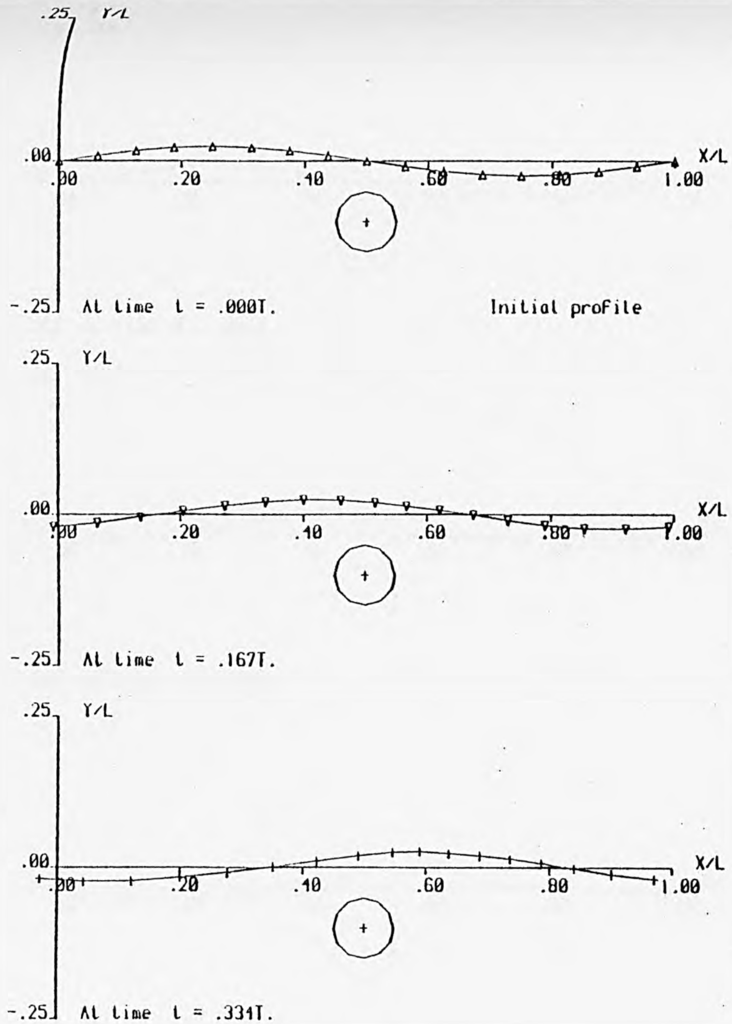

Wave height	= .054m.	Centre X =	.566m.
Wavelength	= 1.132m.	Centre Y =	-.112m.
Undisturbed W.L.=	.555m.	Radius =	.055m.
Order of eq.	= 1		

Fig. A.13.32a

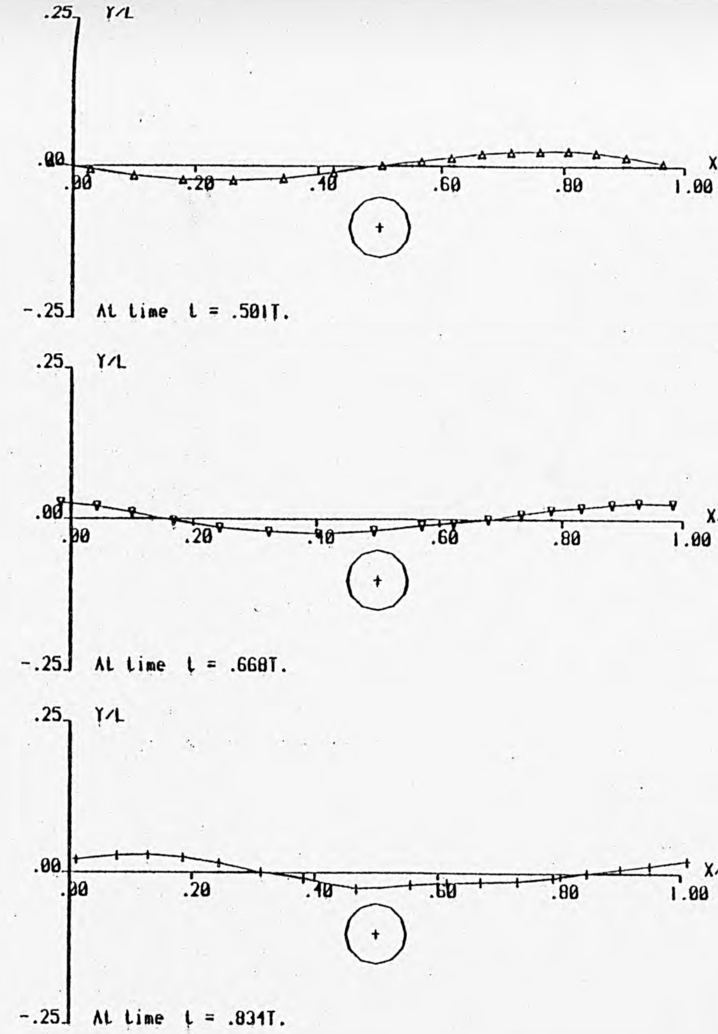

Wave height	= .054m.	Centre X =	.566m.
Wavelength	= 1.132m.	Centre Y =	-.112m.
Undisturbed W.L.=	.555m.	Radius =	.055m.
Order of eq.	= 1		

Fig. A.13.32b

Fig. A.13.32(a - f) A time sequence of wave profiles and auxiliary graphs for case No. 32

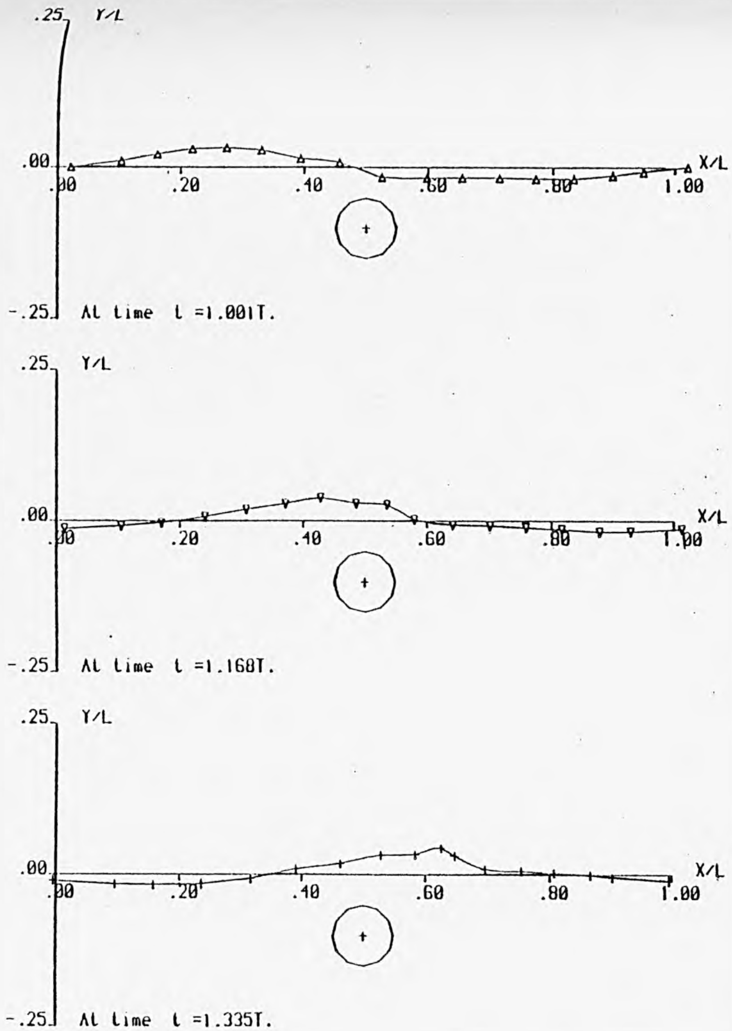

Wave height = .054m.
Wavelength = 1.132m.
Undisturbed W.L.= .555m.
Order of eq. = 1

Centre X = .566m.
Centre Y = -.112m.
Radius = .055m.

Fig.A.13.32c

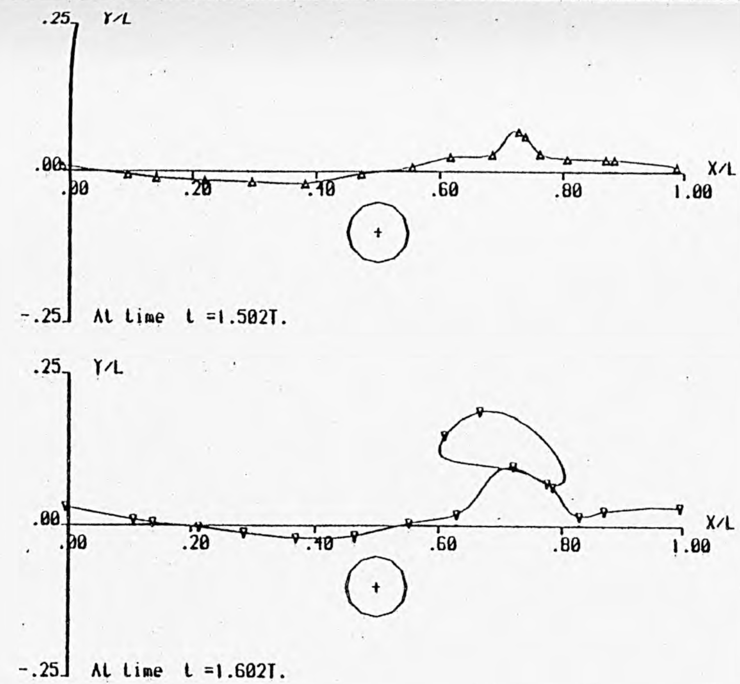

Wave height = .054m.
Wavelength = 1.132m.
Undisturbed W.L.= .555m.
Order of eq. = 1

Centre X = .566m.
Centre Y = -.112m.
Radius = .055m.

Fig. A.13.32d

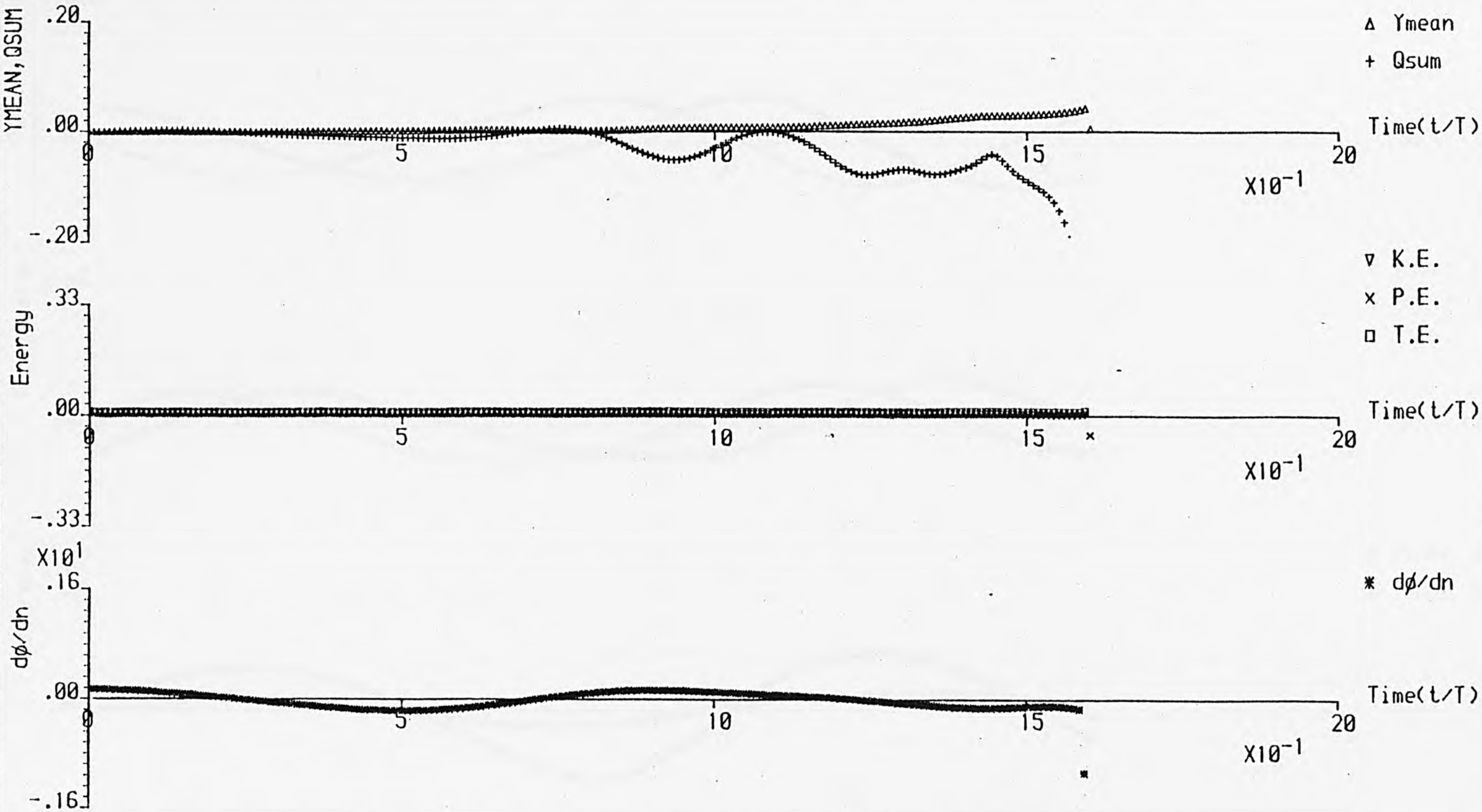

Wave height = .054m. Centre X = .566m.
Wavelength = 1.132m. Centre Y = -.112m.
Undisturbed W.L. = .555m. Radius = .055m.
Order of eq. = 1

Fig. A.13.32e

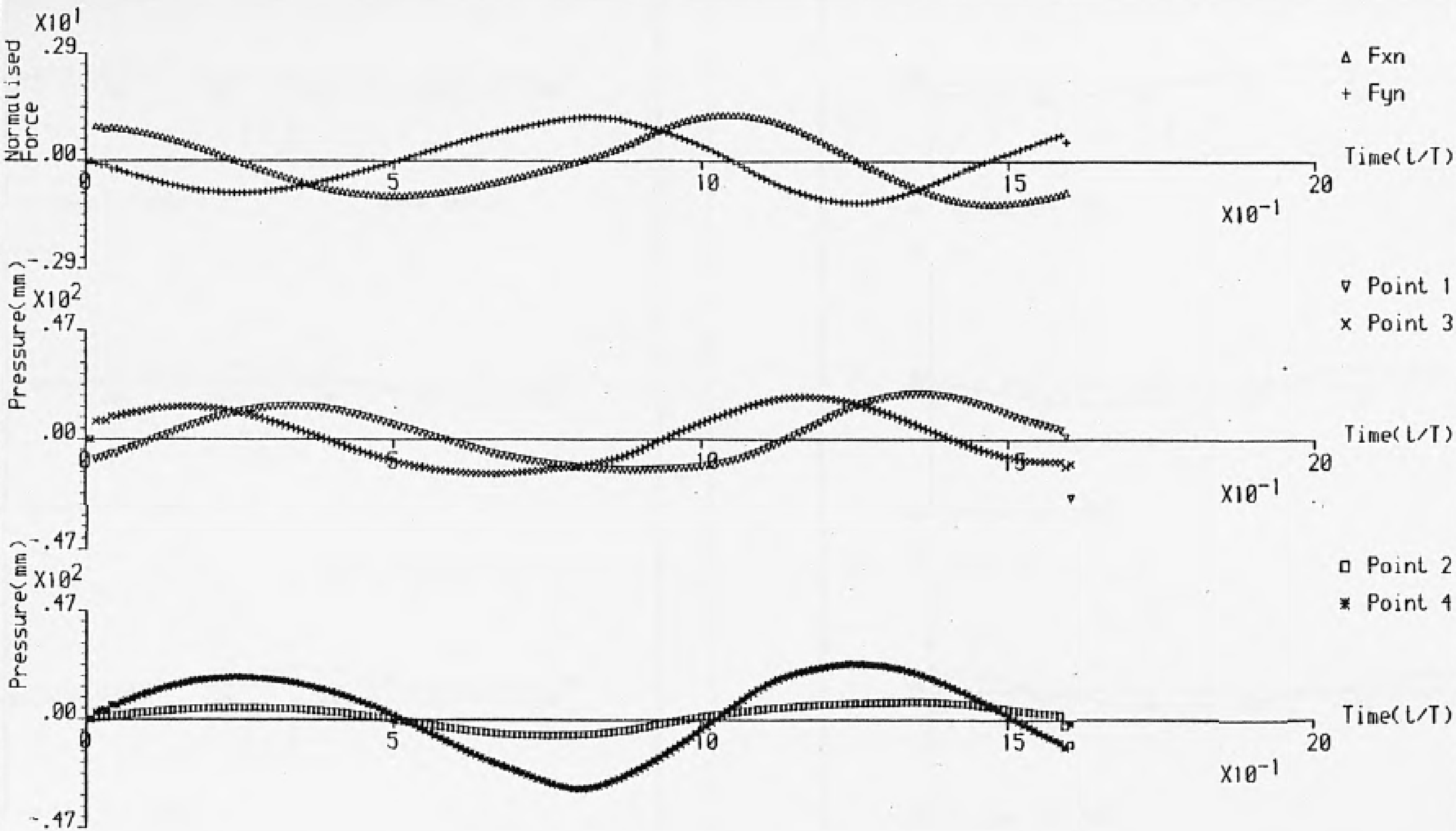

Wave height	=	.054m.	Centre X	=	.566m.
Wavelength	=	1.132m.	Centre Y	=	-.112m.
Undisturbed W.L.	=	.555m.	Radius	=	.055m.
Order of eq.	=	1			

Fig. A.13.32f.

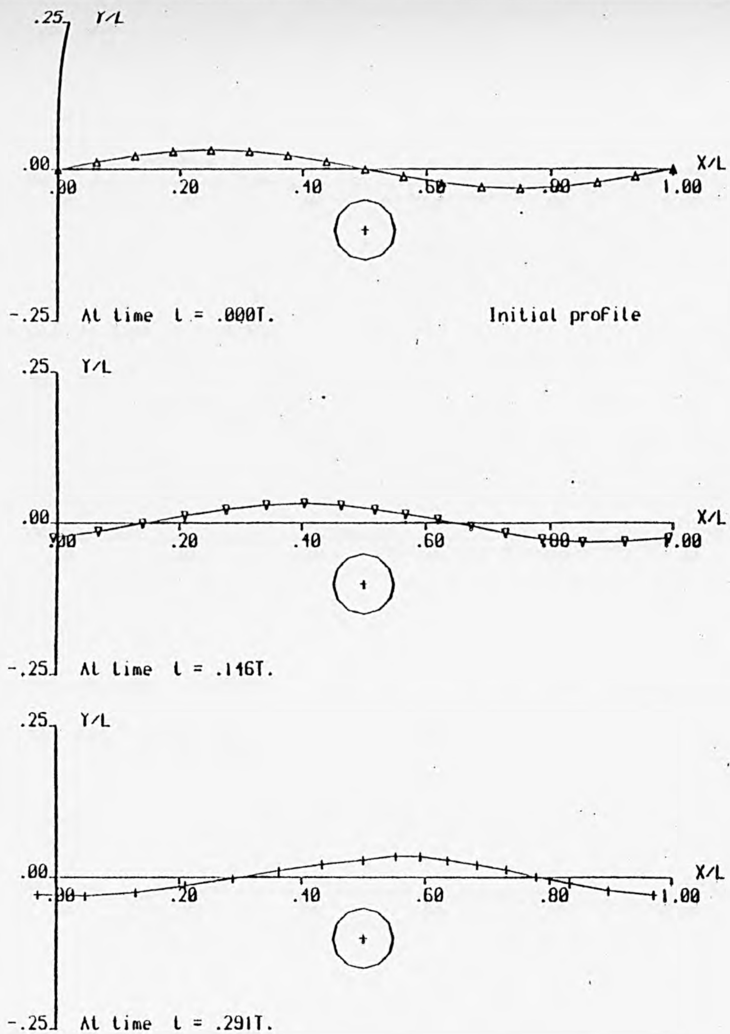

Wave height = .071m.
Wavelength = 1.132m.
Undisturbed W.L.= .555m.
Order of eq. = 1
Centre X = .566m.
Centre Y = -.112m.
Radius = .055m.

Fig. A.13.33a

Fig. A.13.33(a - f) A time sequence of wave profiles and auxiliary graphs for case No. 33

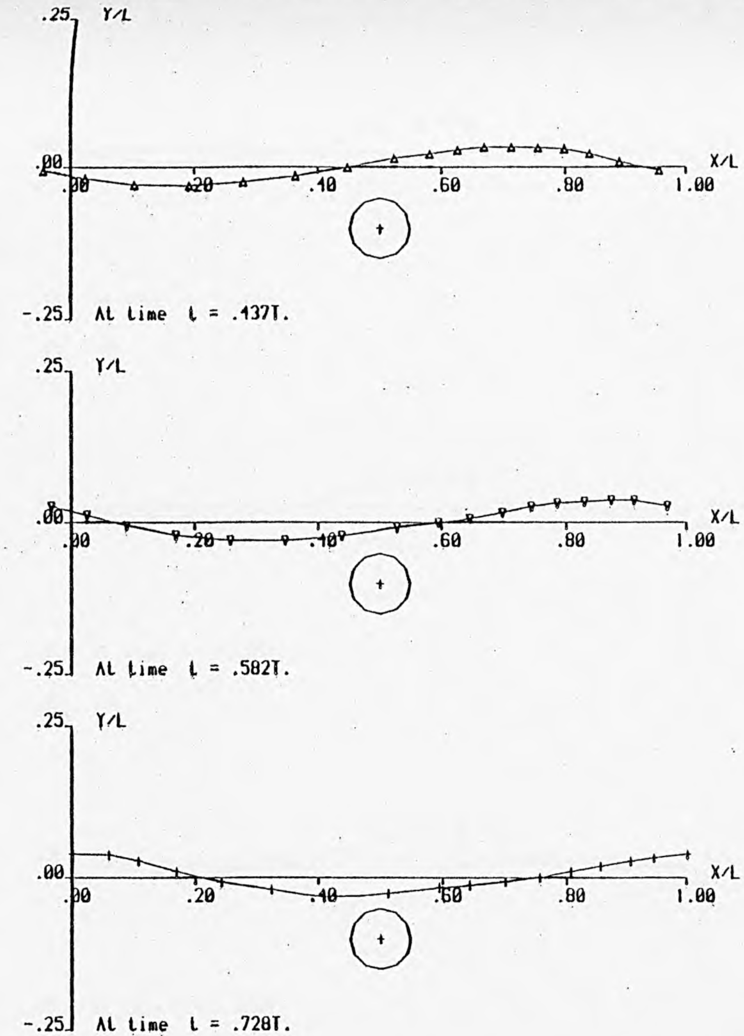

Wave height = .071m.
Wavelength = 1.132m.
Undisturbed W.L.= .555m.
Order of eq. = 1
Centre X = .566m.
Centre Y = -.112m.
Radius = .055m.

Fig. A.13.33b

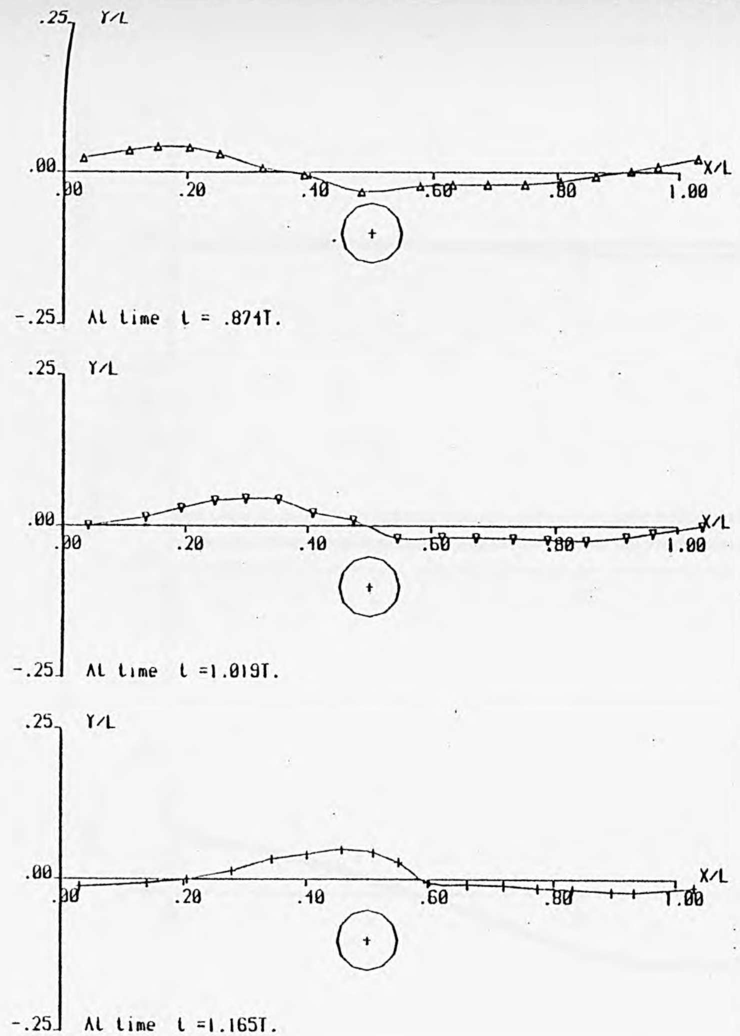

Wave height = .071m.
Wavelength = 1.132m.
Undisturbed W.L.= .555m.
Order of eq. = 1

Centre X = .566m.
Centre Y = -.112m.
Radius = .055m.

Fig. A.13.33c

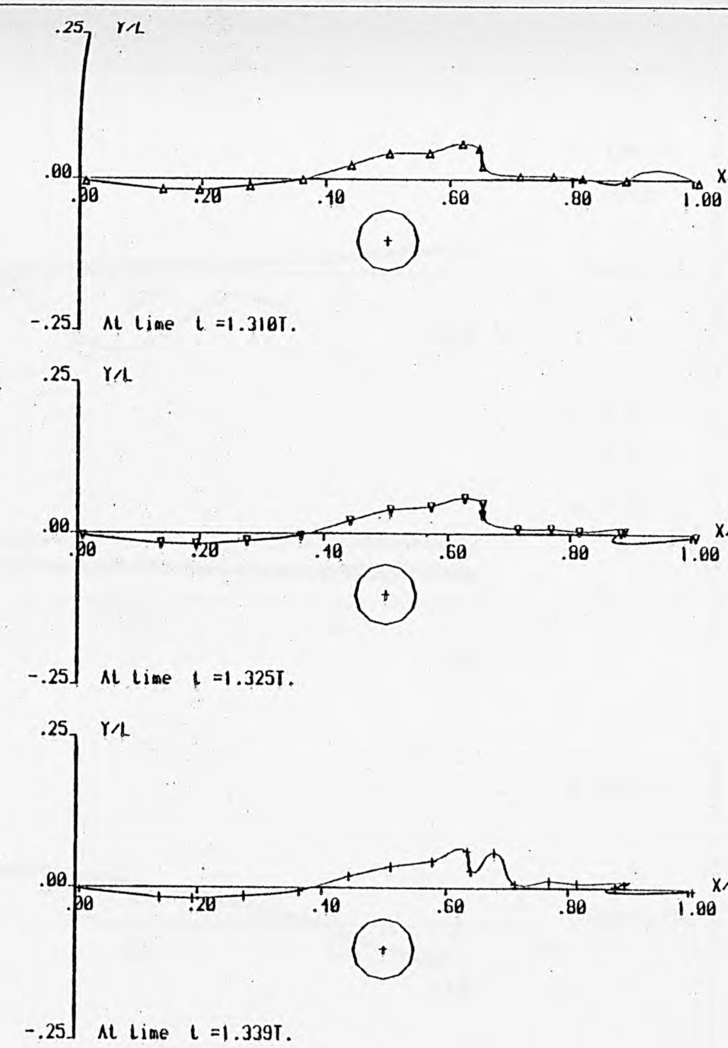

Wave height = .071m.
Wavelength = 1.132m.
Undisturbed W.L.= .555m.
Order of eq. = 1

Centre X = .566m.
Centre Y = -.112m.
Radius = .055m.

Fig. A.13.33d

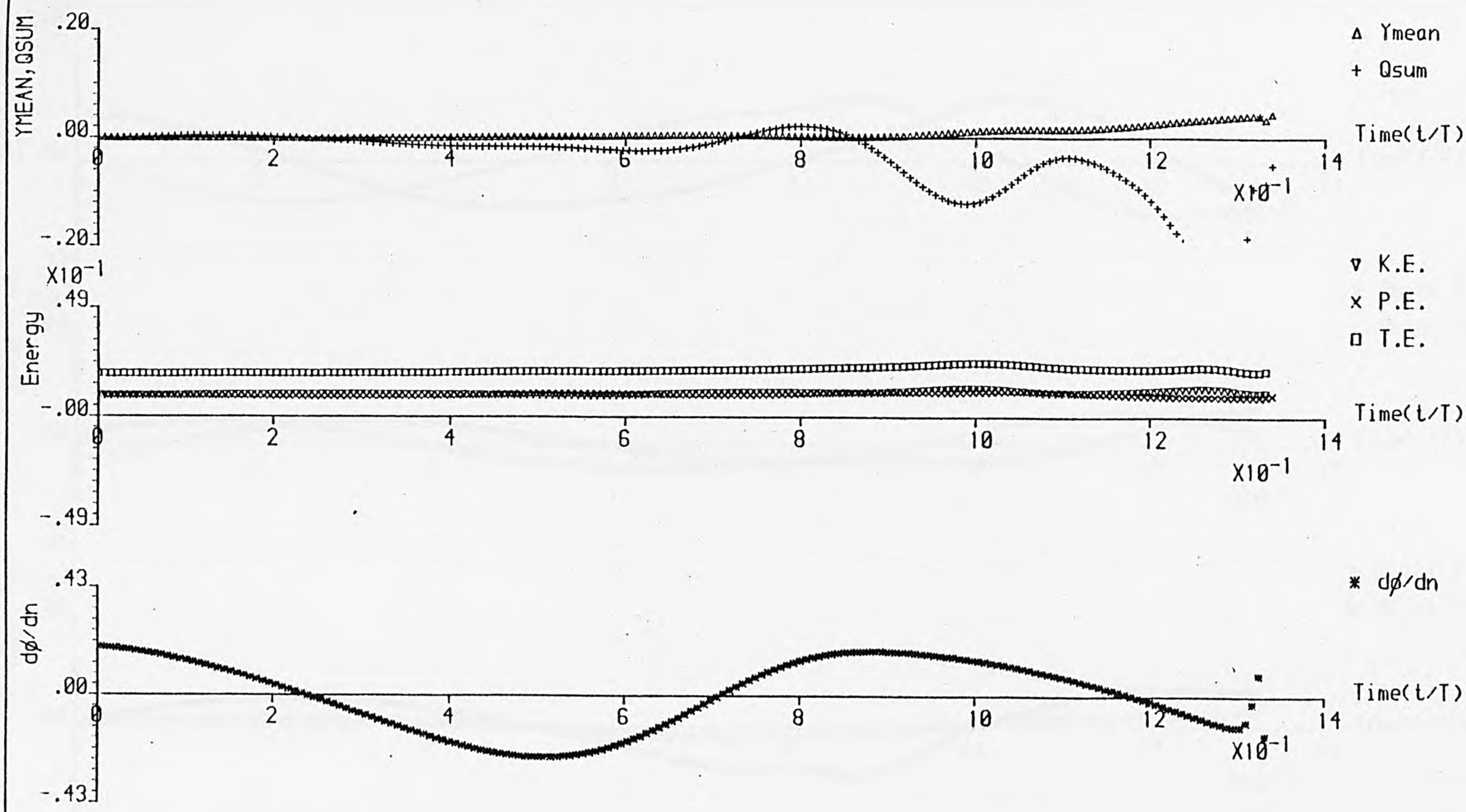

Wave height = .071m. Centre X = .566m.
Wavelength = 1.132m. Centre Y = -.112m.
Undisturbed W.L.= .555m. Radius = .055m.
Order of eq. = 1

Fig. A.13.33e

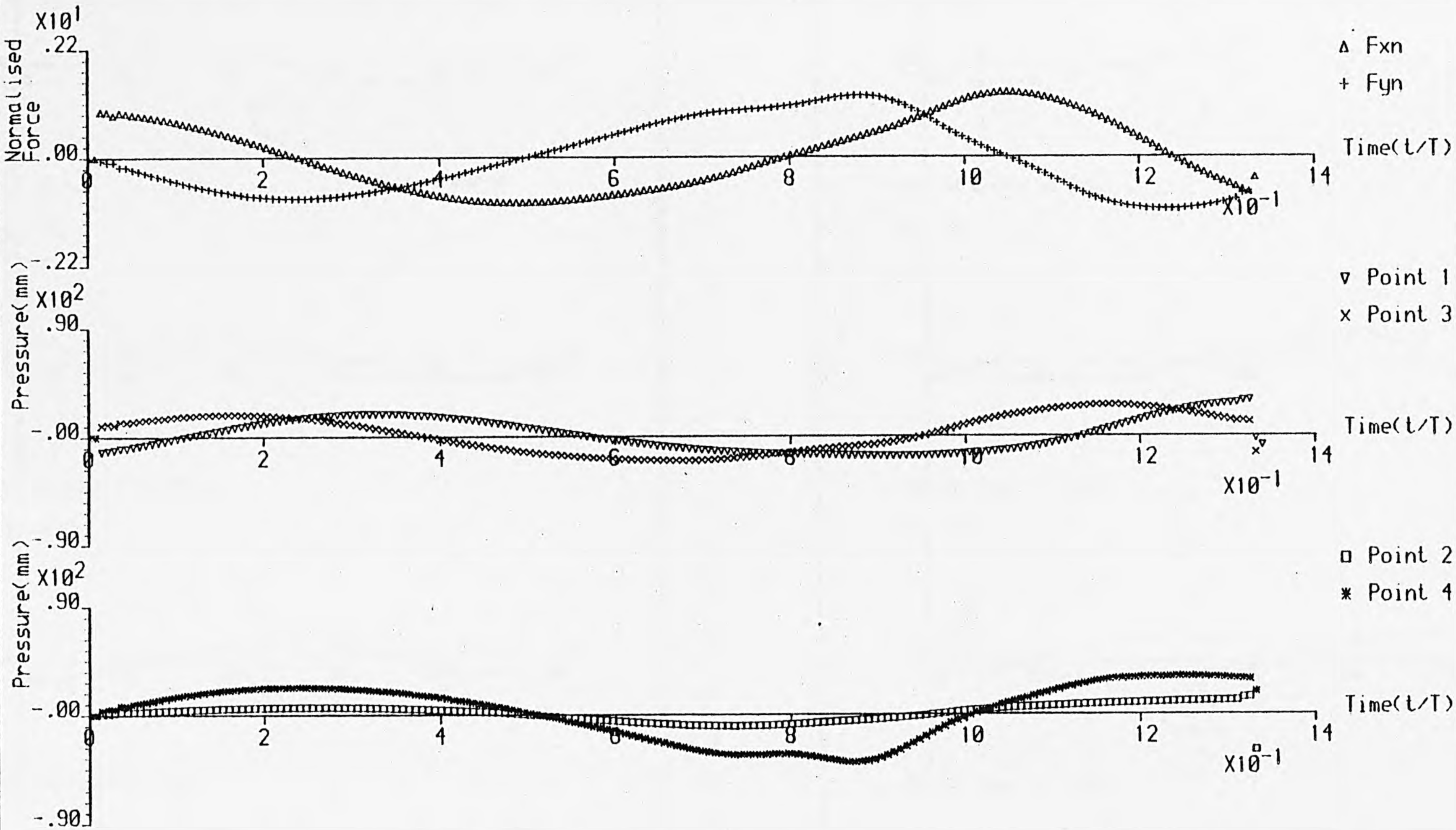

Wave height = .071m. Centre X = .566m.
Wavelength = 1.132m. Centre Y = -.112m.
Undisturbed W.L.= .555m. Radius = .055m.
Order of eq. = 1

Fig.A.13.33f

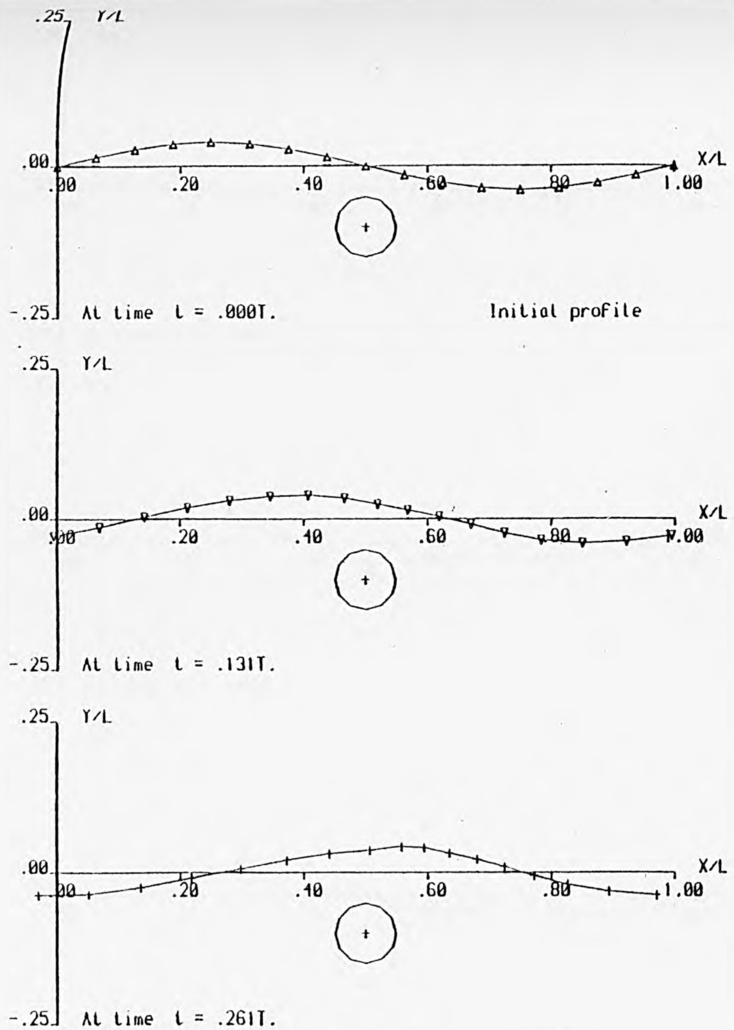

Wave height = .088m.
Wavelength = 1.132m.
Undisturbed W.L.= .555m.
Order of eq. = 1

Centre X = .566m.
Centre Y = -.112m.
Radius = .055m.

Fig. A.13.34a

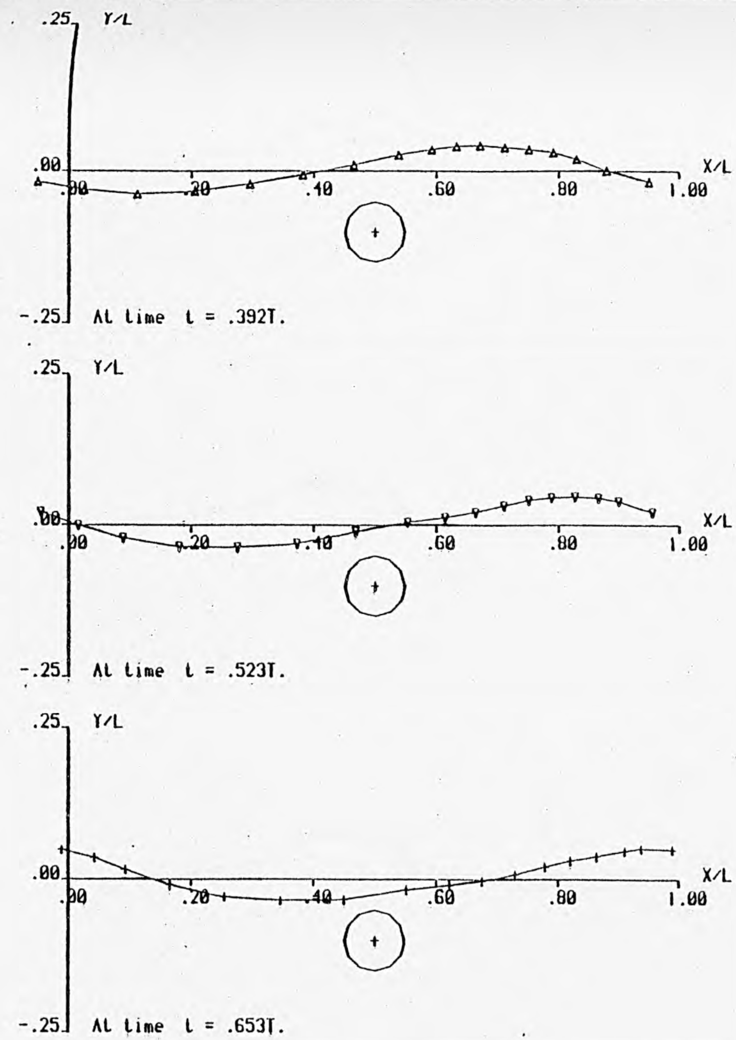

Wave height = .088m.
Wavelength = 1.132m.
Undisturbed W.L.= .555m.
Order of eq. = 1

Centre X = .566m.
Centre Y = -.112m.
Radius = .055m.

Fig. A.13.34b

Fig. A.13.34(a - f) A time sequence of wave profiles and auxiliary graphs for case No. 34

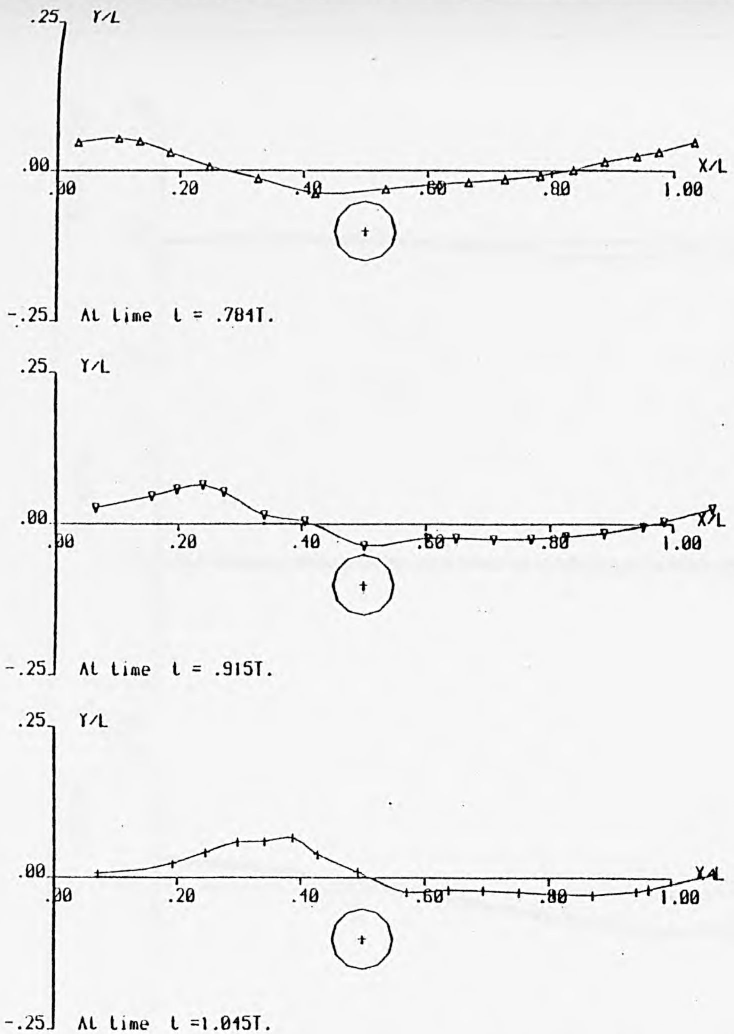

Wave height = .088m.
Wavelength = 1.132m.
Undisturbed W.L.= .555m.
Order of eq. = 1

Centre X = .566m.
Centre Y = -.112m.
Radius = .055m.

Fig. A.13.34c

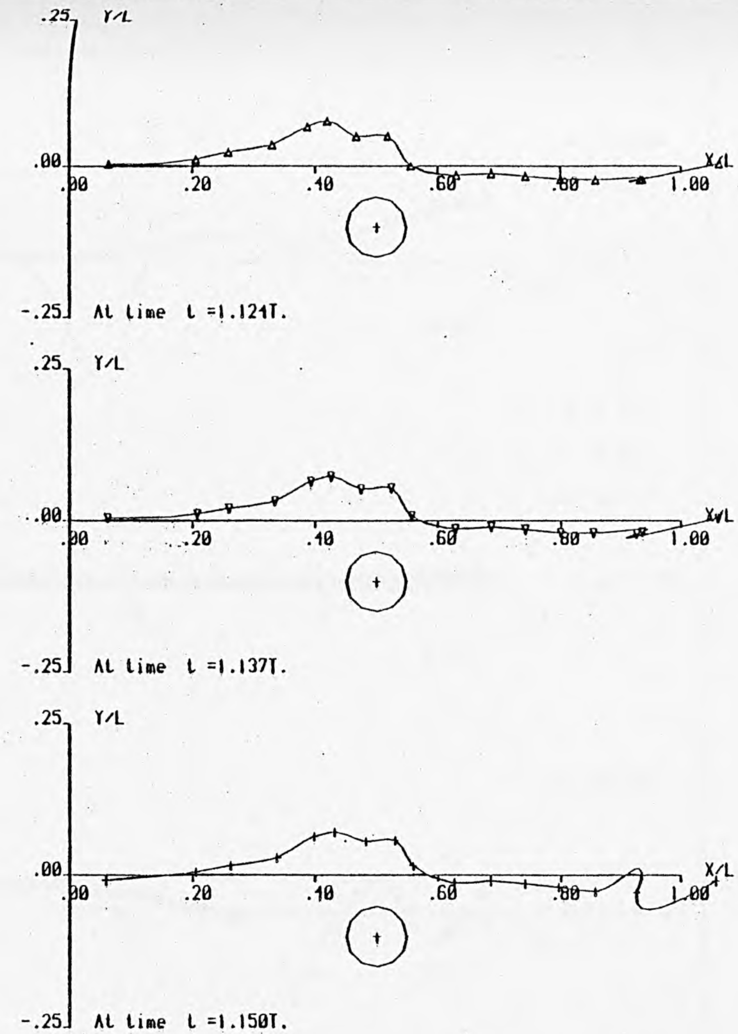

Wave height = .088m.
Wavelength = 1.132m.
Undisturbed W.L.= .555m.
Order of eq. = 1

Centre X = .566m.
Centre Y = -.112m.
Radius = .055m.

Fig. A.13.34d

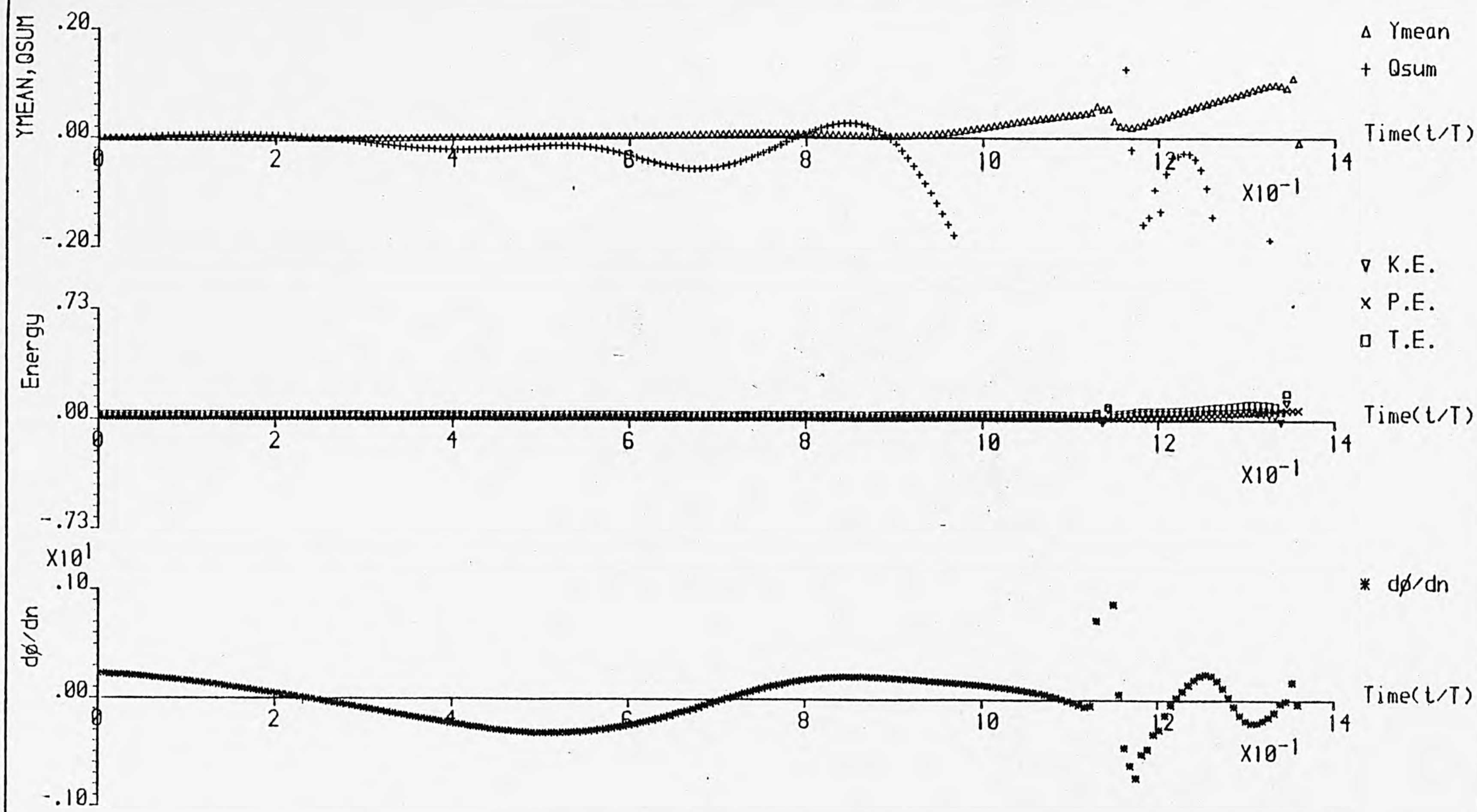

Wave height	=	.088m.	Centre X	=	.566m.
Wavelength	=	1.132m.	Centre Y	=	-.112m.
Undisturbed W.L.	=	.555m.	Radius	=	.055m.
Order of eq.	=	1			

Fig. A.13.34e

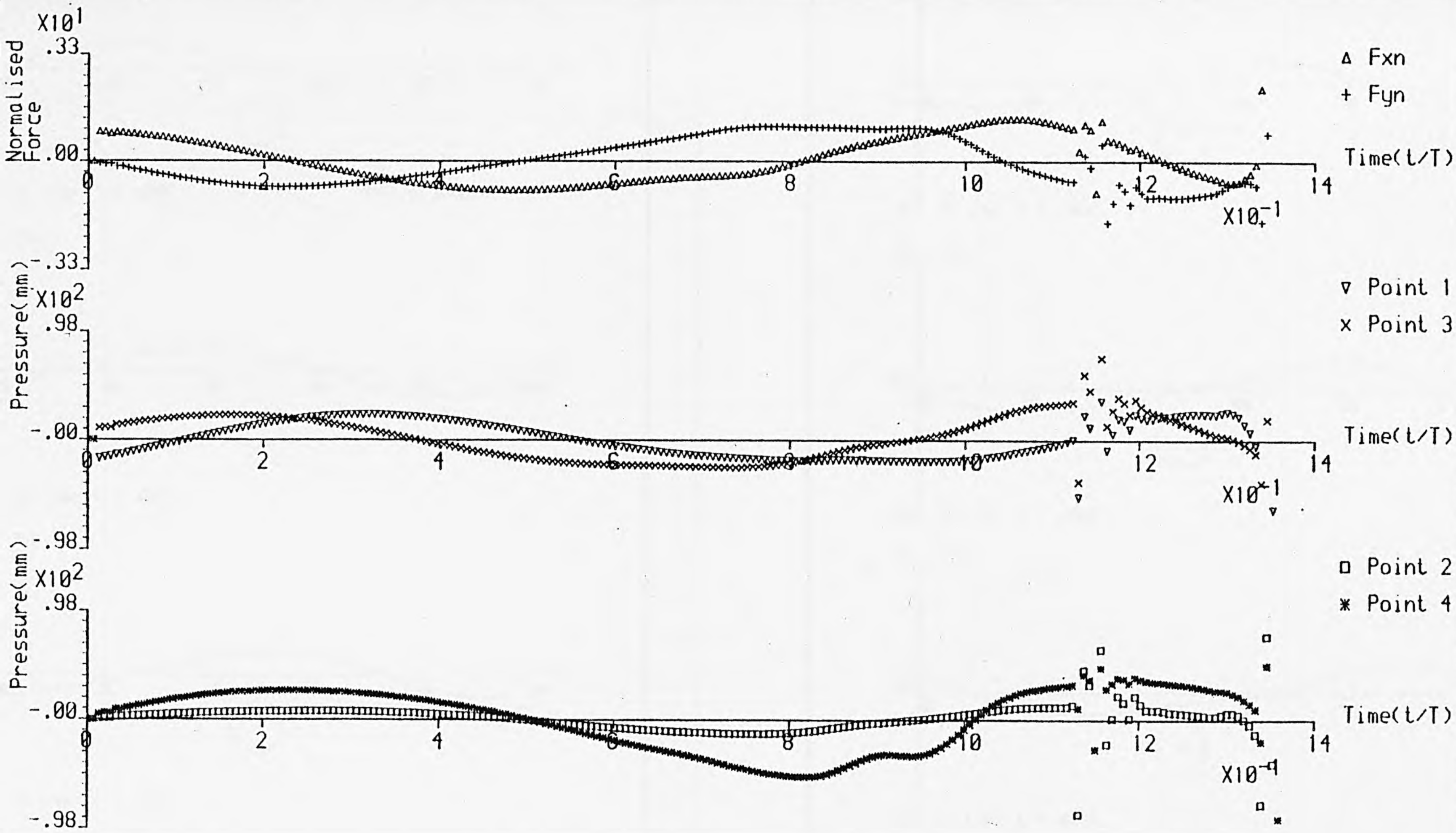

Wave height = .088m. Centre X = .566m.
Wavelength = 1.132m. Centre Y = -.112m.
Undisturbed W.L.= .555m. Radius = .055m.
Order of eq. = 1

Fig. A.13.34f

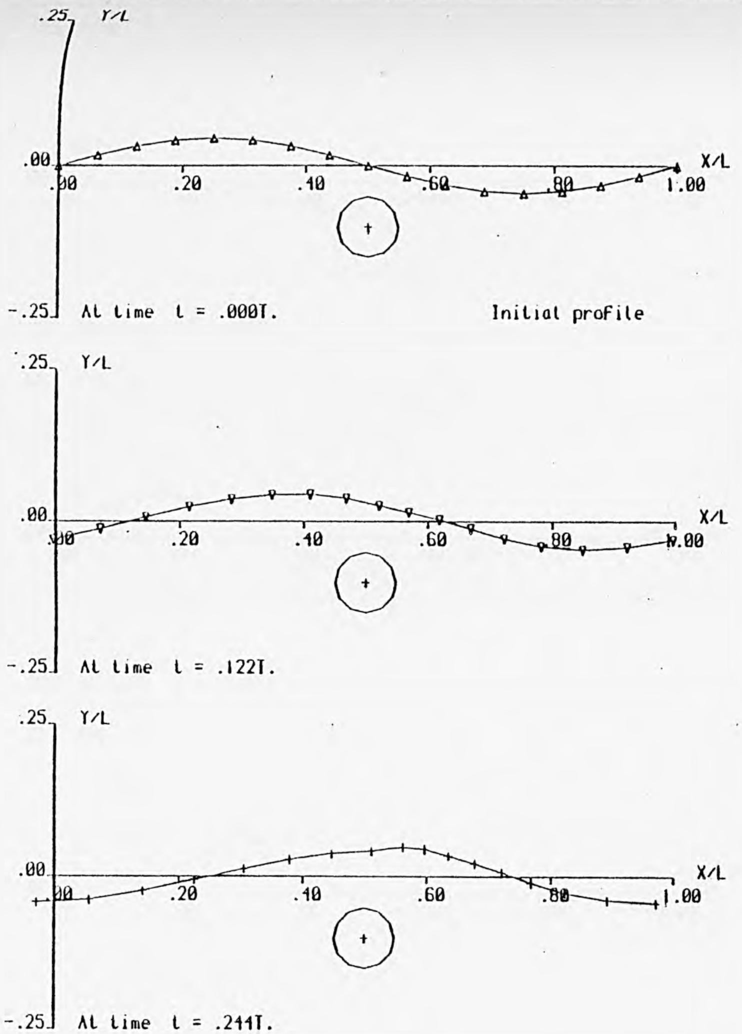

Wave height = .101m.
Wavelength = 1.132m.
Undisturbed W.L.= .555m.
Order of eq. = 1
Fig. A.13.35a

Centre X = .566m.
Centre Y = -.112m.
Radius = .055m.

Fig. A.13.35(a - f) A time sequence of wave profiles and auxiliary graphs for case No. 35

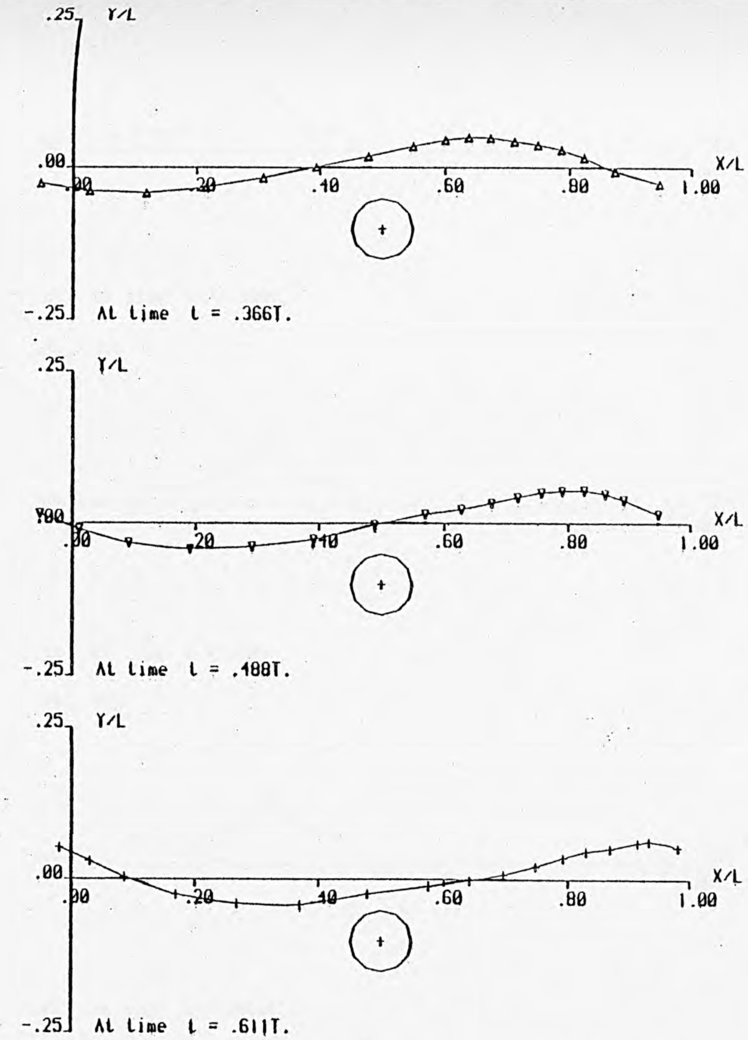

Wave height = .101m.
Wavelength = 1.132m.
Undisturbed W.L.= .555m.
Order of eq. = 1
Fig. A.13.35b

Centre X = .566m.
Centre Y = -.112m.
Radius = .055m.

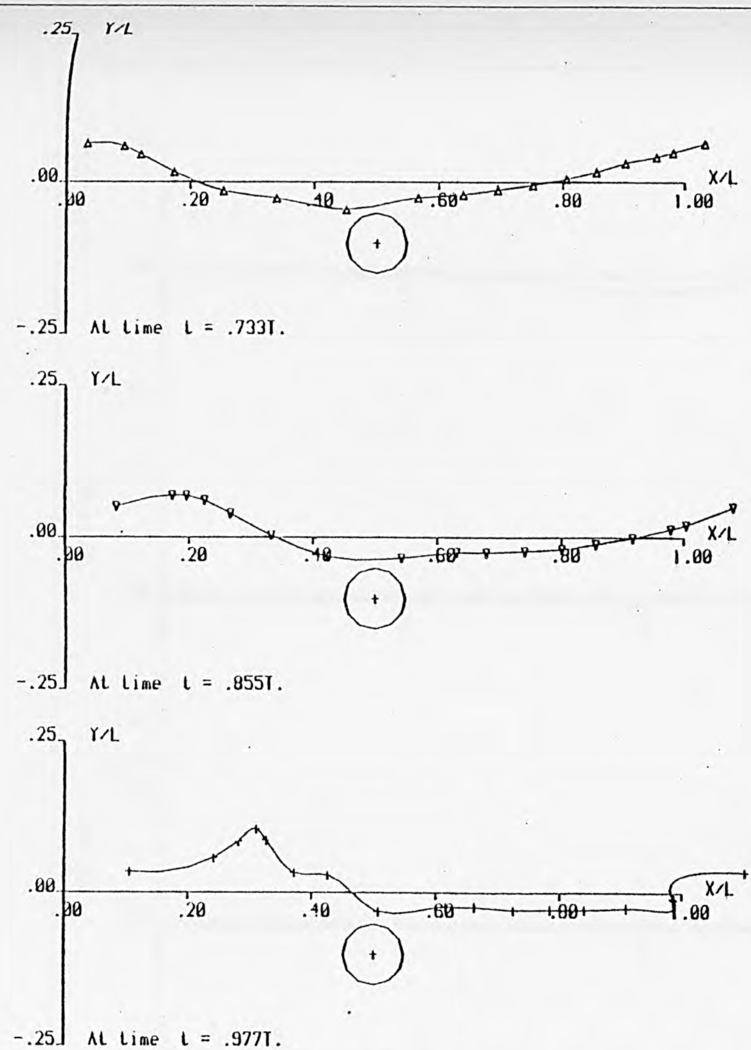

Wave height = .101m.
Wavelength = 1.132m.
Undisturbed W.L.= .555m.
Order of eq. = 1

Centre X = .566m.
Centre Y = -.112m.
Radius = .055m.

Fig. A.13.35c

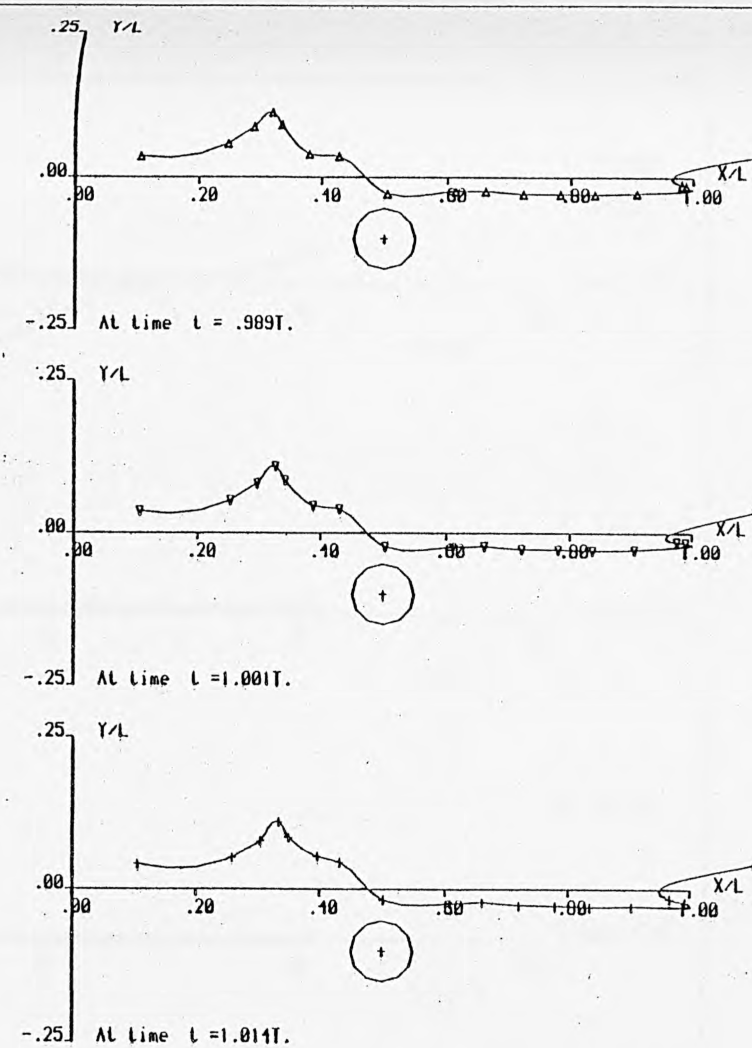

Wave height = .101m.
Wavelength = 1.132m.
Undisturbed W.L.= .555m.
Order of eq. = 1

Centre X = .566m.
Centre Y = -.112m.
Radius = .055m.

Fig. A.13.35d

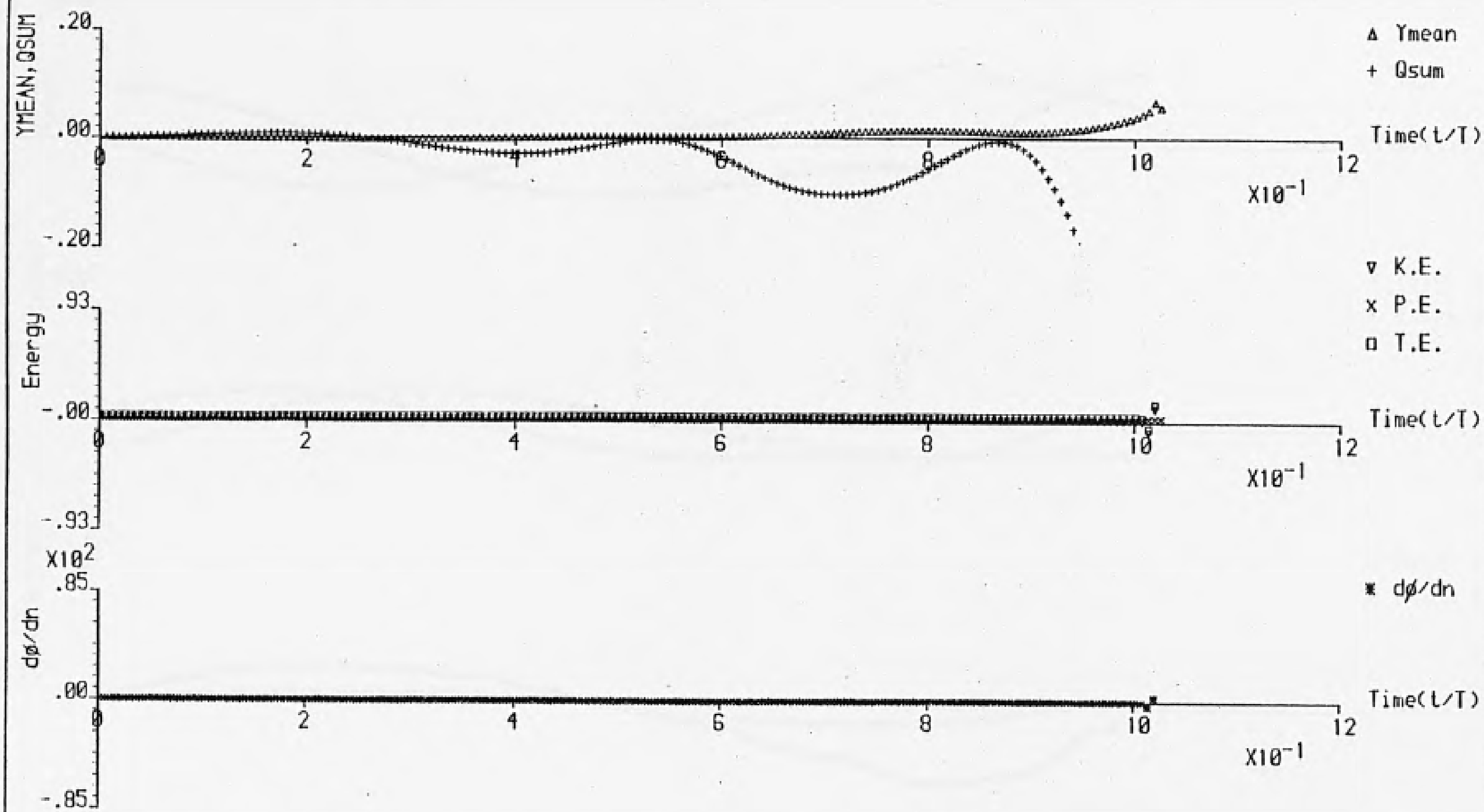

Wave height	=	.101m.	Centre X	=	.566m.
Wavelength	=	1.132m.	Centre Y	=	-.112m.
Undisturbed W.L.	=	.555m.	Radius	=	.055m.
Order of eq.	=	1			

Fig. A.13.35e

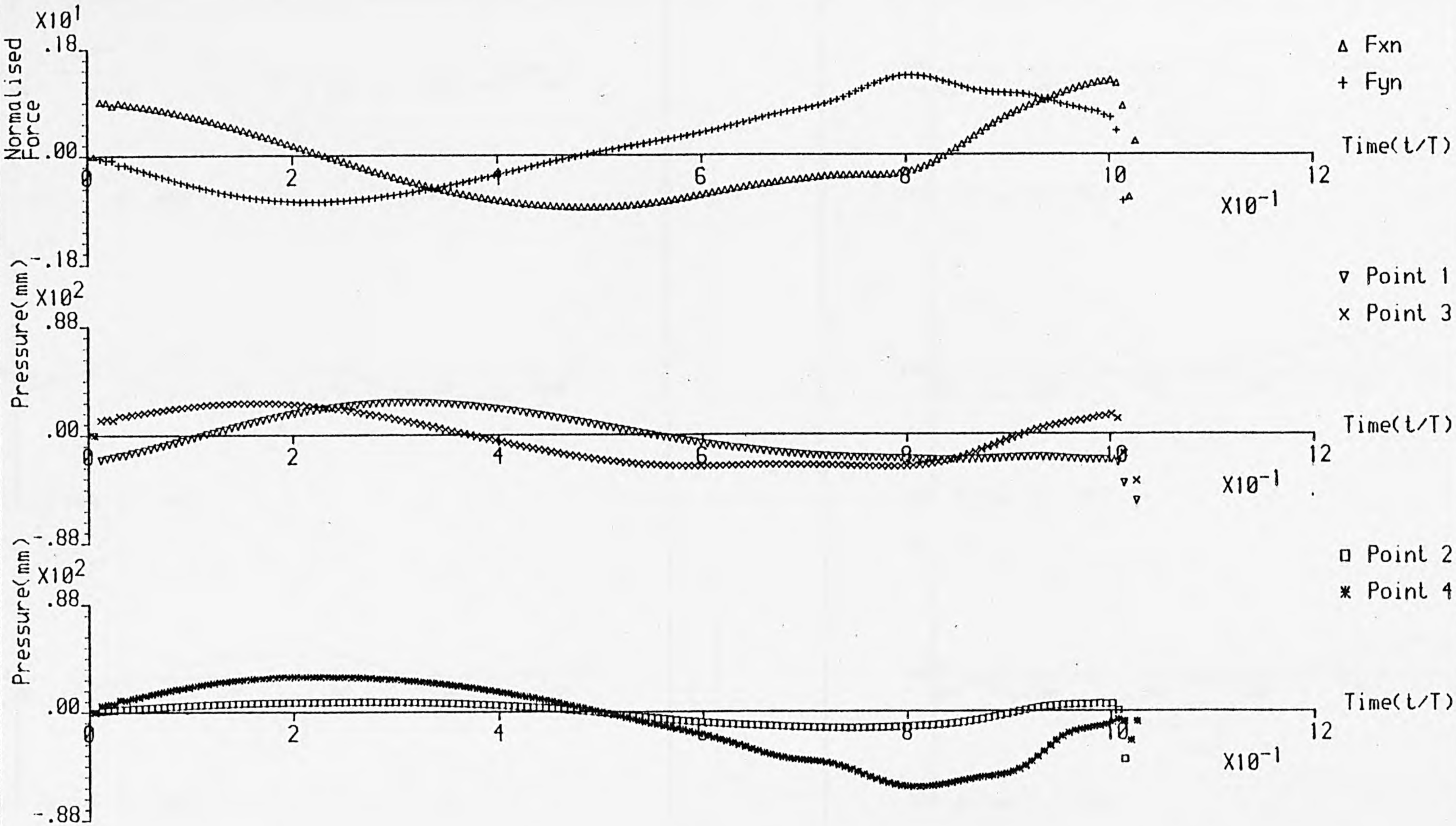

Wave height = .101m. Centre X = .566m.
Wavelength = 1.132m. Centre Y = -.112m.
Undisturbed W.L.= .555m. Radius = .055m.
Order of eq. = 1

Fig. A.13.35f

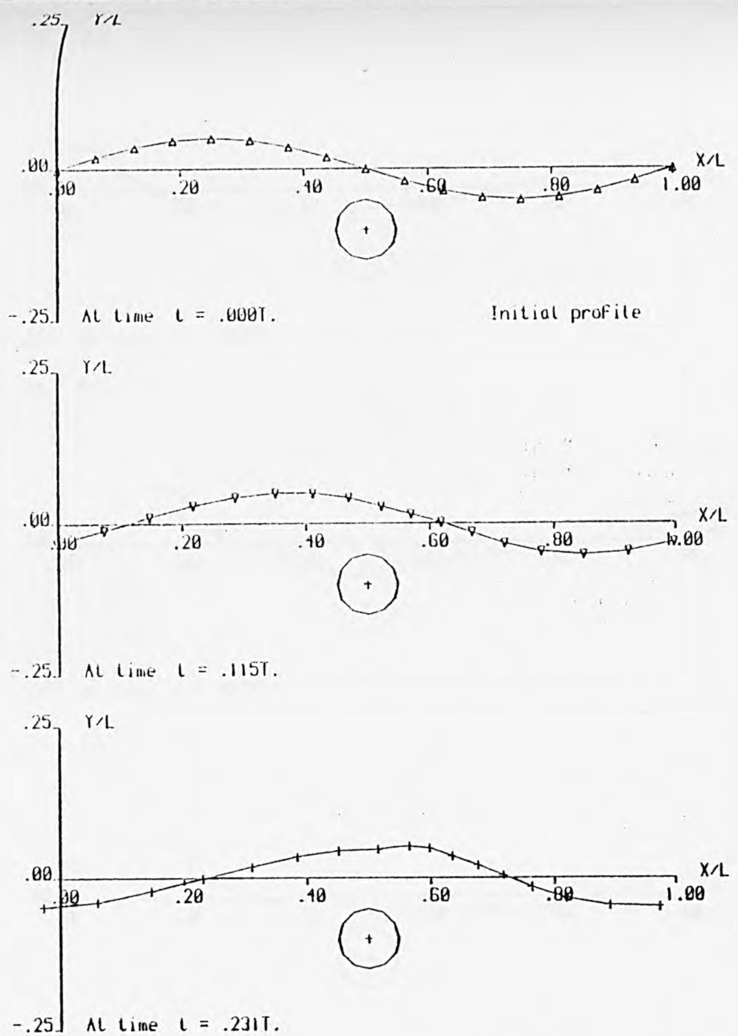

Wave height = .114m.
Wavelength = 1.132m.
Undisturbed W.L.= .555m.
Order of eq. = 1

Centre X = .566m.
Centre Y = -.112m.
Radius = .055m.

Fig. A.13.36a

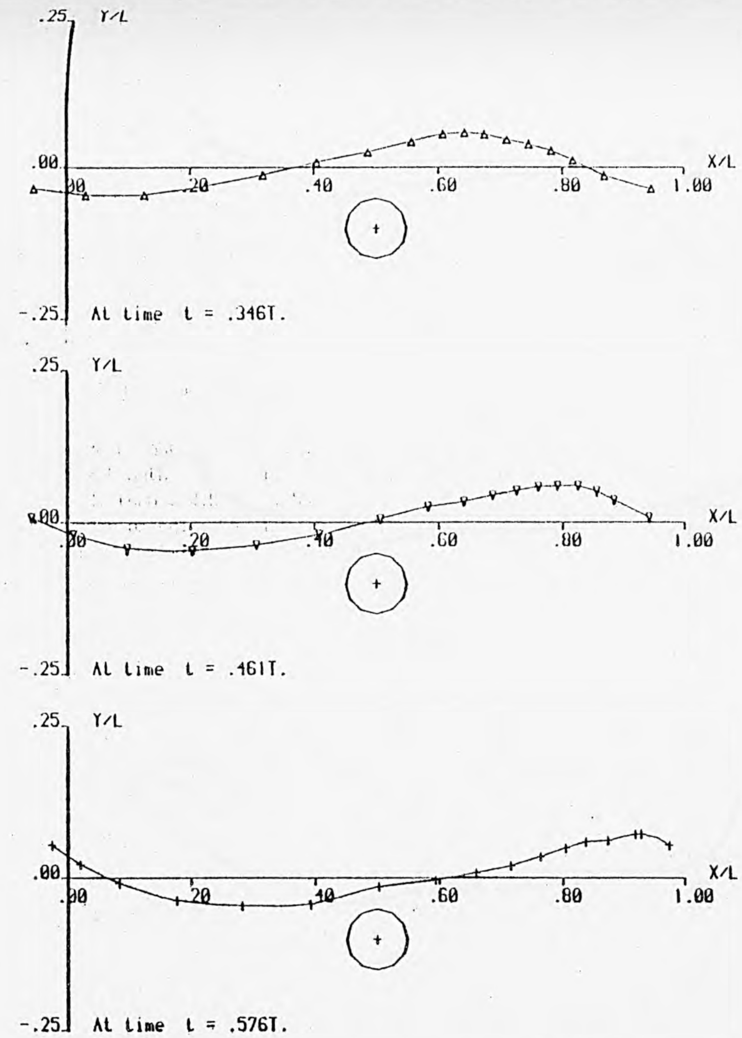

Wave height = .114m.
Wavelength = 1.132m.
Undisturbed W.L.= .555m.
Order of eq. = 1

Centre X = .566m.
Centre Y = -.112m.
Radius = .055m.

Fig. A.13.36b

Fig. A.13.36(a – f) A time sequence of wave profiles and auxiliary graphs for case No. 36

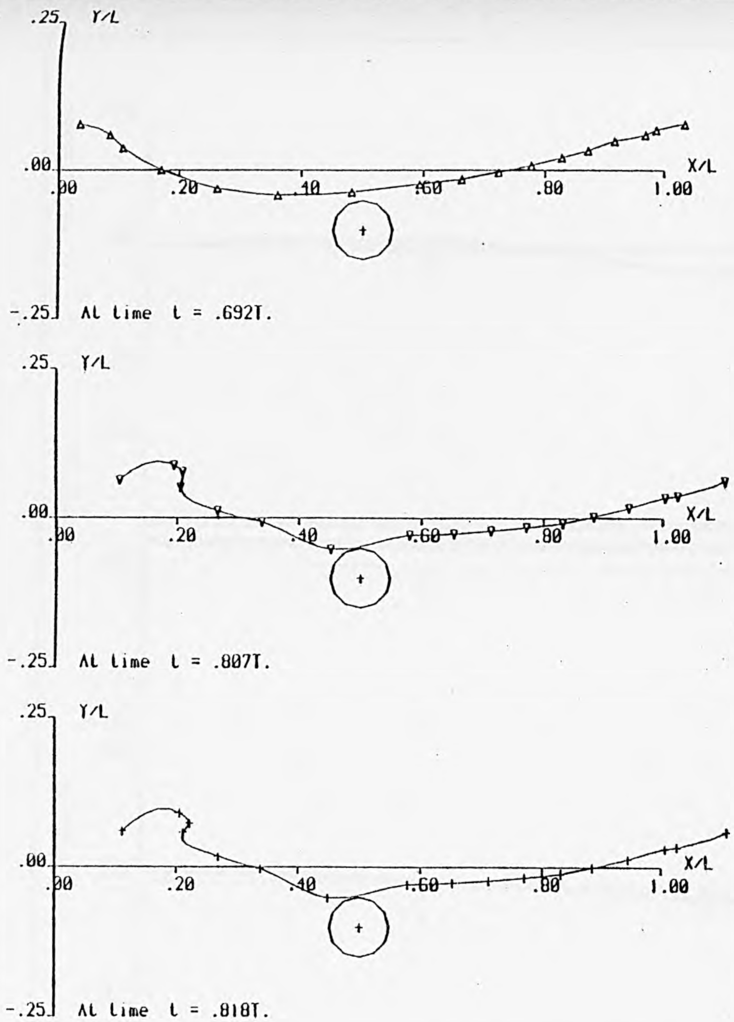

Wave height = .114m.
Wavelength = 1.132m.
Undisturbed W.L.= .555m.
Order of eq. = 1
Centre X = .566m.
Centre Y = -.112m.
Radius = .055m.

Fig. A.13.36c

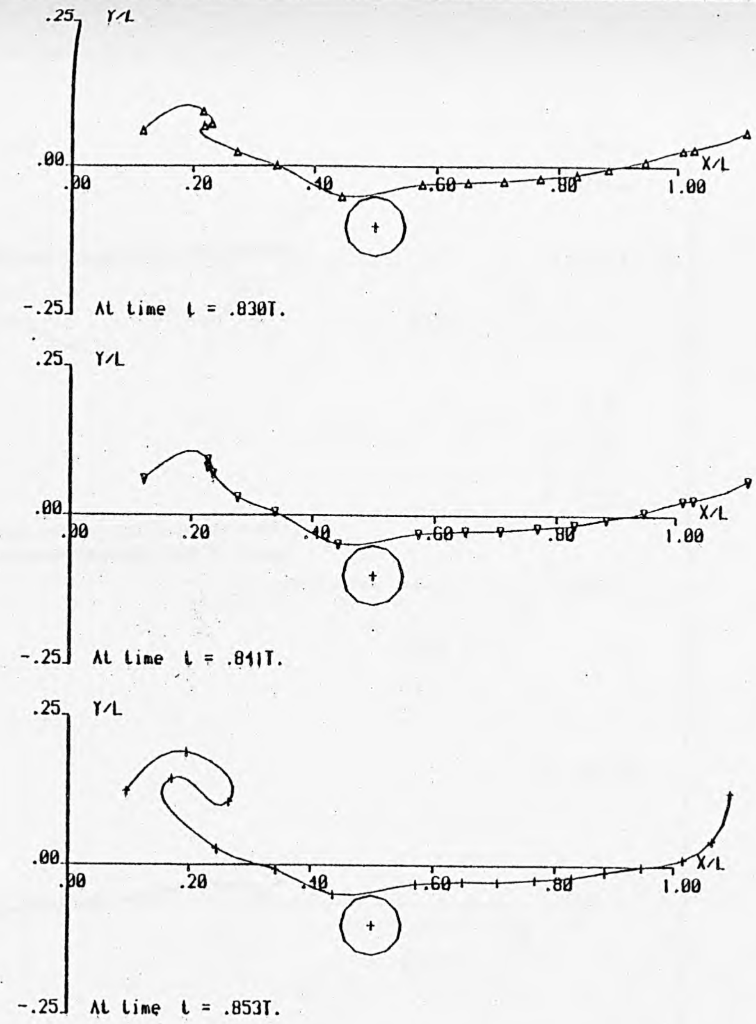

Wave height = .114m.
Wavelength = 1.132m.
Undisturbed W.L.= .555m.
Order of eq. = 1
Centre X = .566m.
Centre Y = -.112m.
Radius = .055m.

Fig. A.13.36d

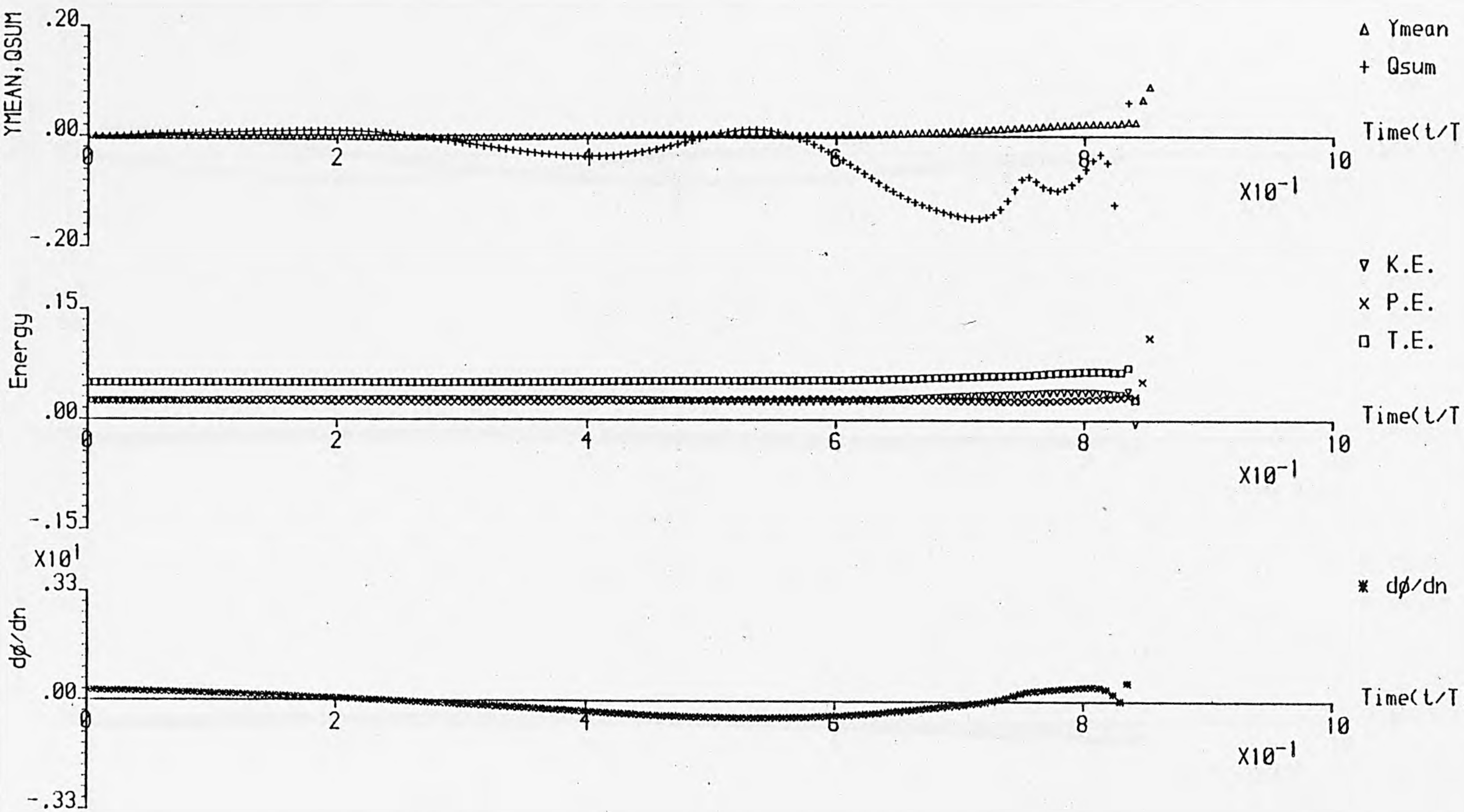

Wave height = .114m. Centre X = .566m.
Wavelength = 1.132m. Centre Y = -.112m.
Undisturbed W.L.= .555m. Radius = .055m.
Order of eq. = 1

Fig. A.13.36e

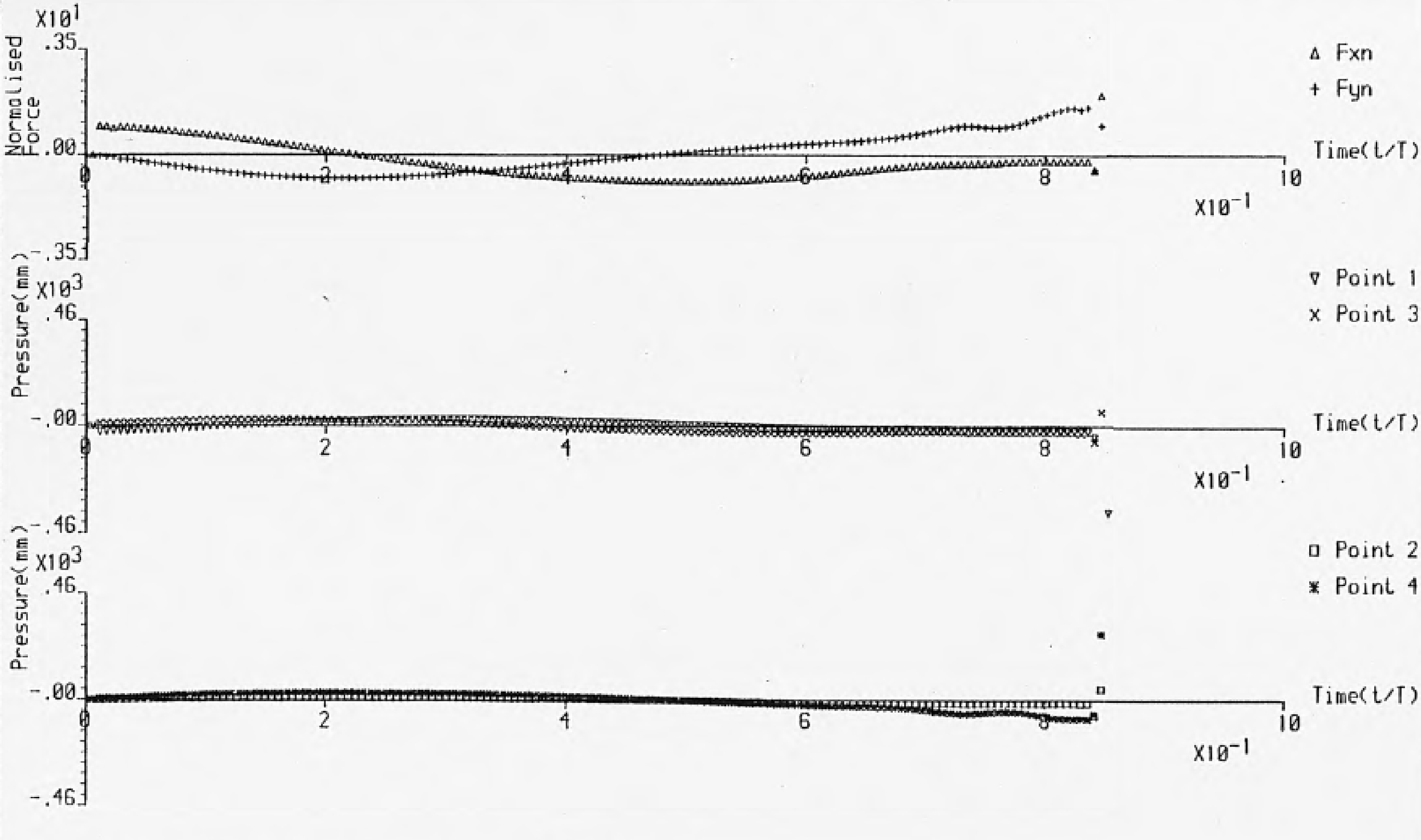

Wave height	= .114m.	Centre X	=	.566m.
Wavelength	= 1.132m.	Centre Y	=	-.112m.
Undisturbed W.L.	= .555m.	Radius	=	.055m.
Order of eq.	= 1			

Fig. A.13.36f

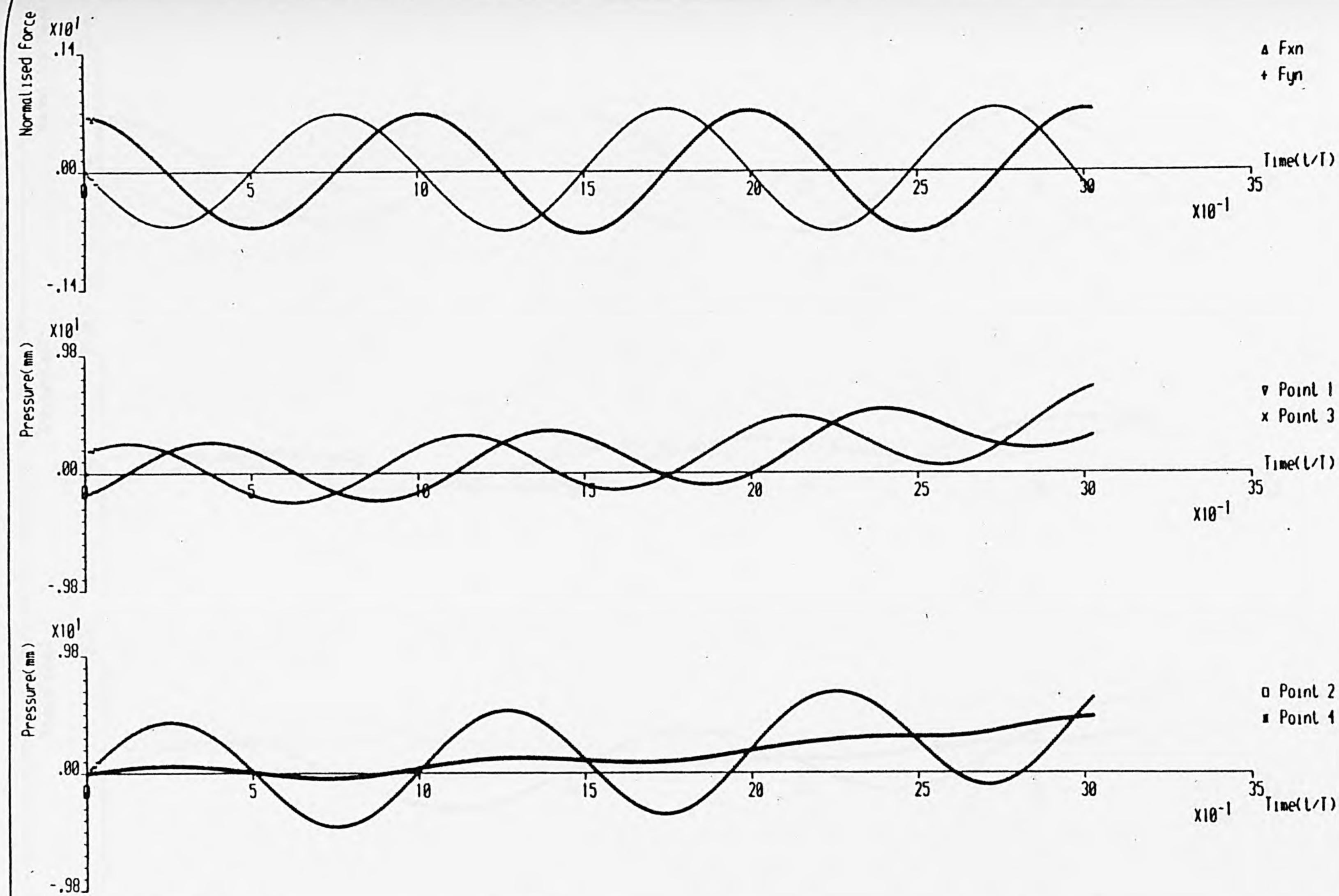

Wave height = .018m.
Wavelength = .835m.
Undisturbed W.L.= .555m.
Order of eq. = 1

Centre X = .417m.
Centre Y = -.180m.
Radius = .055m.

Fig. A.13. 37 Auxiliary graphs for case No. 37

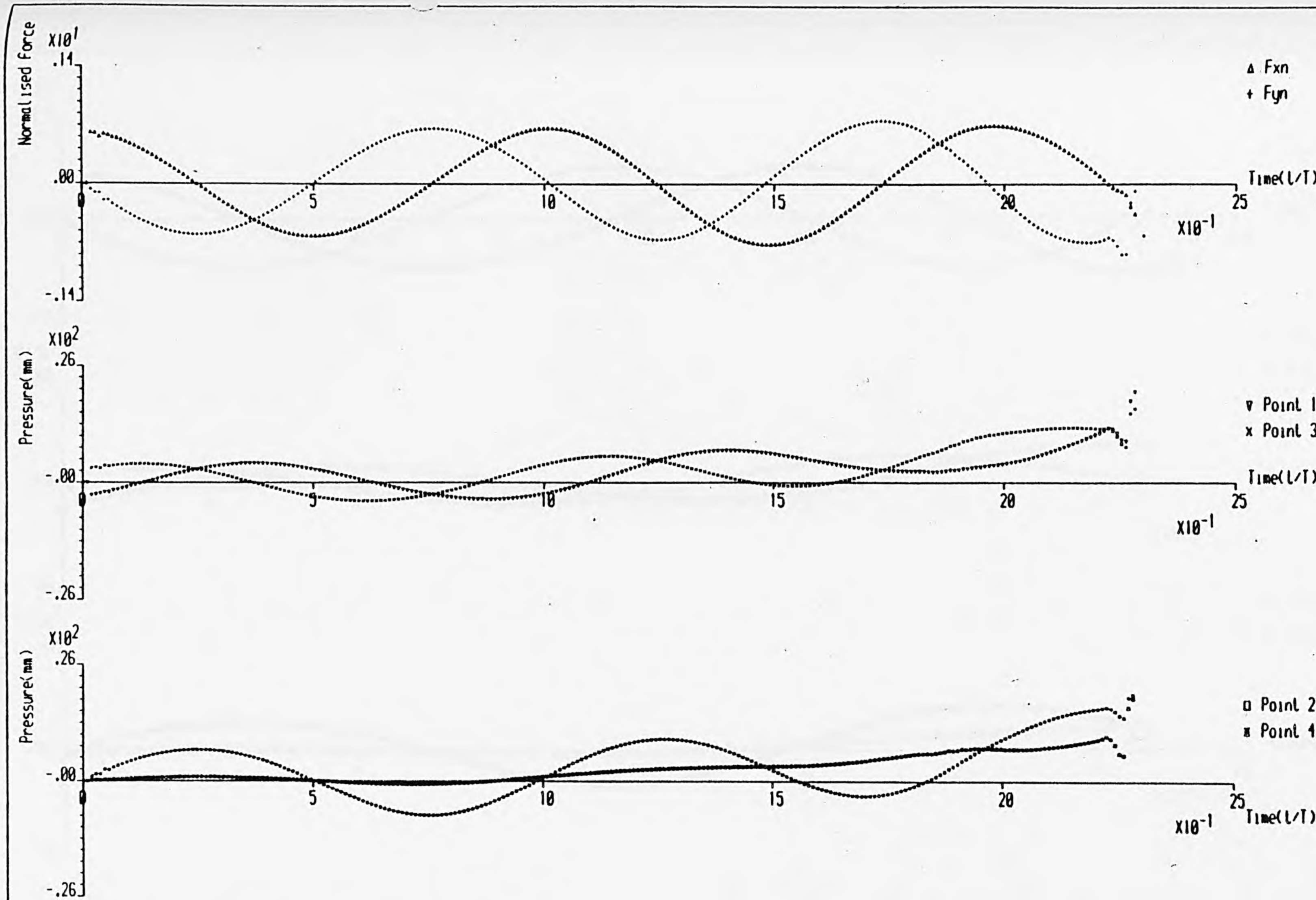

Wave height = .031m.
Wavelength = .835m.
Undisturbed W.L.= .555m.
Order of eq. = 1

Centre X = .417m.
Centre Y = -.180m.
Radius = .055m.

Fig. A.13. 38 Auxiliary graphs for case No. 38

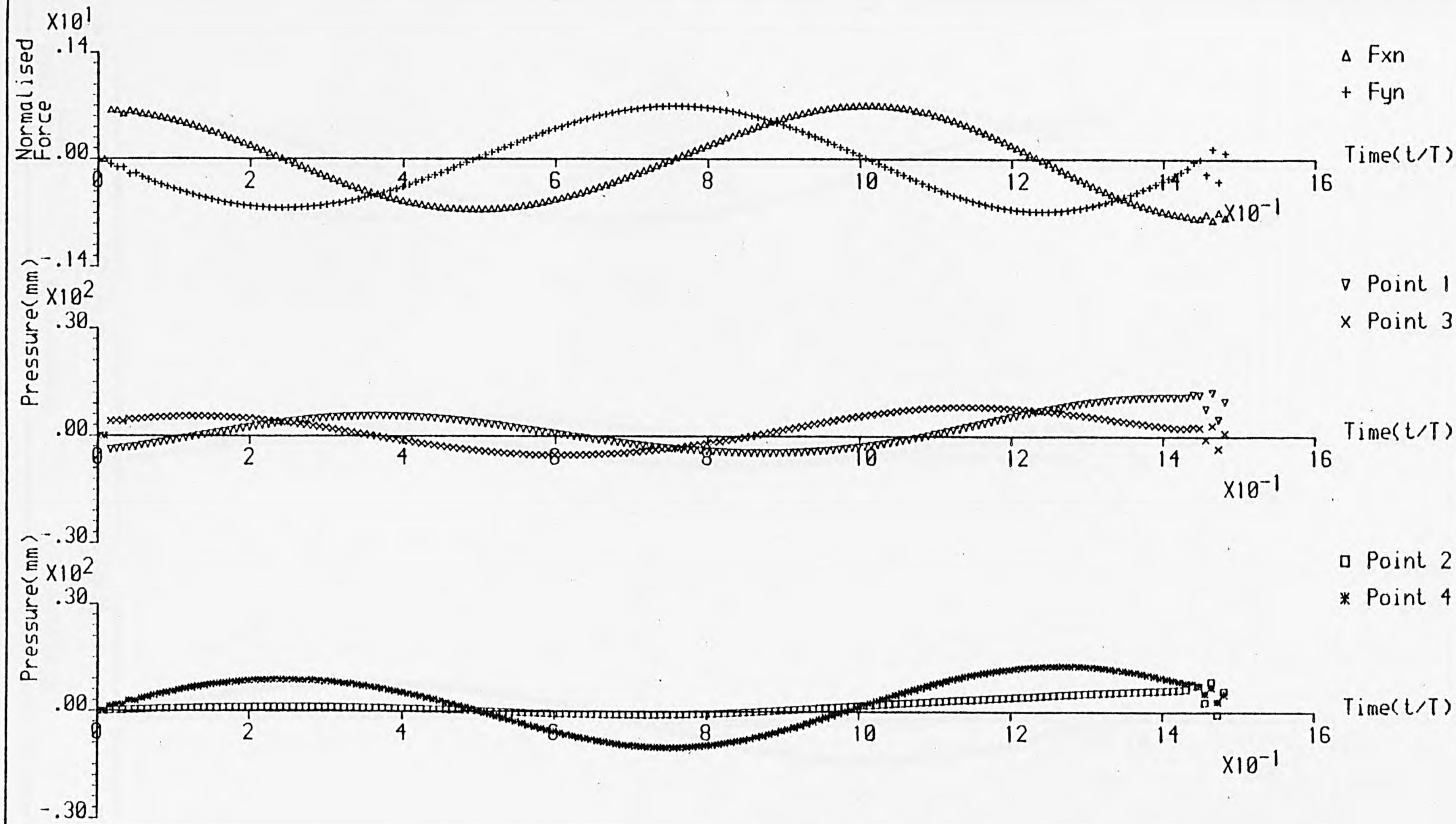

Wave height = .040m. Centre X = .418m.
Wavelength = .835m. Centre Y = -.180m.
Undisturbed W.L.= .555m. Radius = .055m.
Order of eq. = 1

Fig. A.13. 39 Auxiliary graphs for case No, 39

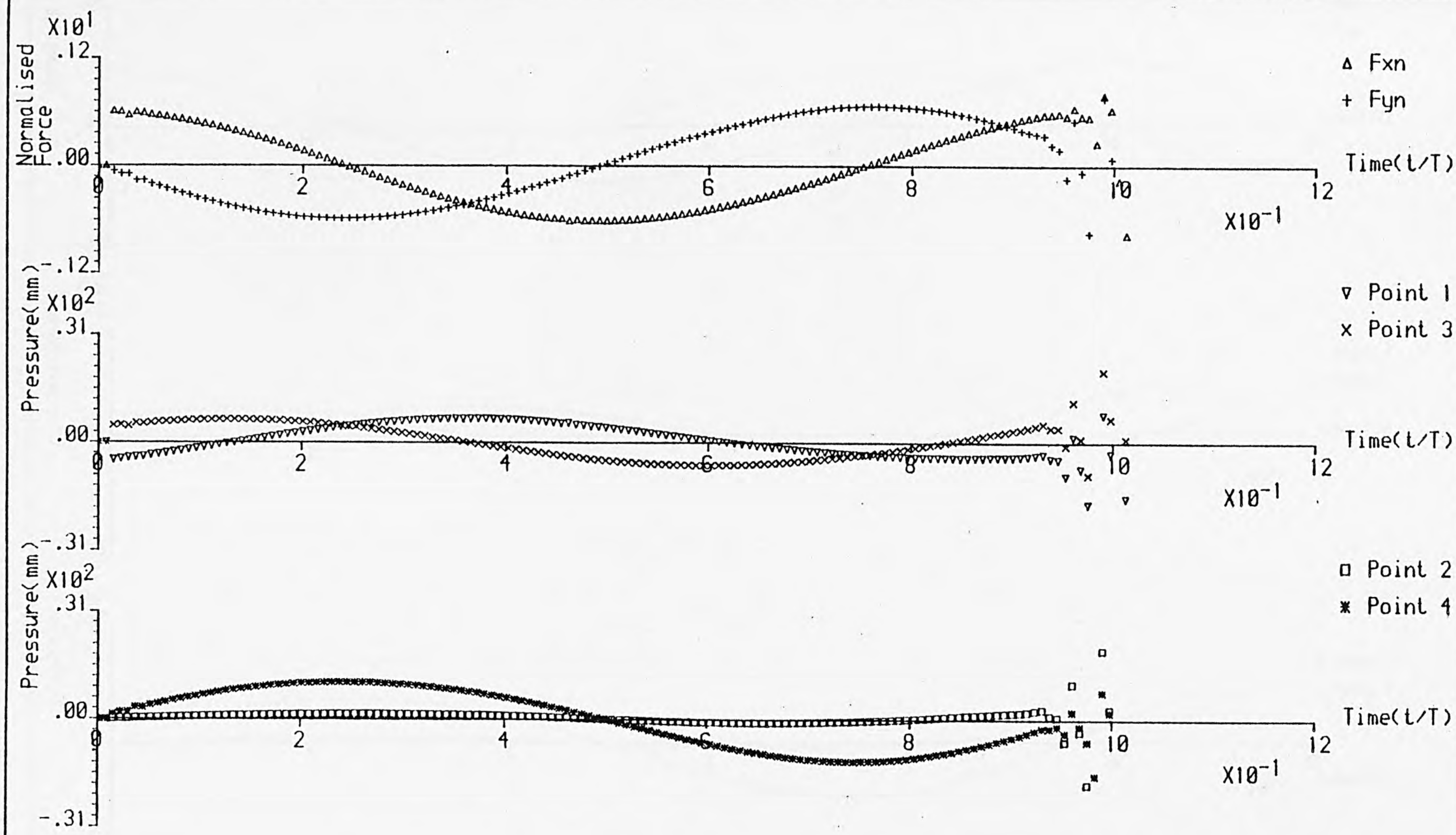

Wave height	= .050m.	Centre X	=	.418m.
Wavelength	= .835m.	Centre Y	=	-.180m.
Undisturbed W.L.	= .555m.	Radius	=	.055m.
Order of eq.	= 1			

Fig. A.13. 40 Auxiliary graphs for case No. 40

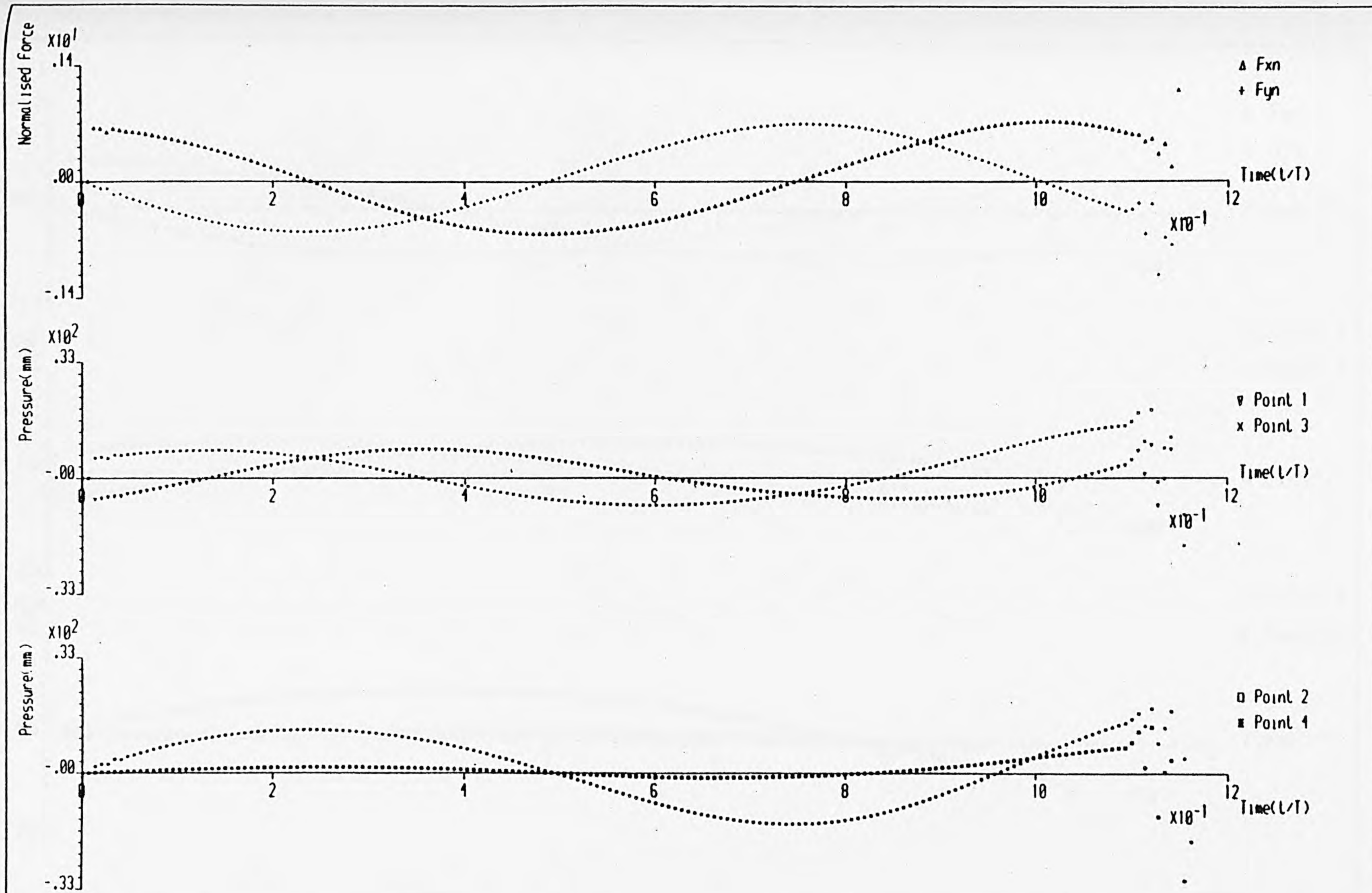

Wave height = .060m.
Wavelength = .835m.
Undisturbed W.L.= .555m.
Order of eq. = 1

Centre X = .417m.
Centre Y = -.180m.
Radius = .055m.

Fig. A.13. 41 Auxiliary graphs for case No. 41

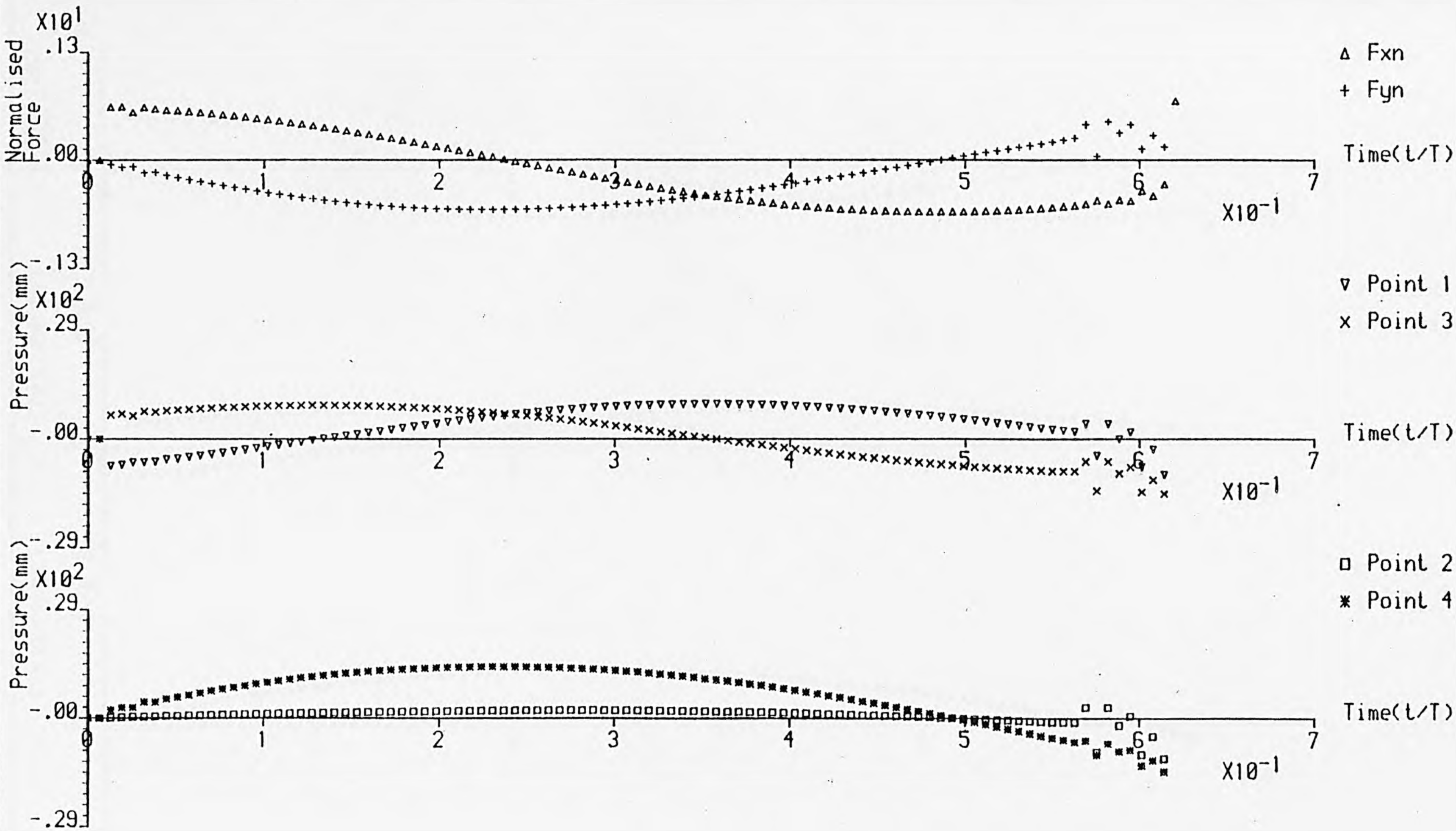

Wave height	=	.068m.	Centre X	=	.418m.
Wavelength	=	.835m.	Centre Y	=	-.180m.
Undisturbed W.L.	=	.555m.	Radius	=	.055m.
Order of eq.	=	1			

Fig. A.13. 42 Auxiliary graphs for case No. 42

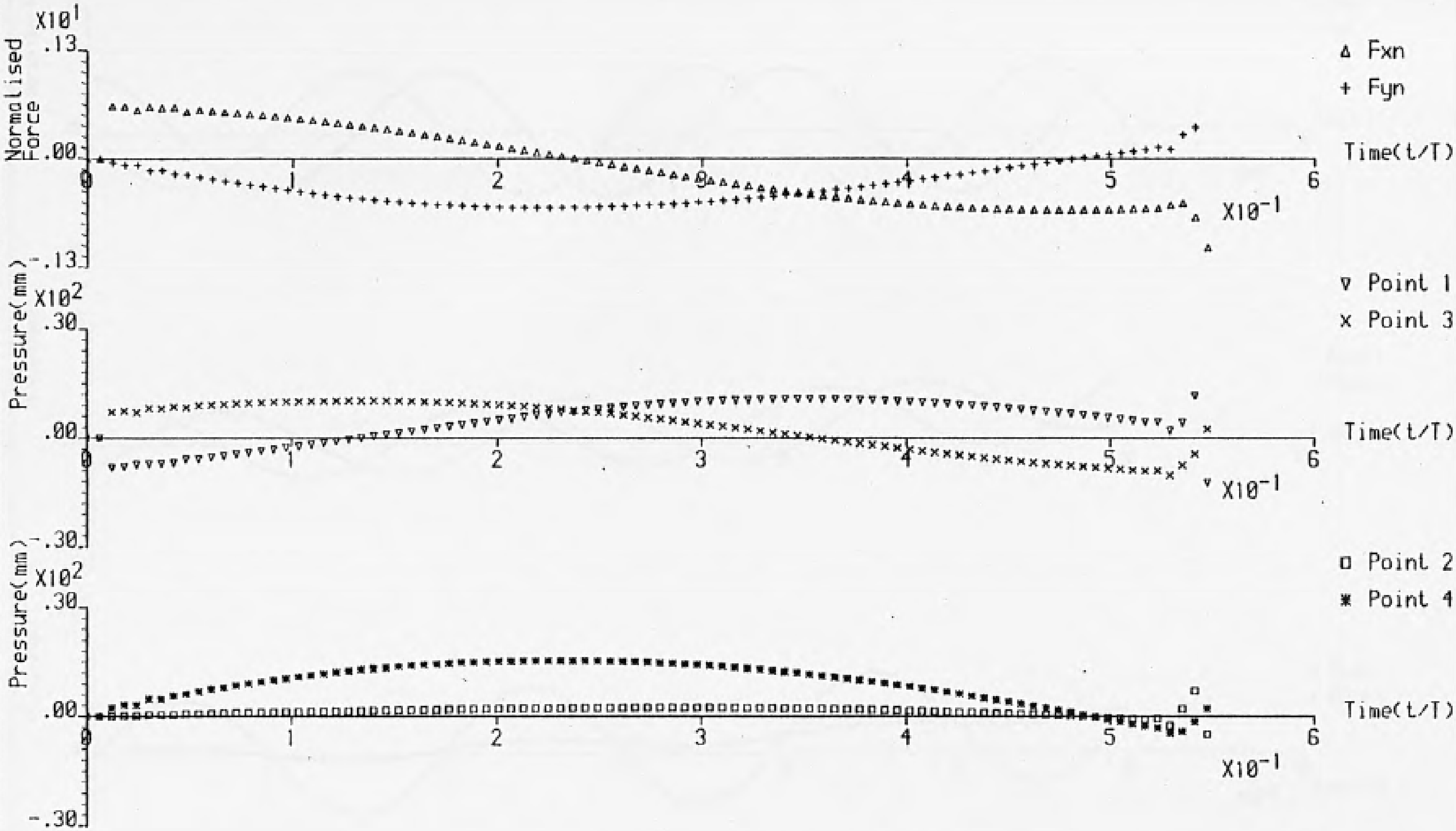

Wave height = .075m. Centre X = .418m.
Wavelength = .835m. Centre Y = -.180m.
Undisturbed W.L.= .555m. Radius = .055m.
Order of eq. = 1

Fig. A.13. 43 Auxiliary graphs for case No. 43

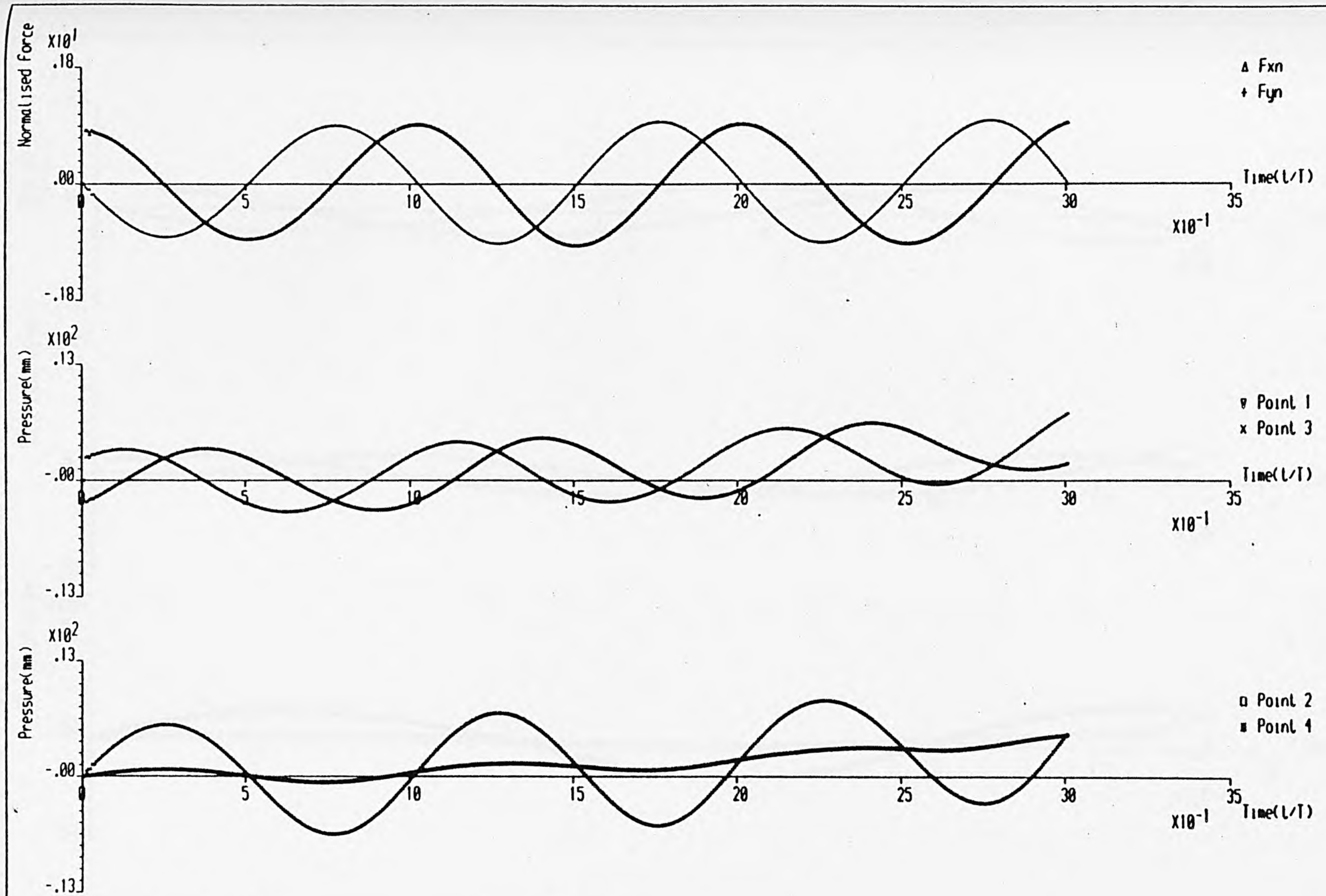

Wave height	= .018m.	Centre X =	.417m.
Wavelength	= .835m.	Centre Y =	-.138m.
Undisturbed W.L.=	.555m.	Radius =	.055m.
Order of eq.	= 1		

Fig. A.13. 44 Auxiliary graphs for case No. 44

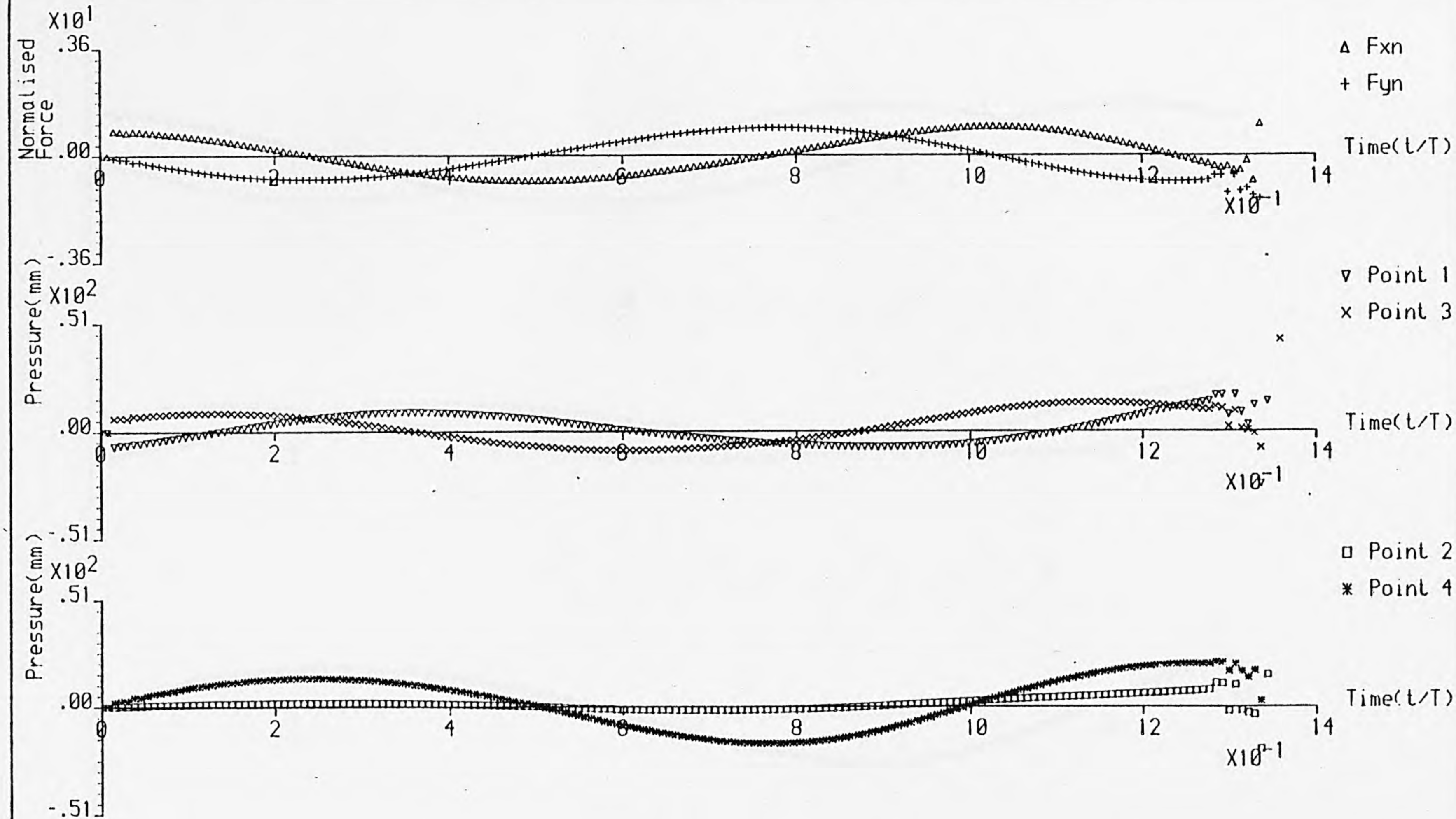

Wave height = .049m. Centre X = .418m.
Wavelength = .835m. Centre Y = -.138m.
Undisturbed W.L.= .555m. Radius = .055m.
Order of eq. = 1

Fig. A.13. 47 Auxiliary graphs for case No. 47

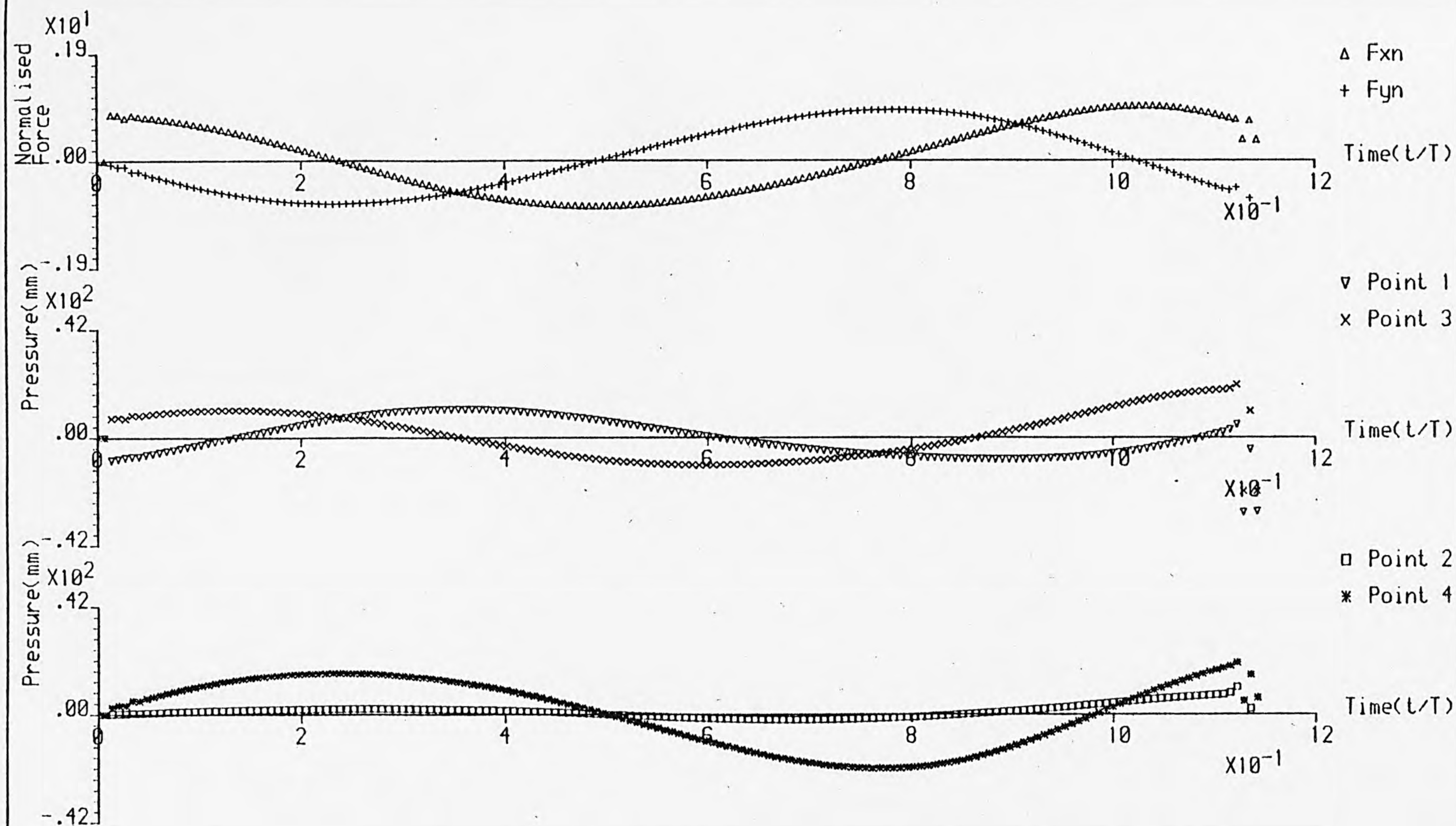

Wave height = .060m. Centre X = .418m.
Wavelength = .835m. Centre Y = -.138m.
Undisturbed W.L.= .555m. Radius = .055m.
Order of eq. = 1

Fig. A.13. 48 Auxiliary graphs for case No. 48

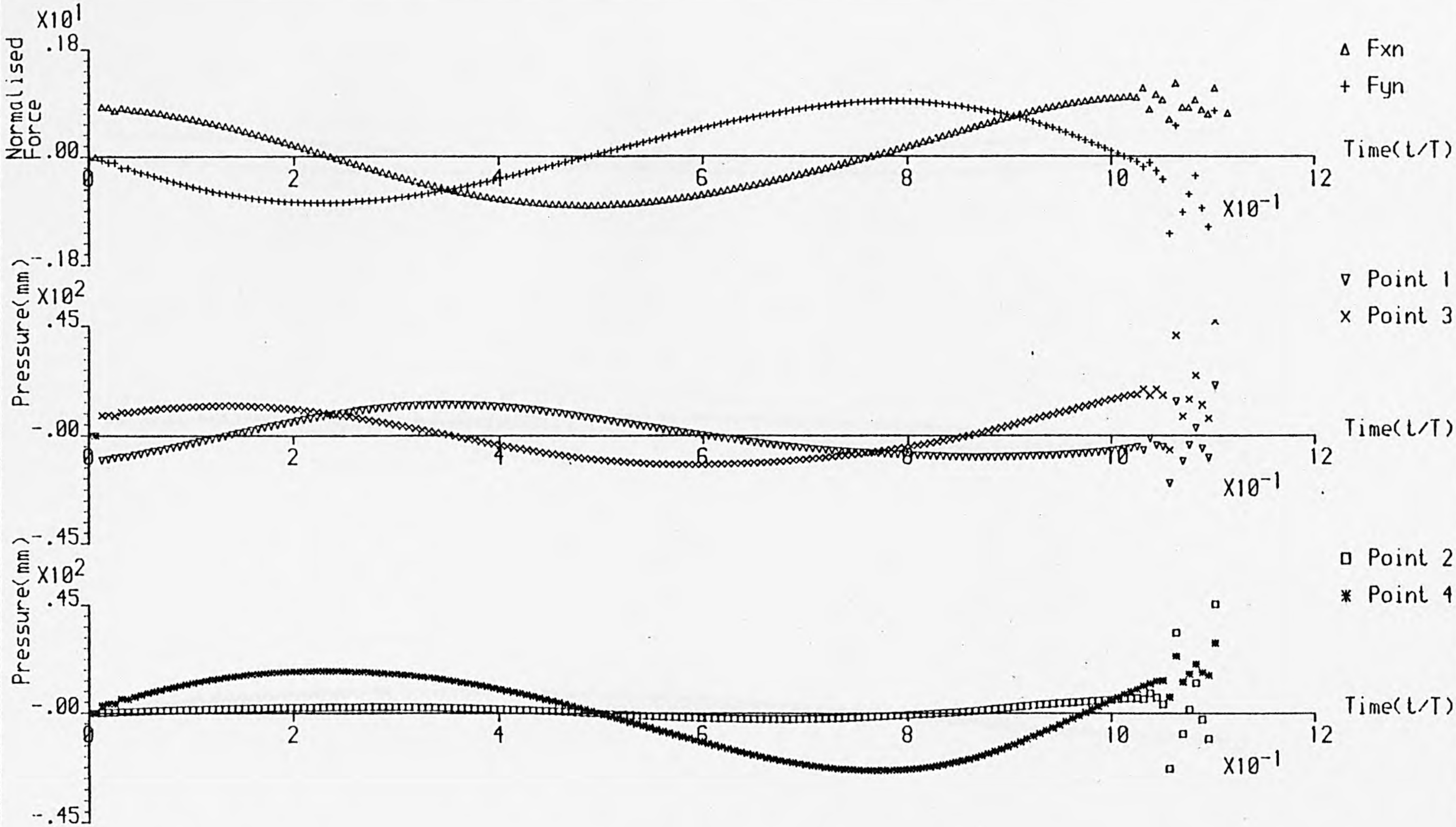

Wave height = .069m. Centre X = .418m.
Wavelength = .835m. Centre Y = -.138m.
Undisturbed W.L.= .555m. Radius = .055m.
Order of eq. = 1

Fig. A.13. 49 Auxiliary graphs for case No. 49

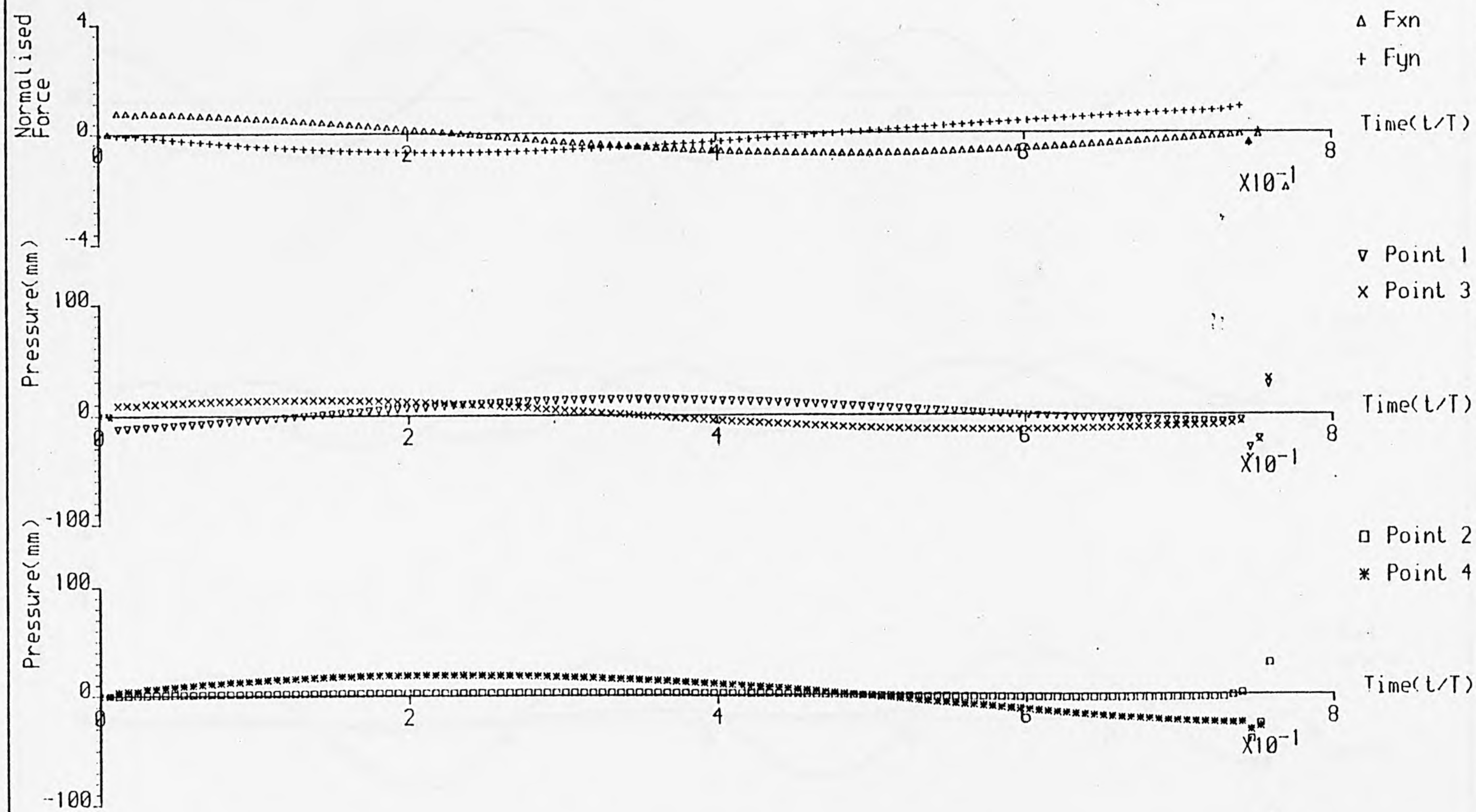

Wave height	=	.077m.	Centre X	=	.418m.
Wavelength	=	.835m.	Centre Y	=	-.138m.
Undisturbed W.L.	=	.555m.	Radius	=	.055m.
Order of eq.	=	1			

Fig. A.13. 50 Auxiliary graphs for case No. 50

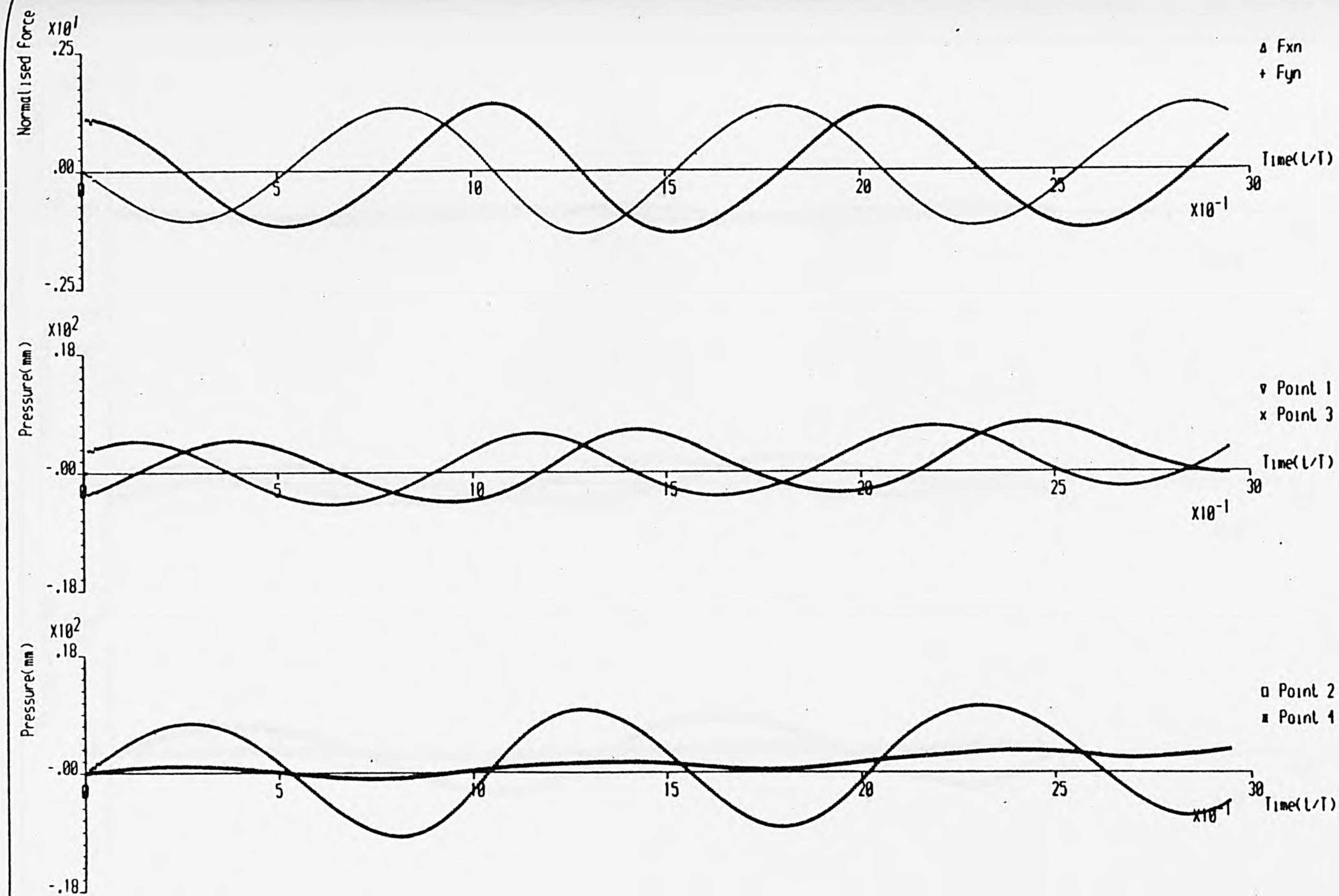

Wave height = .019m.
Wavelength = .835m.
Undisturbed W.L.= .555m.
Order of eq. = 1

Centre X = .417m.
Centre Y = -.097m.
Radius = .055m.

Fig. A.13. 51 Auxiliary graphs for case No. 51

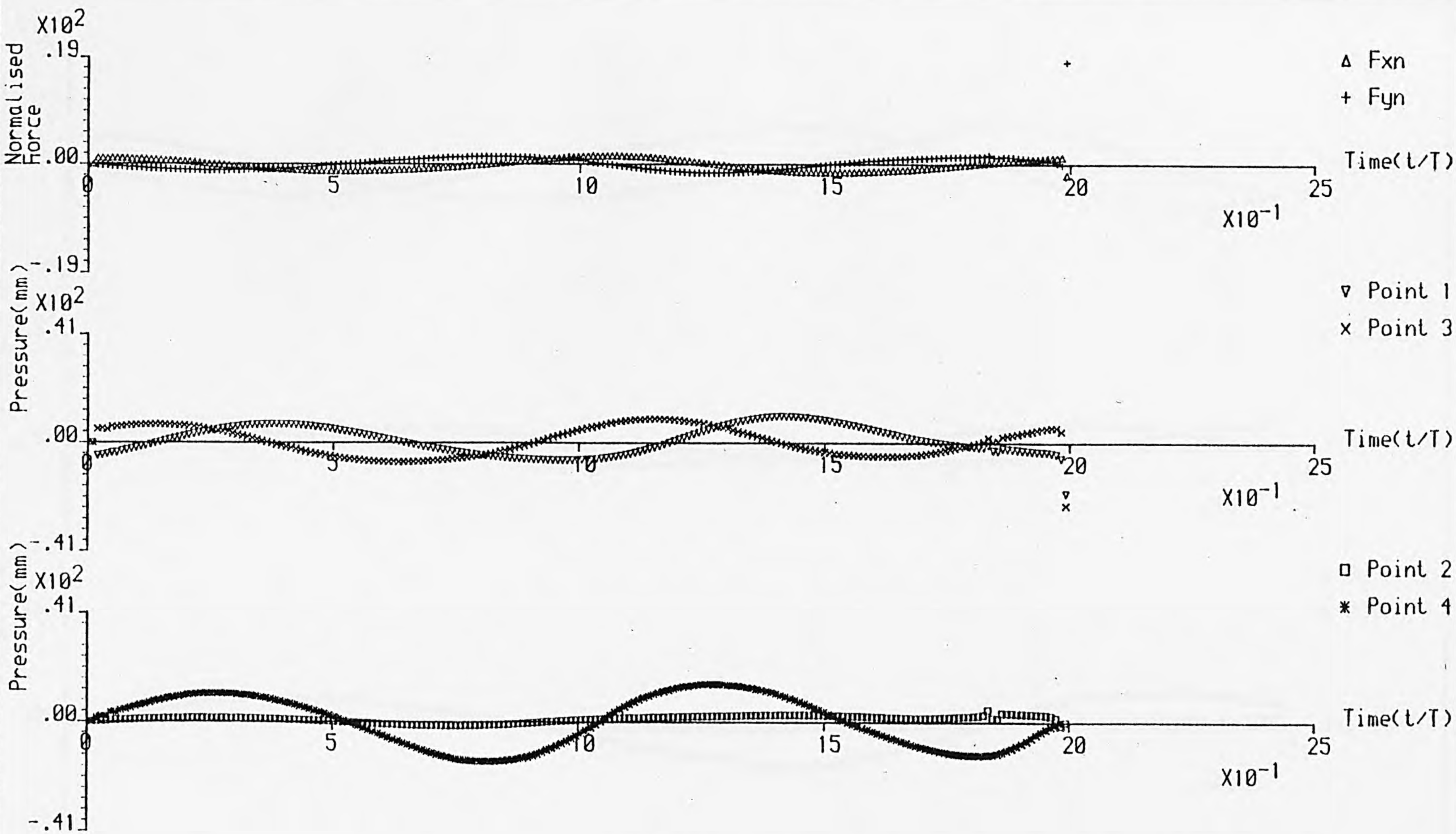

Wave height = .029m. Centre X = .418m.
Wavelength = .835m. Centre Y = -.097m.
Undisturbed W.L.= .555m. Radius = .055m.
Order of eq. = 1

Fig. A.13. 52 Auxiliary graphs for case No. 52

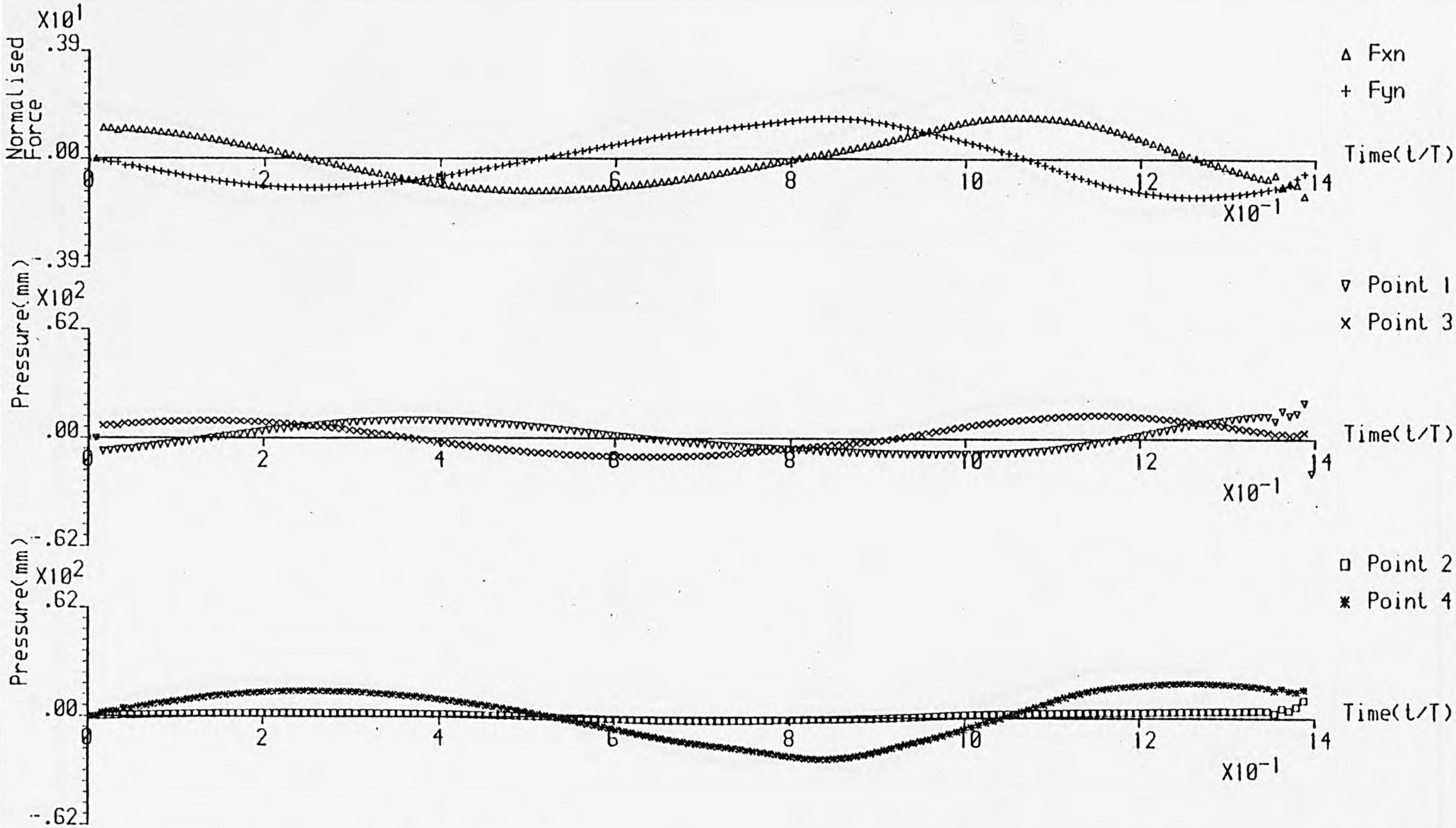

Wave height = .041m. Centre X = .418m.
Wavelength = .835m. Centre Y = -.097m.
Undisturbed W.L.= .555m. Radius = .055m.
Order of eq. = 1

Fig. A.13. 53 Auxiliary graphs for case No. 53

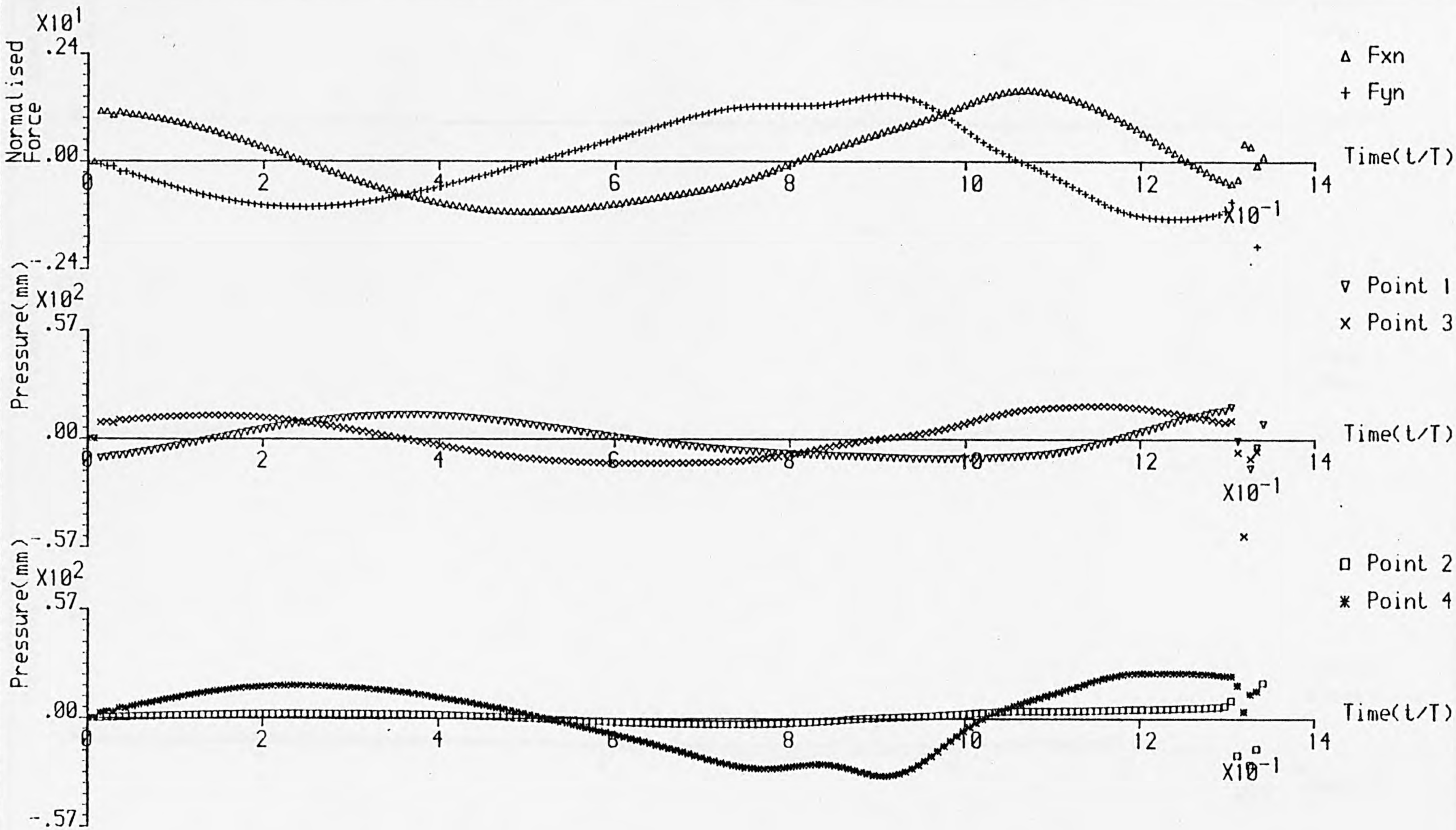

Wave height	=	.052m.	Centre X	=	.418m.
Wavelength	=	.835m.	Centre Y	=	-.097m.
Undisturbed W.L.	=	.555m.	Radius	=	.055m.
Order of eq.	=	1			

Fig. A.13. 54 Auxiliary graphs for case No. 54

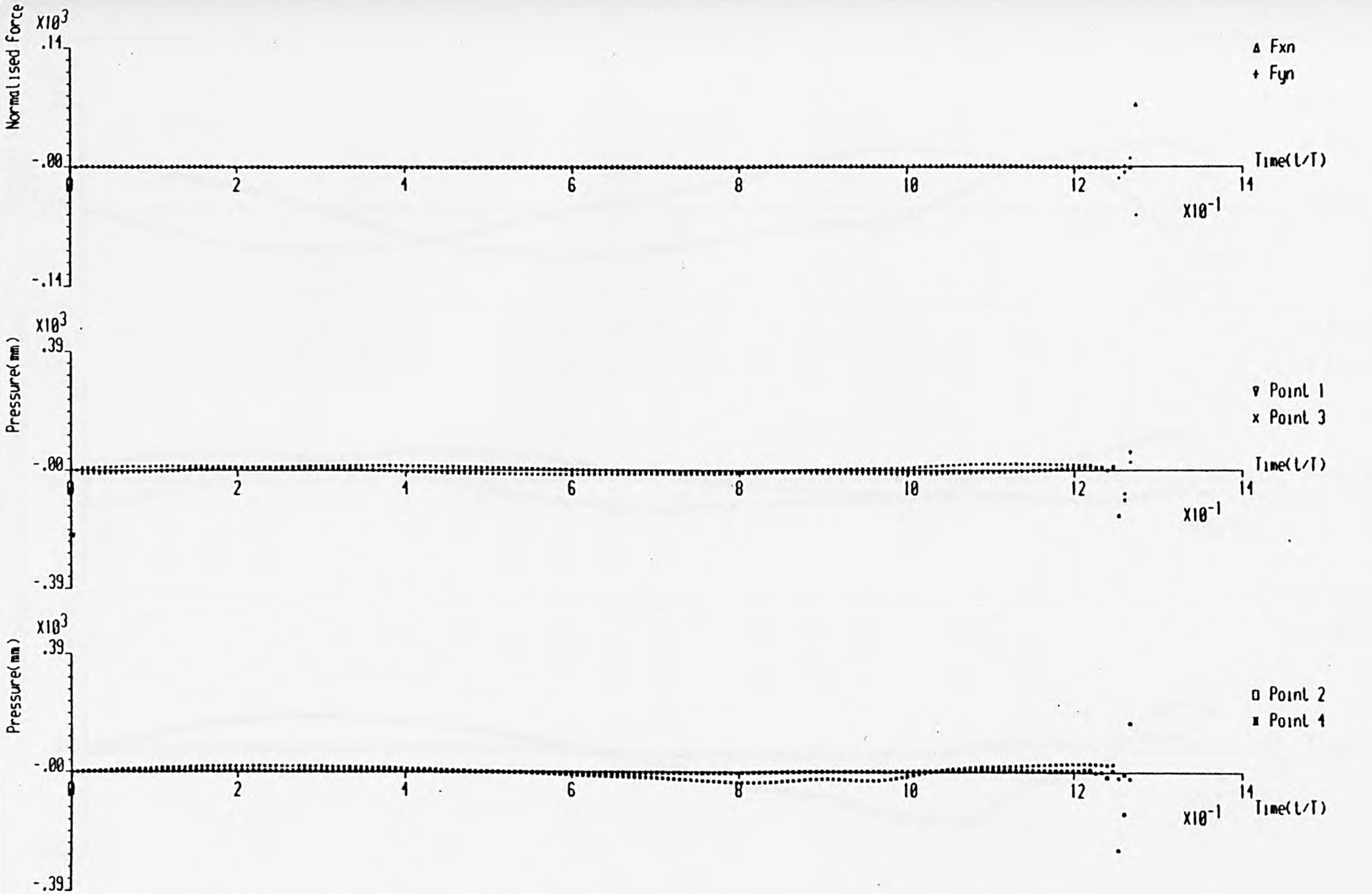

Wave height = .060m.
Wavelength = .835m.
Undisturbed W.L.= .555m.
Order of eq. = 1

Centre X = .417m.
Centre Y = -.097m.
Radius = .055m.

Fig. A.13. 55 Auxiliary graphs for case No. 55

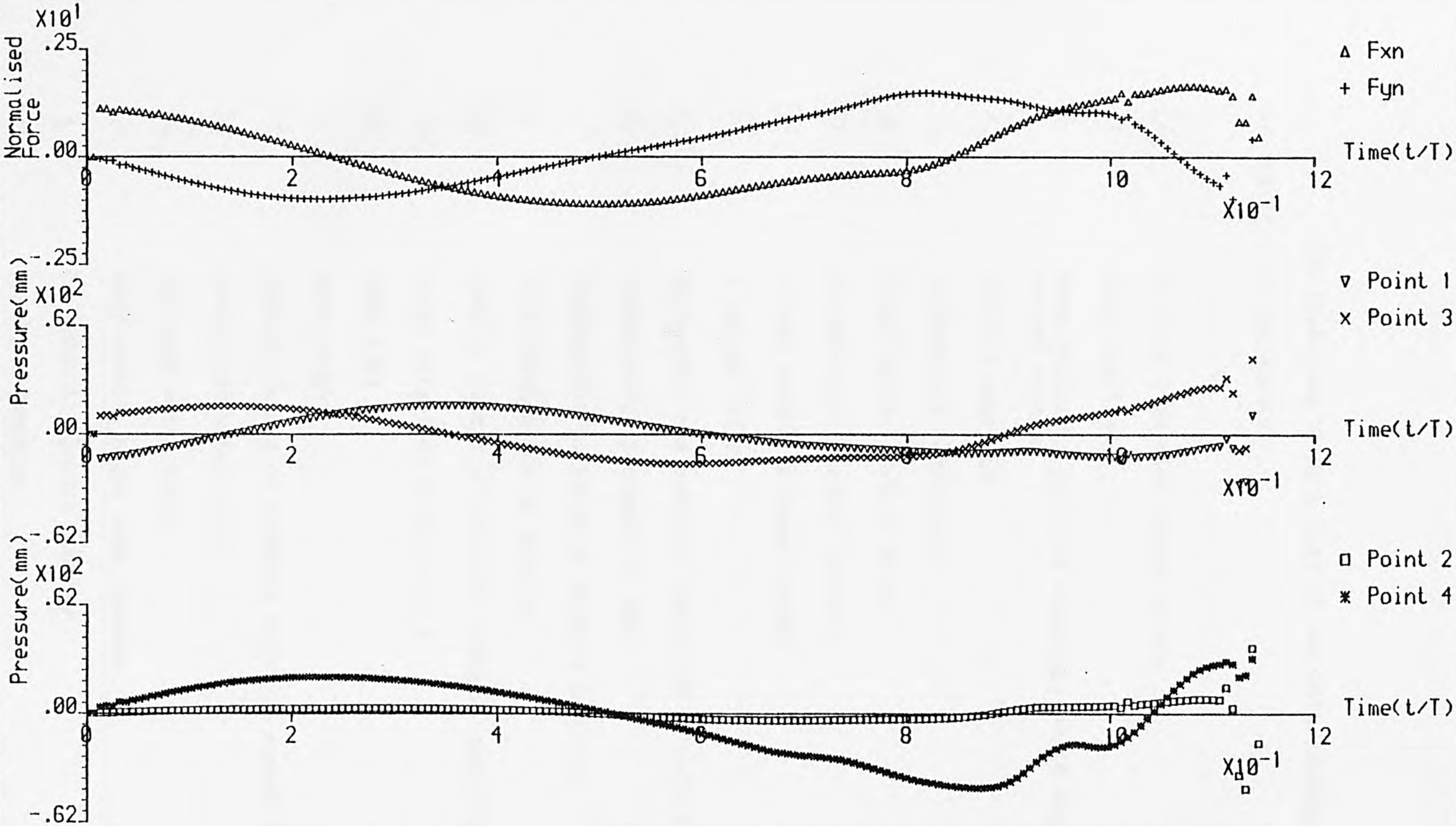

Wave height = .068m. Centre X = .418m.
Wavelength = .835m. Centre Y = -.097m.
Undisturbed W.L.= .555m. Radius = .055m.
Order of eq. = 1

Fig. A.13. 56 Auxiliary graphs for case No. 56

The following shows a list of the main symbols used in the text of the thesis.

$[A]$	A fully populated square matrix
a	Wave amplitude
C	Wave velocity; particle velocity; solid angle; closed contour
C_E	Euler's constant
C_x	Diffraction coefficient
d	Water depth; uniform depth
Ei	Exponential-integral function
$[F]$	Column vector of known values
$\underset{\sim}{F}$	A vector field
F_x, F_y	Horizontal and vertical forces on an object
f_o	Fundamental frequency of wave
g^*	Fundamental solution or Green's function
g	Acceleration due to gravity
$[G]$	Overall matrix of boundary integral equation
GW_k	Gauss weight at Gauss point k
h	Step size
H	Wave height
$[H]$	Overall matrix of boundary integral equation
h_d	Downstream water depth
h_u	Upstream water depth
i	Nodal point; nodal node counter
j	An element; element counter
$\|J\|$	Jacobian function

k	Gauss points counter; a constant
K	A constant in diffusion equation or determining time step length
k	Wave number
k_e	Effective permeability
K_e	Kinetic energy
k_x, k_y	Permeabilities in the directions of orthotrophy
L	Total number of elements on a boundary
ℓ	Length of an element
ln	Natural logarithm
L_c	Number of triangular or rectangular cells
ℓ_i	Direction cosine of outward normal
$\mathcal{L}$	A linear operator
M	Number of Gauss points
m	Counter for triangular element
N	Total number of nodal points on boundary Γ
n	Normal direction at a node on boundary Γ; counter for infinite series
n_e	Outward normal direction at a node on boundary Γ
n_i	Inward normal direction at a node on boundary Γ
N_α	Interpolation function
p	A field point in potential theory; point or node number on wave surface
$\underset{\sim}{p}$	A vector at point p with respect to a set of coordinate axes
p	Pressure
P_e	Potential energy
q	A source point in potential theory
$\underset{\sim}{q}$	A vector at point q with respect to a set of coordinate axes
R	Notation for constant term
r	Radial direction at a point ; radius of circular cylinder
$r(p,q)$	Distance between points p and q
s	Distance between adjacent nodal points on wave surface

S	Simple-layer potential
t	Time variable; tangential direction at a point
t_0, t_1, t_2	Dimensions of time
T	Wave period
U	Function defined in a closed regular region Ω
u	Particle velocity or discharge velocity in x direction
v	Particle velocity or discharge velocity in y direction
V	Function defined in a closed regular region Ω
W	Double-layer potential
ω_i	A set of linearly independent weighting functions
$\{x\}$	Column vector of unknowns
x	Cartesian coordinate system
X	Direction of orthotrophy
X_t	Scale factor for the transformation of orthotropic flow domain to a fictitious isotropic flow domain
Y	Direction of orthotropy
y	Cartesian coordinate system
y_0	Depth of cylinder axis below still water level
Z	Notation for constant term
Γ	Boundary of a domain Ω
γ	Number of nodal points on an element
ξ	Intrinsic coordinate system
α	Angle for orthotrophy; spatial dimension
β	Angle for orthotrophy
η	Vertical displacement of a point on wave surface
σ	Radian wave frequency; simple-layer source density
ϵ	Phase angle; error function
Ω	A domain; a region
Ω_i	Interior domain
Ω_e	Exterior domain
ϕ	Velocity potential; total head in seepage problem

ϕ'	Potential derivative
Γ_I	Internal boundary
μ	Double-layer source density
θ	Direction of potential derivative
∞	Infinity
Δs	Element size
Δt	Time step length
Δx	Element size projected on to the x-axis
$\nabla\phi$	Particle velocity
λ	Wavelength

APPENDIX A. 15 REFERENCES

Acton, F.S. (1970).'Numerical Methods that work'. New York: Harper & Row.

Ahlberg, J.H., Nilson, F.N. and Walsh, J.L. (1976).'The Theory of Splines and their Applications'. New York: Academic Press.

Au, M.C. and Brebbia, C.A. (1982). 'Numerical prediction of wave forces using The Boundary Element Method'. Applied Mathematical Modelling. Vol.6. pp. 218-228.

Au, M.C. and Brebbia, C.A. (1983a). 'Diffraction of Water Waves for Vertical Cylinders using Boundary Elements'. Applied Mathematical Modelling. VOL. 7.

Au, M.C. and Brebbia, C.A. (1983b). "Computation of Wave Forces on three dimensional Offshore Structures". In the Pro. of 4th Int. Conf. on Boundary Element Methods in Engineering. pp.195-217

Bai, K.J. and Yeung, R.W. (1974)'Numerical Solutions to Free-Surface flow Problems'. Tenth Symposium of Navel Hydrodynamics. M.I.T. Ed: Cooper. R.D. and Doroff. S.W.

Brebbia, C.A. (1978).'The Boundary Element Method for Engineers' Pentech Press, London

Brebbia, C.A. and Chang, O.V. (1979).' Boundary Elements Applied to Seepage Problems in Zoned Anisotropic Soils'. Advances in Engineering Software, Vol. 1, No. 3.

Brebbia, C.A. and Walker, S. (1980). 'Boundary Element Techniques in Engineering' . Newnes - Butterworths, London.

Brebbia, C.A. and Wrobel, L.C. (1979). 'Steady and Unsteady Potential Problems using the Boundary Element Method'. In: Recent Advances in Numerical Methods in Fluids. Ed: C. Taylor, Swansea.

Brevig, P., Greenhow, M. and Vinje, T. (1981). 'Extreme Wave Forces on Submerged Cylinders'. Paper presented at the Second Int. Symposium on Wave and Tidal Energy. Cambridge, England.

Butterfield, R. and Tomlin, G.R. (1972). 'Integral Techniques for Solving Zoned Anisotropic Continuum Problems' In: Pro. Int. Conf. on Variational Methods in Engineering. Vol. 2 Ed: C.A. Brebbia and H. Tottenham. Southampton University Press, Southampton.

Carslaw, H. S. and Jaeger, J.C. (1959). 'Conduction of Heat in Solids' 2nd edition. Clarendon Press, Oxford

Chan, R.K. and Street, R.L. (1970). 'SUMMAC - A Numerical Model for Water Waves. Tech. Report, Dept. Civil Engineering , Stanford University, Calif., No. 135.

Chang, Y.P. Kang, C.S. and Chen, D.J. (1973). 'The Use of Fundamental Green's Functions for the Solution of Problems of Heat Conduction in Anisotropic Media'. Int. Journal Heat Mass Transfer Vol. 16, pp. 1905 - 1918, Pergamon Press

Coates, L.E. (1977). 'The Finite Element applied to Fluid Mechanics'. Final Year Project, The City University.

De, S.C.(1955). 'Contributions to the Theory of Stokes Waves'. Proc. Camb. Phil. Soc. Vol. 51,pp. 713 - 736.

Fernandes, J.L.M. and Pina, H.L.G. (1983). 'Unsteady Heat Conduction using the Boundary Element Method' In: The 4th Int. Conf. on Boundary Element Methods in Engineering,pp. 156 - 170.

Gerald, C.F. (1970). 'Applied Numerical Analysis'. Reading. Mass: Addison - Wesley

Isaacson, M. de St. Q. (1982).'Nonlinear-Wave effects on fixed and floating bodies'. J. Fluid Mech. Vol. 120,pp. 267 - 281.

Jaswon, M.A. (1963).'Integral Equation Methods in Potential Theory I'. Proc. Roy. Soc. A. Vol. 275.

Jaswon, M.A. and Symm, G.T. (1977). 'Integral Equation Methods in Potential Theory and Elastostatics'. London Academic Press

Jeffrey, D.C.,Richmond, D.J.E.,Salter, S.H. and Taylor, J.R.M. (1976). 2nd year Interim Report on Edinburgh Wave Power Project. Dept. of Mech. Eng., University of Edinburgh.

Kellogg,O.D. (1954).'Foundations of Potential Theory'. Dover Publications.

Kinsman, B. (1965). 'Wind Waves-their generation and propagation on the ocean surface'. Englewood Cliffs. N.J.: Prentice-Hall.

Lacey, D.J. (1983). 'Wave Obstacle Interaction for A Submerged Horizontal Circular Cylinder'. Ph.D. Thesis, The City University.

Lambe, T.W. and Whitman, R.V. (1969). 'Soil Mechanics'. Wiley, New York.

Lau, C.S. (1980). 'Boundary Element Method'. Undergraduate Project, The City University.

Lennon, G.P., Liu, P.L.F. and Liggett, J.A. (1982). 'Boundary Integral Solution of Water Wave Problems.' Journal of the Hydralic Division, ASCE, Vol. 108, No. HY8.

Liggett, J.A. (1977a). 'Location of Free Surface in Porous Media' Journal of the Hydralics Division. Proceedings of the American Society of Civil Engineers. Vol. 103, No. HY4.

Liggett, J.A. (1977b). 'Lecture Notes on Boundary Integral Equation Method'.

Longuet-Higgins, M.S. and Cokelet, E.D. (1976). 'The Deformation of Steep Surface waves on water I. A numerical method of Computation'. Proc. R. Soc. Lond. A. Vol. 350, pp. 1 - 26.

Longuet-Higgins, M.S. and Cokelet, E.D. (1978). 'The Deformation of Steep surface waves on water II. Growth of Normal-mode instabilities'. Proc. R. Soc. Lond. A. Vol. 364, pp.1-28.

Mei, C.C. (1978). 'Numerical Methods in Water-Wave Diffraction and Radiation'. Annual Review of Fluid Mech. Vol. 10 pp. 393 - 416.

Moon, P. and Spencer, D.E.(1961). 'Field Theory for Engineers'. New York: D. Van Nostrand Company Inc.

Morse, P.M. and Feshbach, H. (1953). 'Methods of Theoretical Physics' 2 vols. New York: MCGraw-Hill.

Newman, J.N. (1980). 'Marine Hydrodynamics'. The MIT Press, London, England.

Ogilvie, T.F. (1963). 'First-and Second-Order Forces on a Cylinder submerged under a free surface'. Journal of Fluid Mechanics. Vol. 16, pp. 451 - 472.

Rizzo, F.J. and Shippy, D.J. (1970). 'A Method of Solution for Certain Problems of Transient Heat Conduction'. AIAA Journal Vol. 8, No. 11.

Salmon, J.R., Liu, P.L.F. and Liggett, J.A. (1980). 'Integral Equation Method for Linear Water Waves'. Journal of the Hydraulics Division, ASCE. Vol. 106, No. HY12 pp. 1995-2010.

Schwartz, L.W. (1974). 'Computer Extension and Analytic Continuation of Stoke's expansion for gravity waves'. J. Fluid Mechanics. Vol. 62, pp. 553 - 578.

Skjelbreia, L. (1958). 'Gravity Waves Stokes' Third Order Approximation Tables of Functions'.

Skjelbreia, L. and Hendrickson, J. (1961). 'Fifth Order Gravity Wave Theory'. Proceedings of the 7^{th} Conf. on Coastal Engineering. Vol. 1, Chapter 10, pp. 184 - 196.

Smirnov, V.I. (1964). 'Integral Equations and Partial Differential Equations, a Course of Higher Mathematics' Vol. IV. Pergamon: London.

Smith, W.D. (1974). 'A Nonreflecting Plane Boundary for Wave Propagation Problems'. Journal of Computational Physics. Vol. 15, pp. 492 - 503.

Symm, G.T. (1963). 'Integral Equation Methods in Potential Theory II'. Proc. Roy. Soc. Lond. A. Vol. 275, pp. 33 - 46.

Vinje, T. and Brevig, P. (1980). 'Numerical Simulation of Breaking Waves'. 3^{rd} Int. Conf. on Finite Elements in Water Resources, University of Miss., Oxford, Miss.

Vinje, T. and Brevig, P. (1981). 'Numerical Calculations of Forces from Breaking Waves'. International Symposium on Hydrodynamics in Ocean Engineering, The Norwegian Institute of Technology.

Wehausen, J.V. and Laitone, E.V. (1960).'Surface Waves.' In Encyclopedia of Physics'. Vol. 9. Berlin-Gottingen-Heidelberg: Springer-Verlag.

Wiegel, R. (1964). 'Oceanographical Engineering'. Englewood Cliffs, N.J.: Prentice-Hall.

Wrobel, L.C.(1981). 'Potential and Viscous Flow Problems using the Boundary Element Method'. Ph.D. Thesis, University of Southampton.

Wrobel, L.C. and Brebbia, C.A. (1979). 'The Boundary Element Method for Steady State and Transient Heat Conduction'. In: First Int. Conf. on Numerical Methods in Thermal Problems. Ed: R.W. Lewis and K. Morgan.